SHRP-A-415

Permanent Deformation Response of Asphalt Aggregate Mixes

Asphalt Research Program
Institute of Transportation Studies
University of California, Berkeley

Strategic Highway Research Program
National Research Council
Washington, DC 1994

SHRP-A-415
Contract A-003A
ISBN 0-309-05850-3
Product no. 1017

Program Manager: *Edward T. Harrigan*
Project Manager: *Rita B. Leahy*
Program Area Secretary: *Juliet Narsiah*
Typesetters: *Laurie Dockendorf, Peggy Blair, Teresa Culver*
Production Editor: *Katharyn L. Bine*

August 1994

key words:
asphalt concrete
creep test
diametral test
dilatancy
mix design and analysis
permanent deformation
repeated load test
rutting
shear test
stiffness
viscoelastic

Strategic Highway Research Program
National Research Council
2101 Constitution Avenue N.W.
Washington, DC 20418

(202) 334-3774

1.5M/NAP/894

Acknowledgments

The research described herein was supported by the Strategic Highway Research Program (SHRP). SHRP is a unit of the National Research Council that was authorized by section 128 of the Surface Transportation and Uniform Relocation Assistance Act of 1987.

Professor Carl L. Monismith of the University of California, Berkeley served as the principal investigator. Dr. R. G. Hicks of Oregon State University and Mr. Fred N. Finn of the University of California, Berkeley served as co-principal investigators. Under the overall direction of Professor Monismith, individual responsibilities for this research were: Dr. J. Sousa and Dr. J. Harvey, equipment development and laboratory testing; Dr. S. Weissman, constitutive relationships; Dr. J. Deacon, Mr. J. Coplantz and Mr. G. Paulsen, data reduction and analysis; Dr. J. Deacon, mix design and analysis framework. Integration of these many efforts into a cohesive final report was accomplished primarily through the effort of Professor Monismith.

The patience and expertise of Laurie Dockendorf, Peggy Blair, and Teresa Culver are gratefully acknowledged. Without their tireless efforts at the keyboard, this report would not have made it to press.

Contents

List of Figures

List of Tables

Abstract

This report describes the research conducted on permanent deformation of asphalt concrete mixes as part of the SHRP Asphalt Research Program. Divided into three sections the report addresses the following: the development of a series of accelerated performance tests to measure the permanent deformation response and a constitutive relationship to define it; validation of the binder properties included in the SHRP binder specification; and the use of the test methodology in an asphalt concrete mix design and analysis system.

Executive Summary

The primary objectives of Strategic Highway Research Program (SHRP) Project A-003A included the development of a series of accelerated performance-related tests for asphalt aggregate mixes and methods for analyzing asphalt aggregate interactions that significantly affect pavement performance. Included within the scope of the A-003A project was permanent deformation development (rutting), one of the major distress mechanisms affecting asphalt pavement performance.

This report, detailing the results of the permanent deformation investigation, is divided into three sections:

Part I provides a summary of the methodology used to select the test equipment (the simple shear test) to define the permanent deformation characteristics of asphalt/binder-aggregate mixes.

Part II includes the following:

- Development of test procedures using the simple shear test to measure permanent deformation response and a constitutive relationship to define this response.
- Validation of the A-002A hypothesis for specification requirements for consideration of permanent deformation.
- Limited validation of the simple shear test(s) for permanent deformation assessment and prediction.

Part III describes the use of the test methodology and results contained in Part II to develop a mix analysis and design system to mitigate rutting. An example of the use of the system for mix design is also included.

To select the test methodology to define permanent deformation response, several candidate procedures were identified and three separate organizations were involved in the evaluation program. Tests included (1) axial and shear creep, and axial and shear repeated load; (2) axial creep following the Federal Highway Administration's (FHWA's) VESYS procedure; and (3) wheel-tracking using equipment developed by the Transport and Road Research Laboratory (TRRL) of Great Britain. The third group of tests was performed by SWK

Pavement Engineering at the University of Nottingham (SWK/UN); the VESYS tests were performed at North Carolina State University (NCSU); all other tests were performed at the University of California at Berkeley (UCB).

In this initial phase, mix variables included asphalt type (temperature susceptibility), asphalt content, aggregate stripping potential, and degree of compaction; other variables included temperature and applied stress magnitude.

The test program at UCB identified a number of important mix characteristics that must capture the permanent deformation characteristics of asphalt/binder-aggregate mixes. These include (1) dilation under shear loading, (2) increase in stiffness with increase in hydrostatic pressure, (3) residual deformation on removal of load, (4) temperature and rate of loading dependence, and (5) the difference between repeated and static loading in terms of accumulated deformation.

The test program at NCSU, which used only the repeated cream (VESYS) test, provided data that indicated that the parameters developed from the test (α, μ) were not sensitive to mix characteristics. Accordingly, this test and associated methodology were not considered.

The test program at SWK/UN was designed to provide results on mixes associated with this initial phase that might serve as indicators of relative performance for mixes tested at NCSU and at UCB; that is, to ensure that the procedure selected would order the mixes in a similar manner. The results were generally as expected, with mixes containing aggregate RB performing better than those with aggregate RL and those containing asphalt AAK-1 performing better than mixes with asphalt AAG-1. Since the test provided a reasonable differentiation of mixes in terms of rutting performance, it was decided to use this test as a part of the validation of the SHRP binder specification criteria.

As the test program at UCB developed and experience was gained with the shear test, the decision was made to use this test for measuring the permanent deformation characteristics of asphalt aggregate mixes, because of the following:

- The results of the literature evaluation stressed the importance of considering directly the effect of shear stresses on the accumulation of permanent deformation. Additional analysis of representative pavement structures indicated that states of stress in the upper part of the pavement near the tire edge could be defined with a test in which both the normal and shear stresses could be controlled independently of each other.

- While one might argue that an axial loading test is sufficient to define the state of stress directly beneath the tire, it is not possible to duplicate, with such a test, the conditions of stress elsewhere so as to directly measure their influence. With the simple shear test it is possible to directly measure the effects of a specific stress state.

- With developments in servo-hydraulic loading and computer control, simultaneous application for shear and normal stresses is feasible and can be

accomplished in a practical manner. Hence, equipment limitations no longer preclude the use of such a test.

- The importance of the dilation characteristics of a mix on permanent deformation response has been stressed. The simple shear test provides a more accurate measure of the dilation characteristics of a mix than an axial loading test, since the normal force generated as the specimen tends to dilate under shear stress application can be directly measured in the simple shear test.

Specimen size and configuration also influenced the decision to select the shear test. For conventional mixes (aggregate of nominal 2.5 cm [1 in.] maximum size) it is desirable to have test specimens that are 15 cm (6 in.) in diameter. Specimens 10 cm (4 in.) in diameter may be used for testing, but estimates of shear modulus may be inaccurate because of end effects. With a 15 cm (6 in.) diameter specimen, an *axial loading test* would require at least a 15 cm (6 in.) specimen height (with polished end surface) and preferably a 30 cm (12 in.) height, i.e., a ratio of height to diameter of 2 to 1 to minimize end effects on material response. On the other hand, a 15 cm (6 in.) diameter specimen for the simple shear test could have a height in the range 5 to 7.5 cm (2 to 3 in.) and provide reasonable results (as will be seen in Part II).

With large stone mixes, specimens of the order of 20 cm (8 in.) in diameter are desirable. Considering the requirements stated above, this makes the simple shear test even more appealing from the standpoint of specimen size.

At the outset of this program, partial factorial experiments were planned for the studies conducted by each of the agencies; these plans were followed at NCSU and SWK/UN. At UCB, however, the planned partial factorial was not followed exactly. Nevertheless, the information gained from each series of experiments led to the conclusion that the simple shear test would provide the best opportunity to define the permanent deformation characteristics of asphalt aggregate mixes.

It was also concluded that none of the existing analysis procedures for pavement response to load would reflect the type of behavior described above. Thus, it was deemed necessary to develop a constitutive relationship for asphalt aggregate mixes that reflected the above-noted characteristics and was compatible with a three-dimensional finite element representation of typical pavement structure, permitting, in turn, the estimation of the accumulation of permanent deformation under repetitive traffic loading. At the same time, it was also necessary to develop the test equipment and procedures that define the parameters contributing to the permanent deformation response of asphalt aggregate mixes.

Part II describes the development of the simple shear test and its potential application in mix analysis and design. In addition, the use of the test to validate a permanent deformation requirement in the SHRP binder specification is presented.

The simple shear test described herein permits simultaneous application of shear and axial loads to cylindrical or square specimens. Confining pressures of up to 690 kPa (100 psi) can

be applied over a temperature range of -10°C to +70°C (14°F to 158°F). Both shear and axial loads can be applied sinusoidally, repetitively, or sustained (creep loading). For sinusoidal loading, frequencies in the range of 0.01 to 20 Hz (approximately 3 decades) are feasible. Repeated loads using a haversine pattern can be applied with a range in time of loading and time intervals between loadings (rest periods). Shear stresses are transmitted to the specimen through end caps that have been bonded to it using an epoxy resin.

A simpler version of the equipment has also been developed. This equipment permits testing only in the upper temperature range. It has the advantage, however, that it could be used in the field as a construction control test since cores from as-constructed pavements could be tested under prescribed conditions at paving sites.

Both sets of equipment permit testing of conventional dense-graded mixes, open-graded mixes, gap-graded (SMA) mixes, and large-stone (up to 3.7 cm [1.5 in.] maximum size) mixes.

To ensure that the test reflects mix response representative of in situ conditions, proper compaction of laboratory specimens is required. While the evidence is not exhaustive, the A-003A team recommends, based on available information, that specimens for permanent deformation testing be cored (or sawed) from slabs prepared by rolling wheel compaction.

Two levels of testing have been recommended. At the first level and for mix design purposes, *the constant height repeated load simple shear test would appear suitable.* With this test, mixes can be selected that will ensure that the design traffic will not cause ruts exceeding a predetermined level (e.g., 1.25 cm [0.5 in.]) with a prescribed level of reliability.

An alternative test is the simple shear test in which a fixed ratio of normal to shear stress is maintained. Difficulties were experienced with deformation measurements in this test and time constraints precluded additional studies to improve the technique. Accordingly, this test was not studied to the same extent as was the constant height test.

The second procedure, which permits the estimation of rut depth for some design traffic volume, requires the performance of a suite of tests at 40°C (104°F) including the following:

- *Uniaxial strain test.* A test in which the axial load is rapidly applied and the confining pressure necessary to maintain a constant diameter of the specimen is measured.

- *Volumetric test.* A test in which the specimen is subjected to a hydrostatic stress state and the associated volume change is determined.

- *Simple shear constant height test.* A test in which a shear stress is rapidly applied while maintaining the specimen at constant height and the corresponding shear strain is measured.

In addition, *frequency sweeps* in shear over a range in frequencies from 0.01 to 10 Hz are performed at 4°C, 20°C, 40°C (39°F, 68°F, 104°F), and possibly 60°C (140°F). The shear stress is adjusted to provide a shear strain of about 0.01 percent and an axial stress is applied to maintain constant height.

The data obtained from these tests are used to define the nonlinear elastic, viscous, and plastic parameters for the constitutive relationship to define mix response.

The three-dimensional constitutive relationship developed from the suite of tests includes (1) nonlinear elastic response to capture the effects of the aggregate structure at higher temperatures, including dilation and stress stiffening; (2) plastic behavior; and (3) temperature and rate of loading dependency.

Results from solutions of representative pavement structures have provided a useful design relationship that relates maximum permanent shear strain in the asphalt aggregate mix $(\gamma_p)_{max}$ to the rut depth at the pavement surface, i.e.,

$$\text{rut depth} = k(\gamma_p)_{max}$$

This relationship can be used to select a limiting value of permanent shear strain in the constant height, repeated load, simple shear tests for mix design purposes.

While significant progress has been made in defining the permanent deformation response of asphalt aggregate mixes using the three-dimensional constitutive relationship noted above, a number of improvements are required. One is to better represent what happens during unloading. It is demonstrated herein that, while the loading portion of the measured data is reasonably represented by the model, improvement in the unloading estimates is required.

Other changes include the following:

- Modification of the elastoplastic component of the constitutive model, to be based on multiplicative decomposition of the deformation gradient.
- Replacement of the Kirchhoff elasticity by a compressible Neo-Hook model in the viscoelastic component of the model.
- Incorporation of plastic deformation in the volume change component to reflect reduction in air void content (compaction) by traffic.
- Incorporation of the modified constitutive model in finite deformation elements (two- and three-dimensional).

Work is also required to define material response in tension as well as in compression. Moreover, to ensure that the development of damage with load repetition is defined, a failure envelope is required.

The validation testing for the SHRP binder specification indicated that binder properties can affect the permanent deformation response of asphalt aggregate mixes. However, aggregate characteristics can be equally or more significant. The results suggest that the influence of asphalt on permanent deformation response is dependent on the loading and environmental conditions to which the mix is subjected. The effect of the asphalt is comparatively small when the mix is subjected to states of stress that amplify the effects of the aggregate; e.g., the field stats of stress (FS) shear test. However, in cases where mix characteristics are such that interparticle friction is low and the mix is subjected to harsh environmental and loading conditions (e.g., 60°C [140°F] and constant height shear test), the influence of the binder becomes more pronounced. When aggregate characteristics or compaction conditions are expected to result in a mix that is susceptible to permanent deformation, selection of a binder that can overcome these deficiencies will be important. Under these circumstances the value of $G^*/\sin\delta$ can be used to screen binders that will provide inferior performance.

From the favorable comparisons of data from the wheel-tracking and simple shear test program, it would appear that the constant height simple shear test is a suitable candidate for improved mix evaluation for design purposes.

The suitability of compound-loading simple shear tests for mix design and analysis was evaluated. Because of the variability in test measurements and relative insensitivity of the measured response to asphalt content, the tests are not considered suitable at this time for routine mix design purposes. However, because mixes are evaluated under different stress states, the compound-loading test does hold promise for mix design and analysis. *Accordingly, it is recommended that such an approach be further evaluated.*

The temperature equivalency concept has been introduced whereby a single temperature for a particular location can be defined for mix analysis and design purposes. It provides an effective way to account for both traffic and environmental effects. For conventional mixes, testing at a single temperature, *the critical temperature*, assures optimum results. Temperature conversion factors, examples of which have been determined in this investigation, provide a simple, convenient way to convert traffic loading to its equivalent at a fixed temperature level, permitting, in turn, direct comparisons between traffic loading in situ and single-temperature, repeated-load testing in the laboratory.

The temperature conversion factors presented in Part II are considered to be first-order approximations since they are based on a layer-strain approach. However, *when applied with care they provide an effective way to account for traffic and climatic effects in mix analysis and design.* It is recommended that the layer-strain analysis be replaced with a more accurate model of permanent deformation coupled with a range of appropriate laboratory test data to support its application, i.e., the suite of tests described.

Consideration has been given to reliability relative to the permanent deformation test. Initial reliability multipliers have been developed for measurements of variability in the constant height, repeated load, simple shear test. The coefficient of variation (CV) obtained from a limited test program is 90 percent (based on a mean square error of about 0.60). As experience is gained with the equipment and improvements made in the deformation measuring systems, it is expected that this value of CV will be reduced. An example of this

has already been demonstrated for the beam fatigue test program wherein CV was reduced from 90 percent for the earlier equipment to about 40 percent with the SHRP-developed beam fatigue unit.

Consideration has been given to relating anticipated traffic on the actual pavement to laboratory traffic estimates, using a limited study of cores from selected General Pavement Studies (GPS) sections for which both rut depths and associated traffic were available. Results of this analysis suggest that a shift factor of about 0.04 should be applied to the traffic, expressed as repetitions at the critical temperature. Comparison with the repetitions corresponding to a preselected level of permanent shear strain (determined from the constant height, repeated load, simple shear test performed at the critical temperature) provide an indication of the suitability of the mix, i.e.,

$$N_{supply} \geq M \bullet N_{demand}$$

where:

	M	=	reliability multiplier,
	N_{demand}	=	$SF(ESALs)_{Tc}$,
	SF	=	shift factor, and
	$(ESALs)_{Tc}$	=	(equivalent single axle load) estimated design traffic repetitions converted to repetitions at critical temperature.

While the results for the shift factor developed from this study appear reasonable, it is recommended that additional analyses be made and the resulting factor (or factors) be validated through wheel-tracking and other forms of accelerated pavement testing. The effects of tire pressure should be included in this study.

A very limited study has been conducted of mixes containing modified binders. It appears that the constant height, repeated load, simple shear test can be used to evaluate the permanent deformation response of mixes containing modified binders as well as mixes containing conventional asphalts. However, validation of this approach should be accomplished through wheel-tracking or other accelerated pavement testing.

The results of the simple shear tests for this study emphasize that, for a given asphalt, not all modifiers are equally effective in improving permanent deformation resistance and that the influence of a specific modifier is asphalt dependent. Thus, it is important to evaluate a particular asphalt/modifier combination with the specific aggregate to ascertain whether the modified binder will improve the permanent deformation resistance of a mix.

Part III describes an innovative design and analysis system to evaluate the resistance of asphalt aggregate mixes to permanent deformation. The system provides an effective methodology to define the impact of asphalt aggregate interactions on pavement rutting. It combines mix testing with traffic loading (repetitions, wheel loads, and tire pressures), environmental conditions (temperature), and the pavement cross section to ensure that permanent deformation will not exceed acceptable limits.

As with the fatigue system, this analysis system assumes that a trial mix has been identified, traffic and environmental conditions have been determined, and the pavement cross section has been designed. It then seeks to judge, with predetermined reliability, in the case of the Level 1 methodology, whether the trial mix will perform satisfactorily in service. Performance in this instance is defined in terms of a limiting rut depth that should not be exceeded when the anticipated traffic is applied. If the particular mix is not satisfactory, the designer has two options available: either the mix can be redesigned, or a more comprehensive testing and analysis program (Level 2) can be performed.

For routine mix designs, the testing and analysis system has been simplified to permit the test program to be completed in one day's time after the test specimens have been prepared. Laboratory testing is limited to simple shear constant height repeated load testing with each specimen requiring one hour of testing at a single temperature. For large projects or unconventional mixes, more extensive testing and analysis are recommended.

Key features of the Level 1 method include the use of temperature conversion factors and reliability considerations. The temperature conversion factors used to convert design equivalent single axle loads (ESALs) to their equivalent at a specific high temperature appear to be an effective way to treat temperature effects without resorting to multiple temperature testing. Time limitations have precluded the development of temperature equivalency factors based on the Level 2 methodology and is an area that should be pursued further. The authors believe that the use of the approach will not change significantly the results reported herein. Nevertheless, this development should be pursued.

Conceptual development of the mix design and analysis system has been completed as a part of the SHRP A-003A effort. Considerable progress has been made toward establishing an implementable package at Level 1. Validation of this approach, however, has been limited. Accordingly, a key task is to demonstrate its ability to discriminate among suitable and unsuitable mixes.

In terms of the test methodology, a limited study has been completed to define the reliability of the simple shear, constant height, repeated load test. Moreover, reliability of the test procedures associated with the Level 2 methodology has not been investigated. Thus, while an initial indication of test variability has been provided for the simple shear, constant height, repeated load test, the authors believe that this can be improved significantly as the test is used in practice.

The Level 2 procedure provides a sound testing and analytical basis for improved rutting prediction. The permanent deformation relationship that has been developed has some limitations, particularly in the representation of plastic behavior, and refinement of this aspect of the model is required. Computations associated with the accumulation of rutting with traffic repetitions using the finite element idealization of the pavement structure are time consuming with today's microcomputer technology. Nevertheless, computers of this type are increasing in speed of computation each year. Thus, one cannot judge by today's standards for computing the efficacy of the type of approach incorporated in the Level 2 methodology. Rather one must look a few years down the road when this approach will be implemented on a large scale in practice.

Part I — Test Method Selection

J. B. Sousa
R. B. Leahy
J. Harvey
C. L. Monismith

1

Introduction

1.1 Background

A major concern today in many parts of the United States is excessive permanent deformation (rutting) in heavy-duty asphalt concrete pavements resulting from frequent repetitions of heavy axle loads, many of which are operating with radial tires having pressures 138 to 172.5 kPa (20 to 25 psi) higher than the bias-ply tires they have replaced (e.g., 724 kPa versus 552 kPa [105 psi versus 80 psi]). Rutting gradually develops with increasing number of load applications and appears as longitudinal depressions in the wheel paths.

These depressions or ruts are of concern for at least two reasons: (1) If the surface is impervious, the ruts trap water and, at depths of about 0.5 cm (0.2 in.), hydroplaning (particularly for passenger cars) is a threat. (2) As the ruts deepen steering becomes increasingly difficult, leading to added danger. Accordingly, it is important that a test procedure be developed that will reasonably predict the propensity of an asphalt paving mix to develop excessive permanent deformation under repeated loading by heavy traffic.

The summary report, Strategic Highway Research Program (SHRP) A-318, prepared as a part of this investigation, contains a detailed review of the available information on numerous aspects of permanent deformation. This information indicates that rutting is caused by a combination of densification (decrease in volume and, hence, increase in density) and shear deformation and can occur in any one or more of the pavement layers as well as the subgrade. Results of trenching studies from the American Association of State Highway Officials (AASHO) Road Test as well as other test tracks indicated that shear deformation rather than densification was the primary rutting mechanism. Studies (e.g., Eisenmann and Hilmer 1987 and Brown and Cross 1989) have shown that in the asphalt-bound layer rut depth is proportional to the number of load cycles (Figure 1.1) and permanent deformation is limited to the upper 100 mm (4 in.) of the mix (Figure 1.2) (Brown and Cross 1989). The results also indicate that, at least for reasonably stiff supporting materials, most pavement rutting is confined to the asphalt concrete layer (Figure 1.2).

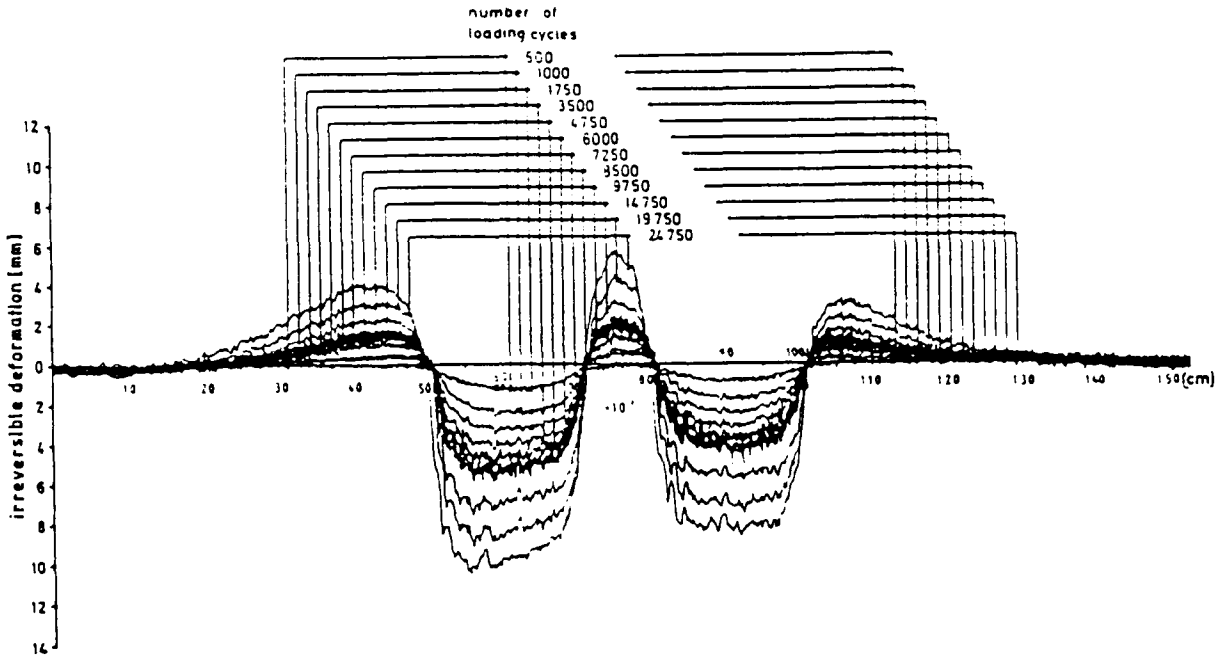

Figure 1.1. Effect of number of passes on transverse surface profile (after Eisenmann and Hilmer 1987)

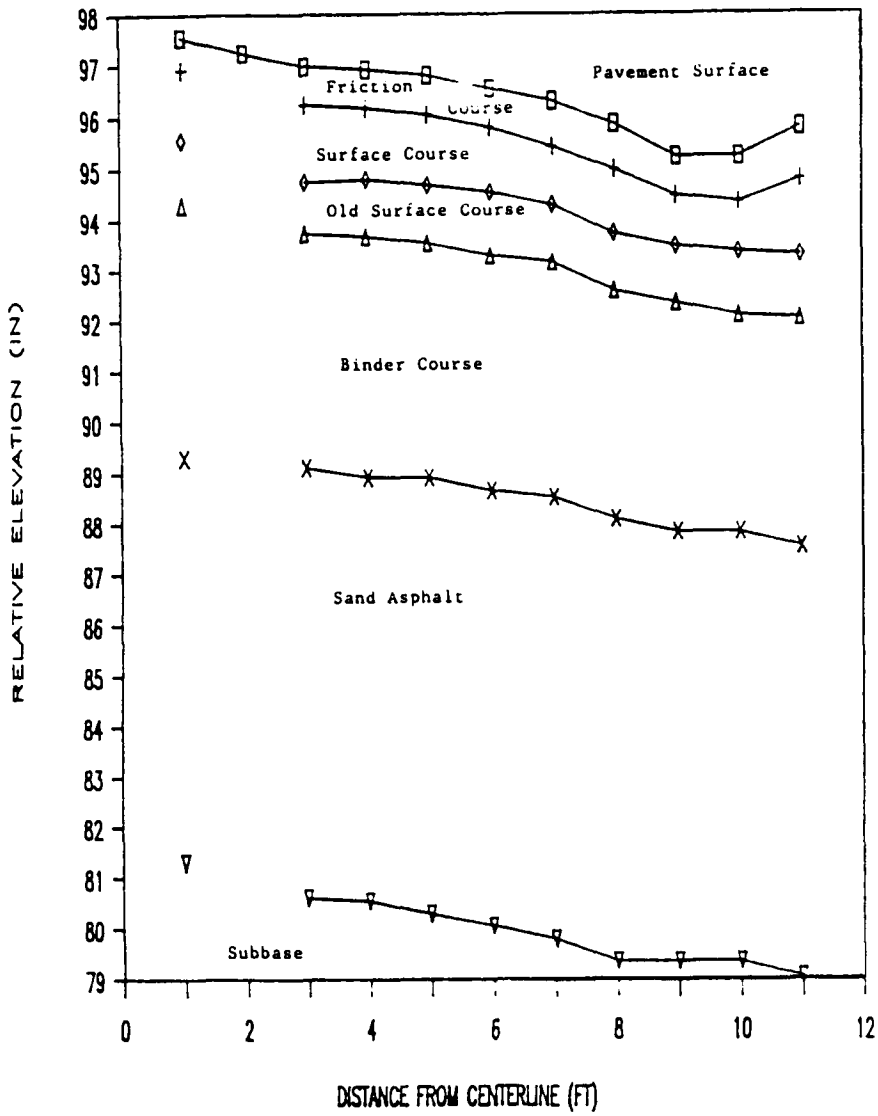

Figure 1.2. Relative layer elevation versus distance from centerline for site with rut depth of about 23 mm (0.9 in.) (after Brown and Cross 1989)

The summary report also provides an evaluation of the factors affecting rutting, including both mix characteristics and test or field conditions (Table 1.1).

With this information as a basis, the research program described in this report was formulated.

1.2 Purpose

This report describes a series of laboratory studies designed to examine the permanent deformation response of asphalt aggregate mixes associated with the *Development of Accelerated Performance Tests for Asphalt Aggregate Mixes.* The goal is to identify suitable laboratory test procedure(s) to characterize permanent deformation response of asphalt aggregate mixes.

1.3 Hypothesis

Permanent deformation in an asphalt concrete layer is caused by a combination of densification (volume change) and shear deformation from the repetitive application of traffic loads. For properly constructed pavements, shear deformations, caused primarily by large shear stresses in the upper portions of the asphalt aggregate layer(s), are dominant.

Pavement rutting cannot be estimated with sufficient accuracy and reliability using current mechanistic procedures, which are based on either linear viscoelastic models or layer-strain algorithms. However, finite element techniques are now available that are well adapted to the analysis of permanent deformation in pavement structures. They can consider the entire rutting zone, including that near the tire walls, and can effectively handle complex constitutive relationships as well as the transverse distribution (wander) of traffic. For the analysis of surface rutting, supporting layers can be represented simplistically, for example, as equivalent linear elastic foundations.

The permanent deformation response of asphalt aggregate mixes to loading must be characterized by a constitutive relationship that is compatible with the finite element idealization used to represent the pavement structure. This relationship must reflect at least the effects of time of loading, temperature, and stress states. The hypothesis is illustrated in Figure 1.3.

Repetitive loading in shear is required to accurately measure, in the laboratory, the influence of mix composition on resistance to permanent deformation. Laboratory tests must closely duplicate the states of stress that are encountered within the entire rutting zone, particularly near the pavement surface and off the loading centerline where shear stresses are relatively greater than normal stresses. Specifically, it is the shear stress or strain invariants that dictate mix response in shear. Because of the accelerating rate at which permanent deformation accumulates at higher temperatures, laboratory testing must be conducted at tempratures that simulate the highest levels expected in the paving mix in service. Furthermore, both laboratory testing and the constitutive relationship must recognize that the accumulation of

Table 1.1. Factors affecting rutting of asphalt concrete mixes

	Factor	Change in Factor	Effect of Change in Factor on Rutting Resistance
Aggregate	Surface texture	Smooth to rough	Increase
	Gradation	Gap to continuous	Increase
	Shape	Rounded to angular	Increase
	Size	Increase in maximum size	Increase
Binder	Stiffness[a]	Increase	Increase
Mix	Binder content	Increase	Decrease
	Air void content[b]	Increase	Decrease
	VMA[c]	Increase	Decrease
	Method of compaction	—[d]	—[d]
Test or field conditions	Temperature	Increase	Decrease
	State of stress/strain	Increase in tire contact pressure	Decrease
	Load repetitions	Increase	Decrease
	Water	Dry to wet	Decrease if mix is water sensitive

[a]Refers to stiffness at temperature at which rutting propensity is being determined. Modifiers may be utilized to increase stiffness at critical temperatures, thereby reducing rutting potential.

[b]When air void contents are less than about 3 percent, the rutting potential of mixes increases.

[c]It is argued that very low VMA (voids in the mineral aggregate) (i.e., less than 10 percent) should be avoided.

[d]The method of compaction, whether laboratory or field, may influence the structure of the system and therefore the propensity for rutting.

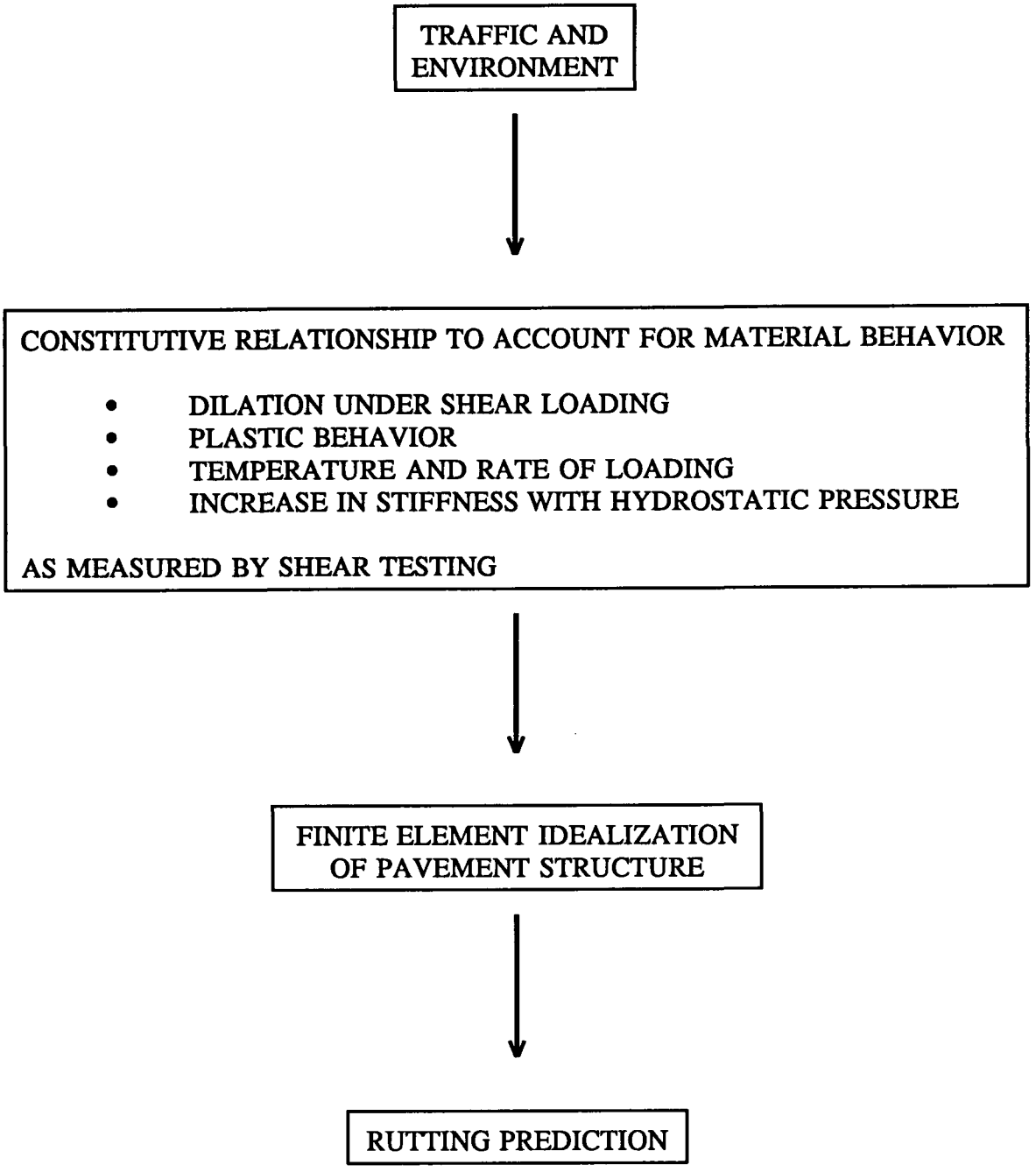

Figure 1.3. Rutting prediction hypothesis

permanent strain in asphalt mixes is a nonlinear function of the number of loading cycles.

2

Background

This section is intended to provide the reader with background information that can clarify the rationale for the experimental design, test selection, and prediction methodology.

2.1 Rutting Prediction

With increased axle loads, tire pressure, and load repetitions, the need exists for a methodology to predict rut depth before construction to minimize potential safety hazards such as hydroplaning. Concomitant with the development of analysis procedures that permit estimates of stresses, strains, and deformations resulting from traffic loads, pavement design systems have evolved that include provisions for rutting considerations. These have been referred to as analytically based, mechanistic, or mechanistic-empirical procedures. Layer-strain and viscoelastic methodologies are currently used to predict the development of permanent deformation in asphalt-bound layers.

2.1.1 Layer-Strain Procedure

The layer-strain method predicts rut depths using permanent deformation characteristics determined from laboratory tests and using an analysis of pavement structure by either linear or nonlinear elastic theory. While nonlinear elastic theory should provide more accurate results, it has not been used extensively because of its complexity. Improvements are necessary to extend the prediction of rut depth from the centerline of the loading to the entire rutting zone. Current laboratory test procedures make use of some form of axial compression test, either creep or repeated loading. If predictions are to be extended beyond the center of the loaded area, the laboratory procedure must incorporate provisions for states of stress that include significant shear components. Such stress states exist off centerline and are particularly important near the tire edges. To account for the sehar stress also implies that new functions relating stress to permanent deformation will be required to take shear stresses into consideration.

2.1.2 Viscoelastic Methodology

In this approach, moving wheel loads can be considered in conjunction with time-dependent material properties to define the states of stress and strain at particular points in the pavement structure. Material properties can be defined in terms of models consisting of finite numbers of Maxwell and Kelvin elements in various arrangements or in terms of generalized compliance relationships. An important advantage of this approach is that moving wheel loads can be directly considered. This results in the correct time-rate of loading to be applied to each material element and permits estimates to be made of the lateral plastic flow of material beneath the moving wheel.

While nonlinear viscoelastic response characteristics may provide a more realistic estimate of pavement response, the associated mathematical complexities have limited past analyses to linear characterizations. However, with advances in computer technology, nonlinear viscoelastic characterization, including plasticity, is feasible and can be used in finite element idealization.

Common to both layer-strain and viscoelastic methodologies are the determination of the states of stress in the pavement structure and the specification of permanent deformation characteristics of the materials in the pavement as a function of stress state, load repetitions, temperatures, etc. The layer-strain method is considered a reasonable approach for predicting rut depth, at least for comparative purposes: it provides the added flexibility of allowing use of either linear or nonlinear elastic theory. Although the viscoelastic method is theoretically more appealing, its complexity and the relatively poor agreement between measured and predicted values to date have not proved it to be superior to the layer-strain method. However, if constitutive relationships are developed based on tests that apply states of stress comparable to those encountered in pavements near the tire edges and if nonlinear viscoelastic models are developed that can incorporate these laws, more accurate predictions are expected.

2.2 Pavement Response

Determining the state of stress and strain in a pavement section under a load is an essential step in any rut-depth predictive methodology. Use of a suitable mathematical model of the pavement system and realistic material properties are closely interrelated.

Difficulties in duplicating the appropriate stress states have been carefully considered by Brown and Bell (1977). They have pointed out that Barksdale (1972) and Romain (1972) related permanent strain to vertical and horizontal stresses. They suggested, furthermore, the use of stress invariants as the most appropriate method of representing the correct stress state for materials characterization. The use of stress invariants is particularly advantageous when considering the tension zone in the bottom of bituminous layers and for predicting rutting away from the axis of symmetry of loading. Following this approach, the stress conditions

at any point can be characterized by the mean normal stress, p, and the octahedral shear stress, τ_{oct}, as follows:

$$p = \frac{1}{3}(\sigma_1 + \sigma_2 + \sigma_3) \tag{2.1}$$

$$\tau_{oct} = \left[\frac{1}{3}\right] \cdot [(\sigma_1 - \sigma_2)^2 + (\sigma_2 - \sigma_3)^2 + (\sigma_3 - \sigma_1)^2]^{\frac{1}{2}} \tag{2.2}$$

where σ_1, σ_2, σ_3 are the principal stresses existing at the point. For simplicity, a shear stress term, q, can be defined as:

$$q = \left[\frac{3}{\sqrt{2}}\right] \cdot (\tau_{oct}) \tag{2.3}$$

In the triaxial compression test, the shear stress, q, is equal to the deviator stress. The mean normal stress, p, is associated with volume change, whereas q is associated with shear distortion. Similarly, the strain invariants corresponding to p and q are volumetric strain (v) and shear strain (ϵ), defined as:

$$v = \epsilon_1 + \epsilon_2 + \epsilon_3 \tag{2.4}$$

where ϵ_1, ϵ_2, and ϵ_3 are the principal strains at the point. In situ permanent strains develop as a result of the combination of volume change and shear distortion.

Variations of p, q, ϵ, and v with depth and radial distance from the centerline for a dual tire assembly can be easily illustrated using multilayer elastic analysis. Using the ELSYM multilayer elastic program (Ahlborn 1972), loads were applied on dual tires with a contact stress of 620 kPa (90 psi). Three-dimensional plots illustrating the variation of p, q, ϵ, and v in the upper part of the pavement section are shown in Figures 2.1 through 2.4.[1]

It is evident that the shear components, q and ϵ, exhibit maximum values close to the surface and near the edges of the tires, indicating a strong tendency for shear distortion. Furthermore, near the surface, the mean normal stress, p, and the volumetric strain, v, decrease with distance from the centerline of the tire, indicating little tendency for volume change. Volume change is associated with poor compaction, and shear strain is associated

[1]Elastic strains ϵ and v have been used because plastic strains that develop in asphalt concrete are approximately proportional to the elastic strains (e.g., McLean and Monismith 1974). Thus the variation in ϵ and v also provides an indication of the variation of the corresponding plastic strains.

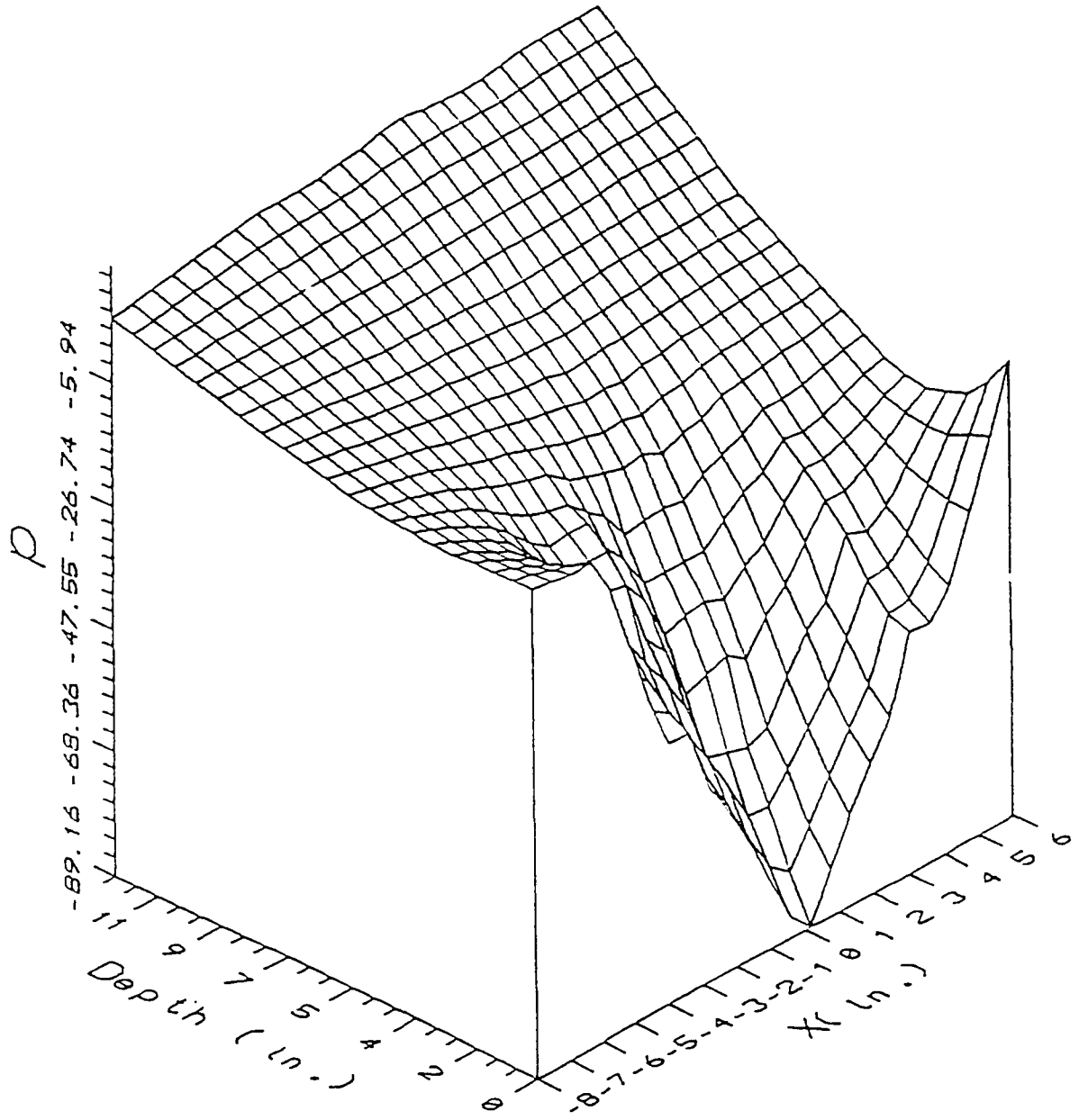

Figure 2.1. Variation of mean normal stress, p, within the pavement section for a dual-wheel assembly

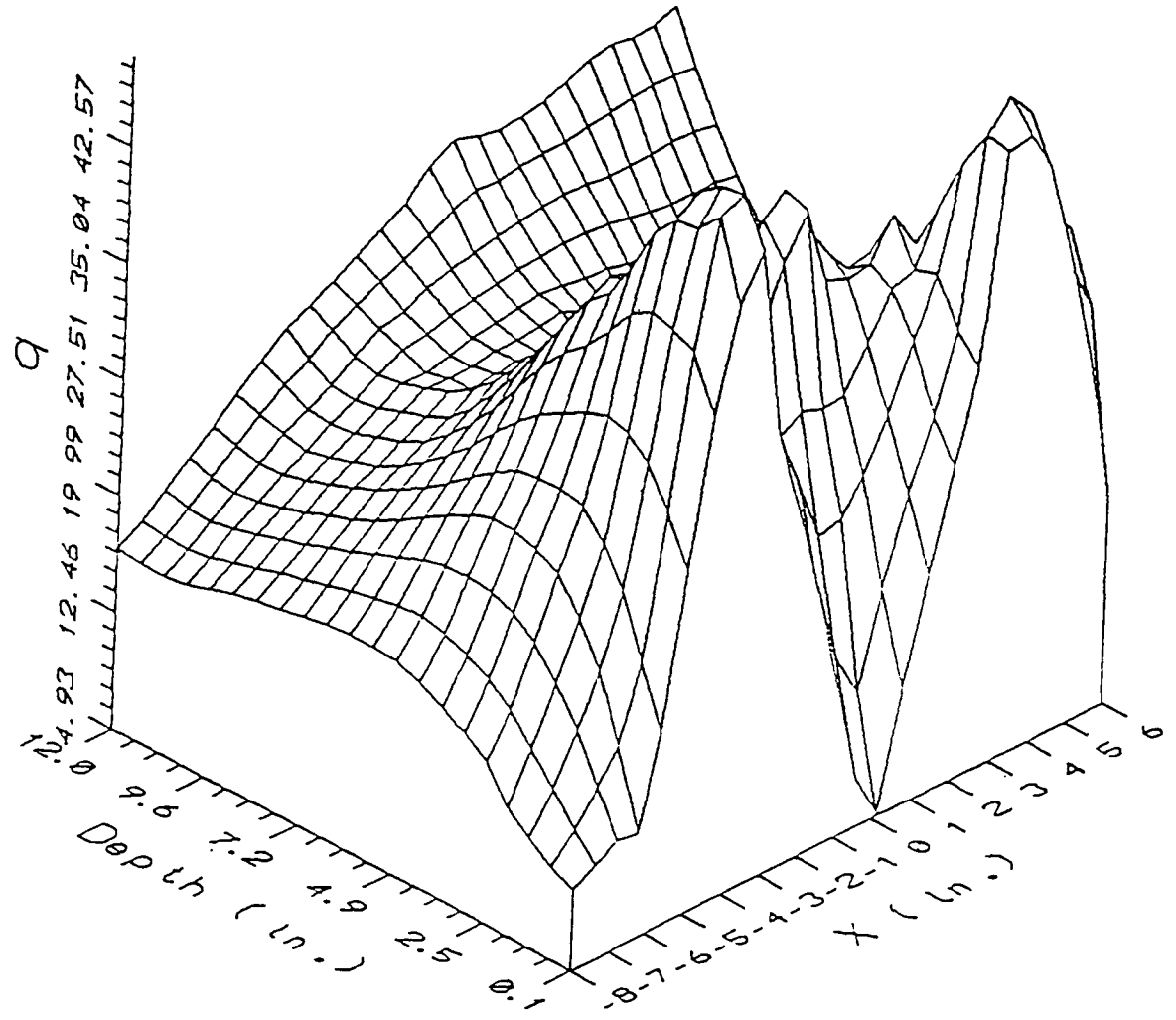

Figure 2.2. Variation of shear stress, q, within the pavement section for a dual-wheel assembly

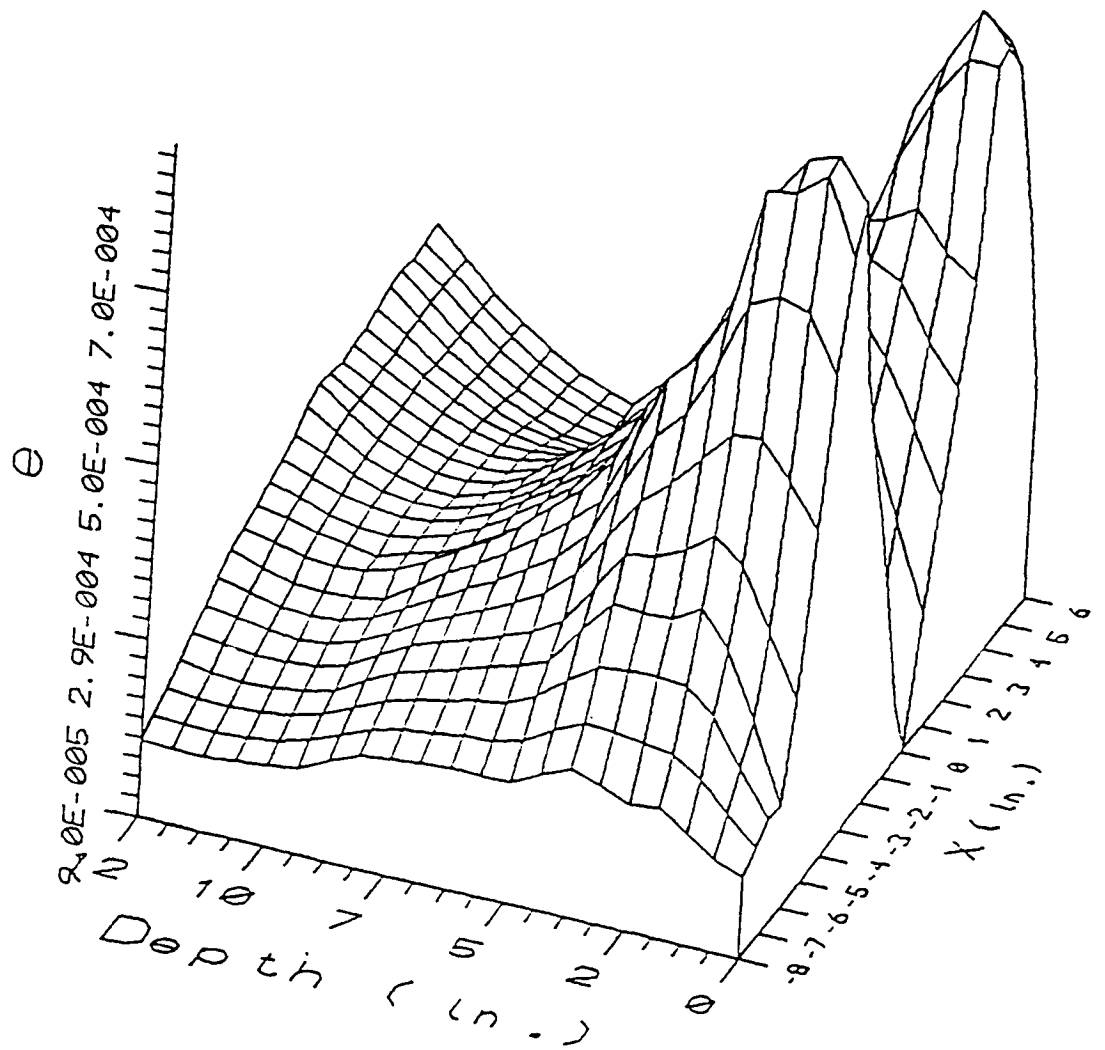

Figure 2.3. Variation of shear strain, ϵ, within the pavement section for a dual-wheel assembly

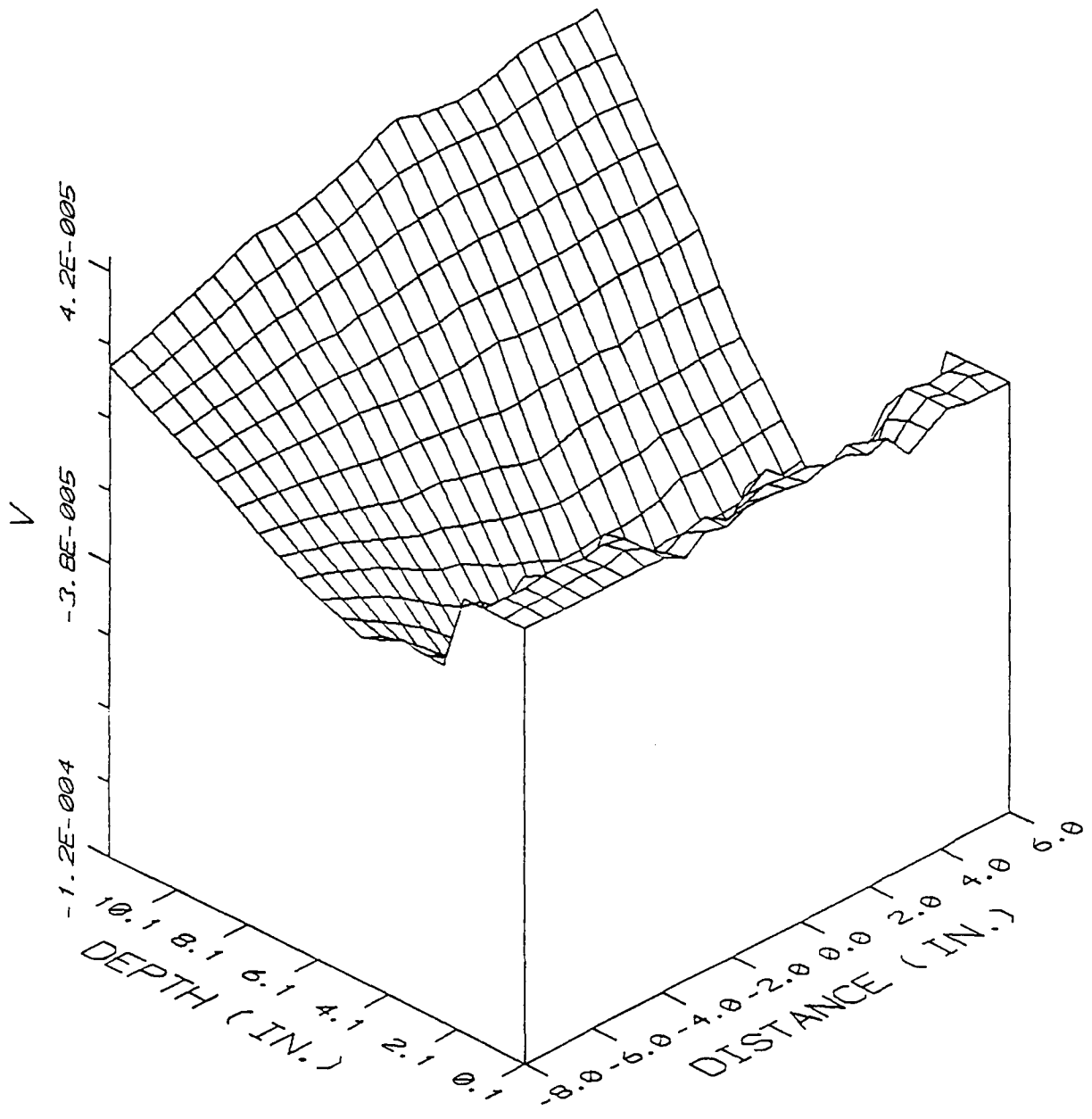

Figure 2.4. Variation of volumetric strain, v, within the pavement section for a dual-wheel assembly

with high shear stresses in the pavement. The advantage of using p and q stress invariants is that tensile and off-axis principal stresses cannot always be directly reproduced in the triaxial test. However, some of the corresponding values of p and q can be, and p and q in the pavement structure can be calculated using elastic layered theory or finite element programs.

Brown and Bell (1977) found that substantial errors in both p and q (and, hence, permanent strain) develop if shear stresses are ignored in the determination of the state of stress, causing underestimation of permanent strain by as much as 40 percent. This highlights the importance of testing materials over the entire range of stresses expected in the field.

2.3 Materials Testing

The development of predictive methods or models requires suitable techniques not only for calculating the response of the pavement to load but also for realistically characterizing the materials. Table 2.1 identifies a wide range of models representative of the permanent deformation behavior of asphalt mixes. They fall into three general categories: (1) empirical regression equations, (2) typical plastic strain laws, and (3) functional equations directly based on laboratory test results. In all cases laboratory tests are performed to determine the representative parameters. From an analysis of these models of permanent deformation, the primary factors affecting rutting are found to be temperature, number of load applications or time of loading, mix properties, and state of stress.

In some of the models, the state of stress is identified as the axial compressive stress (σ_1) and the horizontal stress (σ_2). In fact, however, rutting appears to be more closely related to the shear stress, which can be obtained from (σ_1 - σ_2). Célard (1977) emphasized, based on results of dynamic creep tests, the important effect of shear stress on the rate of permanent deformation (Figure 2.5). For example, in Célard's tests, increasing the shear stress from 0.1 MPa to 0.25 MPa (with the normal stress at 0.1 MPa) increased the rate of permanent deformation from 0.1 to 10 (a 100-fold increase). On the other hand, varying the normal stress from 0.1 to 0.25 MPa (at constant shear stress of 0.1 MPa) did not significantly change the rate of permanent deformation. Similar conclusions can be derived from the work of Brown and Bell (1977) (Figure 2.6).

The overall objective of materials testing should be to reproduce as closely as practical in situ pavement conditions, including the general stress state, temperature, moisture, and general condition of the material. There are four types of tests used to characterize the permanent deformation response of pavement materials.

- uniaxial stress tests: unconfined cylindrical specimens in creep, repeated, or dynamic loading.
- triaxial stress tests: confined cylindrical specimens in creep, repeated, or dynamic loading.

Table 2.1. Summarized overview of the models and permanent deformation equations used by several authors

Author	Pavement Analysis	Permanent Deformation Equation	Variables	Laboratory Test	Observations
Kirwan Snaith Glynn (1977)	DEFPAV Nonlinear finite element Layer strain method	$\epsilon_n = A\Delta^b$	ϵ_n = induced axial permanent strain after an elapsed time N A = function of elapsed time and material b = constant for the material Δ = applied axial compressive stress	Uniaxial compression dynamic loading creep test	Calculated values of rut depth higher than obtained in Nottingham Test Track
Monismith Inkabi Freeme McLean (1977)	ELSYM Layered elastic theory Layer strain method	$\epsilon_z^p = [\delta(T)N^{\alpha}\bar{\sigma}^{n-1}t] \cdot [\sigma_z - \frac{1}{2}(\sigma_x + \sigma_y)]$	ϵ_z^p = vertical permanent deformation $\delta(T)$ = function of temperature α = coefficient determined experimentally N = number of stress repetitions $\bar{\sigma}$ = equivalent stress defined as a function of σ_1, σ_2, and σ_3 t = loading time	Repeated load triaxial compression test	Consideration of traffic axle load and lateral distribution
Brown Bell (1979)	DEFPAV Nonlinear finite element Layer strain method	$\epsilon_p = \left[\frac{q}{a}\right]^b (N)$	ϵ_p = permanent shear strain q = deviator stress a, b = constant N = number of load applications	Axial repeated load tests	Relatively good agreement in test track

Table 2.1 (continued). Summarized overview of the models and permanent deformation equations used by several authors

Author	Pavement Analysis	Permanent Deformation Equation	Variables	Laboratory Test	Observations
Meyer Haas (1977)	FEPAVE II Finite element Layer strain method	$\epsilon_p = f(\sigma_1, \sigma_3, T, AV, N) \pm E$	ϵ_p = axial permanent deformation σ_1 = vertical stress σ_3 = lateral stress T = temperature AV = air voids N = number of load applications E = error of estimate	Repeated load triaxial test	Measured values for rut depth on the Brampton Test Road sections. Good agreement between measured and predicted.
van de Loo (1976)	BISAR Elastic layer theory	$\epsilon_p = c\sigma N^a$	ϵ_p = axial permanent deformation c = constant σ = axial stress level (103.5 kPa [15 psi]) N = number of load applications a = constant	Axial creep test	Basis of SHELL method. Generally overestimates rut depth.
Kenis (1977)	VESYS Probabilistic linear viscoelastic solution	$\epsilon_p(N) = e\mu N^{-\alpha}$	$\epsilon_p(N)$ = permanent strain per pulse α = 1 - S S = slope of the line on a log-log plot of permanent strain versus N e = peak haversine load strain for a load pulse of duration d = 0.1 sec μ = IS/e I = intercept	Uniaxial repeated load tests	Basis of the VESYS approach

Table 2.1 (continued). Summarized overview of the models and permanent deformation equations used by several authors

Author	Pavement Analysis	Permanent Deformation Equation	Variables	Laboratory Test	Observations
Francken (1977)		$\epsilon_p(t) = At^B + C(\exp Dt-1)$ (high stresses) $\epsilon_p(t) = At^B$ (low stresses)	$\epsilon_p(t)$ = permanent strain A,B,C,D = parameters A = $115(\sigma_1-\sigma_3)\lvert E^*\rvert$ B = $.182+.294(\sigma_{VM}-\sigma_{VL})$ σ_{VM} = maximum stress σ_{VL} = plastic failure threshold t = time σ_1 = vertical stress σ_3 = lateral stress $\lvert E^*\rvert$ = modulus	Triaxial dynamic tests	Method used to determine rutting propensity in mixes
Verstraeten Romain Veverka (1982)	ORN093 Elastic layer theory Layer strain theory	$\epsilon_p(t) = A\left[\frac{t}{10^3}\right]^B = \frac{C(\sigma_1-\sigma_3)}{\lvert E^*\rvert * \left[\frac{t}{10^3}\right]^B}$	$\epsilon_p(t)$ = permanent strain at time t (in sec) A = a coefficient depending on the mix composition and on the experimental conditions (stresses, frequency, temperature); it characterizes the susceptibility of the mix to rutting B = a coefficient varying between .14 and .37 C = $f[V_b/(V_b + V_v)]$ $\lvert E^*\rvert$ = modulus of the mix σ_1 = amplitude of vertical stress σ_3 = lateral stress V_b = volume of bitumen V_v = volume of voids	Triaxial dynamic tests	Acceptable correlation with rut depth measure in 16 in-service roads

Table 2.1 (continued). Summarized overview of the models and permanent deformation equations used by several authors

Author	Pavement Analysis	Permanent Deformation Equation	Variables	Laboratory Test	Observations
Huschek (1977)	BISAR Elastic layer theory Layer strain theory	$e_{irr} = c \cdot \sigma t^{A}$ $e_{irr}(T,\Delta t_1,t) = \frac{\sigma \Delta t_1}{[\eta(T,t)]}$ $\eta(T,t) = \frac{t^{1-A}}{(c \cdot A)}$	e_{irr} = permanent deformation c = constant A = consolidation characteristic σ = stress level η = viscosity T = temperature Δt_1 = time of loading	Uniaxial creep tests Cyclic load creep test	Asphalt mix is represented by a Maxwell element: spring and dashpot in series
Thrower (1977)	Viscoelastic theory Separative method	$\dot{e}_{ij} = \frac{\sigma_{ij}}{2\eta}$ i=/j $\dot{e}_{ij} = \frac{\sigma_m}{3\chi} + \frac{(9\sigma_{ij}-\sigma_m)}{18\eta}$	$\dot{e}_{ij}$ = rate of deformation σ_{ij} = state of stress σ_m = isotropic mean stress χ = coefficient of volume viscosity η = coefficient of shear velocity		
Battiato et al. (1977)	MOREL Viscoelastic theory Two layer viscoelastic incompressible system	$J(t) = J_1 t^{\alpha}$ $u_{ik}^{perm} = \frac{1}{\eta_s} g_{ik}(y,z)$	J(t) = creep compliance function t = time J_1 = shear creep parameters α = slope of line on a log-log between J(t) and time u_{ik}^{perm} = permanent deformation η_s = shear viscosity of the Maxwell element in series $g_{ik}(y,z)$ = tensor function	Uniaxial creep tests	Asphalt mix is represented by a Maxwell model

Table 2.1 (continued). Summarized overview of the models and permanent deformation equations used by several authors

Author	Pavement Analysis	Permanent Deformation Equation	Variables	Laboratory Test	Observations
Mahboub Little (1988)		$\frac{\epsilon_{vp}}{N} = a\sigma^b$	ϵ_{vp}/N = accumulated, viscoplastic deformation per cycle σ = peak cyclic stress a,b = regression parameters	Uniaxial creep tests	
Tseng Lytton (1986)		$\epsilon_a = e_0 \exp\left[-\left(\frac{\rho}{N}\right)^b\right]$	ϵ_a = permanent strain N = load cycles ϵ_0,ρ,b = regression parameters	Repeated load testing	
Lai Anderson (1973)		$\epsilon_{vp} = a(\sigma)t^b$	ϵ_{vp} = viscoplastic strain t = time $a(\sigma)$ = $b_1\sigma + b_2\sigma^2$ σ = creep stress b,b_1,b_2 = regression constants	Uniaxial creep tests	
Célard (1977)	ERDT/ESSO Three layer elastic system	$\ln(\dot{\epsilon}) = A + B \cdot \ln(\sigma_{Vm}) + C \cdot \sigma_H + D \cdot T$	$\dot{\epsilon}$ = rate of permanent deformation σ_{Vm} = compressive vertical stress σ_H = compressive horizontal stress A,B,C,D = coefficients T = temperature	Dynamic creep tests	Developed isocreep curves

Table 2.1 (continued). Summarized overview of the models and permanent deformation equations used by several authors

Author	Pavement Analysis	Permanent Deformation Equation	Variables	Laboratory Test	Observations
Khedr (1986)	OSU model	$\frac{\epsilon_p}{N} = A_a N^{-m}$	ϵ_p = permanent strain N = number of load cycles A_a = material properties function of resilient modulus and applied stress m = material parameter	Multistep dynamic tests	
Uzan (1982)		$\epsilon_p(N) = \epsilon_r \mu N^{-\alpha}$	$\epsilon_p(N)$ = permanent strain for Nth repetition ϵ_r = resilient strain N = number of repetitions α, μ = characteristics of materials based on intercept and slope coefficients	Repeated load testing	
Leahy (1989)		Statistically derived predictive models for permanent strain, ϵ_p $\epsilon_p = f(T, \sigma_d, V_{air}, N, \eta_{asp}, P'_{Wasp})$	ϵ_p = plastic strain T = temperature σ_d = deviator stress V_{air} = volume of air η_{asp} = asphalt viscosity P'_{Wasp} = effective asphalt content	Repeated load and creep, axial testing	Determined effect of mix variables on both ϵ_p and ϵ_r

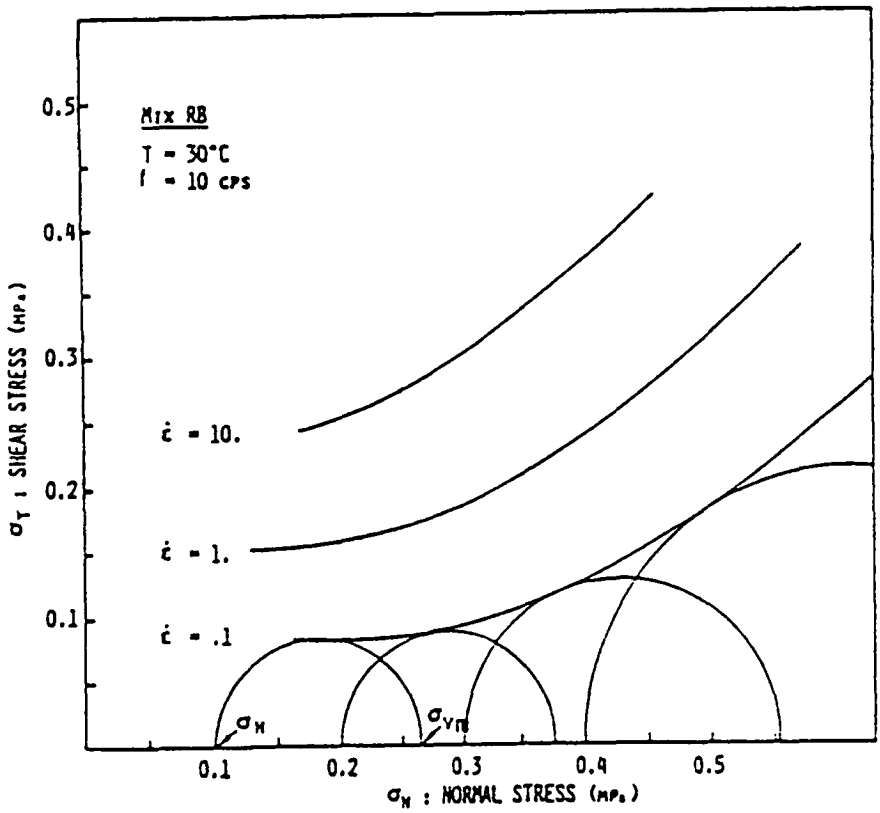

Figure 2.5. Isocreep curves (after Célard 1977)

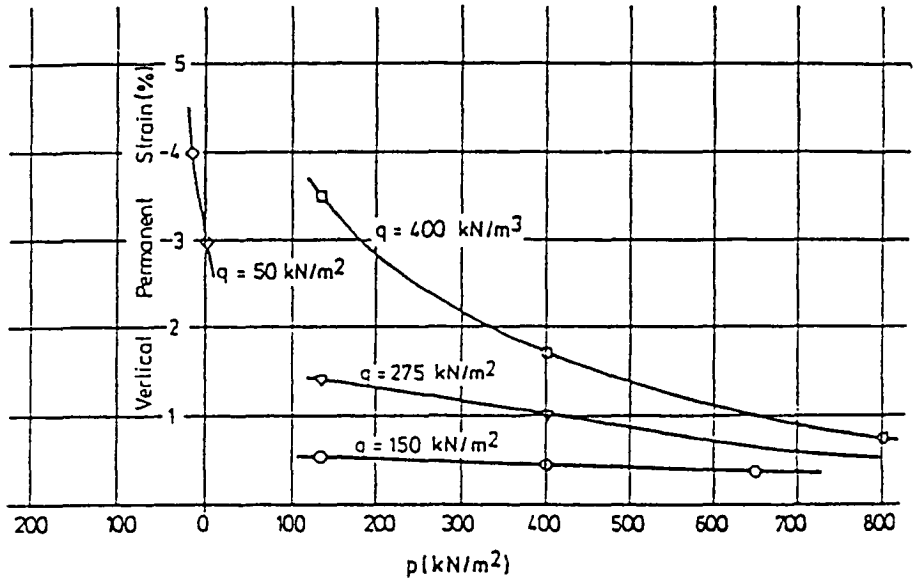

Figure 2.6. Permanent strain in dense bitumen macadam after 1000 cycles as a function of stress conditions (after Brown and Bell 1977)

- diametral tests: cylindrical specimens in creep or repeated loading.
- wheel-track tests: slab specimens or actual pavement cross sections.

2.3.1 Uniaxial and Triaxial Creep Tests

The creep test (unconfined or confined) has been used to measure mix characteristics for a variety of predictive methods. Among its users have been researchers at the Shell Laboratory in Amsterdam. They have conducted extensive studies using the unconfined creep test as a basis for predicting rut depth in asphalt concrete (Van der Loo 1976, Uge and Van der Loo 1974, and Hills 1973). To obtain good comparisons between relative rut depths observed in a test track and those calculated using creep test data, Van der Loo (1974) found that the creep test must be performed at relatively low stress levels — within the linear range of the materials. The need to use a stress level within the linear range has been attributed to the fact that the loading time in situ is small compared to the loading time in the creep test.

Results of the creep test, when expressed as relative deformation (measured change in height divided by original height), are independent of the shape of the specimen and of the ratio of height to diameter, provided the specimen's ends are parallel, flat, and well lubricated. Strain, measured as a function of the loading time at a fixed test temperature, is the usual test output.

This test is the most widely used for determining material properties because of its simplicity and the fact that many laboratories have the necessary equipment and expertise.

2.3.2 Uniaxial and Triaxial Repeated Load Test

A variety of loading systems have been used to measure mix response in repeated loading, ranging from relatively simple mechanical or pneumatic systems to more complex electrohydraulic systems. The more sophisticated systems typically are capable of the following:

- application of repeated axial and lateral stress pulses of any desired shape, in phase with one another, with pulses ranging from 0.01 to 1.0 s;
- application of the axial stress in either tension or compression;
- incorporation of rest periods between stress pulses, ranging from near zero to several seconds; and
- control of temperature within a tolerance of $\pm 0.3°C$ (0.5°F).

The permanent vertical and horizontal strains or deformations are easily measured by LVDTs on the axial ram and lateral strain gauges on the specimen. Resilient modulus, permanent

strain, and Poisson's ratio, as functions of the numbers of load repetitions, can be calculated from these measurements. An important point to note is that pulse shape and duration can greatly influence the measurements: they must duplicate as closely as possible conditions existing in the actual pavement. Estimates of in situ pulse duration and shape, as functions of vehicle speed and depth within the pavement, are available from published charts (Barksdale 1971).

Repeated load tests appear to be more sensitive to mix variables than to creep tests. For example, Barksdale and Miller (1977) reported that, on the basis of Shell creep tests, an increase in the asphalt content of a particular mix from 4.5 to 5.5 percent should not have a significant effect on the rut depth. Results of repeated load triaxial tests on the same mix, however, indicated that such an increase in asphalt content could increase the rut depth by 16 percent (Figure 2.7). On the basis of extensive testing, Barksdale (1972) concluded that repeated load triaxial tests appear to provide a better measure of rutting characteristics than the creep test.

Similar conclusions were drawn by Monismith and Tayebali (1988). They compared the response of three mixes containing conventional and modified binders (AR8000 and AR2000 + 20 percent carbon black microfiller) under both creep and repeated loading (Figure 2.8). For creep loading at 37°C (100°F) and a confining pressure of 207 kPa (30 psi), differences among the mixes were not discernable. Differences were observed, however, in the data for repeated load testing. This study suggests that the repeated loading test may be more appropriate than the creep test to evaluate the permanent deformation characteristics of asphalt mixes.

2.3.3 Triaxial Dynamic Tests

This test was used by Francken (1977) to determine dynamic and creep properties of cylindrical asphalt concrete specimens. A constant lateral pressure was used, and the vertical pressure was varied sinusoidally over a range of frequencies.

Triaxial dynamic tests permit the determination of additional fundamental properties such as the dynamic modulus and the phase angle as functions of the frequency of loading, the number of load cycles, and temperature. Used to characterize the load response of linear viscoelastic materials, the dynamic modulus is the ratio of peak stress to peak strain, while the phase angle, a measure of damping, represents the amount by which strain response lags the applied stress.

Uniaxial and triaxial tests (creep, repeated, and dynamic) have been extensively used for the following reasons:

- Relatively uniform states of stress are applied if proper care is taken in lubricating the ends of the specimens.

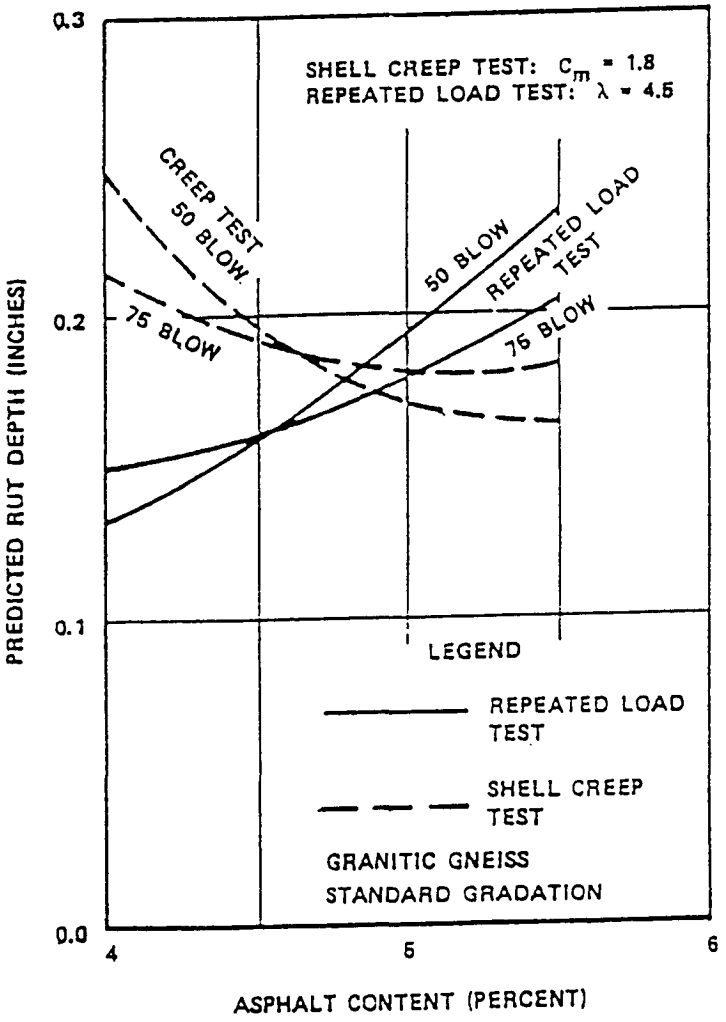

Figure 2.7. Comparison of rut depth predictions from repeated load and creep tests — black base mix (after Barksdale 1977)

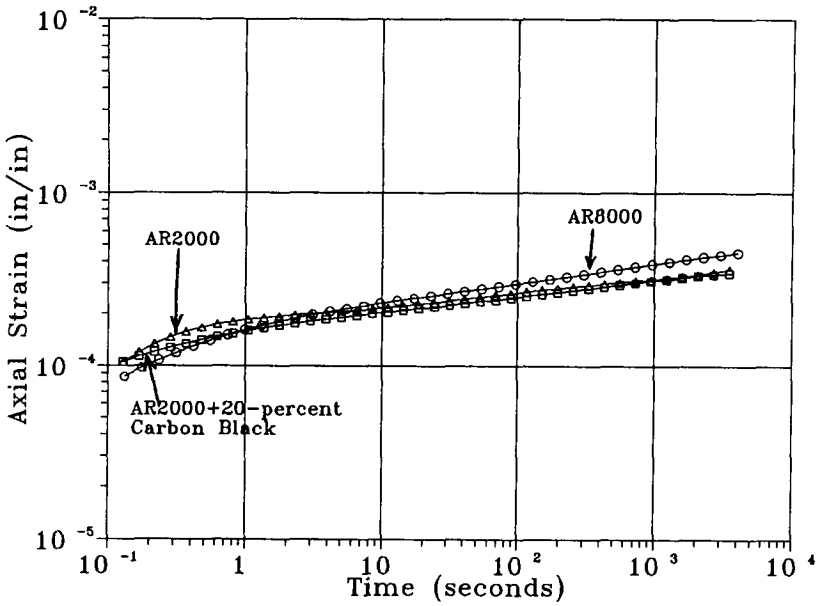

Creep loading

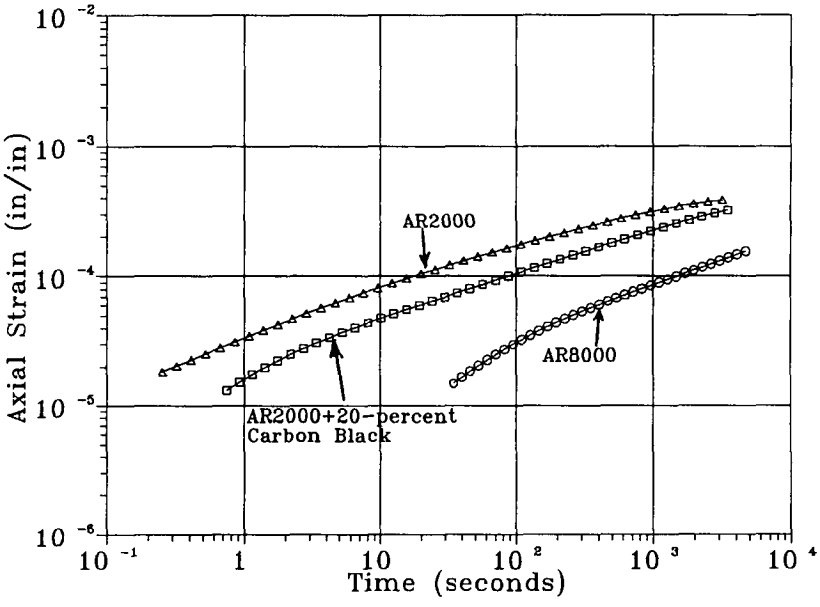

Repeated loading

Figure 2.8. Comparison of three mixes in triaxial compression tests at 37°C (100°F), 207 kPa (30 psi) confining pressure

- A wide range of stress states can be created by varying axial and confining pressures. Some of the states of stress include shear components, and most of the states of stress that are encountered within pavements can be duplicated.

- The tests are relatively easy to implement.

On the basis of a study of computed stresses in idealized pavement, Thrower (1978), however, suggested that limitations inherent in the triaxial test — the relative values of the stress invariants that can be achieved — make it undesirable to rely solely on triaxial testing to define material behavior for predicting pavement performance. He further suggested that another test should be used to investigate properties of materials composing the upper bound layers because the states of stress encountered in upper layers cannot be duplicated in triaxial testing. This test should be able to develop states of stress with relatively higher shear components than the triaxial test.

2.3.4 Diametral Tests

An alternative test procedure for measuring the stiffness of asphalt mixes employs the indirect-tension device originally described by Schmidt (1972). With the indirect load application, most of the specimen is in tension along the vertical diameter, in line with the load. Thus, the stiffness or resistance to load is largely a function of the asphalt binder, and the aggregate has less influence than in triaxial testing. Accordingly, the diametral test may be better suited for repeated load testing associated with modulus measurements than for the longer time periods associated with creep measurements. Without confinement, large loads tend to unrealistically deform the specimen and, if the stress or temperature is too high, creep deformations will accelerate with time.

Diametral testing was deemed inappropriate for permanent deformation characterization for two critical reasons:

1. The state of stress is nonuniform and strongly dependent on the shape of the specimen (Sousa 1990). At high temperature or load, permanent deformation produces changes in the specimen shape that significantly affect both the state of stress and the test measurements.

2. During the test, the only relatively uniform state of stress is tension along the vertical diameter of the specimen. All other states of stress are distinctly nonuniform. It has been recognized that shear stresses contribute significantly to rutting and that laboratory tests must duplicate in situ conditions. Further, shear stresses cause nonlinear behavior in the permanent deformation response of asphalt concrete (Célard 1977). Because of the nonuniform field of shear stresses that result from this load application, deformation measurements cannot be related to a specific stress level.

Khosla and Omer (1985) compared rutting predictions obtained from uniaxial creep tests and from diametral creep tests with values measured from an in-service pavement. Permanent deformation parameters (μ and α), determined from incremental creep tests using both test methods, were used as input to the VESYS computer program. Use of mechanical properties determined by diametral testing almost always resulted in overestimates of pavement rutting.

2.3.5 Torsion Shear Tests on Hollow Cylindrical Specimens

Controlled changes in the magnitude and direction of principal stresses on a material element are extremely difficult to reproduce in the laboratory. With most equipment (e.g., that used for triaxial or plane strain testing), principal stresses are fixed in one direction, and only an interchange of principal stress directions can take place. Rotation of the principal stress axes can only be accomplished in equipment in which shear stresses can be applied to the specimen surfaces. A laboratory simulation of principal stress rotation involves subjecting hollow cylindrical specimens to axial load (W) and torque (M_T), about a central axis, and to internal and external radial pressures, p_i and p_o, respectively (Figure 2.9). Due to the symmetry of the hollow cylindrical specimen, the normal and shear stresses are uniformly applied.

This type of apparatus (Figure 2.10) was used by Sousa (1986) to determine dynamic properties of asphalt concrete under axial and torsional loads. However, the apparatus also offers valuable capabilities in determining permanent deformation characteristics of asphalt concrete under three-dimensional states of stress with reversal of shear stresses. Although the equipment is quite sophisticated and much too complex to be standardized for routine applications, it is very useful as a research tool.

2.3.6 Simple Shear Tests

Simple shear tests are frequently used in the measurement of soil properties. Their widespread use stems from two factors: a greater awareness of the importance of stress-strain anisotropy in geotechnical problems and the simplicity of simple shear testing relative to triaxial testing. The simple shear test approximates field conditions that are characterized by a pure shear stress state. It is the simplest test that permits controlled rotation of the principal axes of stress and strain (Figure 2.11).

The simple shear test has not been extensively used for measuring asphalt concrete properties: however, it appears suitable for investigating the rutting propensity of asphalt concrete because rutting is predominantly caused by plastic shear flow.

Monismith and Tayebali (1988) employed the simple shear test to compare the response of cored specimens obtained from field pavements with the response of specimens compacted with the kneading compactor. Cylindrical specimens, 10 cm (4 in.) in diameter and 6.3 cm (2.5 in.) thick, were tested in the apparatus depicted schematically in Figure 2.12. Although only creep response was measured, the apparatus is also capable of applying repeated or

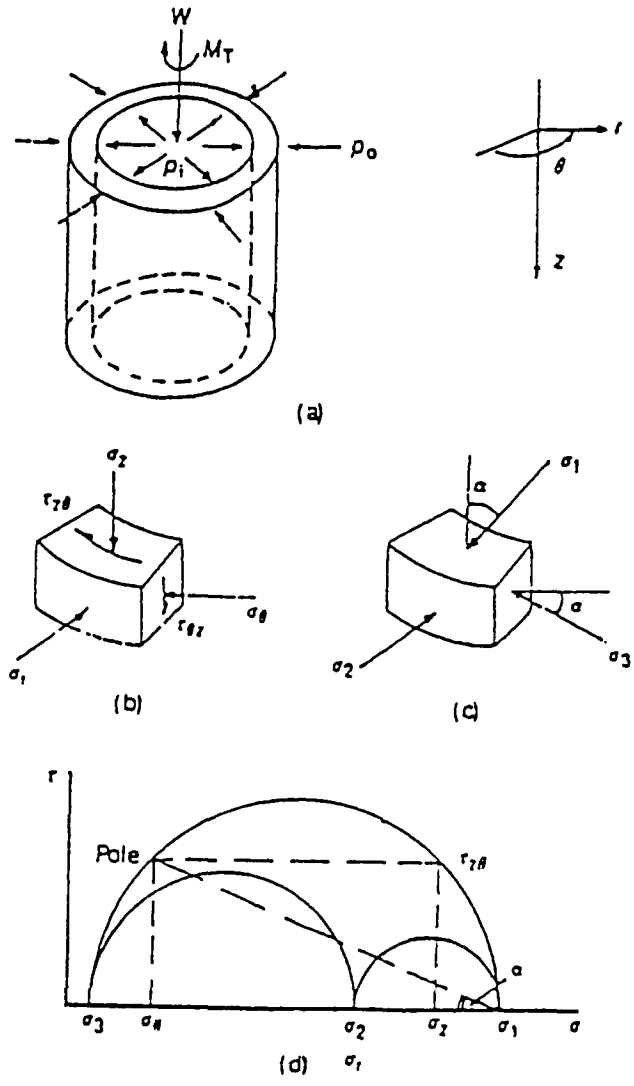

Figure 2.9. Idealized stress conditions in a hollow cylinder test: (a) loading; (b) stresses on wall element; (c) principal stresses on wall element; (d) Mohr circle representation of stresses

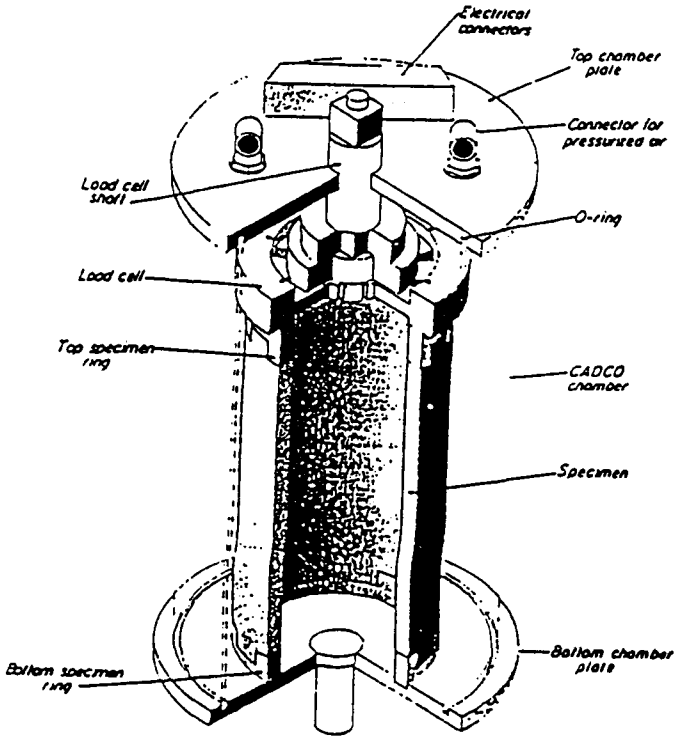

a. Axonometric view

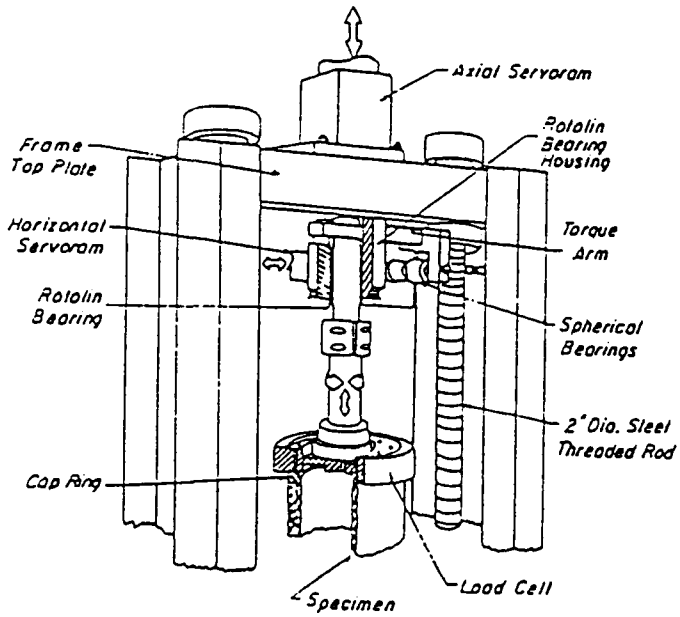

b. Dynamic loading system

Figure 2.10. Hollow cylinder test system

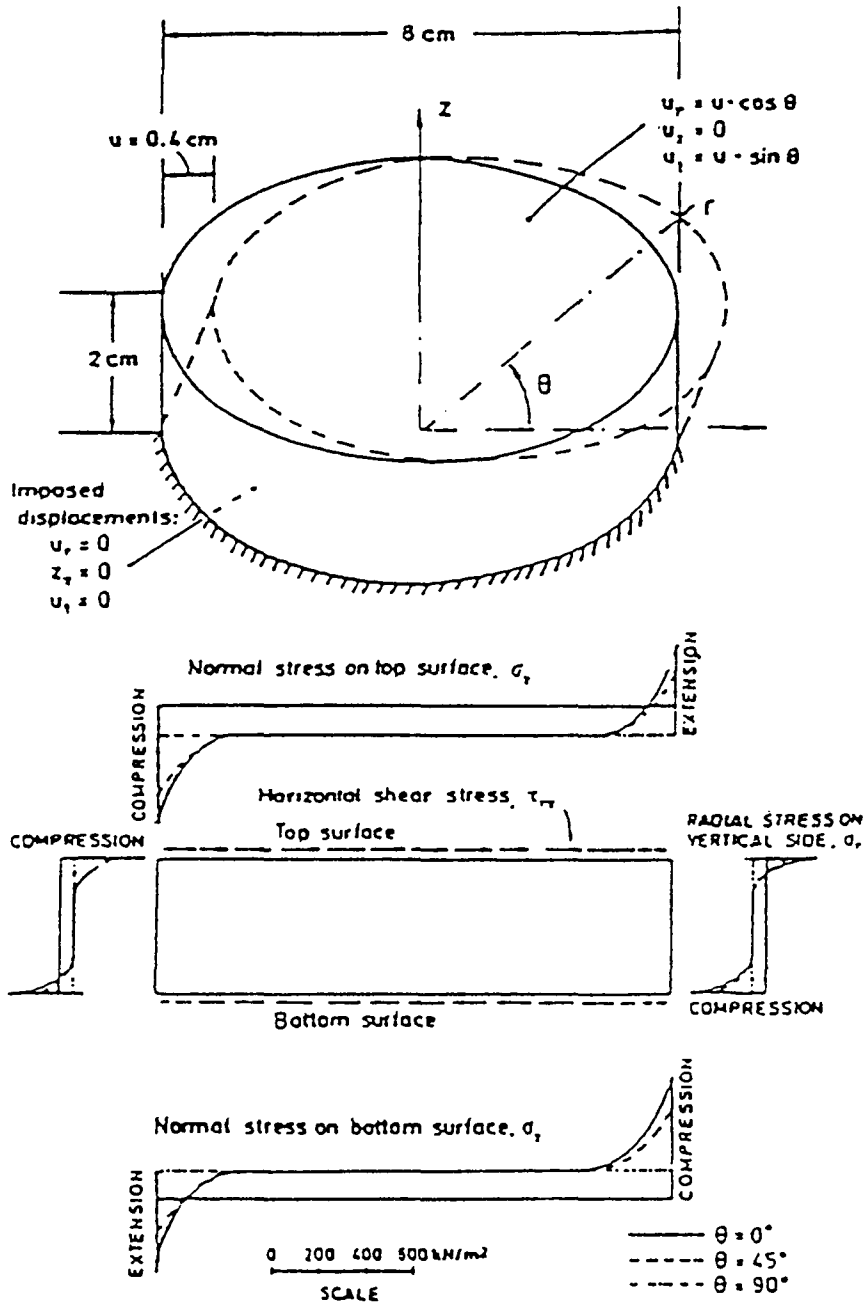

Figure 2.11. Normal stress distribution at specimen boundary (after Lucks et al. 1971)

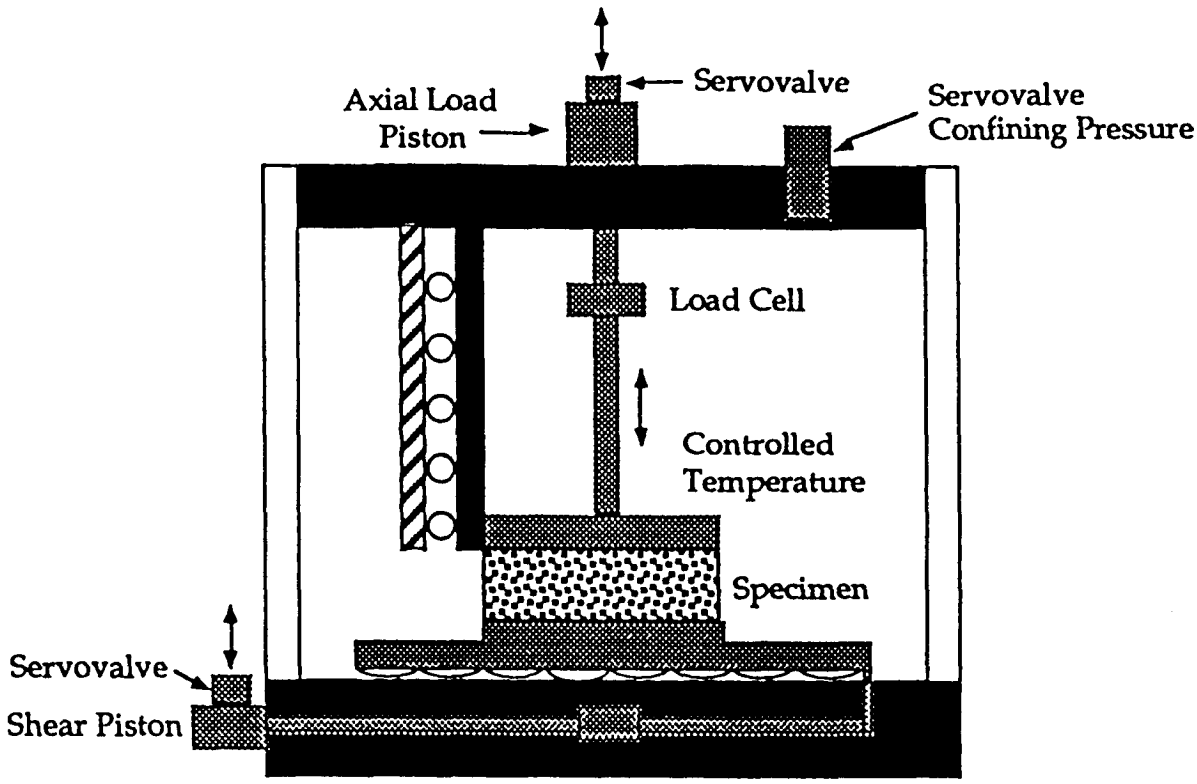

Figure 2.12. Schematic of shear apparatus

dynamic loads over a range of frequencies for the determination of resilient shear modulus, dynamic shear modulus, or shear damping response under stress or strain control and with or without stress reversal.

2.3.7 Wheel-Track Tests

All proposed methods for estimating rutting need further field and test-track validation. A complete mechanistic validation should include determining whether the correct plastic strain profile, with depth and lateral distance, can be estimated.

Bonnot (1986) described procedures used by the Laboratoires des Ponts et Chausées (LCPC) for practical mix design. He has emphasized that, for design applications, laboratory simulation of rutting must duplicate stress conditions in actual pavements. In the LCPC design procedure, a wheel-track test (Figure 2.13) is used for measuring ruts created by the repeated passage of a wheel over prismatic asphalt concrete specimens. The specimen can be removed from an actual pavement but generally is compacted in the laboratory with a pneumatic tire. Rutting is measured by the relative percentage reduction in the thickness of asphalt concrete in the wheel path. Tests are executed over the temperature range of 50°C to 60°C (122°F to 140°F) to reproduce the most unfavorable pavement conditions expected in France.

The Nottingham Pavement Test Facility (Figure 2.14) allows instrumented pavement sections, 4.8 m (16 ft) long and 2.4 m (8 ft) wide, to be constructed in a 1.5 m (5 ft) deep test pit. Testing is carried out under controlled temperatures with a rolling tire, loaded to a maximum of 9 kN (2 tons) and inflated to 500 kPa (73 psi) contact pressure, travelling at speeds up to 16 km/h (10 mph). The facility enables the collection of detailed pavement performance data under carefully controlled conditions.

Full-scale instrumented circular facilities have also been developed in Nantes, France. While circular test tracks may be useful for studying fatigue, there is some concern about their efficacy to study realistically the development of permanent deformation under repeated trafficking. This concern stems in part from the state of stress imposed by the tire in this circular loading path as compared to the stress state which develops from tires following a straight trajectory.

Field test sections on existing roads have also been used to study pavement response. The major advantage of these studies is that they are representative of pavement response under real traffic patterns and environmental conditions. Their major disadvantage is that uncontrolled variables may affect the experiment and confound the interpretation of the test results.

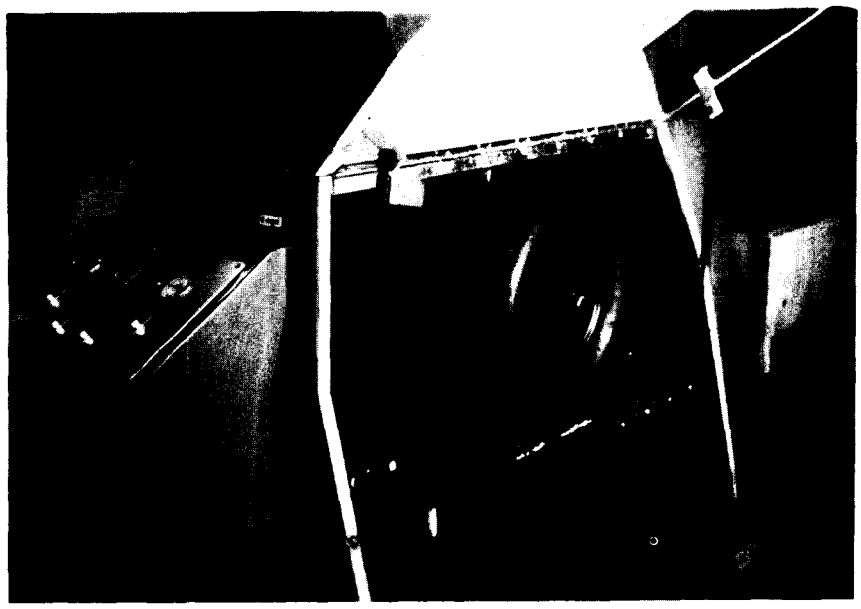

Figure 2.13. LCPC wheel-tracking rutting-test machine (after Bonnot 1986)

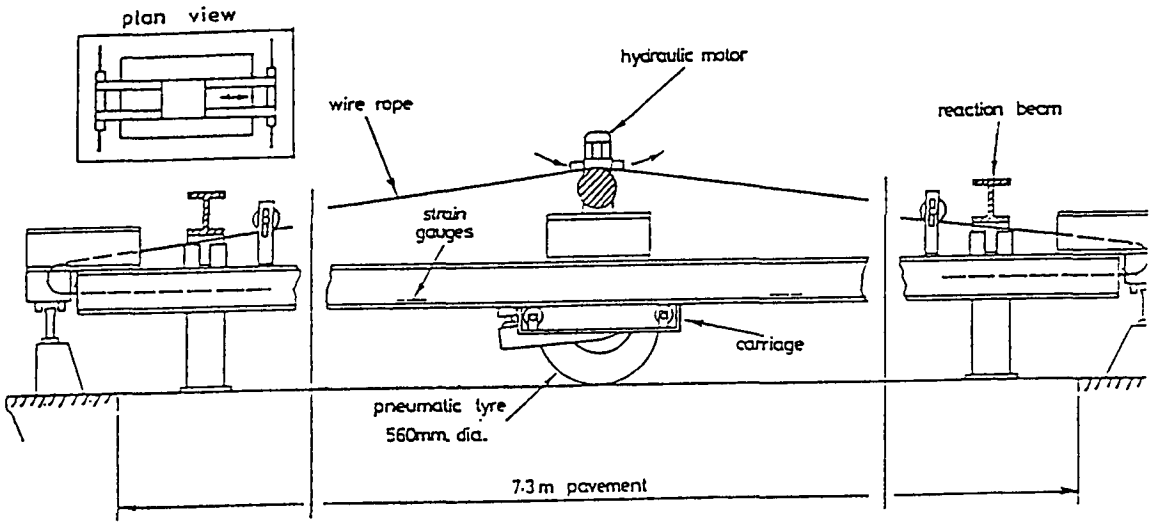

Figure 2.14. Side view of Nottingham pavement testing facility (after Brown and Bell 1979)

2.3.8 Selection of Test Systems

From the information developed and summarized in the preceding section, test methods were evaluated to determine the extent to which each might be effective as a standard testing procedure for measuring material properties representative of rutting in actual pavements. Special emphasis was placed on the ability of each test to represent in situ stress states and, to a somewhat lesser extent, on its simplicity. The two major criteria were as follows:

1. Field Simulation
    - a state of stress representative of the shear stresses causing permanent deformation in situ
    - repeated or dynamic loading (with stress reversal) to approximate in situ traffic loading
    - supplemental data, if possible, useful in mechanistic analyses
2. Simplicity
    - ease of specimen fabrication

- minimum quantities of material for fabricating specimens in the laboratory
- compatibility with equipment currently available in material laboratories
- cost of new equipment or supplemental devices required to adapt existing equipment

Consideration was also given to the factors identified in Table 2.2. The ratings shown in Table 2.2 are by order of preference.[2] Test-track and hollow cylindrical tests are not included in the overall rating because they are considered suitable for research and for the validation of alternate predictive models. Therefore, the shear test is the only test in which shear stresses are directly applied and stress reversal can be easily implemented.

2.4 Summary

Based on information presented in the *Summary Report of Permanent Deformation in Asphalt Concrete* (SHRP A-/IR-91-104), and summarized herein, the conclusions and recommendations with respect to permanent deformation are presented below.

2.4.1 Conclusions

- Shear deformation rather than densification is the primary rutting mechanism.
- Better characterization of the shear properties of asphalt concrete is necessary if accurate predictions of rutting are to be made.
- Since permanent deformation is primarily associated with the shear component, separating the stress state into p (volumetric) and q (shear) components is critical. The variation of q within the pavement structure, particularly near the surface, should be the primary factor in selecting appropriate stress states for laboratory testing.
- Permanent deformation in the asphalt concrete cannot be completely accounted for by the vertical subgrade strain criterion.
- Current analytical models focus on the rut depth under the center line of loading and do not account for shear stresses at the edges of the tires.

[2]Rating 1 (high) - 5 (low)

Table 2.2. Comparison of various test methods for permanent deformation evaluation

Test Method	Sample Shape	Measured Characteristics	Advantages and Limitations	Field Simulation	Simplicity	Overall Ranking
Uniaxial static (creep)	Cylindrical (10 cm [4 in.] diameter, 20 cm [8 in.] high)	• Creep modulus versus time • Strain versus time	• Widespread, well known • Easy to implement; equipment generally available in labs • State of stress contains shear components in the Mohr-Coulomb representation • More technical information provided			
Uniaxial repeated		• Resilient modulus • Permanent deformation versus cycles • Poisson's ratio	• Better expresses traffic conditions • Equipment is more complex	5	1	3
Uniaxial dynamic		• Dynamic modulus • Damping ratio • Poisson's ratio • Permanent deformation versus cycles	• Capability of determining the damping as a function of frequency for different temperatures			
Triaxial static (creep confined)	Cylindrical (10 cm [4 in.] diameter, 20 cm [8 in.] high)	• Creep modulus versus time • Strain versus time	• More states of stress can be obtained • State of stress contains shear components in Mohr-Coulomb representation			
Triaxial repeated		• Resilient modulus • Permanent deformation versus cycles • Poisson's ratio	• Better expresses traffic conditions • Equipment is more complex • Requires a triaxial chamber	4	3 to 4	2
Triaxial dynamic		• Dynamic modulus • Damping ratio • Poisson's ratio • Permanent deformation versus cycles	• Capability of determining the damping as a function of frequency for different temperatures			

Rating 1 (high) – 5 (low)

Table 2.2 (continued). Comparison of various test methods for permanent deformation evaluation

Test Method	Sample Shape	Measured Characteristics	Advantages and Limitations	Field Simulation	Simplicity	Overall Ranking
Test tracks	Slabs	• Rut profile versus number of passages • In-depth strain/stress profile	• States of stress duplicate field conditions • Fundamental material properties cannot be obtained • Good method for verification of predictive models • Requires special equipment that can be costly	1	5	Not suitable for routine use
Diametral static (creep)	10 cm [4 in.] diameter 6.25 cm [2.5 in.] high	• Creep modulus versus time • Permanent deformation versus time	• Easy to implement • Field cores can be easily obtained • Shear stress field not uniform			
Diametral repeated		• Resilient modulus • Permanent deformation versus cycles	• State of stress is predominantly tension • Equipment is relatively simple in static test	5	2	4
Diametral dynamic		• Dynamic modulus • Damping ratio • Permanent deformation versus cycles	• For repeated and dynamic tests, the complexity of the equipment is similar to that of triaxial repeated and dynamic equipment			
Hollow cylindrical	2.5 cm [1 in.] wall thickness 45 cm [18 in.] high 22.5 cm [9 in.] external diameter	• Dynamic axial modulus • Dynamic shear modulus • Axial damping ratio • Shear damping ratio • Axial permanent deformation versus cycles • Shear permanent deformation versus cycles	• Almost all states of stress can be duplicated • Capability of determining damping as a function of frequency for different temperatures for shear as well as axial • Sample preparation is tedious • Expensive equipment • Cores cannot be obtained from pavement	2	5	Not suitable for routine use

Rating 1 (high) – 5 (low)

Table 2.2 (continued). Comparison of various test methods for permanent deformation evaluation

Test Method	Sample Shape	Measured Characteristics	Advantages and Limitations	Field Simulation	Simplicity	Overall Ranking
Simple shear static (creep)	10 cm [4 in.] diameter 6.25 cm [2.5 in.] high	• Shear creep modulus versus time • Shear permanent deformation versus time	• Shear stress can be directly applied to the specimen • Cores can be easily obtained from existing pavements			
Simple shear repeated		• Shear permanent deformation versus cycles • Resilient shear modulus	• Better expresses traffic conditions	3	3 to 4	1
Simple shear dynamic		• Dynamic shear modulus • Shear permanent deformation versus cycles • Damping ratio	• Capability of determining the damping as a function of frequency for different temperatures • Equipment not generally available			

Rating 1 (high) – 5 (low)

- Analytical models differ greatly in their estimation of the variation of permanent strain with depth beneath the pavement surface.

- Both layer-strain and viscoelastic methods are presently used for predicting permanent deformations in pavements.

- The layer-strain method is considered a simplified engineering theory for predicting rut depth, which allows use of either linear or nonlinear elastic theory together with the permanent deformation characteristics of asphalt mixes.

- Comparison of predicted permanent-strain profiles with measurements in test tracks indicate that, in many instances, layer-strain theory overestimates permanent strains in tensile zones. Test-track results suggest that the permanent strain is quite small near the bottom of thick bituminous layers. The preceding suggests a discrepancy between the actual distribution of permanent strain with depth and the theoretically calculated distribution.

- Nonlinear viscoelastic models are more realistic than linear viscoelastic models for predicting permanent deformations but, because of mathematical complexities and difficulty in defining an appropriate material model, the linear model has been most frequently used.

- Although the viscoelastic method is more theoretically sound than the layer-strain approach, it is more complex and has not been shown to be more accurate in estimating permanent deformations observed in pavement in situ.

- Given the complexity of the states of stress and the large number of parameters involved in the analysis, computer programs are required to investigate the response of multilayered systems.

- Finite element methodology has been used to determine the state of stresses in pavements. This technique can better define the propensity for rutting in the entire portion of the pavement structure where rutting can occur.

- A number of models representing the permanent deformation behavior of asphalt mixes have been developed. They can be grouped into three general categories: empirical regression equations, typical plastic strain laws, and models based directly on results of laboratory tests. In all cases, laboratory tests are necessary to determine parameters representative of permanent deformation behavior.

- Although many researchers recognize that shear stress is the main mechanism causing rutting, suitable laboratory test methods and theoretical models are not yet available for properly treating shear-induced permanent deformation.

- Tests presently used to characterize the permanent deformation behavior of pavement materials are of the following general types: uniaxial, triaxial, diametral, and wheel-track. These tests have been designed to evaluate the elastic, viscoelastic, plastic, and strength parameters of asphalt mixes.

2.4.2 Recommendations

The conclusions suggest that significant new developments are required before reliable test procedures, analytical models, and design systems are available. The conclusions provide the basis for development of a theoretically sound analysis procedure and related test methodology that will permit more reliable mix designs and more appropriate modeling of the real conditions under which rutting occurs. Thus, the following recommendations are offered:

- A generalized permanent deformation law should be developed that takes into account the shear stresses developed within the entire zone of permanent deformation. This law should consider states of stress and strain and temperatures encountered in pavement sections at various radial distances from the centerline of loading. A generalized law is needed not only to provide input for predictive permanent deformation models but also to complement mix design procedures. After extensive testing, it is reasonable to expect that a set of constants that uniquely identify an asphalt concrete mix could be determined by just a few tests at selected temperatures and states of stress making the approach attractive for routine mix design.

- The states of stress under which permanent deformation characteristics of materials are obtained in the laboratory should be extended. Laboratory tests should duplicate the states of stress that are encountered within the entire rutting zone, in particular where the shear stress is greater than the normal stress. Accordingly, the propensity of mixes to rut should be measured using equipment capable of directly applying shear stresses.

- To validate the test methods and analytical system, full-scale field tests should be conducted on pavements composed of different structures and subjected to different patterns and characteristics of traffic. Emphasis should be placed on measuring the states of stress and strain in the asphalt concrete layer, including shear deformations.

3

Test Evaluation

Based on the literature evaluation a number of test systems were selected for further study. Three agencies with laboratory test capabilities were utilized: the University of California at Berkeley (UCB), North Carolina State University (NCSU), and SWK Pavement Engineering (University of Nottingham) (SWK/UN) of the United Kingdom. Each agency was assigned the following test systems to be evaluated.

Agency	Test
University of California	• Axial compressive creep • Axial compressive repeated load • Shear creep • Shear repeated load
North Carolina State University	• Axial creep (VESYS procedure)
SWK Pavement Engineering (University of Nottingham)	• Wheel-tracking test (slab specimens measuring 305 mm × 305 mm × 50 mm [12.2 in. × 12.2 in. × 2 in.])

The compaction study (Sousa et al., 1991) had not been completed when this evaluation program began; accordingly, each agency/laboratory prepared its own specimens for test by the method available to that organization and considering specimen size and shape requirements. The various compaction methods used are described in the individual testing programs.

Test performed at UCB were planned to evaluate both the axial and shear loading modes in creep and repeated loading, and to lay the groundwork for the development of a permanent deformation constitutive relationship and an analysis procedure to predict permanent deformation under repetitive traffic loading. It was planned to compare this testing and analysis system with the VESYS procedure, an alternative system that incorporates a unique test series and utilizes linear viscoelastic modeling. The results of wheel-track tests by

SWK/UN were planned to evaluate these two systems. Should neither the UCB-developed nor the VESYS system prove to be acceptable, a primary consideration in evaluating an alternative test system would be its ability to measure fundamental properties necessary for a finite element analysis of a pavement structure.

3.1 Materials

Four asphalt aggregate mixes were used in the test program. They contained MRL aggregates RB and RL and MRL asphalts AAG-1 and AAK-1. Asphalt contents were selected using the Hveem stabilometer test and the U.S. Army Corps of Engineers procedure for 1375 kPa (200 psi) tires (based on the Marshall test).

Table 3.1 contains a summary of selected asphalt properties for the two asphalts that were available at the start of this test program. Asphalt AAG-1, an AR-4000 asphalt cement, is more susceptible to temperature than asphalt AAK-1, an AC-30 asphalt cement. Characteristics of the two aggregates are summarized in Table 3.2. Two aggregate gradations were utilized at NCSU and SWK/UN and are shown in Table 3.3 while only the medium grading was used at UCB. The gradations are also included in the table.

Table 3.4 contains a summary of the asphalt contents used for the four mixes.

3.2 Experiment Design

Initially, the plan was to conduct a series of experiments at UCB on one mix (aggregate RB, asphalt AAG-1, optimum asphalt content, air void content of 4.0 $\pm$ 0.5 percent), at a test temperature of 40°C (104°F), using specimens prepared by rolling wheel compaction. This series is summarized in Table 3.5. The plan was to develop a constitutive relationship that could be used in a finite element idealization to predict the results of tests in other configurations. With this constitutive relationship and finite element idealization, and the tests considered necessary to define the relationship, tests on a second mix were to be performed. For this mix aggregate RB would be used and asphalt AAG-1 would be replaced by asphalt AAK-1.

While the specific systems to be evaluated by UCB depended on the above developments, it was assumed that repeated-load testing in both axial compression and shear would be required. Thus, the following systems would then be evaluated further.

Table 3.1. Asphalt cement properties

Test property	AAG-1	AAK-1
Viscosity/penetration grade	AR-4000	AC-30
SHRP PG grade	PG58-10	PG64-22
Original asphalt		
viscosity @60°C (140°F), poise	1862	3256
viscosity @135°C (275°F), cSt	243	562
Aged asphalt (TFOT)		
viscosity @60°C (140°F), poise	3253	9708
viscosity @135°C (275°F), cSt	304	903

Table 3.2. Aggregate properties

Property	RB Granite, CA	RL Chert, TX
LA Abrasion, %	35.7	17.0

Table 3.3. Aggregate gradation

Sieve Size	Percent passing (by weight)		
	RB, RL		ASTM D3515
	Medium	Coarse	
1 in.	100	100	100
3/4 in.	95	90	90-100
1/2 in.	81	72.5	--
3/8 in.	69	60	56-80
No. 4	49	40	35-65
No. 8	35	27	23-49
No. 16	24	18	--
No. 30	17	10	--
No. 50	12	8	5-19
No. 100	8	5.5	--
No. 200	5.5	3	2-8

Table 3.4. Asphalt contents for four mixes

Aggregate	Asphalt	Asphalt content — percent (by weight of aggregate)	
		Low level	High level
RB	AAG-1	4.9	5.5
	AAK-1	5.1	5.7
RL	AAG-1	4.1	4.8
	AAK-1	4.3	5.0

Table 3.5. Test schedule for developing permanent deformation law

Configuration	Creep Loading	Repetitive Loading	Ramp Loading
Isotropic	• 1 stress	• 1 stress	• 1 stress • 3 rates
Axial compression	• 3 axial stresses • 3 confining stresses	• 3 axial stresses • 3 confining stresses	• 1 stress • 3 rates
Axial tension	• 3 axial stresses • 1 confining stress	• 3 axial stresses • 1 confining stress	• 1 stress • 3 rates
Shear	• 3 shear stresses • 3 axial stresses • 3 confining stresses	• 3 shear stresses • 3 axial stresses • 3 confining stresses	
Hollow cylinder	• 2 shear stresses • 2 axial stresses • 1 confining stress	• 2 shear stresses • 2 axial stresses • 1 confining stress	
Diametral	• 3 axial stresses	• 3 axial stresses	

Agency	Test
University of California	• Axial compressive creep • Shear repeated load
North Carolina State University	• Axial creep (VESYS procedure)
SWK Pavement Engineering (University of Nottingham)	• Wheel-tracking test (slab specimens measuring 305 mm × 305 mm × 50 mm [12.2 in. × 12.2 in. × 2 in.])

As noted above, however, the programs at NCSU and SWK/UN were initiated before the initial program at UCB was completed because of the limited time available.

Table 3.6 summarizes the significant variables for this study. For seven, two-level variables, a complete factorial would consist of 2^7 or 128 treatment combinations. A 1/2 fraction, i.e. 64 treatments, is the smallest that permits estimation of all two-factor interactions. (A 1/4 fraction in 32 runs estimates only 15 of the 21 two-way interactions.) The 1/2 fraction has 35 degrees of freedom associated with higher order interactions. This should be more than enough to adequately estimate testing error without any deliberate replication. It is also possible to split this design into eight blocks of eight runs each, without any loss of information on main effects or two-factor interactions.

Table 3.7 lists the distribution of the numbers of samples for the various test methods at the several laboratories. This assumed that all participating laboratories except the SWK/UN would be investigating seven variables at two levels each. The University of Nottingham's wheel-track test used a constant wheel load, and tests were restricted to only one temperature. This reduced its tests to 2^6 for a full factorial. It was then decided to use a 1/2 fraction with replication, recognizing time and material constraints.

The program shown in Table 3.7 was followed at NCSU. Laboratory specimens were prepared to the specific air void contents using the Corps of Engineers' gyratory testing machine (GTM).

At SWK/UN 32 different mix combinations were tested and specimens were at least replicated (some mix combinations had as many as four specimens on which wheel-tracking tests were performed) for a total of 85 tests. These specimens were prepared using a form of rolling wheel compaction.

As will be seen subsequently, the test program at UCB did not follow the program as shown, although many of the tests enumerated in Tables 3.5 and 3.7 were performed. All specimens were obtained by coring and sawing from large slabs (approximately 61 cm × 61 cm [2 ft × 2 ft] and varying from 7.6 cm to 22.9 cm [3 in. to 9 in.] in height) prepared by rolling wheel compaction.

Table 3.6. Significant mix and test variables for permanent-deformation study

Variable	Level of Treatment			Number of levels (total 2^7)
	1	2	3	
Aggregate				
• Stripping Potential	Low		High	(2)
• Gradation		Medium	Coarse	(2)
Asphalt				
• Temperature Susceptibility	Low		High	(2)
• Grade		Medium		
• Content		Optimum	High	(2)
Compaction				
• Air Voids	4 ± %		8 ± %	(2)
Test Conditions				
• Temperature		40°C (104°F)	60°C (140°F)	(2)[a]
• Stress	Low		High	(2)[b]

[a]Only one level (40°C [104°F]) for wheel-track tests at University of Nottingham (2^6)
[b]Contact pressures of approximately 550 and 825 kPa (80 and 120 psi) for wheel-track tests at University of Nottingham

Table 3.7. Number of samples for permanent deformation factorial design

Complete factorial	$2^7 = 128$
1/2 factorial	64
Total number of samples	256
Estimated time for testing	6-9 months

Laboratory/Test	1/2 Fractional = Total
University of California	
• Axial compressive repeated load[a]	64
• Shear repeated load[a]	64
North Carolina State University	
• Axial creep (VESYS procedure)	64
University of Nottingham	
• Wheel-track test	64
Total	256

[a]Subject to change following initial test system development and evaluation.

3.3 Test Program at University of California at Berkeley

The initial program at UCB was conducted on one mix containing the aggregate RB and the asphalt AAG-1 compacted to air void contents in the range 3.5 to 4.5 percent by the rolling wheel compaction method developed during the compaction study. Tests were performed at 40°C (104°F).

3.3.1 Isotropic Confining Pressure Tests

To investigate mix response under hydrostatic pressure, cylindrical specimens 10 cm (4 in.) in diameter by 20 cm (8 in.) high were subjected to a confining pressure of 410 kPa (60 psi). Radial and axial displacements were measured during loading and unloading.

Figure 3.1 illustrates the variation of the axial and radial strains with time obtained during the loading and unloading phases of a specific test. These data show that, although the level of the confining stress was high, there was little permanent deformation and the specimen did not show any signs of failure. In this figure, the radial and axial strains were identical, indicating isotropic behavior. Accordingly, the model being developed for permanent deformation will assume *isotropic properties*. (N.B. Although the specimens tested exhibited that behavior, it has not been demonstrated that all asphalt concrete specimens will exhibit such characteristics.)

3.3.2 Axial Compression Creep Tests

Axial creep tests were performed on 10 cm (4 in.) diameter by 20 cm (8 in.) high specimens under several stress conditions. Axial stresses ranged from 35 to 180 kPa (5 to 260 psi) and confining pressures of 0, 105, and 205 kPa (0, 15, and 30 psi) were used. The load was applied for one hour and released. The recovery also was monitored for one hour. Axial displacements and changes in the perimeter of each specimen were recorded and axial and radial strains were computed at specific time intervals. Based on these strains, the volumetric and octahedral strains (first and second invariants of the strains) were computed. This test series included 27 specimens.

In the axial creep the first invariant of strain, I_1, was determined from:

$$I_1 = \epsilon_1 + \epsilon_2 + \epsilon_3 = \epsilon_z + 2\epsilon_r \tag{3.1}$$

where: ϵ_z = axial strain, and
ϵ_r = radial strain.

The second invariant of strain, J_2, was determined from:

$$J_2 = \frac{2}{3}(\epsilon_z - \epsilon_r)^2 \tag{3.2}$$

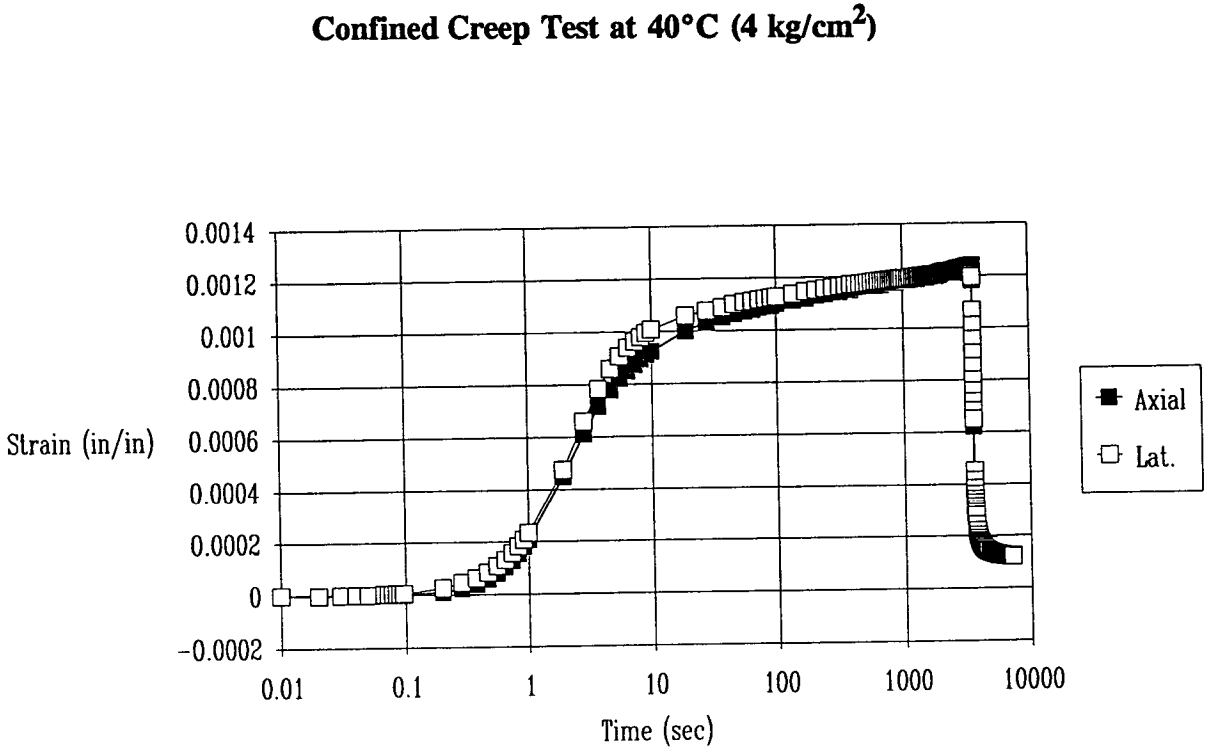

Figure 3.1. Variation of axial and radial strain with time in creep (loading and unloading at 40°C [104°F])

Figures 3.2, 3.3 and 3.4 illustrate the variation of axial strain with both time and stress level. In these tests the axial strain increases at a faster rate after reaching a specific strain level (threshold). It is also important to note that in the recovery phase the magnitude of the nonrecoverable permanent deformation is a significant portion of the total deformation. Variation of the parameter J_2 with time for the three conditions of confinement are shown in Figures 3.5 through 3.7. Comparison of the data for an axial stress of 138 kPa (20 psi), for example (Figure 3.4), shows a significant influence of confining stress on deformation. Thus, in any permanent deformation constitutive relationship that is developed, this phenomenon, which will be termed *stress hardening*, must be reflected.

3.3.3 Shear Creep Tests

These tests were conducted on 10 cm (4 in.) diameter by 15 cm (2 in.) high specimens. Shear stresses varied between 14 and 105 kPa (2 and 15 psi) while the axial stress was either 17 or 35 kPa (2.5 or 5 psi). The apparatus used for this test program did not permit the application of confining pressure. Relative displacements between the caps of the specimens were measured and used to compute volumetric and octahedral strains. A total of 14 specimens were tested in this series.

The first strain invariant, I_1, was determined from:

$$I_1 = \epsilon_z + 2\epsilon_r \tag{3.3}$$

where: ϵ_z = vertical strain, and
ϵ_r = radial strain.

The second strain in variant, J_2, was determined from:

$$J_2 = \frac{2}{3}(\epsilon_z - \epsilon_r)^2 + \frac{1}{2}\gamma^2 \tag{3.4}$$

where: γ = shear strain.

Shown in Figure 3.8 is the shear strain versus time; in Figures 3.9 and 3.10 is the strain invariant J_2 versus time. These figures illustrate the influence of stress state on behavior and highlight the necessity to include the effects of stress hardening in any permanent deformation constitutive relationship developed.

3.3.4 Axial Compression Repeated Load Tests

Repeated load tests were performed on 10 cm (4 in.) diameter by 20 cm (8 in.) high specimens and were applied with a time of loading of 0.1 s and a time interval between loading of 0.9 s. Axial stresses varied between 35 and 1860 kPa (5 and 270 psi) and confining pressures included values of 0, 105, and 210 kPa (0, 15, and 30 psi). In this series 13 specimens were tested.

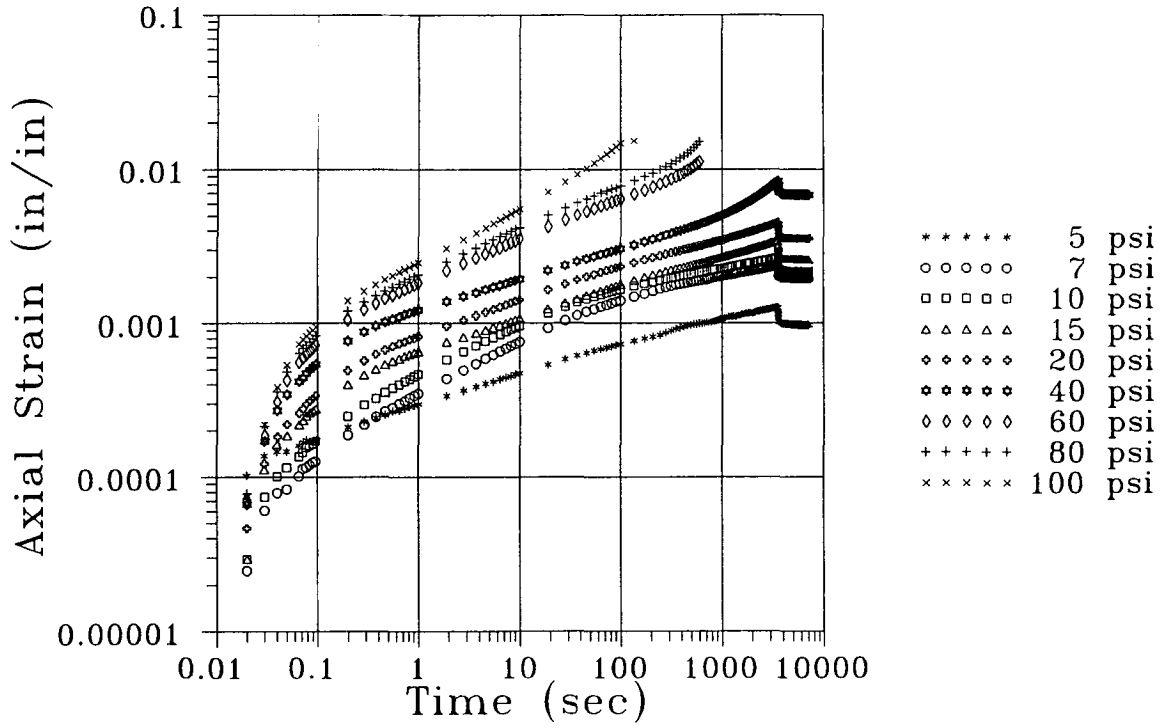

Figure 3.2. Axial strain in unconfined axial creep at 40°C (104°F)

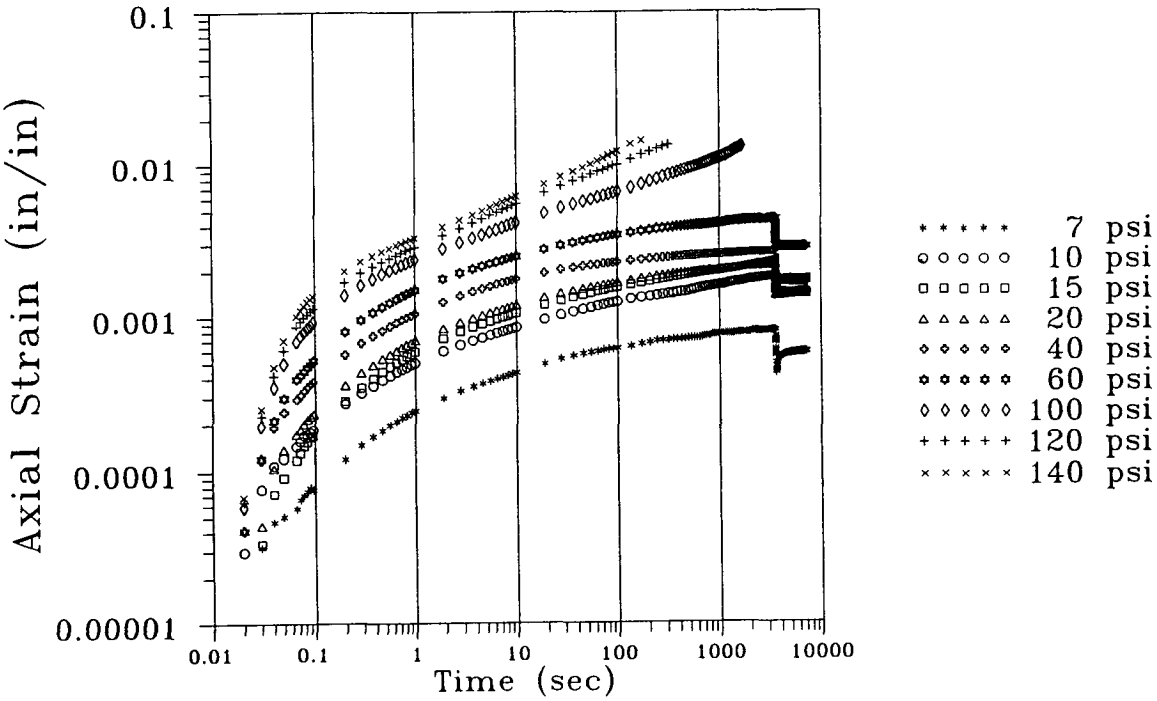

Figure 3.3. Axial strain in confined axial creep (confining pressure = 105 kPa [15 psi]) at 40°C (104°F)

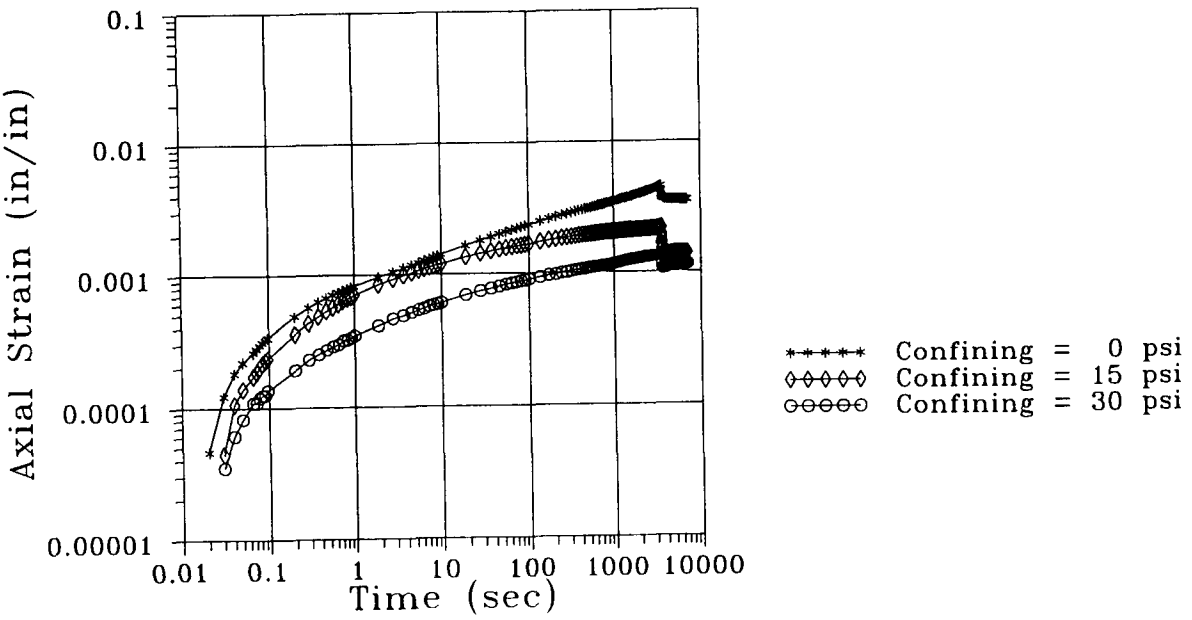

Figure 3.4. Effect of confining pressure on creep behavior at 40°C (104°F)

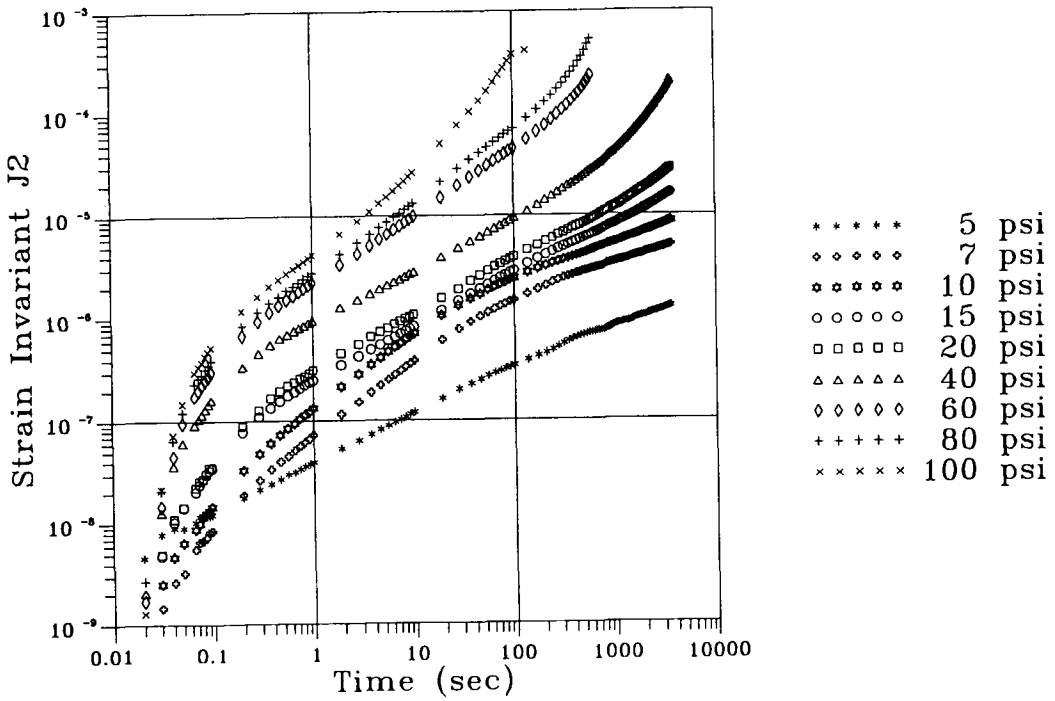

Figure 3.5. Behavior of strain invariant J_2 in unconfined axial creep at 40°C (104°F)

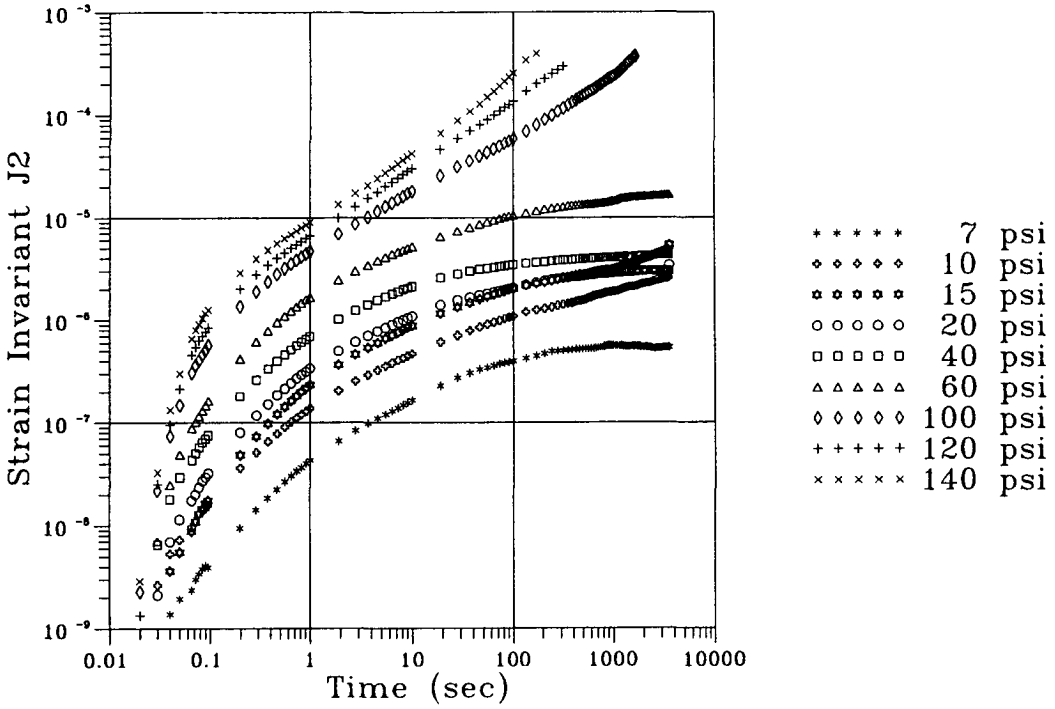

Figure 3.6. Behavior of strain invariant J_2 in confined axial creep at 40°C (104°F) (confining pressure = 105 kPa [15 psi])

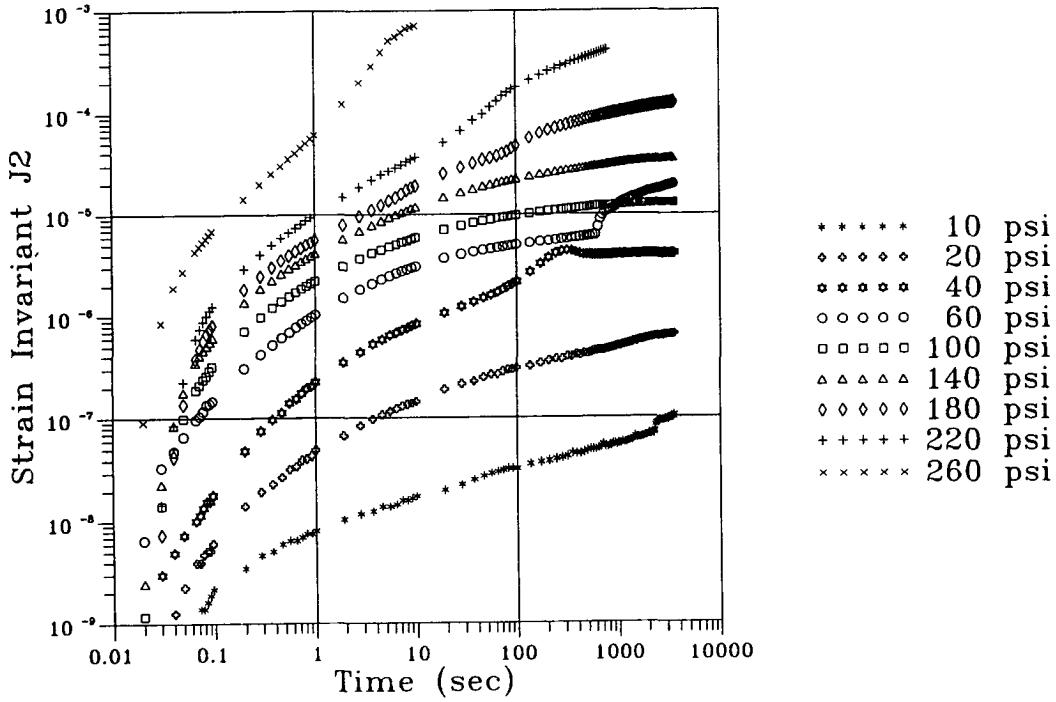

Figure 3.7. Behavior of strain invariant J_2 in confined axial creep at 40°C (104°F) (confined pressure = 210 kPa [30 psi])

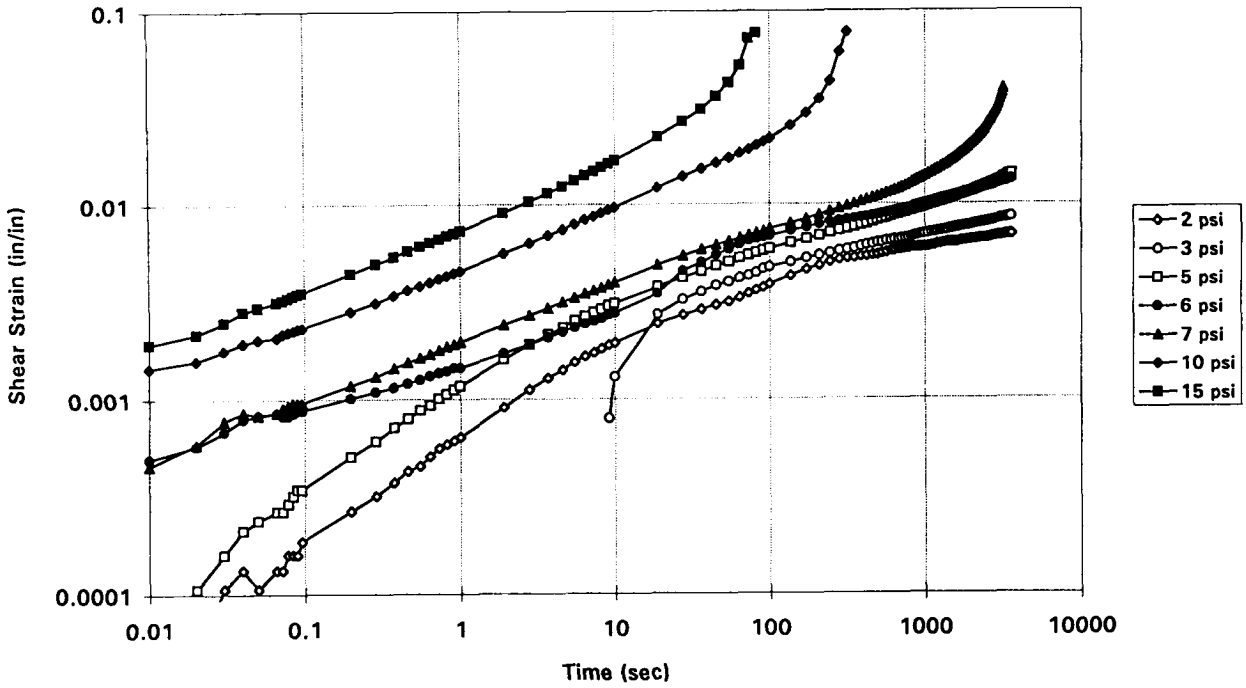

Figure 3.8. Shear strain versus time (35 kPa [5 psi] axial stress)

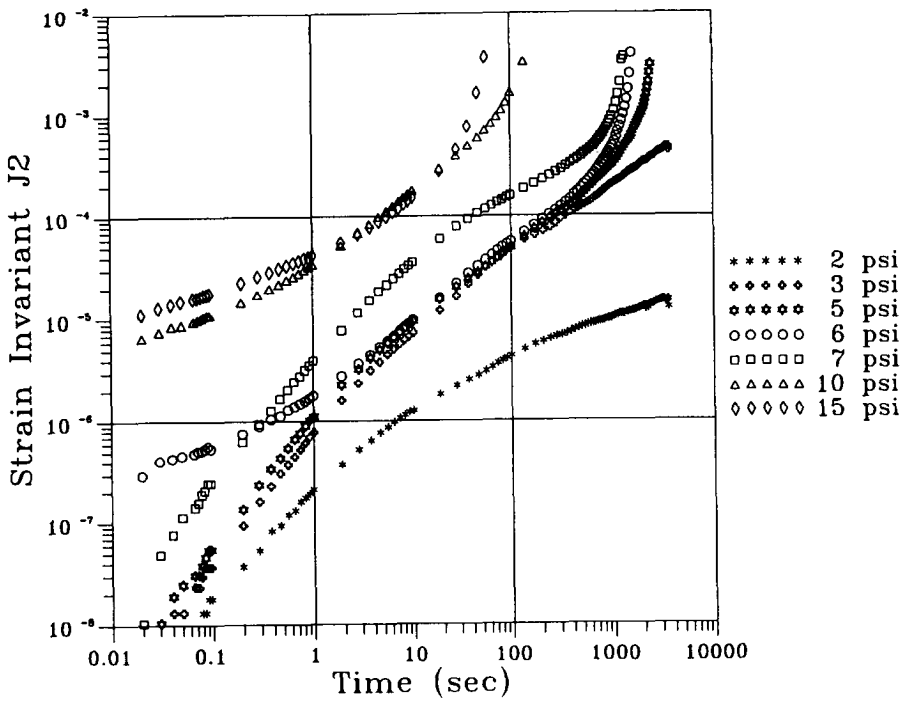

Figure 3.9. Behavior of strain invariant J_2 in shear creep at 40°C (104°F) (axial pressure = 17 kPa [2.5 psi])

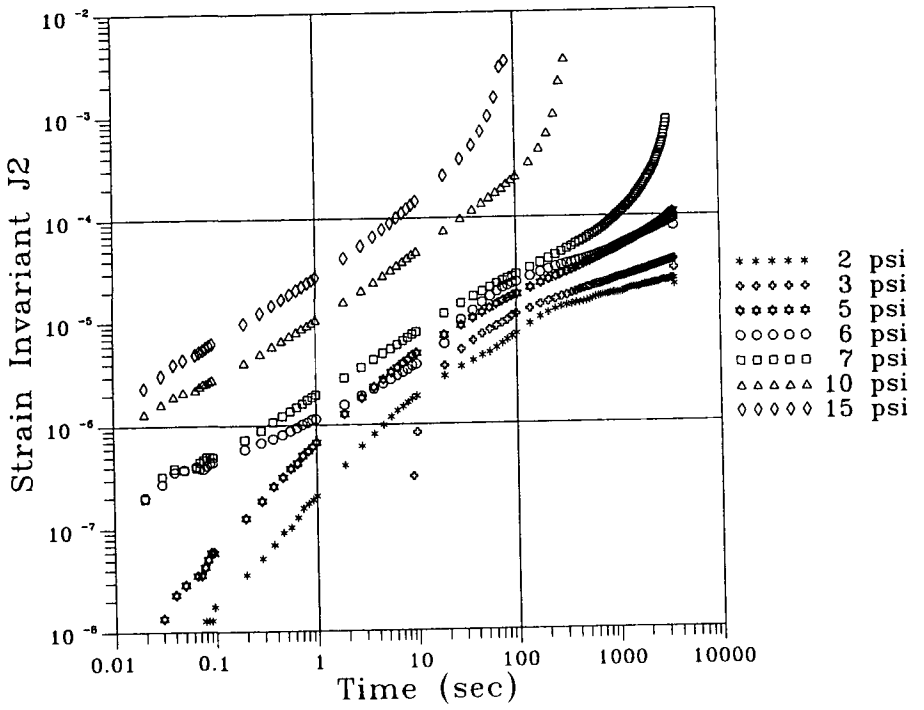

Figure 3.10. Behavior of strain invariant J_2 in shear creep at 40°C (104°F) (axial pressure = 35 kPa [5 psi])

Figures 3.11, 3.12, and 3.13 illustrate the variation of axial strain with load repetitions while Figures 3.14, 3.15, and 3.16 show the variation of the strain invariant J_2 with repetitions.

Comparisons of the strain values, e.g., Figure 3.17, indicate that more deformation occurs in repetitive loading than in creep (e.g., comparison of the strain values at 100 s in creep versus 1,000 repetitions — 1,000 × 0.1 s = 100 s of loading — in repeated loading). The resilient modulus, defined as the quotient of the applied stress and recoverable axial strain, appears to be independent of stress level for the range of axial stresses applied as shown in Figure 3.18.

3.3.5 Repeated Load Shear Tests

This test series was conducted using specimens 10 cm (4 in.) in diameter by 5 cm (2 in.) high. Repeated shear stresses ranging from 14 to 105 kPa (2 to 15 psi) were applied at time of loading of 0.1 s with a time interval between loading of 0.9 s. The static axial stress was either 17 or 35 kPa (2.5 or 5 psi). This series included 14 tests.

Figures 3.19 and 3.20 illustrate the variation of shear strain with number of load applications and Figures 3.21 and 3.22 the variation of the strain invariant J_2 with load applications. The resilient shear modulus, as with the resilient axial modulus, appears reasonably independent of shear stress as seen in Figures 3.23 and 3.24.

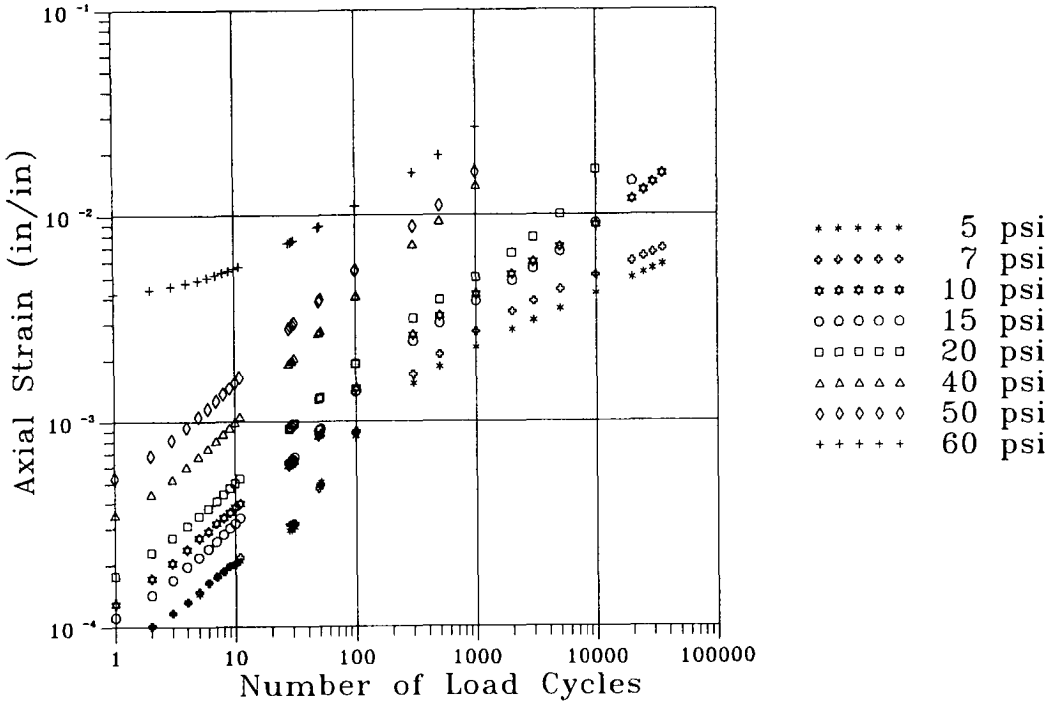

Figure 3.11. Axial strain under repetitive axial load at 40°C (104°F) (confining pressure = 0 kPa [0 psi])

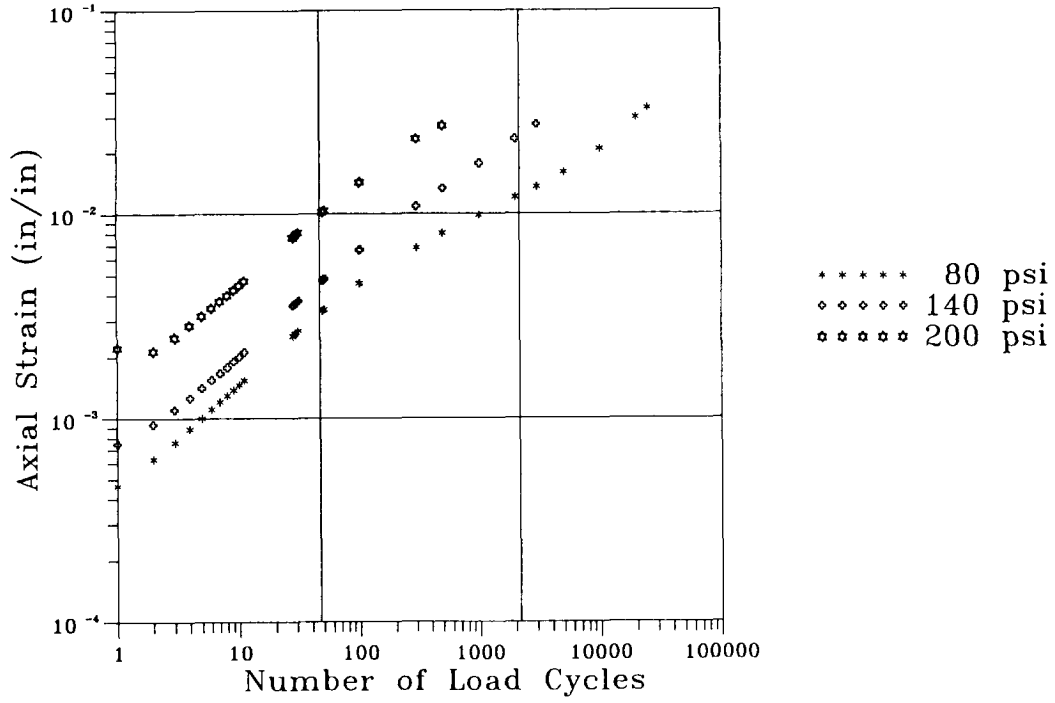

Figure 3.12. Axial strain under repetitive axial load at 40°C (104°F) (confining pressure = 105 kPa [15 psi])

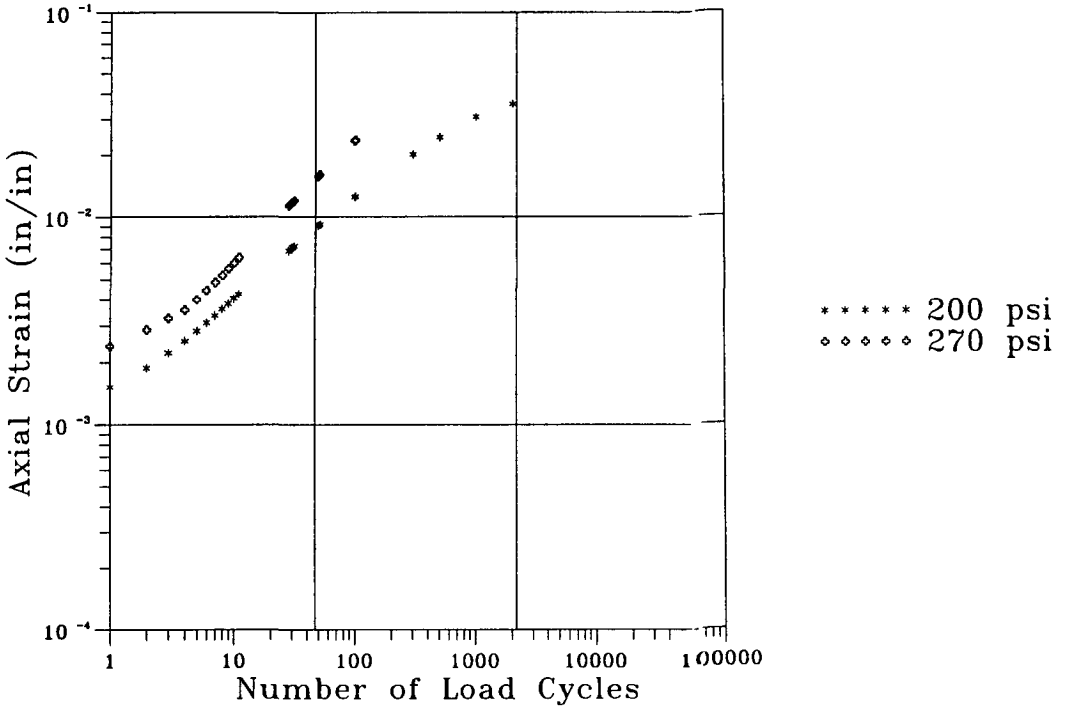

Figure 3.13. Axial strain under repetitive axial load at 40°C (104°F) (confining pressure = 210 kPa [30 psi])

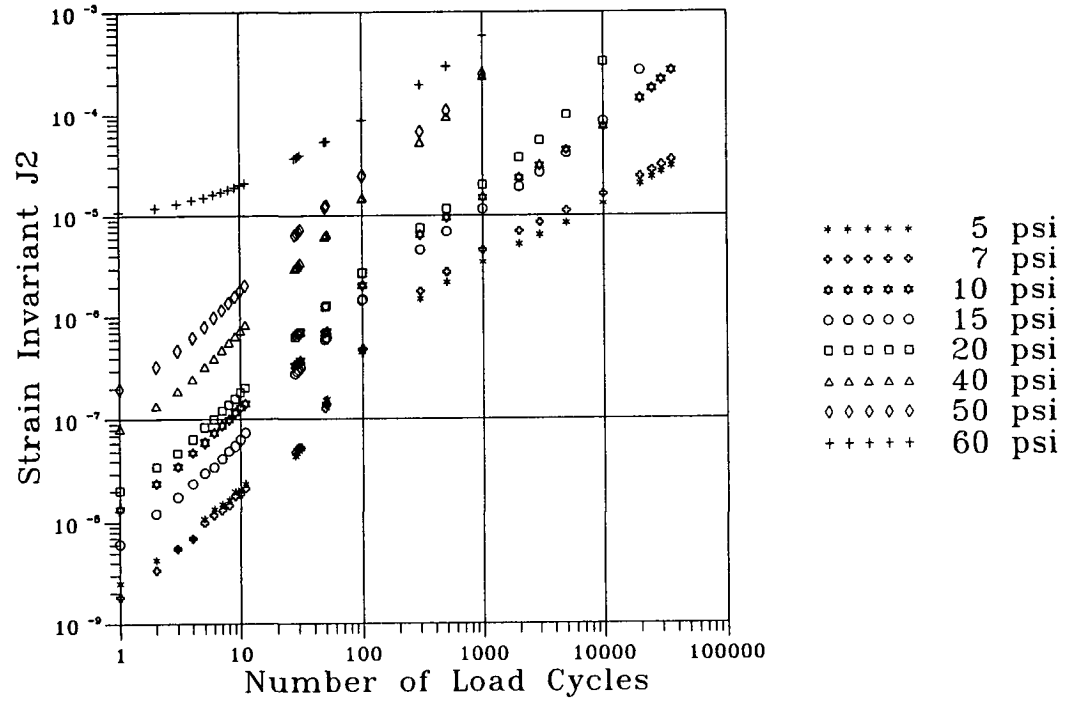

Figure 3.14. Strain invariant J_2, repeated axial load at 40°C (104°F) (confining pressure = 0 kPa [0 psi])

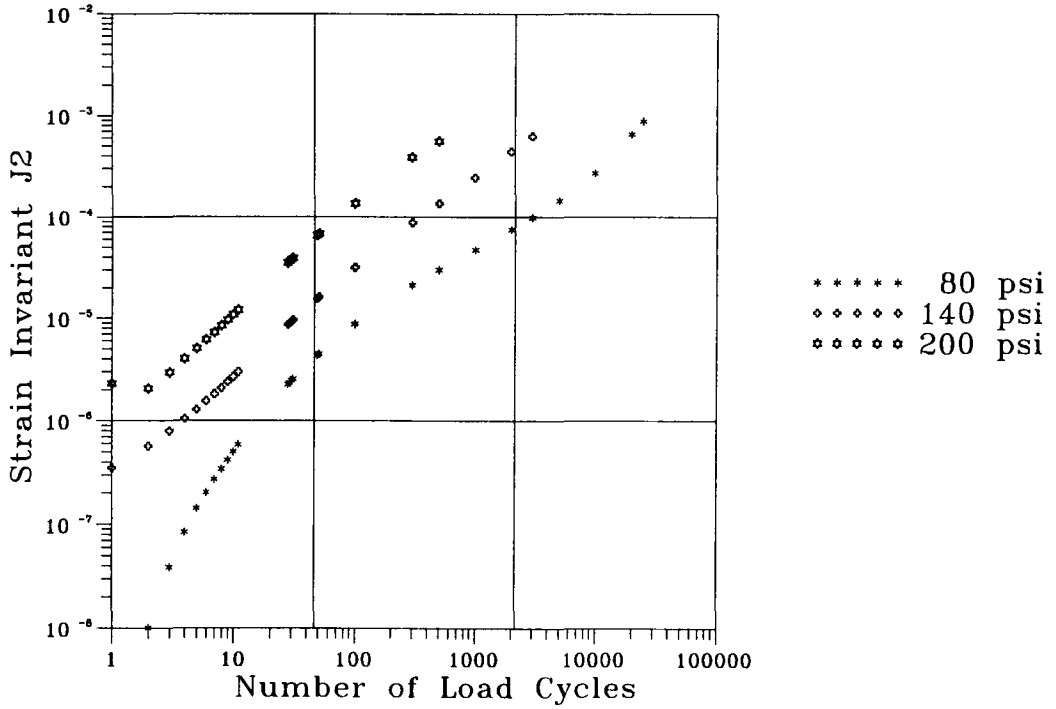

Figure 3.15. Strain invariant J_2, repeated axial load at 40°C (104°F) (confining pressure = 105 kPa [15 psi])

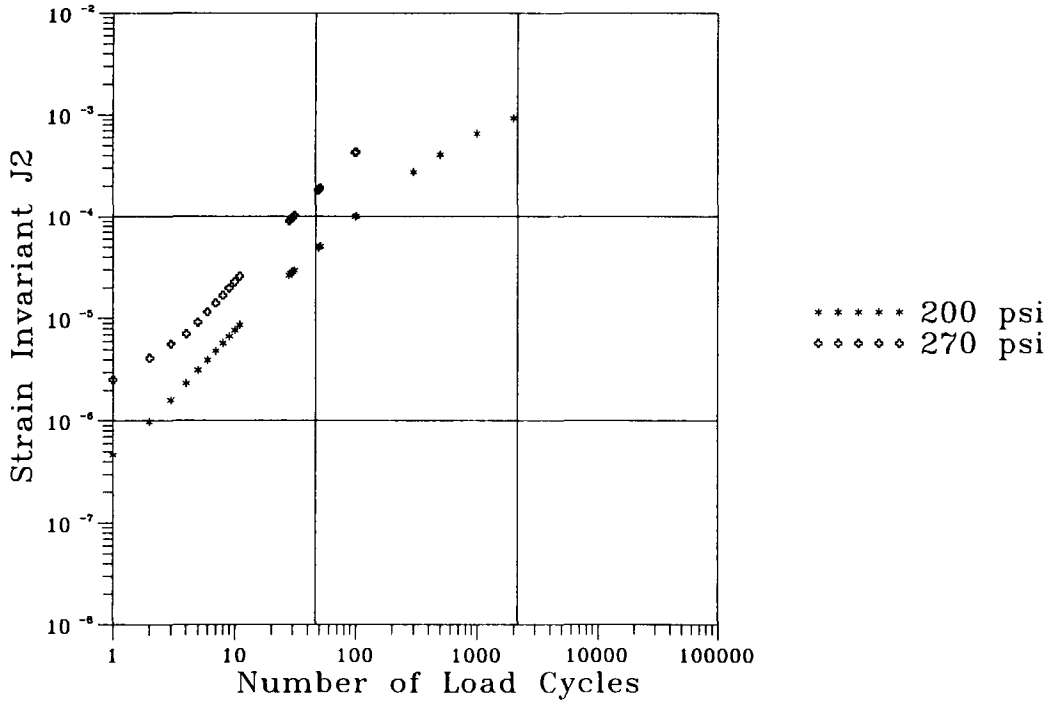

Figure 3.16. Stain invariant J_2, repeated axial load at 40°C (104°F) (confining pressure = 210 kPa [30 psi])

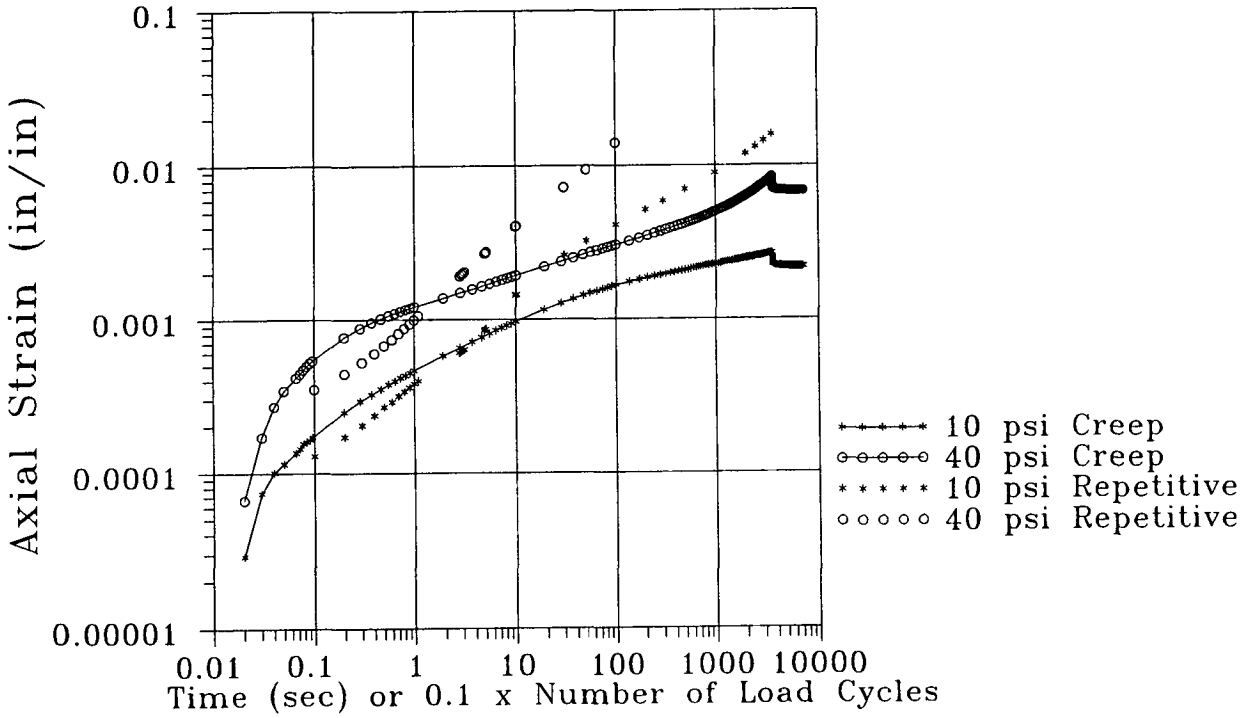

Figure 3.17. Influence of mode of loading (creep versus repeated) on the accumulation of strain at 40°C (104°F), unconfined conditions

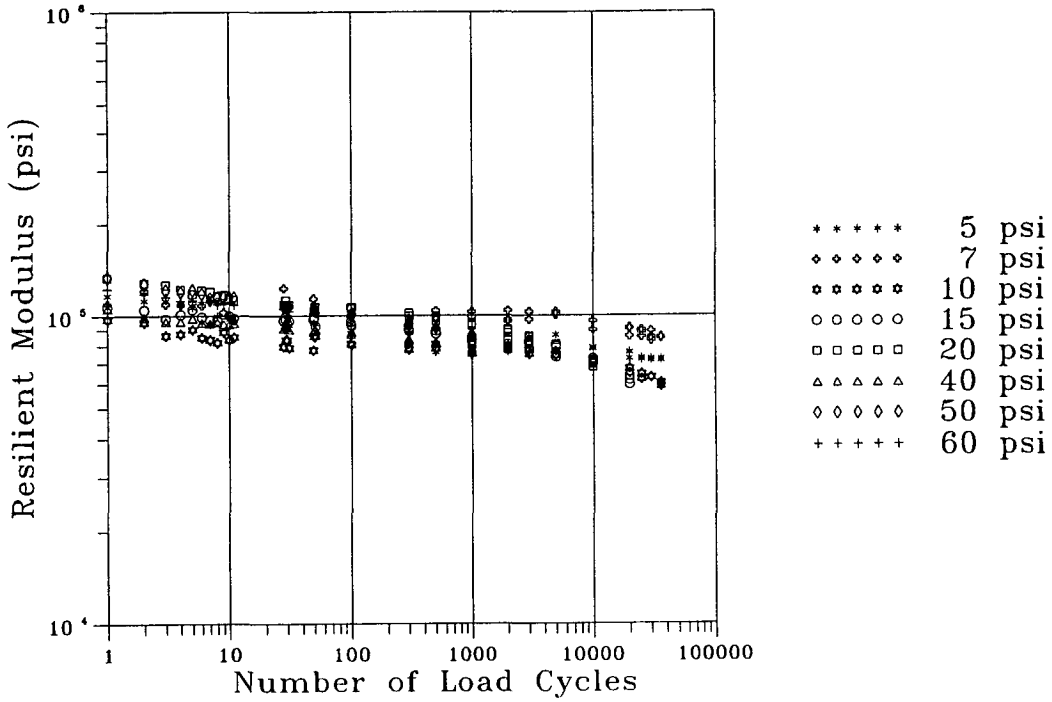

Figure 3.18. Resilient modulus in repetitive axial loading at 40°C (104°F) (confining pressure = 0 kPa [0 psi])

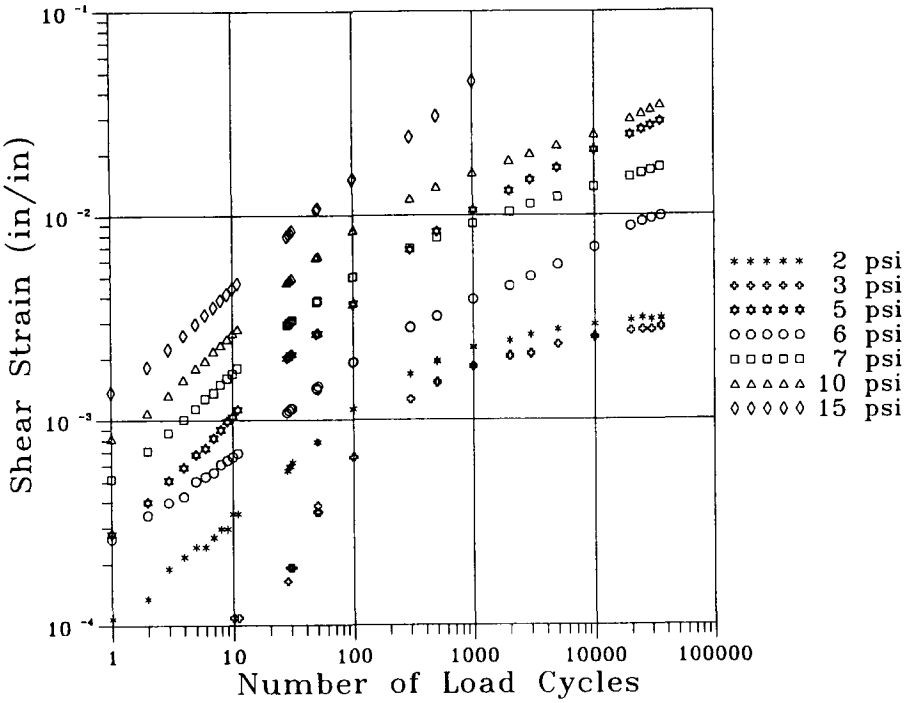

Figure 3.19. Variation of shear strain with load repetitions in repetitive shear at 40°C (104°F) (axial stress = 17 kPa [2.5 psi])

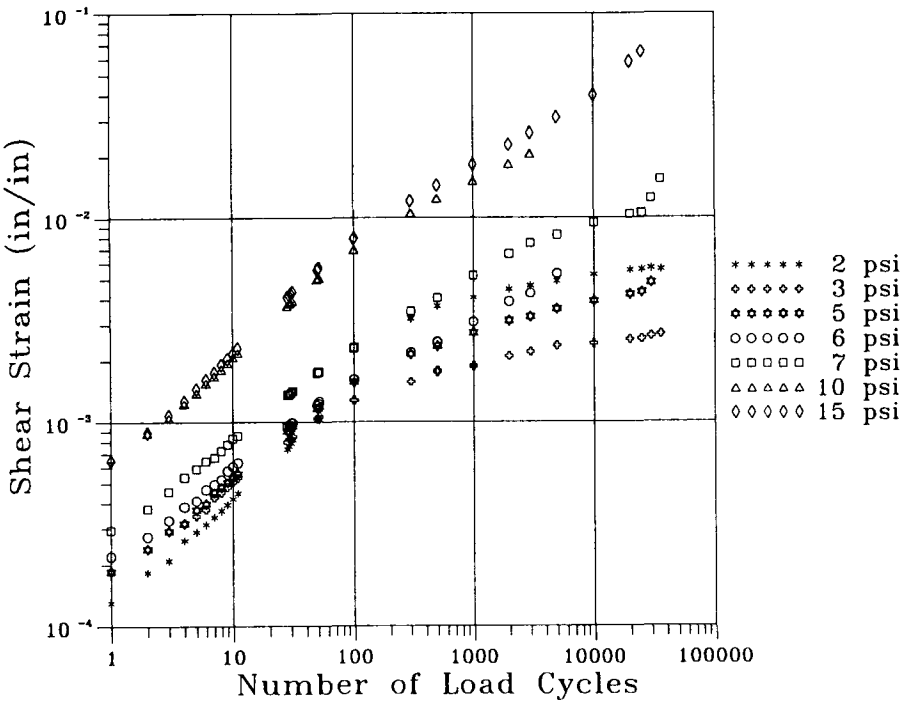

Figure 3.20. Variation of shear strain with load repetitions in repetitive shear at 40°C (104°F) (axial stress = 35 kPa [5 psi])

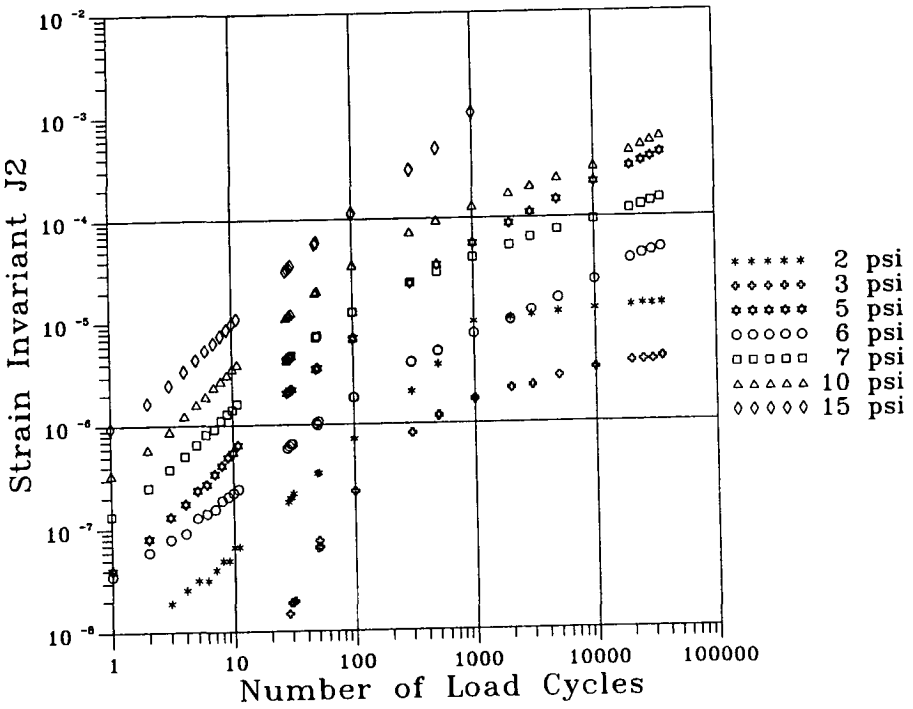

Figure 3.21. Variation of strain invariant J_2 with load repetitions, repeated shear at 40°C (104°F) (axial stress = 17 kPa [2.5 psi])

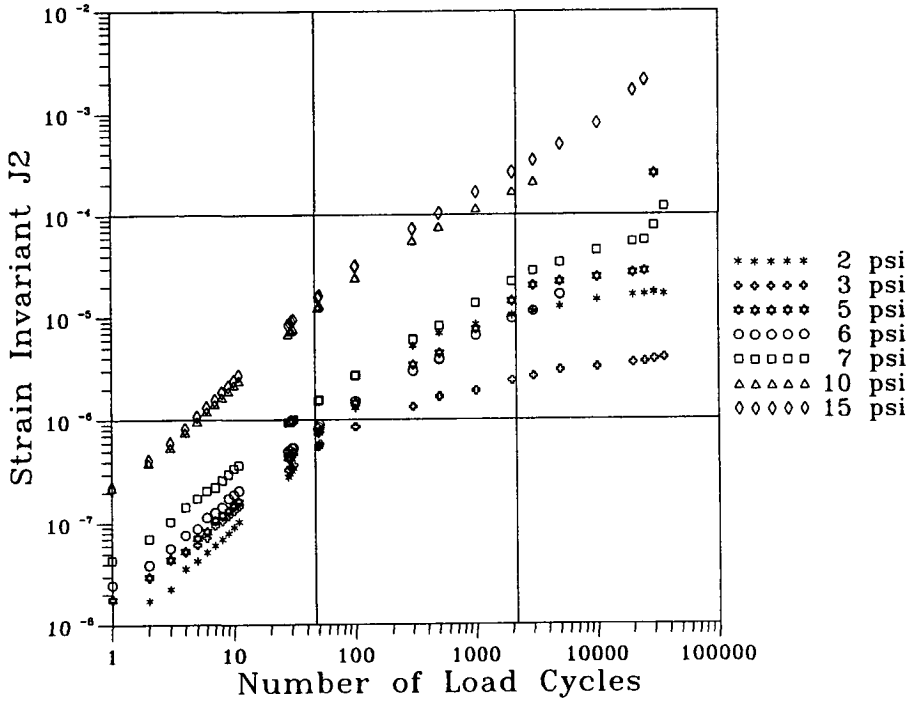

Figure 3.22. Variation of strain invariant J_2 with load repetitions, repeated shear at 40°C (104°F) (axial stress = 35 kPa [5 psi])

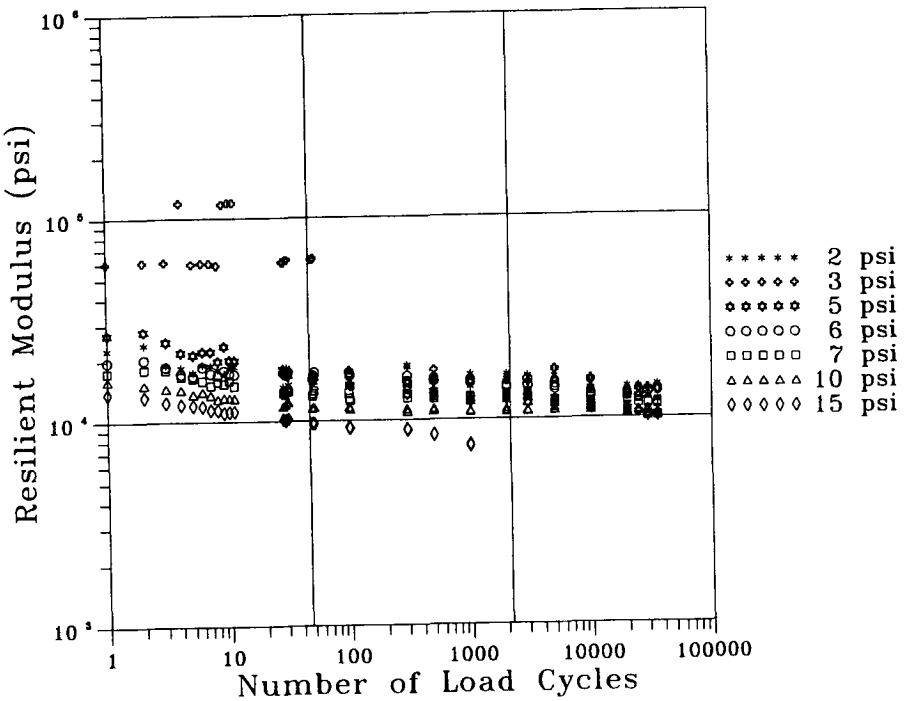

Figure 3.23. Variation of resilient modulus with load repetitions, repetitive shear at 40°C (104°F) (axial stress = 17 kPa [2.5 psi])

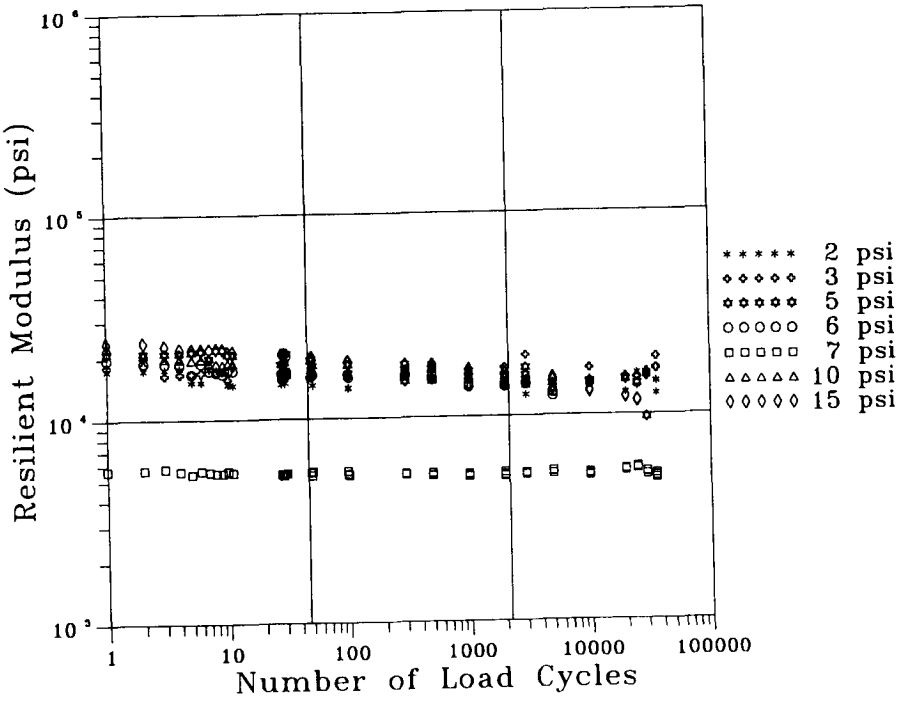

Figure 3.24. Variation of resilient modulus with load repetitions, repetitive shear at 40°C (104°F) (axial stress = 35 kPa [5 psi])

Comparative performance between creep and repetitive loading in shear is the same as in axial loading; that is, for comparable times, more deformation is obtained in repeated loading than in creep.

3.3.6 Volume Change Characteristics

In the compaction study (Sousa et al. 1991) data indicate that mixes may dilate when subjected to shearing deformations. An example from that study is illustrated in Figure 3.25 in which specimens 10 cm (4 in.) diameter by 5 cm (2 in.) high were subjected to a sustained shear stress of 35 kPa (5 psi) while the axial stress was maintained at a constant value of 17 kPa (2.5 psi). In this instance the rate of development of dilation appears dependent on the aggregate structure resulting from different compaction methods.

Analyses of the data from both the axial and shear tests in creep and repeated loading provide considerable evidence for the dilation phenomenon and indicate that it is dependent on state of stress.

The computed volumetric and octahedral strains [first (I_1) and second (J_2) invariants of strains] were plotted as shown in Figures 3.26 through 3.30 for the axial and shear creep tests. For each specimen the plot represents the path to failure. It is interesting to note that the path to failure followed by all the specimens within a set of tests was about the same. The general pattern is a slight volume decrease at first due to densification; then, with further increase in shear strain, an increase in volume (negative volumetric strains indicate volume increase) indicating dilation.

Figures 3.31 and 3.32 illustrate the results for repetitive shear tests. In this instance, for the tests with a 17 kPa (2.5 psi) axial static stress, the strain path varies considerably with the magnitude of the shear strain, exhibiting both compression and dilation, Figure 3.31. With a 35 kPa (5 psi) static axial stress and for the magnitude of the cycle shear stresses applied, only decreases in volume were observed, Figure 3.32. This suggests that it may be possible to apply specific stress states (axial and shear) to produce only specimen densification. For these conditions, the total amount of work applied to the specimen to produce a given densification could also be determined. This may have the potential to permit evaluation of the densification of mixes subjected to different levels of traffic loading (in different environments).

The data from the axial tests have been plotted in another way to illustrate that dilation takes place. The strain ratio (radial strain/axial strain) has been plotted versus octahedral strain, J_2, for the mixes whose test results were shown in Figure 3.33. Strain ratios greater than 0.5 indicate volume increase (dilation).

The phenomenon of dilation is dependent on a number of factors as illustrated herein. While the majority of the data that have been presented demonstrate that dilation does indeed vary with stress state, earlier data (compaction study) suggested that the aggregate structure is also important. As will be seen subsequently, other mix factors also must be considered.

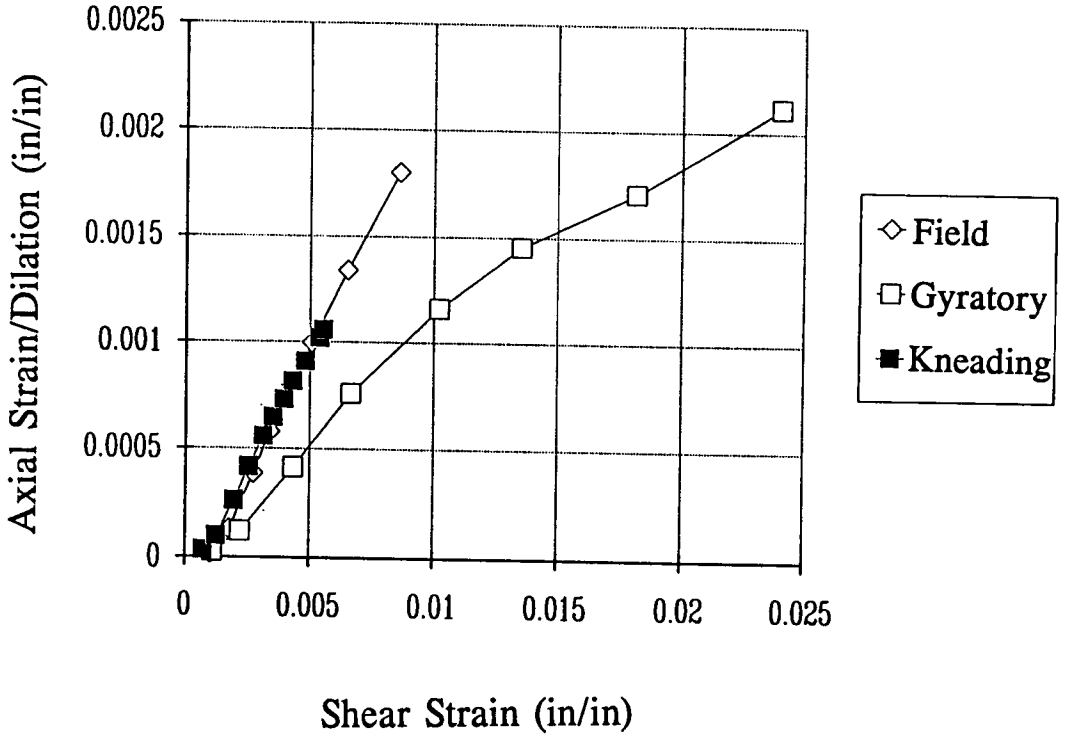

Figure 3.25. Comparative dilational response of I80 field cores to shear creep loading (average of five specimens, each line)

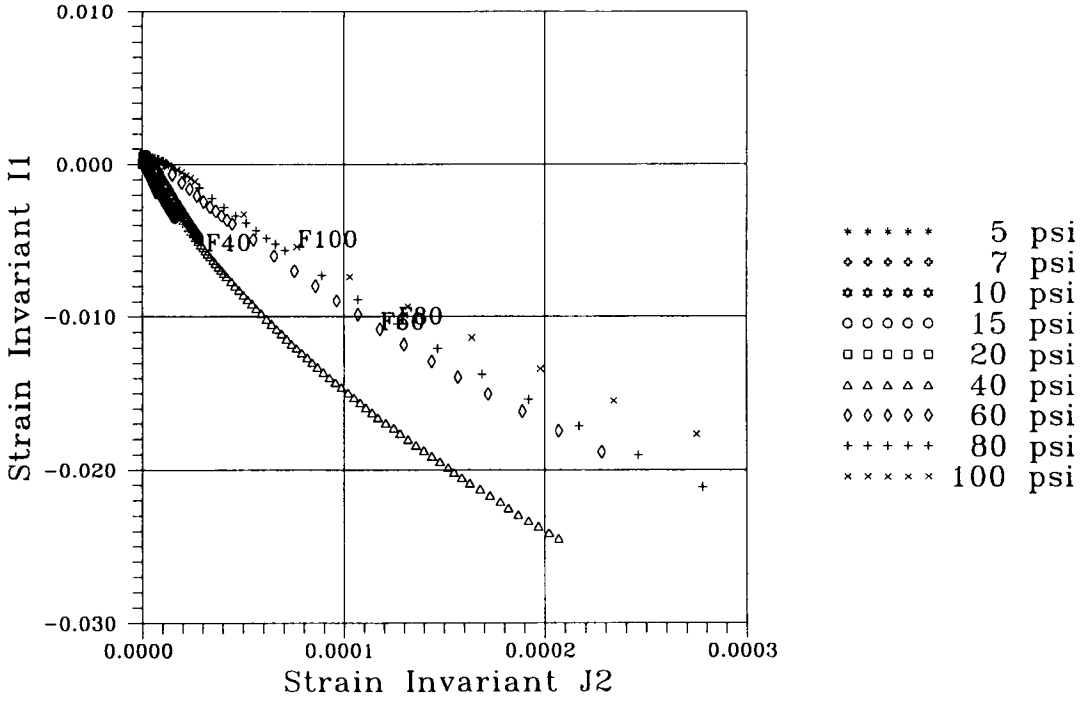

Figure 3.26. Strain invariants I_1 versus J_2 under axial creep at 40°C (104°F) (confining pressure = 0 kPa [0 psi])

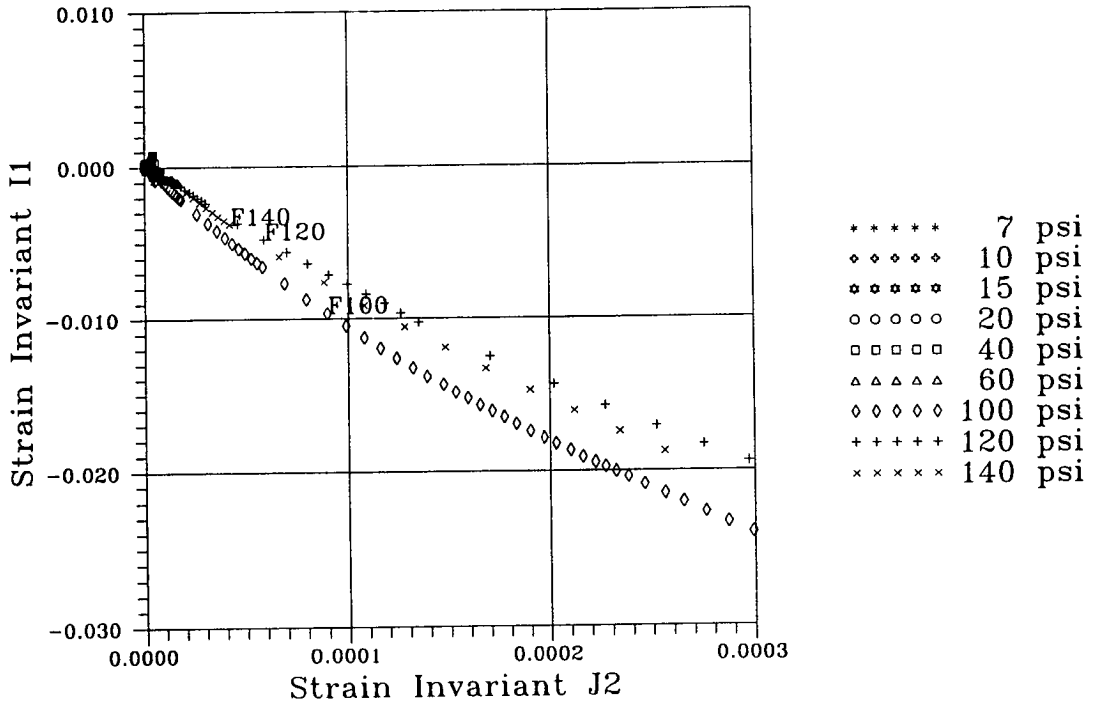

Figure 3.27. Strain invariants I_1 versus J_2 under axial creep at 40°C (104°F) (confining pressure = 105 kPa [15 psi])

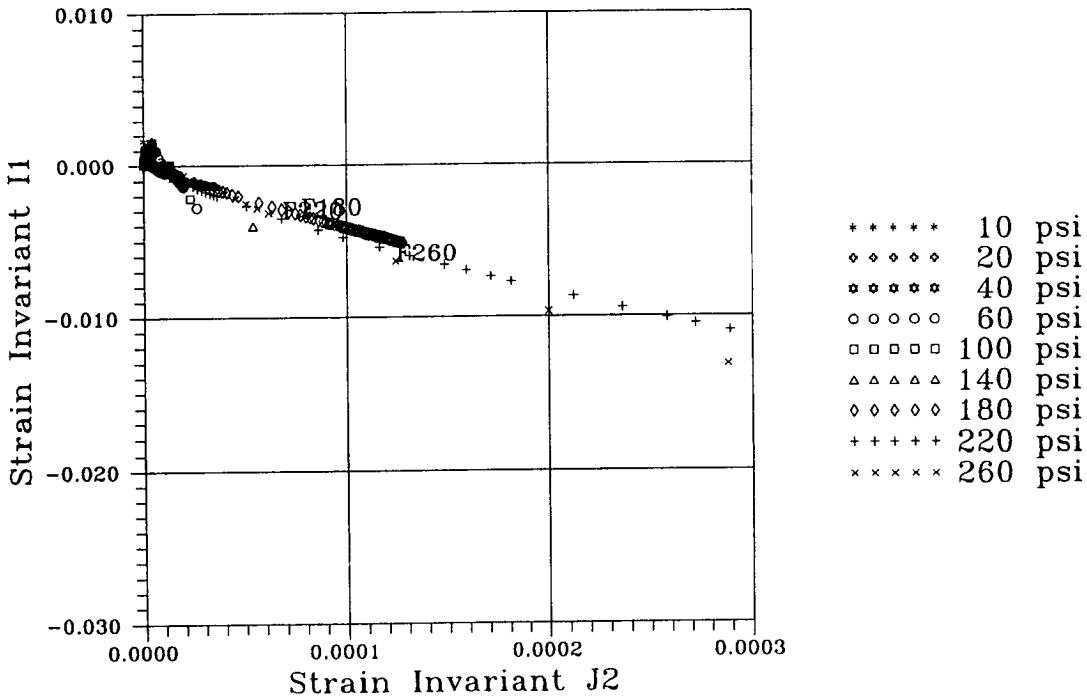

Figure 3.28. Strain invariants I_1 versus J_2 under axial creep at 40°C (104°F) (confining pressure = 210 kPa [30 psi])

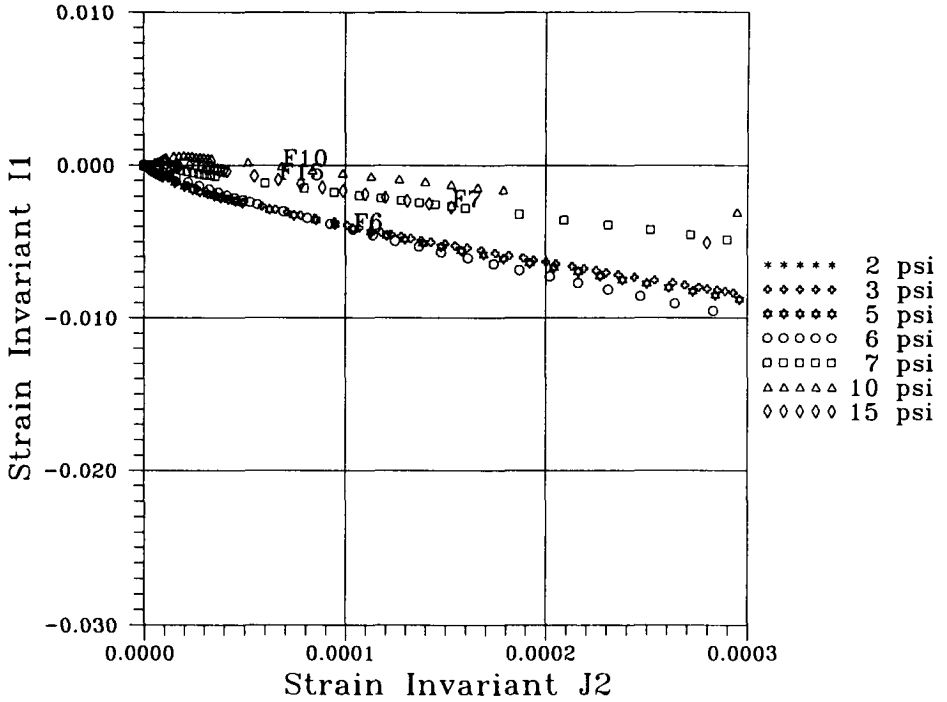

Figure 3.29. Strain invariants I_1 versus J_2 under shear creep at 40°C (104°F) (axial pressure = 17 kPa [2.5 psi])

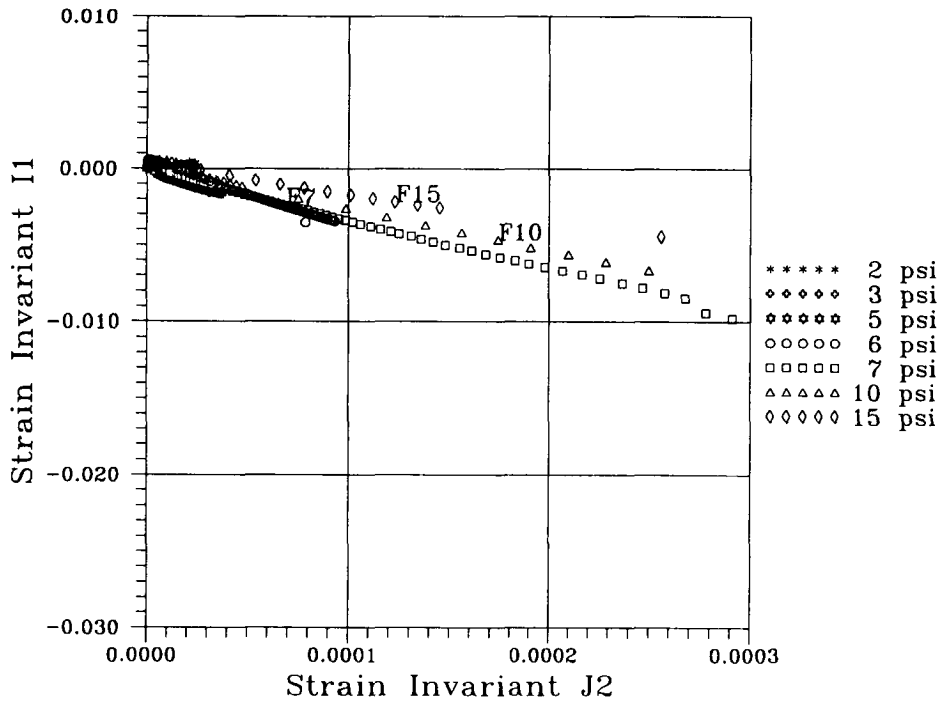

Figure 3.30. Strain invariants I_1 versus J_2 under shear creep at 40°C (104°F) (axial pressure = 35 kPa [5 psi])

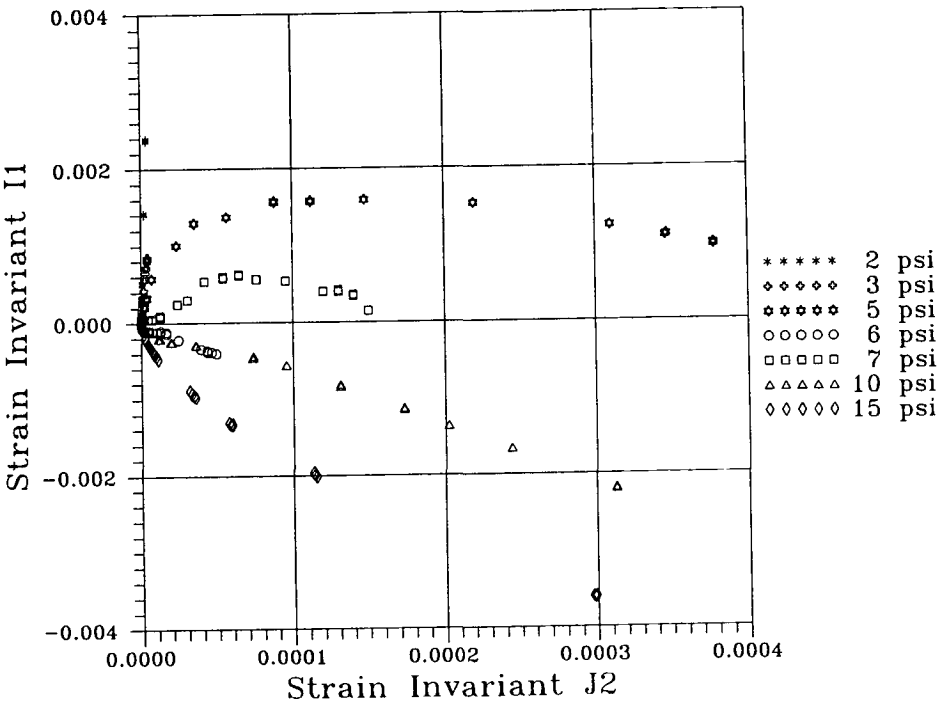

Figure 3.31. Strain invariants I_1 versus J_2 under repetitive shear at 40°C (104°F) (axial pressure = 17 kPa [2.5 psi])

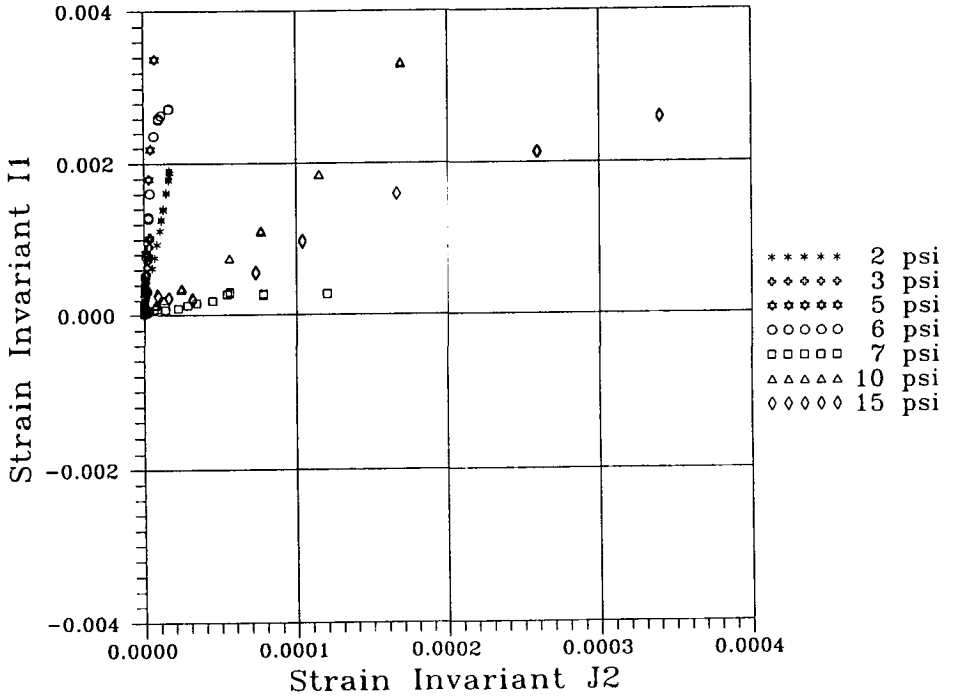

Figure 3.32. Strain invariants I_1 versus J_2 under repetitive shear at 40°C (104°F) (axial pressure = 35 kPa [5 psi])

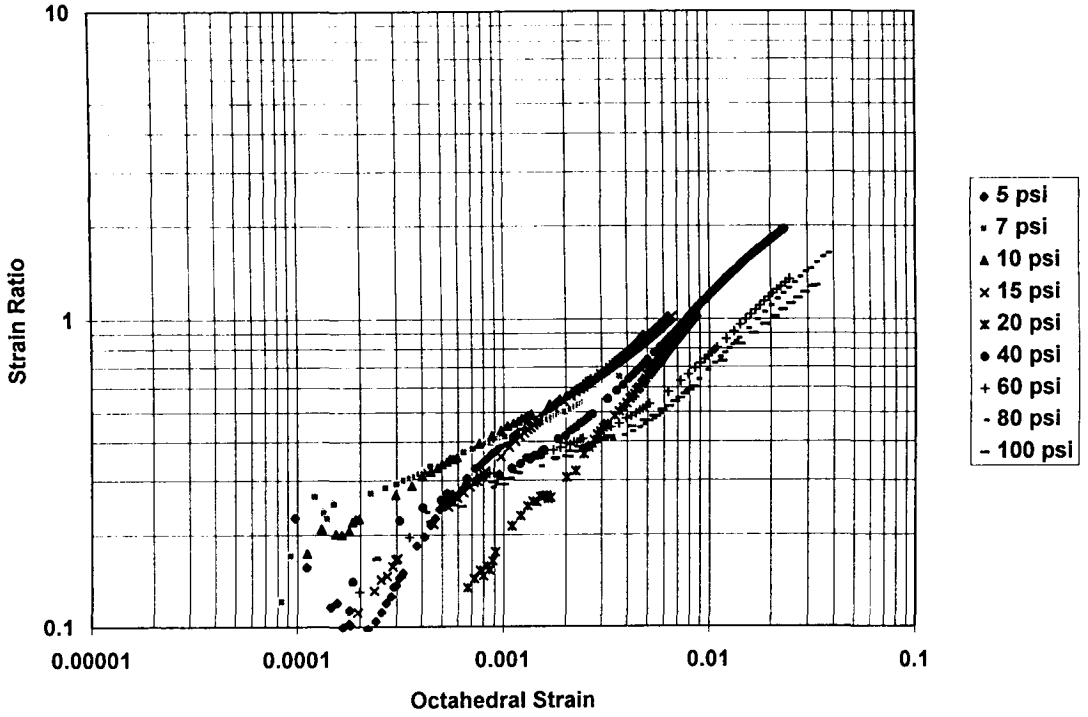

Figure 3.33. Variation of strain ratio with octahedral strain in unconfined compressive creep at 40°C (104°F)

Nevertheless, regardless of the number of factors involved, a constitutive relationship that properly defines the permanent deformation characteristics of asphalt aggregate mixes must incorporate the ability to consider this phenomenon.

3.3.7 Stiffness Tests

A number of different measures of stiffness modulus can be defined for asphalt aggregate mixes and must also be reflected in a constitutive relationship to define their permanent deformation characteristics.

Data for a measure of stiffness termed the resilient modulus have already been presented in Figures 3.18, 3.23, and 3.24, and were obtained in axial and shear repeated loading. These data suggest that, for the conditions considered, the resilient modulus appeared to be sensibly independent of stress level for the range in stresses used.

To define the effects of both *rate of loading* and *temperature*, another series of tests was conducted on hollow cylinders prepared from mixes containing aggregate RB and asphalt AAG-1 (Alavi thesis). The hollow cylinders, 23 cm (9 in.) outside diameter, wall thickness of 2.5 cm (1 in.) and 23 cm (9 in.) high, were obtained by coring from slabs approximately 23 cm (9 in.) thick compacted in three lifts by rolling wheel compaction.

Results of the tests to define the complex modulus, E*, in axial loading, conducted at stress levels to result in comparatively small strains, are shown in Figures 3.34 and 3.35 for mixes containing two different asphalt contents (Table 3.4). Frequencies ranged from 0.01 to 10 Hz and temperatures of 4°, 25°, and 40°C (39°, 77°, and 104°F) were utilized.

The data were shifted to a reference temperature of 40°C (104°F) using the time-temperature superposition process. Results of these shifts are shown in Figure 3.36 for the moduli obtained at two stress levels. In this figure the curves can be shifted to match, suggesting that for these conditions the mix appears to be thermorheologically simple and to respond as a linear viscoelastic material. Moreover, the dynamic modulus, E*, is virtually independent of stress level for the range in stresses considered.

Similar data are shown for the phase angle, ϕ, in Figures 3.37 and 3.38.

The same series of tests was performed in torsional loading to define the dynamic shear modulus, G*, over the same range of temperatures and frequencies. The results of this test series are shown in Figures 3.39 through 3.43. Essentially the same results were obtained as for axial loading; that is, the material can be considered to be linear viscoelastic and thermorheologically simple. There does appear to be some influence of stress level at the longer times of loading as seen in Figure 3.43.

A comparison of the values for E* and G* are shown in Figure 3.44 for the reduced curves at 40°C (104°F). There is some evidence to suggest that, although the curves can be shifted to match as illustrated herein, the values of Poisson's ratio defined from the relation,

$$G^* = \frac{E^*}{2(1 + \nu)} \tag{3.5}$$

may differ from the values for strain ratio defined by measured values of the axial and radial strains obtained during testing (Alavi 1992). This suggests, of course, nonlinear response characteristics. Nevertheless, for this investigation at least, the effects of time of loading and temperature will be treated as illustrated herein and a constitutive relationship to define permanent deformation response should reflect this time of loading and temperature dependency.

Finally, it is interesting to compare the variation of the phase angle, ϕ, defined from axial and torsional loading. The reduced curves at 40°C (104°F) for both modes of loading are shown in Figure 3.45. While the values for the phase angle in shear are larger than for axial loading, the peak values occur at essentially the same frequency. This highlights the influence of the binder on mix response since both mixes contain the same asphalt cement, AAG-1.

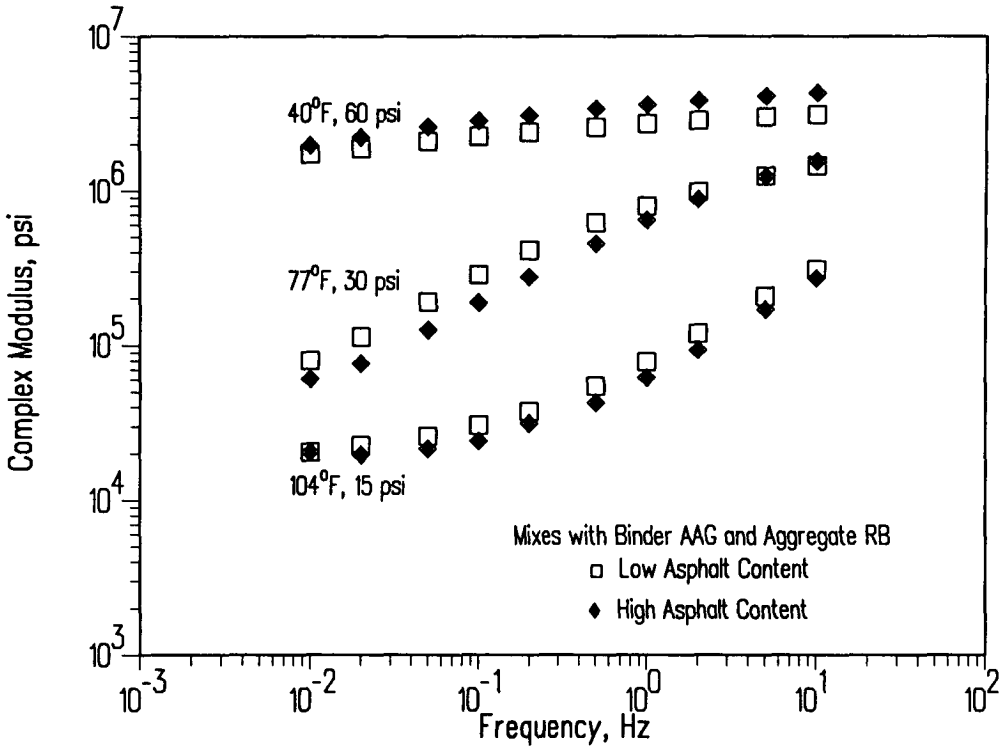

Figure 3.34. Effects of frequency, temperature, and asphalt content on E*, low air void content mixes, high stress level

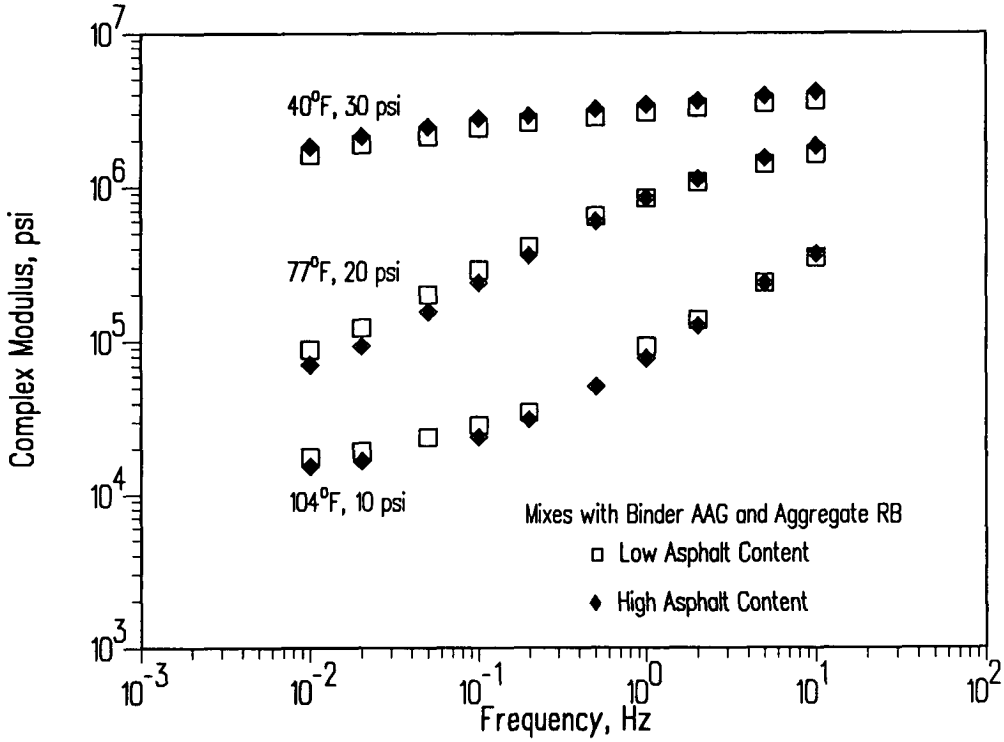

Figure 3.35. Effects of frequency, temperature, and asphalt content on E*, low air void content mixes, low stress level

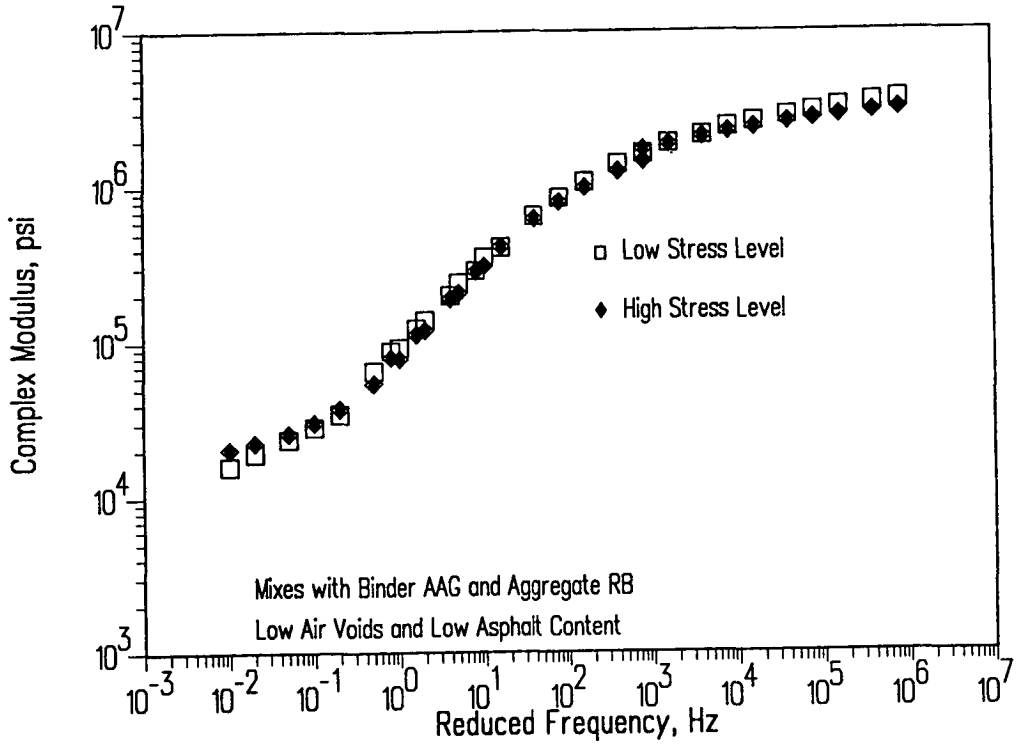

Figure 3.36. Effect of stress level on E*, reduced to 40°C (104°F)

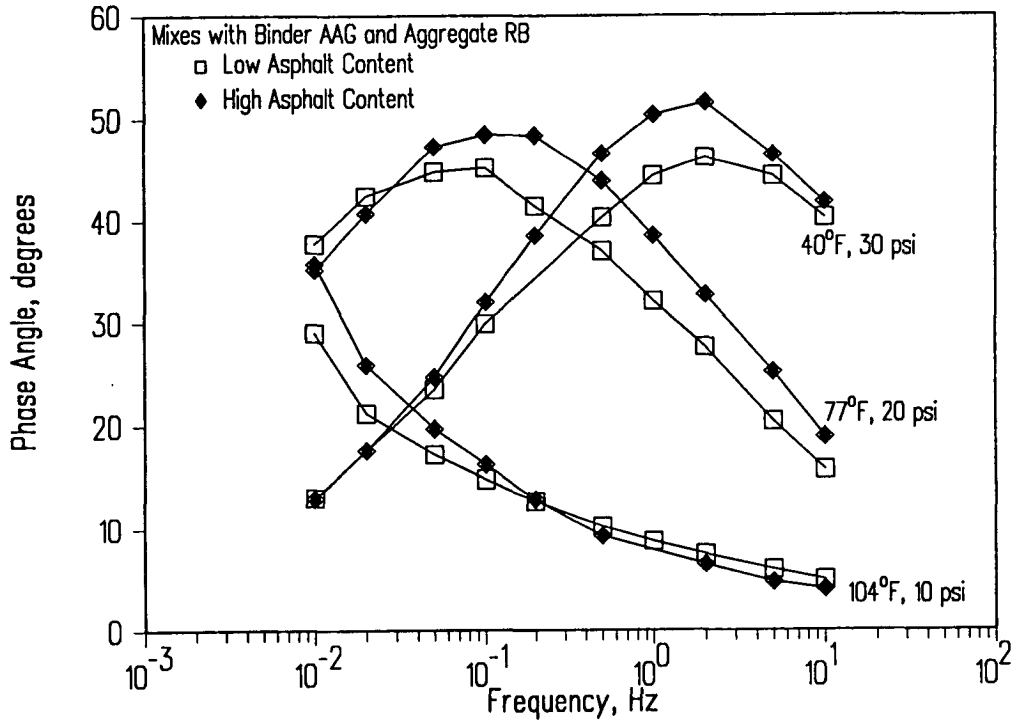

Figure 3.37. Effect of frequency, temperature and asphalt content on axial phase angle, low air void content mixes at low stress level

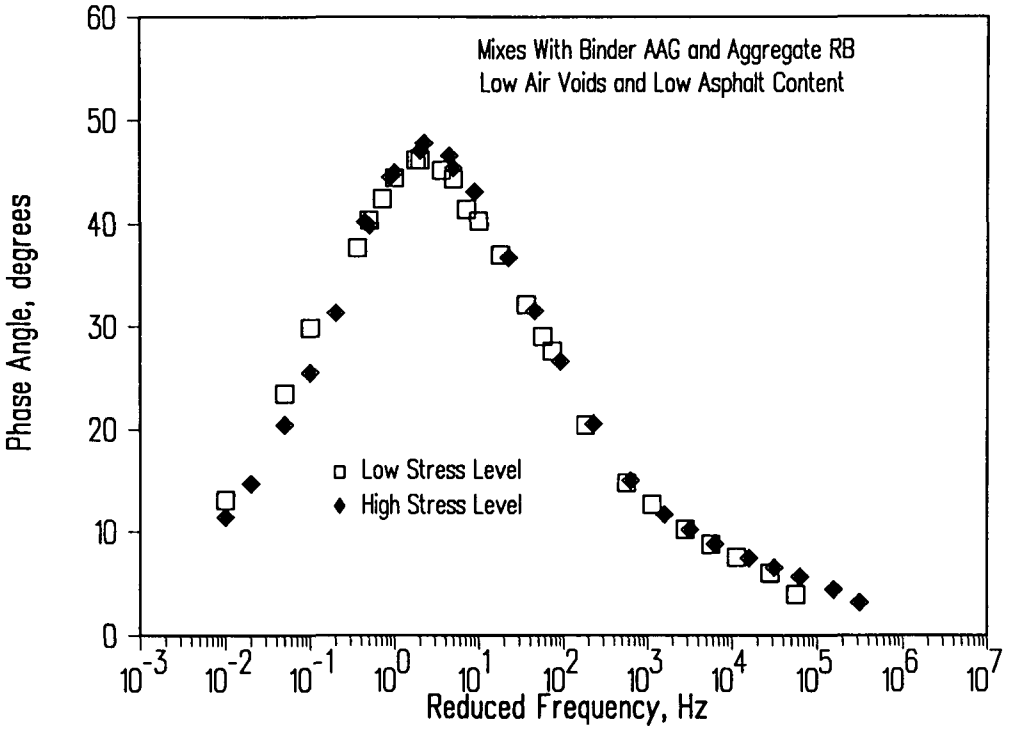

Figure 3.38. Effect of stress level on axial phase angle, reduced to 40°C (104°F)

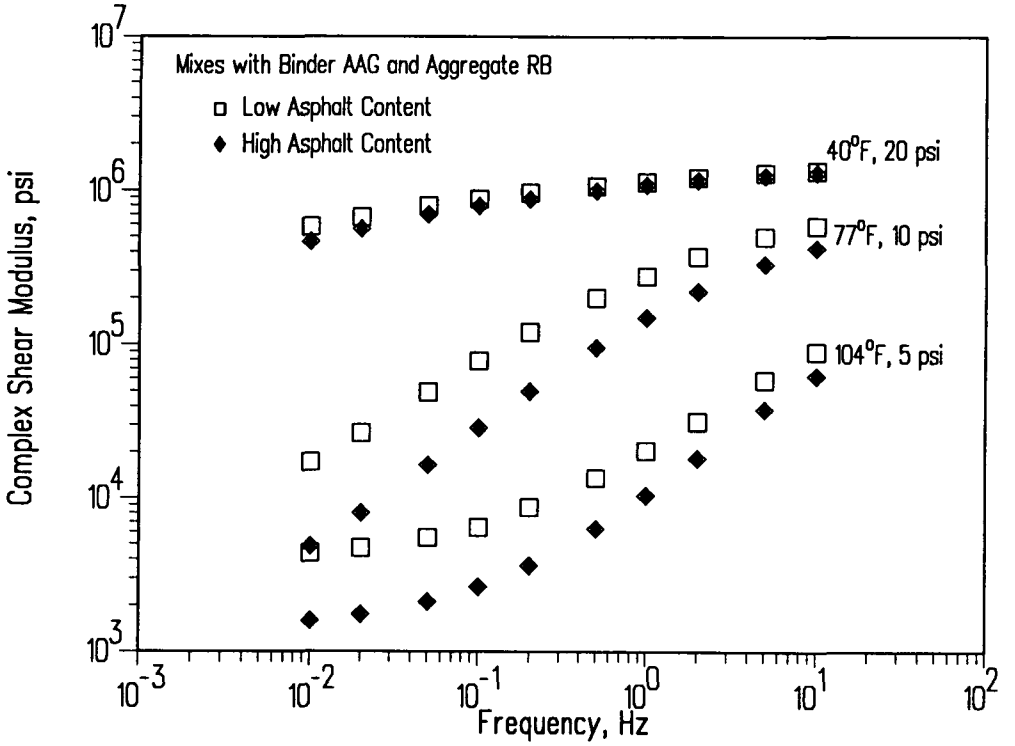

Figure 3.39. Effect of frequency, temperature, and asphalt content on G*, low air void content mixes at high stress level

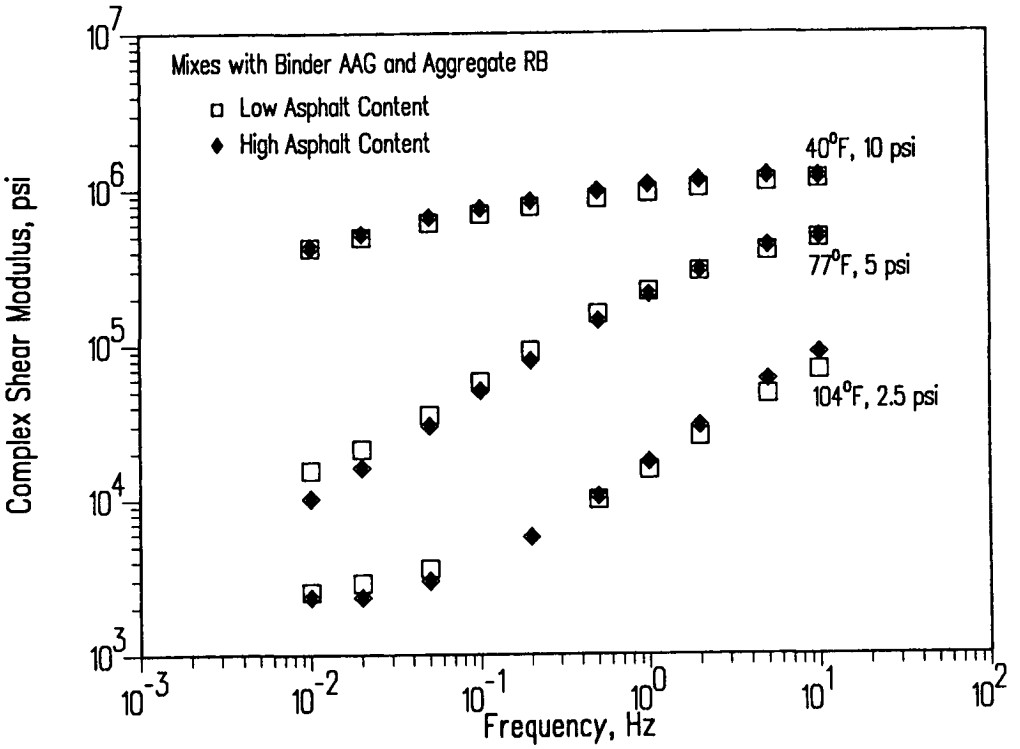

Figure 3.40. Effects of frequency, temperature, and asphalt content on G*, low air void content mixes at low stress level

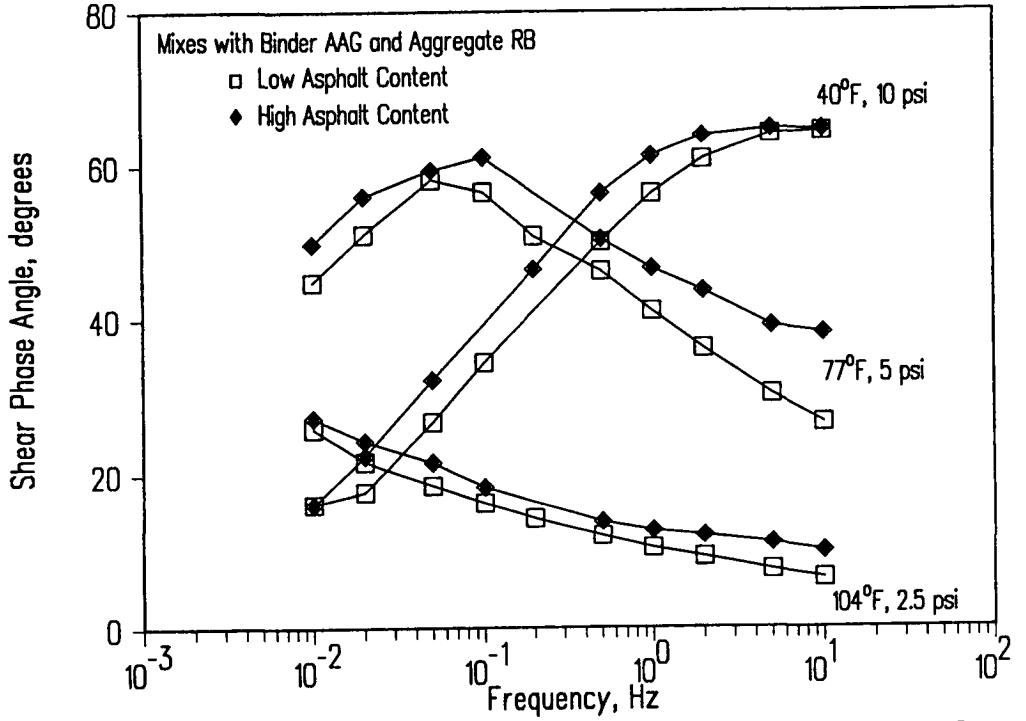

Figure 3.41. Effects of frequency, temperature, and asphalt content on shear phase angle, low air void content mixes at low stress level

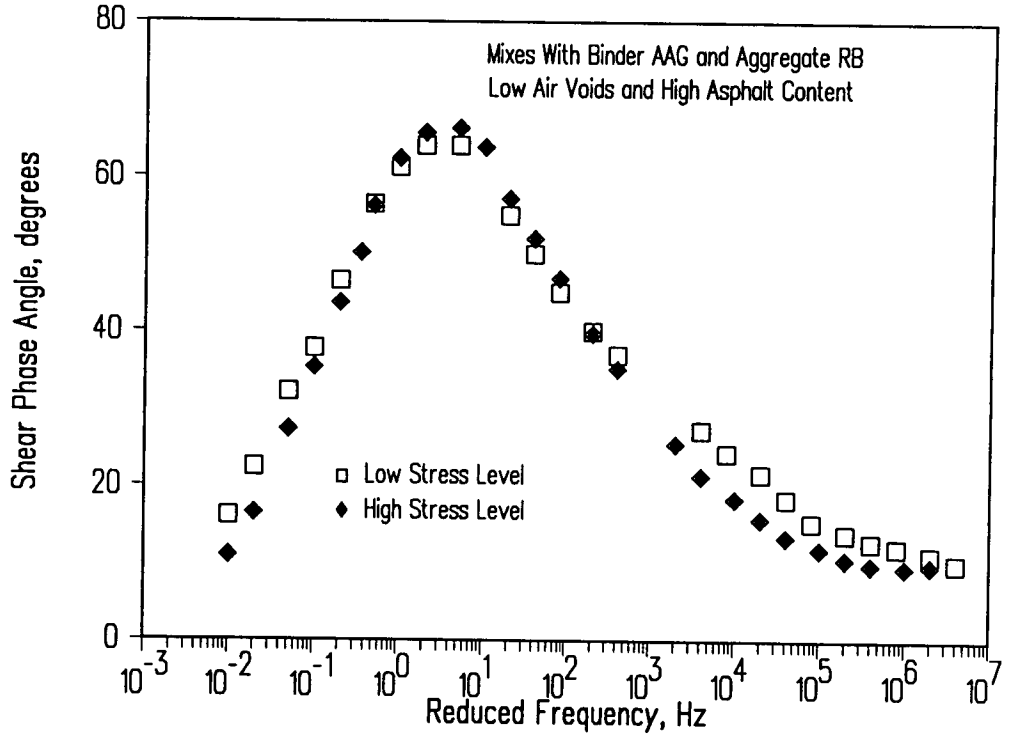

Figure 3.42. Effect of stress level on shear phase angle reduced to 40°C (104°F)

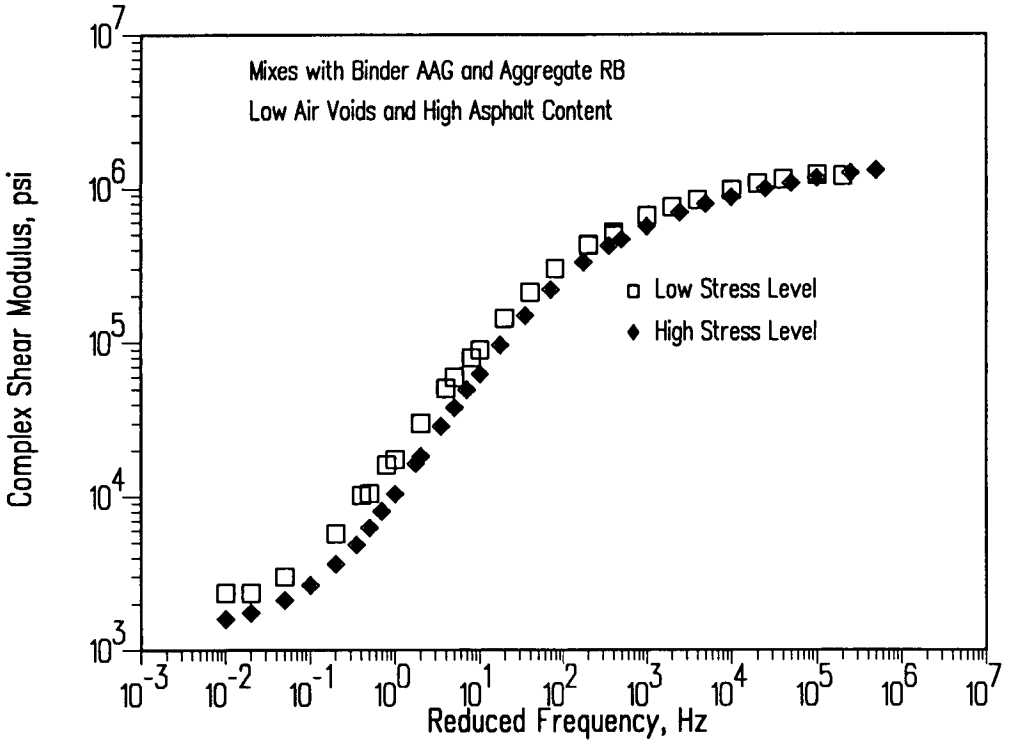

Figure 3.43. Effect of stress level on G* reduced to 40°C (104°F)

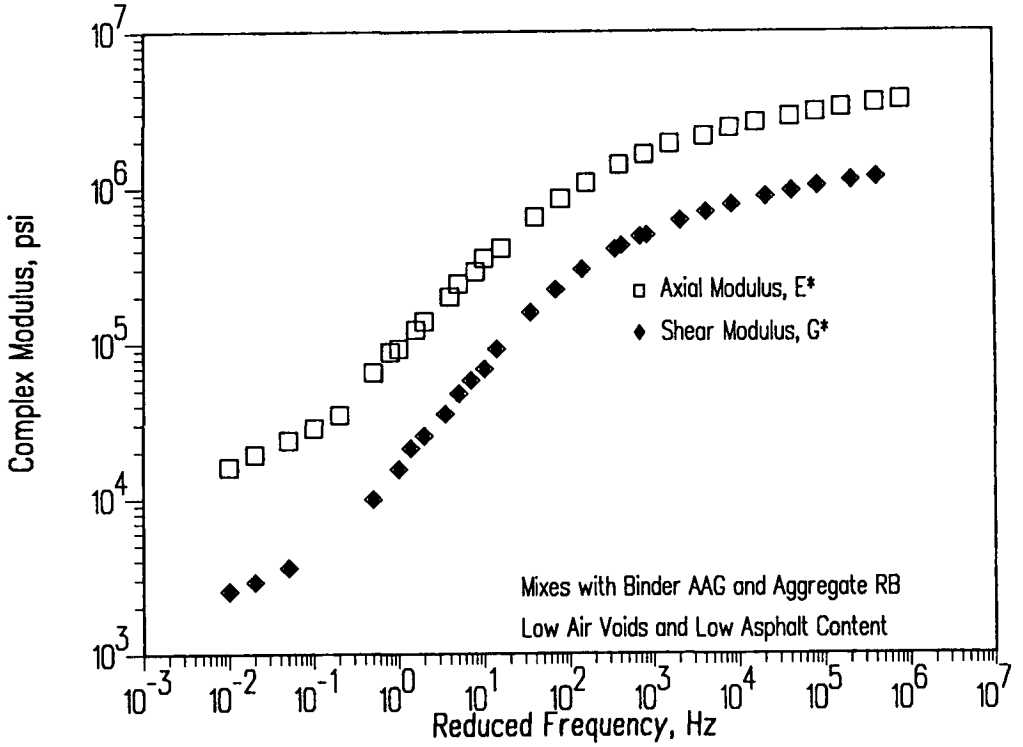

Figure 3.44. Comparison of E* and G*, at low stress level reduced to 40°C (104°F)

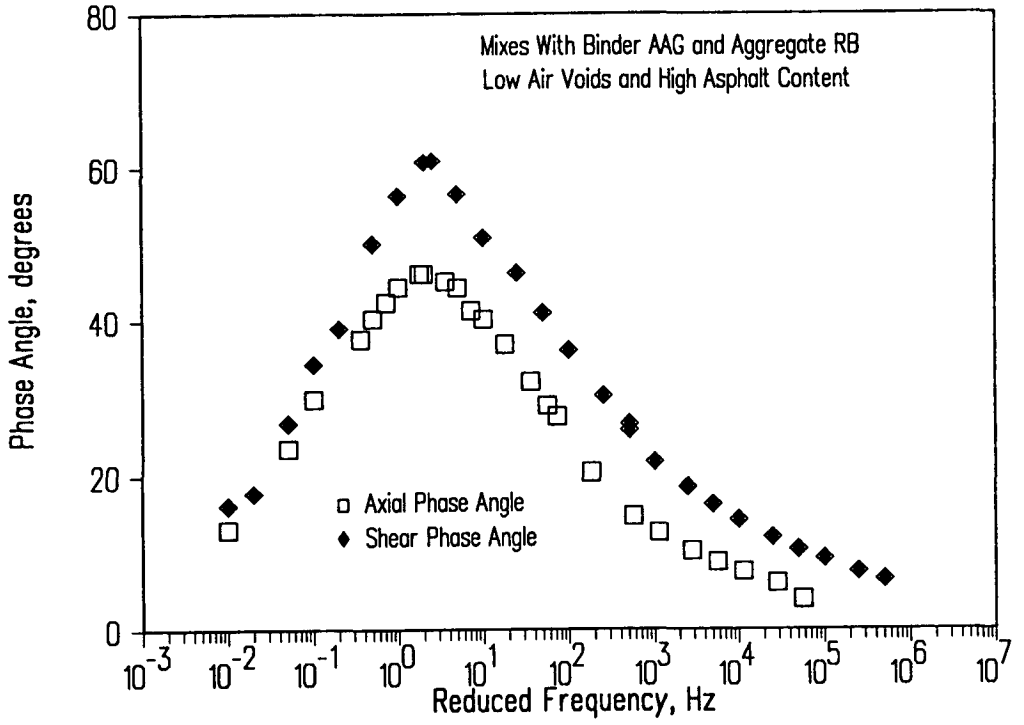

Figure 3.45. Comparison of axial and shear phase angles at low stress level, reduced to 40°C (104°F)

3.3.8 Tests Associated with Factorial Design, Table 3.7

Table 3.7 indicated that a series of repeated load tests would be performed at UCB in both the axial and shear modes and that the form of tests might change as the program developed. While the axial load test equipment and procedures remained essentially the same, the equipment for testing mixes in shear changed as experience was gained and the test results presented earlier were evaluated. Essentially, a new shear test device was developed and this is illustrated schematically in Figure 3.46.

This test unit consists of two orthogonal tables mounted on bearings connected to vertical and horizontal hydraulic actuators as seen in Figure 3.46. Each actuator can be independently controlled from the feedback of either load cells or LVDTs (linearly variable differential transducers). The tables are mounted on V-shaped linear roller preloaded bearings which effectively eliminate the possibility of any cross or unwanted displacements. They are mounted so that the specimen deformations are always achieved with the top and bottom faces parallel. The tables are placed inside a cylindrical chamber in which confining pressures of 690 kPa (100 psi) can be applied. Each of the actuators can apply dynamic loads of up to 13 kN (3000 lb). The hydraulic actuator and servovalves operate at frequencies in the range 0.01 to 20 Hz.

3.3.8.1 Materials

A total of 16 mixes were initially planned for evaluation in this phase. They included, as noted in Table 3.7, two asphalts — AAG-1 and AAK-1; two aggregates — RB and RL; two asphalt contents (optimum and high); and two air void contents — 4 percent ± 1 percent and 8 percent ± 1 percent.

Slabs from which the specimens were obtained were prepared by rolling wheel compaction. From each slab, a number of specimens were cored, including the following: (a) one hollow cylindrical specimen (23 cm [9 in.] high, 18 cm [7 in.] inside diameter, and 23 cm [9 in.] outside diameter); (b) three cylinders 10 cm (4 in.) in diameter by 20 cm (8 in.) high for axial compression tests; (c) seven cylinders 10 cm (4 in.) in diameter by 5 cm (2 in.) high for shear tests; and (d) three cylinders 15 cm (6 in.) in diameter by 5 cm (2 in.) high for shear tests.

3.3.8.2 Test Program

Based on the earlier studies it was decided to include some creep as well as repeated load tests and the resulting program as planned is shown in Table 3.8.

In the shear test series, the A.3 program incorporated a stress state that attempted to duplicate the stress conditions that exist near the tire edge in the upper part of the pavement. These stresses were estimated using a multilayered elastic analysis program. Stress analyses were conducted using a set of dual tires (550 kPa [80 psi] inflation pressure) for a few pavement conditions that might be encountered when the pavement has the highest propensity for rutting (i.e., high pavement temperatures). For each of the conditions,

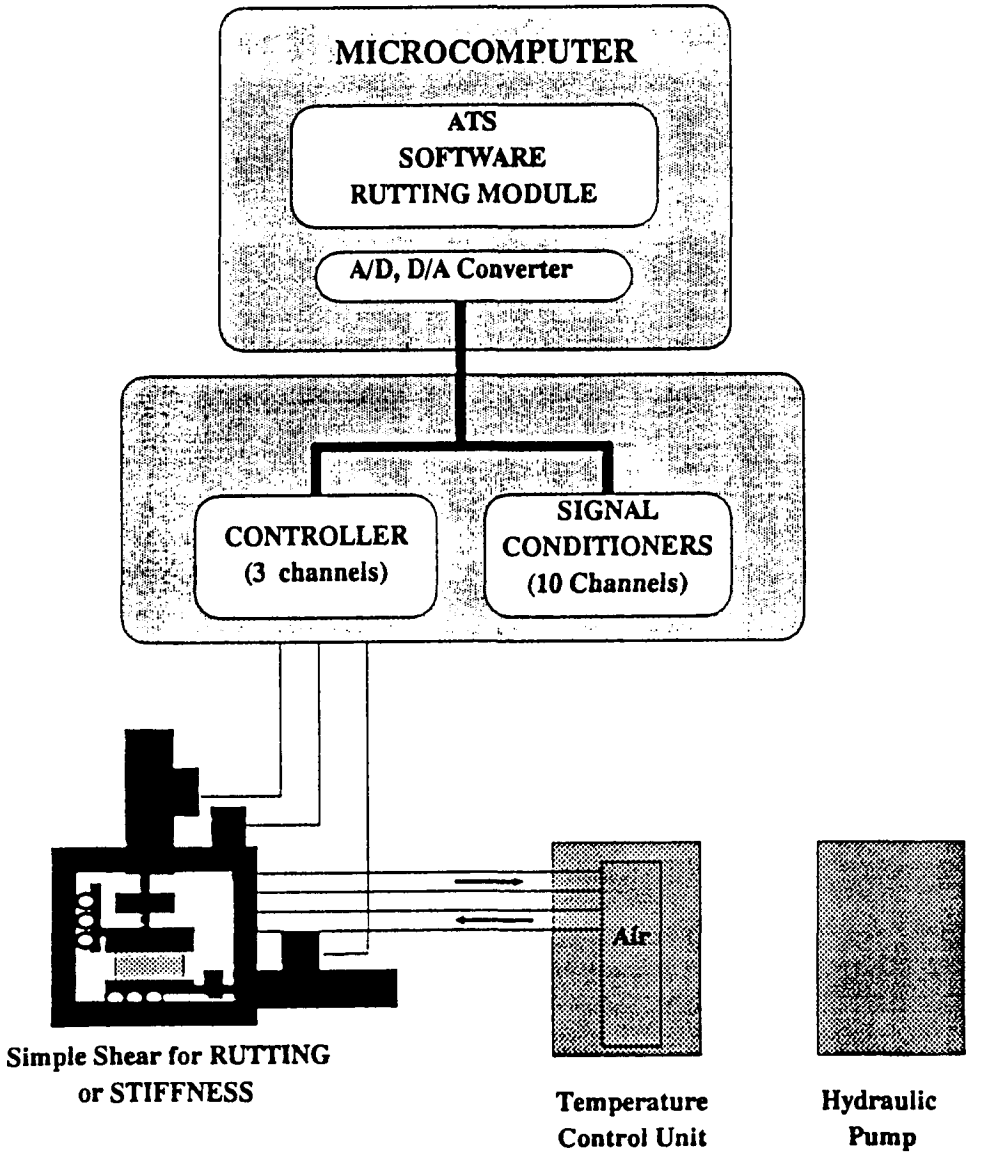

Figure 3.46. Schematic representation of proposed system for rutting evaluation

Table 3.8. Test programs for factorial design mixes

Axial Tests		Shear Tests	
		A Series	B Series
1	Creep and recovery (one hour loading, one hour unloading) σ_1 = 15 psi, σ_3 = 0 psi I_1 (stress) = 15 psi J_2 (stress) = 75 psi^2	Confined creep (one hour loading, one hour unloading) σ_z = 9 psi, σ_x = 2.5 psi τ = 6.5 psi I_1 (stress) = 16.5 psi J_2 (stress) = 75 psi^2	Repeated load shear (shear deformation, no dilation) σ_z = variable to maintain constant height σ_x = 0 psi, τ = 15 psi I_1 (stress) — depends on material response J_2 (stress) — depends on material response
2	Repeated load (0.1 sec on, 0.9 sec off) σ_1 = 15 psi, σ_3 = 0 psi I_1 (stress) = 15 psi J_2 (stress) = 75 psi^2	Repeated load shear, confined (0.1 s on, 0.6 s off) σ_z = 9 psi, σ_x = 17.5 psi τ = 6.5 psi I_1 (stress) = 61.5 psi J_2 (stress) = 75 psi^2	Repeated load shear (shear deformation, with dilation) σ_z = 0 psi, σ_x = 0 psi τ = 15 psi I_1 (stress) = 0 psi J_2 (stress) = 112.5 psi^2
3	Repeated load, confined (0.1 sec on, 0.9 sec off) σ_1 = 30 psi, σ_3 = 15 psi I_1 (stress) = 60 psi J_2 (stress) = 75 psi^2	Repeated load shear, confined (0.1 sec on, 0.6 sec off) σ_z = 30 psi, σ_x = 30 psi τ = 20 psi I_1 (stress) = 120 psi J_2 (stress) = 500 psi^2	Repeated load shear (to duplicate field compaction effects) a. Same as A.3 b. Apply fixed amount of energy associated with traffic c. Same as A.3

Note: 1 lb/in^2 = 6.89 kPa

the states of stress producing the highest octahedral shear stress were identified. The values obtained indicate that near the edge of the tires, the shear stress component of the state of stress is quite important.

Based on the computations, a reasonable state of stress to be duplicated by the confined repeated load shear test is (for a tire with 550 kPa [80 psi] inflation pressure): σ_x — 105 to 140 kPa (15 to 20 psi) static confining pressure; σ_z — 105 to 140 kPa (15 to 20 psi) repetitive axial stress; τ — 140 to 210 kPa (20 to 30 psi) repetitive shear stress; hence, the range in values shown in Table 3.8.

3.3.9 Test Results

Results of the *axial compression creep* tests are presented in Figures 3.47 through 3.50. Although the mixes perform significantly differently, their instantaneous moduli are not very different. As expected, mixes with low voids performed better than mixes with high voids. Mixes with aggregate RB generally performed better than mixes with aggregate RL.

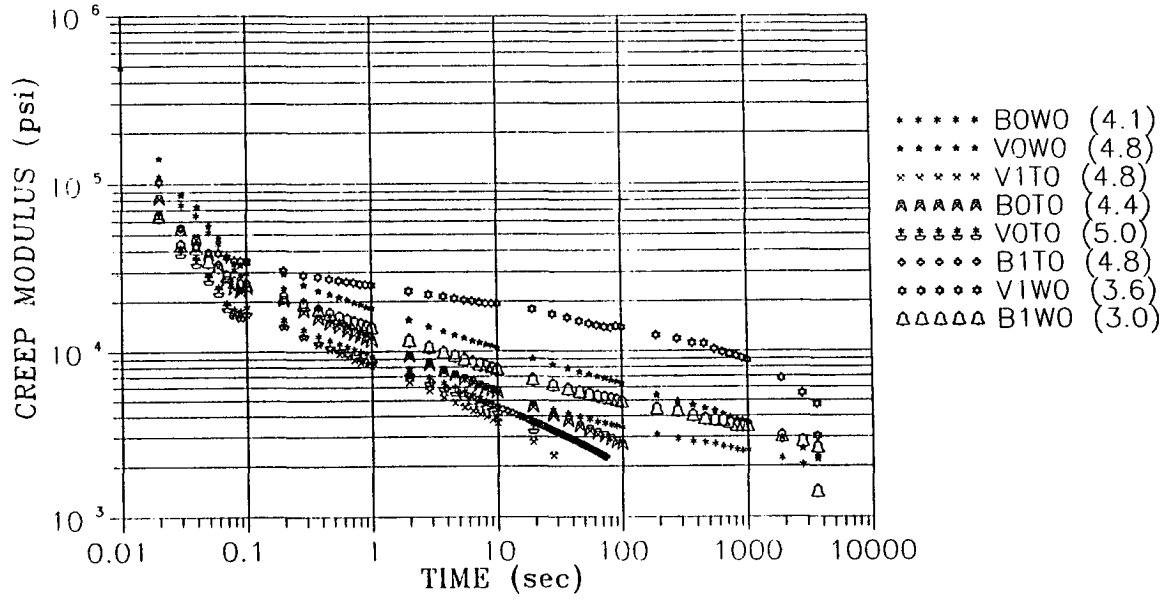

Figure 3.47. Creep modulus versus time; axial creep, 105 kPa (15 psi), at 60°C (140°F); confining pressure, 0 kPa (0 psi); low void content

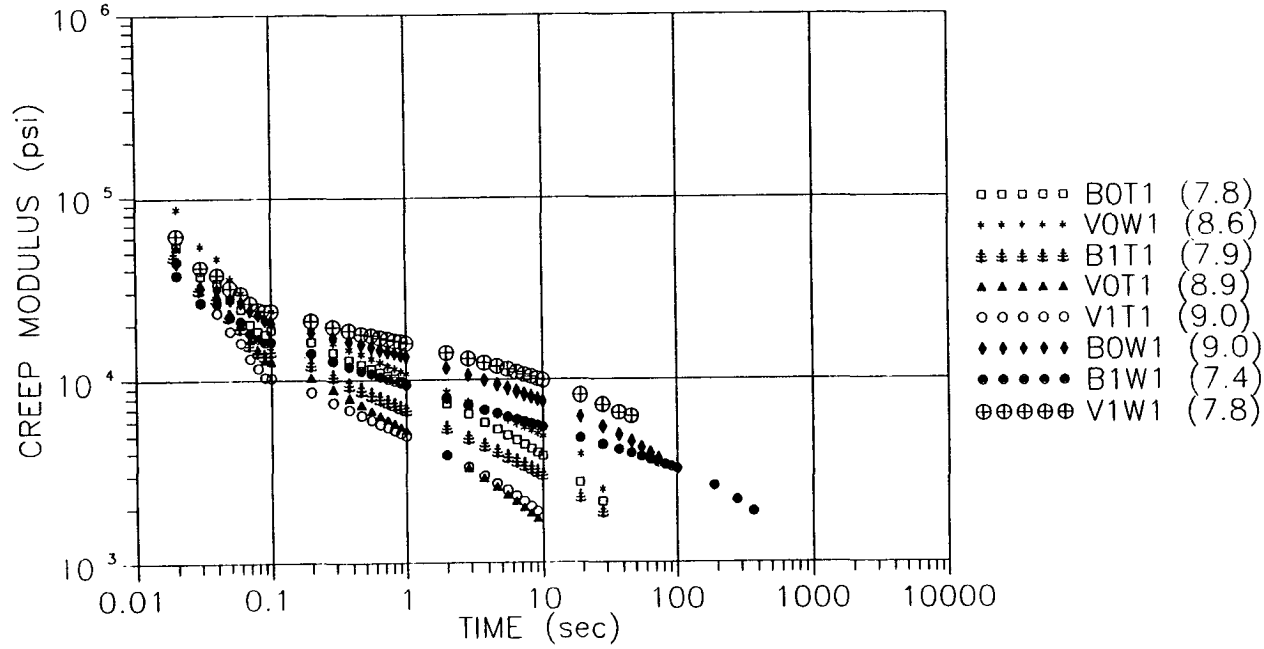

Figure 3.48. Creep modulus versus time; axial creep, 105 kPa (15 psi), at 60°C (140°F); confining pressure, 0 kPa (0 psi); high void content

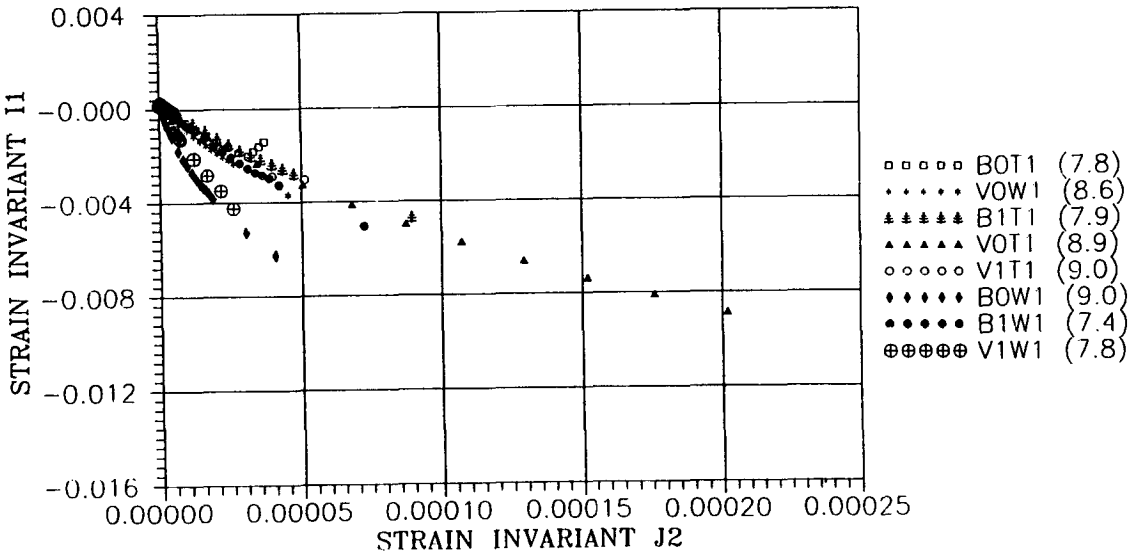

Figure 3.49. Strain invariants I_1 versus J_2, axial creep, 105 kPa (15 psi), at 60°C (140°F); confining pressure, 0 kPa (0 psi); high void content

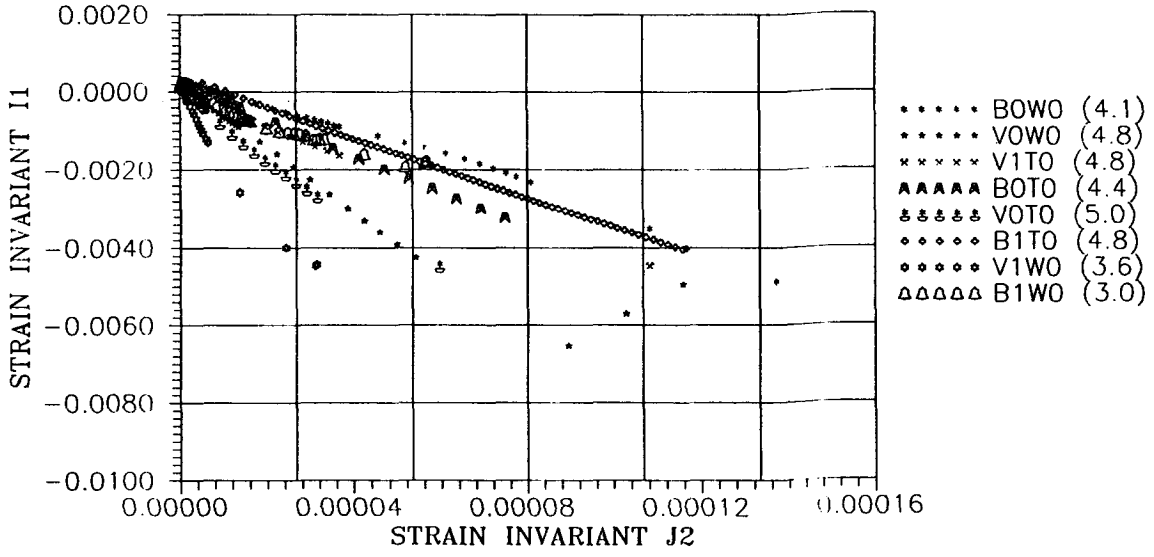

Figure 3.50. Strain invariants I_1 versus J_2, axial creep, 105 kPa (15 psi), at 60°C (140°F); confining pressure, 0 kPa (0 psi); low void content

The I_1 versus J_2 path is identical in all high voids mixes, Figure 3.49, but shows some differences for the low void mixes, Figure 3.50.

Results of the *repeated load axial tests* are presented in Figures 3.51 through 3.57. The behavior of the mix in *unconfined repetitive loading* appears to be controlled in part by the initial strain, Figures 3.51 and 3.52. Both sets of curves show similar parallel lines, although the mix properties vary significantly. The repeated load tests at high void contents, Figure 3.51, clearly separate the mixes containing aggregate RB from the mixes with aggregate RL. These differences are not so marked at low void contents, Figure 3.52. It should be noted, however, that the void differences between specimens being compared could be as much as 2 percent.

Figures 3.53 and 3.54 show the variation of I_1 with J_2 (permanent strain invariants). It is interesting to note that at the high void content the mixes only exhibit dilation and rapidly approach the failure strain threshold limit. At the low void content some of the mixes densify, particularly those containing aggregate RB, thereby providing improved resistance to dilation caused by the shear component of stress. This phenomenon is illustrated in Figures 3.55 and 3.56.

Results of the *confined repeated loading tests* (confining pressure of 105 kPa [15 psi], repeated axial stress of 105 kPa [15 psi]) are shown in Figures 3.58 through 3.65. For these conditions, the mixes exhibited similar response characteristics. All of the mixes tested exhibited a decrease in volume up to 36,000 load repetitions. None reached the threshold strain at which excessive deformation develops.

The repeated load data (confining pressure of 105 kPa [15 psi]) for the mix containing aggregate RB and asphalt AAG-1 provide a broader perspective on behavior since a wider range in deviatoric stresses was utilized. These data illustrate that mixes will dilate if the deviatoric component of the stress tensor is sufficiently large. (Dilation is associated with a negative value of I_1 in these figures.) When the data are plotted in the form I_1 versus J_2, the mixes first exhibit a volume decrease and then a volume increase as the number of repetitions is increased. These data highlight the importance of selecting the proper stress state for laboratory evaluation to ensure that it is representative of that which occurs in situ.

Results for the *constant height repeated load shear tests* are shown in Figures 3.66 through 3.69. For these tests, the vertical actuator maintained constant the reading from an LVDT, which measures the change in height of the specimen. The horizontal actuator was used to apply a haversine wave with a 0.9 kN (200 lb) peak amplitude and a duration of 0.1 s with a rest period of 0.6 s. Load was applied only in one direction; i.e., no reversal of shear stress was imposed. During the test, the specimen was restrained from expanding axially by the force developed by the vertical actuator. Figure 3.66 traces the shear versus axial forces and Figure 3.67 shows the variation of axial force with shear displacement. A specimen with high dilatancy characteristics would develop a larger axial force.

The results presented in Figure 3.68 indicate that the accumulation of permanent shear strain for the eight mixes tested varied by two orders of magnitude. For these data, the number of repetitions to a given strain level, e.g., 0.02, depended not only on the initial permanent

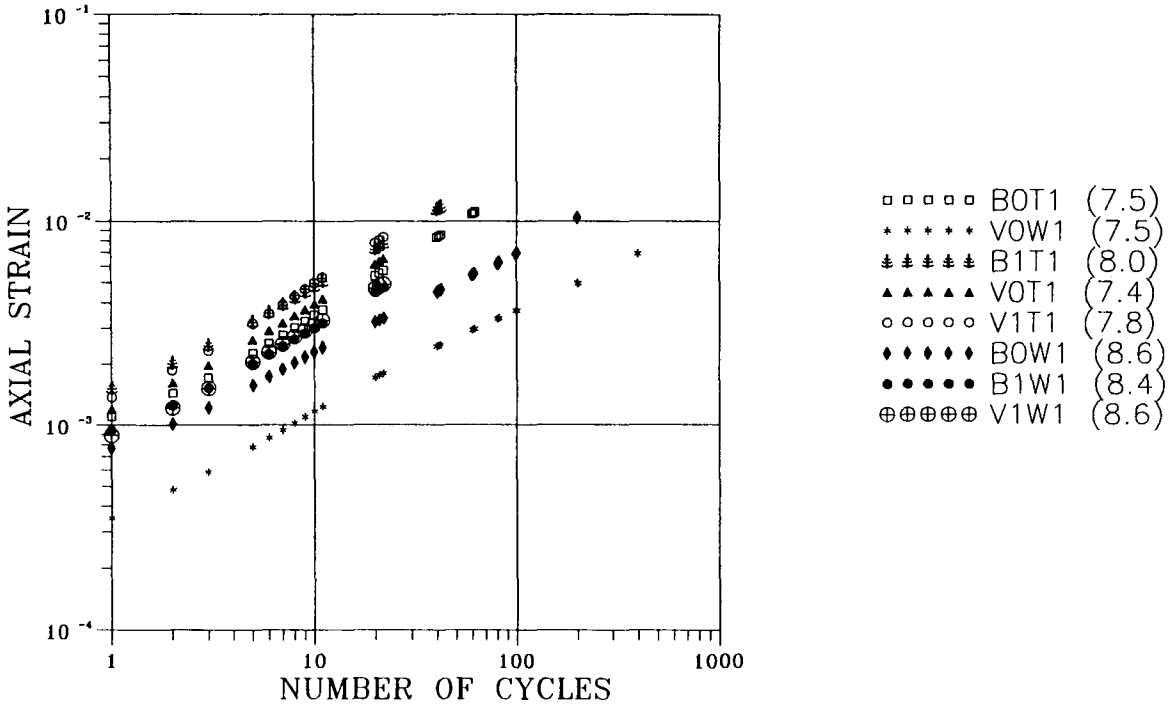

Figure 3.51. Axial strain versus number of stress repetitions; repeated axial load, 105 kPa (15 psi), at 60°C (140°F); confining pressure, 0 kPa (0 psi); high void content

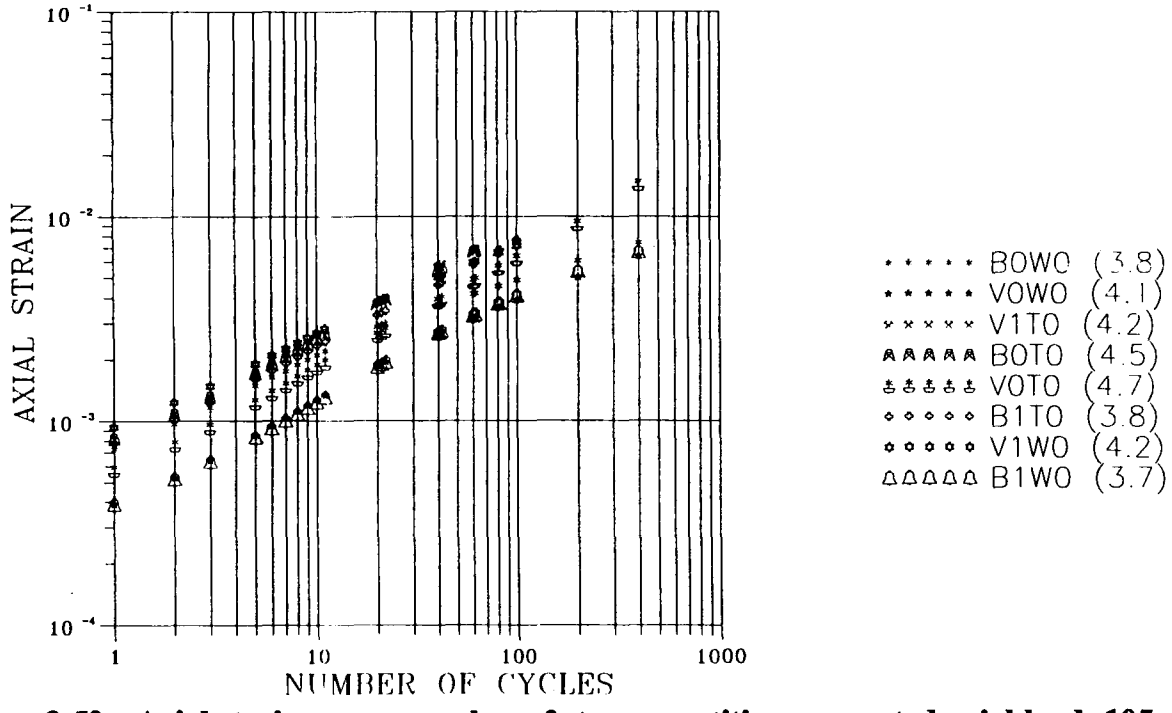

Figure 3.52. Axial strain versus number of stress repetitions; repeated axial load, 105 kPa (15 psi), at 60°C (140°F); confining pressure, 0 kPa (0 psi); low void content

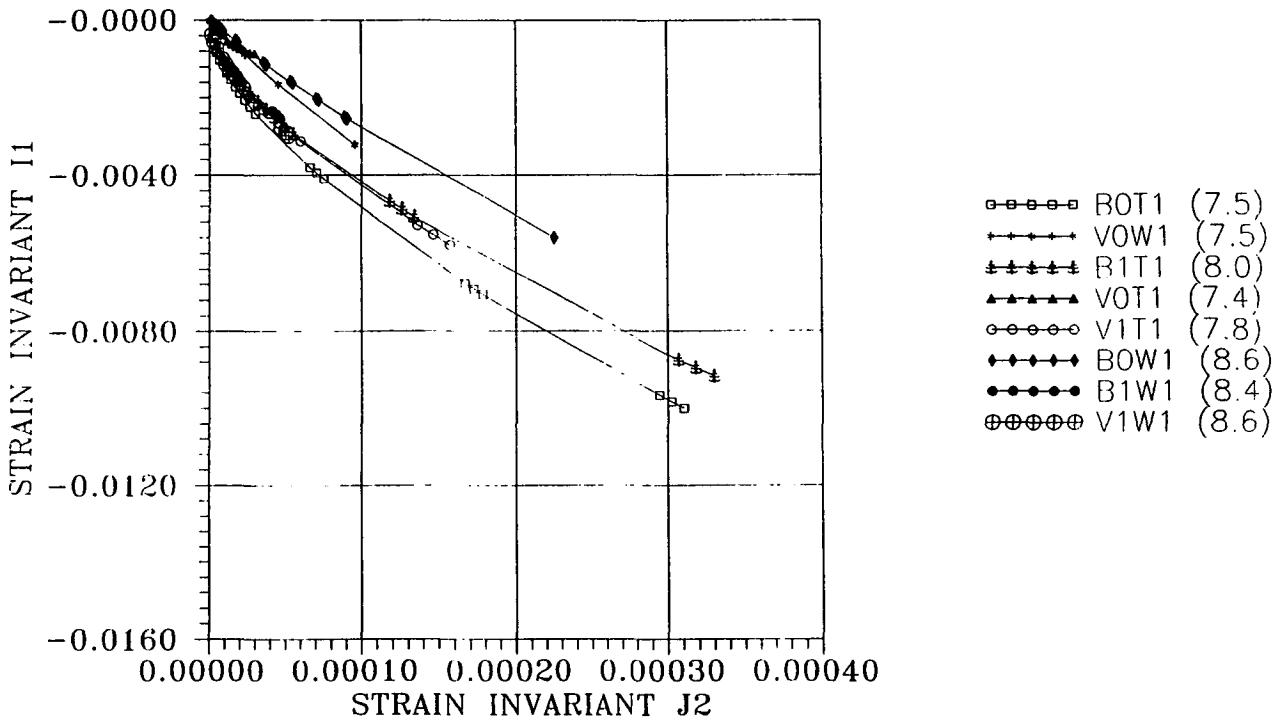

Figure 3.53. Strain invariants I_1 versus J_2; repeated axial load, 105 kPa (15 psi), at 60°C (140°F); confining pressure, 0 kPa (0 psi); high void content

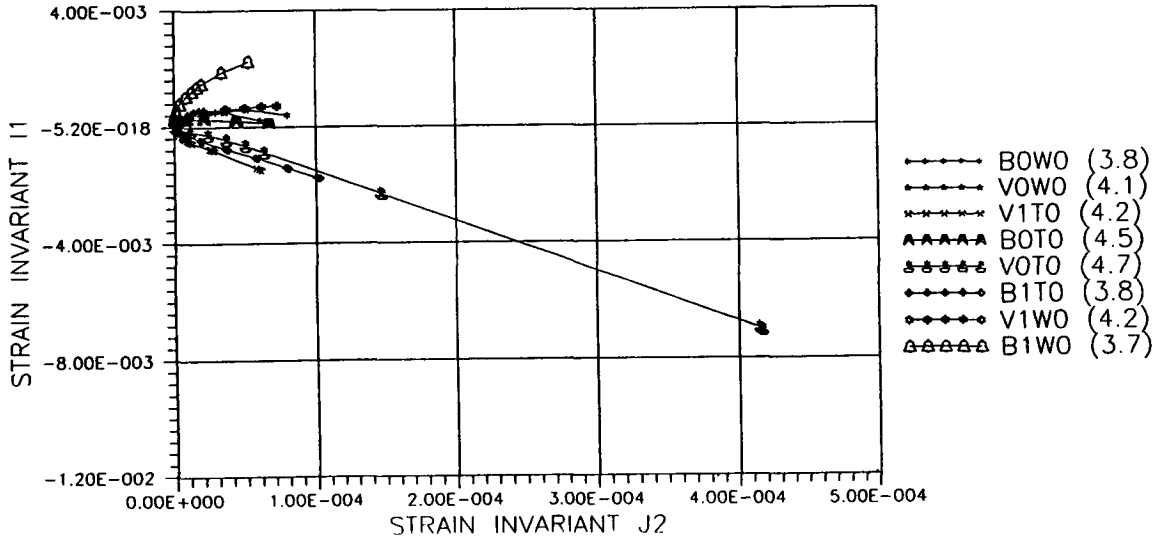

Figure 3.54. Strain invariants I_1 versus J_2; repetitive axial load, 105 kPa (15 psi), at 60°C (140°F); confining pressure, 0 kPa (0 psi); low void content

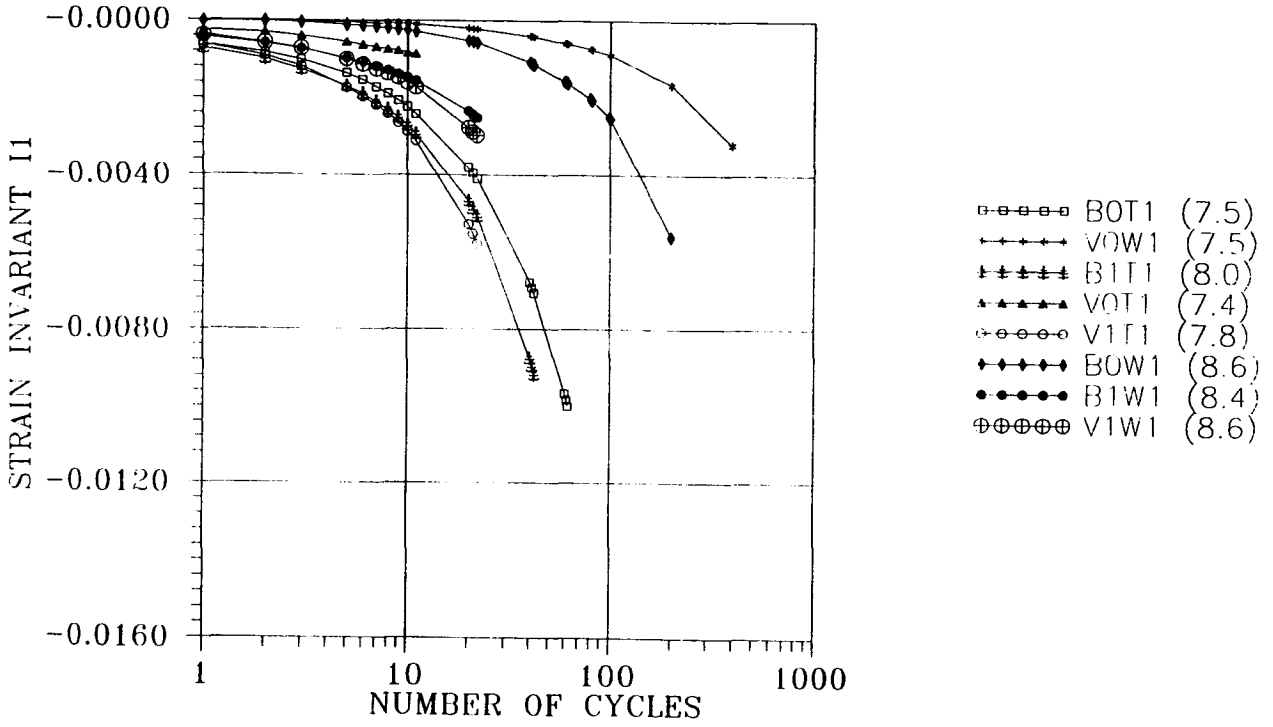

Figure 3.55. Strain invariant I_1 under repetitive axial load, 105 kPa (15 psi), at 60°C (140°F); confining pressure, 0 kPa (0 psi); high void content

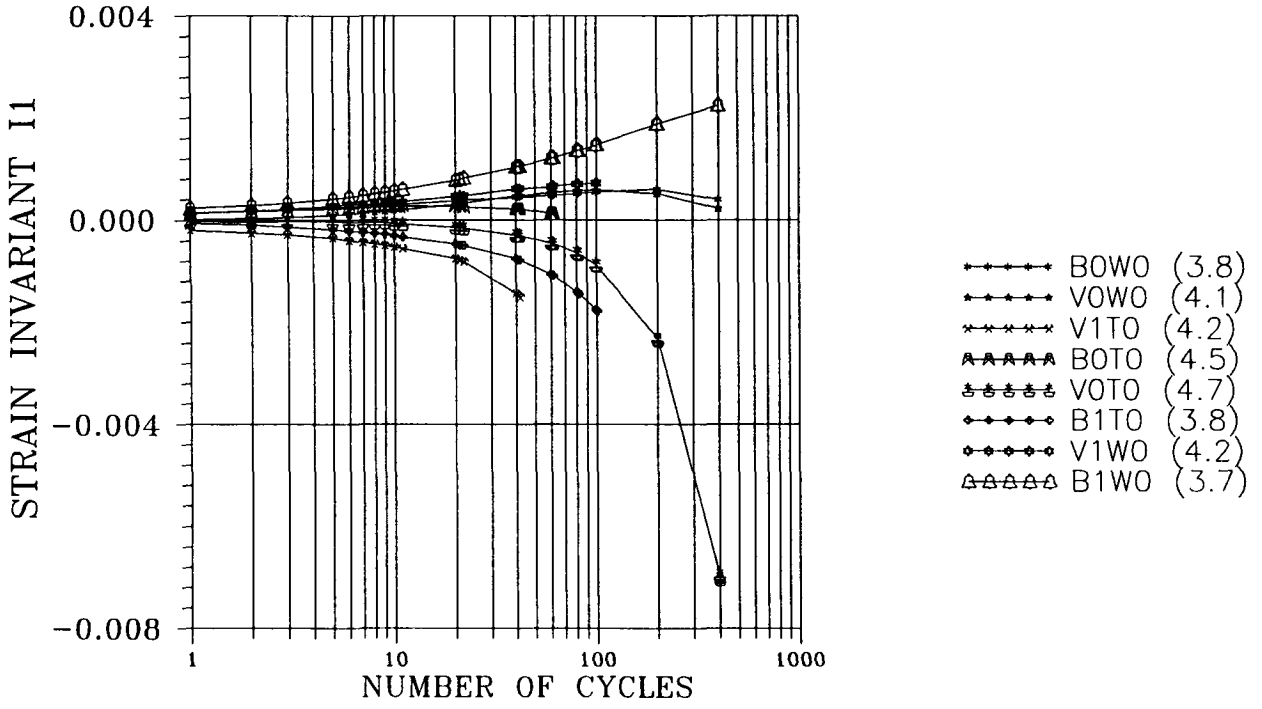

Figure 3.56. Strain invariant I_1 versus number of stress applications; repeated axial load, 105 kPa (15 psi), at 60°C (140°F); confining pressure, 0 kPa (0 psi); low void content

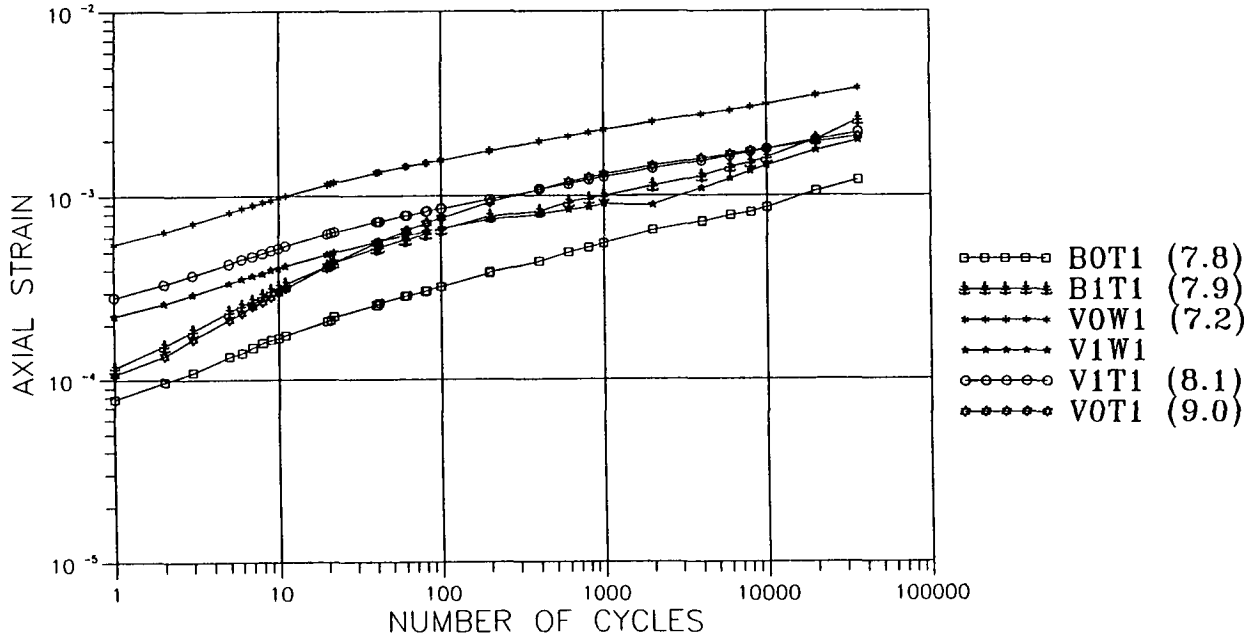

Figure 3.57. Axial strain under repetitive axial load, 105 kPa (15 psi), at 60°C (140°F); confining pressure, 105 kPa (15 psi); high void content

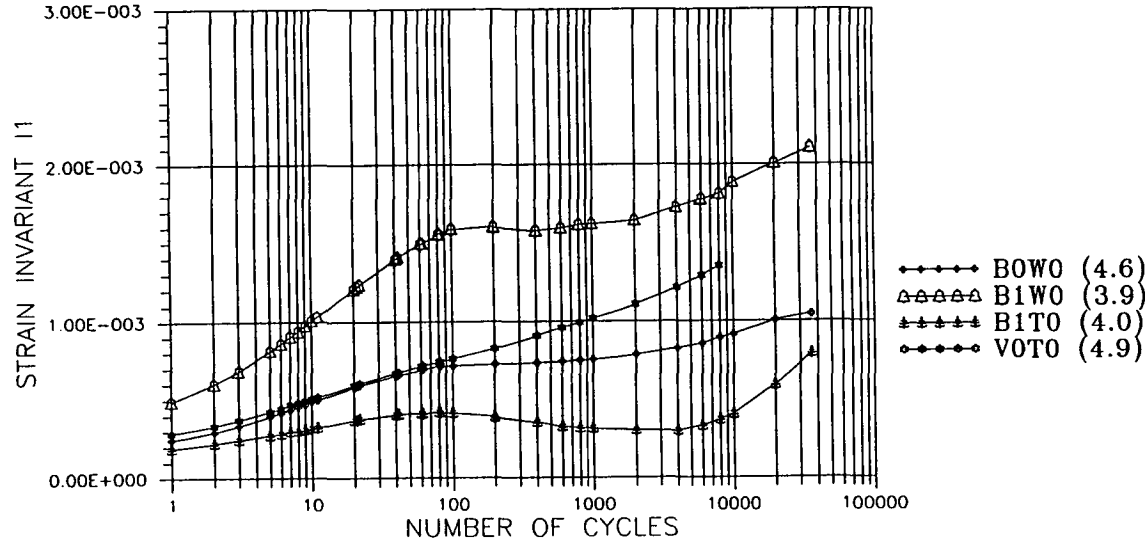

Figure 3.58. Strain invariant I_1 under repetitive axial load, 105 kPa (15 psi), at 60°C (140°F); confining pressure, 105 kPa (15 psi); low void content

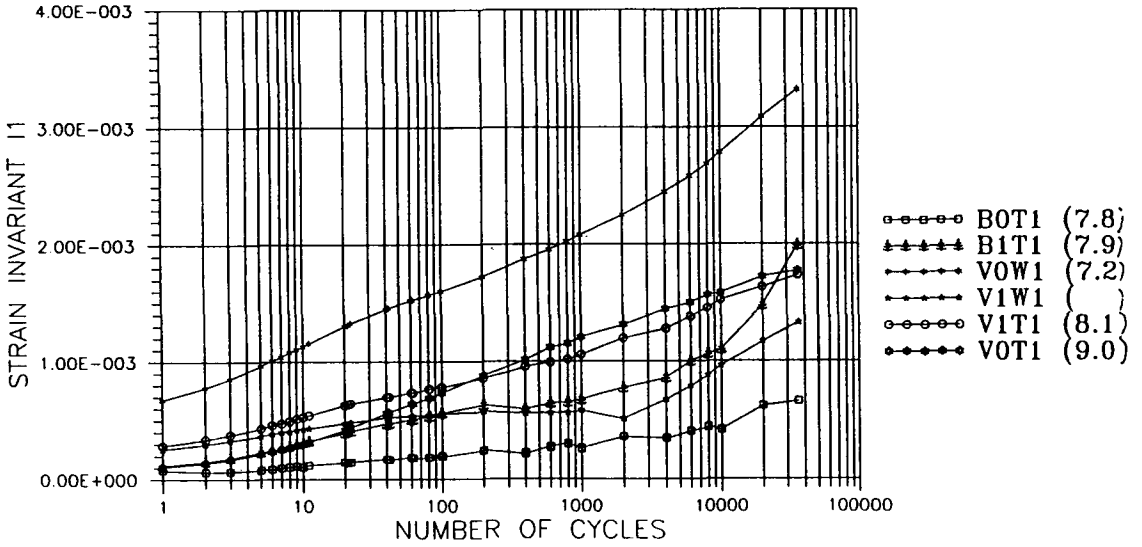

Figure 3.59. Strain invariant I_1 under repetitive axial load, 105 kPa (15 psi), at 60°C (140°F); confining pressure, 105 kPa (15 psi); high void content

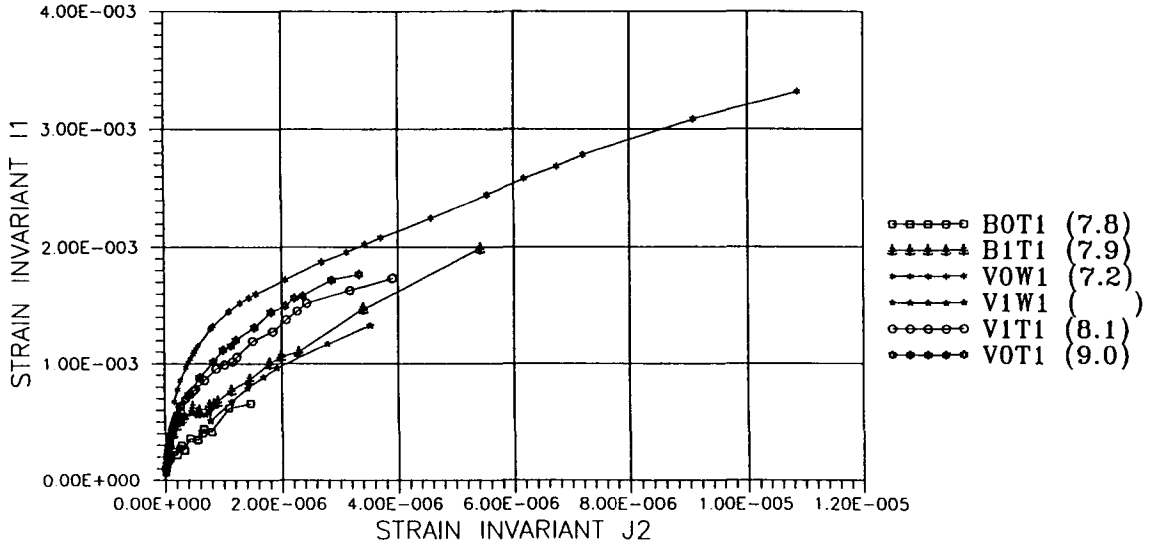

Figure 3.60. Strain invariants I_1 versus J_2 under repetitive axial load, 105 kPa (15 psi), at 60°C (140°F); confining pressure, 105 kPa (15 psi); high void content

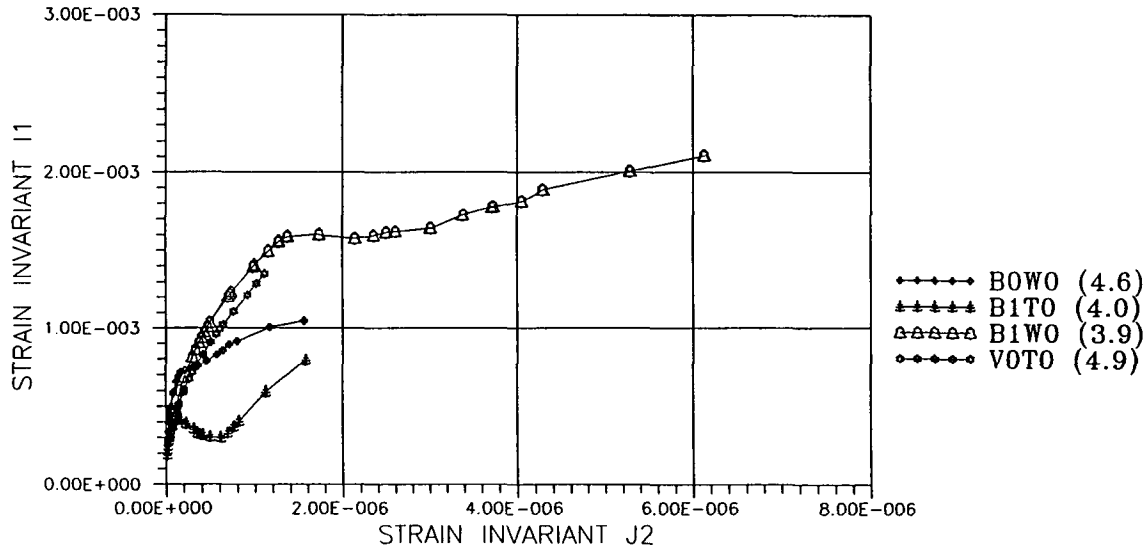

Figure 3.61. Strain invariants I_1 versus J_2 under repetitive axial load, 105 kPa (15 psi), at 60°C (140°F); confining pressure, 105 kPa (15 psi); low void content

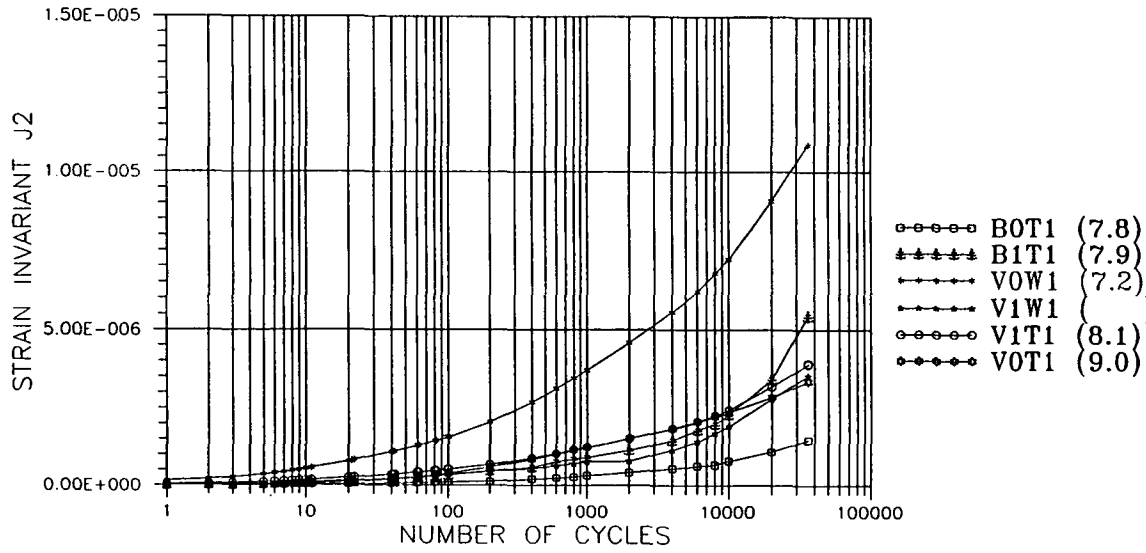

Figure 3.62. Strain invariant J_2 under repetitive axial load, 105 kPa (15 psi), at 60°C (140°F); confining pressure, 105 kPa (15 psi); high void content

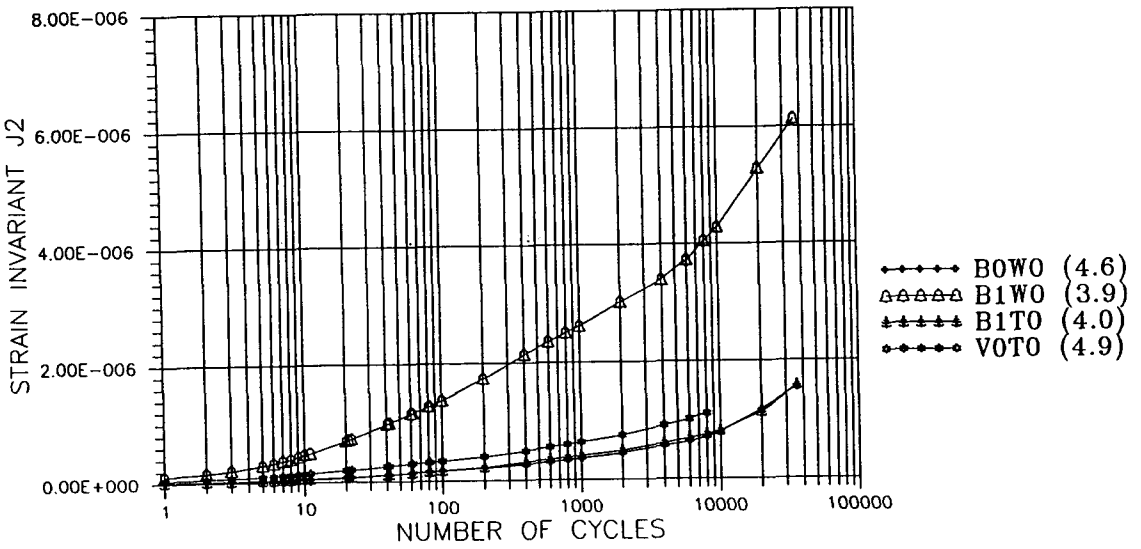

Figure 3.63. Strain invariant J_2 under repetitive axial load, 105 kPa (15 psi), at 60°C (140°F); confining pressure, 105 kPa (15 psi); low void content

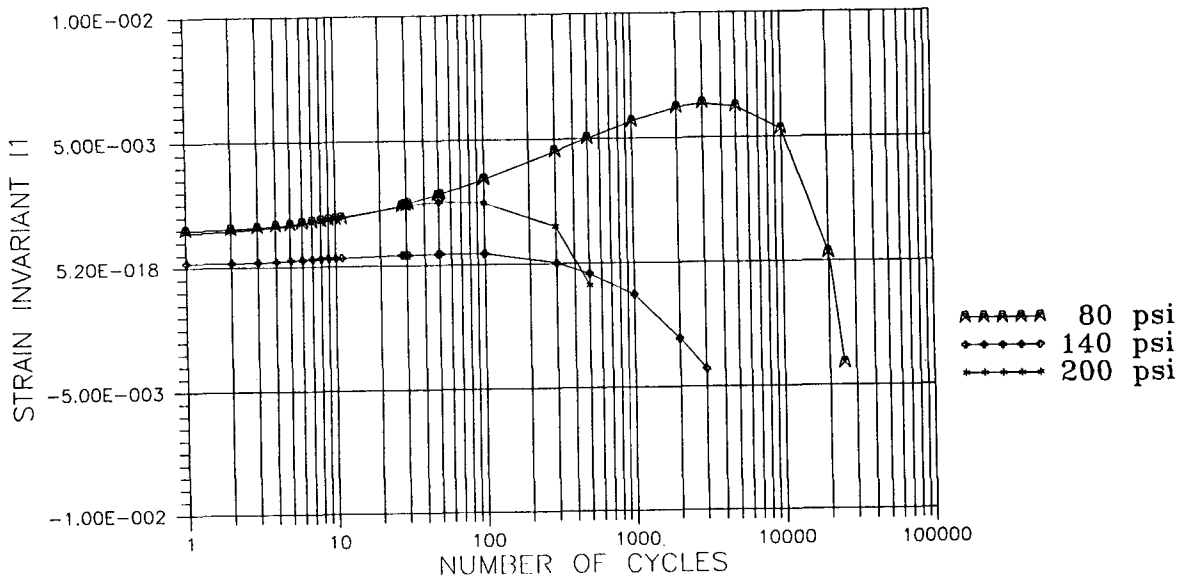

Figure 3.64. Strain invariant I_1 under repetitive axial load at 40°C (104°F); confining pressure, 105 kPa (15 psi)

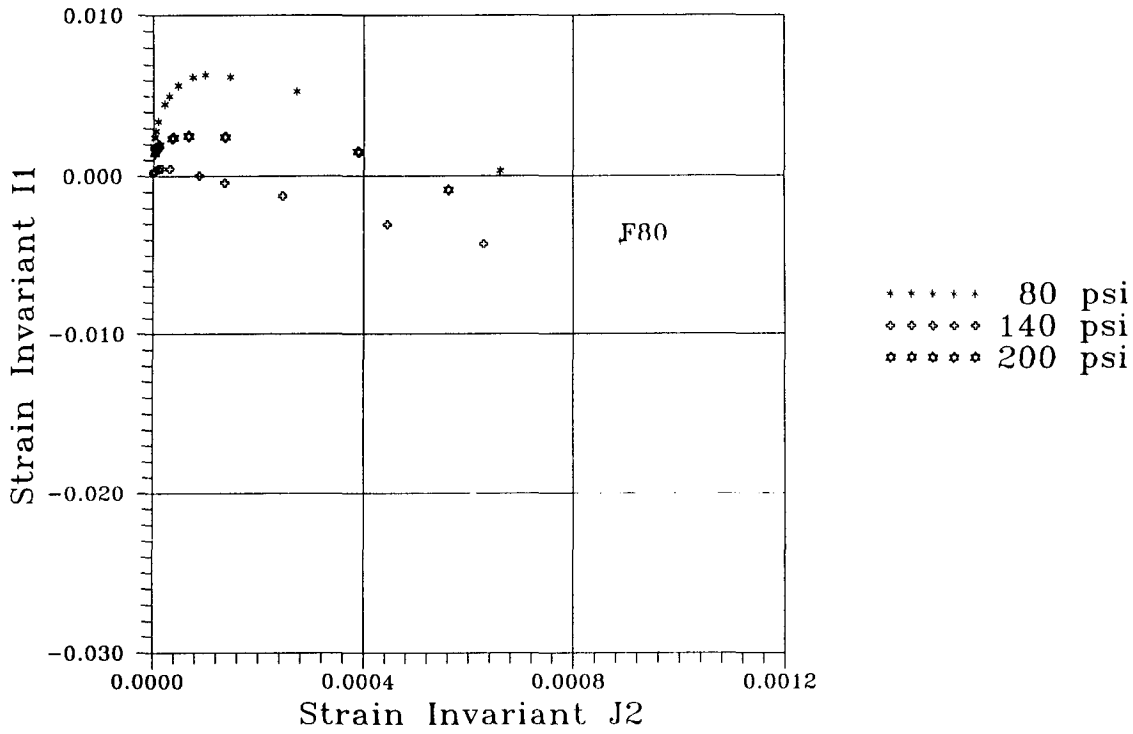

Figure 3.65. Strain invariants I_1 versus J_2 under repetitive axial load at 40°C (104°F); confining pressure, 105 kPa (15 psi)

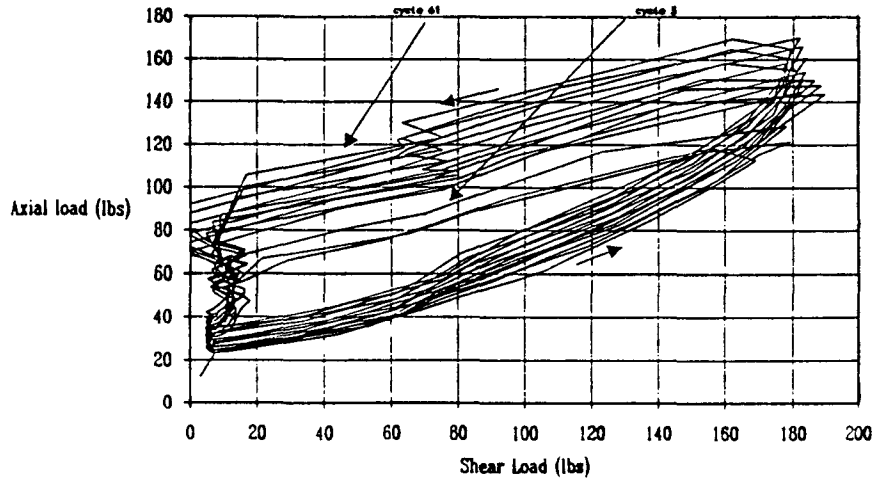

Figure 3.66. Variation of the axial load with the shear load (constant height test)

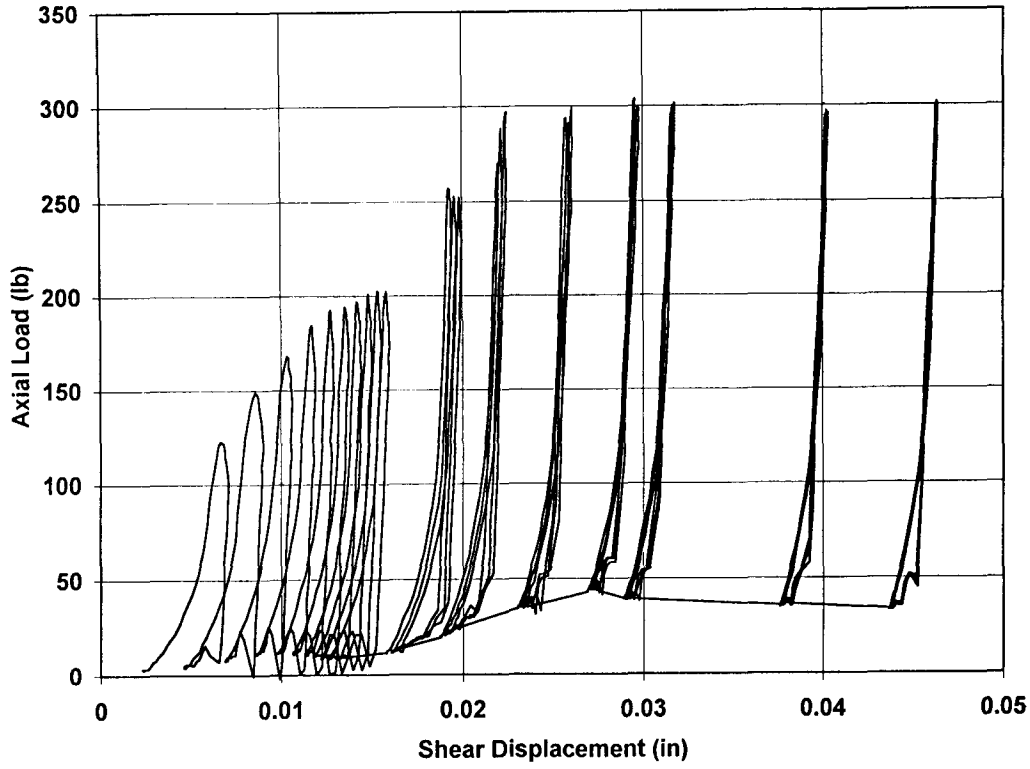

Figure 3.67. Variation of the axial load with the shear displacement (constant height test)

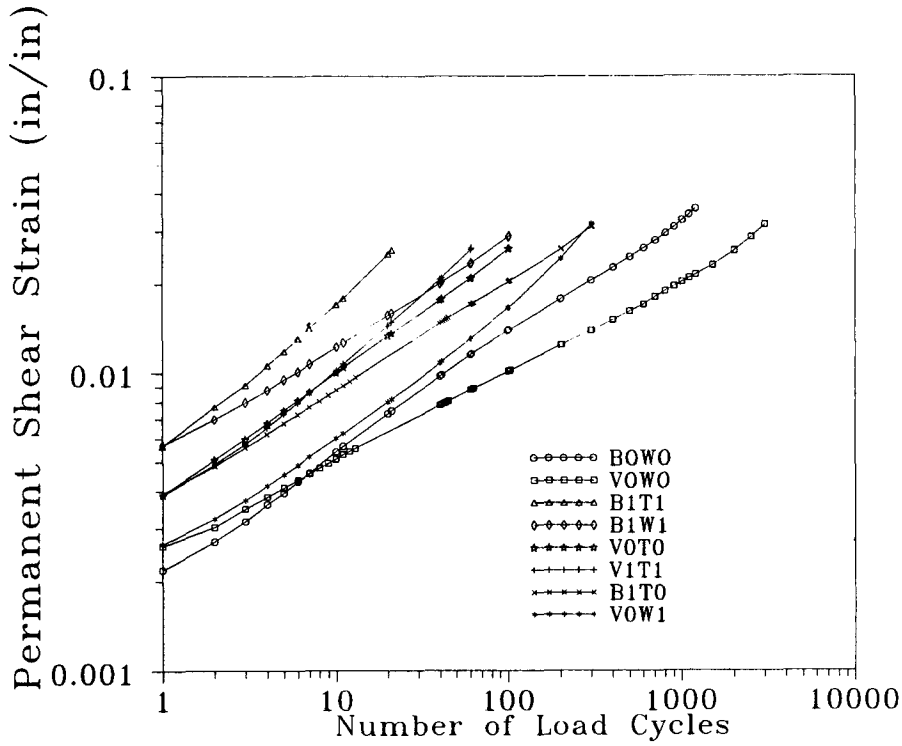

Figure 3.68. Permanent shear strain versus number of load repetitions under repetitive shear at 60°C (140°F) (constant height test)

strain but also on the slope of the line, suggesting that the repetitive shear test may be more sensitive to mix properties than the unconfined repeated axial load test. Figure 3.69 illustrates the variation of I_1 as a function of J_2.

3.4 Test Program at North Carolina State University

As described earlier, the factors investigated at NCSU using the VESYS type test (FHWA 1978) included aggregate type, aggregate gradation, asphalt type, air void content, temperature, and applied stress level. The tests at 40°C (104°F) were performed at axial stress levels of 70 and 140 kPa (10 and 20 psi). At 60°F (140°F), however, only one stress level — 70 kPa (10 psi) — was used since the majority of the specimens failed at an early stage at the 140 kPa (20 psi) stress level.

Specimens, 10 cm (4 in.) in diameter by 20 cm (8 in.) high, were prepared using the Gyratory Testing Machine developed by the U.S. Army Corps of Engineers (ASTM D3387). Uniaxial, incremental, static creep tests were performed using a servo-hydraulic loading system. Details of the test procedure and an analysis of the results performed by the NCSU investigators are contained in Kim et al. (1992).

Although 80 specimens were tested, alpha and mu (α and μ) values were reported for only 65. The ranges in values for alpha and mu were as follows: 0.356 to 0.874; and 0.302 to 2.367, respectively. The average value of alpha was 0.722. For mu the average was 0.843. As shown in Figure 3.70 both alpha and mu are relatively insensitive to changes in air void content. Using various combinations of the minimum, maximum and mean values of alpha and mu, rut depths were calculated using the FHWA's VESYS program. The rut depth calculations were based on the pavement structure shown in Figure 3.71. In addition to alpha and mu, input to the VESYS program included the following; load radius of 4.62 inches; tire pressure of 105 lb/in^2 and 10 million axle loads (80 kN) over 10 years. As illustrated in Figure 3.72, rut depth ranged from approximately 0.1 inch to 800 inches. Unlike alpha and mu which are relatively insensitive to mix parameters, the rut depth calculations are extremely sensitive to alpha and mu. Given the time and budget constraints and the preliminary data analysis, this approach was eliminated from further consideration.

3.5 Test Program at SWK Pavement Engineering/University of Nottingham

The results of this test program are described in the report titled *An Evaluation of the Wheel-Tracking Test as a Means of Assessing Resistance to Permanent Deformation* by J. M. Gibb, P. S. Fell, and S. F. Brown, SWK Pavement Engineering Ltd, UK, September 1991. This section includes a brief summary of that report.

The test program at SWK/UN was designed to provide a set of results for mixes associated with the factorial design and which might serve as relative indicators of performance to be

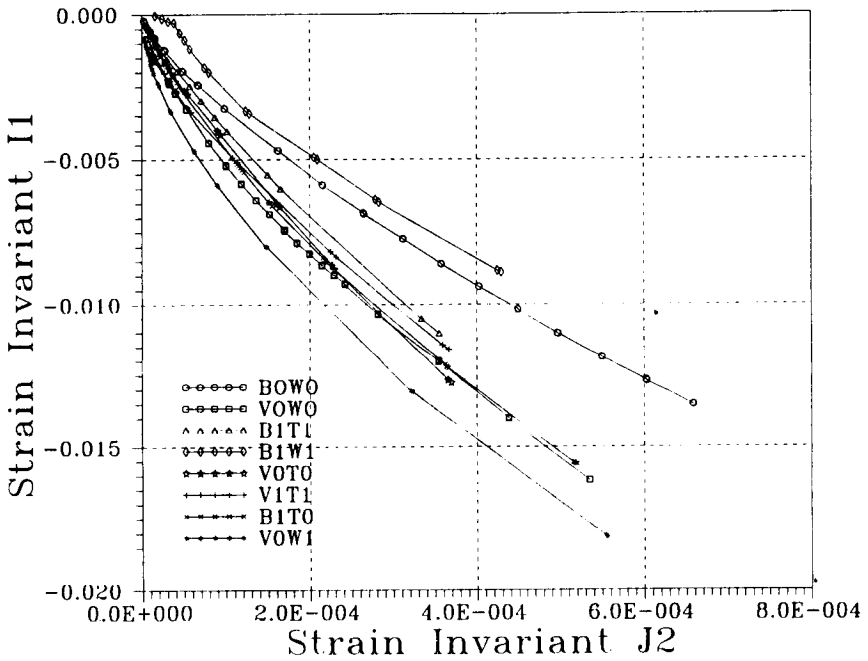

Figure 3.69. I_1 versus J_2 in repetitive shear (constant height) at 60°C (140°F)

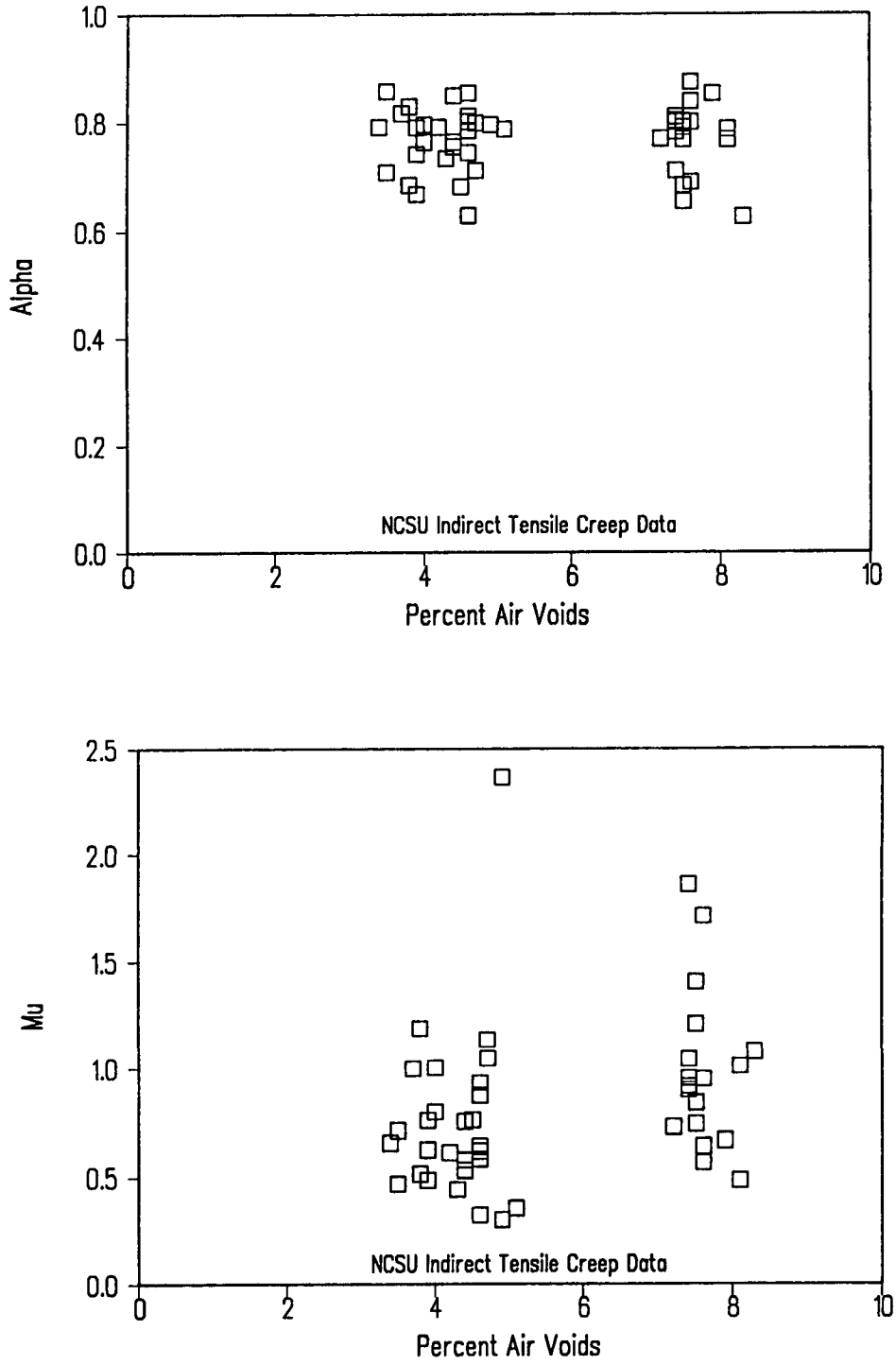

Figure 3.70. Alpha and mu as a function of air void content

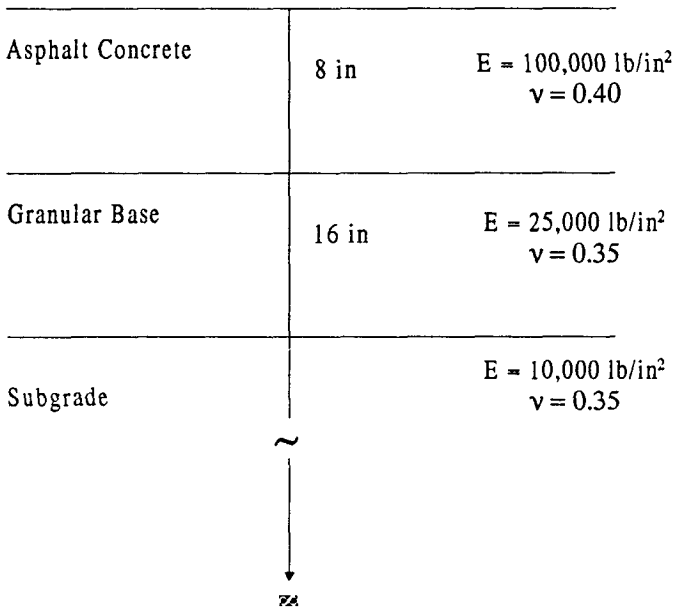

Figure 3.71. VESYS pavement structure

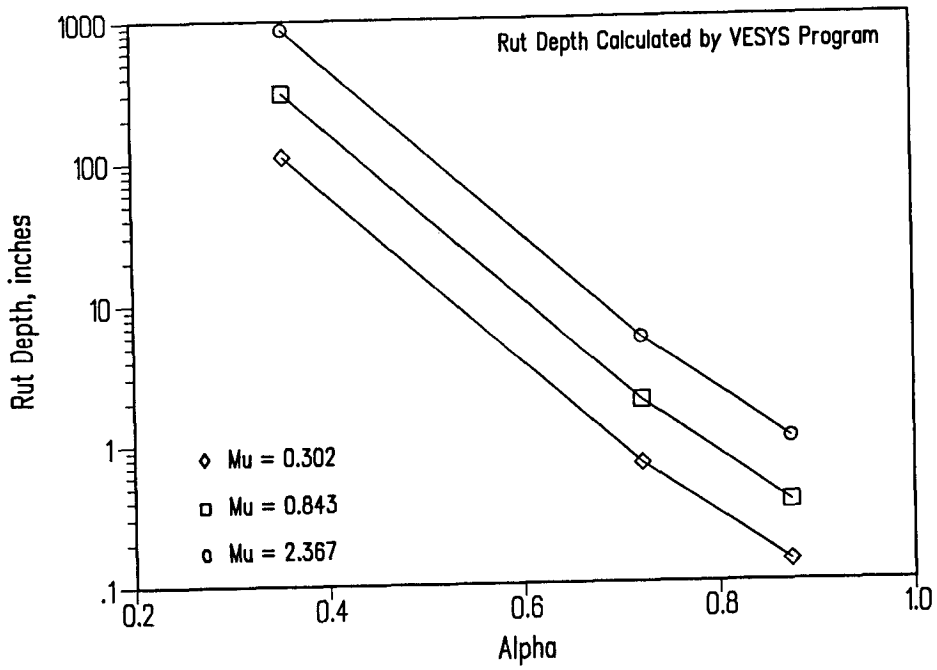

Figure 3.72. Rut depth calculation by VESYS program

expected of mixes tested at NCSU and UCB; that is, to ensure that the procedure selected would order the mixes in an appropriate manner.

The wheel-tracking apparatus used to test slab specimens prepared by rolling wheel compaction is illustrated schematically in Figure 3.73. Table 3.9 contains a listing of the asphalt contents used for the various mixes as well as a UCB mix reference; Table 3.10 lists the variables evaluated in the program. Tests were conducted at one temperature, 40°C (104°F), as noted earlier.

Results of tests on four slabs are shown in Figure 3.74 under the condition of low stress (650 kPa [95 psi]). Rutting rate rather than rut depth has been selected as the parameter to assess performance. This parameter is defined as the gradient of the rut depth versus N relationship over the range 2000 to 4000 passes and was selected to eliminate the effects of start-up errors. Since the rate of tracking was constant, 42 passes per minute, the rutting rate could be expressed in mm/hr. In addition, the rutting rate was normalized by dividing by the contact pressure (since two contact pressures were utilized).

A summary of the results for the eight mixes tested is shown in Table 3.11. Results of the test program were generally as expected, with mixes containing aggregate RB performing better (lower rutting rates) than those with aggregate RL.

While the wheel-track test is useful to compare the relative performance of mixes, the test was not considered further for use in a mix design and analysis since it does not permit a prediction of permanent deformation in situ. It should be noted, however, that this test has been used as a part of the binder validation activities and additional test results on a total of 64 different mixes will be described in Part II of this report.

3.6 Findings and Recommendations

The primary purpose of this investigation was to identify a suitable test or tests to characterize the permanent deformation response of asphalt aggregate mixes. This section summarizes the principal findings and recommendations regarding such a procedure.

3.6.1 Findings Based on Tests at University of California at Berkeley

The test program at UCB included tests in both the axial and shear modes of loading. Test conditions encompassed creep, repeated loading (pulse or haversine load form), and sinusoidal loading in compression and shear, all at various conditions of confining pressure (up to 210 kPa [30 psi]). With the exception of the sinusoidal loading tests (to measure stiffness), the testing was accomplished at temperatures of 40°C and 60°C (104°F and 140°F).

- Results of the limited series of *isotropic confining pressure tests* suggest that it may be reasonable to assume, for permanent deformation determinations, isotropic properties for asphalt aggregate mixes even though all mixes may not

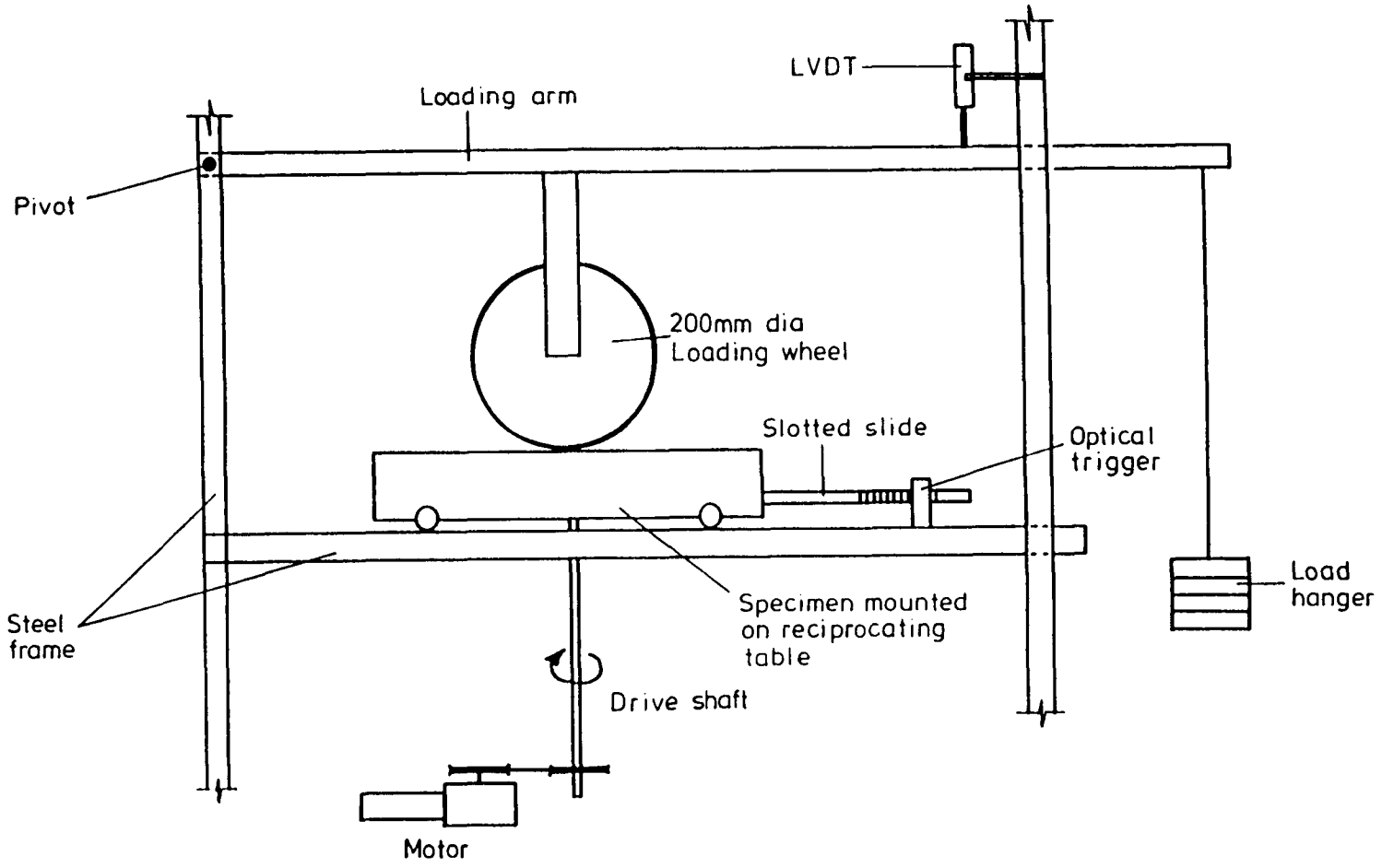

Figure 3.73. Schematic representation of wheel tracking apparatus

Table 3.9. Asphalt contents used in specimen manufacture

Aggregate	Asphalt	Asphalt Content % by Mass of Mix	UCB Mix Reference
RL	AAG	4.1	V0T
RL	AAG	4.8	V1T
RL	AAK	4.3	B0T
RL	AAK	5.0	B1T
RB	AAG	4.9	V0W
RB	AAG	5.5	V1W
RB	AAK	5.1	B0W
RB	AAK	5.7	B1W

Table 3.10. Variables evaluated in test program

Variable	Possible Values	Reference Code	Remarks
Asphalt Type	AAK	B	MRL Reference AAK
	AAG	V	MRL Reference AAG
Asphalt Content	Optimum	0	See Table 3.9
	High	1	See Table 3.9
Aggregate Type	RL	T	MRL Reference RL
	RB	W	MRL Reference RB
Aggregate Gradation	Medium	M	See Table 3.2
	Coarse	C	See Table 3.3
Air Void Content	Low	0	4%
	High	1	8%
Stress Level	Low	0	650 kPa
	High	1	950 kPa

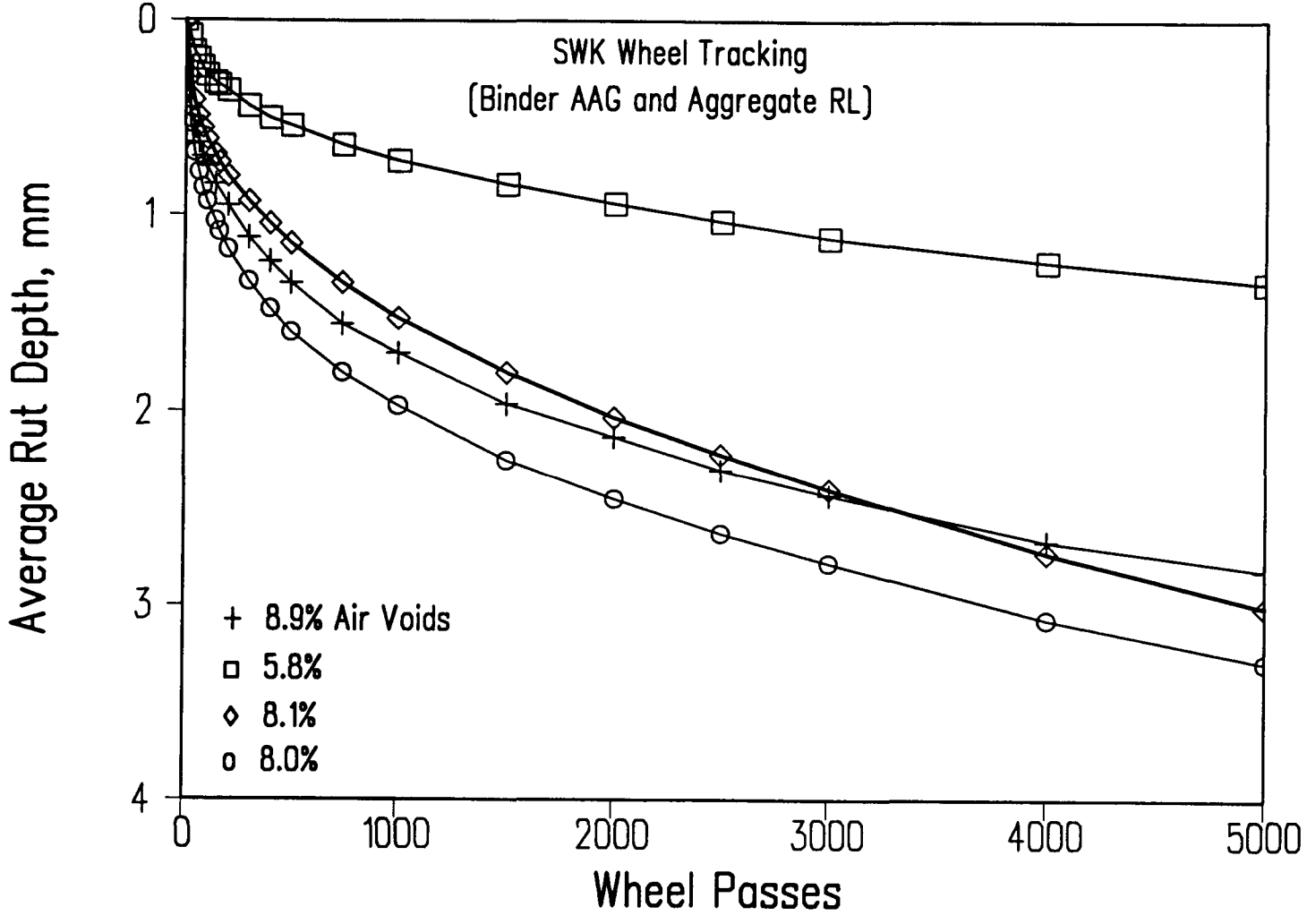

Figure 3.74. A-003A deformation wheel-tracking

Table 3.11. Normalized rutting rate from SWK/Nottingham deformation wheel-tracking tests

UCB Mix Reference	Normalized Rutting Rate (m/GPa.hr)	Standard Deviation (m/GPa.hr)	Coefficient of variation (percent)
B0T (AAK/RL)	0.320	0.138	43.1
B1T (AAK/RL)	0.524	0.312	59.5
V0T (AAG/RL)	1/163	0.274	23.6
V1T (AAG/RL)	1.460	0.456	31.2
B0W (AAG/RB)	0.224	0.121	54.0
B1W (AAK/RB)	0.310	0.236	76.1
V0W (AAK/RB)	0.499	0.182	36.5
V1W (AAG/RB)	0.686	0.186	27.1
		Average	43.9

exhibit such response. Thus, the constitutive relationship to be developed will include this assumption. (N.B., to attempt to incorporate anisotropy in a model at this time, in the light of other important and complex response characteristics, does not appear reasonable from an engineering standpoint.)

- At temperatures of 40°C (104°F) and above, the deformation response of the asphalt aggregate mixes tested was significantly influenced by confining pressure. Thus, a permanent deformation constitutive relationship to be developed must reflect this phenomenon, which has been termed herein *stress hardening*.

- Results of both the creep and repeated load tests indicated significant amounts of permanent deformation upon unloading relative to the total deformation. The nature of the permanent deformation is described in Part II of this report. Nevertheless, the data indicate that it is important that a permanent deformation constitutive relationship include a mechanism to reflect *nonrecoverable deformation* upon unloading.

- Results of creep and repeated load tests in both the axial and shear modes of loading have shown, for comparable times of loading, that more permanent deformation is obtained in repeated loading than in creep for the same stress conditions. A permanent deformation constitutive relationship must therefore reflect this difference.

- *Dilation* was observed in both the axial and shear tests at the temperatures of 40°C and 60°C (104°F and 140°F). This phenomenon, which is strain related, is dependent on a number of factors, including stress state and

aggregate structure. Its influence can normally be neglected at low temperatures because the asphalt aggregate mix is so stiff that conventional traffic loads are not sufficient to generate strains large enough to mobilize the dilational component. However, at higher temperatures, where strains can be significantly higher, dilation becomes an important aspect of permanent deformation response and must be incorporated in any constitutive relationship developed to define this response.

- While there is some evidence of a *threshold strain*, based on results obtained in the axial and shear creep tests, (i.e., a strain level of 1 to 2 percent beyond which the rate of development of strain with time increased more rapidly, this threshold level was not observed in repeated load tests or in the creep tests under conditions of high confinement. The magnitude of the threshold strain may be influenced by test configuration and stress state as well as by mode of loading (i.e., creep versus repeated load). Moreover, this condition may be associated with another failure mode (e.g., micro-cracking or fracture) rather than permanent deformation.

- Results of stiffness measurements from the creep and repeated load tests suggest, for small values of strain, that the stiffness moduli of asphalt aggregate mixes are relatively independent of stress level. Similar results were obtained from dynamic sinusoidal loading tests. These latter tests also indicate that the concept of time-temperature superposition is applicable (i.e., the mixes can be considered to be thermorheologically simple in response) to a reasonable degree. Thus, it appears reasonable to assume, so long as deformations are small, that the stiffness/modulus characteristics of asphalt aggregate mixes can be represented as *thermorheologically simple and linear viscoelastic* when defining the effects of time of loading and temperature. This too must be incorporated in any constitutive relationship to represent the permanent deformation characteristics.

3.6.2 Findings Based on Tests at North Carolina State University

The test program at NCSU included only repeated creep tests (VESYS type) on mixes associated with the factorial design. Results of the tests suggested that the parameters developed from the tests (α, μ) were not sensitive to mix parameters. Accordingly, this test and the associated methodology were eliminated from further consideration.

3.6.3 Findings Based on Tests at SWK Pavement Engineering/University of Nottingham

The test program at SWK/UN was designed to provide results on mixes associated with the factorial design that might serve as relative indicators of the performance to be expected of mixes tested at NCSU and at UCB; that is, to ensure that the procedure selected would order

the mixes in a similar manner. The results were generally as expected with mixes containing aggregate RB performing better than those with aggregate RL and those containing asphalt AAK-1 performing better than mixes with asphalt AAG-1. Since the test provided a reasonable differentiation of mixes in terms of rutting performance it was decided to use this test for validation of the SHRP binder specification criteria.

3.7 Recommendations

As the test program at UCB developed and experience was gained with the shear test, the decision was made to utilize this test for measuring the permanent deformation characteristics of asphalt aggregate mixes. The following paragraphs delineate the reasons for this choice.

The results of the literature evaluation stressed the importance of considering directly the effect of shear stresses on the accumulation of permanent deformation. Additional analysis of representative pavement structures indicated that states of stress in the upper part of the pavement near the tire edge could best be defined with a test where both the normal and shear stresses could be controlled independently of each other.

While one might argue that an axial loading test is sufficient to define the state of stress directly beneath the tire, it is not possible to duplicate, with such a test, the conditions of stress elsewhere in such a manner as to directly measure their influence. With the simple shear test it is possible to directly measure the effects of a specific stress state.

With today's developments in servo-hydraulic loading and computer control, simultaneous application of shear and normal stresses is feasible and can be accomplished in a practical manner. Hence, equipment limitations no longer preclude the use of such a test.

The importance of the dilation characteristics of a mix on permanent deformation response has been stressed. The simple shear test provides a more direct measure of the dilation characteristics of a mix than an axial loading test since the normal force generated as the specimen tends to dilate under shear stress application can be directly measured in the simple shear test.

Specimen size and configuration also influenced the decision to select the shear test. For conventional mixes (nominal 2.5 cm [1 in.] maximum size aggregate) it is desirable to have test specimens that are at least 10 cm (4 in.) and preferably 15 cm (6 in.) in diameter. With a 15 cm (6 in.) diameter specimen, an axial loading test would require at least a 15 cm (6 in.) specimen height (with polished end surfaces) and preferably a 30 cm (12 in.) height, i.e., a height diameter ratio of 2 to 1 to minimize end effects on material response. On the other hand, a 15 cm (6 in.) diameter specimen for the simple shear test could have a height in the range of 5 to 7.5 cm (2 to 3 in.) and provide reasonable results as shown in Part II.

With large stone mixes, specimens of the order of 10 cm (8 in.) in diameter are desirable. Considering the requirements stated above, this makes the simple shear test even more appealing.

Thus, while the experimental program at UCB did not follow exactly the planned partial factorial described at the outset, the information gained from each series of experiments led to the conclusion that the simple shear test would provide the best opportunity to define the permanent deformation characteristics of asphalt aggregate mixes in order to reflect the important characteristics defined by the various tests performed, including the following:

- dilation under shear loading;
- increase in stiffness with increase in hydrostatic pressure;
- negligible volumetric creep;
- residual permanent deformation on removal of load; and
- temperature and rate of loading dependence.

It was also concluded that none of the existing analysis procedures for pavement response to load would reflect the type of behavior described above. Thus, it was deemed necessary to develop a constitutive relationship for asphalt aggregate mixes, reflecting the above-noted characteristics, which would be compatible with a three-dimensional finite element representation of typical pavement structures, permitting, in turn, the estimation of the accumulation of permanent deformation under repetitive traffic loading. At the same time, it was also necessary to develop the test equipment and procedures which define the parameters contributing to the permanent deformation response of asphalt aggregate mixes.

Part II — Development of Permanent Deformation Tests and Associated Analyses; Extended Test Program

J. B. Sousa
S. L. Weissman
J. A. Deacon
J. Harvey
G. Paulsen
C. L. Monismith

4

Introduction

4.1 Background

A primary objective of Strategic Highway Research Program (SHRP) Project A-003A, titled, *Performance Related Testing and Measuring of Asphalt Aggregate Interactions and Mixtures*, was to develop a series of accelerated performance tests (APTs) for asphalt aggregate mixes and methods for analyzing asphalt aggregate interactions that significantly affect pavement performance.

Part I of this report, titled, "Test Method Selection," recommended the simple shear test as the best method to define the permanent deformation characteristics of asphalt aggregate mixes reflecting the literature evaluation and testing conducted in the initial test program.

Part II describes the laboratory studies conducted as part of SHRP Project A-003A in support of the following:

- development of a constitutive relationship to define the permanent deformation response of asphalt aggregate mixes;
- development of test procedures using the simple shear test to measure permanent deformation response;
- validation of A-002A hypotheses for permanent deformation; and
- limited validation of the simple shear tests for permanent deformation assessment and prediction.

This report starts with a brief description of the equipment that was developed to permit the execution of the new tests.

4.2 Objectives

The objective of this report is to document the results of the various phases of permanent deformation testing and analysis of the associated test results under SHRP Project A-003A's extended test program activities.

5

Permanent Deformation Test Equipment

The Universal Testing Machine (UTM) was developed to measure the permanent deformation characteristics of asphalt aggregate mixes. Its comprehensive testing capabilities and accommodation of add-on testing modules permits fatigue and stiffness testing as well as permanent deformation evaluation. A microcomputer system provides feedback closed-loop control to the servo-hydraulic system, confining pressure, test temperature, and data acquisition. The equipment, manufactured as a part of the A-003A contract by James Cox and Sons, Inc., Colfax, California, is shown in Figure 5.1.[3]

The three major components of the UTM are diagrammed in Figure 5.2. In Figure 5.3 the UTM is schematically represented with the simple shear module in place.

A simple shear device, developed for another research project under the auspices of the Civil Engineering Department at Berkeley, served as the prototype for the UTM. This device, Figure 5.4, was also used to conduct a number of tests, the results of which have been used in this investigation.

The next section describes the elements of the UTM and the methodology used to prepare specimens for testing in the UTM.

5.1 Universal Test Machine

The Universal Test Machine is illustrated schematically in Figures 5.2 and 5.3. The testing equipment can perform the following tests:

- dynamic loading — axial and shear loading, with or without confining pressure;

[3]Functional specifications for the equipment may be obtained from the Federal Highway Administration (FHWA) Office of Technology Applications.

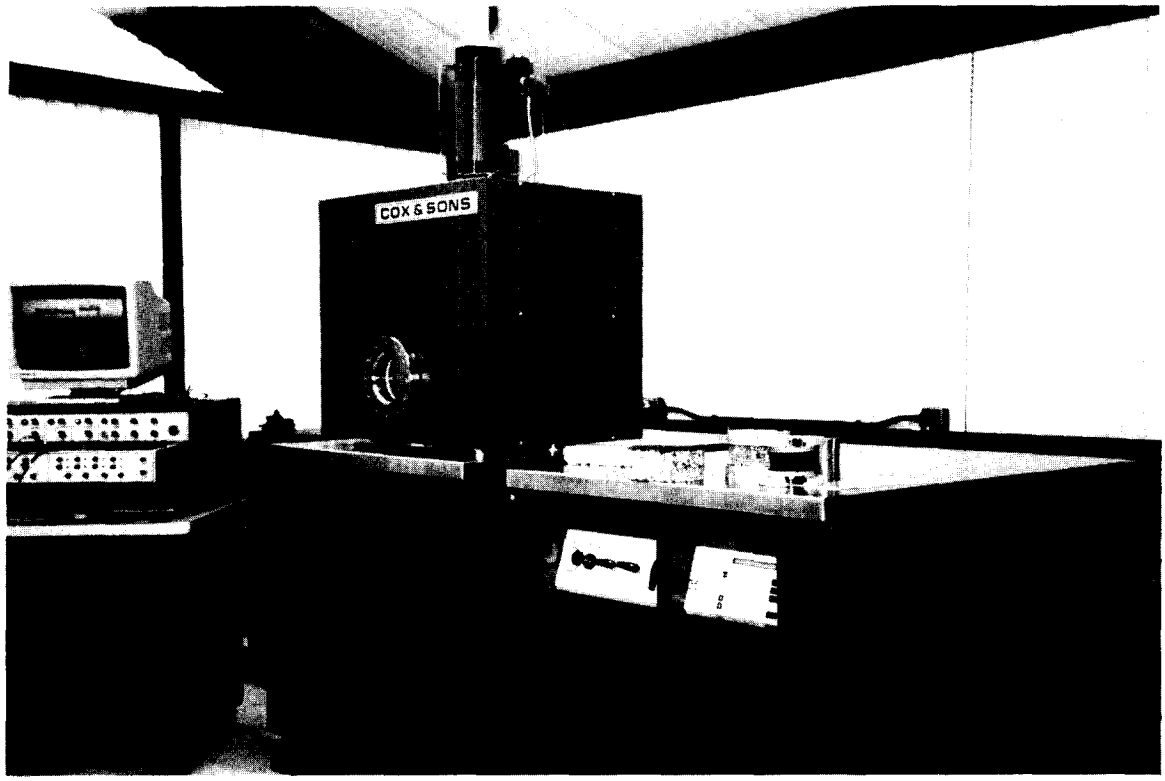

Figure 5.1. Universal Test Machine fabricated by Cox and Sons

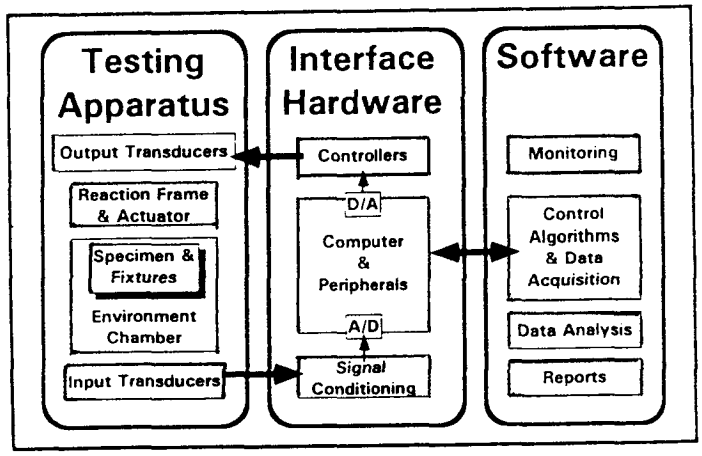

Figure 5.2. Components of UTM

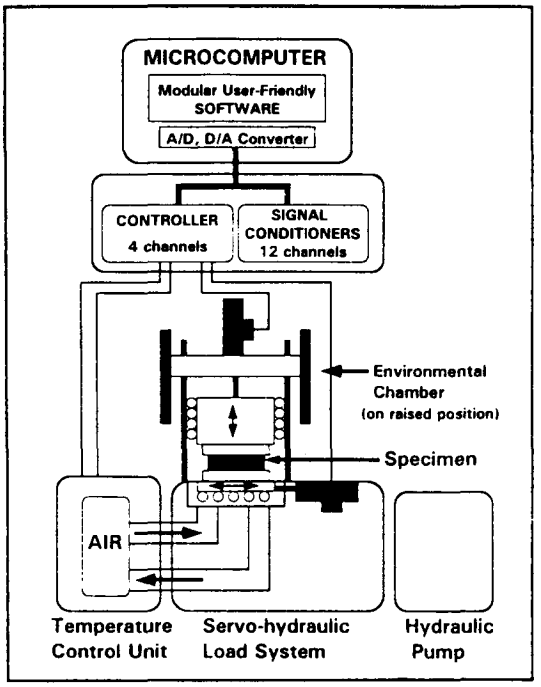

Figure 5.3. UTM schematic

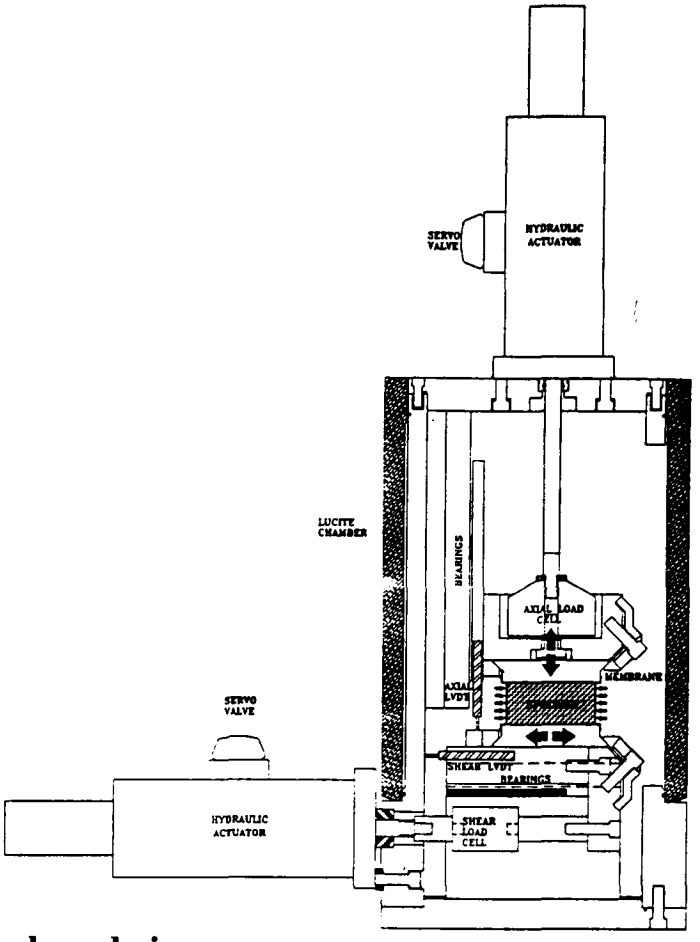

Figure 5.4. Simple shear device

- creep loading — axial and shear loading, with or without confining pressure;
- repetitive loading using a haversine wave form — axial and shear loading with or without confining pressure; and
- constant rate of strain or stress application in the axial and shear modes and constant rate of stress application in the radial direction (confining pressure).

The UTM can perform simple shear and axial tests under creep, repetitive, dynamic, and constant rate of deformation modes of loading. For dynamic loading, frequencies from 0.01 to 20 Hz can be applied. The environmental chamber, which can be automatically positioned, can be pressurized and held at a constant temperature between -10°C and 80°C (14°F and 176°F). The maximum confining pressure in the chamber is 690 kPa (100 psi). The maximum axial load of the machine in 45 kN (10,000 lb) and the maximum shear load is 22.5 kN (5000 lb).

Specimens with dimensions of 20 cm (8 in.) in diameter and 30.5 cm (12 in.) high can be accommodated by the UTM. This permits evaluation of mixes with aggregate sizes of 3.8 cm (1.5 in.).

The UTM test modules can accommodate both cylindrical and rectangular shaped specimens. The specimen, which is fitted with aluminum caps, slides easily into the load testing frame. Computer-controlled hydraulic clamps are then activated by computer to firmly secure the caps to the loading heads. This mounting feature was designed to minimize the time spent in specimen alignment and enhances the user-friendly interface with the UTM.

5.2 Testing in Shear Mode

To test in the shear mode, cylindrical specimens, either 15 cm (6 in.) in diameter by 5 cm (2 in.) high or 20 cm (8 in.) in diameter by 7.5 cm (3 in.) high, are obtained by coring from slabs prepared in the laboratory by rolling wheel compaction (Harvey 1991). A special double-bladed saw (Figure 5.5) is used to produce the 5 cm (2 in.) or 7.5 cm (3 in.) high specimens.[4]

[4]Ideally, the specimen diameter-to-height ratio should exceed three to minimize bending effects. Furthermore, finite element analyses (Appendix A) indicate that the error in the estimate of the shear modulus is no more than 10 percent for specimens with a minimum diameter of 15 cm (6 in.). Although a 10 cm (4 in.) diameter specimen having a diameter-to-height ratio greater than or equal to three would minimize the effects of bending, the end effects due to the lack of complementary shear stresses would likely result in an estimate error of the shear modulus greater than 10 percent. Therefore, testing a 15 cm (6 in.) diameter is recommended.

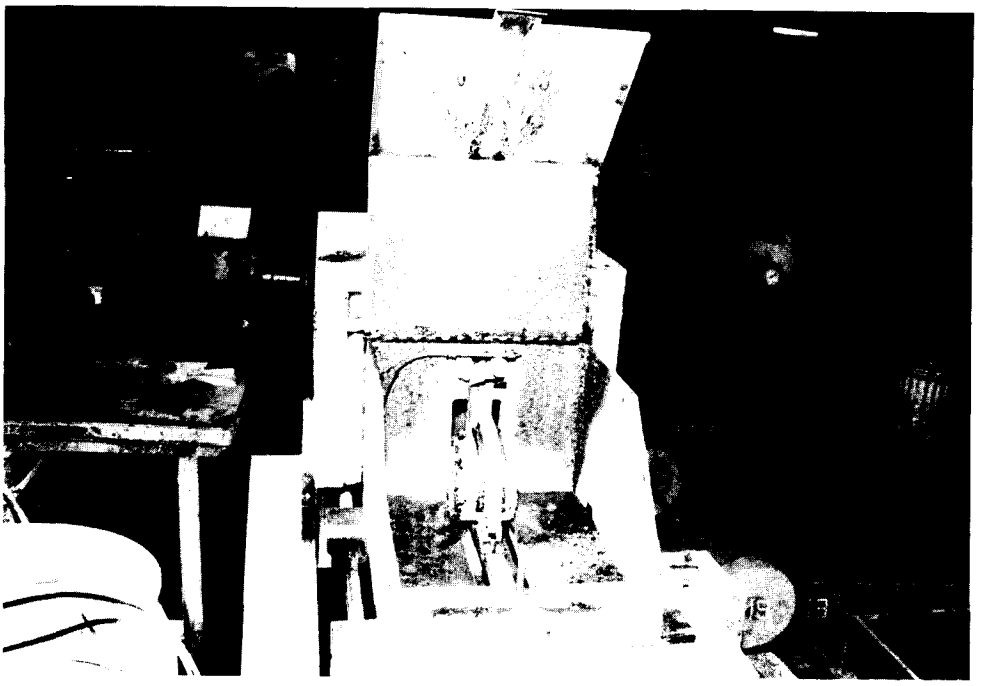

Figure 5.5. Double-bladed saw

The test specimens are glued to aluminum caps, top and bottom, using either an epoxy binder or hydrastone. This process is performed in a special jig to ensure that the end caps are parallel. The equipment, shown in Figure 5.6, is separate from the UTM.

As noted earlier, hydraulic clamps in the UTM permit easy mounting of the shear specimen in the test frame. Figure 5.7 illustrates a specimen with caps in place just prior to placement in the loading system. Also shown in this figure is a linearly variable differential transducer (LVDT) used to measure shear displacements. If confining pressure is required in the test, a latex membrane 0.64 mm (0.025 in.) thick is mounted around the specimen.

The equipment monitors and acquires test data from the following:

- LVDTs mounted inside the two actuators,
- LVDTs and load cells mounted inside the vertical and horizontal tables,
- LVDTs mounted on specimens to measure axial, shear, and change in circumference deformations, and
- pressure transducer to monitor the confining pressure.

N.B. The UTM was designed to satisfy a very wide range of requirements. With the development and implementation of new specifications, it is very likely that the range in

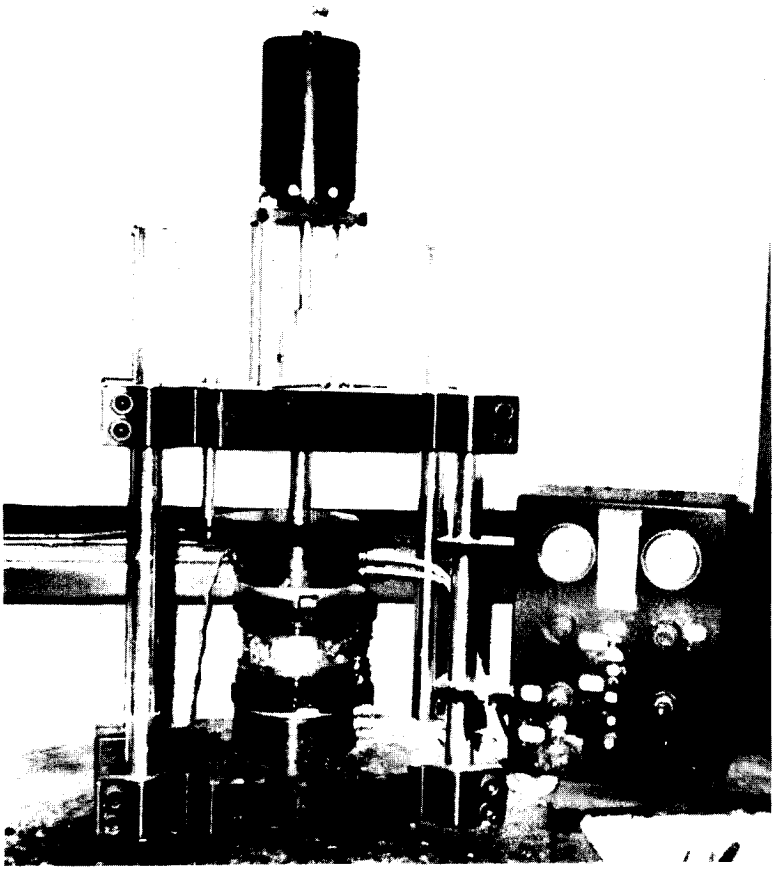

Figure 5.6. Gluing device

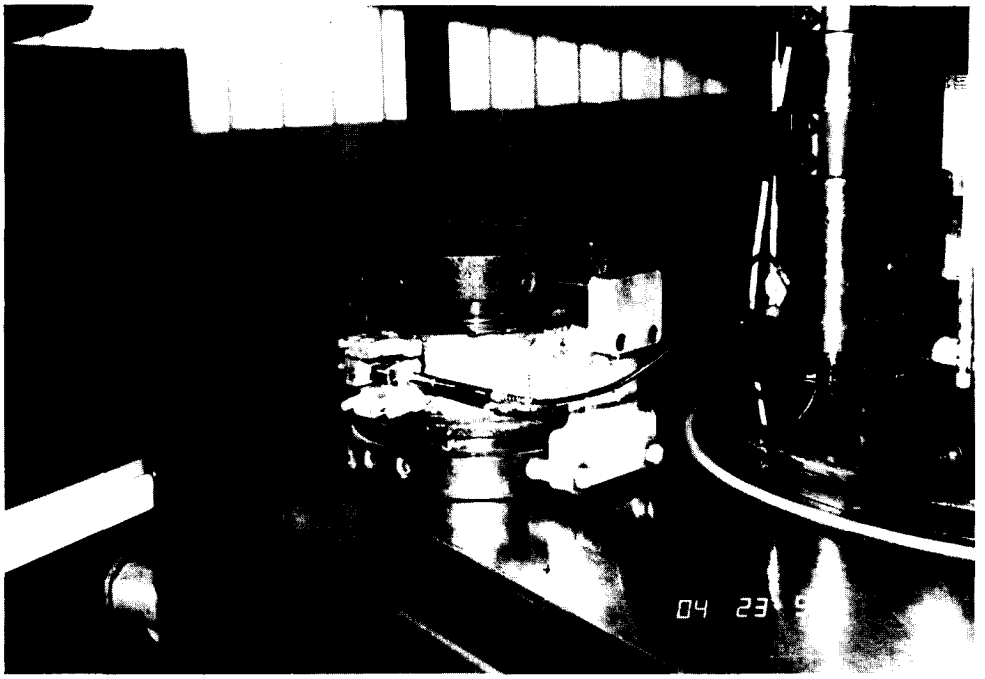

Figure 5.7. Specimen with caps glued

requirements will be substantially narrowed. In this case, and based on the experience gained with the UTM and the simple shear device, a potential development from the UTM would likely be a stand-alone simple shear device, which is portable and much cheaper. The reduced size and ease of use of this improved simple shear device would make it a likely candidate for quality control tests conducted in the field.

5.3 Specimen Preparation

For permanent deformation testing, the method used to compact the specimen can have a significant influence on its behavior in shear loading. Accordingly, the method of compaction used is important.

The purpose of any laboratory compaction process is to simulate, as closely as possible, the actual compaction produced in the field. Factors such as particle orientation and aggregate interlock, void content and structure, and the number of interconnected voids should be considered in the selection of a compaction device. During the past five years a number of researchers, including the A-003A Project team, have investigated the relationship between compaction (laboratory and field) and expected performance; highlights of some of these studies are reported in subsequent paragraphs to provide the basis for selection of one compaction method recommended for use with this mix design and analysis system.

As a part of National Cooperative Highway Reasearch Program Project 9-6(1) (von Quintus et al. 1991), various methods of compaction were investigated. While the 9-6(1) researchers indicated a preference for the Texas gyratory compactor (although the data were limited and confounded by variation in void content and laboratory methods used to simulate aging), they noted that rolling wheel compaction gave comparable results to those obtained using the gyratory compactor.

It should be noted that the steel wheel simulator used by NCHRP 9-6(1) researchers is not the same as used in the A-003A project. The NCHRP investigators considered the particular steel wheel simulator to be "relatively unsophisticated in comparison to the typical European type compactors...."

In a subsequent study for SHRP, Button et al. (1992) prepared specimens in the laboratory using three different compaction methods, including the Texas gyratory, the Exxon rolling wheel, and the rotating base Marshall hammer. While the researchers concluded that the Texas gyratory most often produced specimens similar to field cores, the results must be qualified because of significant differences in air void contents of compacted specimens.

As a part of the A-003A program, gyratory (Texas type), kneading, and rolling wheel compaction procedures were investigated (Sousa et al. 1991).

The gyratory compactor was found to place excessive emphasis on the asphalt binder and to inaccurately portray the role of asphalt aggregate interaction in the performance of properly constructed pavements. Furthermore, the shapes and dimensions of specimens produced by gyratory compactors are limited. Although the kneading compactor is more adaptable for

producing a larger variety of sizes and shapes, it may create a more stable aggregate structure than is commonly developed by conventional construction practice, thereby failing to capture the role of the asphalt binder in properly performing pavements. Because the response of rolling-wheel specimens to test loads is typically between that of gyratory and kneading specimens, rolling-wheel compaction is best suited for preparing laboratory specimens. Among the methods investigated, it appears to duplicate field-compacted mixes quite well.

In another study comparing the same three methods of compaction (Harvey 1992) it was concluded:

> "Gyratory, rolling, and kneading compaction produce specimens that are significantly different with respect to resistance to repetitive shear permanent deformation test results, with average results differing by more than an order of magnitude between each method for conventional asphalts. This indicates that selection of laboratory compaction method will have at least as much effect on mix performance as aggregate type, binder type, fines content, or air void content."

European experience has proven the practicality and superiority of rolling-wheel compaction. It is the recommended form of specimen preparation in France and is a major component of the LCPC mix design/evaluation methodology (Bonnot 1986). Studies in the United Kingdom (Brown and Cooper 1980, Nunn 1978) as well as the Royal Dutch Shell Laboratory, Amsterdam (Van Dijk 1975), also demonstrated the effectiveness of rolling-wheel compaction.

Rolling-wheel compaction is intuitively appealing for its obvious similarity to field compaction processes. Moreover, extensive studies have demonstrated that it produces uniform specimens with engineering properties similar to those of cores extracted from recently constructed pavements. Rolling-wheel compaction is a comparatively easy procedure to use and enables rapid fabrication of specimens in suitable numbers and shapes for a comprehensive mix design and analysis system. Because specimens produced by rolling-wheel compaction are cored or sawed from a larger mass, all surfaces are cut. Cut surfaces are desirable because air voids can be more accurately measured, comparisons with specimens extracted from in-service pavements are more accurate, specimens are more homogenous, and test results are likely to be less variable. Rolling-wheel compaction also has the advantage that specimens containing large-size aggregate can be produced without difficulty.

Based on these studies as well as on an evaluation of international experience, it is strongly recommended that rolling-wheel compaction be used for the preparation of laboratory specimens of an asphalt aggregate mix that are to be evaluated as a part of a comprehensive asphalt aggregate mix design/analysis system.

All of the specimens tested in this portion of the report have been obtained from slabs prepared by rolling wheel compaction (Harvey 1991) by coring and sawing; thus, all surfaces are cut.

6

Constitutive Relationship for Permanent Deformation Response of Asphalt Aggregate Mixes

It was concluded in Part I that it would be necessary to develop a constitutive relationship to define the permanent deformation response of asphalt aggregate mixes that would reflect the following characteristics:

- dilation under shear loading;
- increase in stiffness with increase in hydrostatic pressure;
- negligible volumetric creep;
- residual permanent deformation on removal of load; and
- temperature and rate of loading dependence.

In addition, test procedures are required to properly define these characteristics for use in the constitutive relationship.

It was emphasized in Part I that the constitutive relationship must be compatible with a three-dimensional finite element representation of typical pavement structures so that the accumulation of permanent deformation (rutting) could be determined for repetitive traffic loading.

This chapter provides a summary of the following:

- analytical developments to formulate the constitutive relationship;
- a description of the test procedures using the shear device;
- results and analyses of tests of 16 mixes following the developed procedures;
- limited validation of the constitutive relationship by comparing measured and predicted results in the constant height repetitive load simple shear test; and
- an explanation of the use of the constitutive relationship to predict rutting in pavement structures containing selected mixes from the group of 16 tested in this phase.

6.1 Proposed Constitutive Law

This section presents both the original and enhanced constitutive laws used to model asphalt aggregate mixes. Initially a nonlinear viscoelastic model was considered adequate to represent the response of asphalt concrete. An analysis of the data revealed that this type of response was not sufficient to capture the observed behavior. Accordingly, the viscoelastic model was enhanced with an elastoplastic model. Both developments are summarized in this section.

6.1.1 Nonlinear Viscoelastic Model

The proposal to use a nonlinear viscoelastic constitutive relationship was motivated by the observations noted above regarding mix behavior, that is, the following:

- Shear loading leads to change in volume (i.e., volumetric and deviatoric processes are coupled, also known as dilation).
- The effective shear modulus increases under hydrostatic pressure.
- It is temperature dependent.
- Its volumetric creep is negligible.
- Residual permanent deformation is observed after the load has been removed (i.e., the material is inelastic).

In addition, there are two points regarding the microstructure of asphalt aggregate mixes that pertain to what follows. The first is that dilatancy and hardening under hydrostatic pressure are associated with aggregate skeletons. The second is that aggregate behavior is insensitive to temperature and loading history (i.e., it is not rate dependent). The asphalt binder, on the other hand, is sensitive to both temperature and rate of loading. Therefore, it is natural to associate dilatancy and hardening with the spring, and temperature and rate dependency with the dashpot.

The model adopted to capture the main attributes of mixes consists of a number of three-dimensional Maxwell elements (Figure 6.1) in parallel. However, in view of the nonlinear nature of mixes, each Maxwell element is assumed to be composed of a nonlinear spring and a nonlinear dashpot.

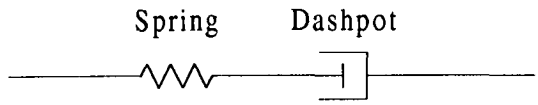

Figure 6.1. A one-dimensional schematic of a Maxwell element

First, consider the spring (i.e., the elastic component) in a typical Maxwell element. To achieve the desired coupling and hardening, the strain energy function is expanded in a Taylor series (in terms of the strain invariants, i.e., the material is assumed to be initially isotropic) and truncate terms of order greater than four. Thus, the strain energy function is assumed as:

$$W(\epsilon^e) := \frac{1}{2} C_1 I_1^2 + C_2 I_2 + \frac{1}{3} C_3 I_1^3 + C_4 I_1 I_2 + C_5 I_3 + \frac{1}{4} C_6 I_1^4 + C_7 I_1^2 I_2 + C_8 I_1 I_3 + \frac{1}{2} C_9 I_2 \tag{6.1}$$

where C_1 through C_9 are material constants and ϵ^e is the elastic strain tensor. I_1, I_2, and I_3 are the elastic strain tensor invariants given by:

$$I_1(\epsilon) := \text{trace}(\epsilon), \quad I_2(\epsilon) := \frac{1}{2}[I_1^2 - \epsilon:\epsilon], \quad I_3(\epsilon) := \det(\epsilon) \; ; \tag{6.2}$$

and ϵ^e is a function of the total strain, ϵ, and the viscous (i.e., inelastic) strain, ϵ^i, is given by:

$$\epsilon^e := \epsilon - \epsilon^i \tag{6.3}$$

To complete the description of the elastic component, the stress tensor, σ, is defined as:

$$\sigma := \partial_\epsilon W(\epsilon^e) \tag{6.4}$$

Second, consider the dashpot in a typical Maxwell element. In this case, the equilibrium equation is given in the form of a rate equation of the following form:

$$\dot{\epsilon}^i := \left[1 + \frac{q^n}{\alpha^n}\right] \eta^{-1} \partial_\epsilon W(\epsilon^e) \tag{6.5a}$$

or

$$\dot{\epsilon}^i := \left[1 - \frac{q^n}{\alpha^n}\right]^{-1} \eta^{-1} \partial_\epsilon W(\epsilon^e) \tag{6.5b}$$

where α and n are material constants, the internal (damage) variable, q, is defined as:

$$q := \max(q_\tau) \qquad 0 \leq \tau \leq t \tag{6.6}$$

and q_τ is given by:

$$q_\tau := (\epsilon^i : \epsilon^i)_\tau^{\frac{1}{2}} \tag{6.7a}$$

when Equation 6.5b is used, by:

$$q_\tau := (\dot{\epsilon}^i : \eta : \dot{\epsilon}^i)_\tau^{\frac{1}{2}} \tag{6.7b}$$

and η, the initial viscosity, is a rank four tensor given in component form by:

$$\eta_{ijkl} := \lambda^v \delta_{ij}\, \delta_{kl} + \mu^v(\delta_{ik}\, \delta_{jl} + \delta_{il}\, \delta_{jk}) \tag{6.8}$$

where λ^v and μ^v are temperature-dependent material constants.

The laboratory tests performed during the course of this investigation as well as the majority of test data available in the literature suggest that a good description of mix temperature dependence is achieved if the material is assumed to thermorheologically simple. This temperature dependency can be easily accommodated in the model if the η is assumed to be given by:

$$\eta = \eta_0 e^{\frac{C_T (T - T_0)}{T_0\, T}} \tag{6.9}$$

where C_T is a material constant, T and T_0 are the current and reference temperatures (in Kelvin degrees), respectively, and η_0 is given by Equation 6.8 with λ^v and μ^v evaluated at the reference temperature.

The two models proposed for the rate equation, Equations 6.5a and b, differ in the definition of the damage parameter, q, (i.e., they differ in the evolution of the viscosity). The first model is based on the maximum attained inelastic strain, while the second is based on the maximum attained inelastic strain rate. From a computational standpoint, the second model leads to a symmetric algorithmic tangent matrix, while the first leads to a nonsymmetric one; thus, the second model is more attractive. In addition, the dashpot (whose viscosity's evolution is described by q) is a rate-dependent element. Therefore, the second approach seems to be more appropriate.

Finally, the global model is obtained when a number of the nonlinear Maxwell elements, described above, are assembled in parallel.[5] This constitutive law, with either of the damage models, captures many of the characteristics of mixes. However, when applied to model cyclic loading, most of the strain is recovered during the unloading. This behavior does not fit the test data obtained in the study. Therefore, to improve the model, it has been enhanced to include an additional elastoplastic branch in parallel with the Maxwell elements. This elastoplastic model is described in the following section.

6.1.2 Elastoplastic Model

It is commonly accepted in the literature that aggregate materials can be described by rate-independent elastoplastic constitutive laws. In addition, as was stated above, aggregate materials dilate and the effective shear modulus is pressure dependent. Finally, the repetitive constant height shear tests conducted with the simple shear equipment suggest that the dilation effect is elastic (no residual axial force was measured during the unloaded period). Therefore, a rate-independent elastoplastic model based on J_2-plasticity was adopted. This model consists of an elastic component described by the strain energy function given in Equation 6.1, and the classical rate-independent von Mises plasticity model with associative flow rule, and linear isotropic and kinematic hardening law.

To elaborate on the constitutive law, the evolution of the plastic strain must be described. To this end, the elastic tensor, **C** (a rank four tensor), is introduced, defined as:

$$\mathbf{C} := \partial_{\epsilon\epsilon} \mathbf{W} \tag{6.10}$$

and is assumed to possess the following symmetries: $C_{ijkl} = C_{klij} = C_{ijlk} = C_{jilk}$. Next, let $f(\sigma,\mathbf{q})$ be the yield function, where $\mathbf{q}$ represents the hardening parameters. An admissible state is such that:

$$f(\sigma, \mathbf{q}) \leq 0 \tag{6.11}$$

The surface $f(\sigma,\mathbf{q}) = 0$ is known as the yield surface in stress space. The evolution of the plastic strain and hardening parameters, referred to as the flow rule and hardening law, respectively, are given for the case of associative plasticity (the case considered in this work) by:

$$\begin{cases} \dot{\epsilon}^p &= \dot{\gamma}\, \partial_\sigma f(\sigma,\mathbf{q}) \\ \dot{\mathbf{q}} &= -\dot{\gamma}\, \mathbf{D} \partial_q f(\sigma,\mathbf{q}) \end{cases} \tag{6.12}$$

---

[5]Note that all Maxwell elements sharing the same total strain, ϵ. ϵ^e, and ϵ^i, on the other hand, are evaluated independently for each Maxwell element.

where **D** is the matrix of generalized plastic moduli. $\dot{\gamma}$ is referred to as the consistency parameter, and is assumed to obey the following Kuhn-Tucker complementary conditions:

$$\dot{\gamma} \geq 0 \ , \ f(\sigma,\mathbf{q}) \leq 0 \ , \text{ and } \dot{\gamma} f(\sigma,\mathbf{q}) = 0 \tag{6.13}$$

In addition, $\dot{\gamma}$ is constrained to satisfy the consistency requirement.

$$\dot{\gamma} \dot{f}(\sigma,\mathbf{q}) = 0 \tag{6.14}$$

Finally, the elastoplastic tangent, C^{ep}, relating the stress rate, $\dot{\sigma}$, to the total strain rate, $\dot{\epsilon}$, is introduced. Consider a point on the yield surface in stress space (i.e., f=0). By Equation 6.13, $\dot{f} \leq 0$ where the case of $\dot{f} = 0$ corresponds to neutral loading (i.e., loading with no change in the plastic strain) and plastic loading. Thus, by the chain rule:

$$\dot{f} = \partial_\sigma f: \dot{\sigma} + \partial_q f \cdot \dot{q} = \partial_\sigma f: \mathbf{C}: \dot{\epsilon} - \dot{\gamma}(\partial_\sigma f: \mathbf{C}: \partial_q f + \partial_q f \cdot \mathbf{D} \partial_q f) \leq 0 \tag{6.15}$$

and:

$$\dot{f} = 0 \Leftrightarrow \dot{\gamma} = \frac{\langle \partial_\sigma f: \mathbf{C}: \epsilon \rangle}{\partial_\sigma f: \mathbf{C}: \partial_\sigma f + \partial_q f \cdot \mathbf{D} \partial_q f} \tag{6.16}$$

where $\langle x \rangle = \frac{1}{2}(x + |x|)$ is the ramp function. From the above, the following relation between the stress rate and the total strain rate is obtained:

$$\dot{\sigma} = \mathbf{C}^{ep}: \dot{\epsilon} \tag{6.17}$$

where $\mathbf{C}^{ep}$, the elastoplastic tangent matrix, is given by:

$$\mathbf{C}^{ep} := \begin{cases} \mathbf{C} & \text{if } \dot{\gamma} = 0 \\ \mathbf{C} - \dfrac{\mathbf{C}:\partial_\sigma f \otimes \mathbf{C}:\partial_\sigma f}{\partial_\sigma f: \mathbf{C}: \partial_\sigma f + \partial_q f \cdot \mathbf{D} \partial_q f} & \text{if } \dot{\gamma} > 0 \end{cases} \tag{6.18}$$

It is customary in J_2 plasticity to take the hardening vector, $\mathbf{q}$, as $\mathbf{q} := \{\alpha, \bar{\mathbf{q}}\}$ where α is the equivalent plastic strain that defines isotropic hardening and $\bar{\mathbf{q}}$ defines the center or kinematic hardening of the von Mises yield surface. The yield function, flow, and hardening rules are given by:

$$\begin{cases} f(\sigma, \mathbf{q}) = \|\eta\| - \sqrt{\frac{2}{3}}\, K(\alpha) \\ \dot{\epsilon}^p = \dot{\gamma}\, \frac{\eta}{\|\eta\|} \\ \dot{\bar{\mathbf{q}}} = \dot{\gamma}\, \frac{2}{3}\, H'(\alpha)\, \frac{\eta}{\|\eta\|} \\ \dot{\alpha} = \dot{\gamma} \sqrt{\frac{2}{3}} \end{cases} \tag{6.19}$$

respectively. In the above equations, $\eta := \text{dev}\,[\sigma] - \bar{\mathbf{q}}$, $\text{tr}[\bar{\mathbf{q}}]:=0$, and $H'(\alpha)$ and $K(\alpha)$ are the kinematic and isotropic hardening moduli, respectively. It follows from Equation 6.19 that

$$\alpha := \int_0^t \sqrt{\frac{2}{3}}\, \|\dot{\epsilon}^p(\tau)\| d\tau \tag{6.20}$$

which is the standard definition of equivalent plastic strain. Finally, the following definition was adopted for $H'(\alpha)$ and $K(\alpha)$:

$$H'(\alpha) := (1-\beta)\bar{H} \quad \text{and} \quad K(\alpha) := \sigma_y + \beta \bar{H} \alpha \quad \text{with} \quad \beta \in [0,1] \tag{6.21}$$

where σ_y, $\bar{H}$, and β are material constants determined from the data.

6.2 Mix Characterization Procedures

To define the various parameters in the constitutive relationship, a series of tests was devised using the simple shear device. The tests consisted of a battery of three tests at one temperature — a constant height shear test, a uniaxial strain test, and a volumetric (hydrostatic pressure) test — and frequency sweeps in shear over a range of temperatures. A repeated load constant height simple shear test was also performed to serve as a check on the parameters determined from the four tests; this final test, in effect, served as a validation of the methodology.

For the initial test series, the constitutive relationship, as noted earlier, was developed to represent nonlinear viscoelastic response and the tests were conducted on four mixes to check the effectiveness of representing mix response in this manner. From the results of this initial test series it was necessary to enhance the model by including an additional elastoplastic

branch in parallel with the Maxwell elements. Tests conducted on the 16 mixes of the expanded test series were interpreted in this manner.

At the same time it was considered desirable to determine an appropriate size of specimen in order to minimize the effects of the absence of shear stresses on the vertical faces of the simple shear specimens. Accordingly, finite element analyses were performed on specimens with a range in dimensions to ascertain at what minimum size the influence of the noncomplementary shear stress state would be negligible from an engineering standpoint. The results of these analyses are included in Appendix A. The analysis indicates that for a specimen height of 5 cm (2 in.) and diameter of 15 cm (6 in.) the error in the estimate of shear modulus is less than 10 percent.

6.2.1 Nonlinear Elastic Parameters

The battery of three tests performed at one temperature permit determination of the nonlinear elastic parameters defined by the coefficients C_1 through C_9. The suite of tests and associated parameters are shown schematically in Figure 6.2.

6.2.1.1 Simple Shear Constant Height Test.

This test permits the direct determination of three parameters that define the nonlinear elastic response (i.e., C_2, C_4, C_9). The test requires the use of two hydraulic actuators — one to apply the shear stress to the specimen at a rate of 70 kPa/sec (10 psi/sec); the other, under feedback from an LVDT measuring the relative displacement between the specimen caps, to ensure that constant height is maintained in the specimen (within $\pm$ 0.001 mm [0.00005 in.]).

The analysis is based on the assumption that a pure shear state of strain is obtained when $\epsilon_{12} = \epsilon_{21} = \epsilon_0$ and all other strain components are zero. For this situation:

$$\sigma_{11} = -C_4\epsilon_0^2 \tag{6.22}$$

$$\sigma_{12} = -C_2\epsilon_0 - C_9\epsilon_0^3 \tag{6.23}$$

$$\sigma_{33} = -(C_4 + C_5)\,\epsilon_0^2 \tag{6.24}$$

where σ_{11} is the axial stress developed to maintain the height constant and σ_{12} is the shear stress imposed. Unfortunately σ_{33} cannot be measured; thus, C_5 cannot be directly obtained from the test.

Simple Shear

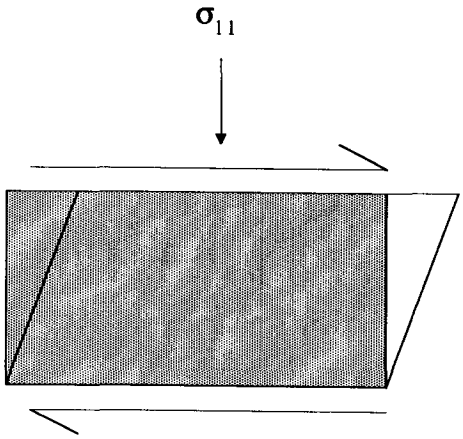

C_2, C_4, C_9

Uniaxial Strain

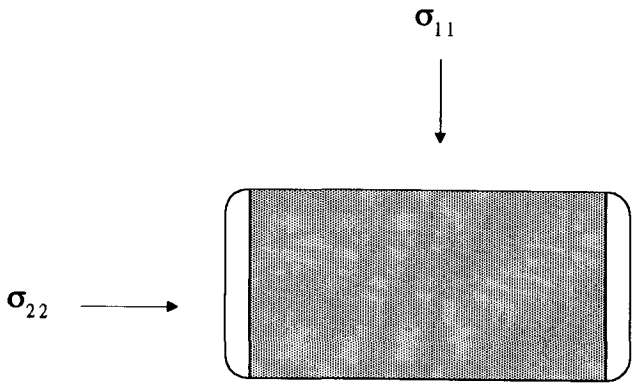

C_1, C_3, C_6, C_7

Figure 6.2. Permanent deformation – coefficients developed

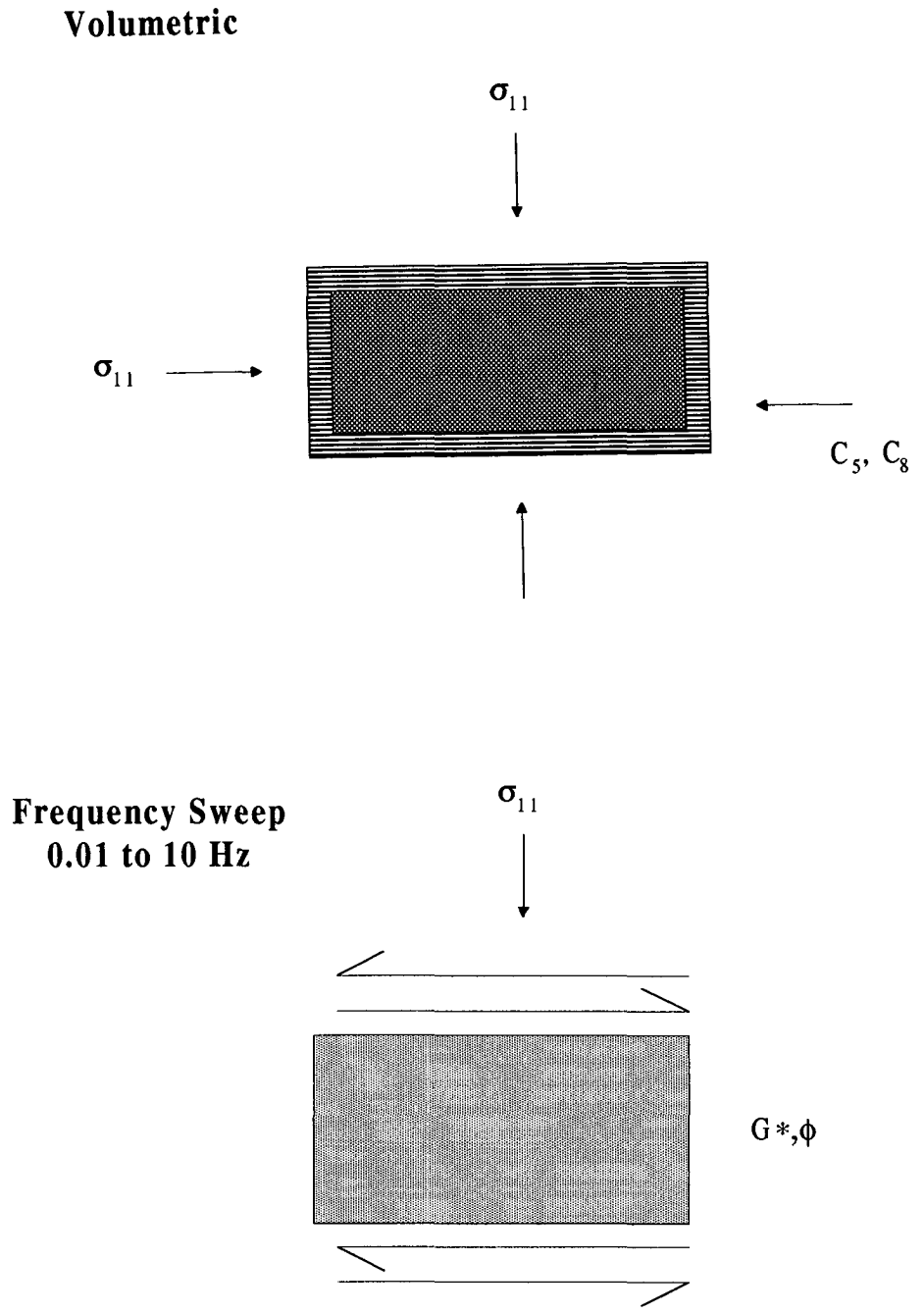

Figure 6.2 (continued). Permanent deformation – coefficients developed

6.2.1.2 Uniaxial Strain Test

This test permits the direct determination of C_1, C_3, C_6, and C_7 and also provides a check for C_2 and C_4 (obtained from the constant height simple shear test) since the only nonzero strain component is $\epsilon_{11} = \epsilon_0$. This assumes that there is no viscous deformation contributing to the response. (N.B. If there is viscous deformation, the constant height simple shear and uniaxial strain tests must be executed at the same rate.) In this test the vertical actuator is programmed to ramp the deviatoric axial stress on the sample at a rate of 70 kPa (10 psi) per second, while pneumatic servovalves control the confining pressures under feedback from an LVDT measuring the change in perimeter of the specimen. The pneumatic servovalves are programmed to maintain a constant perimeter; thus, the change in confining pressure at each instant is just enough to compensate for the bulging of the specimen, insuring a uniaxial state of strain.

The state of stress is given by:

$$\sigma_{11} = C_1\epsilon_0 + C_2\epsilon_0^2 + C_6\epsilon_0^3 \tag{6.25}$$

$$\sigma_{22}=(C_1+C_2)\epsilon_0 + (C_3 + C_4)\epsilon_0^2 + (C_6+C_7)\epsilon_0^3 \tag{6.26}$$

where σ_{11} is the axial stress, σ_{22} is the confining stress, and ϵ_0 is the axial strain; all other stress components are zero.

6.2.1.3 Volumetric (Hydrostatic) Test

Results of this test, and the constants obtained from the simple shear and uniaxial strain tests, permit the two remaining constants, C_5 and C_8, to be determined. A check of the sum of constants C_1 and C_2 also can be obtained from the volumetric test. In this test the specimen is completely enveloped in a latex membrane and placed inside a pressure cell. The cell pressure is tamped at a rate of 70 kPa (10 psi) per second and the change in perimeter is measured.

The confining pressure (σ_{22}) and the radial strain ($\epsilon_0 = \delta/2\pi r$ where δ = change in perimeter and r=radius of specimen) can be computed from the test data. In the volumetric test the state of strain can be expressed as $\epsilon_{11} = \epsilon_{22} = \epsilon_{33} = \epsilon_0$, and the state of stress defined by the following expression:

$$\sigma_{22} = (3C_1+2C_2)\epsilon_0 + (9C_3+9C_4+C_5)\epsilon_0^2 + (27C_6+36C_7+4C_8+6C_9)\epsilon_0^3 \tag{6.27}$$

6.2.2 *Viscoelastic Parameters*

Viscoelastic response characteristics can be determined from the *simple shear constant height test* (included in the battery of tests) to define the nonlinear elastic response characteristics. This test, as noted above, is performed at one temperature, such as 40°C (104°F). To define the influence of temperature on mix response, *frequency sweeps* can be performed over a range in temperatures.

Currently, the test is performed at temperatures ranging from 4°C to 60°C (39°F to 140°F) (e.g., 4°C, 20°C, 40°C, and 60°C [39°F, 68°F, 104°F, and 140°F]) in the sequence from low to high under controlled shear strain conditions (amplitude = 0.025 mm/mm [0.0001 in./in.]) and at constant height (± 0.001 mm [0.00005 in.]). At a particular temperature the tests are executed from high to low frequency (10, 5, 2, 1, 0.5, 0.2, 0.1, 0.05, 0.02, and 0.01 Hz).

In this test an imposed sinusoidal strain X at a frequency ω and at a strain amplitude Xa

$$X = X_a \sin(\omega t) \tag{6.28}$$

will generate a sinusoidal stress P (where t represents time and δ the phase angle):

$$P = P_a \sin(\omega t + \delta) \tag{6.29}$$

from which the complex shear modulus, G*, can be determined, i.e.

$$G^* = \frac{P_a}{X_a} \tag{6.30}$$

At each frequency and temperature, the complex modulus, G*, and the phase angle, δ, are computed from the average of at least three cycles. Master curves can be developed on the assumption that the mix is thermorheologically simple. This assumption appears reasonable for the small deformations used in the test. In the determination of the master curve, the C_1 and C_2 coefficients of the WLF equation can be determined

$$\log a_T = - \frac{C_1(T-T_{ref})}{C_2+T-T_{ref}} \tag{6.31}$$

where: a_T = horizontal shift factor and
T = corresponding absolute temperature in degrees Kelvin,

which provides a measure of the effects of temperature on mix response. The value of G* at high frequencies is related to the coefficient C_2 by the relationship:

$$C_2 = -2G^* \tag{6.32}$$

thus serving as a check on the interpretation of the various test data to define mix parameters.

6.2.3 Plastic Parameters

The constant height shear test in creep provides the test data from which the plastic parameters are selected. The next section describes the process for determination of the constitutive constants, including the computation of the plastic parameters.

6.3 Determination of Constitutive Constants

The procedure described in this section is that used to approximate the behavior of the 16 mixes tested as a part of the extended study. The model concept, defined earlier, is illustrated schematically in Figure 6.3.[6] As can be seen, the constitutive law consists of two independent components, a rate-independent elastoplastic component and a linear viscoelastic component. The two components shear the total strain, and the total stress is obtained by summing the stress from each component.

Before proceeding with the determination of the constitutive constants, it is important to note that the contribution of each individual Maxwell element to the total stress is insignificant for time periods larger than its characteristic time. This point is illustrated in Figure 6.4, where relaxation curves for three Maxwell elements are presented. Additionally, the following two assumptions are introduced regarding the elastoplastic behavior at low total strain levels. First, no plastic flow is present. Second, linear elasticity is assumed (i.e., the contribution from the higher order terms in the strain energy function is negligible).

In view of the above observation and assumptions it is possible to use the first loading cycle in the constant height shear creep test to determine the constants associated with the Maxwell elements (recall that isochoric viscoelastic behavior is assumed). To this end the creep curve is linearly extrapolated (in log-log scale) to 1.0E+6 seconds. The viscoelastic model is assumed to consist of eight Maxwell elements with characteristic times of 1.0E-2, 1.0E-1, 1.0E+0,..., 1.0E+5 seconds. Thus, at 1.0E+6 seconds only the plastic branch contributes to the stress and can be computed. Next, using the following regression equation, the elastic

---

[6]The first test series was conducted using mixes containing aggregates RB and RL and asphalts AAG-1 and AAK-1. Interpretation of these test results was made according to the initial formulation of the constitutive relationship (i.e., without the elastoplastic component). Results of this study are included in Appendix B. The decision was made to add the elastoplastic component based on these results and initial interpretation of the data for the 16 mixes.

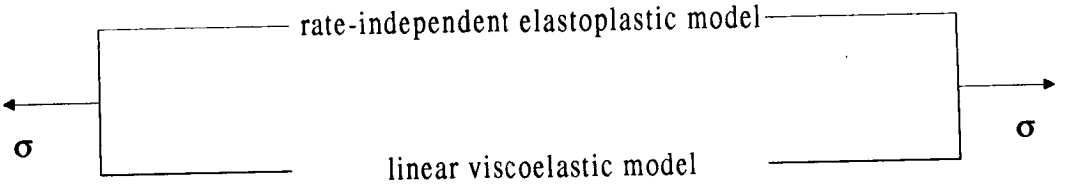

a.) General concept

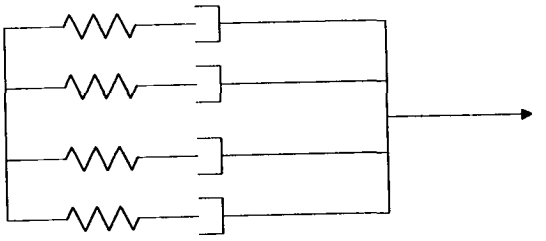

b.) Representative example

Figure 6.3. The constitutive concept, one-dimensional schematics

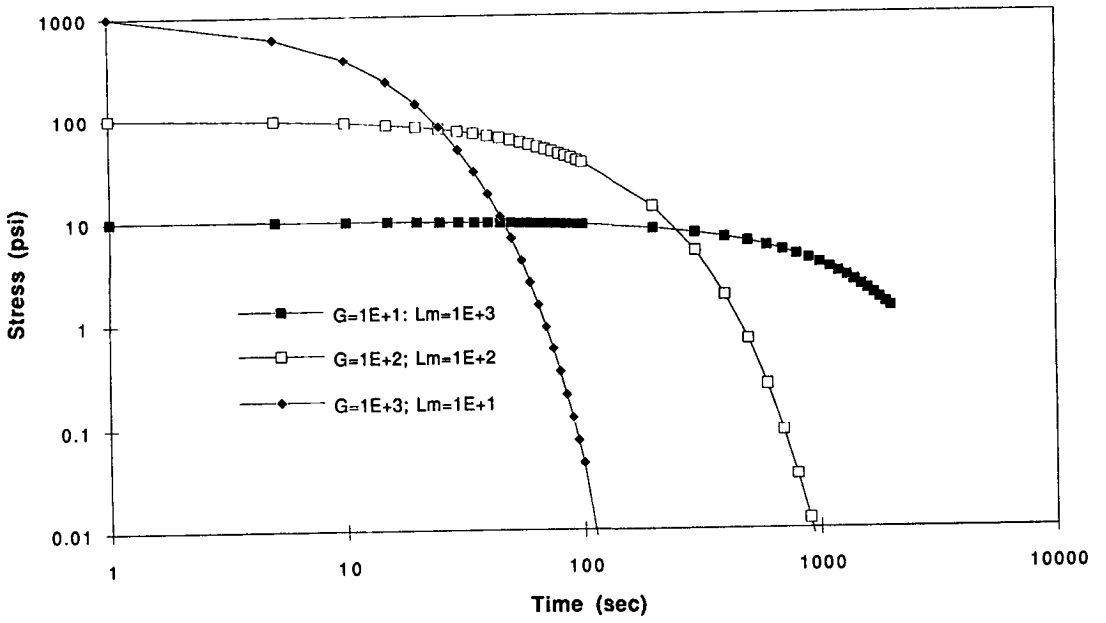

Figure 6.4. Relaxation curves for three different Maxwell elements

components of all Maxwell elements can be computed (recall that a Maxwell element is completely defined by its elastic coefficient and characteristic time).

$$G_i = \frac{\sigma_{total}}{\gamma_n} - \sum_{i=n+1}^{nM} G_i - G_{ep} \tag{6.33}$$

where nM is the number of Maxwell elements (organized by increasing characteristic time); n is the current Maxwell element; σ_{total} is the total shear stress measured (this was the input to the test); γ_n is the measured engineering shear strain at time = characteristic time of the nth Maxwell element; and G_{ep} is the "shear modulus" of the plastic branch ($C_2 = -2G_{ep}$).

Next, the remainder of the constants required for the elastoplastic branch are computed. These include C_1, C_3, C_4, C_5,...,C_8, C_9, σ_y, β, and $\bar{H}$. Given the strain histories measured in the laboratory tests, these parameters are selected to provide the best fit for the stress histories in the constant height shear creep test, the hydrostatic pressure test, and the uniaxial strain test. In this procedure it is important to note that since an isochoric plastic flow is assumed, the plastic parameters (i.e., σ_y, β, and $\bar{H}$) do not affect the volumetric test prediction, and have only a marginal effect on the uniaxial strain test (the uniaxial strain test is expected to be more affected if a real state of uniaxial strain will be achieved). Finally, the plastic parameters are selected from the constant height shear creep test. Specifically, given the stress and strain histories, and the viscoelastic model (as previously determined), it is possible to establish the stress versus strain curve for the plastic branch, and thus approximate these parameters. Unfortunately, however, the procedure provides a good approximation of $\beta \cdot \bar{H}$ but not of each one independently. Therefore, based on the experience developed in determining these parameters, β was set to 0.5, a value that appeared to provide the best results.

6.4 Test Data Interpretation

This section presents the results of tests on 16 mixes. For each mix, the tests consisted of a constant height shear test (creep loading), a uniaxial strain test, a hydrostatic test, and a repeated load constant height simple shear test (0.1 s load duration and 0.6 s interval between load applications). In addition, frequency sweeps were performed on 14 of the 16 mixes. These data were used to develop the material constants consistent with the constitutive relationship presented earlier.

An evaluation of the test results is made prior to presenting the material constants for the 16 mixes so that these results may be viewed in proper perspective.

6.4.1 Materials

Sixteen asphalt aggregate mixes were used in this test program. They contained MRL aggregates RD or RH and MRL asphalts, AAC-1, AAG-1, AAK-1, and AAM-1. Asphalt

contents for the mixes were selected based on the Hveem stabilometer test. Normally, the asphalt content would be selected for each asphalt to be used with a specific aggregate with the asphalt content varying with the stiffness of the asphalt at the test temperature (60°C [140°F]) for the stabilometer test). However, in this case the asphalt content was based on the average of tests with mixes containing asphalts AAG-1 and AAK-1. The asphalt contents are as follows:

Aggregate	Asphalt content (percent) by weight of aggregate	Asphalt content (percent) by weight of mix
RD	4.5	4.3
RH	5.2	4.9

Properties of the asphalts are summarized in Tables 6.1 and 6.2. Table 6.1 contains a summary of conventional test properties while Table 6.2 lists the rheological properties determined by the A-002A contractor at temperatures and times of loading corresponding to tests performed in this contract.

6.5 Evaluation of Test Results

6.5.1 Constant Height Shear-Creep

In this test a 5 cm (2 in.) high by 15 cm (6 in.) diameter specimen is loaded in three cycles. First, the specimen is loaded by a 14 kPa (2 psi) shear stress for a period of 1000 s, followed by 1000 s of no load. Second, a 28 kPa (4 psi) shear stress is applied for a period of 100 s followed by a period of 100 s with no load. Finally, a shear stress of 70 kPa (10 psi) is applied for a period of 100 s, followed by 100 s with the load removed. The three steps are performed in a continuous sequence. Throughout the test, the specimen's height is maintained constant. Also, since the specimen is glued at its top and bottom to steel plates, the lateral strain is highly restrained. Sample strain and stress histories, recorded for the mix containing asphalt AAK and aggregate RD (4 percent air voids), are presented in Figures 6.5 through 6.7.

An examination of the constant height shear test data (creep) suggests the following: the dilation is elastic (axial stress develops instantaneously), and the residual axial stress is negligible, (see Figure 6.7); and very small strain recovery is observed (Figure 6.5). These two observations are the motivation for the change in the constitutive law as detailed earlier. Also, a quadratic increase in the axial stress as a function of the applied shear stress is measured, a characteristic shared by the proposed constitutive law. The actual axial stress value, however, appears to achieve an unexpectedly high value. If this trend is extrapolated, at the level of 140 kPa (20 psi) shear stress, under constant height conditions, an axial stress of about 280 kPa (40 psi) would develop. (N.B. While this shear stress cannot be attained

Table 6.1. Asphalt binder properties

Test/property	MRL Asphalt			
	AAC-1	AAG-1	AAK-1	AAM-1
Viscosity/penetration grade	AC-8	AR4000	AC-30	AC-20
SHRP PG grade	PG58-16	PG58-10	PG64-22	PG64-16
Original asphalt				
viscosity at 60°C (140°F), poise	419	1862	3256	1992
viscosity at 135°C (275°F), cSt	179	243	562	569
Aged asphalt				
viscosity at 60°C (140°F), poise	1014	3253	9708	3947
viscosity at 135°C (275°F), cSt	239	304	930	744

Table 6.2. Asphalt binder properties[a] provided by A-002A contractor

Asphalt Source	G*(kPa)		tanδ		G'(kPa)		G"(kPa)		G*/sinδ (kPa)	
	40°C (104°F)	60°C (140°F)	40°C (104°F)	60°C (140°F)	40°C (104°F)	60°C (140°F)	40°C (104°F)	60°C (140°F)	40°C (104°F)	60°C (140°F)
AAC-1	88	2.66	3.88	11.37	22	0.23	85	2.65	90	2.67
AAG-1	146	4.31	8.66	49.53	17	0.87	145	4.31	147	4.31
AAK-1	137	8.44	2.33	4.06	54	2.02	126	8.20	149	8.69
AAM-1	113	4.86	2.44	7.13	43	0.68	105	4.81	123	4.90

[a]After TFOT at 40°C (104°F) or 60°C (140°F) and 10 rad/s.

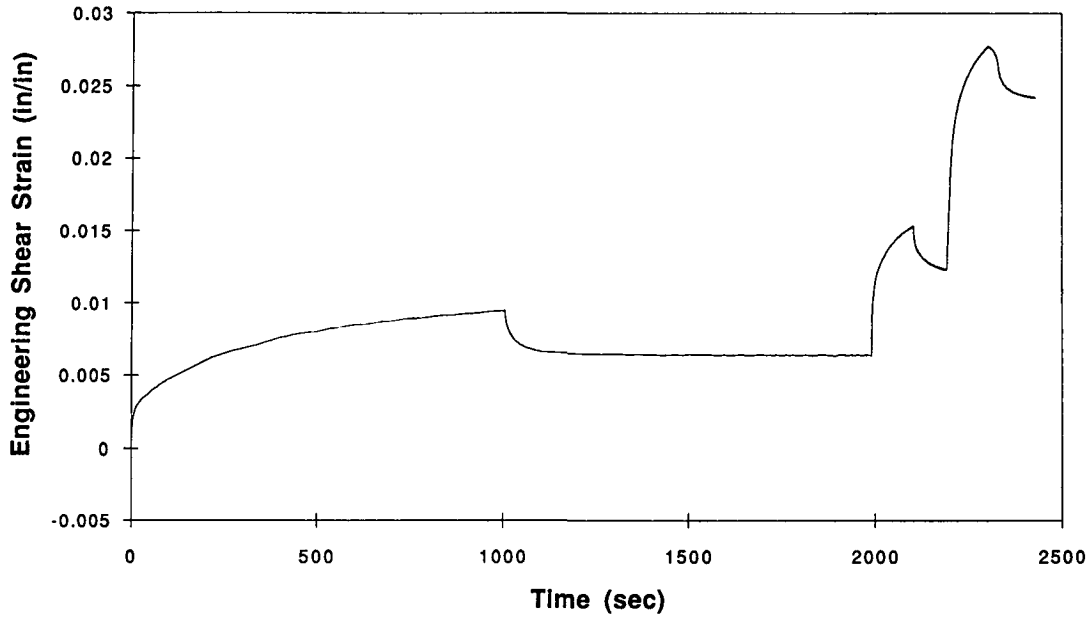

Figure 6.5. Engineering shear strain history, constant height shear test

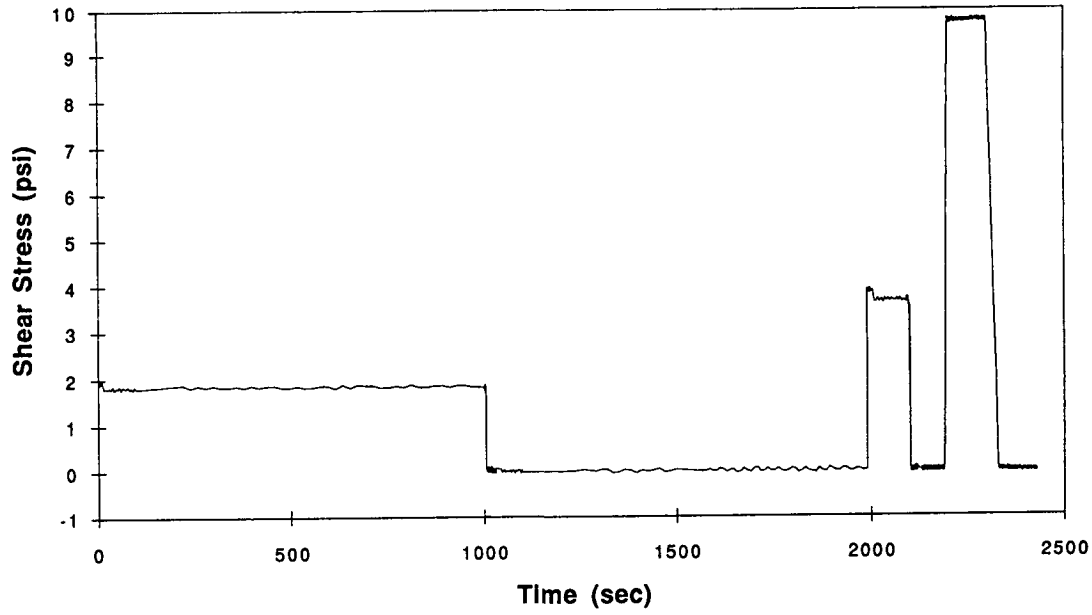

Figure 6.6. Shear stress, constant height shear test

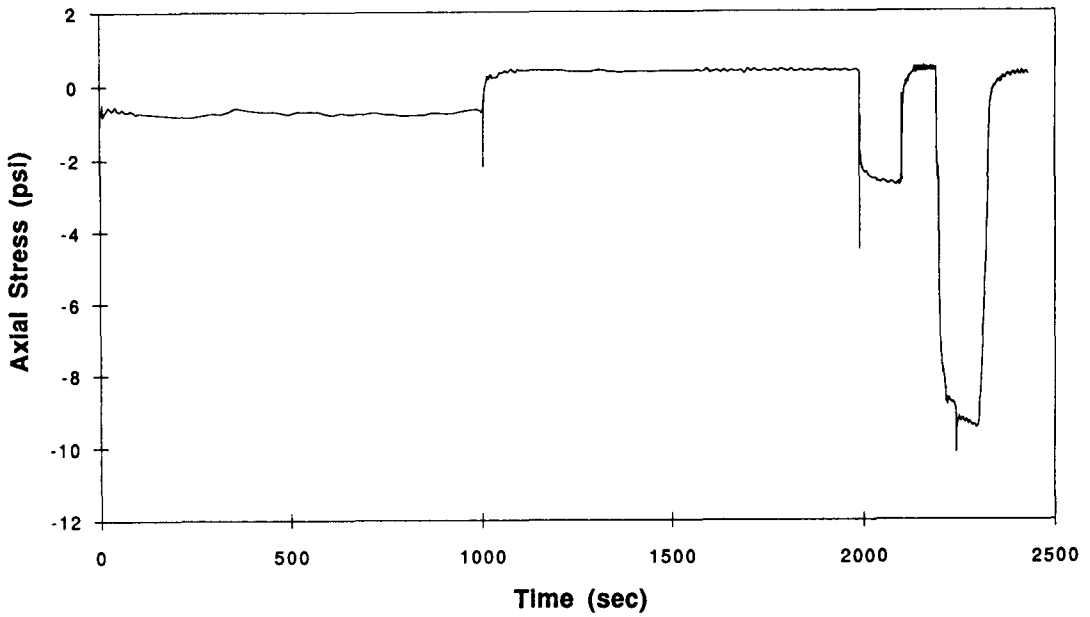

Figure 6.7. Axial stress, constant height shear test

in the laboratory it occurs under the edge of the tires. It may be worthwhile to investigate test conditions under which higher shear stresses might be obtained.

6.5.2 Uniaxial Strain

A specimen of the same dimensions as that used for the constant height shear test is used also for the uniaxial strain test. The specimen is loaded by a compressive axial load while a lateral pressure is applied to keep the diameter constant. The load is applied for 100 s. The histories of the applied radial and axial stresses, and the measured axial strain are given in Figures 6.8 and 6.9, respectively.

The results show a significant residual strain (more than 90 percent of the maximum attained strain remains as residual strain). An explanation of this large residual strain is a significant loss of air voids during the test (note the large deviatoric stress component which results in dilation).

6.5.3 Hydrostatic Pressure

Once again the same specimen dimensions were used. The specimen is subjected to a 690 kPa (100 psi) confining pressure for a period of 100 s, at which time the pressure is removed. The histories of the axial and radial strains, and the hydrostatic pressure are presented in Figures 6.10 and 6.11, respectively.

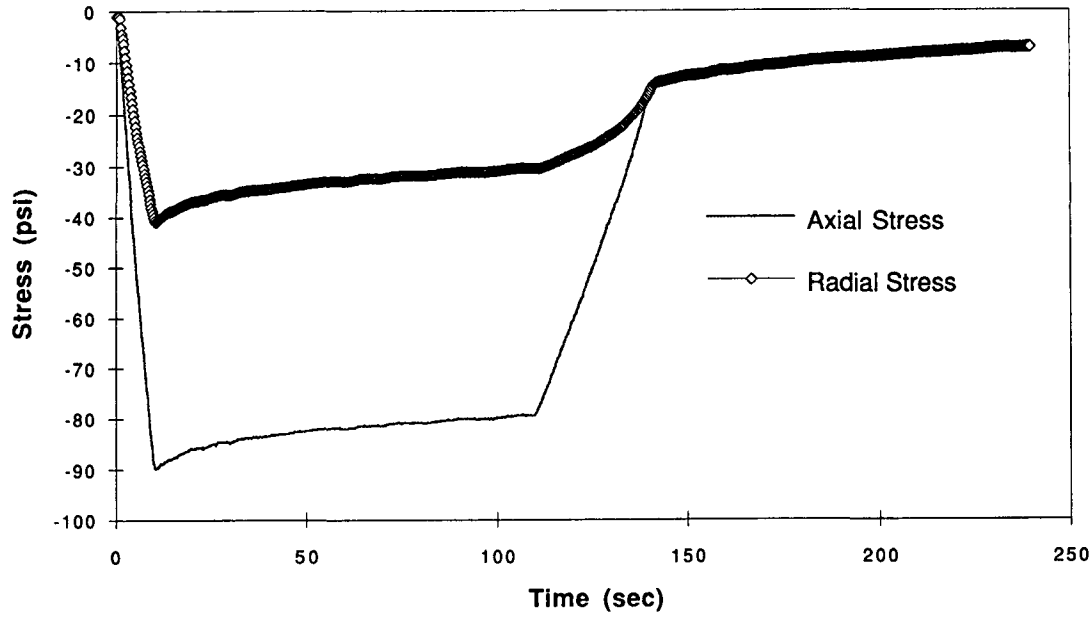

Figure 6.8. Axial and radial stress histories, uniaxial strain test

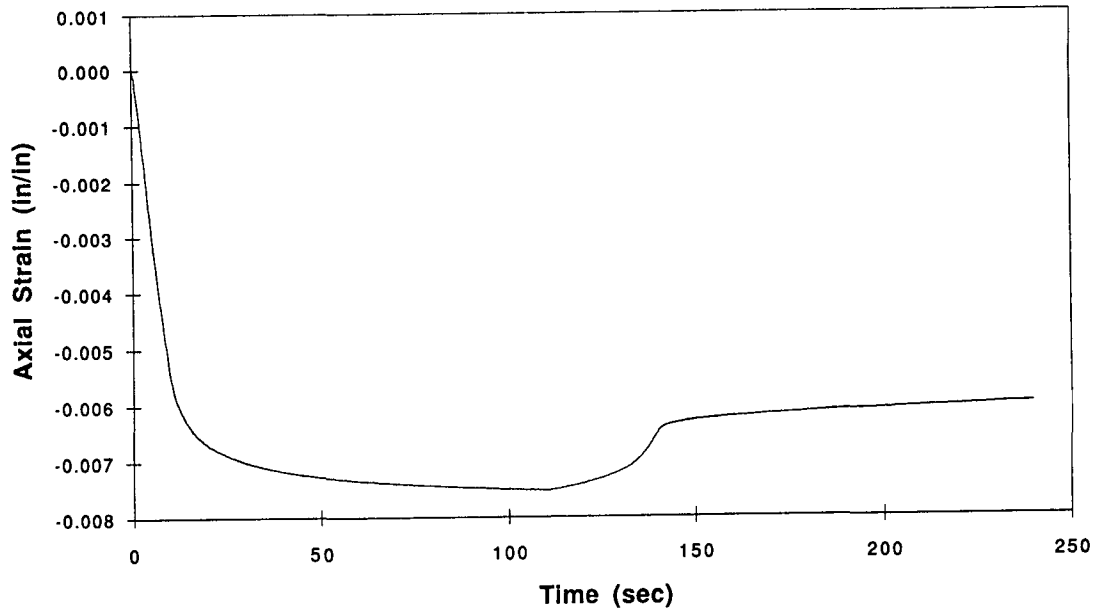

Figure 6.9. Axial stress, uniaxial strain test

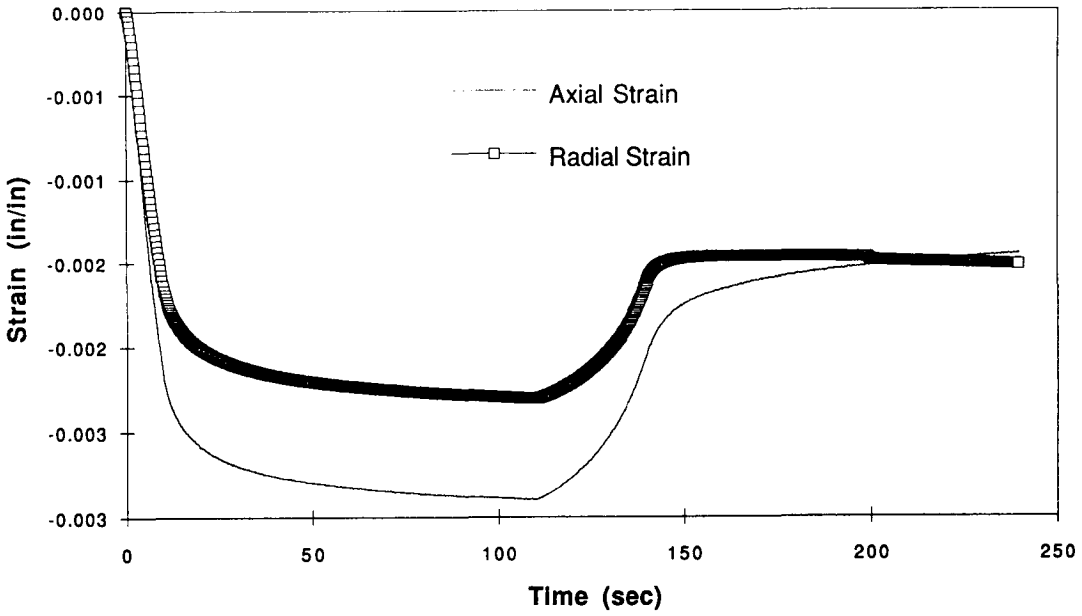

Figure 6.10. Axial and radial strains, hydrostatic pressure test

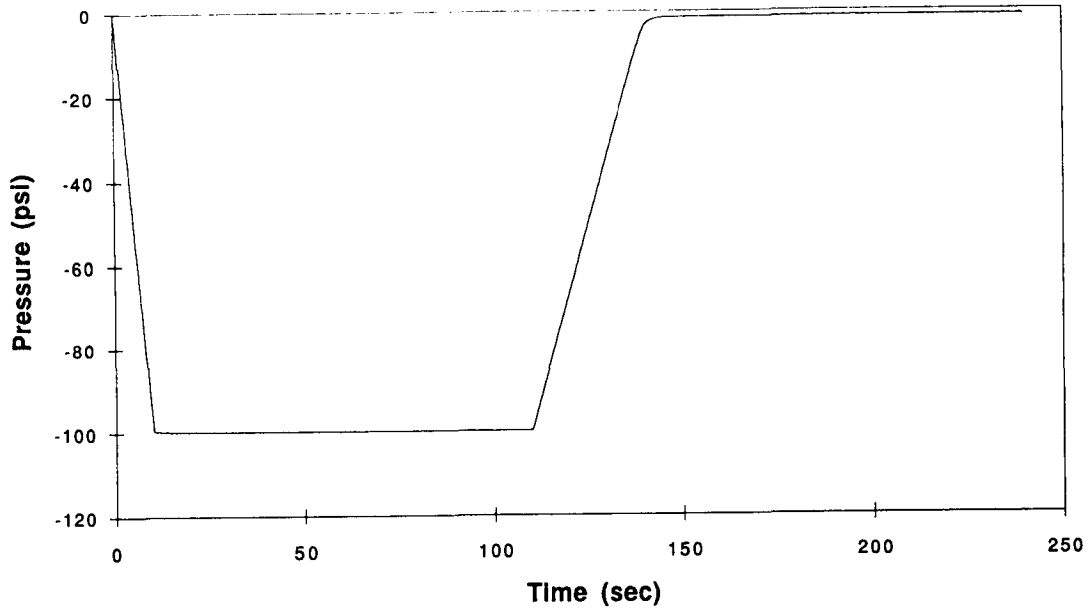

Figure 6.11. Hydrostatic pressure, hydrostatic pressure test

As can be seen from Figure 6.10, there is a significant difference between the axial and radial strains during specimen loading. After the specimen is unloaded, however, the measured radial and axial strains are practically the same. This difference may be due to the instrumentation used (the two should have been the same for the entire history). Attributing higher reliability to the axial strain measurement, it was decided to use the axial strain in determining material constants.

6.5.4 Constant Height Shear — Cyclic Loading

The same specimen geometry is used in this test. A loading cycle consists of 0.1 s of load applied (load varies from 0 to 48 kPa [7 psi] with a sine wave), followed by 0.6 s of no load. The history of the shear and axial stress for the first nine cycles is shown in Figure 6.12, and for cycles 3997 to 4000 in Figure 6.13. The axial strain history is shown in Figures 6.14 and 6.15 for cycles 1 through 9, and 3997 through 4000, respectively.

Figures 6.12 and 6.13 show that the axial stress is considerably smaller than the applied shear stress. This result stands in sharp contrast with that reported for the constant height shear test (creep), which was used to determine the material constants. Moreover, comparing the axial stress (Figures 6.12 and 6.13) and axial strain (Figures 6.14 and 6.15) histories reveals the same patterns with the expected time lag between the two. This correlation suggests that the axial stress measured is affected mostly by the axial strain, and not by dilation. Moreover, the correlation between the axial stress and strain oscillations within each loading cycle suggests that the axial force due to dilation is negligible. (For other materials where the strain oscillations are smaller, the axial stress reported is indeed negligible.)

An examination of the specimens after the cyclic loading test reveals in many a crack that appears to run (at 45°C [113°F]) through the specimen. This result is expected in view of the imperfect boundary conditions of the test. However, the data are meaningless once the crack has developed; cracking can influence the measurements. Thus, it is important to examine specimens at the conclusion of testing. If cracking is observed its effects may be considered in the interpretation of the test results.

6.6 Material Constants

The combination of nonlinear viscoelastic and elastoplastic models presented above provides the ingredients necessary to model mix behavior. However, the model is too complex (i.e., there are far too many material constants to be determined). This difficulty can be resolved once it is observed that the axial force measured during the shear cyclic loading (constant height condition enforced) is negligible in comparison with that measured during the creep loading. Based on this observation, it can be argued that the time-dependent response (i.e., due to the asphalt binder) is closely approximated by a linear viscoelastic model. Consequently, it is possible to replace the nonlinear springs associated with the Maxwell elements with linear springs. This simplifies the representation as shown in Figure 6.3.

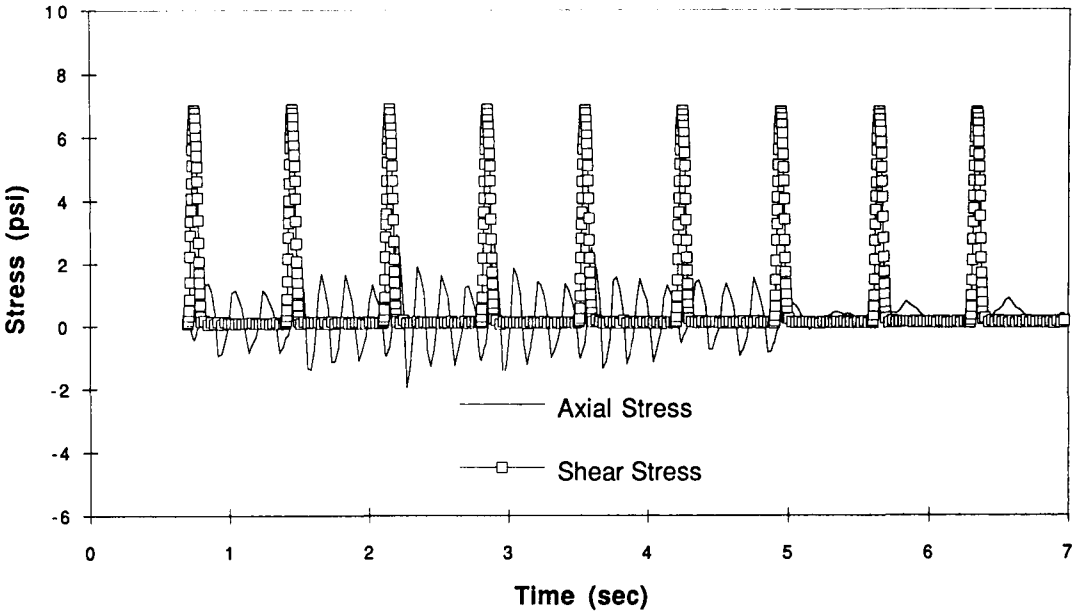

Figure 6.12. Axial and shear stresses, cycles 1 through 9 (constant height shear)

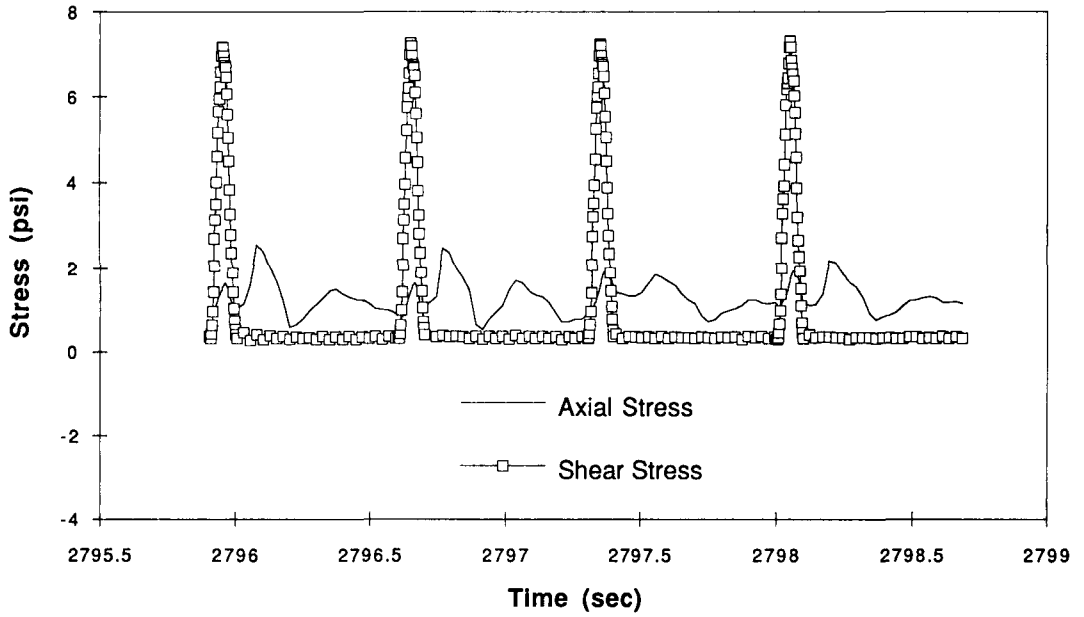

Figure 6.13. Axial and shear stresses, cycles 3997 through 4000 (constant height shear)

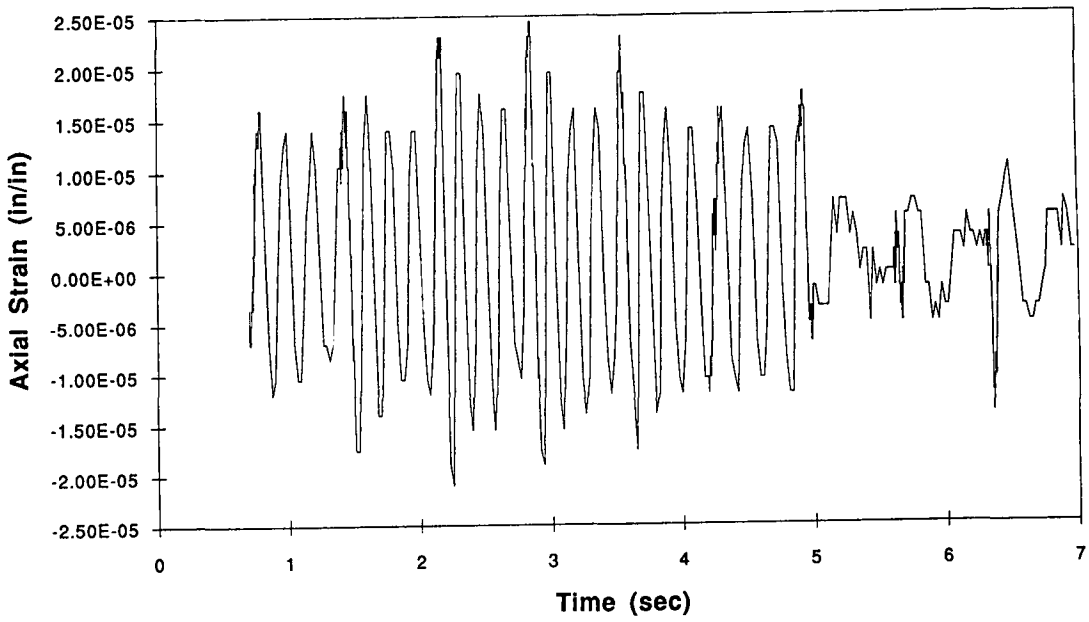

Figure 6.14. Axial strain for the first nine cycles (constant height shear)

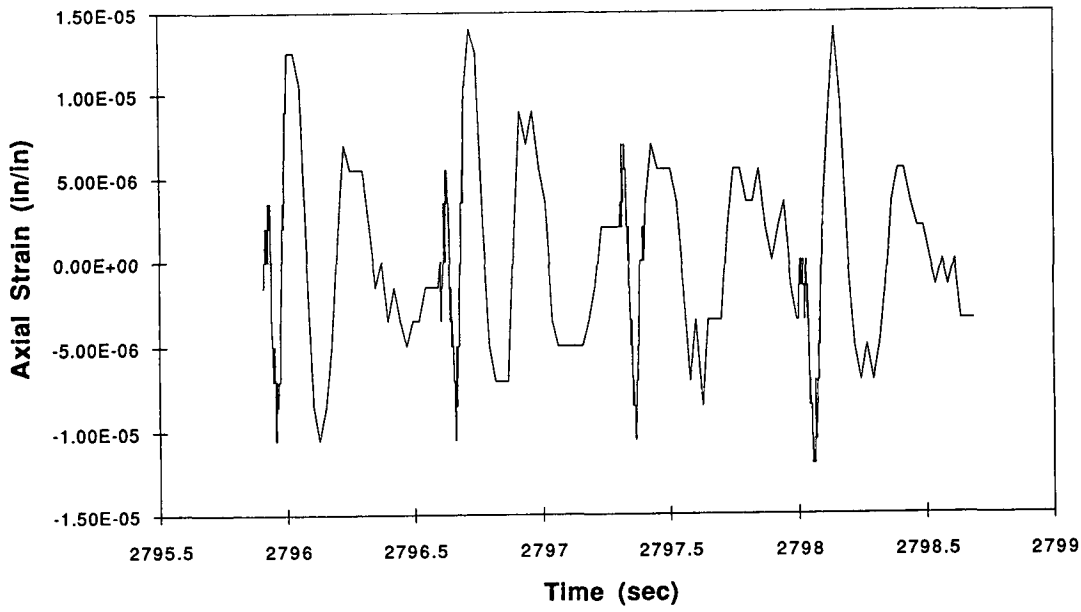

Figure 6.15. Axial strain, cycles 3997 through 4000 (constant height shear)

This option was taken in developing the material constants presented below. Furthermore, the damage model developed was not activated. This choice was motivated by the desire to further simplify the model and the by lack of information regarding the evolution of damage to the binder. (See comments regarding the cyclic loading test in the previous sections.)

A total of 16 mixes, as noted earlier, were evaluated. The coding for the mixes is summarized in Table 6.3. Material constants for these mixes are summarized in Tables 6.4 through 6.27. As an example, the fits obtained for the mix with binder AAC, aggregate RD at high void content are shown in Figures 6.16 through 6.20.

6.7 Simulations of Repeated Load Constant Height Simple Shear Test

The objective of these simulations was to evaluate and validate the material constant determined for the 16 mixes and displayed in the previous section. For each of 16 mixes, a finite element simulation of a specimen subjected to cyclic shear loading (constant height condition imposed) was performed. (Each cycle consists of a sine wave of mean value and amplitude of 24 kPA [3.5 psi] at 10 Hz for 0.1 s, followed by 0.6 s of no load.) The simulations are of perfect test conditions (i.e., shear traction was applied to all appropriate surfaces). In view of the cracks that developed in the specimens tested in the laboratory, this difference plays a significant role and leads to a markedly different behavior. (Note that the model does not account for the development of cracks; moreover, a better approximation of the boundary conditions will not lead to a much closer approximation of the laboratory tests.)

Evolutions of predicted residual engineering shear strains in the mixes are shown in Figures 6.21 through 6.24 (organized by binder). From these simulations it appears that for all four binders the mixes are relatively insensitive to the air void content when aggregate RD is used (i.e., almost the same results are predicted for p0 and p1 mixes). Otherwise, no clear conclusions can be drawn.

For each of the 16 mixes, the predicted residual engineering shear strain is compared with that measured in the corresponding laboratory experiment (Figures 6.25 through 6.40). As expected, based on the discussion above, the agreement is not very good. The initial point (i.e., the residual engineering shear strain at the end of the first cycle) lies above the measured one (typically 100 to 500 percent). The initial slope (in log-log space), however, is typically the same, and it diverges as the number of cycles is increased. This is an expected result in view of the cracks that developed in the specimens tested.

6.8 Permanent Deformation Predictions in a Pavement Section

The material constants summarized in Tables 6.4 through 6.27 have been used in finite element simulations of loading on the pavement section shown in Figure 6.41. The objectives of these simulations are (1) to evaluate the performance of each mix in a pavement structure; and (2) to establish a relation between the maximum engineering shear

Table 6.3. Mix designation

Asphalt	Aggregate	Approximate Air Void Content, Percent[a]
AAK-1	RD	3.7
AAK-1	RD	6.5
AAK-1	RH	4.5
AAK-1	RH	7.0
AAC-1	RD	3.8
AAC-1	RD	6.5
AAC-1	RH	4.2
AAC-1	RH	6.0
AAM-1	RD	4.6
AAM-1	RD	7.5
AAM-1	RH	4.2
AAM-1	RH	7.6
AAG-1	RD	4.9
AAG-1	RD	7.8
AAG-1	RH	4.7
AAG-1	RH	7.5

[a]These values represent the midpoint of the range in air void content for the specimens obtained from one slab.

Table 6.4. Elastic constants for plastic branch for binder AAK

	Aggregate RD, Low Voids	Aggregate RD, High Voids	Aggregate RH, Low Voids	Aggregate RH, High Voids
C_1	5.06E+02	5.06E+02	6.38E+03	4.25E+03
C_2	-2.53E+02	-5.06E+02	-2.13E+03	-2.13E+03
C_3	-5.06E+04	-5.06E+04	-3.83E+06	-4.25E+06
C_4	5.06E+04	2.02E+05	1.06E+06	8.51E+05
C_5	0.00E+00	0.00E+00	0.00E+00	0.00E+00
C_6	1.26E+08	2.53E+08	2.13E+08	2.13E+07
C_7	-5.06E+07	-3.79E+07	-4.25E+07	-4.25E+07
C_8	5.06E+07	5.06E+07	3.40E+08	4.25E+07
C_9	5.06E+05	5.06E+05	4.24E+06	4.25E+05

Table 6.5. Elastic constants for plastic branch for binder AAC

	Aggregate RD, Low Voids	Aggregate RD, High Voids	Aggregate RH, Low Voids	Aggregate RH, High Voids
C_1	4.36E+03	1.28E+03	3.54E+04	1.01E+04
C_2	-1.64E+02	-3.22E+02	-5.06E+03	-5.06E+03
C_3	-2.73E+06	-2.96E+06	-2.53E+05	-5.06E+04
C_4	1.09E+05	2.96E+05	1.26E+06	1.26E+06
C_5	0.00E+00	0.00E+00	0.00E+00	0.00E+00
C_6	5.46E+06	4.74E+08	5.06E+06	2.02E+08
C_7	-7.64E+07	-2.37E+08	-5.06E+07	-2.53E+07
C_8	1.09E+07	5.92E+07	5.06E+06	5.06E+06
C_9	1.09E+06	8.88E+06	5.06E+07	5.06E+06

Table 6.6. Elastic constants for plastic branch for binder AAM

	Aggregate RD, Low Voids	Aggregate RD, High Voids	Aggregate RH, Low Voids	Aggregate RH, High Voids
C_1	2.68E+03	2.76E+03	3.41E+02	1.72E+02
C_2	-5.61E+03	-3.28E+03	-1.58E+02	-7.92E+01
C_3	-2.81E+06	-2.29E+06	-1.12E+05	-2.31E+05
C_4	1.12E+06	8.19E+05	1.12E+05	4.62E+04
C_5	0.00E+00	0.00E+00	0.00E+00	0.00E+00
C_6	2.81E+08	4.14E+07	2.80E+08	4.62E+08
C_7	-2.81E+07	-3.28E+06	-1.12E+08	-4.62E+06
C_8	2.81E+07	3.28E+05	1.12E+08	4.62E+06
C_9	2.81E+07	6.55E+07	5.60E+06	4.62E+05

Table 6.7. Elastic constants for plastic branch for binder AAG

	Aggregate RD, Low Voids	Aggregate RD, High Voids	Aggregate RH, Low Voids	Aggregate RH, High Voids
C_1	1.05E+04	1.01E+04	5.78E+01	3.42E+02
C_2	-5.61E+06	-5.06E+02	-8.09E+02	-2.84E+02
C_3	-2.10E+06	-3.37E+05	-1.16E+06	-4.26E+05
C_4	1.75E+06	3.37E+05	1.16E+05	7.10E+04
C_5	0.00E+00	0.00E+00	0.00E+00	0.00E+00
C_6	6.31E+08	1.69E+07	2.89E+08	2.13E+08
C_7	-4.21E+08	-2.53E+07	-1.16E+07	-3.55E+07
C_8	7.01E+08	1.69E+07	1.16E+07	1.42E+06
C_9	7.02E+05	1.69E+05	1.16E+06	1.42E+04

Table 6.8. Plastic parameters for binder AAK

	Aggregate RD, Low Voids	Aggregate RD, High Voids	Aggregate RH, Low Voids	Aggregate RH, High Voids
σ_y	1.00E+00	1.00E+00	1.50E+00	1.50E+00
β	5.00E−01	5.00E−01	5.00E−01	5.00E−01
$\bar{H}$	1.00E+03	1.00E+03	6.50E+02	6.50E+02

Table 6.9. Plastic parameters for binder AAC

	Aggregate RD, Low Voids	Aggregate RD, High Voids	Aggregate RH, Low Voids	Aggregate RH, High Voids
σ_y	2.00E+00	1.00E−03	3.00E+00	3.00E+00
β	5.00E−01	5.00E−01	5.00E−01	5.00E−01
$\bar{H}$	5.00E+02	5.00E+02	2.00E+03	2.00E+03

Table 6.10. Plastic parameters for binder AAM

	Aggregate RD, Low Voids	Aggregate RD, High Voids	Aggregate RH, Low Voids	Aggregate RH, High Voids
σ_y	3.00E+00	3.00E+00	1.00E+00	5.00E−01
β	5.00E−01	5.00E−01	5.00E−01	5.00E−01
$\bar{H}$	2.00E+03	2.00E+03	1.00E+02	2.50E+02

Table 6.11. Plastic parameters for binder AAG

	Aggregate RD, Low Voids	Aggregate RD, High Voids	Aggregate RH, Low Voids	Aggregate RH, High Voids
σ_y	3.00E+00	1.50E+00	1.00E+04	1.00E+00
β	5.00E−01	5.00E−01	5.00E−01	5.00E−01
$\bar{H}$	1.50E+03	1.00E+03	5.00E+01	2.50E+02

Table 6.12. Plastic constants for Maxwell elements for binder AAK

	Aggregate RD, Low Voids	Aggregate RD, High Voids	Aggregate RH, Low Voids	Aggregate RH, High Voids
C_1	4.47E+05	4.47E+05	9.73E+04	9.73E+04
C_2	-1.34E+05	-1.34E+05	-5.00E+04	-5.00E+04

Table 6.13. Plastic constants for Maxwell elements for binder AAC

	Aggregate RD, Low Voids	Aggregate RD, High Voids	Aggregate RH, Low Voids	Aggregate RH, High Voids
C_1	4.82E+05	1.18E+06	4.47E+05	4.47E+05
C_2	-2.00E+05	-4.00E+04	-1.34E+04	-1.34E+05

Table 6.14. Plastic constants for Maxwell elements for binder AAM

	Aggregate RD, Low Voids	Aggregate RD, High Voids	Aggregate RH, Low Voids	Aggregate RH, High Voids
C_1	1.32E+05	1.17E+05	1.50E+06	5.14E+05
C_2	-1.00E+05	-5.00E+04	-2.00E+05	-2.50E+05

Table 6.15. Plastic constants for Maxwell elements for binder AAG

	Aggregate RD, Low Voids	Aggregate RD, High Voids	Aggregate RH, Low Voids	Aggregate RH, High Voids
C_1	5.44E+05	1.00E+06	5.00E+04	3.35E+05
C_2	-3.00E+05	-6.00E+05	-1.00E+04	-2.00E+05

Table 6.16. Viscous parameters for binder AAK

	Aggregate RD, Low Voids	Aggregate RD, High Voids	Aggregate RH, Low Voids	Aggregate RH, High Voids
V_1	1.62E+08	2.00E+08	8.00E+07	8.00E+07
V_2	2.21E+06	3.31E+06	8.00E+05	8.00E+05

Table 6.17. Viscous parameters for binder AAC

	Aggregate RD, Low Voids	Aggregate RD, High Voids	Aggregate RH, Low Voids	Aggregate RH, High Voids
V_1	1.77E+08	2.83E+09	1.00E+08	1.00E+08
V_2	3.62E+06	5.68E+06	1.00E+04	1.00E+04

Table 6.18. Viscous parameters for binder AAM

	Aggregate RD, Low Voids	Aggregate RD, High Voids	Aggregate RH, Low Voids	Aggregate RH, High Voids
V_1	2.35E+08	5.00E+08	5.00E+07	5.00E+07
V_2	1.00E+04	1.00E+04	3.98E+06	3.42E+06

Table 6.19. Viscous parameters for binder AAG

	Aggregate RD, Low Voids	Aggregate RD, High Voids	Aggregate RH, Low Voids	Aggregate RH, High Voids
V_1	1.38E+09	1.00E+07	5.00E+08	1.00E+08
V_2	1.00E+03	1.00E+06	1.00E+07	1.11E+06

Table 6.20. Elastic weights for Maxwell elements for binder AAK

	Aggregate RD, Low Voids	Aggregate RD, High Voids	Aggregate RH, Low Voids	Aggregate RH, High Voids
α_1	3.67E−04	3.67E−04	4.14E−03	4.14E−03
α_2	6.24E−04	6.34E−04	8.17E−03	8.17E−03
α_3	1.10E−03	1.10E−03	1.62E−02	1.62E−02
α_4	2.61E−03	2.61E−03	3.17E−02	3.17E−02
α_5	4.23E−03	4.23E−03	6.59E−02	6.59E−02
α_6	1.92E+02	1.92E−02	1.70E−01	1.70E−01
α_7	1.71E−01	1.72E+03	7.00E−01	7.00E−01
α_8	8.00E−01	8.00E−01	1.00E+00	1.00E+00

Table 6.21. Elastic weights for Maxwell elements for binder AAC

	Aggregate RD, Low Voids	Aggregate RD, High Voids	Aggregate RH, Low Voids	Aggregate RH, High Voids
α_1	3.89E−04	1.81E−03	3.67E−04	3.67E−04
α_2	5.28E−04	2.37E−03	6.34E−04	6.34E−04
α_3	7.20E−04	3.11E−03	1.10E−03	1.10E−03
α_4	9.70E−04	4.02E−03	2.61E−03	2.61E−03
α_5	1.40E−03	4.98E−03	4.23E−03	4.23E−03
α_6	5.53E−03	4.16E−02	1.92E−02	1.92E−02
α_7	8.92E−02	9.36E−01	1.72E−01	1.72E−01
α_8	9.00E−01	0.00E+00	8.00E−01	8.00E−01

Table 6.22. Elastic weights for Maxwell elements for binder AAM

	Aggregate RD, Low Voids	Aggregate RD, High Voids	Aggregate RH, Low Voids	Aggregate RH, High Voids
α_1	1.02E−02	1.15E−02	4.85E−04	3.31E−04
α_2	1.40E−02	1.55E−02	6.96E−04	5.67E−04
α_3	1.92E−02	2.10E−02	1.00E−03	9.79E−04
α_4	2.59E−02	2.81E−02	1.42E−03	1.62E−03
α_5	4.93E−02	3.42E−02	2.48E−03	1.93E−03
α_6	1.22E−01	1.07E−01	1.55E−02	6.03E−03
α_7	7.32E−01	7.50E−01	1.77E−01	1.13E−01
α_8	0.00E+00	0.00E+00	8.00E−01	1.12E+00

Table 6.23. Elastic weights for Maxwell elements for binder AAG

	Aggregate RD, Low Voids	Aggregate RD, High Voids	Aggregate RH, Low Voids	Aggregate RH, High Voids
α_1	2.68E−03	7.84E−04	3.67E−04	1.76E−04
α_2	3.71E−03	1.15E−03	4.83E−04	1.98E−04
α_3	5.16E−03	1.69E−03	6.39E−04	2.24E−04
α_4	3.71E−03	3.36E−03	8.05E−04	2.85E−04
α_5	2.17E−03	1.64E−02	9.96E−04	5.00E−04
α_6	1.41E−02	3.10E−02	8.33E−03	9.63E−03
α_7	1.62E−01	3.37E−01	1.87E−01	1.53E−01
α_8	1.20E+00	6.07E−01	8.00E−01	8.34E−01

Table 6.24. Viscous weights for Maxwell elements for binder AAK

	Aggregate RD, Low Voids	Aggregate RD, High Voids	Aggregate RH, Low Voids	Aggregate RH, High Voids
β_1	8.25E−01	8.25E−01	8.02E−01	8.02E−01
β_2	1.42E−01	1.42E−01	1.58E−01	1.58E−01
β_3	2.47E−02	2.47E−02	3.14E−02	3.14E−02
β_4	5.86E−03	5.86E−03	6.15E−03	6.15E−03
β_5	9.51E−04	9.51E−04	1.28E−03	1.28E−03
β_6	4.31E−04	4.31E−04	3.29E−04	3.29E−04
β_7	3.86E−04	3.86E−04	1.36E−04	1.36E−04
β_8	1.80E−04	1.80E−04	4.00E−05	4.00E−05

Table 6.25. Viscous weights for Maxwell elements for binder AAC

	Aggregate RD, Low Voids	Aggregate RD, High Voids	Aggregate RH, Low Voids	Aggregate RH, High Voids
β_1	8.64E−01	8.69E−01	8.25E−01	8.25E−01
β_2	1.17E−01	1.13E−01	1.42E−01	1.42E−01
β_3	1.60E−02	1.49E−02	2.47E−02	2.47E−02
β_4	2.15E−03	1.93E−03	5.86E−03	5.86E−03
β_5	3.10E−04	2.39E−04	9.50E−04	9.50E−04
β_6	1.23E−04	1.99E−04	4.31E−04	4.31E−04
β_7	1.98E−04	4.49E−04	3.86E−04	3.86E−04
β_8	2.00E−04	0.00E+04	1.80E−04	1.80E−04

Table 6.26. Viscous weights for Maxwell elements for binder AAM

	Aggregate RD, Low Voids	Aggregate RD, High Voids	Aggregate RH, Low Voids	Aggregate RH, High Voids
β_1	8.63E−01	8.65E−01	8.56E−01	8.29E−01
β_2	1.18E−01	1.17E−01	1.23E−01	1.42E−01
β_3	1.62E−02	1.58E−02	1.77E−02	2.45E−02
β_4	2.19E−03	2.12E−03	2.50E−03	4.05E−03
β_5	4.16E−04	2.58E−04	4.37E−04	4.84E−04
β_6	1.03E−04	8.09E−05	2.74E−04	1.51E−04
β_7	6.17E−05	5.66E−05	3.13E−04	2.84E−04
β_8	0.00E+00	0.00E+00	1.41E−04	2.82E−04

Table 6.27. Viscous weights for Maxwell elements for binder AAG

	Aggregate RD, Low Voids	Aggregate RD, High Voids	Aggregate RH, Low Voids	Aggregate RH, High Voids
β_1	8.63E−01	8.51E−01	8.68E−01	8.86E−01
β_2	1.19E−01	1.25E−01	1.14E−01	9.96E−02
β_3	1.66E−02	1.83E−02	1.51E−02	1.12E−02
β_4	1.19E−03	3.64E−03	1.91E−03	1.43E−03
β_5	6.99E−05	1.78E−03	2.36E−04	2.51E−04
β_6	4.53E−05	3.37E−04	1.97E−04	4.84E−04
β_7	5.21E−05	3.66E−04	4.44E−04	7.71E−04
β_8	3.86E−05	6.59E−05	1.89E−04	4.19E−04

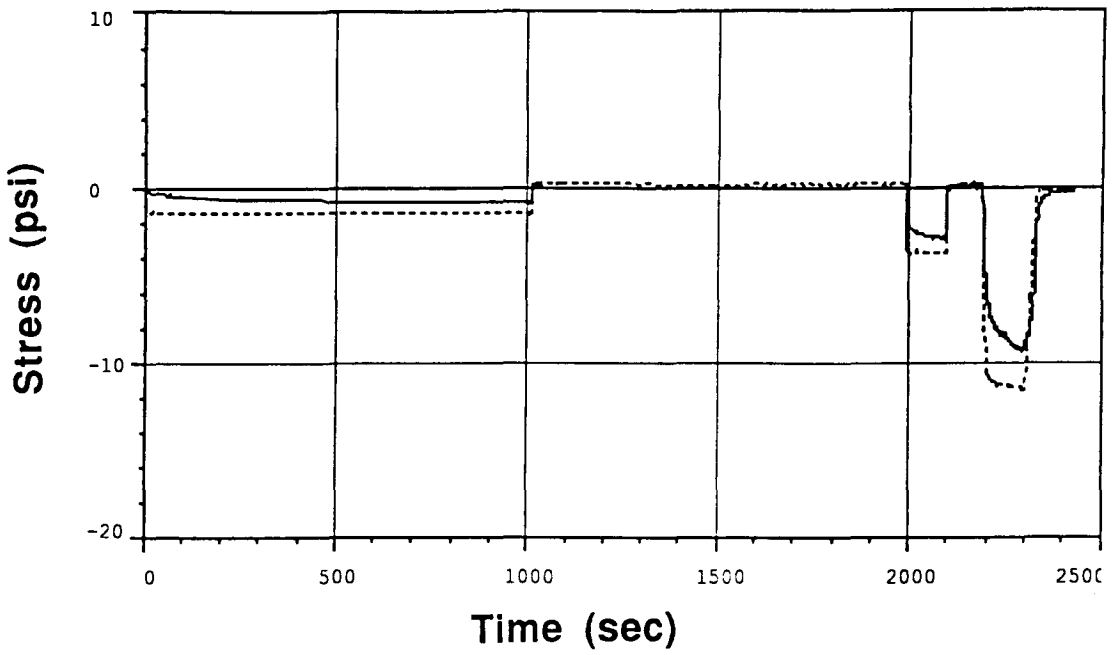

Figure 6.16. Axial stress fit, constant height shear test

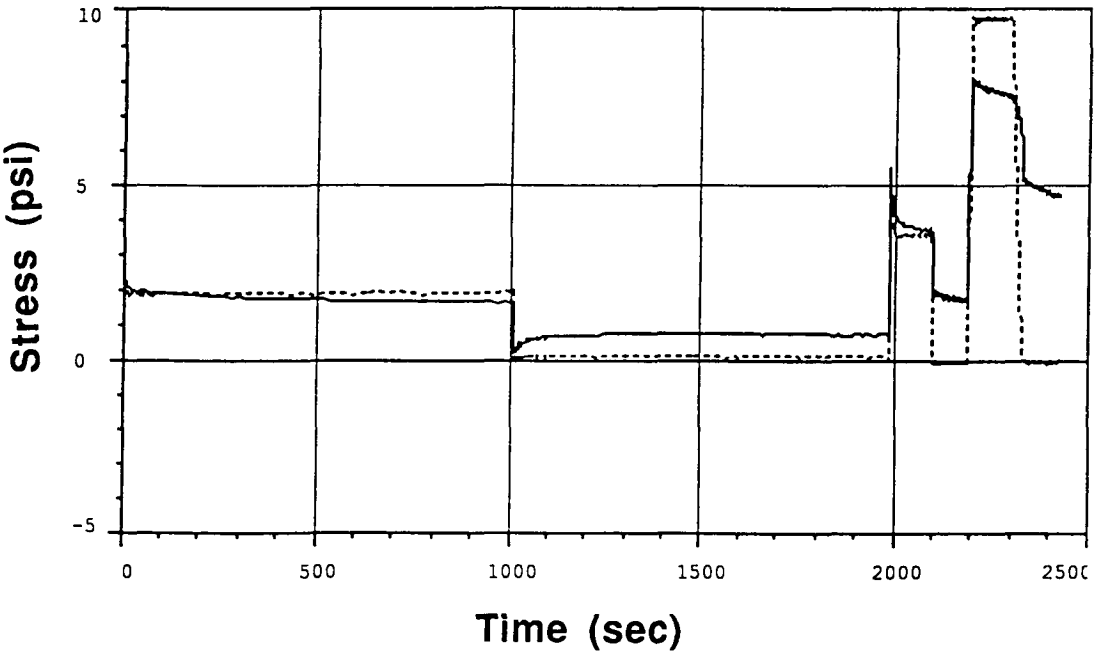

Figure 6.17. Shear stress fit, constant height shear test

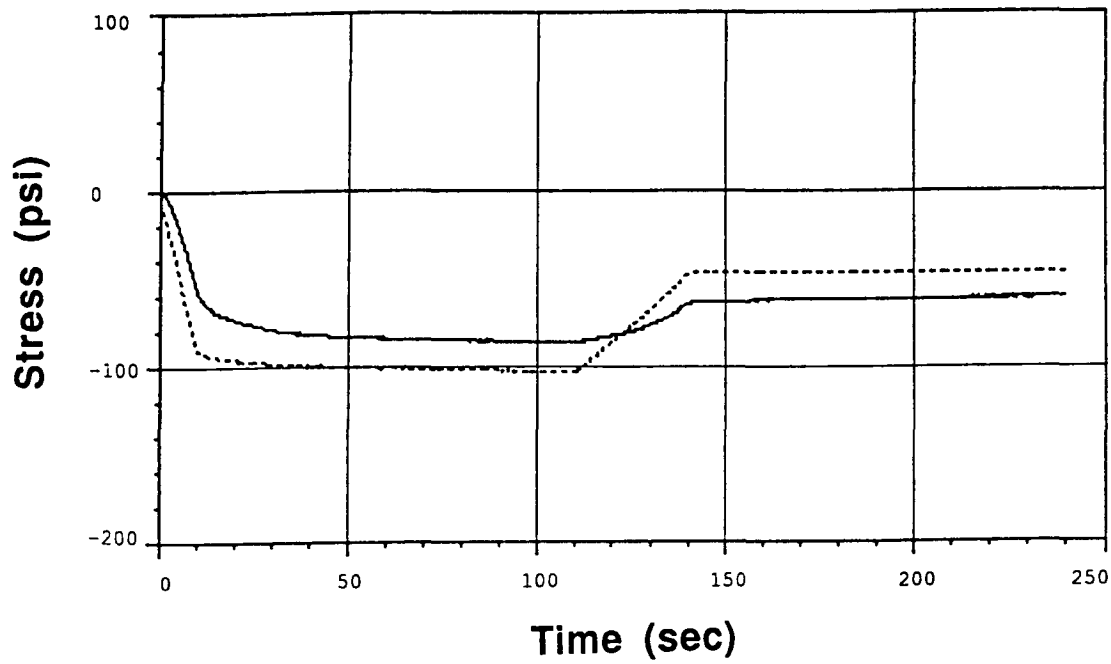

Figure 6.18. Axial stress fit, uniaxial strain test

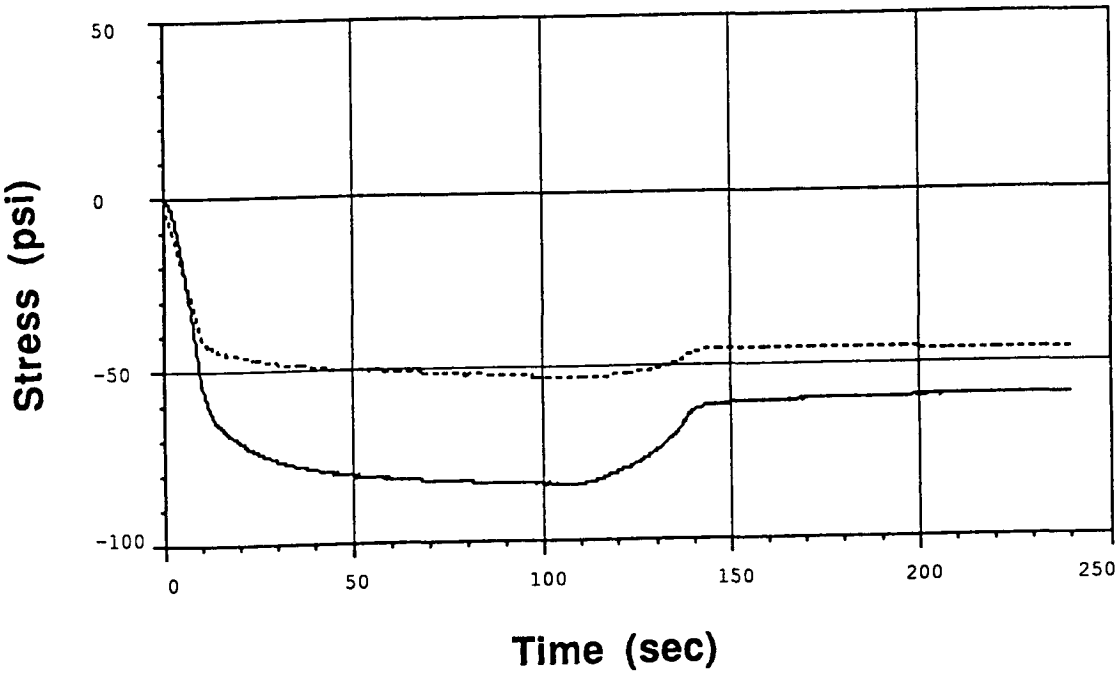

Figure 6.19. Radial stress fit, uniaxial strain test

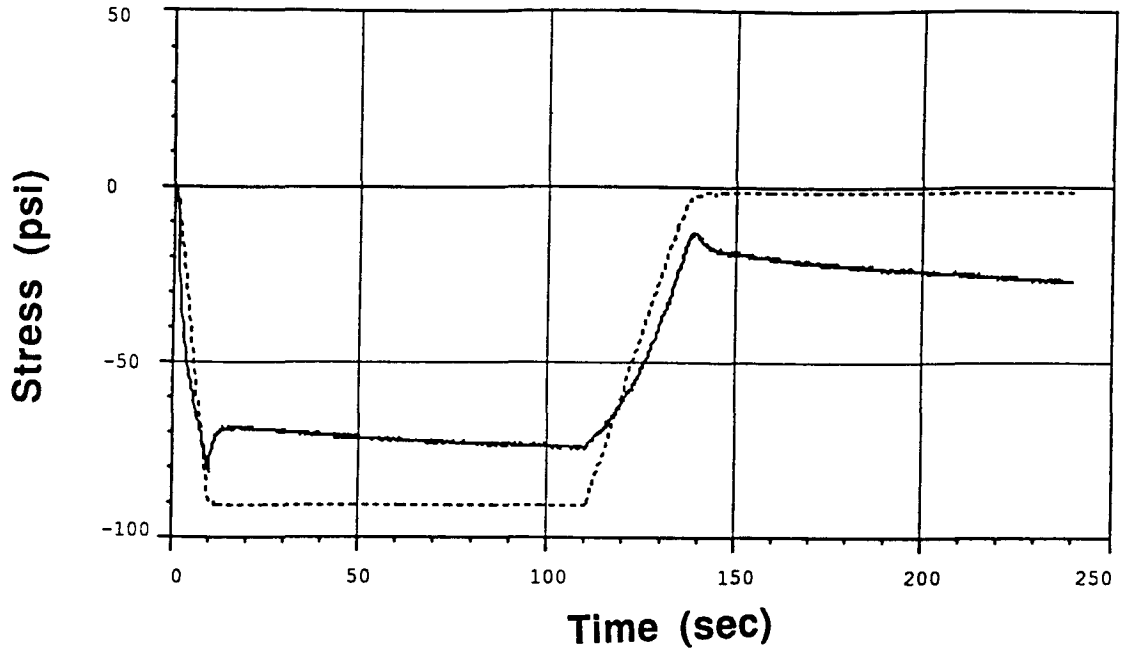

Figure 6.20. Hydrostatic pressure fit, volumetric test

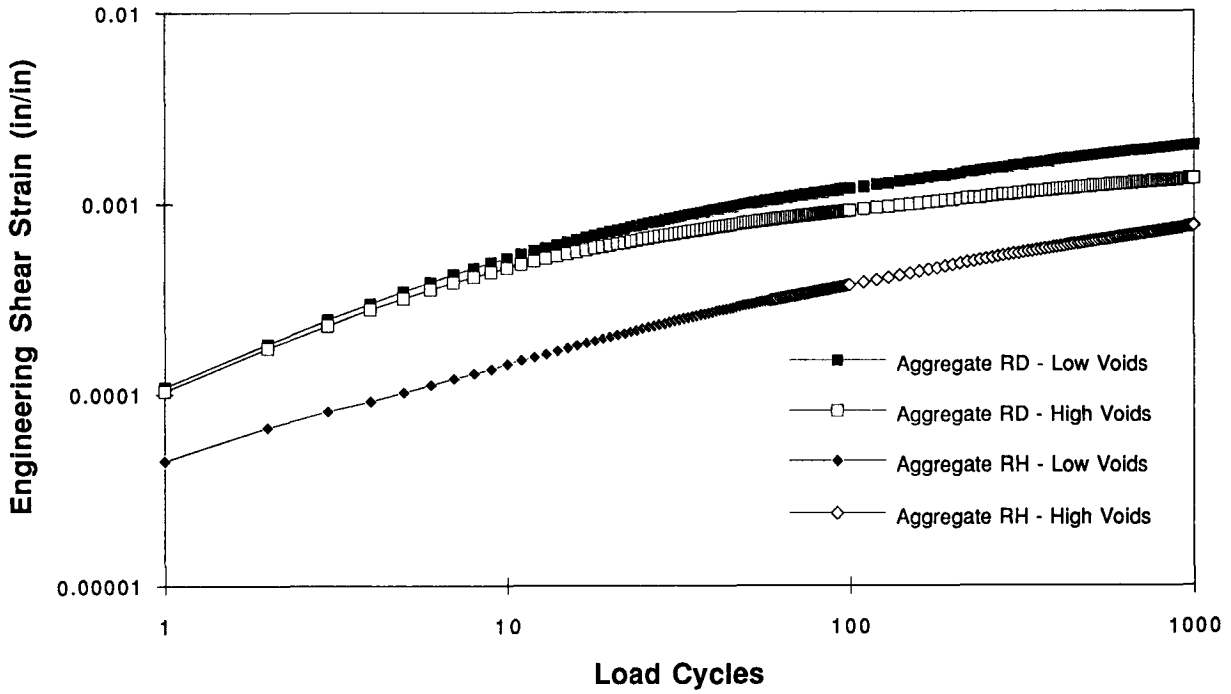

Figure 6.21. Evolution of the residual engineering shear strain in a finite element simulation of a constant height shear test for binder AAK

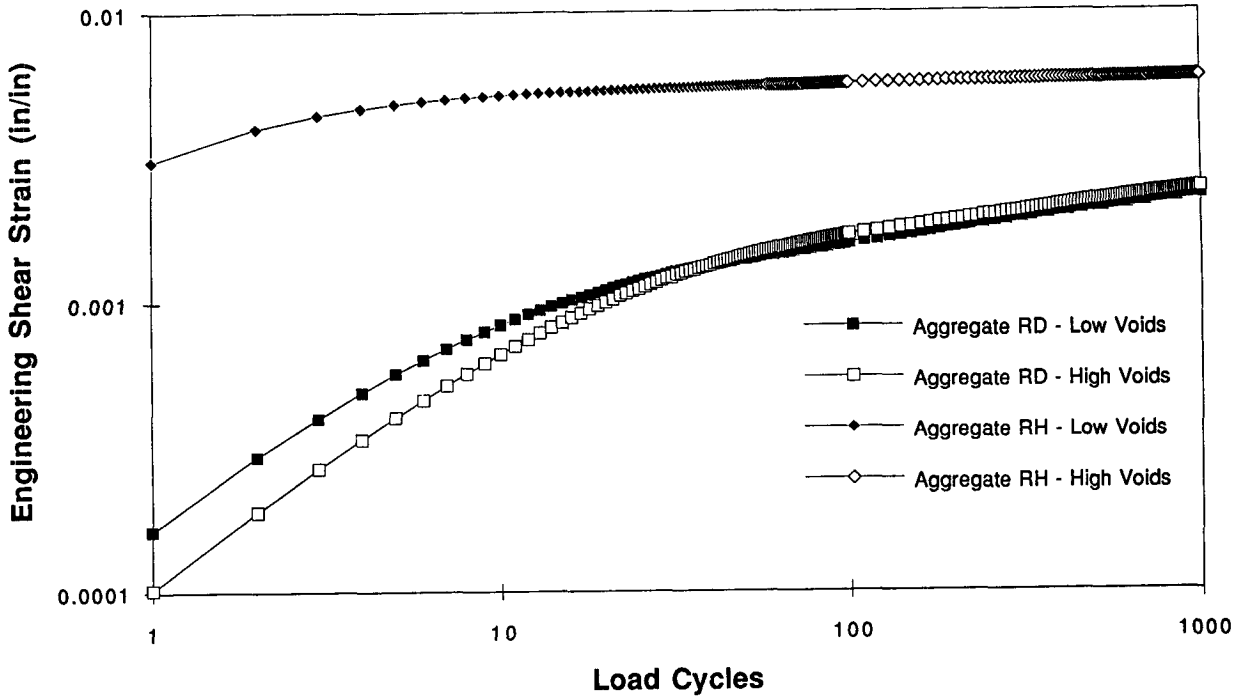

Figure 6.22. Evolution of the residual engineering shear strain in a finite element simulation of a constant height shear test for binder AAC

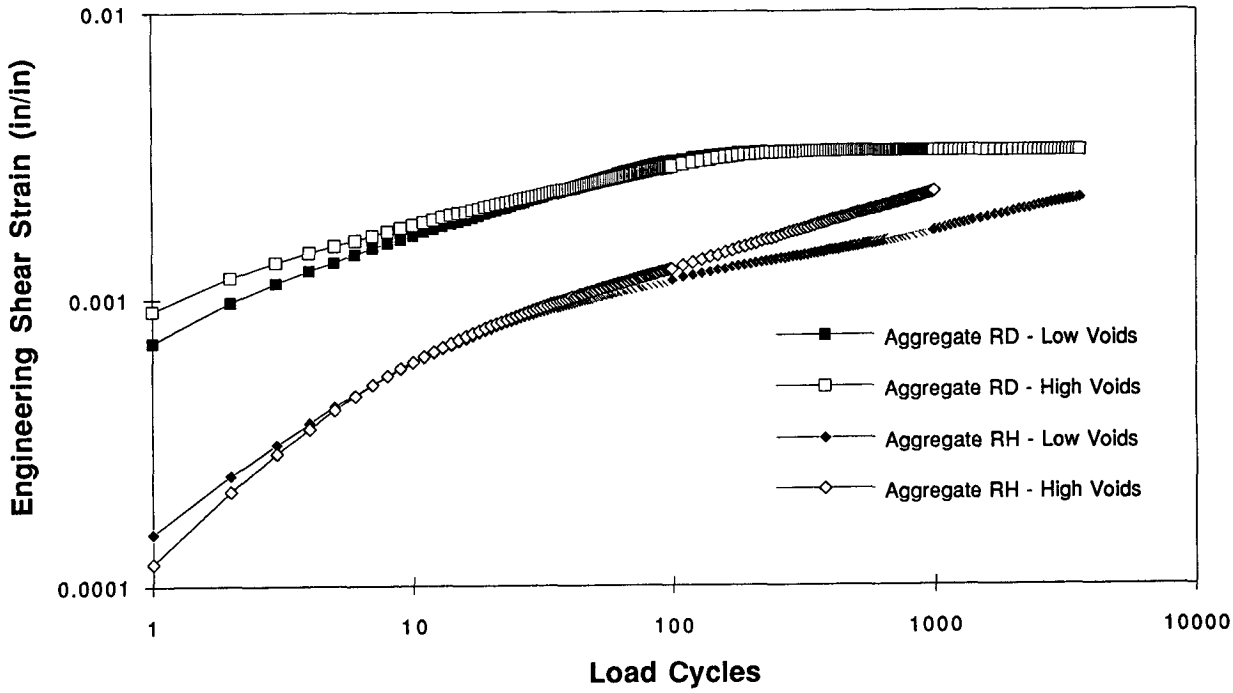

Figure 6.23. Evolution of the residual engineering shear strain in a finite element simulation of a constant height shear test for binder AAM

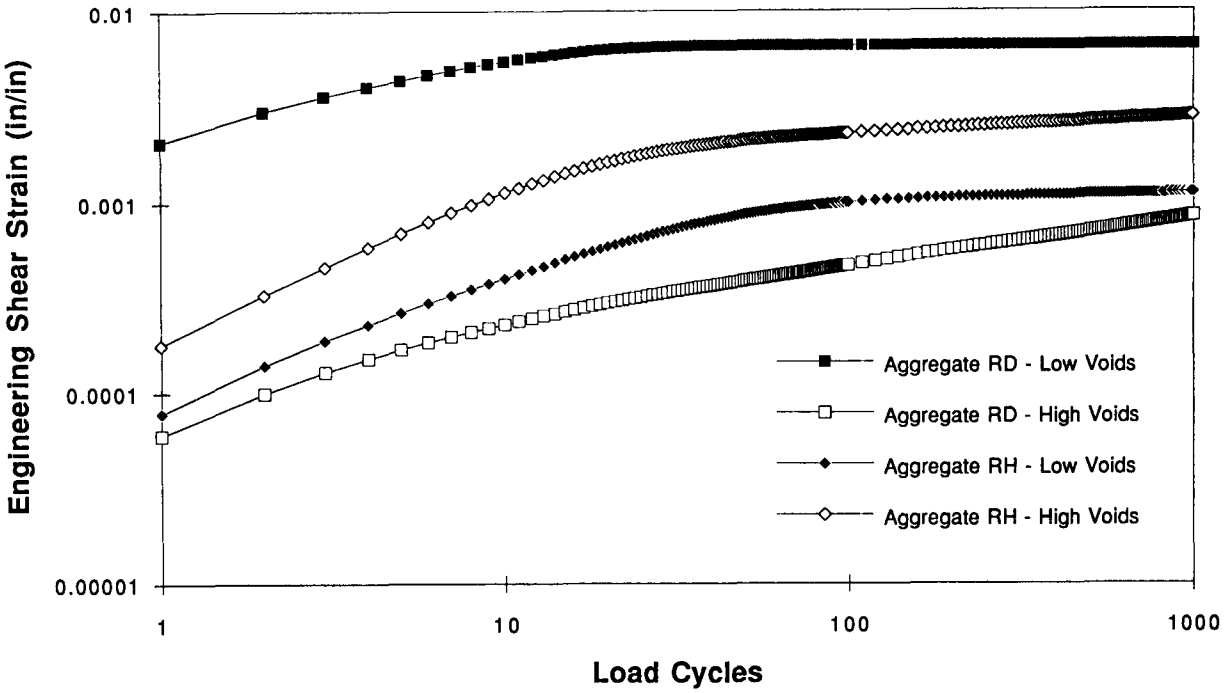

Figure 6.24. Evolution of the residual engineering shear strain in a finite element simulation of a constant height shear test for binder AAG

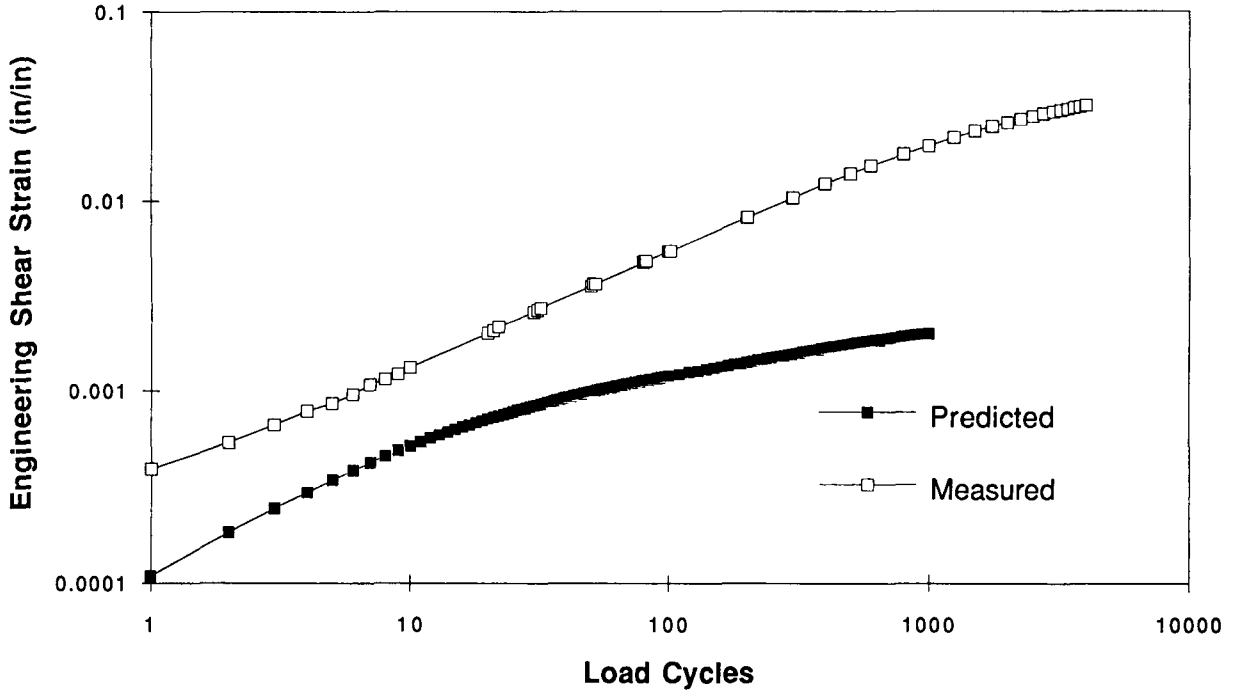

Figure 6.25. Comparison of the predicted and measured residual shear strain for binder AAK, aggregate RD, low void mix

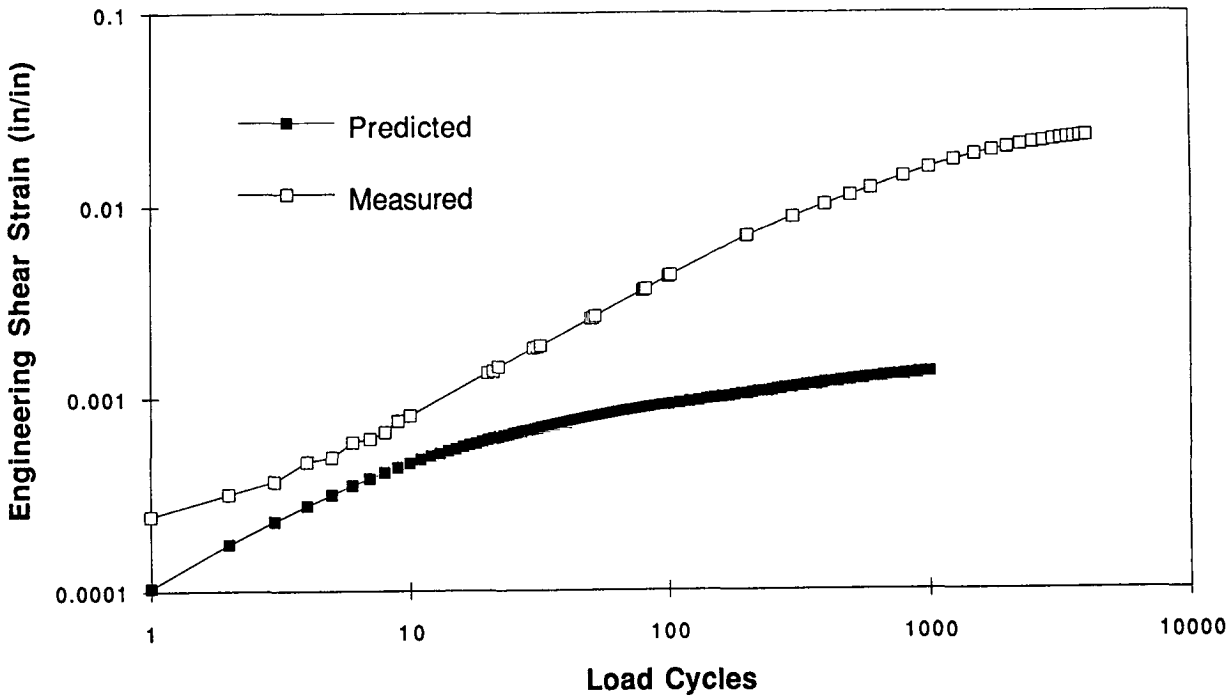

Figure 6.26. Comparison of the predicted and measured residual shear strain for binder AAK, aggregate RD, high void mix

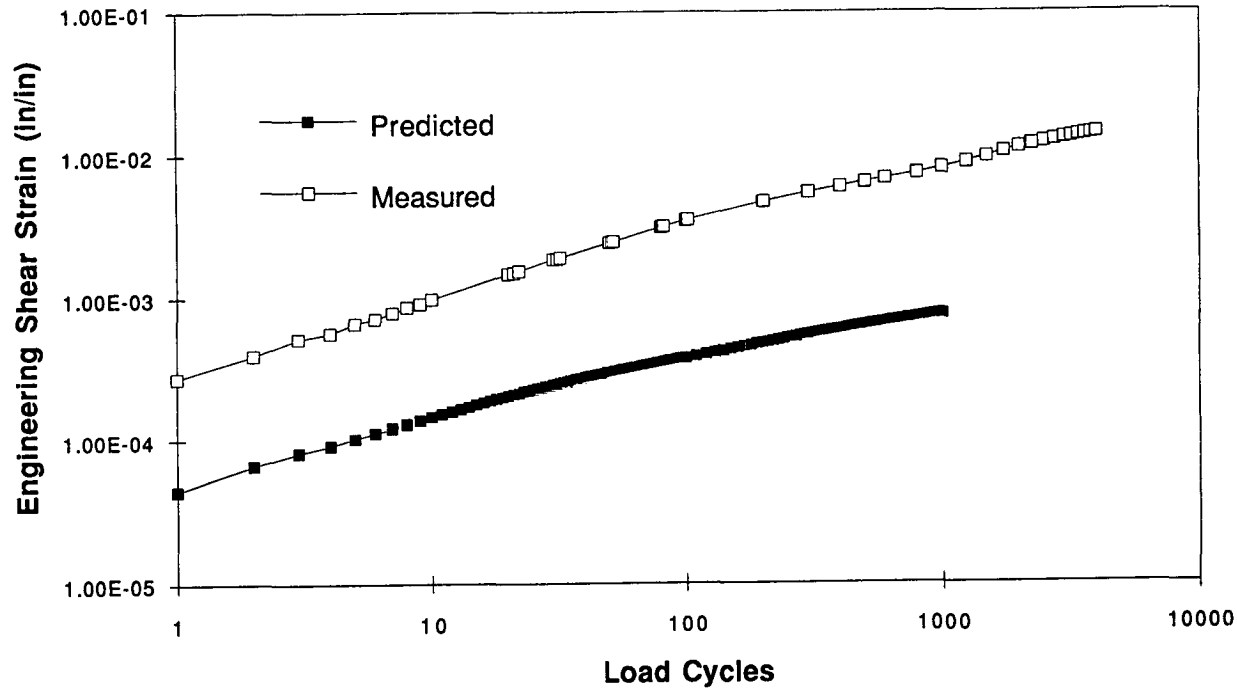

Figure 6.27. Comparison of the predicted and measured residual shear strain for binder AAK, aggregate RH, low void mix

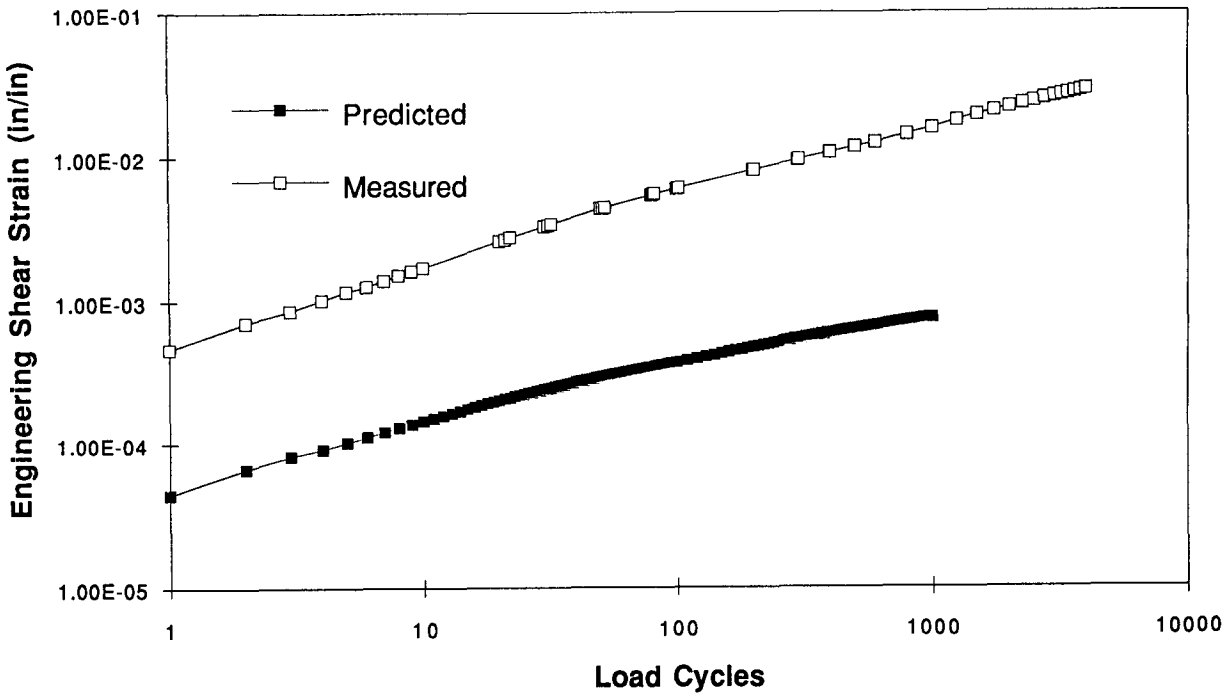

Figure 6.28. Comparison of the predicted and measured residual shear strain for binder AAK, aggregate RH, high void mix

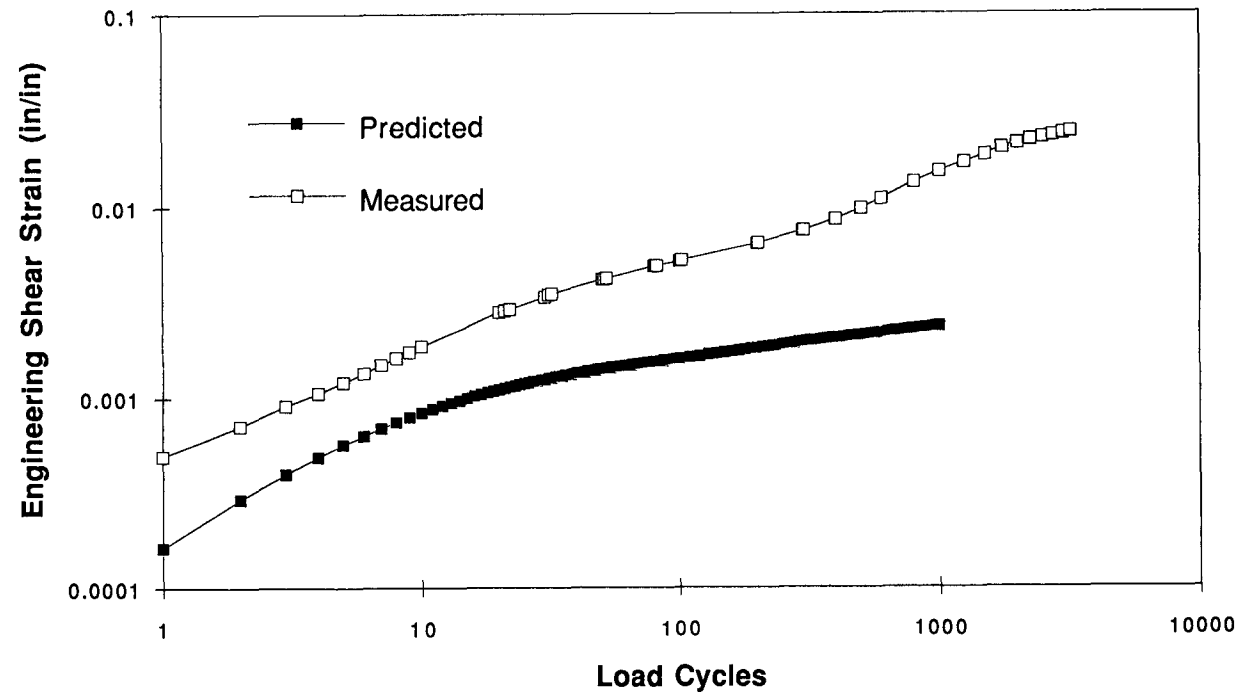

Figure 6.29. Comparison of the predicted and measured residual shear strain for binder AAC, aggregate RD, low void mix

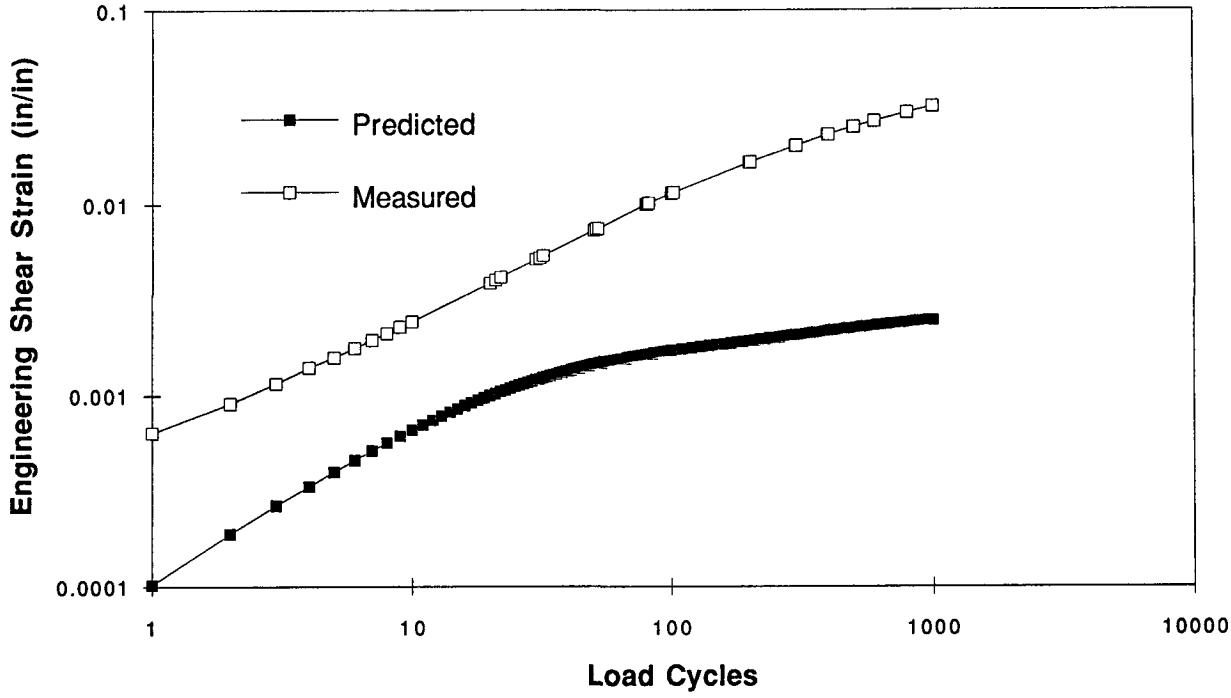

Figure 6.30. Comparison of the predicted and measured residual shear strain for binder AAC, aggregate RD, high void mix

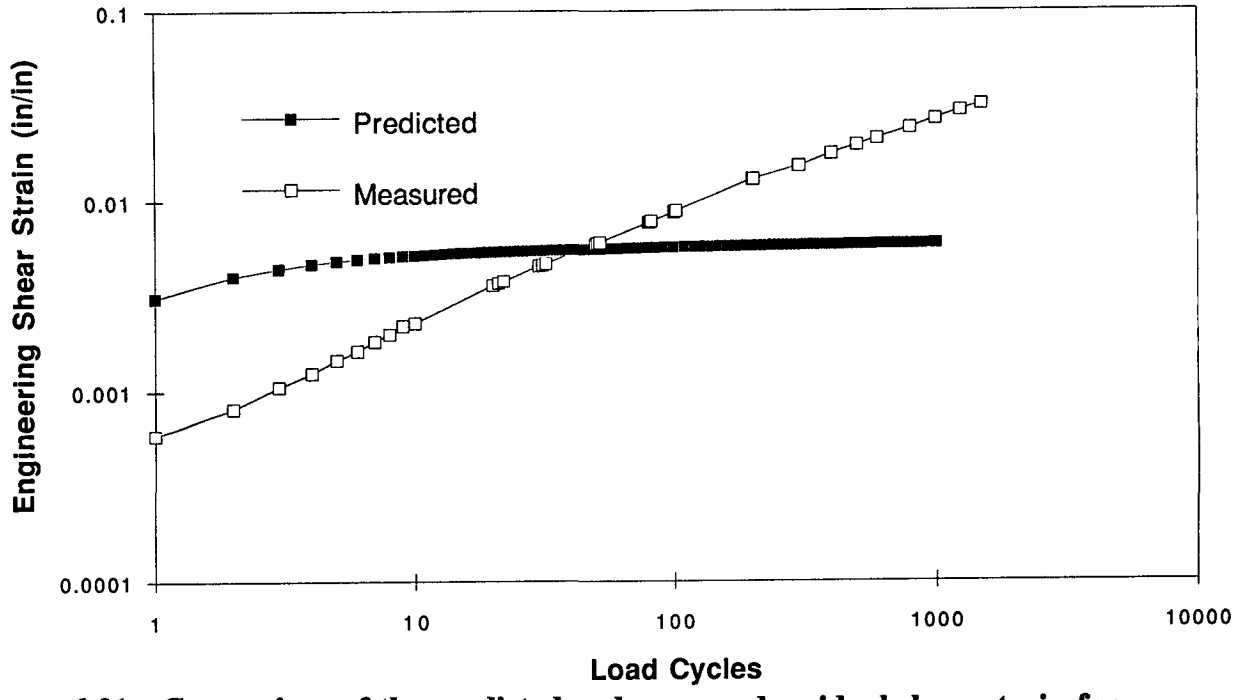

Figure 6.31. Comparison of the predicted and measured residual shear strain for binder AAC, aggregate RH, low void mix

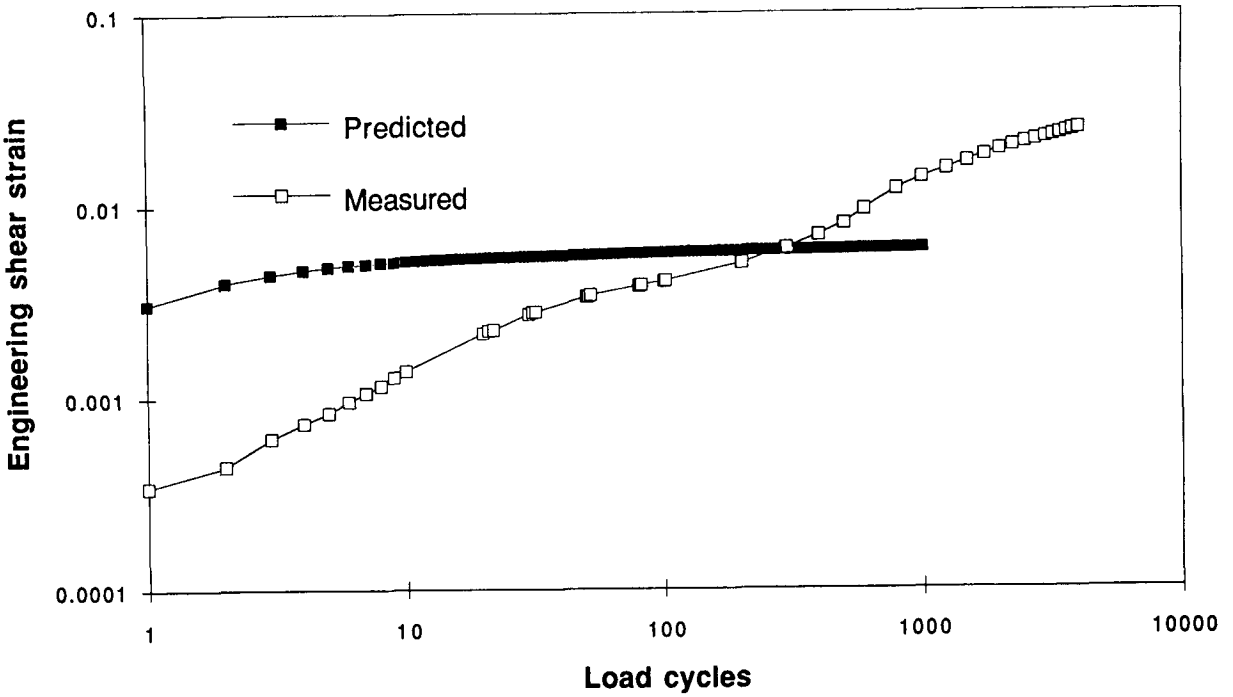

Figure 6.32. Comparison of the predicted and measured residual shear strain for binder AAC, aggregate RH, high void mix

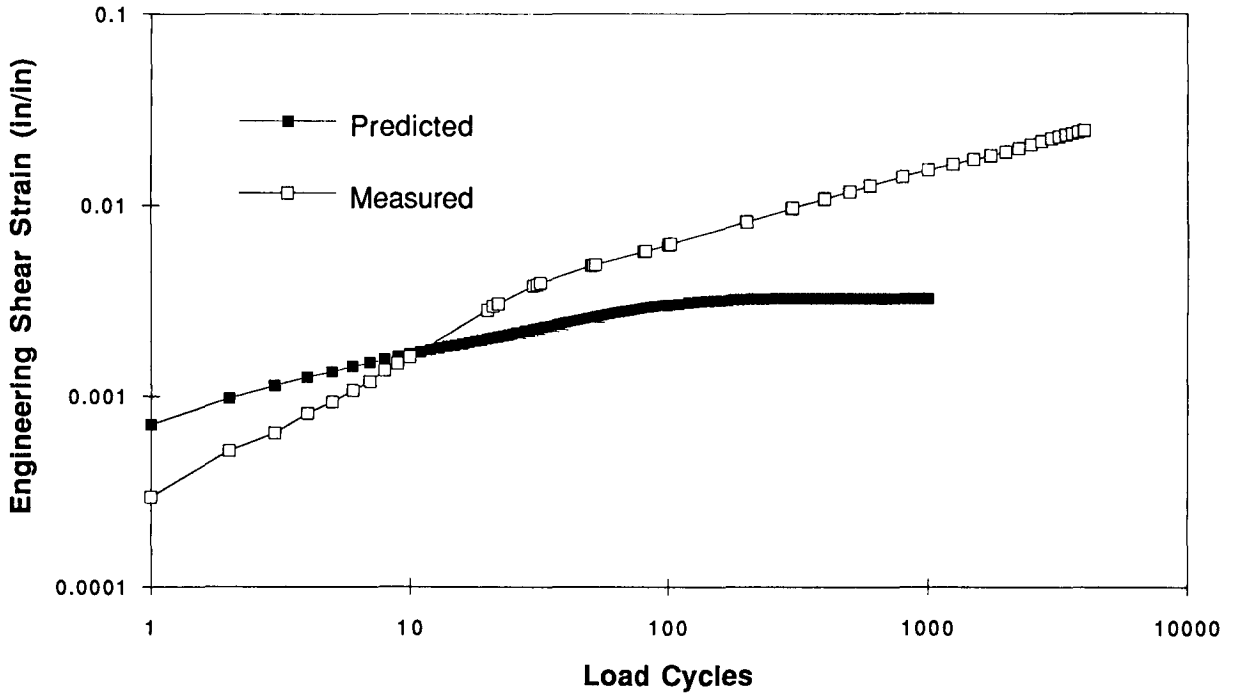

Figure 6.33. Comparison of the predicted and measured residual shear strain for binder AAM, aggregate RD, low void mix

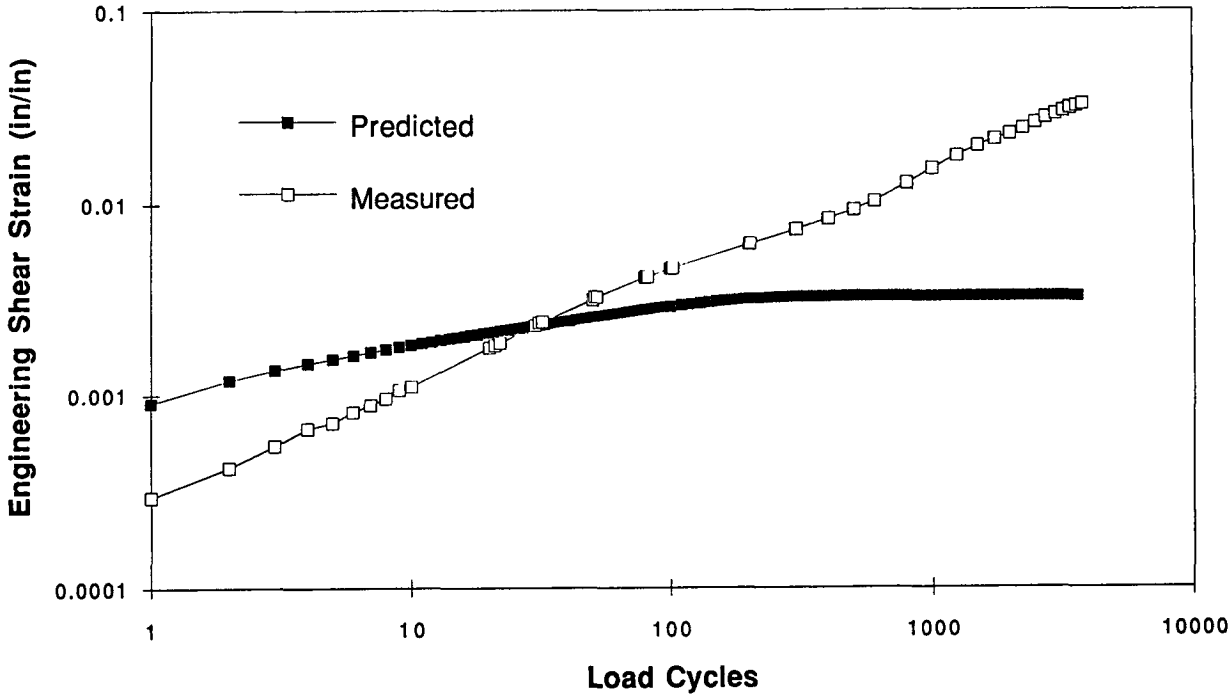

Figure 6.34. Comparison of the predicted and measured residual shear strain for binder AAM, aggregate RD, high void mix

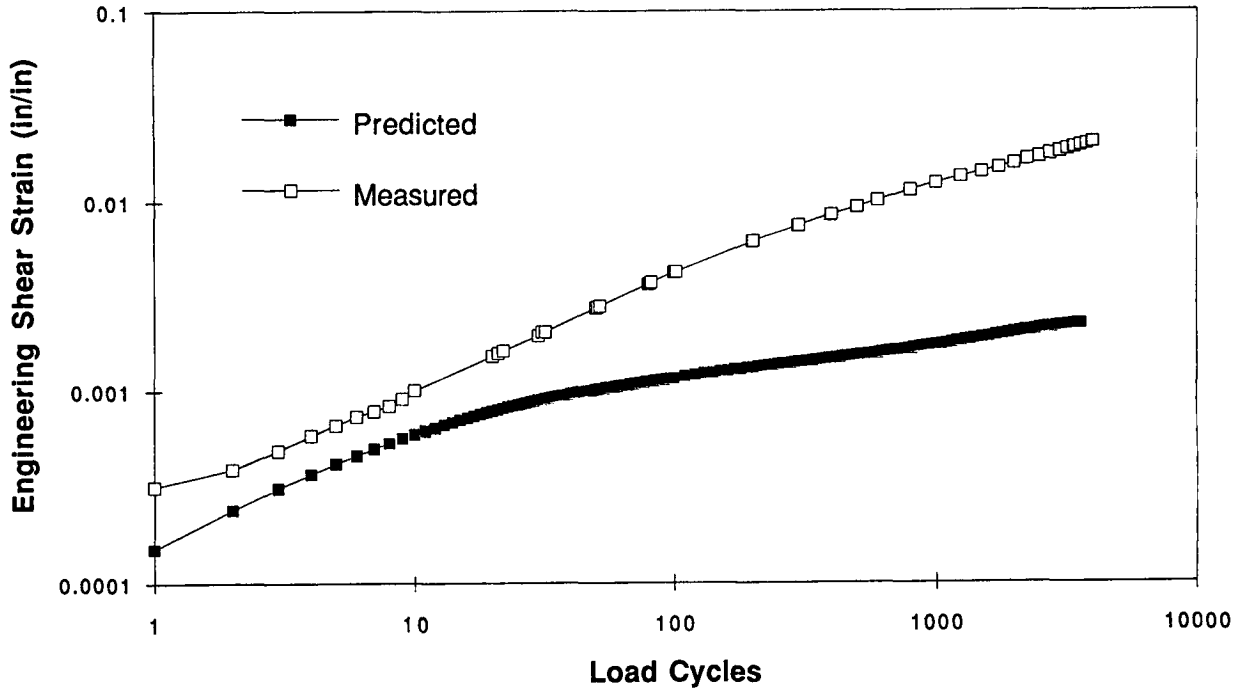

Figure 6.35. Comparison of the predicted and measured residual shear strain for binder AAM, aggregate RH, low void mix

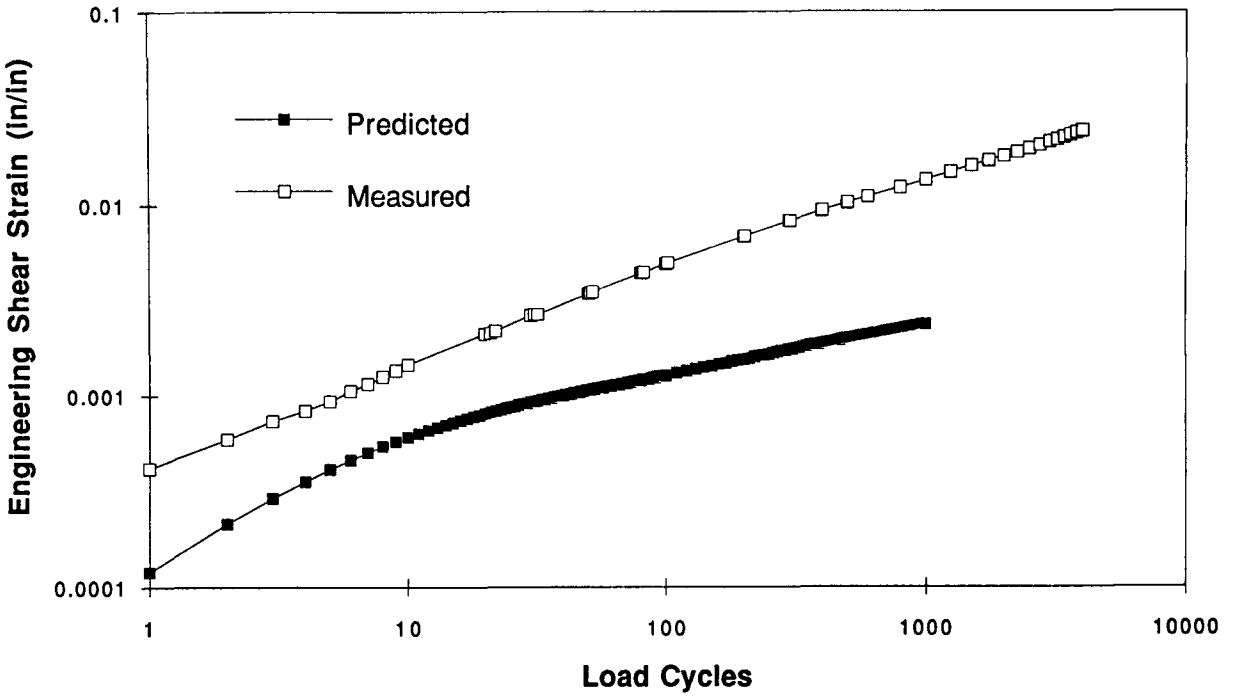

Figure 6.36. Comparison of the predicted and measured residual shear strain for binder AAM, aggregate RH, high void mix

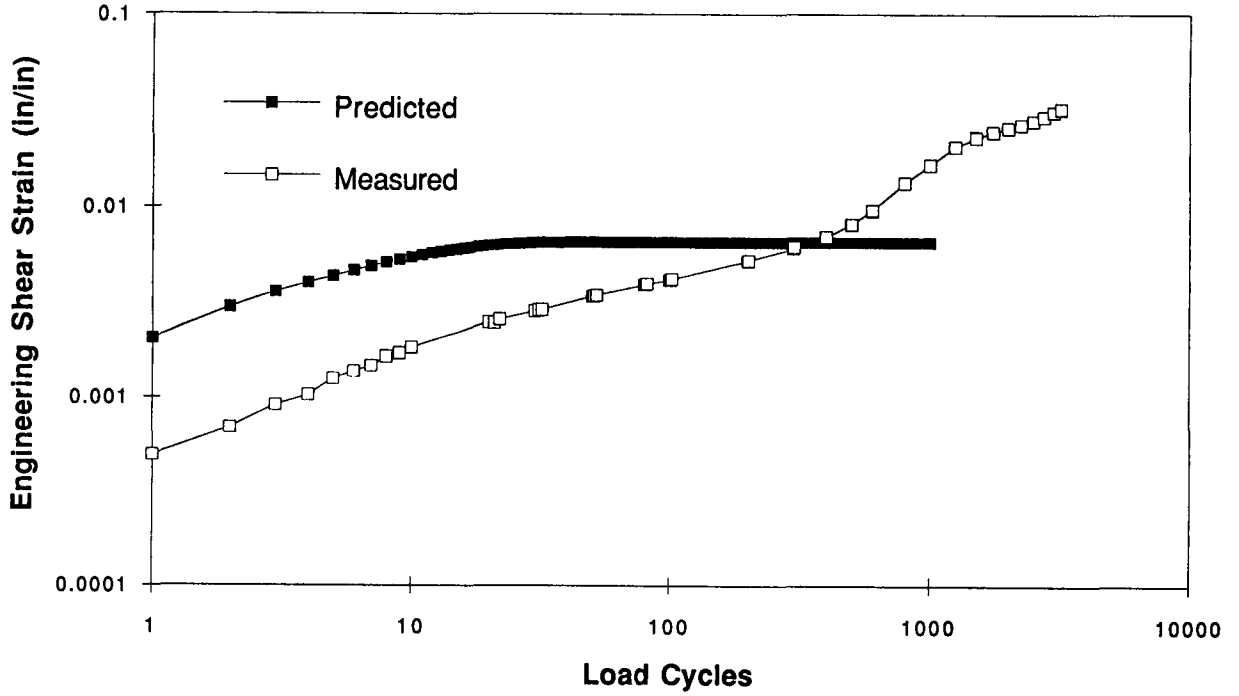

Figure 6.37. Comparison of the predicted and measured residual shear strain for binder AAG, aggregate RD, low void mix

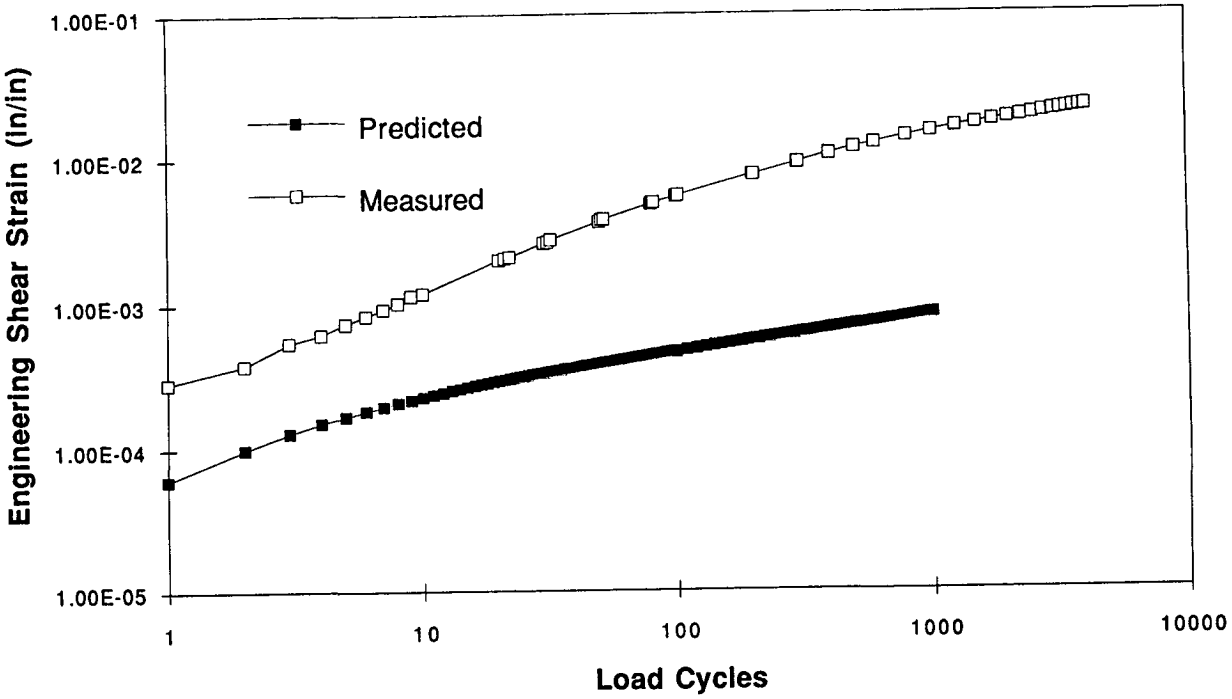

Figure 6.38. Comparison of the predicted and measured residual shear strain for binder AAG, aggregate RD, high void mix

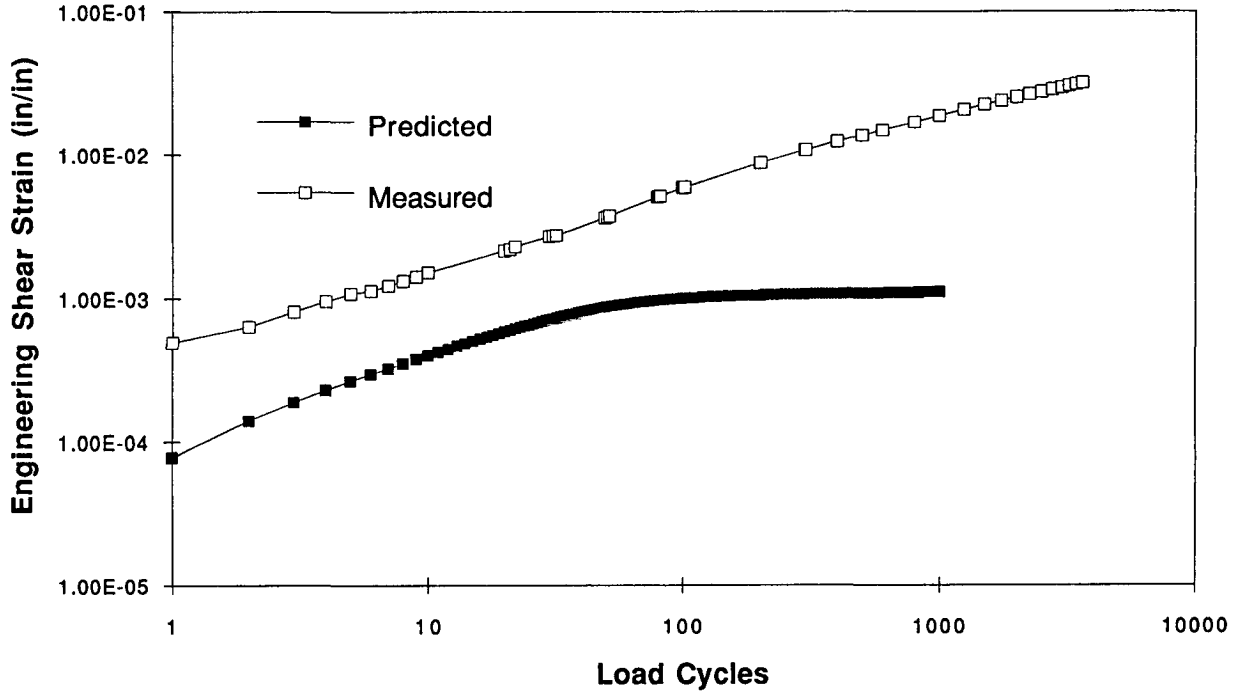

Figure 6.39. Comparison of the predicted and measured residual shear strain for binder AAG, aggregate RH, low void mix

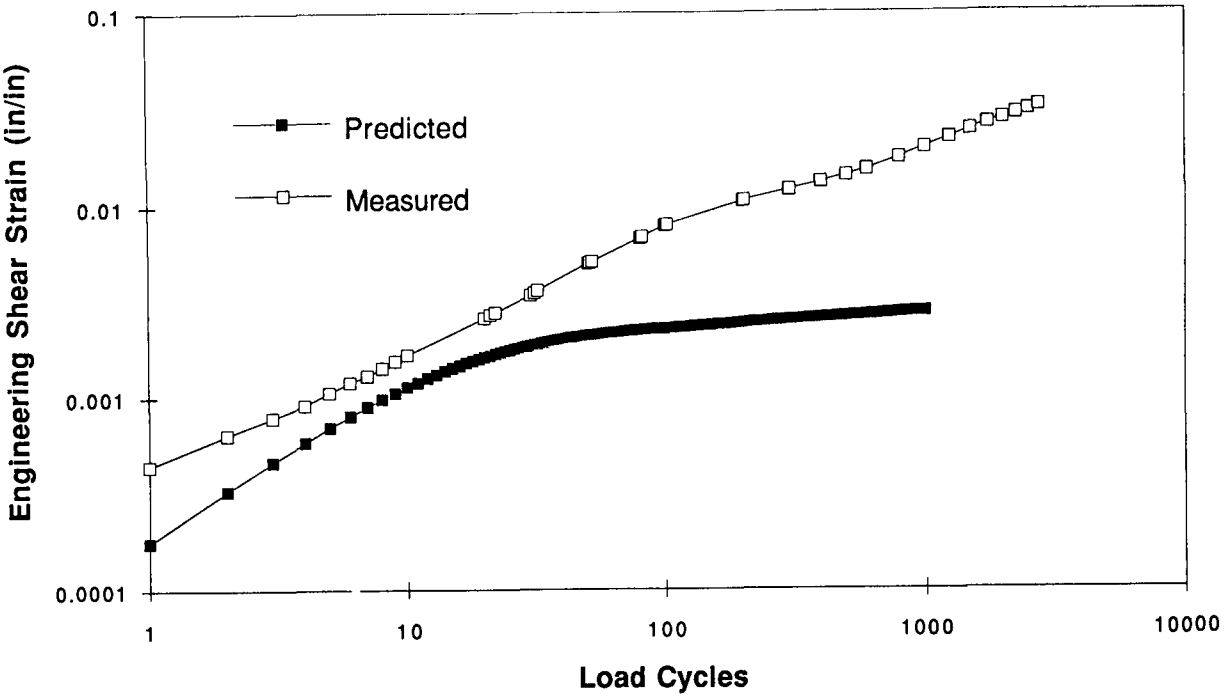

Figure 6.40. Comparison of the predicted and measured residual shear strain for binder AAG, aggregate RH, high void mix

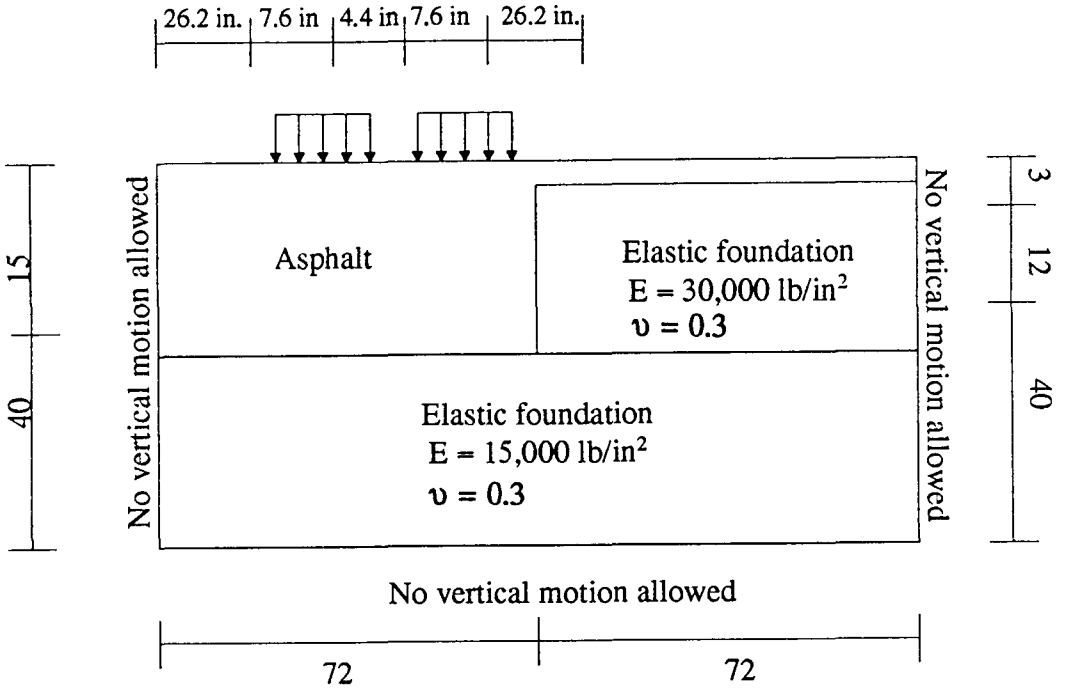

(N.B. All dimensions are in inches.)

Figure 6.41. Pavement cross section used for permanent deformation predictions

strain and the rut depth. This relation pays an important role in the procedures proposed subsequently to evaluate mix performance in actual pavements. To this end, the evolution of the rut depth, for all 16 mixes, is presented in Figures 6.42 through 6.45 (organized by binder). Next, the histories of the maximum residual engineering shear strain at the end of each cycle is plotted in Figures 6.46 through 6.49 (once again organized by binder), followed by the ratio between the rut depth and maximum engineering shear strain presented in Figures 6.50 through 6.53. Finally, the stress and strain distributions in the pavement section are presented for cycle 300 first at the time of maximum application of the load in Figures 6.54 through 6.60, and at the end of the cycle in Figures 6.61 through 6.67. All results hsown in Figures 6.54 through 6.67 are for binder AAM and aggregate RD at low voids.

In Chapter 7, these results will be compared with the results of wheel-tracking tests on the same mixes obtained by SWK/UN.

The results presented in Figures 6.50 through 6.53 illustrate a useful relationship that will be used as a part of a mix design/evaluation procedure and described subsequently in this report. The results shown in these figures were derived from the computations presented in Figures 6.42 through 6.49.

For the 38 cm (15 in.) thick asphalt concrete pavement shown in Figure 6.41, the following relationship between rut depth and maximum permanent shear strain was determined:

$$\text{Rut depth (in.)} = 11 \cdot (\gamma_p)_{max} \tag{6.34}$$

where: $(\gamma_p)_{max}$ = Maximum permanent shear strain, in./in.

(N.B. For some mixes containing aggregate RH the coefficient could be slightly larger.)

This relationship confirms earlier analyses performed on the same pavement structure without a shoulder. Moreover, this earlier study included analyses for tire pressures of 1375 kPa and 3437 kPa (200 psi and 500 psi) as well as 690 kPa (100 psi). Results of this earlier study are reported in Appendix C.

In this same appendix are included two sets of analyses for (1) three asphalt concrete mixes[7], of varying thickness 10 cm to 20 cm (4 in. to 8 in.) resting in a portland cement concrete pavement; and (2) the same mixes of varying thickness 10 cm to 30 cm (4 in. to 12 in.) resting on an untreated aggregate base and subgrade.

If Equation 6.34 is expressed as

$$\text{Rut depth} = K(\gamma_p)_{max} \tag{6.35}$$

[7]These mixes with binders AAK, AAM and AAG, and aggregrate RD showed a range in permanent deformation response.

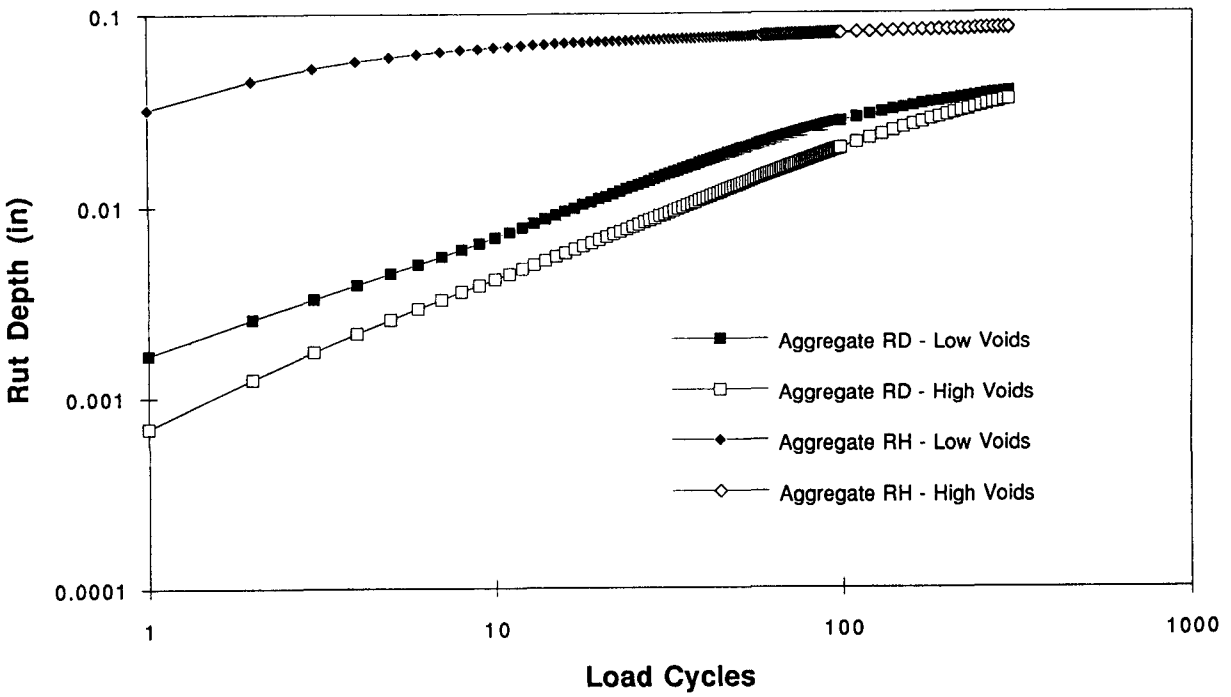

Figure 6.42. Rut depth development in a standard pavement under cyclic loading, binder AAK

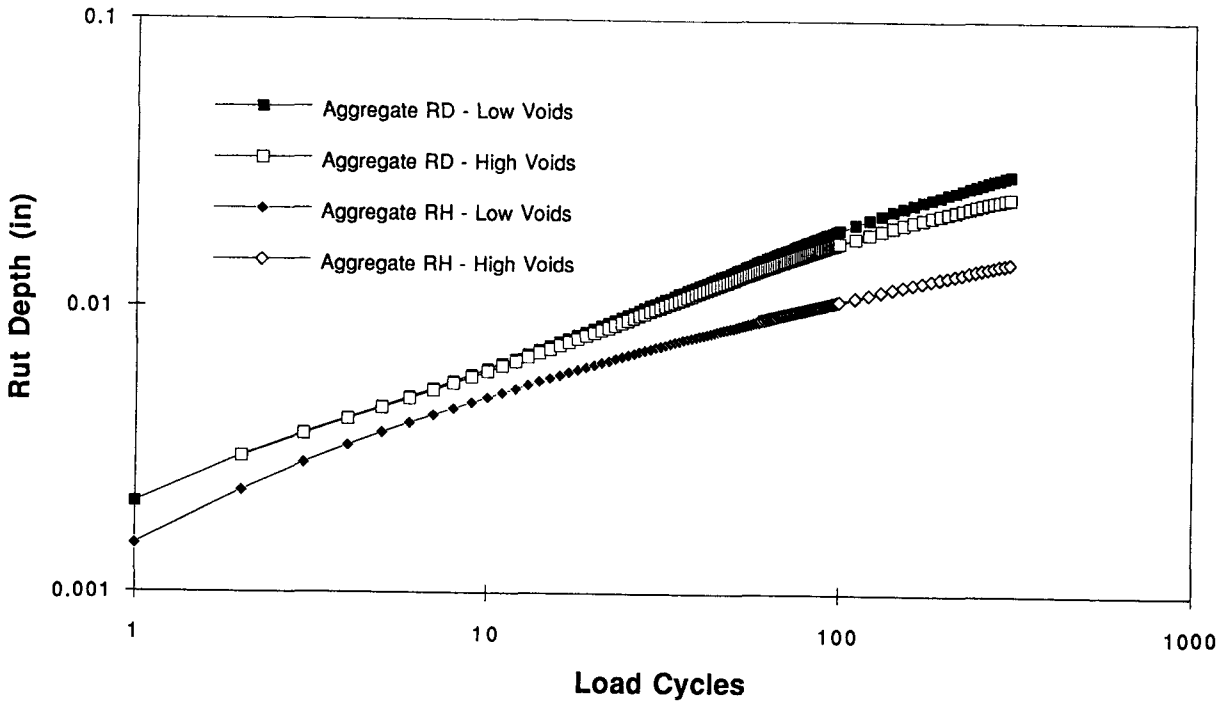

Figure 6.43. Rut depth development in a standard pavement under cyclic loading, binder AAC

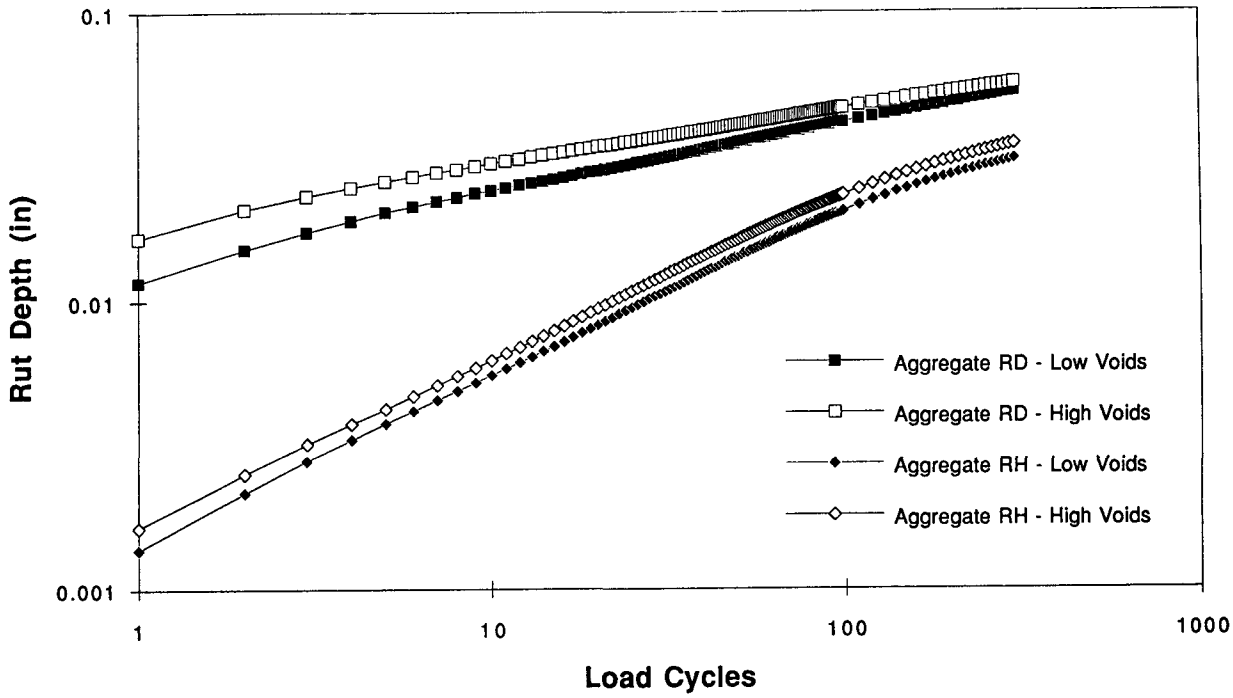

Figure 6.44. Rut depth development in a standard pavement under cyclic loading, binder AAM

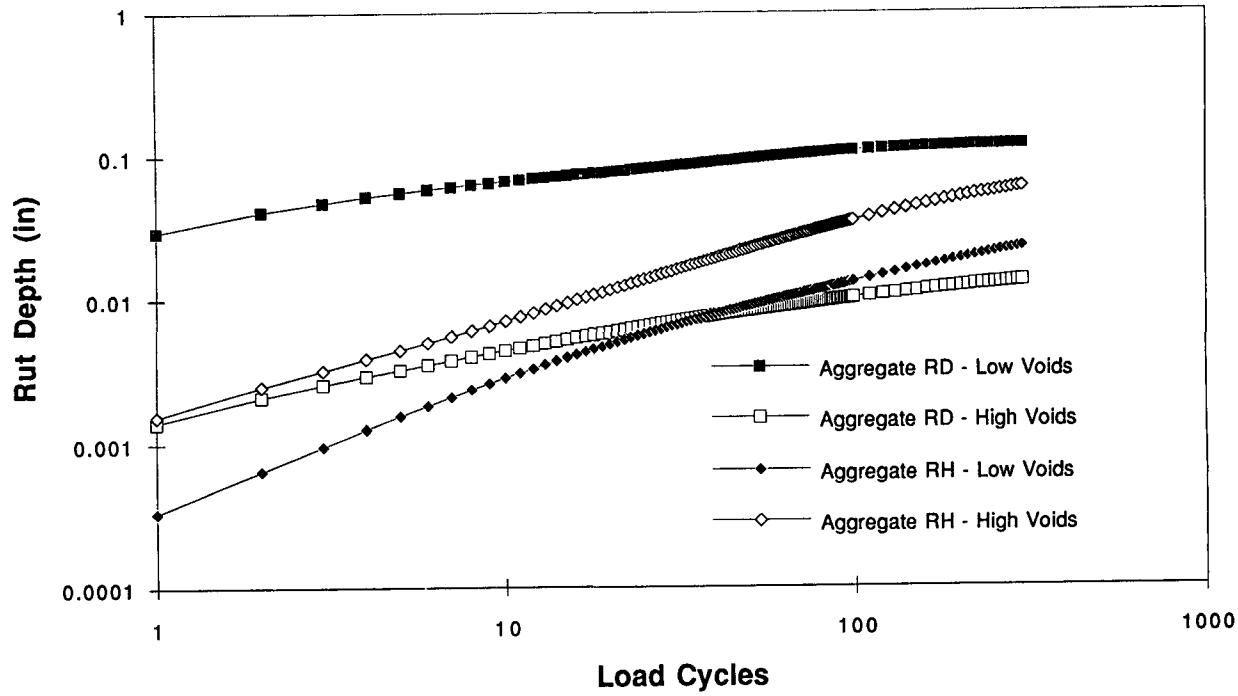

Figure 6.45. Rut depth development in a standard pavement under cyclic loading, binder AAG

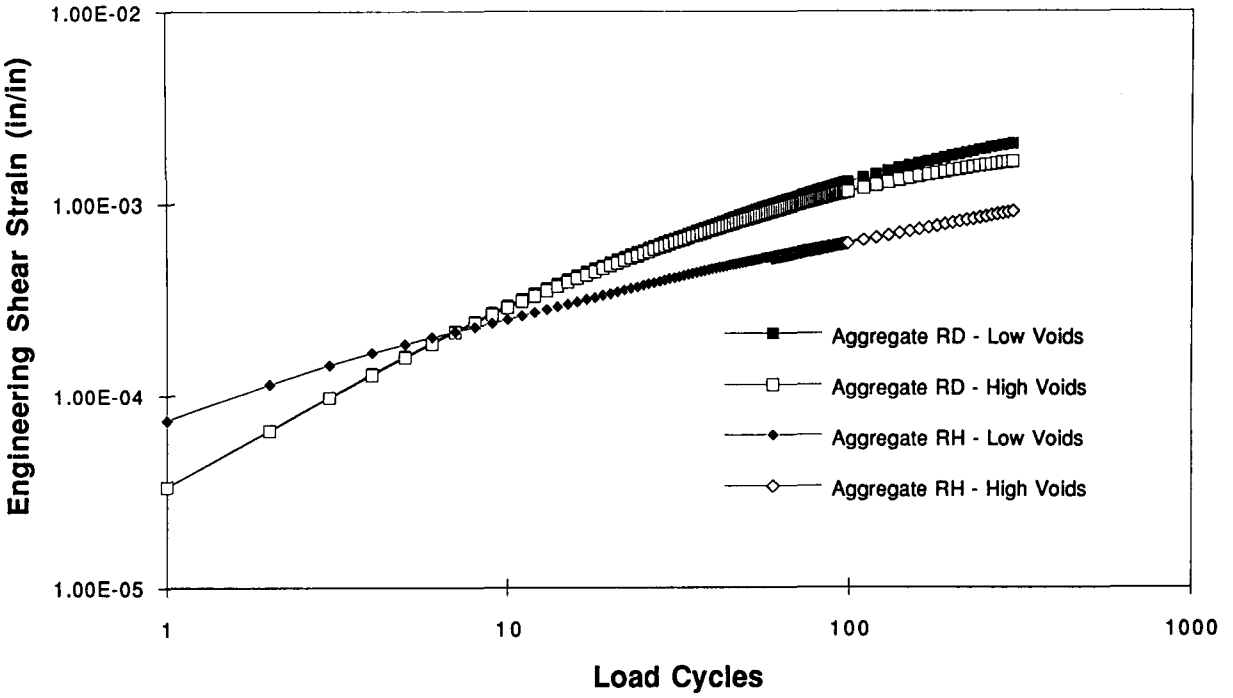

Figure 6.46. Maximum shear strain in a standard pavement under cyclic loading, binder AAK

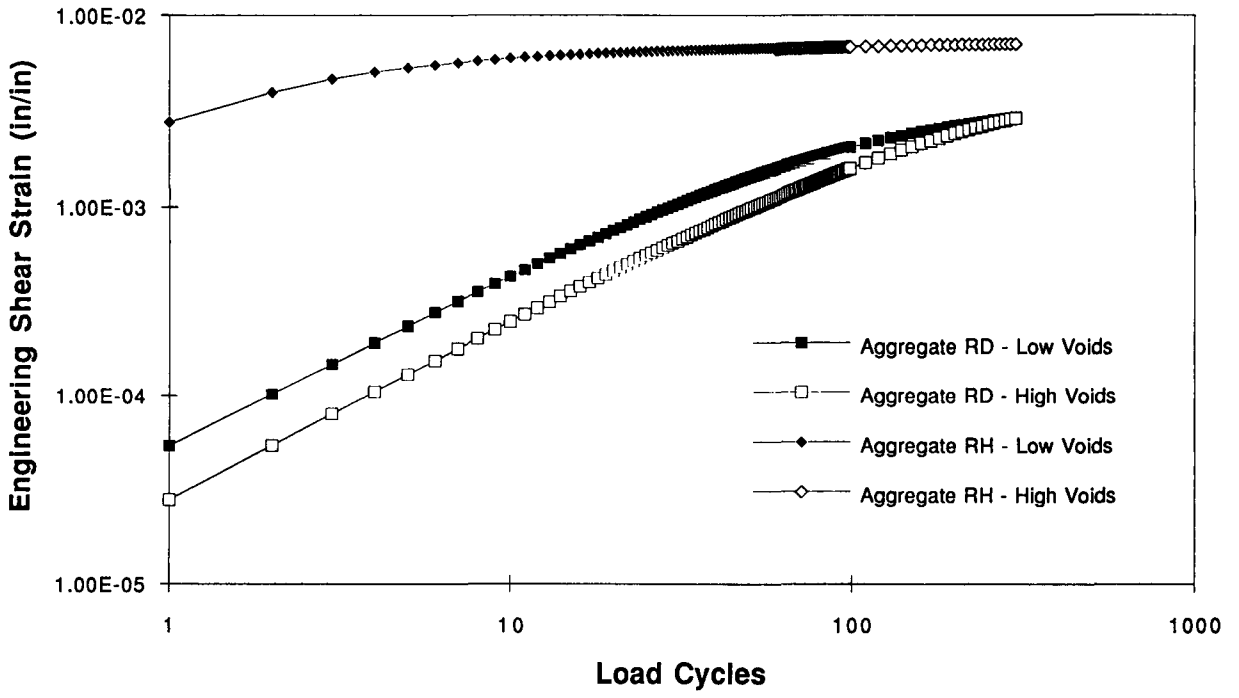

Figure 6.47. Maximum shear strain in a standard pavement under cyclic loading, binder AAC

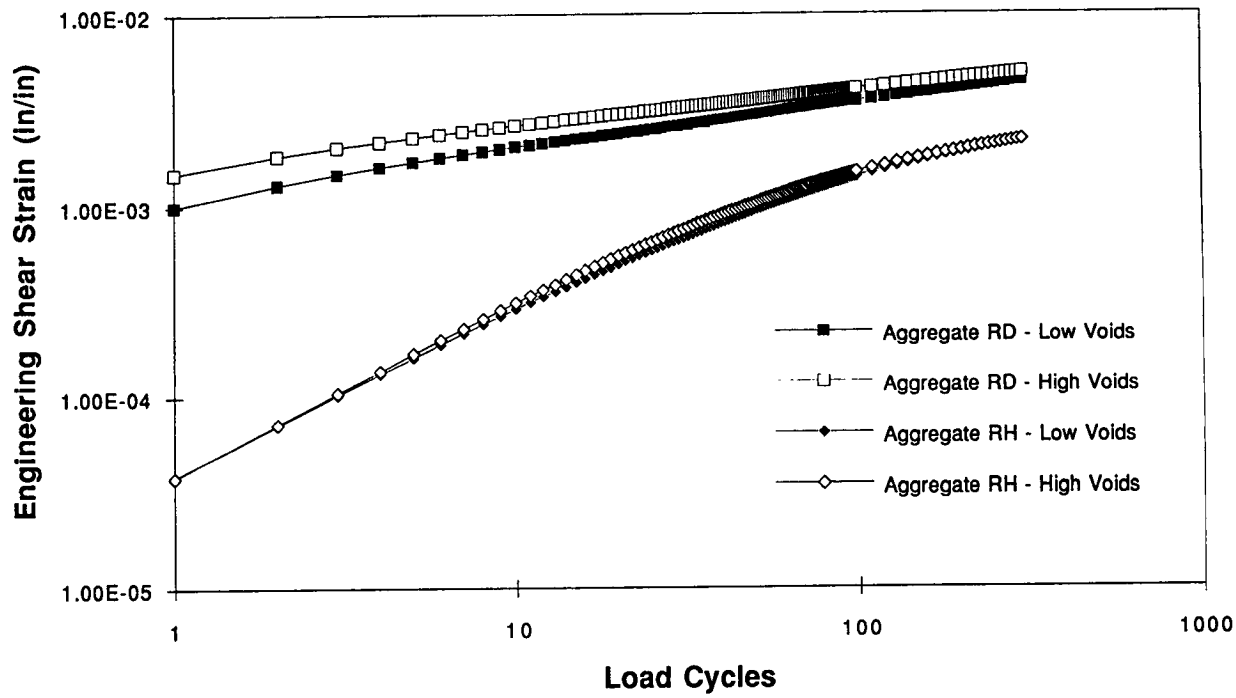

Figure 6.48. Maximum shear strain in a standard pavement under cyclic loading, binder AAM

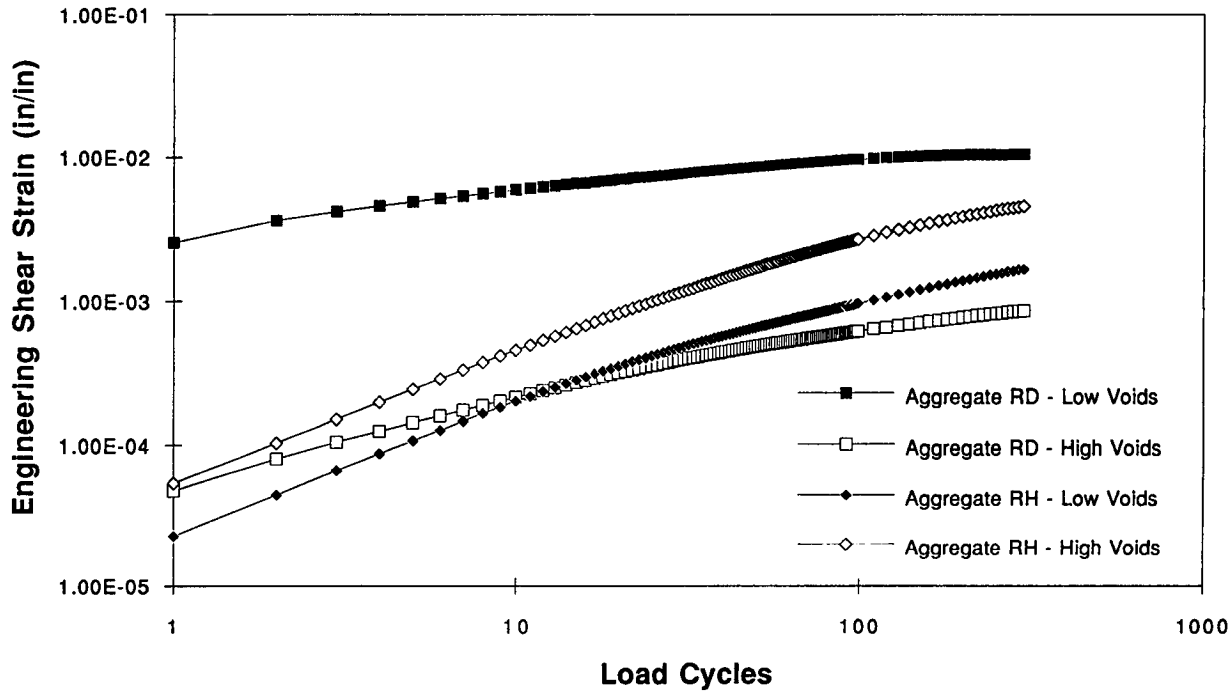

Figure 6.49. Maximum shear strain in a standard pavement under cyclic loading, binder AAG

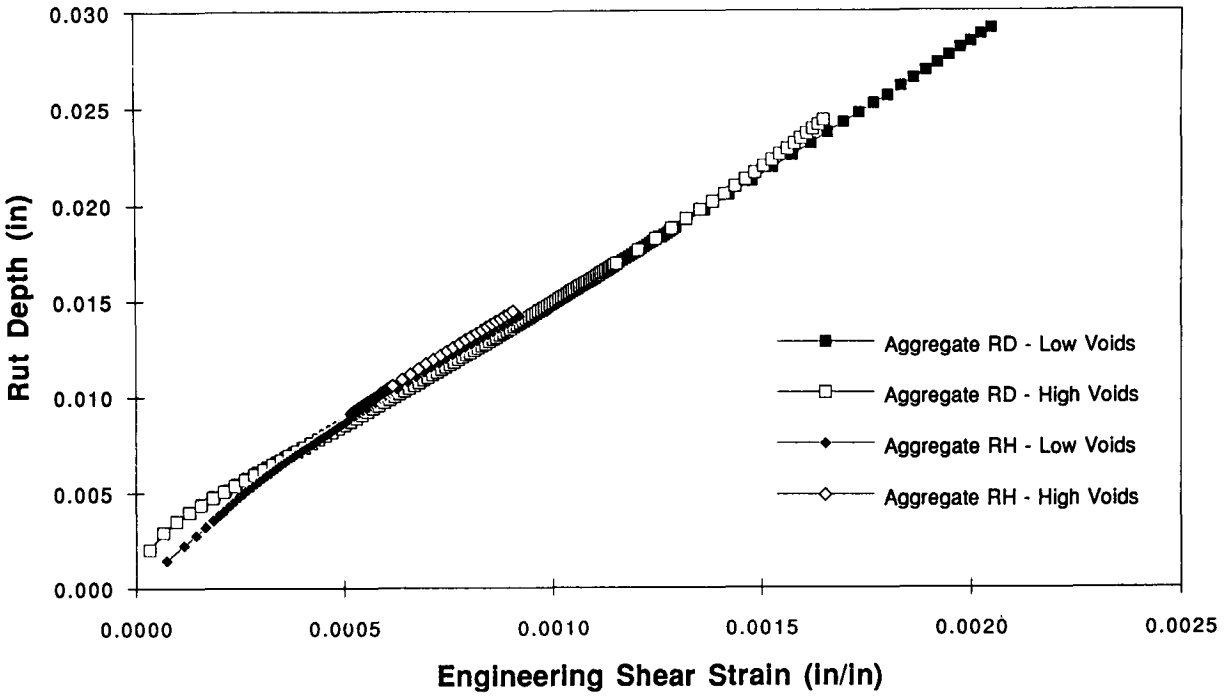

Figure 6.50. Ratio between the rut depth and maximum shear strain in a standard pavement under cyclic loading, binder AAK

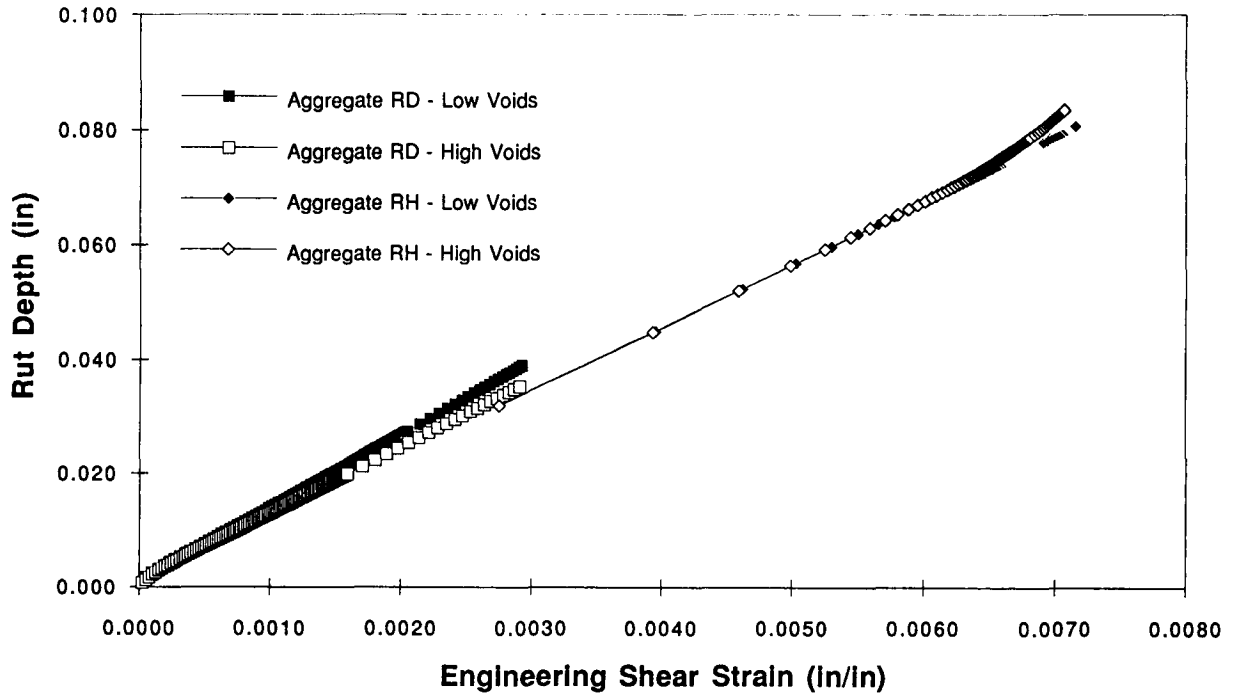

Figure 6.51. Ratio between the rut depth and maximum shear strain in a standard pavement under cyclic loading, binder AAC

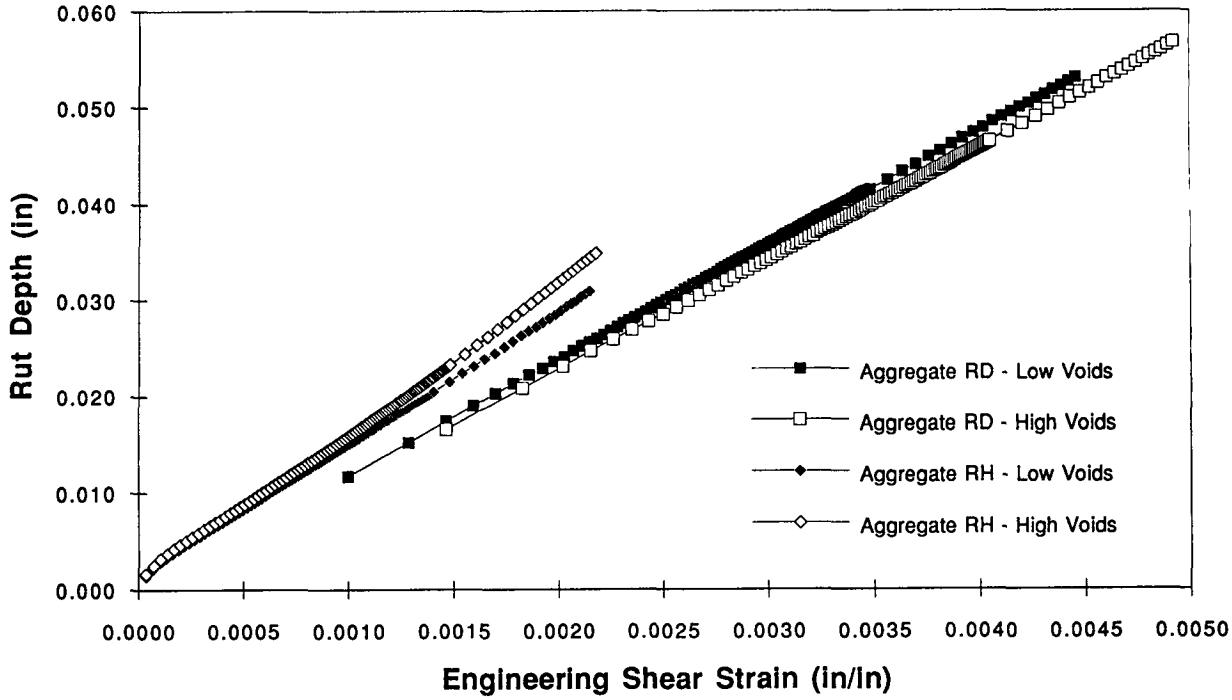

Figure 6.52. Ratio between the rut depth and maximum shear strain in a standard pavement under cyclic loading, binder AAM

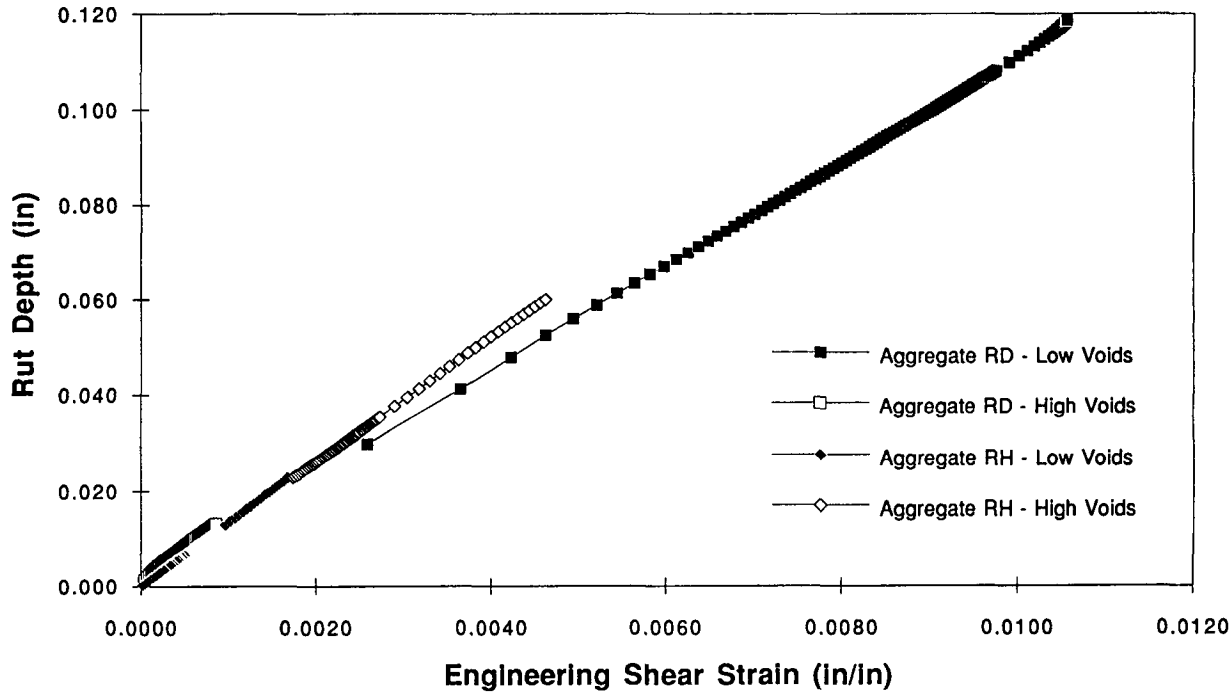

Figure 6.53. Ratio between the rut depth and maximum shear strain in a standard pavement under cyclic loading, binder AAG

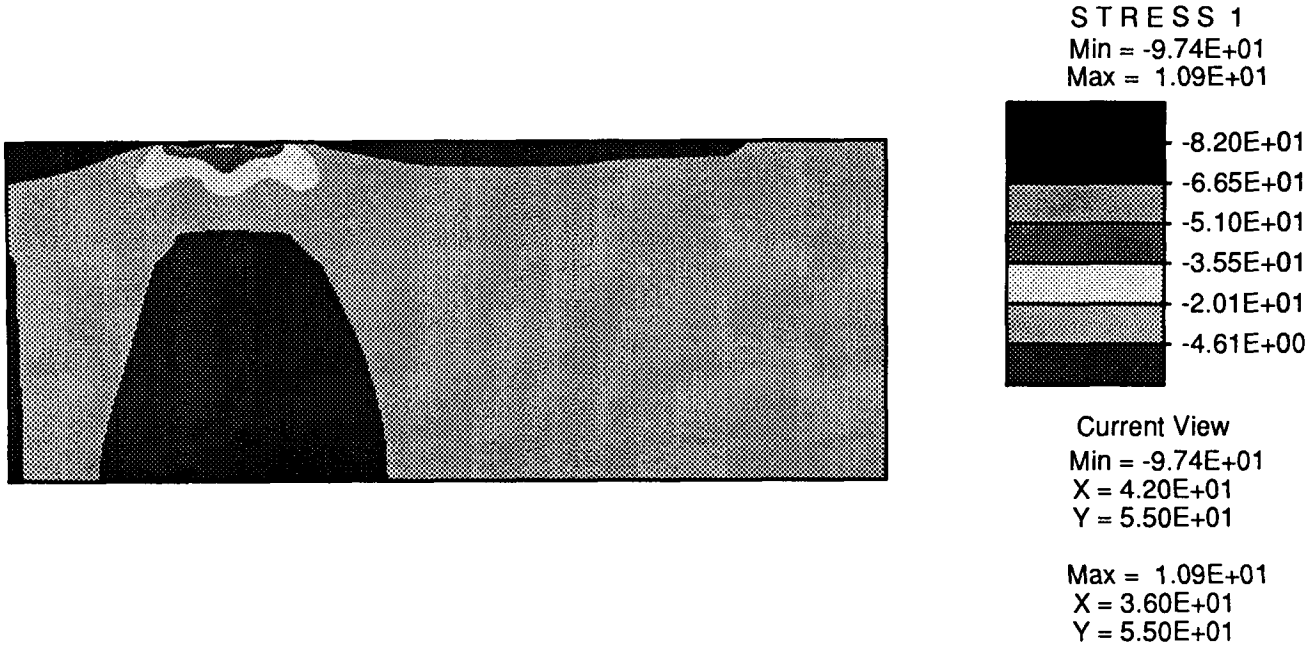

Figure 6.54. σ_{xx} **distribution, cycle 300, load on**

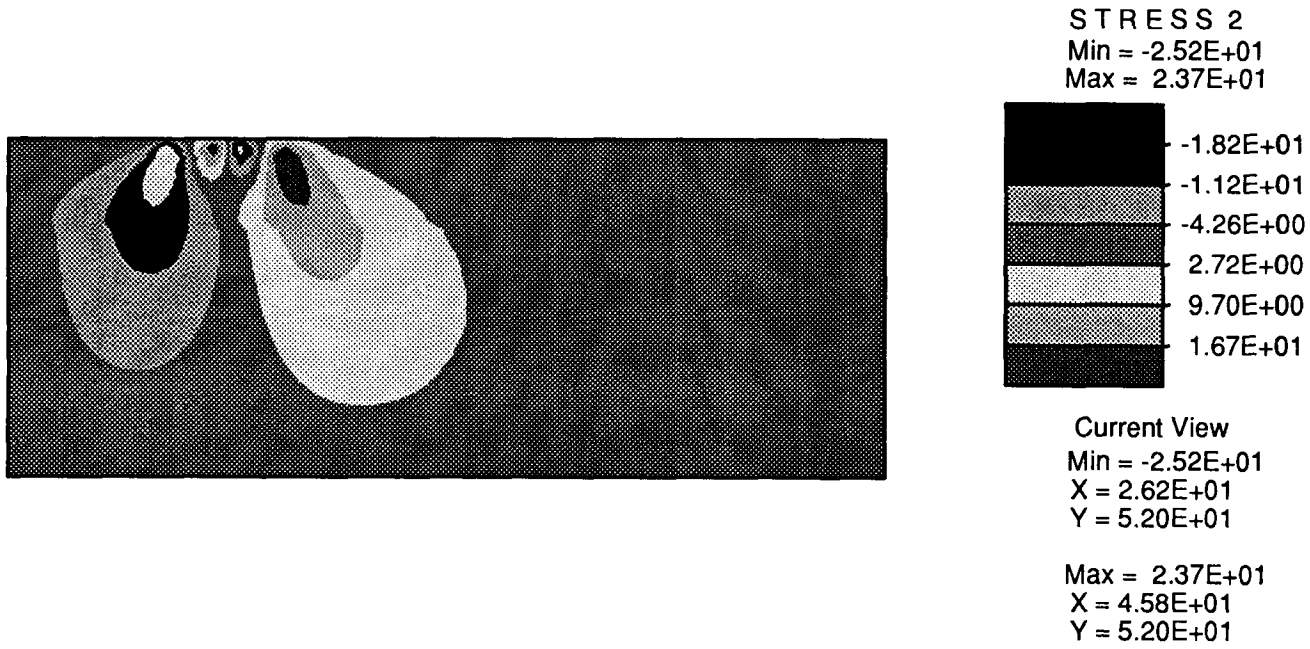

Figure 6.55. σ_{xy} **distribution, cycle 300, load on**

Figure 6.56. σ_{yy} **distribution, cycle 300, load on**

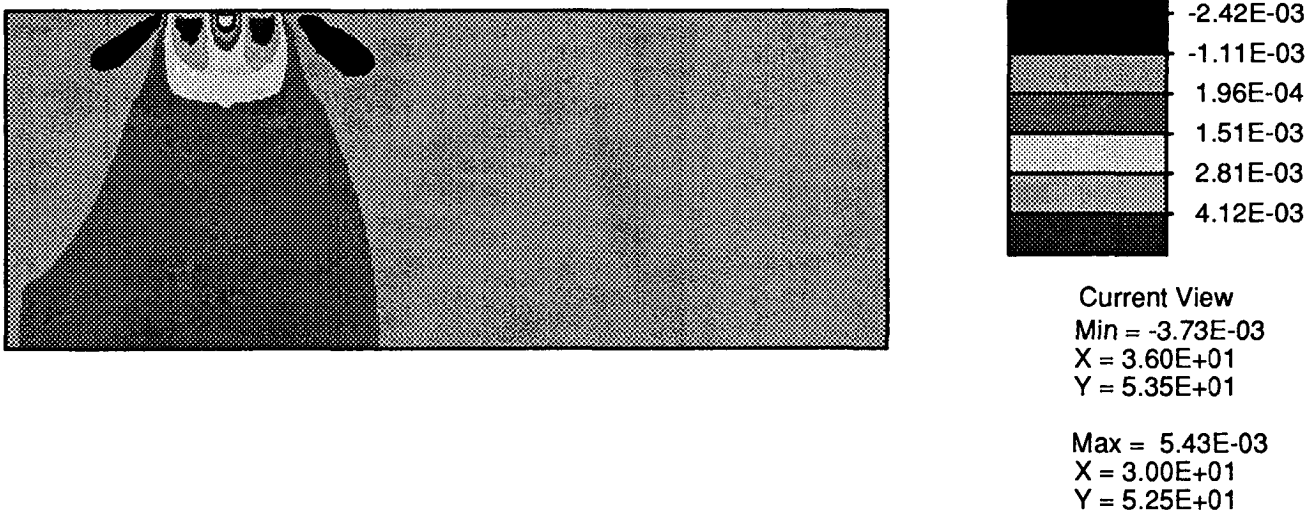

Figure 6.57. ϵ_{xx} **distribution, cycle 300, load on**

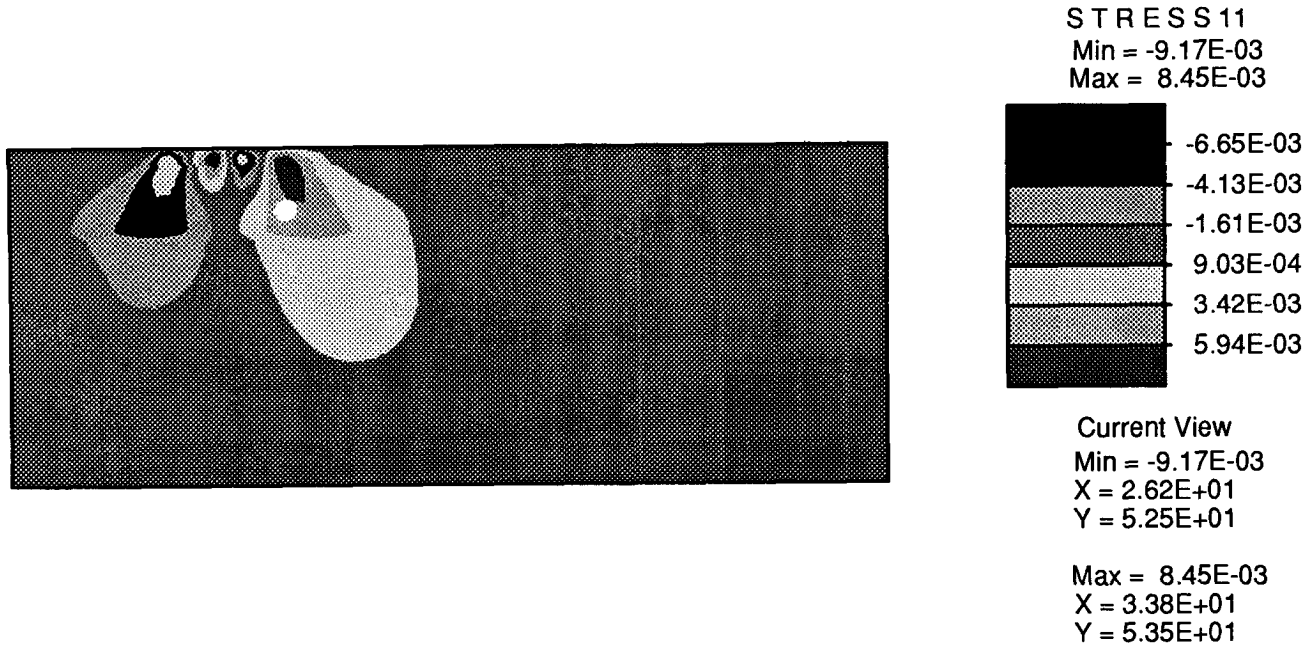

Figure 6.58. ϵ_{xy} **distribution, cycle 300, load on**

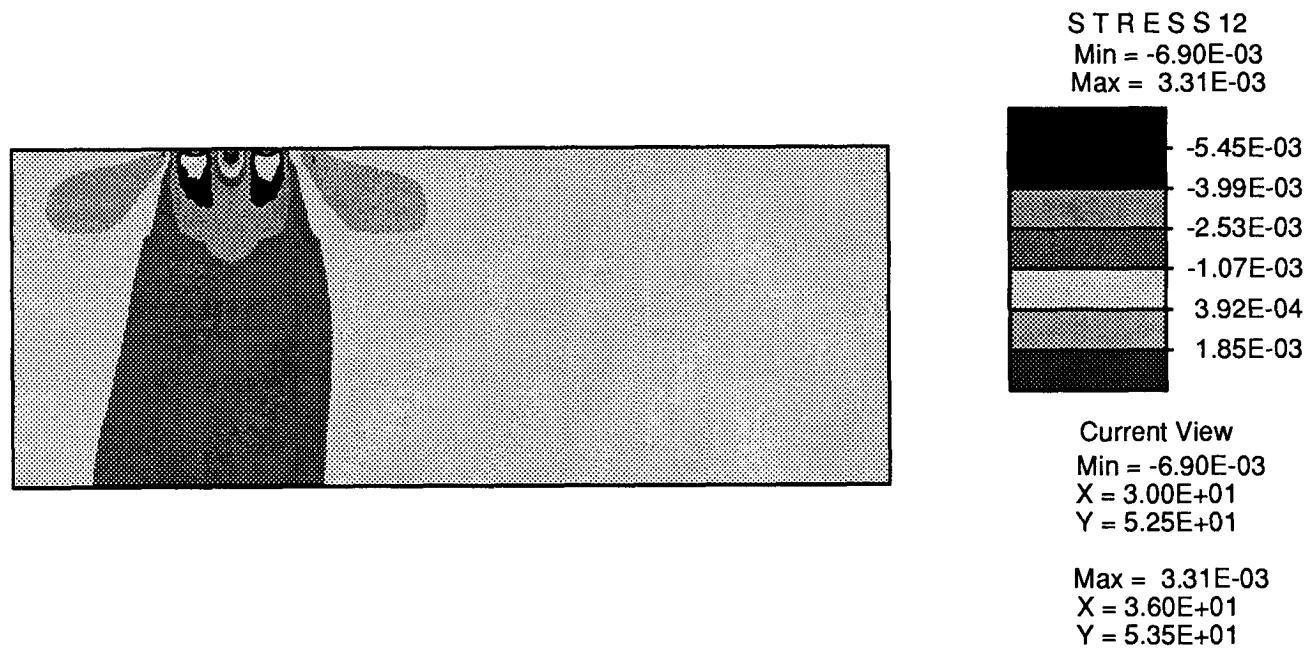

Figure 6.59. ϵ_{yy} **distribution, cycle 300, load on**

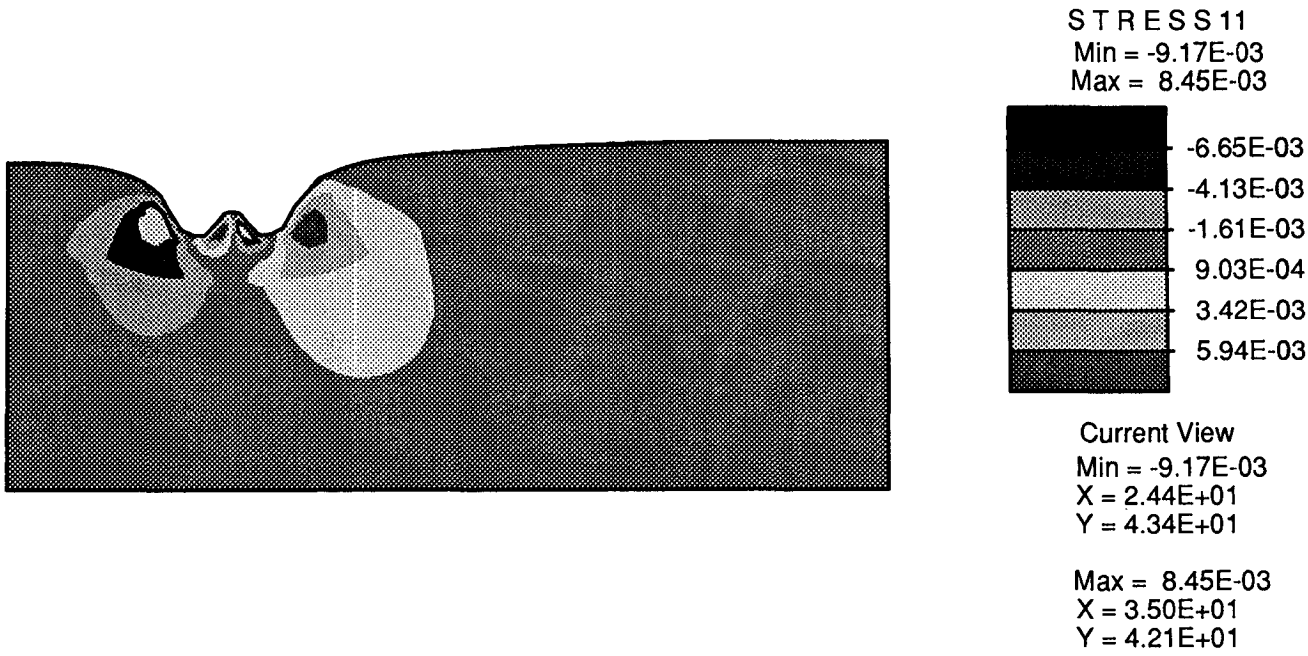

Figure 6.60. ϵ_{xy} **distribution plotted on the deformed configuration (amplified 100 times), cycle 300, load on**

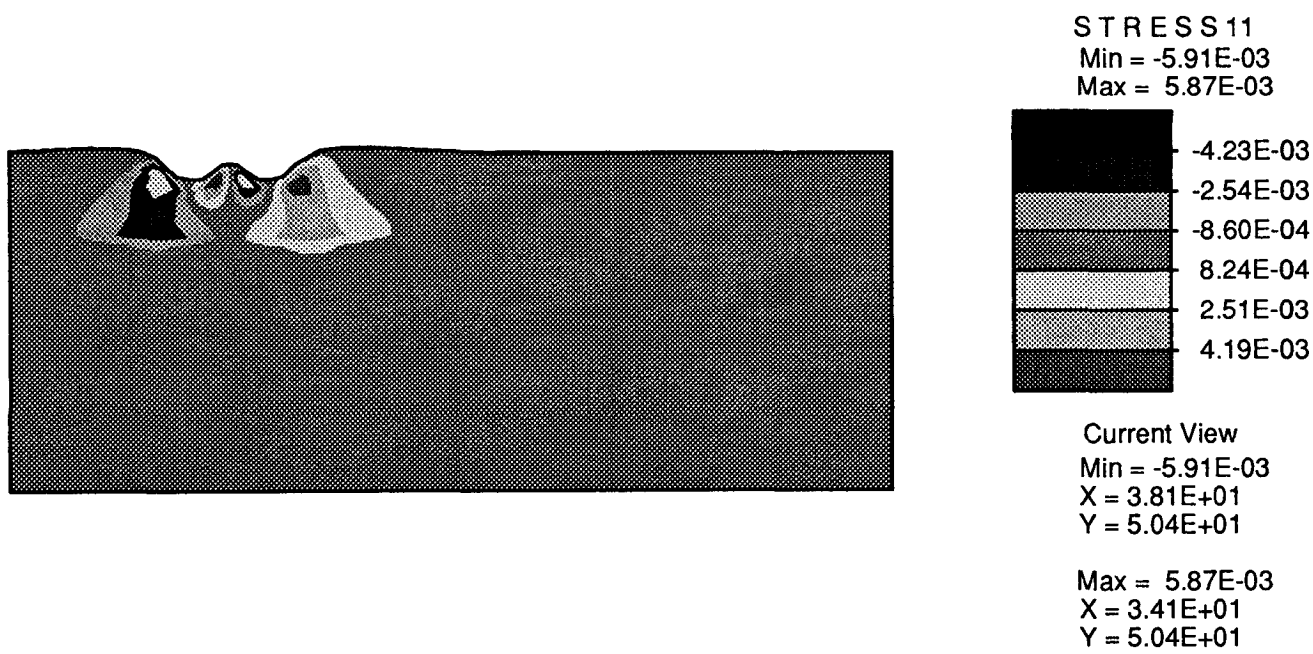

Figure 6.61. ϵ_{xy} **distribution plotted on the deformed configuration (amplified 100 times), cycle 300, load off**

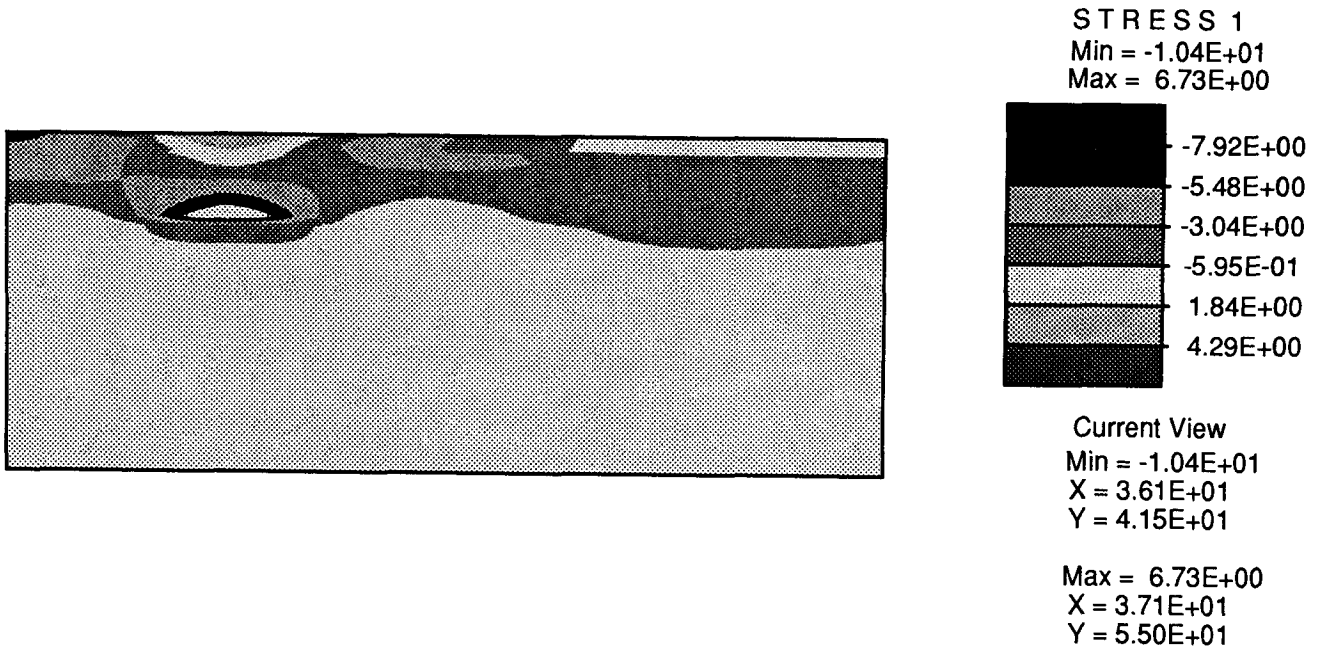

Figure 6.62. σ_{xx} **distribution, cycle 300, load off**

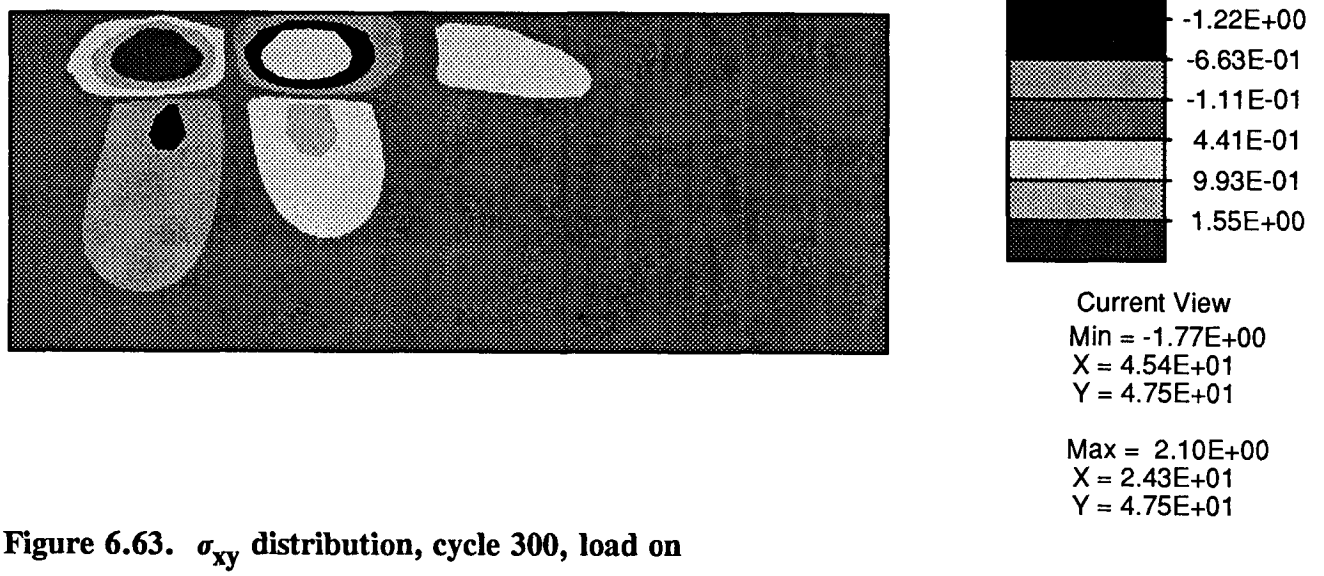

Figure 6.63. σ_{xy} **distribution, cycle 300, load on**

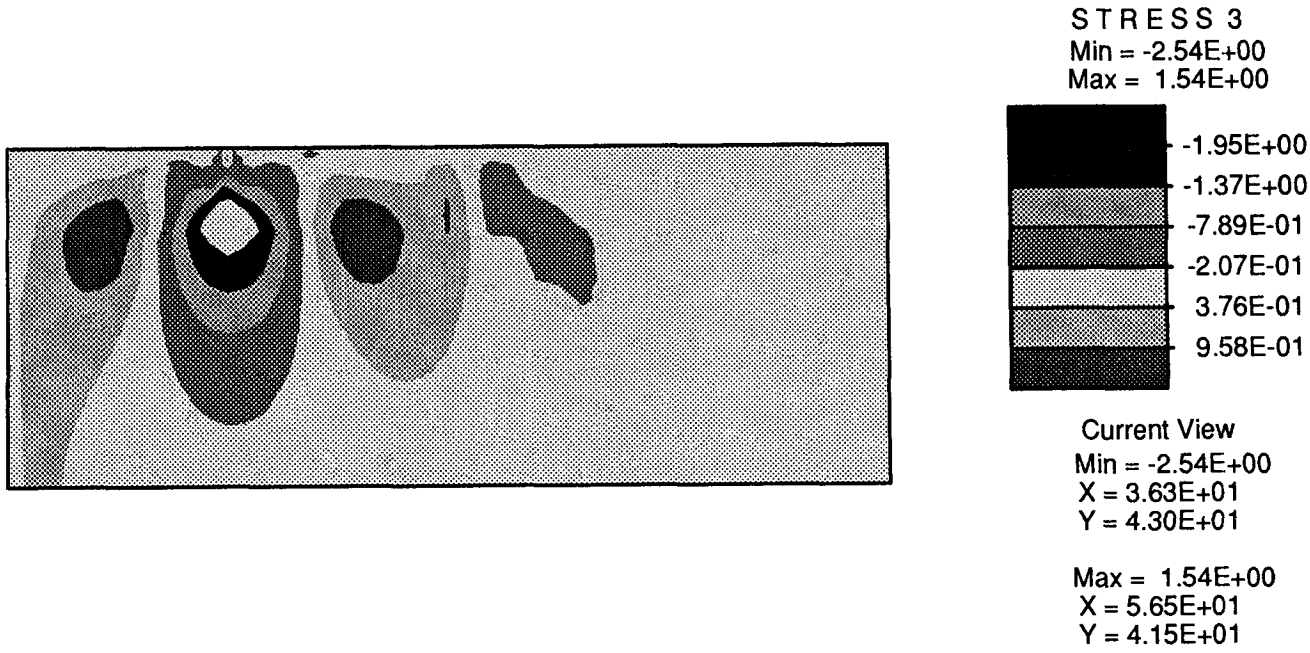

Figure 6.64. σ_{yy} **distribution, cycle 300, load off**

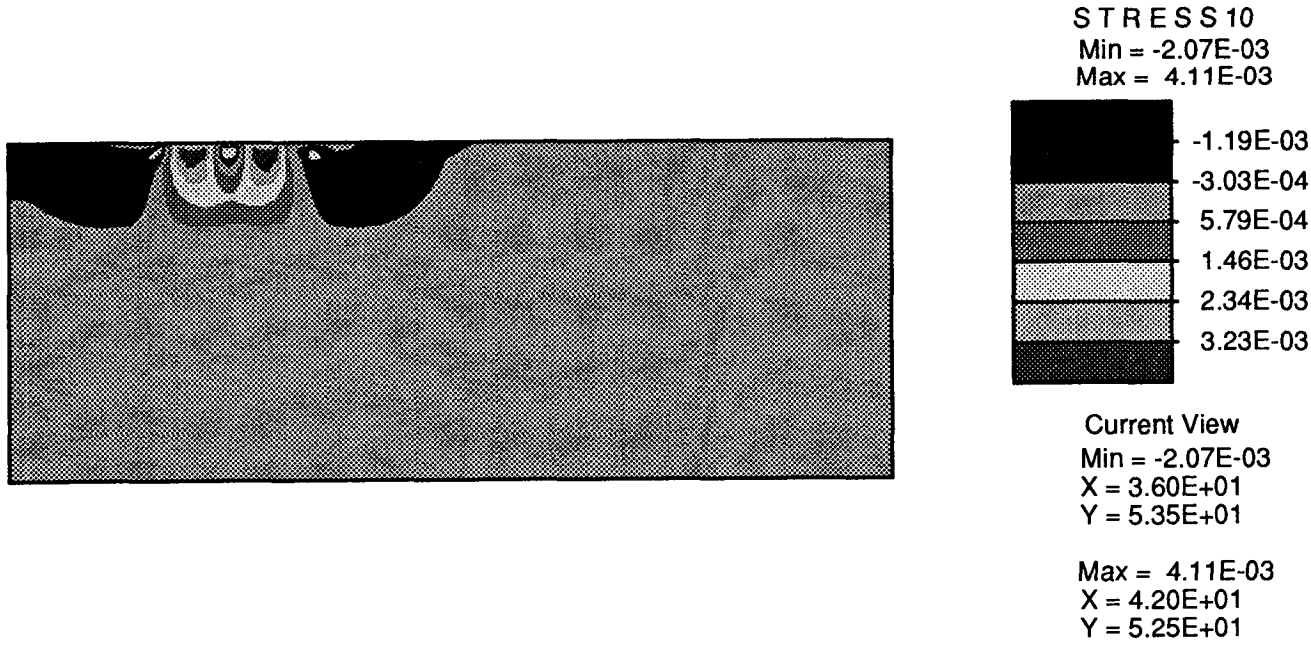

Figure 6.65. ϵ_{xx} **distribution, cycle 300, load off**

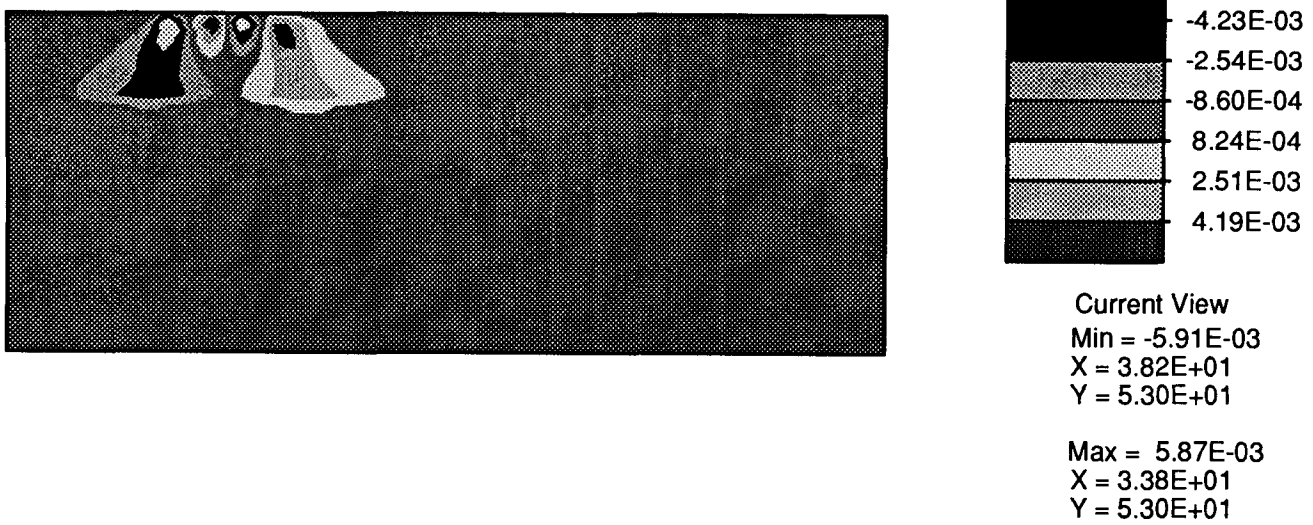

Figure 6.66. ϵ_{xy} **distribution, cycle 300, load off**

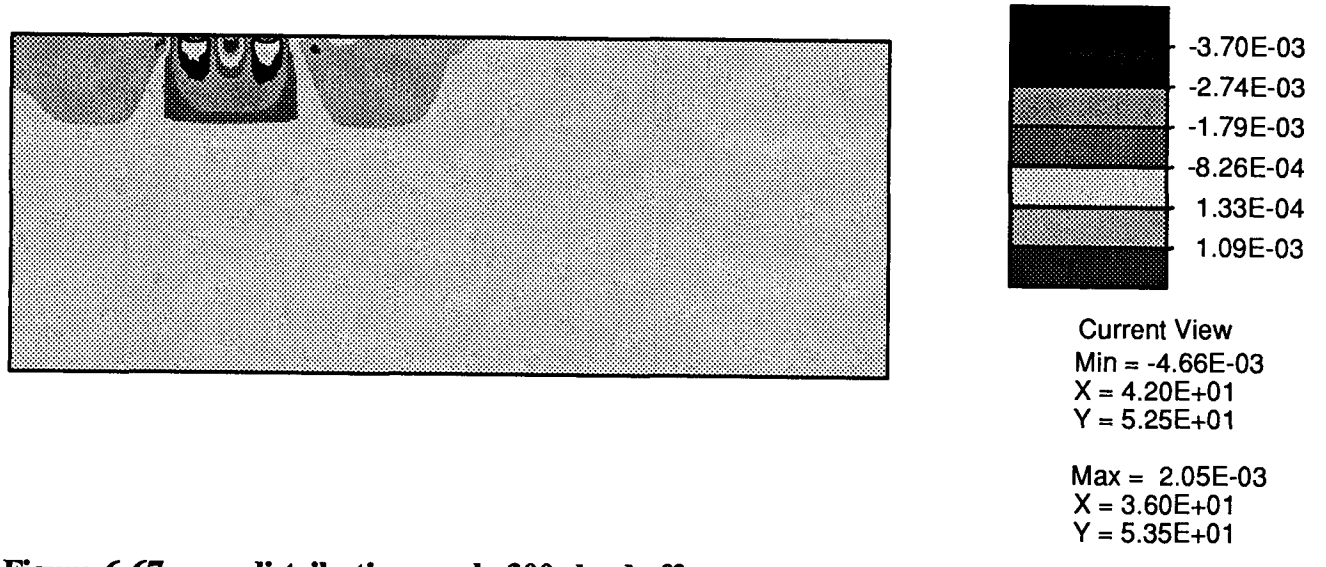

Figure 6.67. ϵ_{yy} **distribution, cycle 300, load off**

then the value of K might be of the order of 3 to 4 for a 10 cm (4 in.) thick asphalt concrete layer resting on either a granular base or portland cement concrete layer and increasing as the asphalt concrete layer thickness increases to the value shown in Equation 6.34 for the 38 cm (15 in.) thick layer.

These computations pass the test of engineering reasonableness since one would expect the underlying layer to have an increasing influence on the asphalt-bound layer as its thickness is decreased. It must be emphasized, however, that results are based on elastic response in the lower layers. Nevertheless, it is not anticipated that significantly different results for the relationships represented by Equations 3.34 and 3.35 would be obtained for other types of response.

6.9 Permanent Deformation Estimates for Mixes Subjected to Repetitive Loading in Wheel-tracking Device

To validate the approach described, it was planned to compare the results of predictions with those obtained under moving wheel load conditions. A special wheel-tracking device was designed to permit the application of a wheel load of constant magnitude moving at a constant velocity on the mix.

N.B. Unfortunately the wheel-tracking equipment was not completed at the time of the preparation of this report; accordingly, only the results of the finite element simulations are presented herein. The slabs of the mixes have been prepared. When the wheel-tracking device is obtained, the results of the test will be made available as an addendum to this report.

For the analyses reported in this section, a decision had to be made regarding the loading period based on the design wheel velocity, since the wheel-track device was not yet operational. Therefore, a period of 5 s was assumed between load applications, and the loading period was assumed to be 0.025 s for mixes using asphalts designated as b and c binders, and 0.03 s for the other mixes (in both cases the load is assumed to follow a sine wave). A tire pressure of 690 kPa (100 psi) was assumed. Development of rutting with load repetitions for each of the 16 mixes is presented in Figures 6.68 through 6.71 (organized by binder); evolution of the maximum shear strain with load repetitions is plotted in Figures 6.72 through 6.75. Computations for each mix were carried to 300 stress repetitions.

6.10 Summary

The objective of this phase of the research program was to develop a constitutive relationship to define the permanent deformation response of asphalt aggregate mixes over a range in loading and temperature conditions, which could be used in a finite element simulation to predict the development of permanent deformation in a mix when used in an actual pavement structure and subjected to repeated trafficking.

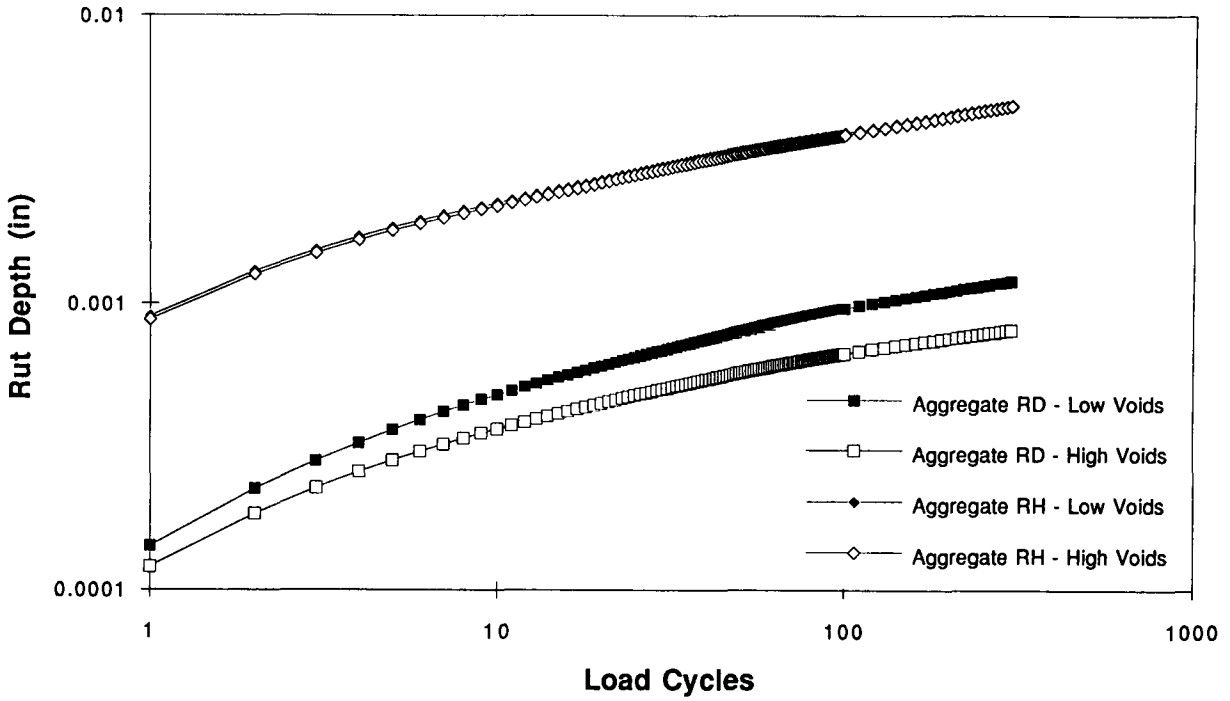

Figure 6.68. Rut development in the wheel-track device, binder AAK

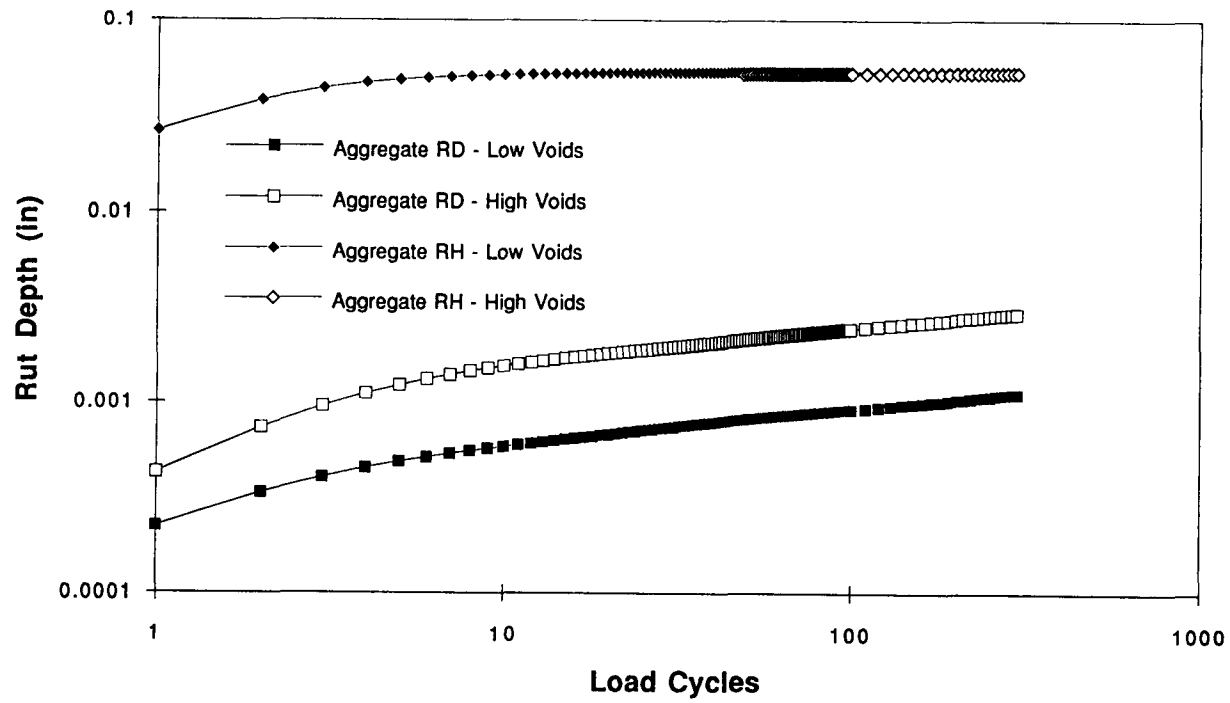

Figure 6.69. Rut development in the wheel-track device, binder AAC

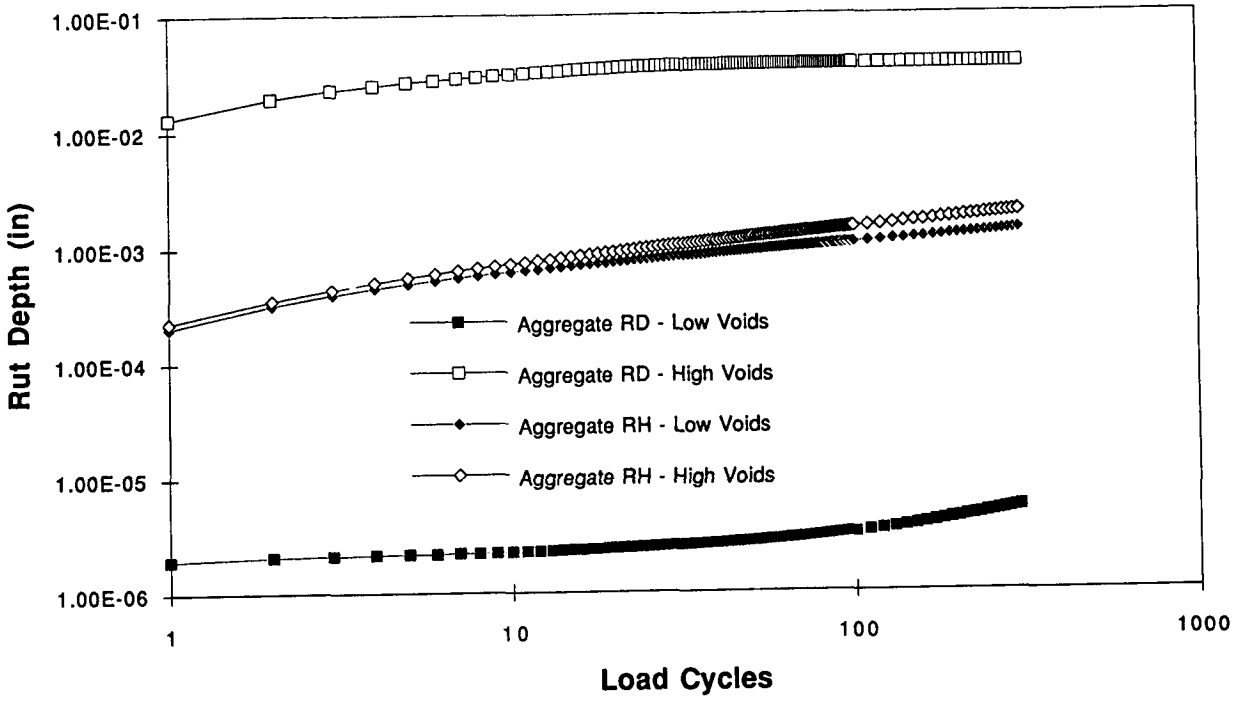

Figure 6.70. Rut development in the wheel-track device, binder AAM

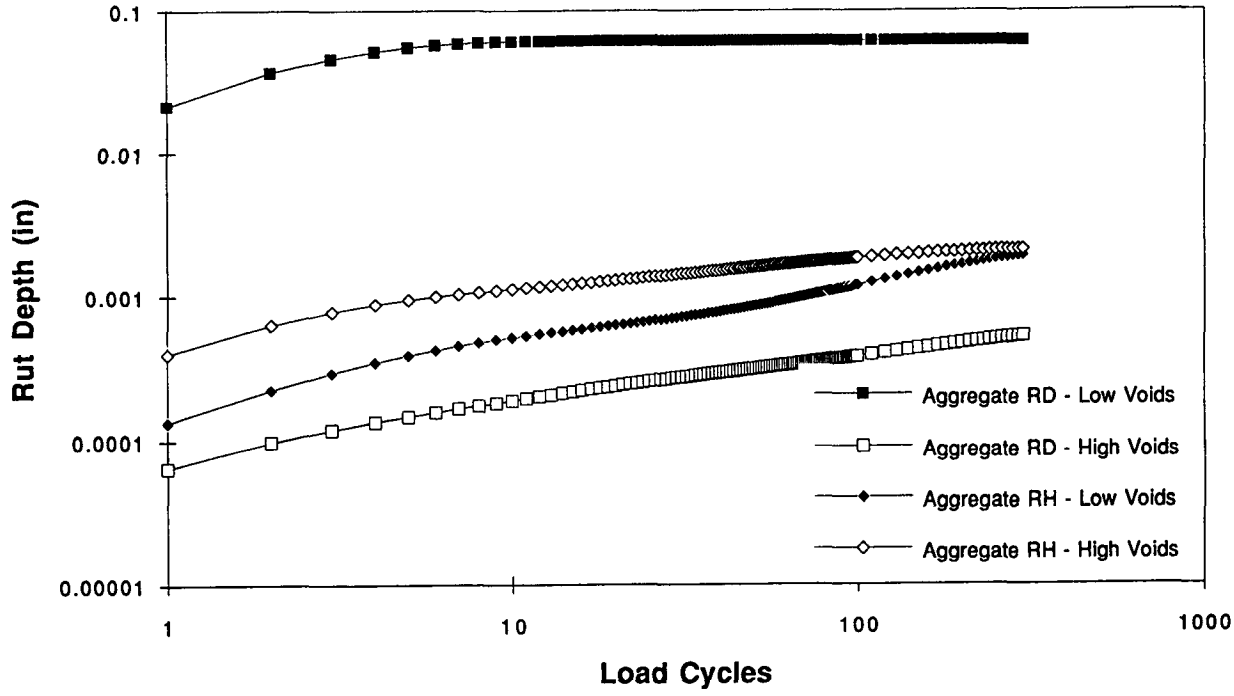

Figure 6.71. Rut development in the wheel-track device, binder AAG

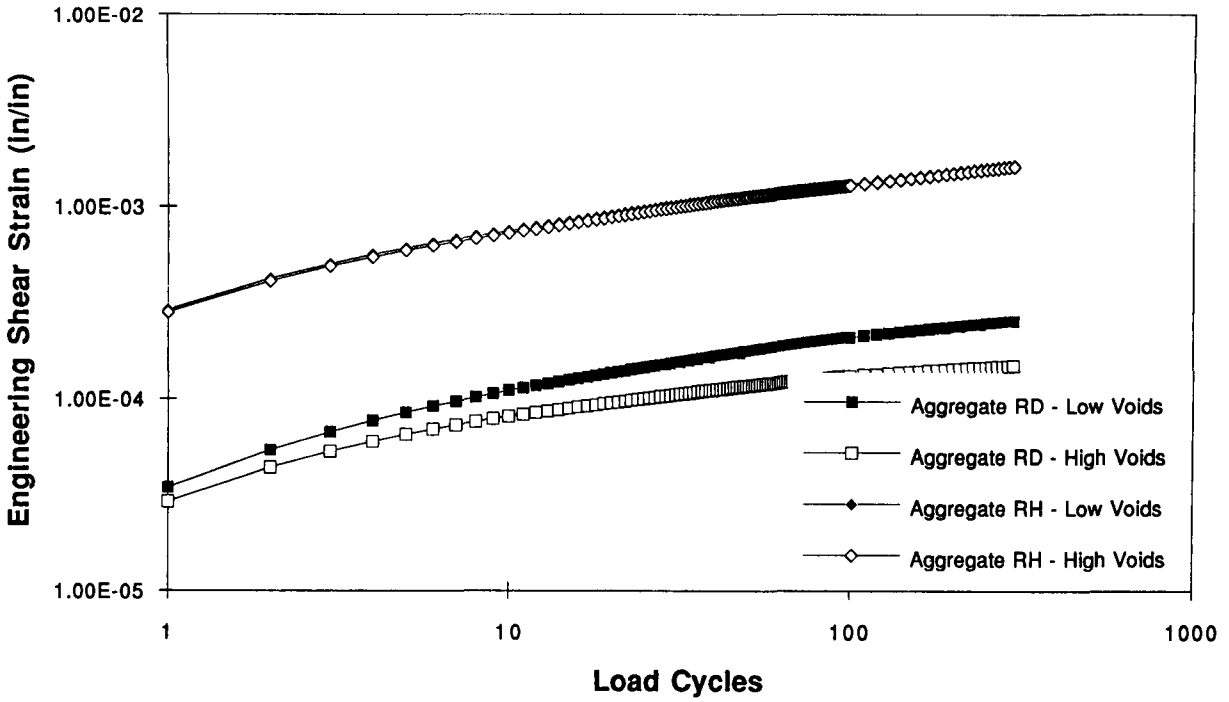

Figure 6.72. Maximum residual shear strain in the wheel-track device, binder AAK

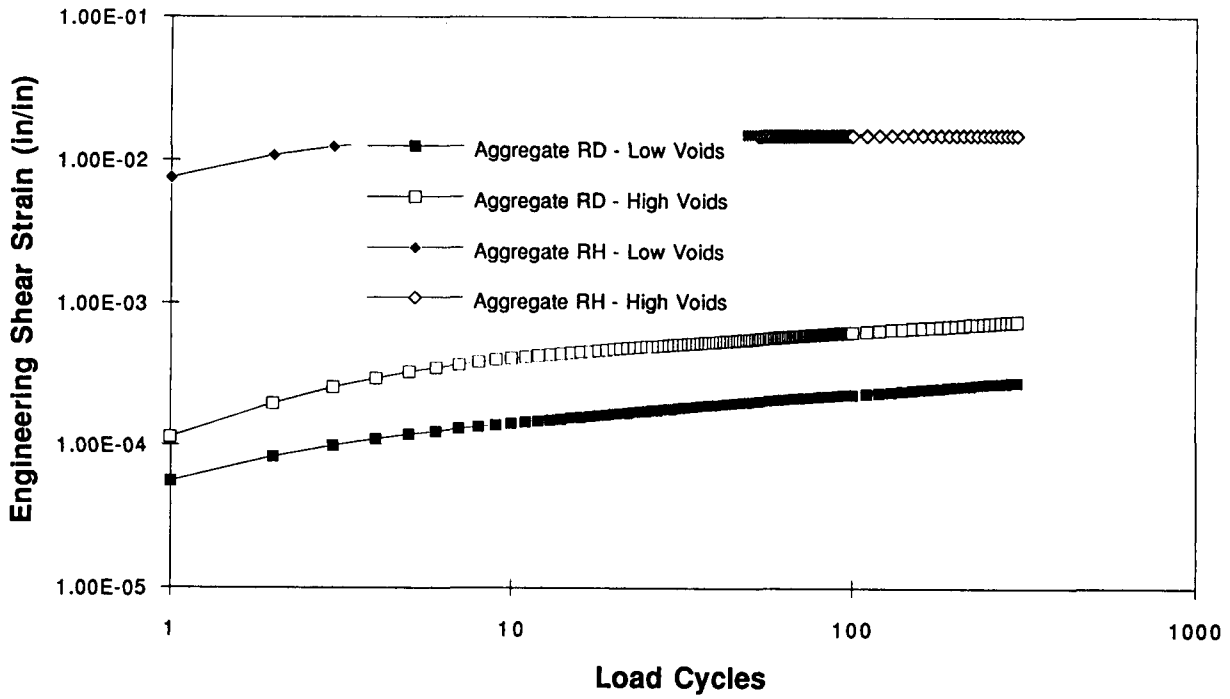

Figure 6.73. Maximum residual shear strain in the wheel-track device, binder AAC

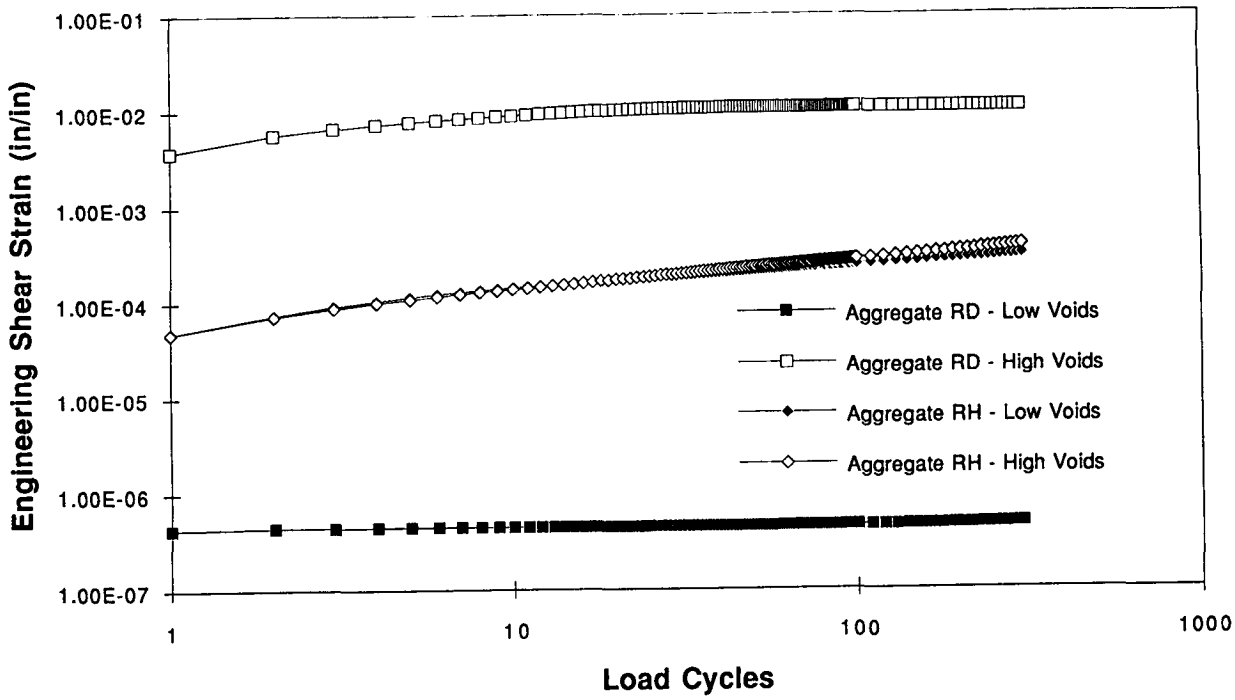

Figure 6.74. Maximum residual shear strain in the wheel-track device, binder AAM

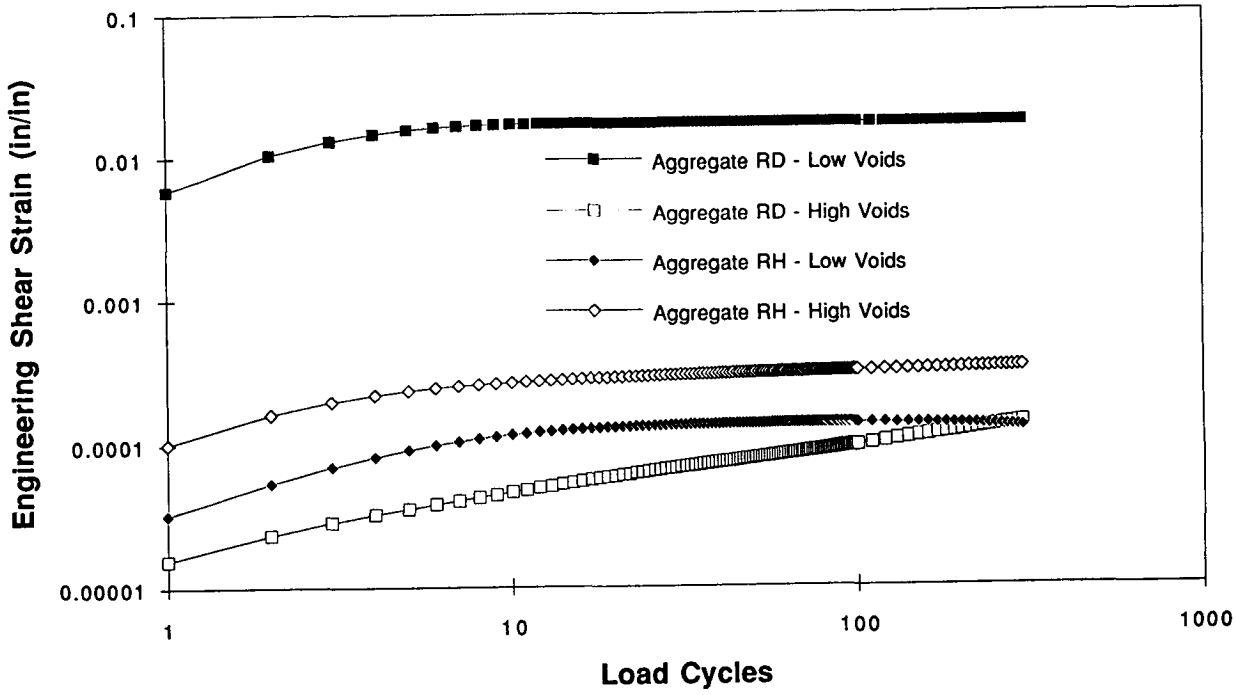

Figure 6.75. Maximum residual shear strain in the wheel-track device, binder AAG

The underlying idea of this approach is that, for each mix, a single set of material constants can be obtained which, when used in a finite element simulation, will provide a good approximation to any boundary value problem. These constants have been developed by providing the best fit possible, for the proposed constitutive law, to a simple set of tests; the constants have then been used in the simulation of the cyclic loading.

The results show that the correlation between the prediction and test data has room for improvement. The reasons for this shortcoming are partly due to the constitutive law, and partly due to the test data (as discussed earlier). The proposed constitutive model suffers from a number of known shortcomings. First, it does not account for microcrack development. Second, the plastic model used, while having the advantage of simplicity, fails to capture some of the mix characteristics (most prominently the fact that the residual strain is too small).

To provide a better approximation of asphalt concrete mix behavior, an investigation should proceed on the two fronts of testing and modeling. It would be desirable to evaluate only one or two mixes; these tests should be very carefully monitored. For example, careful attention must be directed to the determination of the initiation of macrocracks (microcracks are assumed to be present in the virgin material).

From the constitutive model standpoint, it is important that the model be extended to include damage due to cracking. To this end, finite deformation kinematics must be assumed (to ensure frame invariance). It is also proposed to uncouple the viscous portion into volumetric and deviatoric response (the volumetric part can be assumed to be rate independent). Also, a simpler elastic model (i.e., with fewer than nine parameters) should be sought. (It is interesting to note that dilation is automatically induced as a second-order effect when finite motions are concerned.) Finally, the plastic model should be replaced. In this respect it is noted that classical models used in geomechanics for cohesionless soils are probably not suitable for asphalt concrete.

In spite of these limitations relative to the constitutive relationship, the associated test methodology developed, and the analyses that were performed, some very useful results have been obtained — results that have the potential to permit significant advances to be made in the mix design/analysis process.

The relationship between maximum permanent shear strain and rut depth, expressed by Equation 6.34, provides an extremely useful tie between laboratory-measured response and field performance. This will be discussed in Chapter 11. Moreover, the analyses presented in Appendix C indicate that the relationship is valid, *from an engineering standpoint,* over a range of tire contact pressures. The fact that the coefficient K in Equation 6.35 is dependent on layer thickness means that the equation also passes the *test of engineering reasonableness.* The information presented shows that K varies from 11 for thick asphalt-bound layers to about 4 for a 10 cm (4 in.) layer of asphalt concrete resting on a portland cement concrete slab, a decrease that one would anticipate.

The analyses also show that the maximum shear stress and shear strain occur a short distance below the pavement surface at the edge of the tire. This is illustrated in Figures 6.55 and

6.58. The location of the stresses and strains suggest that it would be desirable, from a simplified mix design/analysis standpoint in which only one temperature for testing might be utilized, to select the pavement temperature occurring at this depth, estimated to be about 5 cm (2 in.).

In Part III of this report a hierarchical structure for mix design/analysis is presented utilizing the results of the investigation described in this chapter.

7

Mix Testing Associated with Validation of the Proposed SHRP Binder Specifications

In the permanent deformation test program, as compared to the fatigue test program, validation of the Strategic Highway Research Program (SHRP) binder specification was accomplished through a separate test program that included use of the wheel-tracking device at SWK Pavement at the University of Nottingham (SWK/UN) and the simple shear device at the University of California at Berkeley (UCB). Results of this program have been described in a separate report, *Relationship Between Asphalt Properties and Asphalt Aggregate Mix Performance — Stage I Validation,* (SHRP 1994). Some of the results and additional analysis not included in the report will be presented herein, since they contribute to the overall objectives of this phase of the study and provide some insight on the role of the binder relative to the permanent deformation characteristics of mixes.

7.1 Wheel-Track Testing

In this study, a wheel-tracking device was used to simulate the stress conditions caused by a dynamic wheel load on the pavement surface. A full factorial experiment was designed to allow all main factors and two-factor interactions to be tested. The factorial matrix consisted of 16 asphalts, two aggregates, and two air void levels, resulting in a total of 64 cells. All mixes were prepared at a fixed asphalt content near the optimum determined in accordance with ASTM D1560 and 1561. After mixing, they were placed in an oven at 135°C (275°F) for four hours. Mixes were prepared by rolling wheel compaction to produce specimens with target air void contents of 4 and 7 percent. The factorial experiment is summarized below:

Factor	Levels
Asphalt Source	AAA, AAB, AAC, AAD, AAF, AAG, AAK, AAL, AAM, AAV, AAW, AAX, AAZ, ABA, ABC, ABD
Aggregate Source	RD, RH
Air Voids	4%, 7% (target levels)
Replicates	1/cell (16 binders × 2 aggregates × 2 void contents)
Total No. of Tests	64

The wheel-tracking tests were performed by SWK/UN. A wheel, fitted with a solid rubber tire, passed over the top of a 200 mm (8 in.) diameter cylindrical core specimen (obtained from the slab-specimen prepared by rolling wheel compaction) at a frequency of approximately 3 Hz or 20 rad/s. Wheel-track tests were conducted at a temperature of 40°C (104°F) and each test was run for a duration of 5000 load passes (approximately two hours). Tests were performed with an applied load of approximately 620 N. The contact area of the tire measured 850 mm^2 (34 in^2), that gives a corresponding contact stress of approximately 730 kPa (105 psi).

Two rutting parameters were measured from the wheel-track test data: normalized rut rate and total rut depth. The normalized rut rate is the rate of increase in rut depth (mm/hr) between 2000 and 4000 load passes divided by the contact stress of the wheel. The total rut depth is the average rut depth (mm) at the end of the test, i.e., after 5000 passes. SWK staff considered rut rate to be a more reliable indicator of permanent deformation performance because it is less likely to be affected by initial start-up errors and, perhaps, additional compaction of the specimen during the initial stages of the test. Results of this test program are summarized in Appendix D.

Comparison of the results of the wheel-tracking analyses presented in Figures 6.68 through 6.71 with corresponding test results from the SWK/UN wheel-tracking tests are shown in Table 7.1. While the computed values were determined for a different type of equipment and specimen configuration than the University of Nottingham device, presumably, similar types of response might be expected. Examination of the table indicates general trends in the calculated response (with the exception of the low void mix of binder AAG and aggregate RD) to be about the same as the measured response. It is interesting to note that for this mix a comparatively large initial deformation was obtained but the rate of accumulation is comparatively small.

Also included in the table are the results for the rutting rate. Unfortunately no more definitive comparative results appear to be obtained for this parameter than for rut depth.

Table 7.1. Comparisons of permanent deformation response of 16 mixes tested in SWK/UN wheel-tracking device and computed response of the same mixes in a simulation of UCB wheel-tracking device

	SWK/UN Wheel-tracking Test — 5000 Passes		Finite Element Simulation — UCB Wheel-Tracking Device — 300 Passes	
	Rut depth (mm)	Rut rate (mm/MPa/hr)	Rut depth (mm)	Rut rate (mm/pass[a] × 10^{-6})
BM0	1.69	0.37	0.71	1.02
BM1	1.79	0.60	0.61	0.60
BP0	1.96	0.43	0.36	4.39
BP1	1.24	0.32	0.36	4.37
CM0	1.14	0.25	0.89	0.89
CM1	1.23	0.23	0.81	2.18
CP0	4.64	1.49	2.03	1.38
CP1	5.59	1.53	2.03	1.37
MM0	1.46	0.22	1.27	0.01
MM1	1.09	0.29	1.35	0.90
MP0	1.24	0.27	0.68	1.32
MP1	2.03	0.49	0.79	2.32
VM0	1.14	0.25	2.54	0.18
VM1	2.46	0.82	0.30	0.63
VP0	1.44	0.36	0.51	3.07
VP1	3.77	0.97	1.45	0.98

[a]Average slope of line between 150 and 300 passes.

Rutting rates have also been computed for the results presented in Figures 6.68 through 6.71 and are shown in Table 7.1 as well. In this instance a straight line has been assumed between 150 and 300 repetitions and the rutting computed as the slope of the line. Results are plotted in Figure 7.1. The lines connect pairs of data, e.g., the low and high void content mixes containing aggregate RD and asphalt AAG-1.

7.2 Simple Shear Testing

Simple shear tests were conducted on a number of the mixes tested in the SWK/UN wheel-track testing device. Cylindrical specimens 15 cm (6 in.) in diameter by 5 cm (2 in.) high were utilized.

A full factorial experiment was designed to allow all main effects and two-factor interactions to be evaluated. The factorial matrix consisted of nine asphalts, two aggregates and two air void levels, resulting in a total of 36 cells.[8] The factorial experiment is summarized below:

Factor	Levels
Asphalt Source	AAB, AAC, AAD, AAG, AAK, AAM, AAV, AAZ, ABC
Aggregate Source	RD, RH
Air Voids	4 percent, 7 percent (target levels)
Replicates	1/cell (9 binders × 2 aggregates × 2 void levels × 2 test conditions)
Test Condition	constant height or field state of stress
Total No. of Tests	72

The response variables were as follows: load cycles to 2 percent strain, ($N_{2\%}$ — number of shear load cycles at which the asphalt aggregate mix specimen exhibits 2 percent cumulative permanent shear strain); and cumulative permanent shear strain, ($\Sigma\gamma_p$ — cumulative permanent shear strain after a constant number of load cycles).

A total of 72 shear tests were performed; half of the specimens in this study were tested under a *constant height* condition (CH) and the other half were tested under a *field state of stress* (FS) condition. The CH shear test is sensitive to elastic and viscous characteristics of the asphalt binder, and it also measures the effect of dilatancy. The FS shear test incorporated loading conditions thought to represent the state of stress occurring in an asphalt concrete layer near the edge of a truck tire and were based on a finite element analysis of a

[8]No replicates were provided; the three-factor interaction of asphalt source, aggregate source, and air voids were used as an estimate of experimental error.

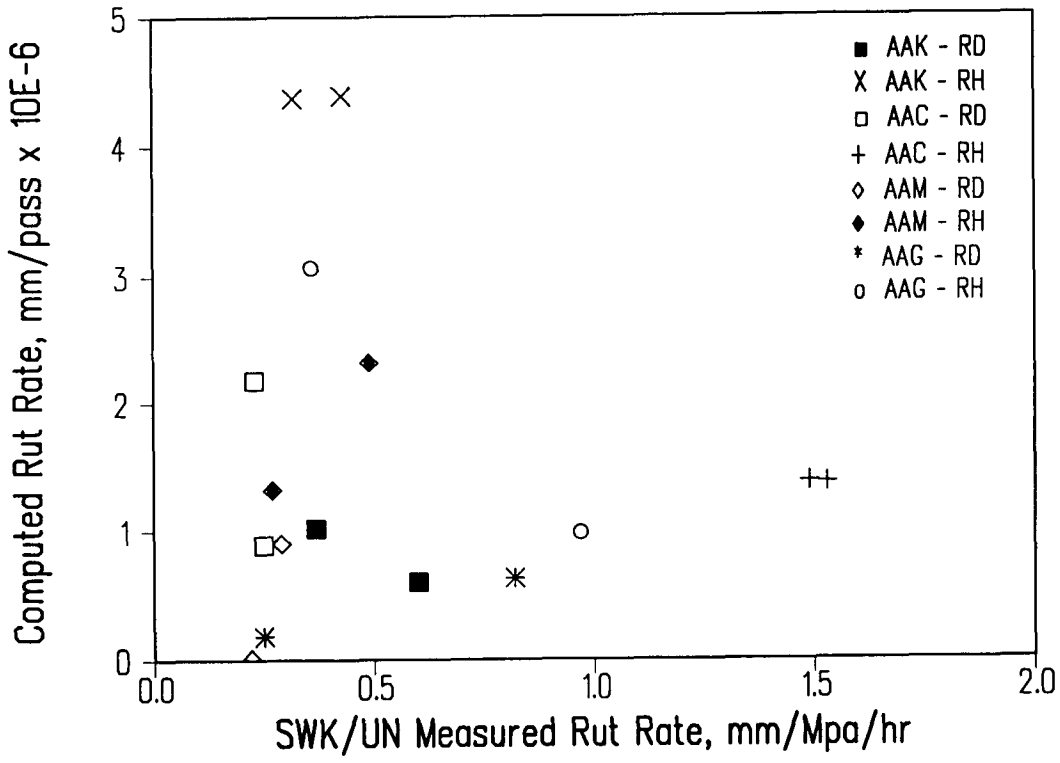

Figure 7.1. Comparison of rut rates in SWK/UN wheel-tracking test with more computed for simulations of the same mixes loaded in the UCB wheel-tracking device

pavement structure shown in Appendix C. The results of the analysis are shown in Figures 7.2 through 7.7.

The CH shear test applied a cyclic (haversine) shear stress of 105 kPa (15 psi) ± 10 percent to the specimens. The load pulse duration was 0.1 s with 0.6 s between load pulses. In addition, vertical compressive loads were applied as necessary to maintain the original specimen height throughout the test duration. As noted earlier the magnitude of the vertical compressive load is a function of the specimen's propensity to dilate under shear loading. Shear strain was calculated from the difference between displacements measured by two LVDTs located ± 1.27 cm (0.5 in.) on each side at mid-height of the specimen. Each test was scheduled to run for 3600 load cycles. However, many were stopped prior to reaching this number of load cycles if the specimen exhibited 4 percent permanent shear strain or if failure occurred.

For the FS test, based on the analyses shown in Figures 7.2 through 7.4, a cyclic shear stress of 173 kPa (25 psi) ± 10 percent and a cyclic compressive axial stress of 345 kPa (50 psi) ± 10 percent were simultaneously applied, both with load pulse durations of 0.1 s and 0.6 s between load pulses. In addition, a constant confining pressure of 140 kPa (20 psi) was applied to the specimen. Each test was also scheduled to run for 3600 load cycles; all but three of the FS tests completed the scheduled 3600 cycles.

Two shear response parameters were calculated from each of the above shear test conditions for comparison with asphalt binder properties: the number of load cycles at which the specimen exhibited two percent cumulative permanent shear strain, ($N_{2\%}$); and the cumulative permanent shear strain after a constant number of load cycles, or $\Sigma\gamma_p$.

For CH tests, $\Sigma\gamma_p$ values at 32 load cycles were used in the following analyses. This was the highest number of load cycles that allowed all specimens to be included in the analyses. Similarly, for FS tests, $\Sigma\gamma_p$ values at 602 load cycles were used.

Although binders and asphalt aggregate mixes were both tested at a temperature of 60°C (140°F), they were tested at substantially different loading frequencies: binders were tested at a loading frequency of 10 rad/s (1.6 Hz) and the mixes at 62.8 rad/s (10 Hz). Thus, it is possible that the binders in the asphalt aggregate mixes exhibited more of their elastic nature and less of their viscous nature, due to the faster loading, than the binders tested alone (i.e., in the asphalt binder tests).

Figures 7.8 and 7.9 illustrate the variation of permanent shear strain for similar specimens in the simple shear repetitive constant height tests and the simple shear repetitive test using the field state of stress. Results are reasonably consistent.

Figures 7.10 and 7.11 illustrate that variation in permanent shear strain for four mixes (aggregates RD and RH) and two void contents in constant height and field state of stress tests. The results suggest that the tests are sensitive to mix variables.

A comparison between the performance of mixes subjected to the field state of stress and constant height tests is presented in Figure 7.12. Although the specimens were similar, there

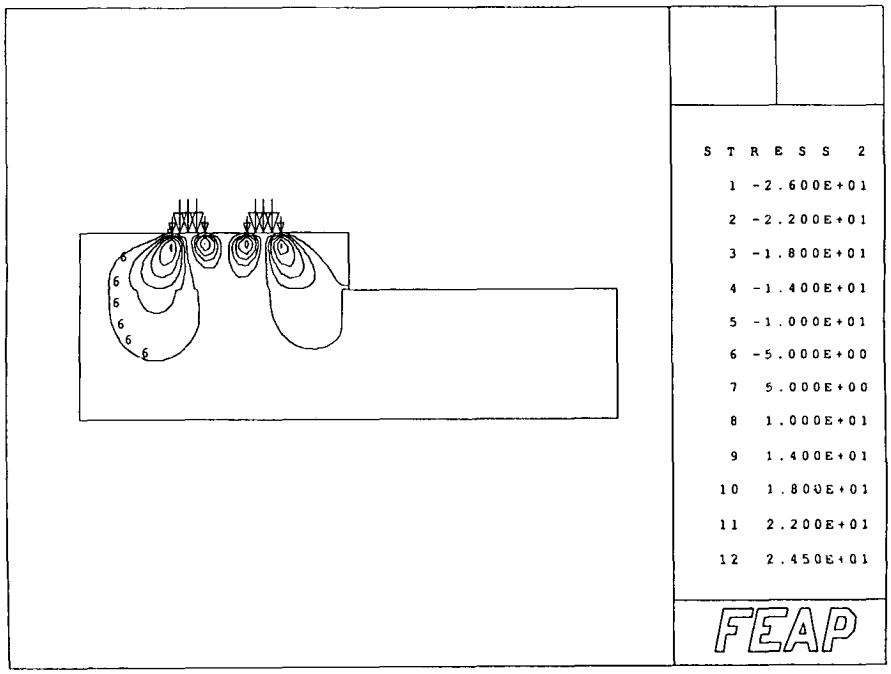

Figure 7.2. Shear stress, σ_{xy}, distribution

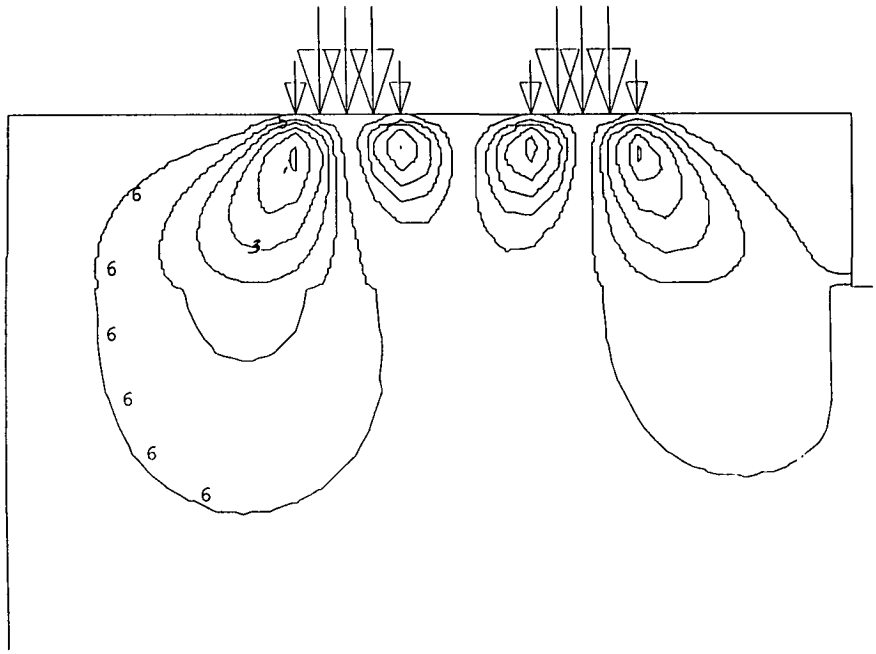

Figure 7.3. Enlarged view of Figure 7.2

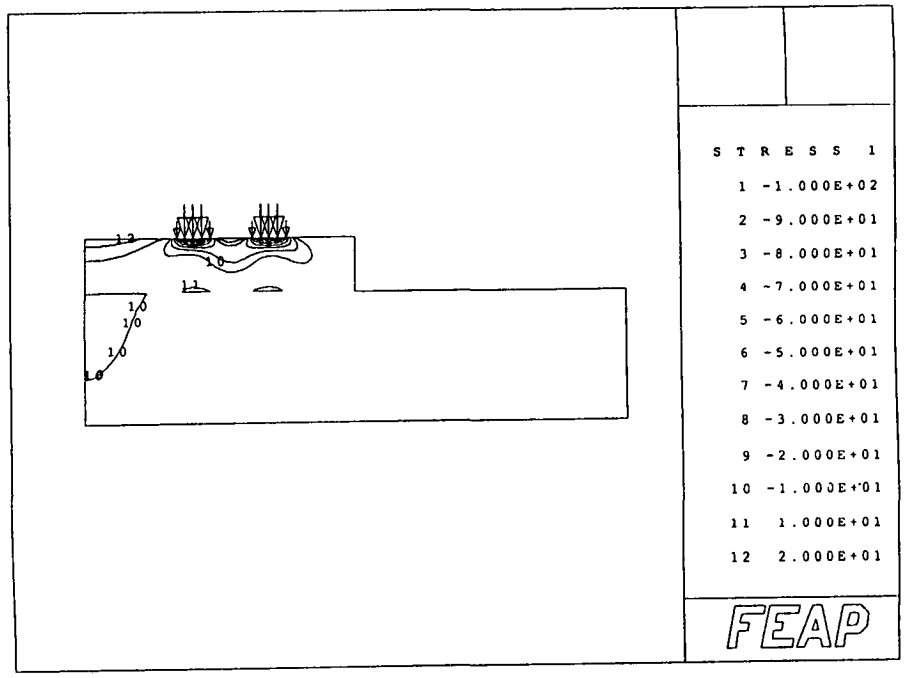

Figure 7.4. Horizontal stress, σ_{xx}, distribution

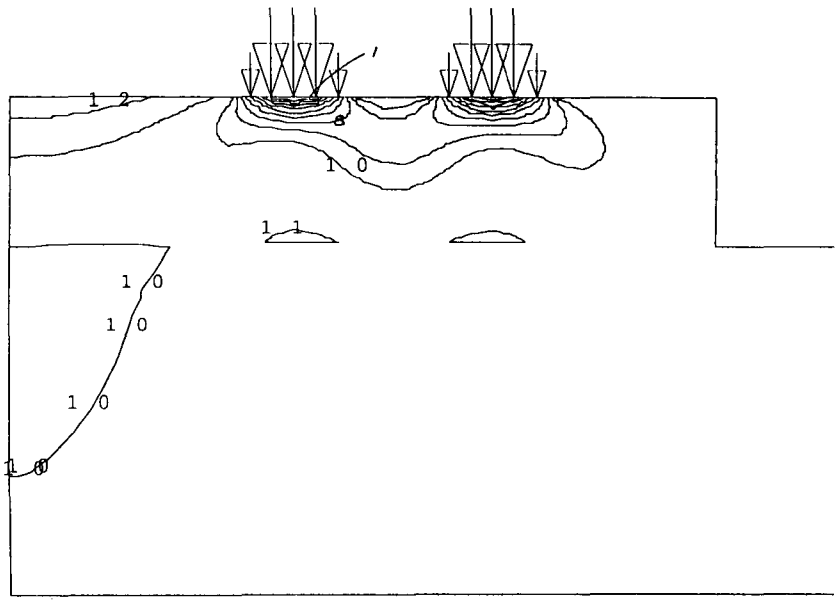

Figure 7.5. Enlarged view of Figure 7.4

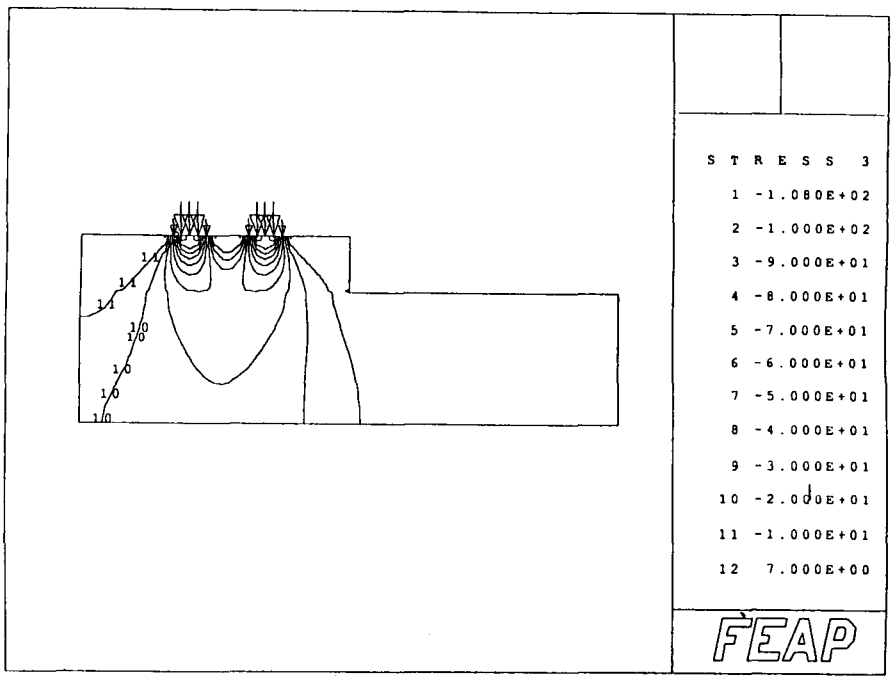

Figure 7.6. Vertical stress, σ_{yy}, distribution

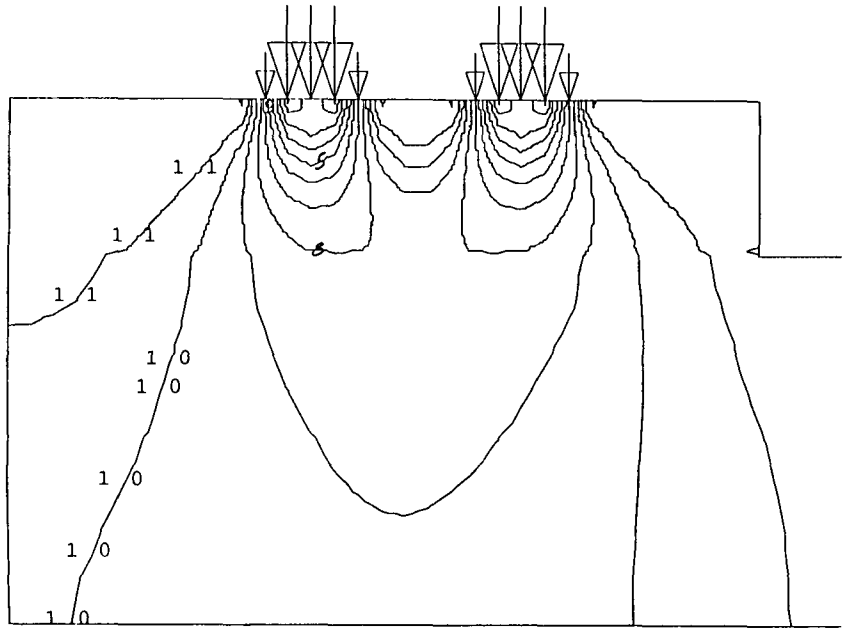

Figure 7.7. Enlarged view of Figure 7.6

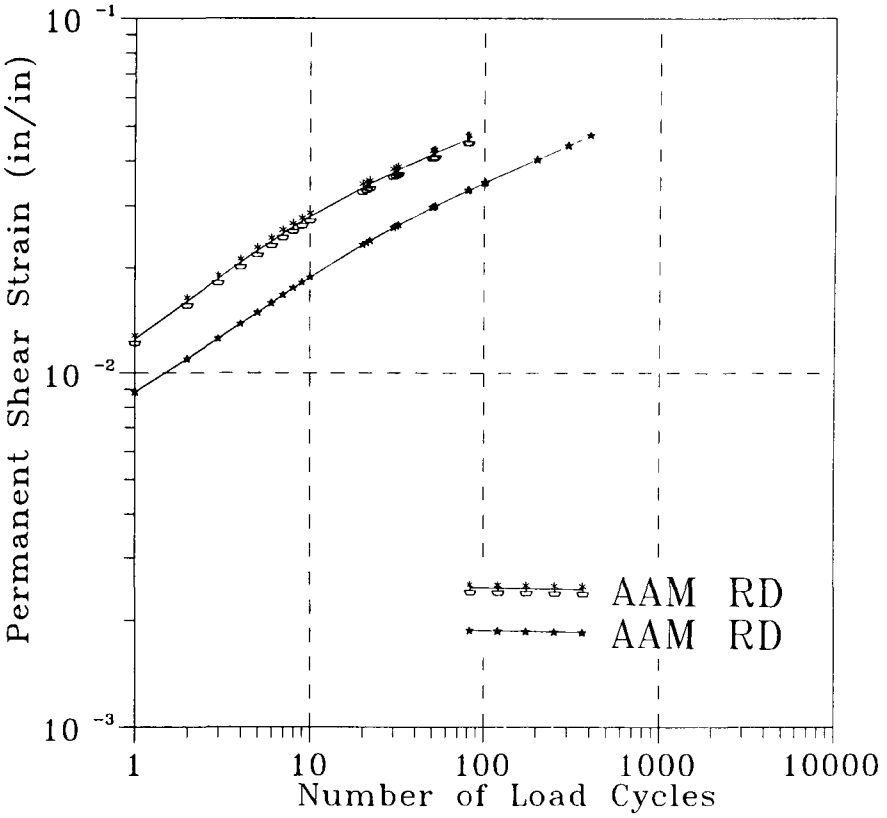

Figure 7.8. Permanent shear strain versus number of repetitions; constant height tests

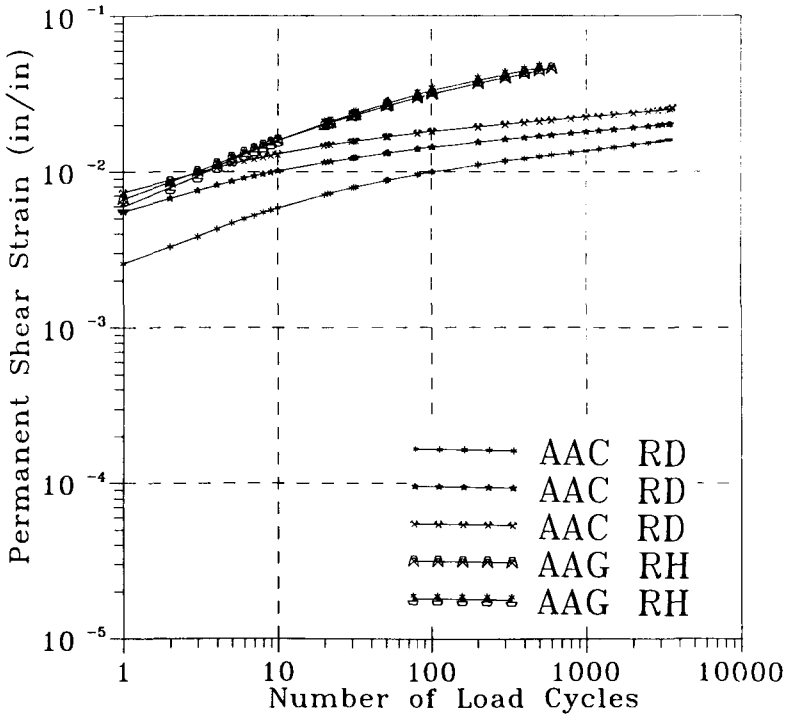

Figure 7.9. Permanent shear strain versus number of repetitions; field tests

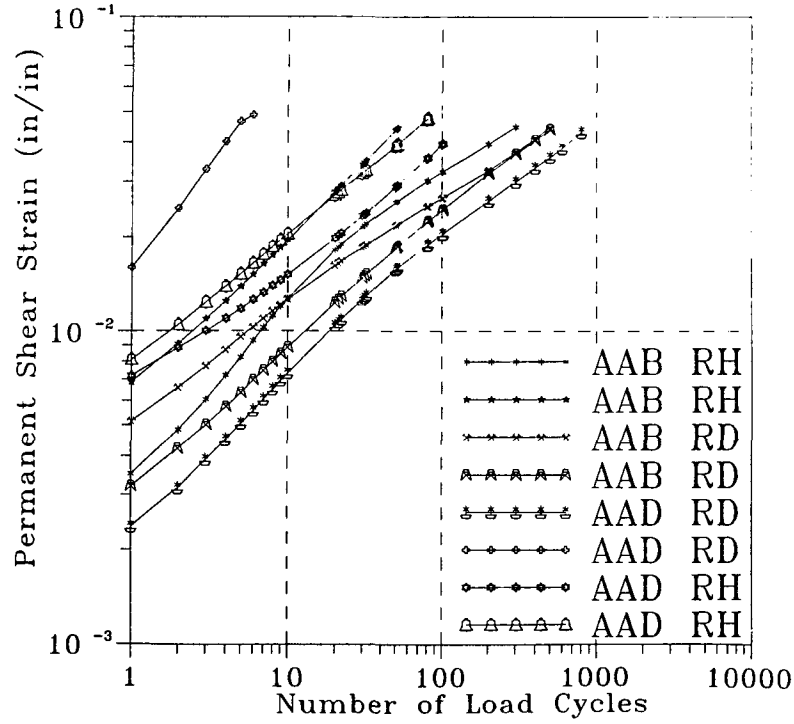

Figure 7.10. Permanent shear strain versus number of repetitions; constant height tests

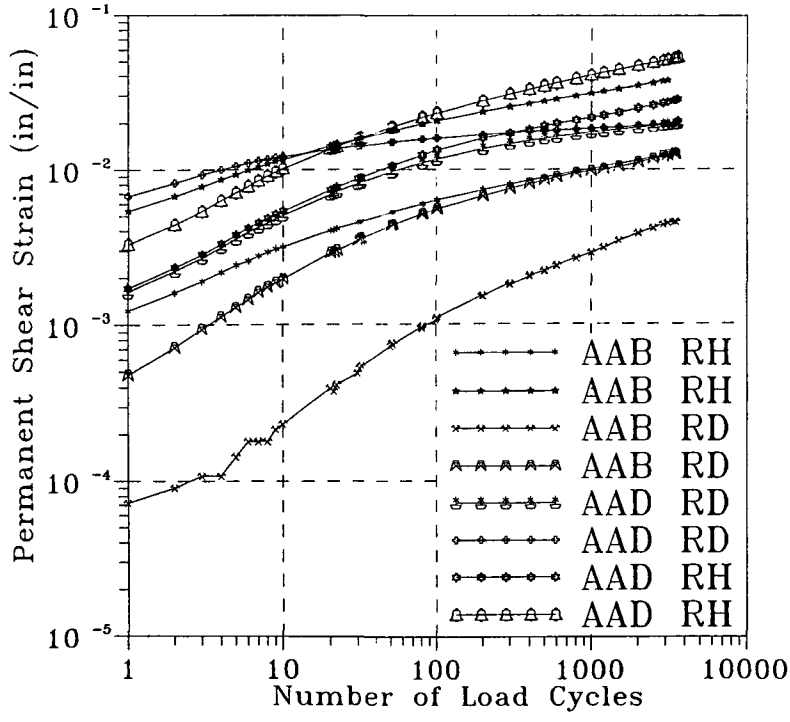

Figure 7.11. Permanent shear strain versus number of repetitions; field tests

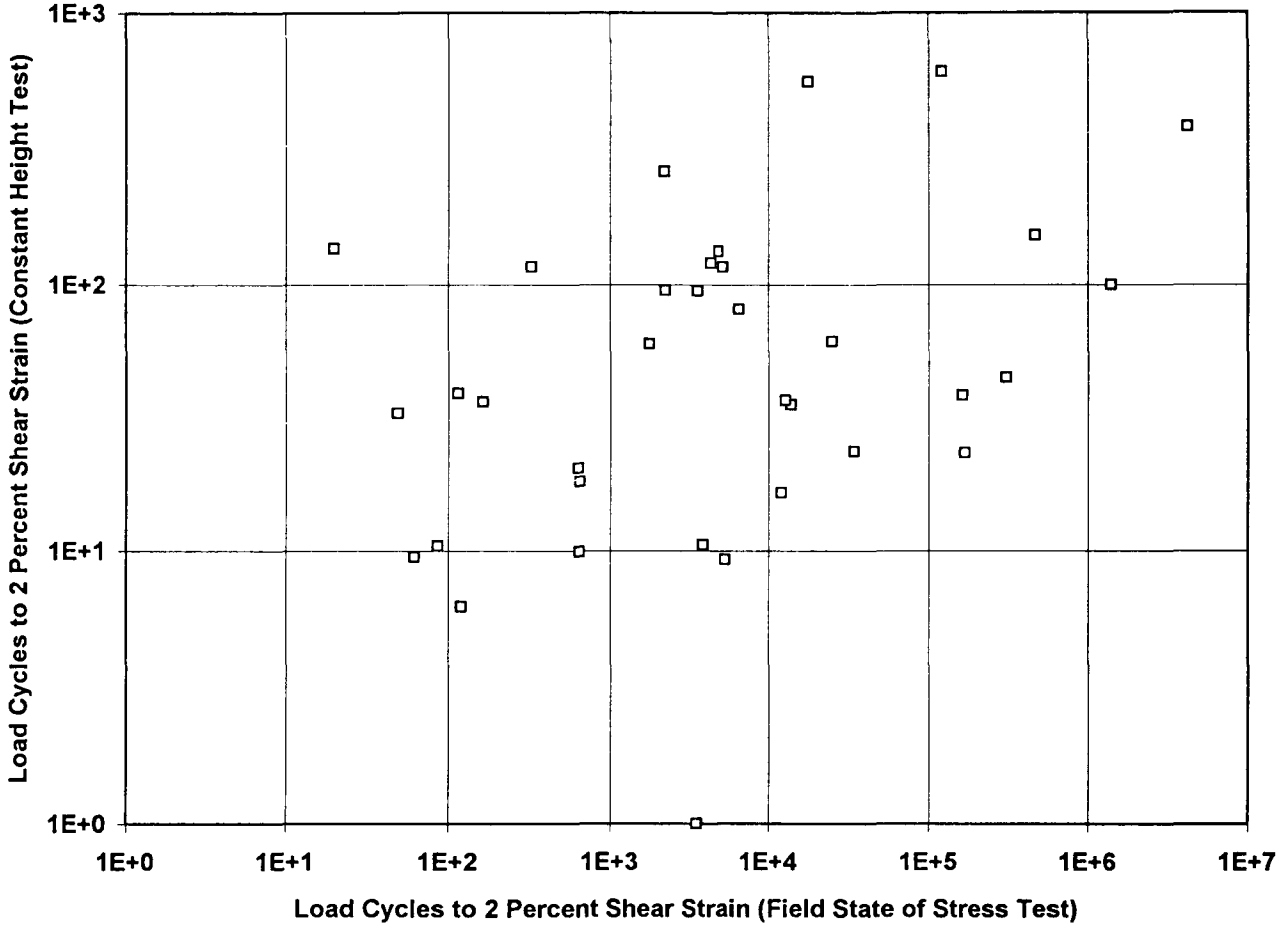

Figure 7.12. Comparison between the number of repetitions to reach 0.02 shear strain in constant height tests and the number of repetitions to reach 0.02 shear strain under the field state of stress

does not appear to be any relationship between the two experiments, indicating that the ranking of a mix depends on the state of stress.

A summary of the results for the various permanent deformation tests is shown in Table 7.2. Asphalt stiffness data were obtained on specimens (subjected to thin film oven test [TFOT] aging prior to testing) at a time of loading of 10 rad/s. Results of the constant height simple shear tests versus $G^*/\sin\delta$ at 60°C (140°F) are shown in Figures 7.13 and 7.14 for mix with low and high void contents respectively. Considerable scatter is apparent in the data. The relationship between load repetitions to 2 percent strain and $G^*\sin\delta$ for mixes containing aggregate RH and tested at the high void content appears to be the most consistent.

Additionally, various relationships among the data were examined. Since void content was a variable, it was decided to perform the comparisons at a single void content, selected as 5.5 percent and determined by logarithmic interpolation of the data for each mix.

These results are summarized in Table 7.3. The only relationships that have been included are those between N at 2 percent strain in the simple shear constant height test, and rut rate and rut depth in the SWK/UN wheel-tracking tests. These are shown in Figures 7.15 and 7.16. These results suggest that the constant height test may be a useful simple test to define the rutting propensity of mixes.

The results of this study indicate that binder properties can affect the shear response of asphalt aggregate mixes. However, aggregate characteristics can be equally or more significant. Specific findings include the following:

- Better relationships between asphalt binder properties and mix shear response ($N_{2\%}$ or $\Sigma\gamma_p$) were observed for mixes tested under CH conditions than for mixes tested under FS conditions. This is likely due to the significant influence of aggregate in the FS shear test. The confining pressure in the FS shear test provides stability to the aggregate skeleton of the mix. This minimizes strains in the asphalt binder that reduce the influence of the binder properties. The results of an analysis of variation (ANOVA) support this hypothesis (SHRP 1994); the influences of binder properties and air void level are less pronounced in the FS shear test. The CH shear test, however, confines specimen deformation in only one direction (i.e., the height of the specimen remains constant). Aggregate particles are allowed to slide past each other during shear loading, causing larger strains in the asphalt, that reflect more the influence of the binder.

- The strongest relationship between asphalt binder properties and mix shear response was observed for mixes containing RH aggregate and 7 percent air voids. This suggests that when mix characteristics are such that they result in low interparticle friction, the influence of asphalt binder properties becomes more significant. Aggregate RD is a quarry stone that is 100 percent crushed; RH is a partially crushed river gravel that would be expected to provide less interparticle friction than RD. This underscores the influence of aggregate characteristics on permanent deformation.

Table 7.2. Summary of wheel-track rutting tests and simple shear tests for 9 mixes containing aggregates RD and RH and 9 MRL asphalts

Specimens			Simple Shear—Constant Height		Simple Shear Field Stress State		SWK/UN Wheel-Tracking Test		G*/sinδ (asphalt) kPa at 10 rad/s	
Asphalt	Aggregate	Void Level	V_{air} (%)	Reps to 2% strain	V_{air} (%)	Reps to 2% strain	Rut depth (mm)	Normalized rutting rate (mm/Pa/hr)	40°C (104°F)	60°C (140°F)
AAB-1	RD	0	3.3	39	3.5	162,406	0.34	1.38	80	3.25
AAC-1	RD	0	3.7	609	5.1	120,862	0.25	1.14	90	2.67
AAD-1	RD	0	5.1	95	4.7	3577	0.33	1.18	76	3.86
AAG-1	RD	0	4.3	261	4.3	2212	0.25	1.14	147	4.31
AAK-1	RD	0	3.5	117	3.5	5178	0.37	1.69	149	8.69
AAM-1	RD	0	4.8	152	3.7	466,837	0.29	1.09	123	4.90
AAV	RD	0	4.6	120	3.3	4327	0.36	1.46	39	1.33
AAZ	RD	0	4.3	100	4.7	1,402,470	0.26	1.26	94	4.29
ABC	RD	0	4.6	381	2.3	4,172,338	0.20	0.92	95	5.92
AAB-1	RD	1	9.1	61	9.0	25,325	0.42	2.60		
AAC-1	RD	1	7.3	36	8.8	13,811	0.23	1.23		
AAD-1	RD	1	10.6	1	11.0	3533	0.43	2.32		
AAG-1	RD	1	6.5	81	6.9	6534	0.82	2.46		
AAK-1	RD	1	6.8	133	6.7	4869	0.60	1.79		
AAM-1	RD	1	7.8	45	7.8	307,340	0.22	1.46		
AAV	RD	1	7.0	11	6.7	3846	0.53	2.30		
AAZ	RD	1	7.2	37	7.8	12,793	0.57	1.91		
ABC	RD	1	7.4	23	5.3	168,945	0.25	1.06		

Table 7.2 (continued). Summary of wheel track rutting tests and simple shear tests for 9 mixes containing aggregates RD and RH and 9 MRL asphalts

Specimens			Simple Shear—Constant Height		Simple Shear Field Stress State		SWK/UN Wheel-Tracking Test		G*/sinδ (asphalt) kPa at 10 rad/s	
Asphalt	Aggregate	Void Level	V_{air} (%)	Reps to 2% strain	V_{air} (%)	Reps to 2% strain	Rut depth (mm)	Normalized rutting rate (mm/Pa/hr)	40°C (104°F)	60°C (140°F)
AAB-1	RH	0	7.8	25	2.9	34,542	0.31	1.34		
AAC-1	RH	0	4.9	9	5.3	5321	1.49	4.64		
AAD-1	RH	0	5.4	20	5.0	627	1.06	3.19		
AAG-1	RH	0	2.6	136	2.3	20	0.36	1.44		
AAK-1	RH	0	2.7	117	2.1	324	0.32	1.24		
AAM-1	RH	0	4.5	560	4.6	17,725	0.27	1.24		
AAV	RH	0	3.1	18	2.6	641	0.62	2.09		
AAZ	RH	0	2.4	95	4.6	2245	0.51	2.23		
ABC	RH	0	2.8	60	3.1	1785	0.35	1.04		
AAB-1	RH	1	7.8	10	8.7	86	0.60	2.89		
AAC-1	RH	1	7.6	10	7.1	637	1.53	5.59		
AAD-1	RH	1	6.8	10	6.0	62	1.18	3.70		
AAG-1	RH	1	8.9		7.6	79	0.97	3.77		
AAK-1	RH	1	6.5	36	5.7	162	0.43	1.96		
AAM-1	RH	1	8.5	33	6.5	49	0.49	2.03		
AAV	RH	1	6.4	6	5.6	119	0.77	2.52		
AAZ	RH	1	7.0	17	6.0	12,067	0.75	2.62		
ABC	RH	1	6.0	39	6.6	114	0.58	1.48		

Table 7.2 (continued). Summary of wheel track rutting tests and simple shear tests for 9 mixes containing aggregates RD and RH and 9 MRL asphalts

Specimens			Simple Shear—Constant Height		Simple Shear Field Stress State		SWK/UN Wheel-Tracking Test		G*/sinδ (asphalt) kPa at 10 rad/s	
Asphalt	Aggregate	Void Level	V_{air} (%)	Reps to 2% strain	V_{air} (%)	Reps to 2% strain	Rut depth (mm)	Normalized rutting rate (mm/Pa/hr)	40°C (104°F)	60°C (140°F)
AAB-1	RH	0	7.8	25	2.9	34,542	0.31	1.34		
AAC-1	RH	0	4.9	9	5.3	5321	1.49	4.64		
AAD-1	RH	0	5.4	20	5.0	627	1.06	3.19		
AAG-1	RH	0	2.6	136	2.3	20	0.36	1.44		
AAK-1	RH	0	2.7	117	2.1	324	0.32	1.24		
AAM-1	RH	0	4.5	560	4.6	17,725	0.27	1.24		
AAV	RH	0	3.1	18	2.6	641	0.62	2.09		
AAZ	RH	0	2.4	95	4.6	2245	0.51	2.23		
ABC	RH	0	2.8	60	3.1	1785	0.35	1.04		
AAB-1	RH	1	7.8	10	8.7	86	0.60	2.89		
AAC-1	RH	1	7.6	10	7.1	637	1.53	5.59		
AAD-1	RH	1	6.8	10	6.0	62	1.18	3.70		
AAG-1	RH	1	8.9		7.6	79	0.97	3.77		
AAK-1	RH	1	6.5	36	5.7	162	0.43	1.96		
AAM-1	RH	1	8.5	33	6.5	49	0.49	2.03		
AAV	RH	1	6.4	6	5.6	119	0.77	2.52		
AAZ	RH	1	7.0	17	6.0	12,067	0.75	2.62		
ABC	RH	1	6.0	39	6.6	114	0.58	1.48		

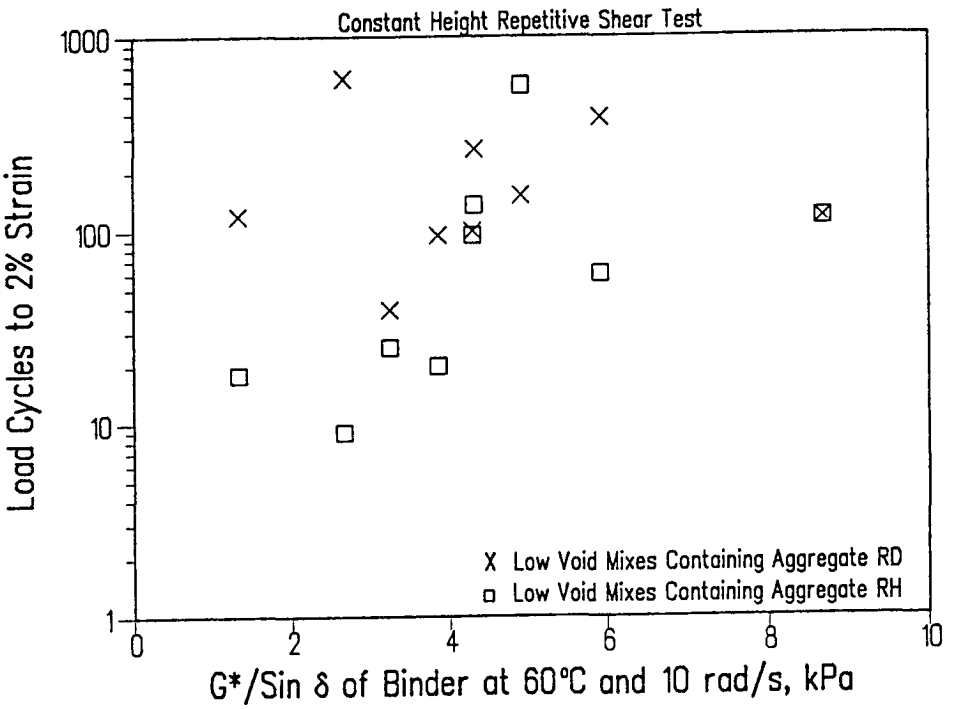

Figure 7.13. Relationship between N at 2 percent strain in constant height repeated load simple shear test and G*/sinδ at 60°C (140°F) for mixes containing aggregates RD and RH; low void content

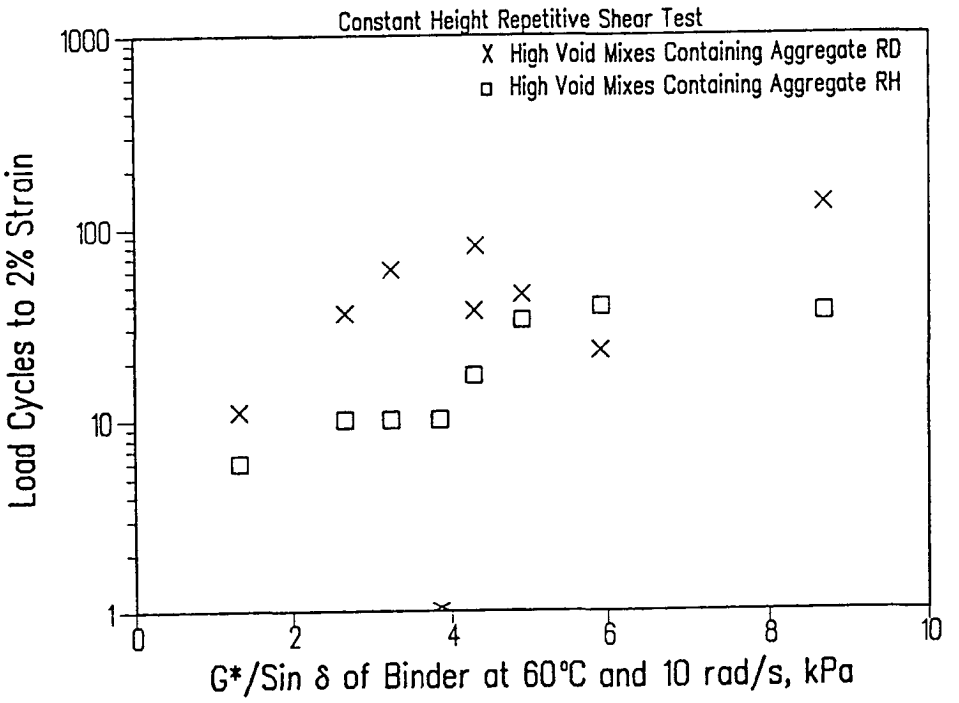

Figure 7.14. Relationship between N at 2 percent strain in constant height repeated load simple shear test and G*/sinδ at 60°C (140°F) for mixes containing aggregates RD and RH; high void content

Table 7.3. Measurements of mixes containing aggregates RH and RD and nine MRL asphalts with results interpolated to 5.5 percent voids

Asphalt Type	Aggregate Type	Load Repetition to 2% strain (CH)	Load Repetition to 2% strain (FS)	Rut Rate (mm/Pa/in.)	Rut Depth (mm)	G*/sinδ (kPa at 10 rad/s)
AAV	RD	33	4063	0.443	1.861	39
AAD-1	RD	60	3573	0.339	1.264	76
AAB-1	RD	46	81,434	0.368	1.746	80
AAC-1	RD	259	62,860	0.244	1.166	91
AAM-1	RD	99	402,940	0.263	1.208	122
AAG-1	RD	145	3802	0.453	1.675	147
AAK-1	RD	126	4986	0.498	1.751	149
AAZ	RD	72	293,037	0.338	1.447	94
ABC	RD	53	432,445	0.234	1.017	95
AAV	RH	7	155	0.744	2.446	39
AAD-1	RH	17	352	1.089	3.310	76
AAB-1	RH	24	25,331	0.321	1.394	80
AAC-1	RH	9	3649	1.497	4.796	91
AAM-1	RH	225	2659	0.327	1.453	122
AAG-1	RH		41	0.606	2.389	17
AAK-1	RH	49	194	0.398	1.739	149
AAZ	RH	30	6889	0.660	2.483	94
ABC	RH	43	220	0.514	1.360	95

Note: CH = constant height test.
FS = field state of stress test.

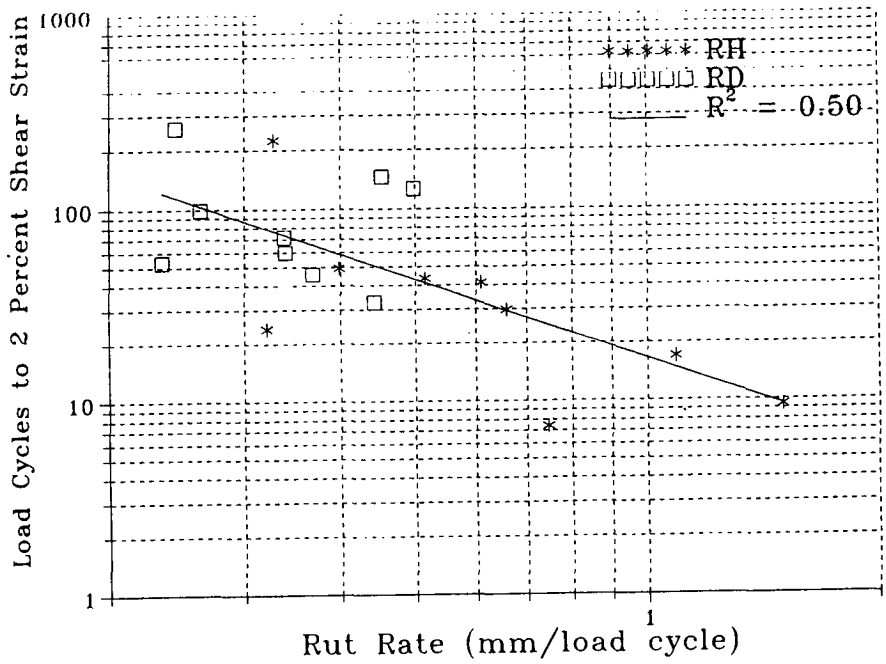

Figure 7.15. Number of repetitions to reach 2 percent shear strain in constant height tests versus the rutting rate for RD and RH materials (adjusted to 5.5 percent voids)

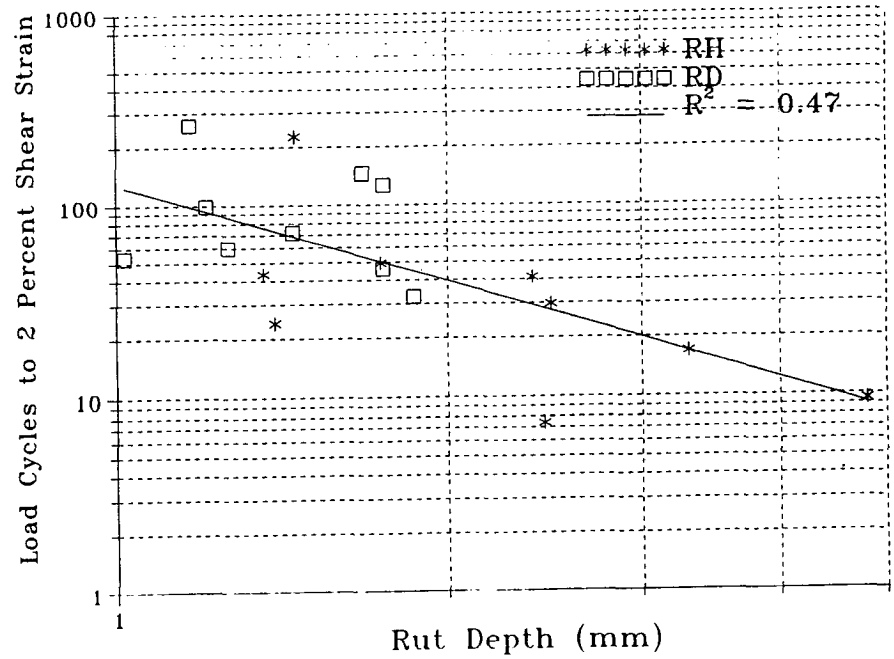

Figure 7.16. Number of repetitions to reach 2 percent shear strain in constant height tests versus the rut depth for RD and RH materials (adjusted to 5.5 percent voids)

In general these results suggest that the influence of asphalt on permanent deformation response is highly dependent on the conditions to which the mix is subjected. Results reported elsewhere (SHRP 1994) showed the effect of asphalt was significant but that its influence was small compared to the influence of aggregate, especially when the mix was tested at lower temperatures (e.g., 40°C [104°F]) or was subjected to states of stress that amplified the aggregate influence (e.g., FS shear test).

7.3 Summary

While the wheel-track and simple shear test programs were developed to assess the validity of the parameter $G^*/\sin\delta$ in the binder specifications proposed by the A-002A contractor, the studies have also provided some assistance in selecting a simplified test to define the permanent deformation response. From the information presented, particularly the relationships between data obtained from the wheel-tracking test and the constant height simple shear test, the constant height repeated load simple shear test would appear to serve as a suitable candidate for improved mix evaluation.

In addition, in the absence of validation data from the UCB wheel-tracking device, some comparisons have been made between the results of the data obtained from the wheel-tracking tests and computed parameters from the same mixes using a battery of tests in the simple shear device and the finite element simulation of the mixes in the UCB wheel-tracking device. While the results are not as good as one hopes for, in general the results for the two separate programs indicate reasonable correspondence, thus suggesting that the constitutive relationship and finite element simulation have the potential to predict performance — i.e., the development of permanent deformation with repeated traffic loading.

8

Compound Loading Tests

A series of tests was conducted in compound loading to assess the feasibility of such an approach to mix evaluation and design to mitigate permanent deformation. As noted earlier, cyclic shear testing is considered by the A-003A researchers to be the most promising procedure for accelerated performance testing to define resistance to permanent deformation of asphalt aggregate mixes.

For this program two types of testing were evaluated: (1) a test in which a constant ratio between the normal and shear pulses is maintained, referred to herein as *normal loading*; and (2) a test in which a constant specimen height is maintained by adjusting the normal stress pulse as necessary to ensure this condition, called *constant height loading*. A third type in which confining pressure is applied was considered to be unnecessarily complex for routine testing purposes (used in the validation studies described in Chapter 7) and was not considered in this study.

This investigation compares normal and constant height loading in a common design environment in which all mix components except asphalt content have been selected. Air void content is also treated as a variable. The objectives were as follows:

- to assess the sensitivity of cyclic shear measurements to mix properties;
- to determine whether cyclic shear tests are useful for those aspects of mix design related to asphalt and air void contents;
- to determine the variability of cyclic test measurement; and
- to evaluate normal and constant height tests with regard to their suitability as accelerated performance tests for the analysis and design of asphalt aggregate mixes.

8.1 Methodology

Asphalt AAG-1 and aggregate RB (medium gradation) were used throughout. Asphalt contents were 4.5, 4.9, 5.5, and 6.0 percent by weight of aggregate, and air void contents were grouped into three categories, 2.5 through 3.5 percent, 4.5 through 5.5 percent, and 6.5 through 7.5 percent. Ranges of both asphalt content and air void content were considered to be sufficiently large to affect mix performance.

Data were available for 18 mixes under normal loading and 18 under constant height loading. Specimens were nominally 15 cm (6 in.) in diameter and 5 cm (2 in.) in height.

All testing was performed at 50°C (122°F). Compound loading was applied throughout: the pattern was 400 cycles of 14 kPa (2 psi) shear stress, 600 cycles of 28 kPa (4 psi) shear stress, 800 cycles of 42 kPa (6 psi) shear stress, and 1000 cycles of 56 kPa (8 psi) shear stress. Although each compound loading sequence was performed three times, analyses reported herein were limited to the first sequence. Shear displacements were measured cap-to-cap and a 3.8 cm (1.5 in.) (rather that 5 cm [2 in.]) gauge length was assumed for computing strains. The ratio of normal-to-shear stresses in the normal testing was nominally 1.5 for all levels of shear stress. The basis for this stress ratio is included in Appendix E.

8.2 Measurements and Analysis

Tables 8.1 through 8.4 summarize stress conditions for each of the tests. That average shear stress was variable from one specimen to the next and failed to reach targeted levels precisely is inconsequential to the analysis. In constant height testing, mix properties determine the ratio of normal-to-shear stress, as is readily apparent from Table 8.4.

Appendix F contains traces of inelastic strain measurements as a function of the number of load cycles for each of 36 tests. Careful examination of these traces yields the following observations: (1) obvious discrepancies between test replicates were limited to one data set, (2) results were not consistent across the variables of interest (asphalt and air void content), (3) replicate measurements were often quite different.

Shear modulus was found to be relatively insensitive to either asphalt content or air void content (Tables 8.5 and 8.6 and Figures 8.1 and 8.2). Just how shear modulus may be influenced by asphalt and air void contents from these tests and at this elevated temperature is unclear.

Shear modulus generally increases with stress level and, as expected, the effect seems to be most pronounced at low asphalt contents. Results of calibrating the following equation are summarized in Tables 8.7 and 8.8.

Table 8.1. Variation of average shear stress in normal tests

Asphalt Content (Percent)	Air Void Content (Percent)	Average Shear Stress (psi)			
		Block 1 (400 cycles)	Block 2 (600 cycles)	Block 3 (800 cycles)	Block 4 (1000 cycles)
4.5	2.5-3.5	1.92	3.85	5.69	7.67
		1.90	3.83	5.73	7.64
4.9	2.5-3.5	1.92	3.86	5.71	7.86
		1.92	3.93	6.02	8.17
5.5	2.5-3.5	1.90	3.89	6.01	8.30
6.0	2.5-3.5	1.89	3.93	5.91	8.02
4.5	4.5-5.5	1.89	3.87	5.77	8.00
		1.89	3.87	6.04	8.15
4.9	4.5-5.5	1.89	3.80	5.77	7.84
		1.92	3.93	6.18	8.14
5.5	4.5-5.5	1.92	3.91	6.44	8.34
6.0	4.5-5.5	1.96	3.89	5.75	7.88
4.5	6.5-7.5	1.92	3.82	5.76	7.64
		1.93	3.94	5.90	7.66
4.9	6.5-7.5	1.89	3.86	5.71	7.66
5.5	6.5-7.5	1.89	3.87	5.75	7.82
		1.92	3.92	6.09	8.30
6.0	6.5-7.5	1.96	3.82	5.87	7.97

Table 8.2. Variation of normal-to-shear stress ratio in normal tests

Asphalt Content (Percent)	Air Void Content (Percent)	Ratio of Average Normal Stress to Average Shear Stress			
		Block 1 (400 cycles)	Block 2 (600 cycles)	Block 3 (800 cycles)	Block 4 (1000 cycles)
4.5	2.5-3.5	1.51	1.49	1.52	1.54
		1.54	1.48	1.49	1.53
4.9	2.5-3.5	1.52	1.49	1.54	1.46
		1.50	1.50	1.47	1.44
5.5	2.5-3.5	1.53	1.54	1.50	1.47
6.0	2.5-3.5	1.55	1.47	1.54	1.50
4.5	4.5-5.5	1.55	1.52	1.48	1.47
		1.52	1.52	1.48	1.44
4.9	4.5-5.5	1.54	1.51	1.52	1.46
		1.51	1.49	1.44	1.47
5.5	4.5-5.5	1.52	1.58	1.44	1.43
6.0	4.5-5.5	1.48	1.49	1.57	1.60
4.5	6.5-7.5	1.52	1.56	1.51	1.50
		1.50	1.46	1.51	1.53
4.9	6.5-7.5	1.54	1.47	1.51	1.50
5.5	6.5-7.5	1.54	1.51	1.50	1.50
		1.48	1.46	1.49	1.46
6.0	6.5-7.5	1.51	1.50	1.57	1.53

Table 8.3. Variation of average shear stress in constant height tests

Asphalt Content (Percent)	Air Void Content (Percent)	Average Shear Stress (psi)			
		Block 1 (400 cycles)	Block 2 (600 cycles)	Block 3 (800 cycles)	Block 4 (1000 cycles)
4.5	2.5-3.5	1.93	3.87	5.92	8.32
		1.89	5.87	5.71	7.86
4.9	2.5-3.5	1.93	4.04	5.83	7.83
		1.92	3.92	6.10	8.33
5.5	2.5-3.5	1.91	3.87	5.95	7.95
6.0	2.5-3.5	1.92	3.96	6.08	8.16
4.5	4.5-5.5	1.90	3.85	5.98	8.41
		1.90	3.98	6.06	8.05
4.9	4.5-5.5	1.91	3.91	6.18	8.15
		1.96	3.84	5.84	7.82
5.5	4.5-5.5	1.94	3.83	5.87	7.85
6.0	4.5-5.5	1.93	3.84	5.85	7.85
4.5	6.5-7.5	1.96	4.67	5.91	7.78
4.9	6.5-7.5	1.93	3.97	6.12	8.22
5.5	6.5-7.5	1.91	3.87	5.93	8.11
		1.90	3.88	6.08	8.25
6.0	6.5-7.5	1.91	4.00	5.71	7.66
		1.99	3.90	5.76	6.23

Table 8.4. Variation of normal-to-shear stress ratio in constant height tests

Asphalt Content (Percent)	Air Void Content (Percent)	Ratio of Average Normal Stress to Average Shear Stress			
		Block 1 (400 cycles)	Block 2 (600 cycles)	Block 3 (800 cycles)	Block 4 (1000 cycles)
4.5	2.5-3.5	0.095	0.092	0.179	0.492
		0.074	0.034	0.067	0.292
4.9	2.5-3.5	0.133	0.166	0.428	0.516
		0.100	0.146	0.456	0.584
5.5	2.5-3.5	0.111	0.076	0.094	0.172
6.0	2.5-3.5	0.295	0.738	0.906	0.910
4.5	4.5-5.5	0.068	0.100	0.522	0.713
		0.212	0.516	0.699	0.758
4.9	4.5-5.5	0.106	0.143	0.490	0.618
		0.172	0.643	0.908	0.896
5.5	4.5-5.5	0.186	0.556	0.781	0.822
6.0	4.5-5.5	0.176	0.663	0.923	0.920
4.5	6.5-7.5	0.121	2.278	1.021	0.961
4.9	6.5-7.5	0.156	0.222	0.530	0.625
5.5	6.5-7.5	0.066	0.076	0.314	0.565
		0.087	0.217	0.615	0.687
6.0	6.5-7.5	0.215	0.718	0.907	0.941
		0.479	0.949	0.934	0.904

Table 8.5. Effect of asphalt and air void contents on average shear modulus in normal tests

Asphalt Content (Percent)	Air Void Content (Percent)	Average Shear Modulus (Psi)				
		Block 1 (400 cycles)	Block 2 (600 cycles)	Block 3 (800 cycles)	Block 4 (1000 cycles)	Blocks 2-4
4.5	2.5-3.5	8600	7800	7200	7200	7400
		6700	6800	7400	8100	7500
4.9	2.5-3.5	3800	3400	4200	5100	4300
		5400	5900	6800	7400	6800
5.5	2.5-3.5	5700	5400	5400	5400	5400
6.0	2.5-3.5	4400	5100	5700	6300	5800
4.5	4.5-5.5	6700	5900	5600	6500	6000
		8000	8200	9200	9700	9200
4.9	4.5-5.5	7100	7000	7300	7500	7300
		7200	7500	8400	8600	8200
5.5	4.5-5.5	7000	6900	7600	8000	7500
6.0	4.5-5.5	3200	3400	3500	3900	3600
4.5	6.5-7.5	5800	5600	6100	6800	6200
		6000	6100	6800	7200	6700
4.9	6.5-7.5	8600	7900	7300	7700	7600
5.5	6.5-7.5	6800	6200	5800	6500	6100
		6000	6000	7200	7500	7000
6.0	6.5-7.5	4900	5600	6200	6800	6000

Table 8.6. Effect of asphalt and air void contents on average shear modulus in constant height tests

Asphalt Content (Percent)	Air Void Content (Percent)	Average Shear Modulus (Psi)				
		Block 1 (400 cycles)	Block 2 (600 cycles)	Block 3 (800 cycles)	Block 4 (1000 cycles)	Blocks 2-4
4.5	2.5-3.5	8300	7300	7900	9200	8200
		4400	4500	3100	3700	3600
4.9	2.5-3.5	8100	8900	9000	9200	9100
		5600	5800	7100	8100	7200
5.5	2.5-3.5	6700	5300	4700	4700	4800
6.0	2.5-3.5	5000	5600	5900	6000	5900
4.5	4.5-5.5	6000	4700	6000	7500	6200
		3800	5300	5700	5800	5600
4.9	4.5-5.5	6500	5400	6300	6900	6300
		3700	4000	4700	5200	4700
5.5	4.5-5.5	3800	4600	5100	5400	5000
6.0	4.5-5.5	4600	5200	5300	5400	5300
4.5	6.5-7.5	3900	2600	4000	4800	3900
4.9	6.5-7.5	7000	6900	7600	7600	7400
5.5	6.5-7.5	8200	7000	7300	7700	7400
		5300	5100	5800	6000	5700
6.0	6.5-7.5	2500	3300	3500	3900	3500
		3200	3700	3800	4000	3800

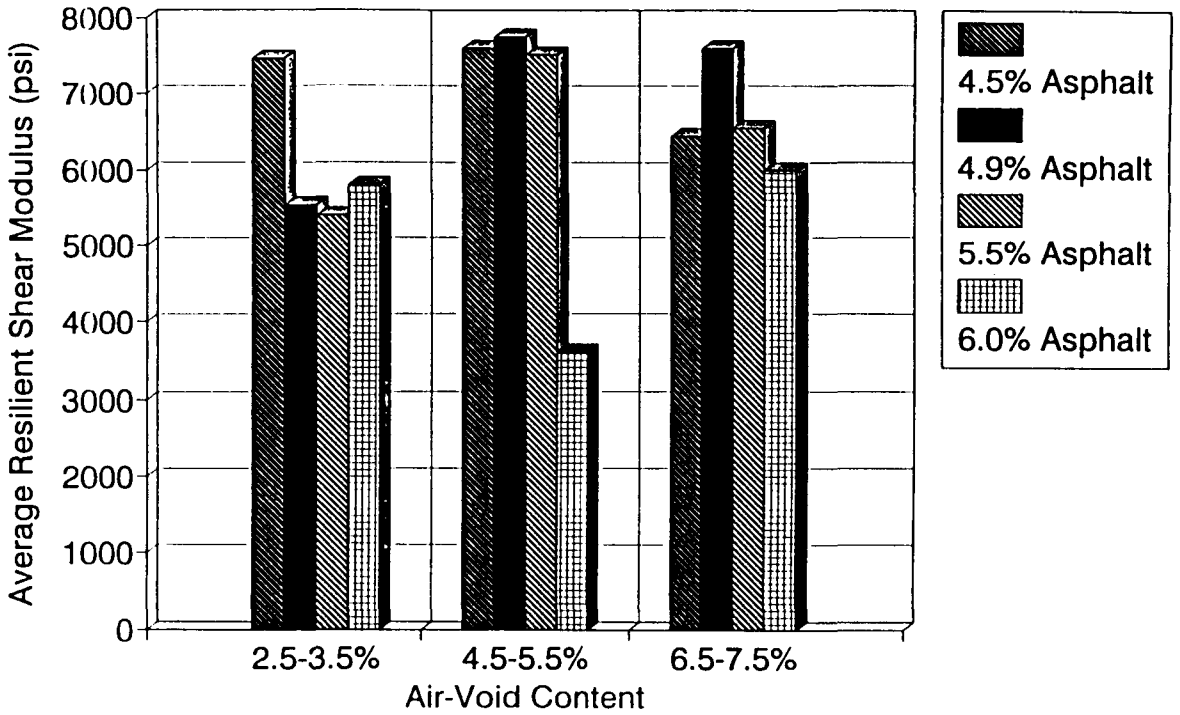

Figure 8.1. Average shear modulus, compound normal loading

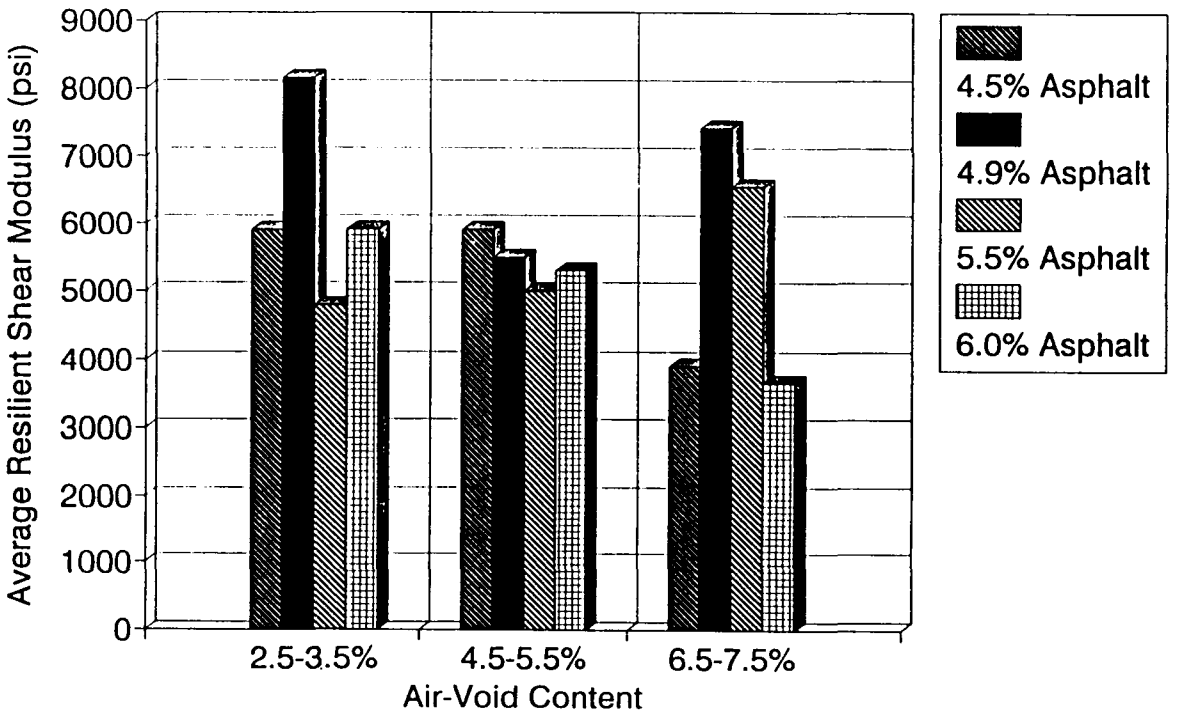

Figure 8.2. Average shear modulus, compound constant height loading

Table 8.7. Shear modulus calibrations for normal tests

Asphalt Content (Percent)	Air Void Content (Percent)	Least-Squares Calibration		
		C_1	C_2	R^2
4.5	2.5-3.5	8114	-126	0.35
		5479	342	0.84
4.9	2.5-3.5	1720	427	0.91
		4680	341	0.89
5.5	2.5-3.5	5293	17	0.00
6.0	2.5-3.5	3961	293	0.86
4.5	4.5-5.5	4963	173	0.40
		6977	347	0.82
4.9	4.5-5.5	6529	124	0.46
		6684	245	0.67
5.5	4.5-5.5	5883	259	0.78
6.0	4.5-5.5	2765	141	0.58
4.5	6.5-7.5	4409	309	0.86
		4887	307	0.82
4.9	6.5-7.5	7759	-34	0.01
5.5	6.5-7.5	5583	93	0.14
		4906	330	0.75
6.0	6.5-7.5	4422	309	0.75

Table 8.8. Shear modulus calibrations for constant height tests

Asphalt Content (Percent)	Air Void Content (Percent)	Least-Squares Calibration		
		C_1	C_2	R^2
4.5	2.5-3.5	5453	442	0.84
		395	498	0.82
4.9	2.5-3.5	8392	110	0.16
		3909	508	0.92
5.5	2.5-3.5	5570	-116	0.30
6.0	2.5-3.5	5178	109	0.41
4.5	4.5-5.5	2272	624	0.95
		4830	128	0.37
4.9	4.5-5.5	3947	373	0.85
		2914	296	0.86
5.5	4.5-5.5	3894	195	0.76
6.0	4.5-5.5	5122	32	0.08
4.5	6.5-7.5	235	588	0.60
4.9	6.5-7.5	6261	187	0.42
5.5	6.5-7.5	6416	154	0.41
		4299	222	0.77
6.0	6.5-7.5	2488	185	0.51
		3211	107	0.14

$$G = C_1 + C_2\tau \tag{8.1}$$

where G is the shear modulus in psi and τ is the shear stress in psi. In the regression analysis the first loading block (14 kPa [2 psi]) was omitted.

The added confinement of the normal loading would be expected to result in greater moduli for normal than for constant height loading. Figure 8.3 generally (but not conclusively) confirms this expectation.

Effects of asphalt and air void contents on inelastic strain measurements are tabulated in Tables 8.9 and 8.10. Figures 8.4 and 8.5 depict composite results (cumulative inelastic strain after 2800 cycles of compound loading) graphically. The significant effects that had been anticipated, especially for air void content, are simply not evident in these depictions. The largest asphalt content at all air void contents does seem to produce the largest inelastic strains, and, although the evidence is mixed, larger air voids seem to yield larger strains.

Regression equations of the following form were fitted to the measurements produced by each test:

$$\gamma = C_1\tau^{C_2}N^{C_3} \tag{8.2}$$

where γ is the inelastic shear strain, τ is the shear stress, N is the number of loading cycles from the beginning of the loading block, and the C's are regression coefficients. Data produced during the first loading block (14 kPa [2 lb/in^2]) were excluded from the calibrations, and the analysis assumed that results from each load block were independent of prior loading. Calibration results are tabulated in Tables 8.11 and 8.12.

Resistant mixes would generally be expected to experience small initial inelasticities (small C_1) as well as small increments with each loading cycle (small C_3). Figures 8.6 and 8.7 generally confirm the expected relationship between C_1 and C_3 and suggest somewhat stronger correlations from normal testing than from constant height testing.

Interestingly, there is also a relationship — although an apparently counterintuitive one — between C_2 and C_3 (Figures 8.8 and 8.9). More resistant mixes (small C_3) experience larger permanent strains as a result of stress increases than do less resistant mixes. The four negative stress exponents under normal loading were unexpected and remain unexplained. The 11 negative exponents under constant height loading likely reflect the increased confinement (larger ratio of normal-to-shear stress) under larger shear stresses.

The regression equations (Tables 8.11 and 8.12) were used to predict the number of load cycles under a 42 kPa (6 psi) shear stress that could be sustained without exceeding an inelastic shear strain of 2 percent. This is the kind of approach that has been anticipated in the recommended mix analysis and design system. Results, shown graphically in Figures 8.10 and 8.11, suggest that increased asphalt content (and possibly increased air void

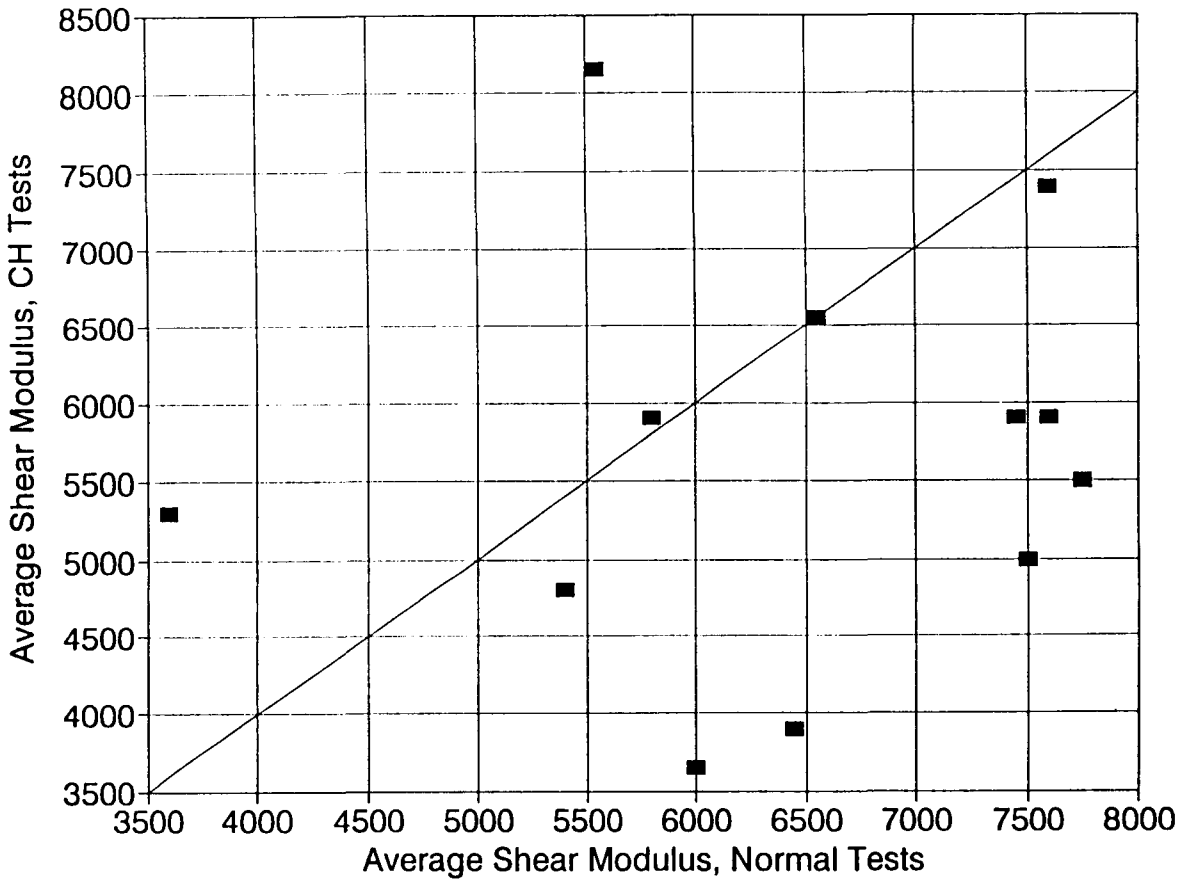

Figure 8.3 Average shear moduli in compound normal tests versus compound constant height tests

Table 8.9. Effect of asphalt and air void contents on inelastic shear strain in normal tests

Asphalt Content (Percent)	Air Void Content (Percent)	Inelastic Shear Strain (Percent)				
		Block 1 (400 cycles)	Block 2 (600 cycles)	Block 3 (800 cycles)	Block 4 (1000 cycles)	All Blocks (2800 cycles)
4.5	2.5-3.5	0.016	0.049	0.092	0.452	0.610
		0.043	0.115	0.407	0.518	1.083
4.9	2.5-3.5	0.056	0.450	1.081	0.775	2.362
		0.292	0.604	0.592	0.551	2.039
5.5	2.5-3.5	0.021	0.127	0.534	0.516	1.198
6.0	2.5-3.5	0.345	1.363	1.346	1.437	4.491
4.5	4.5-5.5	0.031	0.066	0.298	0.829	1.221
		0.138	0.308	0.596	0.606	1.648
4.9	4.5-5.5	0.053	0.122	0.345	0.495	1.015
		0.166	0.399	0.481	0.495	1.542
5.5	4.5-5.5	0.006	0.136	0.168	0.228	0.538
6.0	4.5-5.5	0.158	0.686	0.818	1.268	2.931
4.5	6.5-7.5	0.103	0.197	0.401	0.580	1.280
		0.023	0.173	0.419	0.436	1.050
4.9	6.5-7.5	0.032	0.051	0.143	0.365	0.594
5.5	6.5-7.5	0.016	0.051	0.290	0.734	1.091
		0.080	0.635	1.620	2.160	4.495
6.0	6.5-7.5	0.781	1.607	1.367	2.333	6.088

Table 8.10. Effect of asphalt and air void contents on inelastic shear strain in constant height tests

Asphalt Content (Percent)	Air Void Content (Percent)	Inelastic Shear Strain (Percent)				
		Block 1 (400 cycles)	Block 2 (600 cycles)	Block 3 (800 cycles)	Block 4 (1000 cycles)	All Blocks (2800 cycles)
4.5	2.5-3.5	0.273	0.372	0.804	0.699	2.148
		0.004	0.703	0.378	1.478	2.555
4.9	2.5-3.5	0.508	0.734	0.762	0.750	2.754
		0.142	1.132	1.032	0.808	3.114
5.5	2.5-3.5	0.018	0.080	0.397	0.573	1.069
6.0	2.5-3.5	1.073	1.290	1.061	1.202	4.624
4.5	4.5-5.5	0.021	0.625	1.276	0.913	2.834
		0.156	1.484	1.019	0.960	3.619
4.9	4.5-5.5	0.125	0.415	0.978	1.044	2.563
		0.393	1.835	1.755	1.983	5.967
5.5	4.5-5.5	1.426	1.942	1.782	---	---
6.0	4.5-5.5	1.474	1.326	1.264	1.289	5.352
4.5	6.5-7.5	0.173	2.144	2.493	1.862	6.672
4.9	6.5-7.5	0.430	0.639	0.962	1.287	3.317
5.5	6.5-7.5	0.060	0.212	0.855	1.069	2.195
		0.029	0.923	1.254	1.383	3.589
6.0	6.5-7.5	0.586	2.684	2.873	---	---
		1.069	2.760	3.196	---	---

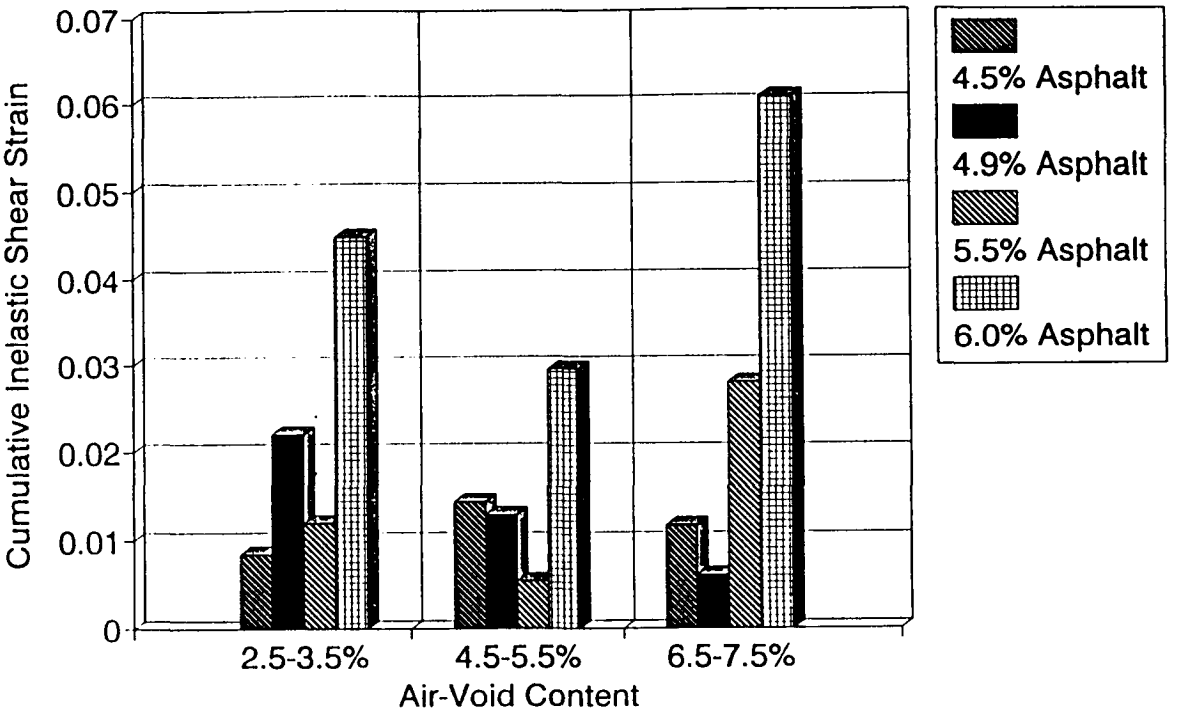

Figure 8.4. Cumulative inelastic shear strain at 2800 cycles; compound normal loading

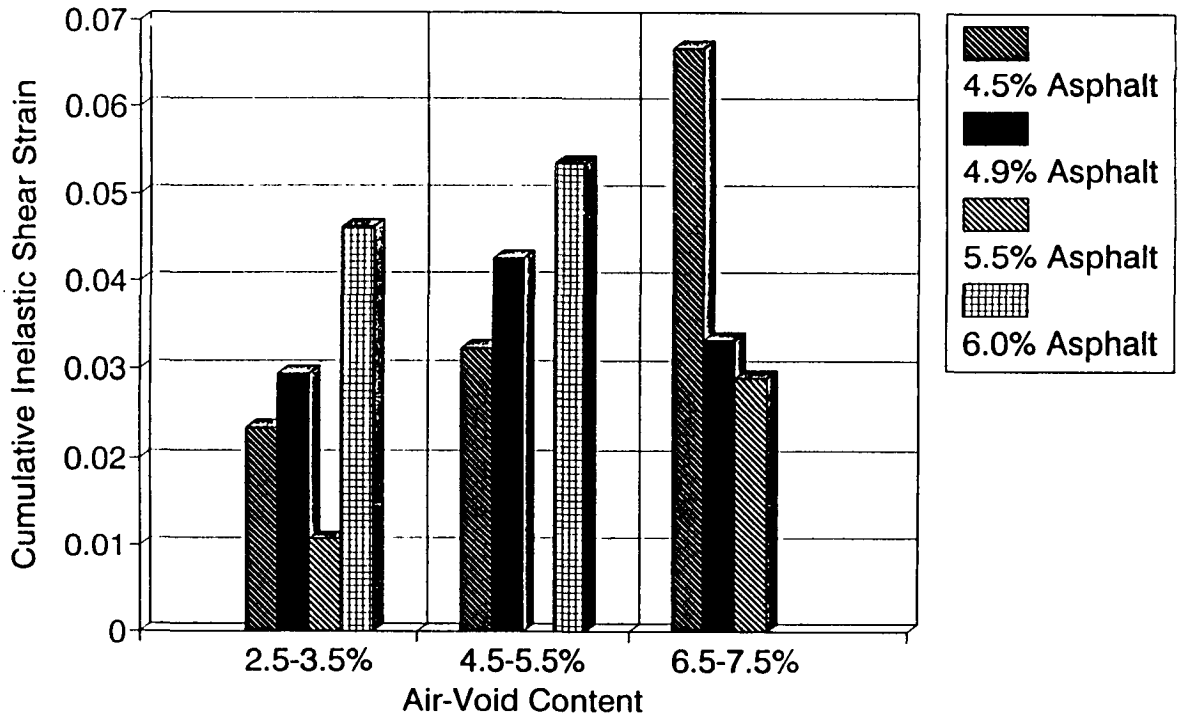

Figure 8.5. Cumulative inelastic shear strain at 2800 cycles; constant height loading

Table 8.11. Inelastic shear strain calibrations for normal tests

Asphalt Content (Percent)	Air Void Content (Percent)	Least-Squares Calibration			
		C_1	C_2	C_3	R^2
4.5	2.5-3.5	2.808×10^{-6}	2.292	0.314	0.87
		1.844×10^{-5}	1.141	0.474	0.91
4.9	2.5-3.5	2.041×10^{-4}	---	0.551	0.80
		4.306×10^{-4}	-1.011	0.684	0.96
5.5	2.5-3.5	5.557×10^{-5}	0.882	0.399	0.69
6.0	2.5-3.5	5.116×10^{-4}	-0.646	0.677	0.99
4.5	4.5-5.5	1.087×10^{-6}	2.744	0.441	0.97
		9.115×10^{-5}	0.280	0.533	0.95
4.9	4.5-5.5	1.836×10^{-5}	1.248	0.433	0.96
		2.208×10^{-4}	-0.330	0.546	0.98
5.5	4.5-5.5	1.134×10^{-4}	---	0.415	0.94
6.0	4.5-5.5	9.676×10^{-5}	---	0.690	0.95
4.5	6.5-7.5	4.473×10^{-5}	0.596	0.511	0.97
		3.399×10^{-5}	0.632	0.526	0.95
4.9	6.5-7.5	3.088×10^{-6}	2.044	0.379	0.94
5.5	6.5-7.5	1.106×10^{-6}	2.717	0.431	0.95
		1.456×10^{-5}	1.400	0.643	0.92
6.0	6.5-7.5	1.308×10^{-3}	-1.784	0.823	0.96

Table 8.12. Inelastic shear strain calibrations for constant height tests

Asphalt Content (Percent)	Air Void Content (Percent)	Least-Squares Calibration			
		C_1	C_2	C_3	R^2
4.5	2.5-3.5	1.241×10^{-4}	0.321	0.510	0.91
		2.182×10^{-5}	0.753	0.672	0.76
4.9	2.5-3.5	4.415×10^{-4}	-0.857	0.667	0.99
		8.783×10^{-4}	-0.862	0.601	0.99
5.5	2.5-3.5	2.835×10^{-6}	2.018	0.509	0.94
6.0	2.5-3.5	6.218×10^{-4}	-0.911	0.697	0.99
4.5	4.5-5.5	1.334×10^{-4}	0.458	0.507	0.82
		2.321×10^{-3}	-1.412	0.624	0.99
4.9	4.5-5.5	1.025×10^{-4}	0.589	0.490	0.93
		8.254×10^{-4}	-0.726	0.664	0.99
5.5	4.5-5.5	9.610×10^{-4}	-0.923	0.699	0.98
6.0	4.5-5.5	8.057×10^{-4}	-0.983	0.684	0.99
4.5	6.5-7.5	5.708×10^{-3}	-1.479	0.618	0.94
4.9	6.5-7.5	1.098×10^{-4}	---	0.675	0.99
5.5	6.5-7.5	4.353×10^{-5}	1.270	0.396	0.85
		2.874×10^{-4}	-0.218	0.623	0.98
6.0	6.5-7.5	1.335×10^{-3}	-0.728	0.655	0.98
		6.754×10^{-4}	-0.640	0.748	0.99

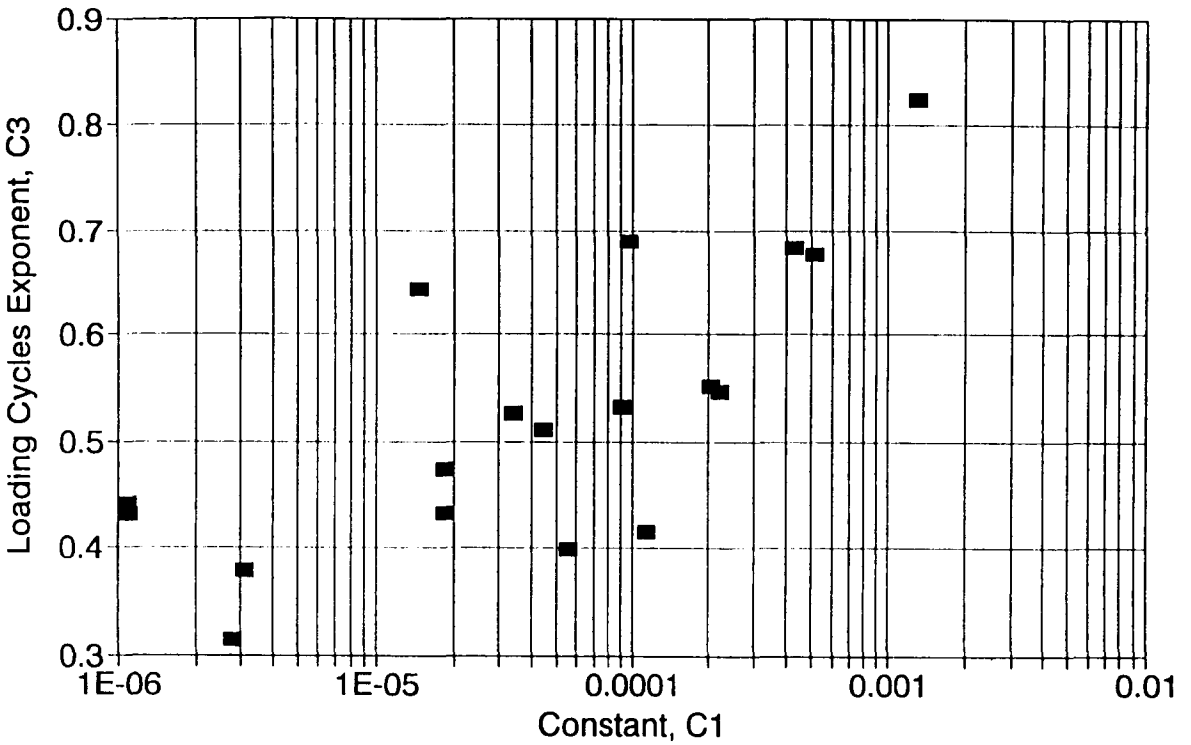

Figure 8.6. C_1 versus C_3 regression relationships, compound normal loading

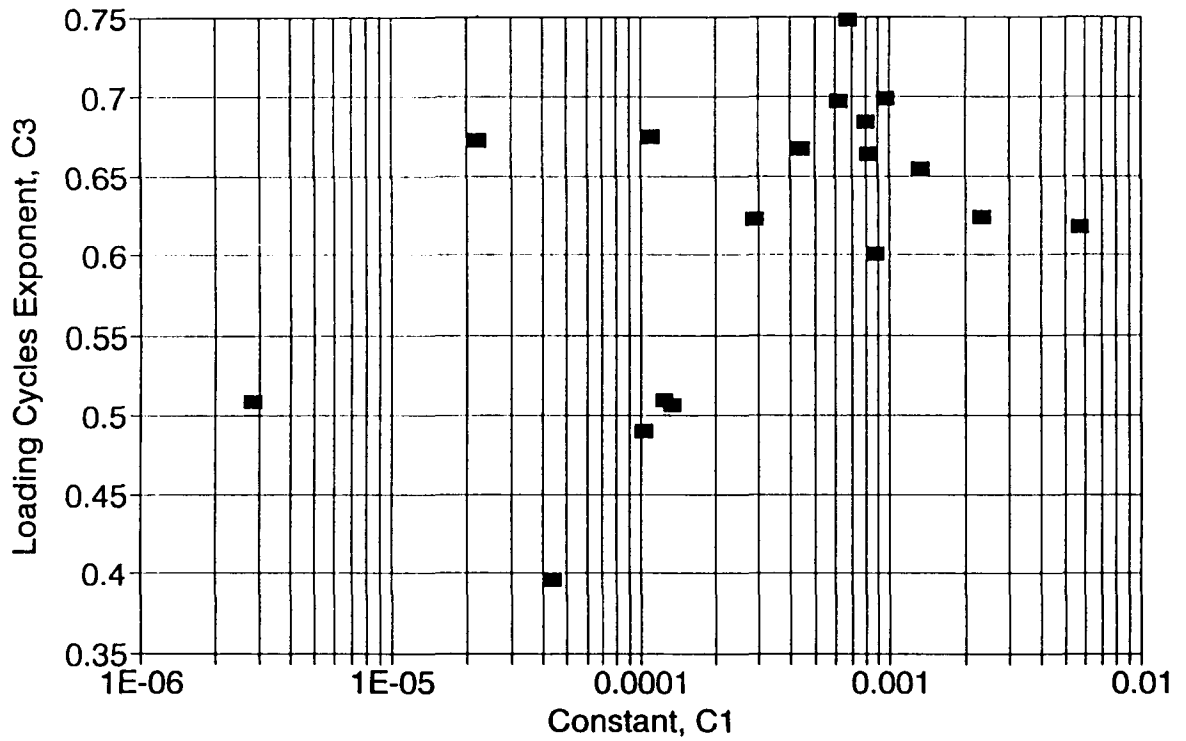

Figure 8.7. C_1 versus C_3 regression relationships, compound constant height loading

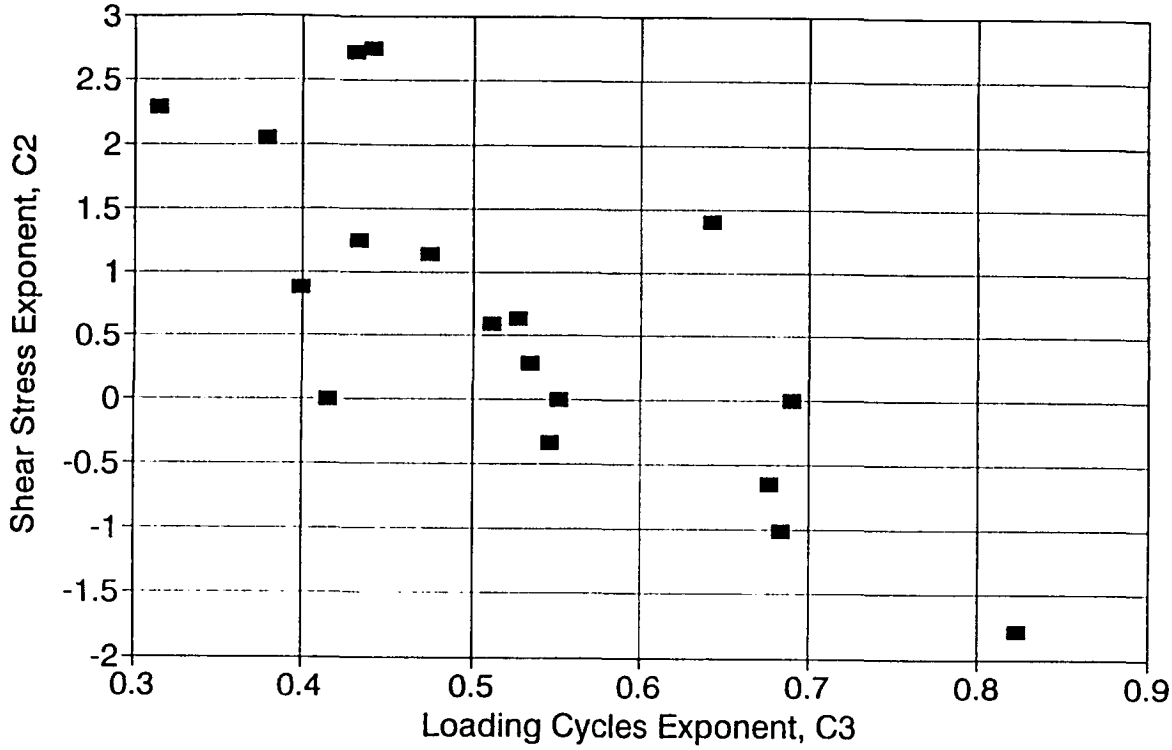

Figure 8.8. C_2 versus C_3 regression relationships, compound normal loading

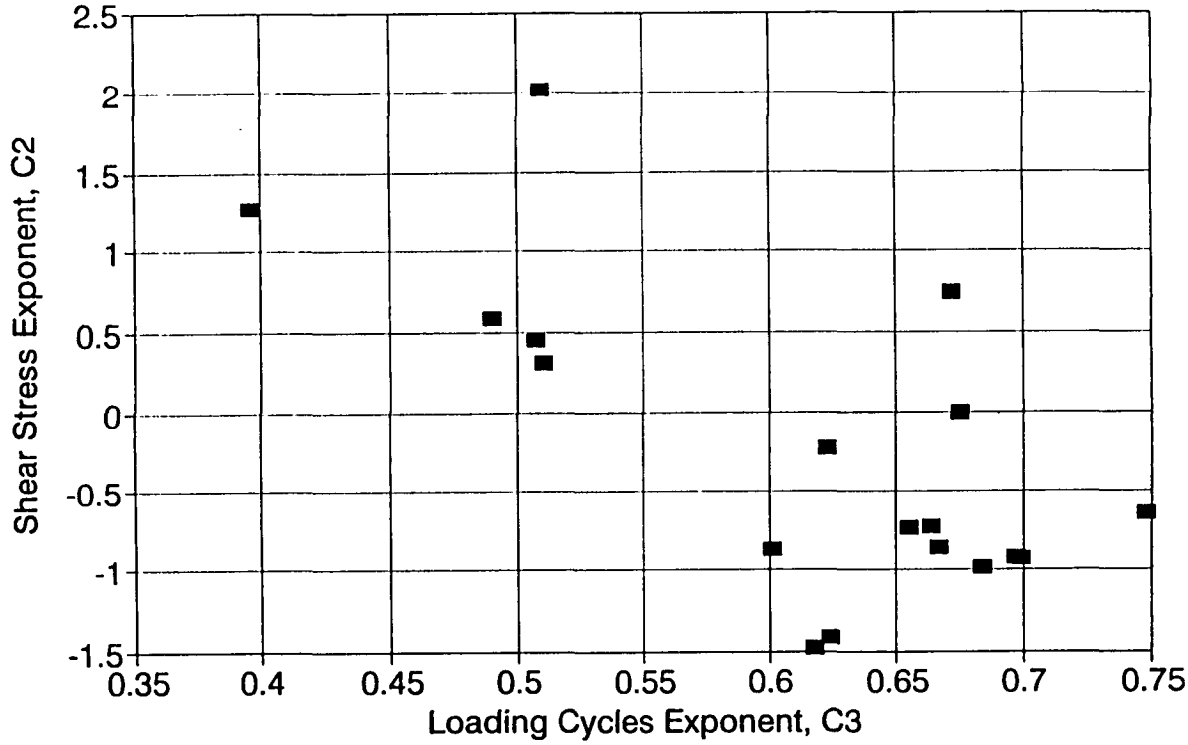

Figure 8.9. C_2 versus C_3 regression relationships, compound constant height loading

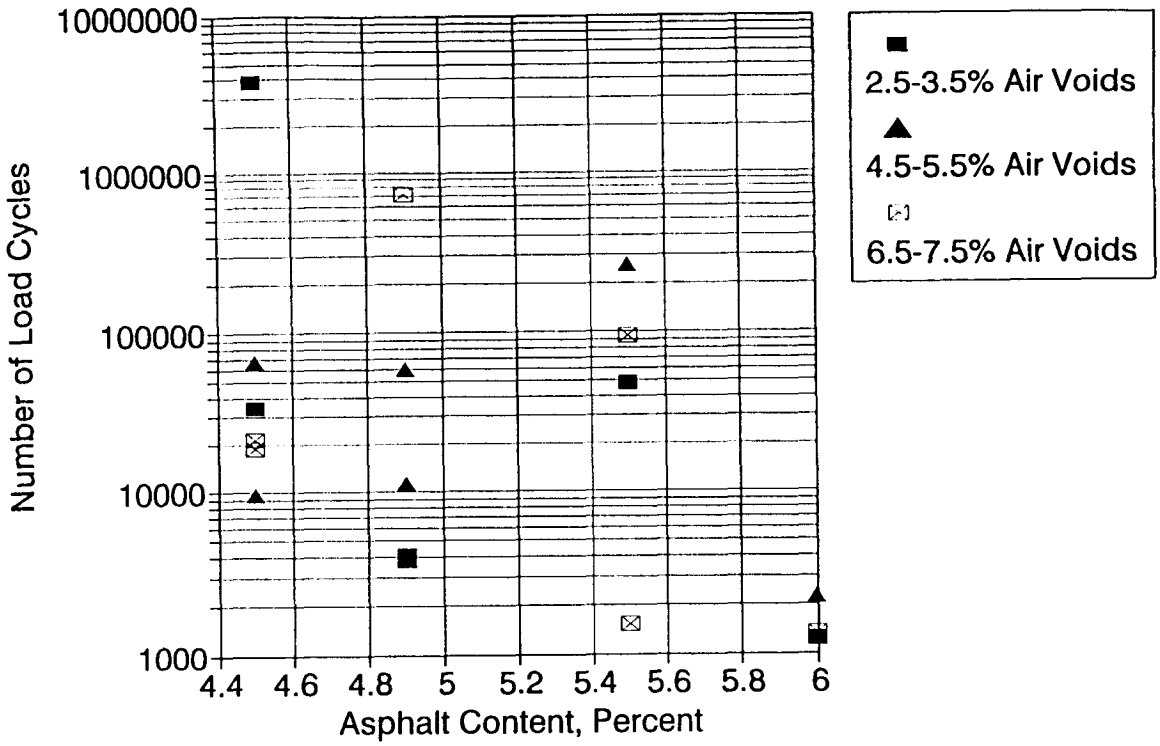

Figure 8.10. Predicted cycles to 2 percent shear strain, normal loading, 6 psi shear stress

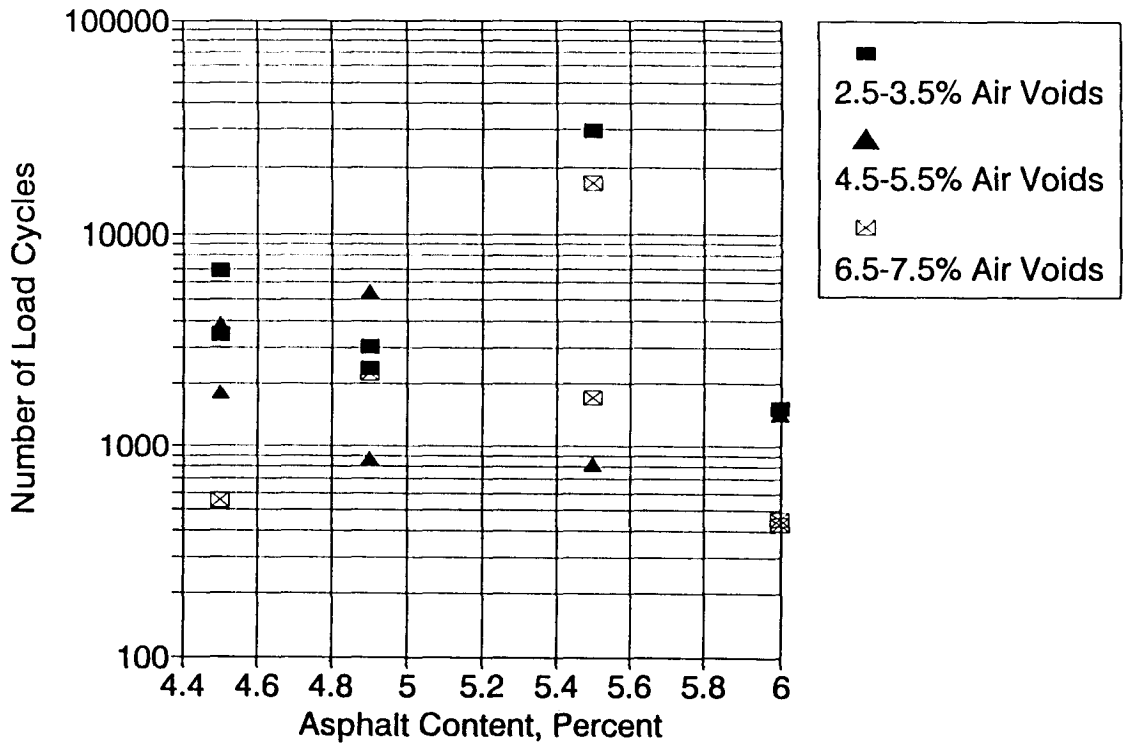

Figure 8.11. Predicted cycles to 2 percent shear strain, constant height loading, 6 psi shear stress

content) is detrimental to mix performance. However, the results are mixed and the evidence is in no way compelling.

Table 8.13 summarizes a final attempt to determine if this experiment helps to define the role of asphalt content in the resistance of mixes to permanent deformation. Results tabulated in each cell represent either a single test or average of two tests when replicates were available. Results are reasonable when comparing 4.5 percent and 6.0 percent asphalt. In between, however, inconsistencies are enormous.

Useful information could possibly be developed from testing of this nature and extent, if measurements were used to calibrate a model whose form was *known* to correctly account for the effects of asphalt and air void contents.

Replicate testing permits determination of measurement variability associated with these cyclic shear tests. Further analysis is required if variability estimates for cyclic shear testing are to be derived from this experiment.

8.3 Summary

While the approach described herein, i.e. the use of compound loading, appears to be promising for mix evaluation, time constraints did not permit satisfactory resolution of the problems encountered.

While the variability was not quantified, it may have been affected by the method used to measure the deformations, that was cap-to-cap rather than directly on the specimen. As a result of this test program, a different deformation measuring system was developed and used for subsequent measurements, e.g., those described in Chapter 6. In addition, for the normal tests, the method used to measure deformation could contribute to the variability in these tests. The plates and mounting targets for the LVDTs were not perfectly smooth nor precisely perpendicular to each other. Thus changes in one axis (e.g. change in height due to loading) would lead to changes in displacement in the normal direction, indicating that strain had developed even though none actually occurred. It should be noted that if such a test is planned for use, a new system of deformation measurements will be required, e.g., the use of a laser-type device to measure deformation.

Because of variability in test measurements and their relative insensitivity to asphalt content, these tests do not appear suitable at this time for selecting the asphalt content for routine mix designs.

The difference, if any, between normal and constant height tests is not striking. Two observations about the constant height testing are noted: (1) the variability in ratio of normal- to-shear stress from one mix to the next, and (2) the frequency with which inelastic strain accumulation was less in compound-loading blocks of greater stress and greater number of load applications. Both may influence the selection of laboratory stresses to represent field conditions as closely as possible.

Table 8.13. Effect of asphalt content on selected mix response measures (4.5 through 5.5 percent air void contents)

Test	Property	Asphalt Content (Percent)			
		4.5	4.9	5.5	6.0
Normal	Measured γ (%) at 2800 cycles	1.43	1.28	0.54	2.93
	Measured shear modulus (psi)	7600	7750	7500	3600
	Calculated cycles (to 2% strain under 6-psi shear)	38,500	35,200	259,000	2200
	Loading cycles exponent, C_3	0.49	0.49	0.42	0.69
Constant Height	Measured γ (%) in Block 3	1.15	1.37	1.78	1.26
	Measured shear modulus (psi)	5900	5500	5000	5300
	Calculated cycles (to 2% strain under 6-psi shear)	2850	3170	820	1440
	Loading cycles exponent, C_3	0.56	0.58	0.70	0.68

The *observed effects of asphalt and air void content on inelastic shear strain seem more realistic from constant height testing than from normal testing*. However, neither testing produced definitive patterns.

In spite of the limitations it should be noted that this type of approach may hold promise for mix design and analysis purposes. Accordingly, it is suggested that such an approach is a fruitful avenue for further evaluation.

9

Temperature Considerations in Mix Analysis and Design

The purpose of the study described in this chapter is to develop and demonstrate a technique for incorporating the effects of in situ temperature in the mix design process for permanent deformation without adding significantly to the complexity of testing and analysis.

As with fatigue cracking, the destructive effects of highway traffic for permanent deformation development can be expressed in terms of equivalent single axle loads (ESALs). Load equivalency factors have proven to be indispensable for expressing the relative destructive effects of the wide variety in over-the-road axle loadings and for determining the number of repetitions of a standard, 80 kN (18,000 lb), single-axle load that is equivalent to the traffic volume anticipated in service.

Extending the equivalency concept into the temperature domain offers considerable promise for conveniently and accurately treating the complexity of the in situ temperature environment in mix evaluation. Factors are required with which the design ESAL is converted to its equivalent at a *single* temperature. Use of a single temperature significantly reduces the testing and analysis effort required in evaluating mix performance. Even routine mix designs can accurately reflect the thermal environment anticipated in situ. Thus the temperature equivalency approach offers the potential for simplifying testing and analysis, with a resulting increase in productivity and reduced costs, and increasing predictive accuracy.

Described herein is the process that is included in the Strategic Highway Research Program (SHRP) A-003A mix analysis and design system[9] for treating temperature conditions and the development of the various factors necessary to implement that process.

---

[9]Described in Part III of this report.

9.1 Approach

As originally conceived, this investigation concentrated on the development of a set of temperature equivalency factors, patterned after the American Association of State Highway and Transportation Officials (AASHTO) load equivalency procedure, that could be used to easily account for traffic level and environmental temperatures in mix fatigue and permanent deformation analyses. The temperature equivalency factor is a multiplicative factor used to convert the number of load applications at one temperature, i, to an equivalent number of load applications at a standard reference temperature, s. Thus,

$$\Sigma \, TEF_i \times ESAL_i = \text{Equivalent } ESAL_s \tag{9.1}$$

in which TEF_i is the temperature equivalency factor for the *i*th temperature interval and $ESAL_i$ is the design ESALs accumulating during the *i*th temperature interval. The temperature equivalency concept theoretically requires independence of the effects of both multiple temperature levels as well as the order in which they occur. Because such independence has not yet been validated, the temperature equivalency factors developed herein can only be considered to represent first-order approximations.

As shown by the following equation, the computation of temperature equivalency factors requires simulations of pavement life at different temperatures:

$$TEF_i = N_s/N_i \tag{9.2}$$

in which N_s is the number of load repetitions to failure at the standard reference temperature and N_i is the number of load repetitions to failure at the *i*th temperature. Failure refers to a permanent surface deformation of 1.25 cm (0.5 in.). Pavement life was modeled using multilayer elastic analysis (ELSYM) to estimate the stress/strain states within hypothetical pavement structures. The layered-strain procedure was used together with repeated-load triaxial compression test results to estimate the effect of load repetitions on permanent surface deformation. The simulated traffic load was the standard AASHTO 80 kN (18,000 lb), single-axle load.

Temperature equivalency factors must be computed for a specific geographic location (that is, temperature environment) and a specific pavement structure. There are two primary tasks. The first is to estimate temperature profile throughout the pavement structure, and the second is to correlate pavement life (number of repetitions to failure) with the pavement temperature profile. The Federal Highway Administration's Integrated Climatic Model (Lytton et al. 1990) was used to compute temperature profiles (depth increments of 5 cm [2 in.]) for each of 4380 hours in a typical year. Elimination of one-half of the 8760 total hours in each year significantly reduced the computational effort without sacrificing accuracy. The temperature profile for each of the 4380 hours was then characterized by two quantities, the temperature at the critical pavement location and a temperature gradient. For permanent deformation, the critical location, that is near the pavement surface, was somewhat arbitrarily selected to be a depth of 5 cm (2 in.). The temperature gradient in °C per inch was defined as:

$$(T_B - T_{2"})/D \tag{9.3}$$

in which T_B is the temperature at the bottom of the asphalt layer, $T_{2"}$ is the temperature at a 5 cm (2 in.) depth, and D is the thickness of the asphalt layer less 5 cm (2 in.).

The pavement-life computations sought to relate pavement life to temperature and temperature gradient. Approximately 10 temperature categories and approximately 10 temperature-gradient categories were analyzed, a total of approximately 100 combinations. For each of these combinations, the average temperature profile for those of the appropriate 4380 hours was analyzed. All pavements were composed of two layers, an upper asphalt layer supported by a uniform foundation. To properly account for temperature effects, the asphalt layer was further subdivided into four sublayers of varying temperatures and, hence, varying stiffnesses. Deviator stresses were computed at 2.5 cm (1 in.) depth increments throughout the asphalt layer. To ensure that the critical condition was examined, computations included locations at the center of the dual tire set, at the center of one tire of the dual set, and at an outer edge of one of the tires.

Using layered-strain procedures, permanent surface deformation is estimated as follows:

$$\Sigma\, \epsilon_p \cdot (\text{thickness}) \tag{9.4}$$

in which ϵ_p is the vertical permanent strain in a layer increment, thickness refers to the increment, and Σ represents summation over all the increments within the asphalt layer. For all computations reported herein, 2.5 cm (1 in.) thickness increments were used. The permanent strain was in turn calculated from a laboratory-calibrated expression of the following type (Leahy 1989):

$$\epsilon_p = C_1 \cdot N_p^{C_2} \cdot \sigma_d^{C_3} \cdot T^{C_4} \tag{9.5}$$

in which ϵ_p is the permanent strain, N_p is the number of load repetitions, σ_d is the deviator stress, T is the temperature, and the C's are experimentally determined constants. Because failure was associated with a permanent surface deformation of 1.25 cm (0.5 in.), a trial-and-error process was necessary to determine the appropriate permanent deformation life.

The objective of these computations was to develop generalized relationships between pavement life and both temperature and temperature gradient so that a life corresponding to each of the 4380 simulated hours could be estimated. The approximately 100 sets of calculations provided a suitable database for calibrating regression equations of the following form:

$$\text{Ln}(N) = A_1 + A_2 \cdot T + A_3 \cdot G + A_4 \cdot T^2 + A_5 \cdot G^2 + A_6 \cdot T \cdot G \tag{9.6}$$

in which N is the number of load repetitions to failure in permanent deformation, T is the temperature at the critical pavement location (5 cm [2 in.] depth for permanent deformation),

G is the temperature gradient as defined above (Equation 9.3), and the A's are regression estimates.

Finally, after determining the appropriate temperature categories for which temperature equivalency factors were desired, pavement life was estimated for each of the 4380 hours using Equation 9.6; the 4380 hours were grouped according to the preselected temperature categories; average pavement lives were computed for each category; and temperature equivalency factors were computed by entering these average lives into Equation 9.2.

The above process was repeated for nine climatic regions spanning the continental United States and for one pavement structure (20 cm [8 in.]). In this analysis, the 20 cm (8 in.) thickness was considered to be sufficient to confine most of the rutting to the asphalt layer. A dual-tire load of 40 kN (9000 lb) with a contact pressure of 585 kPa (85 psi) and a 30 cm (12 in.) center-to-center tire spacing was used throughout.

9.2 Pavement Temperatures

The approach taken herein required the simulation of pavement temperature profiles through the 20 cm (8 in.) asphalt surface every other hour throughout a typical year. The Federal Highway Administration's *Integrated Model of the Climatic Effects on Pavements* (Lytton et al. 1990) was well suited to this task. This computer program can simulate pavement temperatures for any time period up to one year in length. Necessary data for nine climatic regions is built into the program's database so that, for many purposes, climatological data need not be independently collected and inputted. Unfortunately, output for a specific run is limited to one particular hour of each day. This required 12 runs to analyze a specific site and pavement-structure combination and, at 15 to 20 minutes per run on 486-based computers with processor speeds of 25 to 33 MHz, the time to complete the temperature simulations for each situation totaled about 4 hours.

Pavement profiles were produced for the 20 cm (8 in.) surface in each of the nine climatic regions. Default characteristics for both material properties and climatic conditions were used throughout. Minimum daily air temperature was assumed to occur at 6:00 a.m. and maximum daily air temperature at 3:00 p.m. For the simulations, a time step of 0.125 hours was used, and the node spacing (vertically) was 5 cm (2 in.) in the top 50 cm (20 in.) and 15 cm (6 in.) in the next 3.2 m (126 in.). Constant deep ground temperatures for the nine regions are shown in Table 9.1.

The ASCII output files from the temperature simulations served as the input to a series of simple BASIC-language programs that were used for data manipulations and summaries. Table 9.2, illustrative of the kinds of possible summaries, shows the frequency distributions of temperatures at critical locations within the pavement as a function of climatic region.

Table 9.1. Constant deep ground temperature

Region	Temperature (°C)
IA (Boston, MA, and Chicago, IL)	10.0
IB (Little Rock, AR, and Washington, DC)	15.6
IC (Atlanta, GA, and San Francisco, CA)	21.1
IIA (Fargo, ND, and Lincoln, NE)	10.0
IIB (Oklahoma City, OK)	18.3
IIC (Dallas, TX)	21.1
IIIA (Billings, MT, and Reno, NV)	7.2
IIIB (Las Vegas, NV, and San Angelo, TX)	18.3
IIIC (San Antonio, TX)	21.1

Table 9.2. Frequency distribution of temperatures at 5 cm (2 in.) depth in 20 cm (8 in.) pavement (percent)

Mid-Range Temp. (°C)	Region								
	IA	IB	IC	IIA	IIB	IIC	IIIA	IIIB	IIIC
-12.5				2.24					
-10.0				3.58					
-7.5				5.68	0.02		0.04		
-5.0	1.96			6.46	0.04		1.10		
-2.5	4.47			4.95	0.11		3.31		
0.0	12.44	1.07		7.78	2.56		10.18		
2.5	5.39	4.63	0.20	3.95	4.45	0.43	7.21	0.55	
5.0	5.20	5.39	3.26	3.86	5.02	2.15	6.39	2.21	0.25
7.5	5.11	6.21	5.94	4.11	5.66	3.49	6.12	3.47	1.78
10.0	5.23	6.94	7.88	4.25	6.37	5.04	6.23	4.73	3.68
12.5	5.34	6.42	9.11	4.45	6.21	5.80	6.23	5.50	5.23
15.0	5.73	6.37	9.93	4.91	6.03	6.78	6.57	6.58	6.46
17.5	6.46	6.42	10.27	5.52	6.05	6.89	7.90	6.85	7.74
20.0	8.47	6.87	12.83	7.17	6.51	7.03	7.99	6.89	8.29
22.5	8.61	8.10	9.47	7.19	7.40	7.51	6.05	7.21	8.74
25.0	6.39	9.93	7.81	5.59	9.68	9.29	6.19	8.74	11.14
27.5	5.71	7.15	6.28	5.00	7.42	10.75	4.54	10.71	11.14
30.0	3.33	6.53	5.02	3.54	6.23	7.51	4.00	7.24	9.02
32.5	4.54	4.54	4.95	3.90	5.48	6.89	3.20	6.76	7.62
35.0	3.63	5.09	5.20	3.20	3.77	5.27	3.56	5.84	4.45
37.5	1.96	3.10	1.83	2.65	4.50	4.61	3.17	3.93	5.91
40.0		4.92			3.17	4.18		4.98	3.31
42.5		0.94			3.31	4.32		3.31	4.66
45.0						2.03		3.93	0.57
47.5								0.57	

9.3 Temperature Effects on Pavement Life

To make the computations tractable, models are required that relate pavement life to both temperature and temperature gradient. To develop these models, a number of standard temperature profiles, defined by temperature level and by temperature gradient, were developed. For the 20 cm (8 in.) pavement examined herein, 72 profiles were identified, consisting of all possible combinations of nine levels of temperature (ranging from -5° to 35°C (23 to 95°F) in 5°C (9°F) increments) and eight levels of gradient (ranging from -1.5° to 0.6°C per inch in 0.3°C per inch increments). For each category of temperature and temperature gradient, the temperature profile to be analyzed was determined by averaging over the applicable 4380 hours of data and the nine climatic regions. Multilayered elastic analysis was used to estimate the stress and strain conditions within the pavement structure under the 40 kN (9000 lb), dual-tire load.

As described in Chapter 6, the A-003A approach to calculating permanent deformation in pavement structures uses a finite-element analysis that incorporates nonlinear viscoelastic surface properties and requires a suite of laboratory tests, including constant height simple shear, uniaxial strain, volumetric, and shear frequency sweeps. In lieu of this approach, which had neither been well tested nor sufficiently well refined at the time of this investigation, a conventional layered-strain analysis was used to develop pavement life versus temperature and temperature gradient models.

Once again it was desirable to calibrate the necessary models using a mix that was considered typical of paving mixes in the United States. Table 9.3 summarizes those mix properties that were selected as being characteristic of typical mixes. The dynamic modulus-temperature relationship was taken from work reported by Akhter and Witczak (1985). After adjustment, using the mix properties of Table 9.3, this relationship is as follows:

$$E = 100{,}000 \cdot 10^{(1.691635 - 0.00815T - 0.0000618\,T^2)} \qquad (9.7)$$

where E is the dynamic modulus of the asphalt mix in psi and T is the temperature in °F.

Work by Leahy (1989) provided the basis for relating permanent strain to number of load repetitions, temperature, and deviator stress. For the mix properties of Table 9.3, this relationship is as follows:

$$\log \epsilon_p = -12.3469 + 0.408 \log N_p + 6.865 \log T + 1.107 \log \sigma_d \qquad (9.8)$$

where ϵ_p is the permanent strain in inch/inch, N_p is the number of load cycles, T is the temperature in °F, and σ_d is the deviator stress in psi (or 90 psi, whichever is greatest). The basis for this relationship was repeated-load triaxial testing of 251 specimens, including two aggregate types and two asphalt types. Unfortunately, Leahy's testing was limited to temperatures at and below 35°C (95°F). Thus, considerable extrapolation is required to reach some of the temperatures at which rutting occurs in hotter climates.

Table 9.3. Mix properties for permanent deformation investigation

Property	Value
f - frequency, Hz	10
Vis - viscosity @ 70°F, × 10^6 poise	1.5
Peff - percent effective asphalt by volume	12
Pair - percent air by volume	4
Pabs - percent of asphalt absorbed by weight of aggregate	0.5
PP200 - percent passing #200 sieve	5
PR4 - percent retained on #4 sieve	50
PR3/8 - percent retained on 3/8" sieve	30
PR3/4 - percent retained on 3/4" sieve	5

All analysis was limited to one pavement structure having an asphalt surface of sufficient thickness to minimize the likelihood of significant rutting within subsurface layers. The specific section that was evaluated is defined in Table 9.4. The asphalt surface was treated as four layers, and the modulus of elasticity of each layer was determined using Equation 9.7, based on its midthickness temperature. Pavement life, the number of repetitions resulting in a permanent deformation at the surface of 1.25 cm (0.5 in.), was calculated using the layered-strain approach of Equation 9.4 combined with the permanent strain relationship of Equation 9.8. In this trial-and-error process, eight 2.5 cm (1 in.) layers were used to represent the 20 cm (8 in.) surface course and the mid-thickness deviator stresses were calculated both directly and, as necessary, by interpolation.

Table 9.4. Simulation parameters

Layer	Property	Value
Asphalt Surface	Thickness (in.)	8
	Number of Layers	4
	Modulus of Elasticity (psi)	Varies with temperature and temperature gradient
	Poisson's Ratio	0.35
Subgrade	Modulus of Elasticity (psi)	20,000
	Poisson's Ratio	0.40

The purpose of these computations was to develop models relating permanent deformation life to both temperature and temperature gradient in the asphalt layer. The resulting models, containing only statistically significant terms, are summarized as follows:

- For temperatures at a depth of 5 cm (2 in.) less than 25°C (77°F) (R^2 = 0.993)

$$Ln(N_{0.5"}) = 28.0936 - 0.82261T - 5.0689G + 0.0099138T^2 + 0.10840TG \quad (9.9)$$

where $N_{0.5"}$ = cycles to 1.25 cm (0.5 in.) permanent deformation, T = temperature ($T_{2"}$) in °C at 5 cm (2 in.) depth, and G = temperature gradient in °C per inch [($T_{8"}$-$T_{2"}$)/6].

- For temperatures at a depth of 5 cm (2 in.) of 25°C (77°F) or more (R^2 = 0.994)

$$Ln(N_{0.5"}) = 26.6040 - 0.64020T - 4.2074G + 0.0046575T^2 + 0.069677TG \quad (9.10)$$

As indicated by R^2 values, all of the calibrations were highly significant in the statistical sense just as they were for the fatigue calibrations. Figure 9.1 provides graphical illustrations of the relationship between the regression estimate and the permanent deformation life estimates from the previously described calculations.

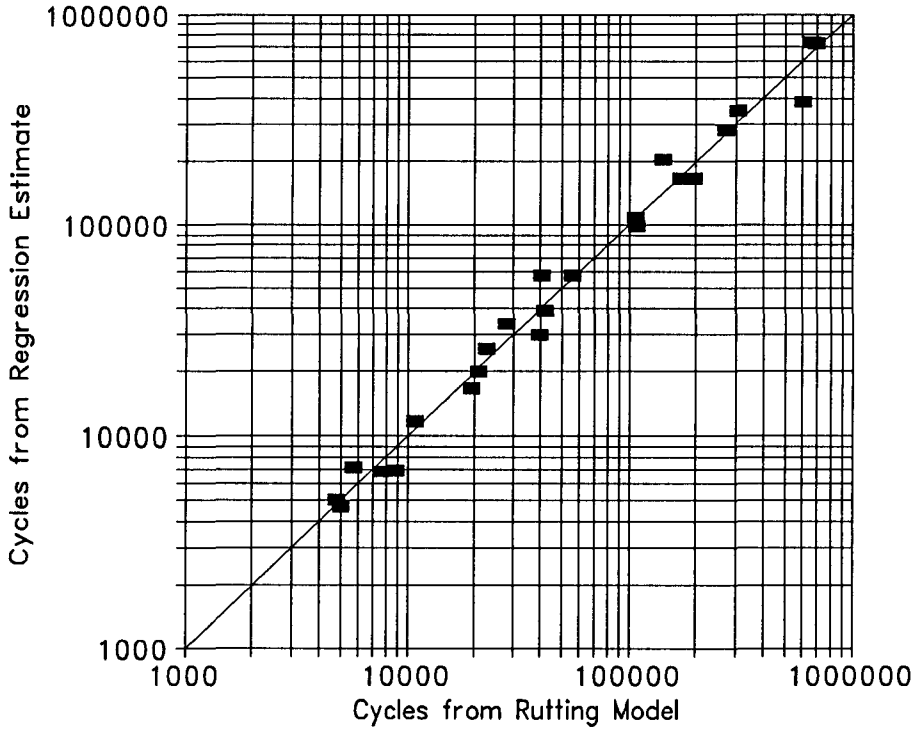

Figure 9.1. Accuracy of permanent deformation model

9.4 Temperature Factors

The primary attribute of the temperature equivalency approach is that both the testing and the bulk of the routine analyses are limited to a single temperature. The matter of mix analysis and design is thus a rather simple one given the proper choice of the testing temperature and the availability of applicable temperature equivalency factors. For atypical (e.g., modified binders) mixes, particularly those with atypical temperature sensitivities, a more complex routine that requires testing at multiple temperatures is required. Multiple-temperature testing may also be desired for large paving projects to increase the accuracy of the evaluations. The matter of multiple temperature testing is briefly discussed below.

9.4.1 Testing at a Single Temperature

Some of the factors to be considered by each mix design agency in selecting the standard reference temperature for single-temperature testing include the following:

- Testing time will be minimized if the test temperature promotes early failure in laboratory testing.
- Accuracy will be maximized if the test temperature is near that to which in situ pavements are most vulnerable to damage.
- Efficiency will be maximized if a single test temperature can be used regardless of structural design and regardless of where the paving project is located within the design agency's jurisdiction.
- Testing will be easier and less expensive if the test temperature provides comfortable working conditions and can be accurately controlled.

The ideal testing temperature would be one that could be used by any design agency without regard to distress mechanism, specific pavement structure, or project location. Candidate temperatures include, among others, the effective temperature, the critical temperature, and the maximum temperature. The effective temperature is defined as that temperature at which loading damage accumulates at the same average rate in service as in the laboratory. Thus, when testing at the effective temperature, there is a one-to-one correspondence between laboratory and in-service loading cycles. The critical temperature is defined as that temperature at which the largest amount of damage occurs in service. For purposes of this investigation, the critical temperature was more specifically defined to be that temperature integer at the midpoint of a 5°C (41°F) temperature range within which the largest amount of damage accumulates. Table 9.5 summarizes the effective, critical, and maximum temperatures for nine climatic regions within the continental United States.

Table 9.5. Key temperatures at 2 inch depth for permanent deformation analysis

Region	Temperature in °C		
	Effective	Critical	Maximum
IA	27.7	35	37.6
IB	33.0	40	41.8
IC	29.3	35	37.5
IIA	28.3	36	38.4
IIB	34.2	42	43.7
IIC	36.0	43	45.7
IIIA	30.1	36	38.6
IIIB	37.2	44	46.6
IIIC	35.1	42	44.3
Mean	32.3	39.2	41.6

The critical temperature — or a standard temperature near the critical temperature — is considered to be the optimal temperature for laboratory testing because it minimizes error associated with variations in mix temperature sensitivity and because of its accelerated rate of damage accumulation. Remaining calculations focus on the critical temperature but include a standard temperature of 35°C (95°F) for permanent deformation.

9.4.2 Temperature Equivalency Factors

Temperature equivalency factors, computed using Equation 9.2, are summarized in Table 9.6. The reference temperature for permanent deformation is 35°C (95°F) (Table 9.6). Detailed examination of the table reveals temperature equivalency factors (TEFs) for permanent deformation increase monotonically with increases in temperature, and temperature equivalency factors are relatively independent of climate.

9.4.3 Temperature Conversion Factors

Equation 9.1, using temperature equivalency factors such as those of Table 9.6, is used to convert the design ESALs to its equivalent at the standard reference temperature. Before the computation can be performed, however, the designer must estimate the number (or proportion) of the design ESALs that accumulate during each temperature interval. In the absence of detailed frequency distribution data, it seems reasonable to assume that damaging

Table 9.6. Temperature equivalency factors in permanent deformation (referenced to 35°C [95°F] at 5 cm [2 in.] depth)

Mid-Range Temp. (°C)	Region								
	IA	IB	IC	IIA	IIB	IIC	IIIA	IIIB	IIIC
-12.5				3.0e-11					
-10.0				1.2e-10					
-7.5				1.0e-10	1.3e-07		5.7e-09		
-5.0	4.8e-08			2.3e-10	4.4e-08		4.2e-08		
-2.5	6.5e-08			1.5e-09	5.0e-08		1.1e-07		
0.0	8.4e-08	6.3e-07		1.8e-08	3.1e-07		2.2e-07		
2.5	1.5e-07	2.6e-06	1.5e-05	1.3e-07	9.8e-07	1.3e-05	4.8e-07	1.5e-05	
5.0	3.1e-07	5.3e-06	3.3e-05	3.2e-07	2.1e-06	2.0e-05	1.2e-06	2.3e-05	9.4e-05
7.5	7.0e-07	9.9e-06	1.0e-04	7.3e-07	2.5e-06	6.5e-05	5.0e-06	7.2e-05	1.8e-04
10.0	1.5e-06	1.8e-05	1.2e-04	2.4e-06	1.6e-05	7.2e-05	2.1e-05	7.9e-05	3.5e-04
12.5	1.3e-05	7.4e-05	2.5e-04	7.5e-05	5.7e-05	1.7e-04	8.5e-05	1.9e-04	6.6e-04
15.0	4.4e-04	3.1e-04	5.6e-04	2.7e-04	2.6e-04	2.8e-04	3.3e-04	2.4e-04	1.2e-03
17.5	1.6e-03	1.1e-03	2.4e-03	1.1e-03	1.0e-03	1.1e-03	1.7e-03	7.9e-04	1.7e-03
20.0	7.0e-03	4.3e-03	9.1e-03	5.2e-03	3.9e-03	3.8e-03	4.9e-03	3.1e-03	4.8e-03
22.5	0.021	0.017	0.021	0.018	0.015	0.013	0.013	0.011	0.017
25.0	0.042	0.049	0.041	0.038	0.053	0.045	0.035	0.036	0.061
27.5	0.102	0.108	0.091	0.095	0.122	0.144	0.080	0.136	0.164
30.0	0.179	0.239	0.177	0.181	0.270	0.245	0.165	0.228	0.344
32.5	0.475	0.434	0.402	0.443	0.566	0.527	0.494	0.510	0.630
35.0	1.000	1.000	1.000	1.000	1.000	1.000	1.000	1.000	1.000
37.5	2.364	2.012	2.007	2.324	2.561	1.912	2.956	1.702	2.464
40.0		4.419			4.967	3.714		4.015	4.559
42.5		7.197			11.391	8.585		7.597	9.876
45.0						17.069		16.594	15.991
47.5								24.673	

truck traffic is uniformly distributed over time. Thus, in the context of mix evaluation, this suggests that a daytime hour is reasonably similar to a nighttime hour in terms of truck traffic, that a wintertime hour is reasonably similar to a summertime hour, and so forth.

The assumption that truck traffic is uniformly distributed through time permits the computation of a temperature conversion factor as follows:

$$TCF = \Sigma f_i \times TEF_i \tag{9.11}$$

in which TCF is the temperature conversion factor, f_i is the frequency associated with the *i*th temperature interval, and TEF_i is the temperature equivalency factor for the *i*th temperature interval. Computation of the equivalent ESALs at the standard reference temperature then requires only a single multiplication as follows:

$$\text{Equivalent ESAL}_s = \text{TCF x Design ESAL} \tag{9.12}$$

in which Equivalent $ESAL_s$ is the equivalent number of ESALs at the standard reference temperature, s, and Design ESAL represents the design traffic loading.

Temperature conversion factors for the 20 cm (8 in.) pavement evaluated herein are summarized in Table 9.7. For comparative purposes, reference temperatures include both the critical temperature for each condition as well as a standard temperature of 35°C (95°F). Also shown in the table is the percentage of damage that occurs within a range of 5°C (41°F) centered on the reference temperature. A large percentage is desirable because it minimizes potential error associated with atypical mix temperature sensitivities. Approximately 64 to 77 percent of the permanent deformation damage occurs within a 5°C (41°F) interval centered on the critical temperature. The critical temperature is the best choice for permanent deformation testing.

9.4.4 Testing at Multiple Temperatures

Testing and analysis at multiple temperatures become necessary when evaluating mixes of atypical temperature sensitivity—that is, those for which standard temperature equivalency and conversion factors are not applicable—and desirable for important paving projects demanding the utmost in accuracy. The objective of the testing would be to recalibrate Equations 9.7 and 9.8. Following these recalibrations, temperature equivalency and conversion factors would be determined by procedures such as those employed herein.

Testing temperatures should be carefully chosen so that they are compatible with the capabilities of laboratory test equipment and so that they span the range within which much of the damage occurs in situ. Calculations reported herein (Table 9.8) suggest that most of the damage occurs within a temperature range as small as 15°C (59°F). An even smaller range may eventually prove to be sufficient for permanent deformation. At the present, however, it appears that testing in the range of 30°C to 45°C (86°F to 113°F) is likely to be adequate for the vast majority of locations within the continental United States.

Table 9.7. Temperature conversion factors for permanent deformation (20.3 cm [8 in.] pavement)

Region	Reference Temperature: 35°C (95°F)		Reference Temperature: Critical	
	Temperature Conversion Factor	Percent Damage Within 5°C (41°F) Range	Temperature Conversion Factor	Percent Damage Within 5°C (41°F) Range
IA	0.1262	70.2	0.1262	70.2
IB	0.4800	20.6	0.0993	69.8
IC	0.1517	74.2	0.1517	74.2
IIA	0.1466	56.2	0.1006	76.6
IIB	0.7486	16.4	0.0707	67.8
IIC	1.4443	9.4	0.1224	64.2
IIIA	0.1817	47.4	0.1218	76.2
IIIB	1.1627	7.0	0.1337	68.5
IIIC	1.0486	13.4	0.1162	67.3
Mean	0.6100	35.0	0.1158	70.5
Coefficient of Variation (%)	78.6	72.8	18.9	5.7

Table 9.8. Extent of damage accumulation in suggested temperature ranges

Region	Percent Damage Within Indicated Temperature Range
	Permanent Deformation (30° through 45°C)
IA	89.6
IB	95.4
IC	89.3
IIA	91.3
IIB	97.4
IIC	92.3
IIIA	94.4
IIIB	78.7
IIIC	96.3
Mean	91.6

9.5 Application of Temperature Factors in Mix Analysis and Design

Temperature equivalency or conversion factors are applied in the SHRP A-003A mix analysis and design process to convert in-service traffic loading (expressed in ESALs) to its equivalent at the preselected reference temperature. These equivalent traffic loading cycles are compared with mix resistance as measured by laboratory repeated load testing at the same reference temperature to determine the acceptability of specific mixes. For basic level, permanent deformation analysis, a constant height simple shear device operated in a repeated-load mode is recommended, as seen in Part III of this report. The laboratory environment is calibrated to in situ conditions by applying an empirically determined shift factor, and a suitable multiplier is applied to satisfy reliability requirements. The procedure has been fully documented in Part III of this report.

9.6 Summary

The primary objective of this study has been to demonstrate the efficacy of the temperature equivalency concept for use in mix analysis and design. Techniques have been developed by which traffic loading in situ can be expressed in terms of its equivalent at a single reference temperature. This provides a simple but effective way to accurately account for both traffic and environmental effects in mix analysis and design.

Single-temperature testing is sufficient for routine mix analysis with mixes of typical temperature sensitivity. Setting the testing temperature to correspond with the critical temperature (appropriate to the geographical location and structural section) ensures optimum results.

Temperature conversion factors provide a simple, convenient way to convert traffic loading to its equivalent at a fixed temperature level. As a result, direct comparisons can be made between traffic loading in situ and single-temperature repeated load testing in the laboratory.

For permanent deformation evaluation, testing and analysis at the critical temperature is an effective way to reduce the influences of climatic variations throughout the continental United States.

When multiple-temperature testing is necessary, the range of test temperatures can be reasonably small. On average in the nine climatic regions spanning the continental United States, temperatures in the range of 30°C to 45°C (86°F to 113°F) encompass the range within which an average of about 92 percent of the rutting occurs. These findings are expected to depend on mix type, and they may be refined based on future work with a wider variety of mix types.

The temperature equivalency and conversion factors are considered to be first-order approximations that, with care, provide an effective way to account for traffic and climate effects in mix analysis and design. They form an integral part of a mix analysis and design system that has been developed by SHRP Project A-003A. The next important requirement

is to replace the layered-strain analysis with a more accurate model of permanent deformation, coupled with a range of appropriate laboratory test data to support its application. A more suitable permanent deformation model will also allow investigation of the independence of the effects of both multiple temperature levels as well as the order in which they occur and the development of a possible refinement, if needed. Additional development is also warranted to incorporate the effects of climate on subgrade support and to identify the variety of mixes for which standard temperature equivalency and conversion factors are applicable. Finally, an investigation of the temporal (hourly, daily, and seasonally) variation in traffic loading is necessary to validate the assumption that damaging traffic loads are uniformly distributed through time.

10

Reliability

As discussed in the report on fatigue response (Tayebali et al. 1993), decisions about anticipated mix performance cannot be made with absolute certainty. Accordingly, reliability analysis offers a procedure whereby an acceptable level of risk can be incorporated into the mix analysis and design process. In this instance reliability is considered to be the probability that the mix will provide satisfactory performance for the design period. Acceptable levels of risk (1- probability level) are the choice of the engineer. In this discussion reliability levels of 60, 80, 90, and 95 percent are considered and correspond to risk levels of 40, 20, 10, and 5 percent respectively. While higher levels of reliability reduce the chances of accepting deficient mixes, there is a likelihood that the number of acceptable mixes may be reduced and higher costs may result.

10.1 Approach

The same approach used to consider reliability for fatigue is used for permanent deformation. That is, a multiplier greater than one is applied to the traffic demand such that the ability of the mix to carry the traffic results in a rut depth that does not exceed some prescribed value (e.g., 1.25 cm [0.5 in.]). This can be stated as follows:

$$N_{supply} \geq M \cdot N_{demand} \qquad (10.1)$$

where:

N_{supply}	=	estimated repetitions to a limiting prescribed rut depth (e.g., 1.25 cm [0.5 in.]);
N_{demand}	=	applied traffic demand; and
M	=	reliability multiplier (greater than 1) whose magnitude is dependent upon variabilities of the estimated repetitions to a prescribed rut depth and the traffic demand; together with the desired reliability of the design.

As with fatigue response it is convenient to use logarithmic transformations in modeling permanent deformation response; accordingly Equation 10.1 can be rewritten as follows:

$$\text{Ln}\,(N_{supply}) \geq \text{Ln}\,(N_{demand}) + \delta \qquad (10.2)$$

where: δ = an increment (>0) whose value is equal to Ln (M); and
Ln = natural logarithmic function.

The increment δ increases with increase in reliability level as well as with increases in the variabilities of the estimated number of repetitions to a prescribed rut depth (N_{supply}) and traffic demand (N_{demand}). The variability of N_{supply} can be estimated from repeated load simple shear constant height test data generated during this phase of the study and described subsequently. The variability of N_{demand} must be estimated from input supplied by the traffic engineer.

10.1.1 Calculation of Variability of N_{supply} as Measured in Constant Height Repeated Load Simple Shear Tests

To determine the variability of measurements obtained from the constant height repeated load simple shear tests (the test recommended for use in the Level 1 approach to mix analysis and design as described in Part III of this report), data from an experiment to evaluate the feasibility of the constant height test for mix design purposes will be utilized.

Assumptions associated with the use of this data include the following:

- The measurement of interest is the number of cycles to reach a shear strain of 5 percent.
- The number of cycles to 5 percent strain has a log normal distribution.

10.1.1.1 Experimental Testing

The experiment included mixes containing aggregate RB and asphalt AAG-1. Four asphalt contents (4.5, 4.9, 5.5, and 6.0 percent) were examined and, for each, varying compaction levels produced a range of air-void contents. All tests were executed at 50°C (122°F) and at a cyclic shear stress of 70 kPa (10 psi) (0.1 s on and 0.5 s off). In the analysis reported herein, three of 34 tests were discarded, two because they gave values two orders of magnitude above all others (possibly as a result of loosened LVDTs) and one because the shear stress was off target. Laboratory data relevant to this analysis are summarized in Table 10.1.

Table 10.1. Experimental data

Asphalt Content (Percent by Weight of Aggregate)	Air-Void Content (Percent)	Cycles to 5 Percent Strain
4.5	2.8	2722
	3.2	5598
	4.8	3798
	5.3	1872
	6.0	258
	6.9	1868
	7.1	723
4.9	2.8	1595
	3.0	3979
	4.9	3067
	6.0	671
	5.1	754
	7.1	1580
	7.2	432
	7.5	369
5.5	3.3	2366
	3.7	1900
	3.7	1936
	4.2	1960
	5.5	279
	5.5	422
	7.1	1967
	8.7	812
6.0	1.8	505
	2.5	829
	3.0	468
	5.7	884
	5.9	661
	6.1	152
	6.8	419
	7.0	164

10.1.1.2 Analysis

Because the experimental program did not include replicate testing, estimates of variance of test measurements require some form of modeling. Because of the complexity of air void and asphalt content effects, both main and interactive, individual models were calibrated for each asphalt content. Although trends in the raw data, illustrated by Figures 10.1 through 10.4, indicate that cycles to 5 percent strain are generally diminished by increasing air void content, they give little clue as to the form of the Ln{Cycles}-% Air relationship. As a result, first-, second-, and third-order polynomials were fitted to the data. The calibrations ignored mixes having air void contents less than 3 percent because of the scarcity of data in

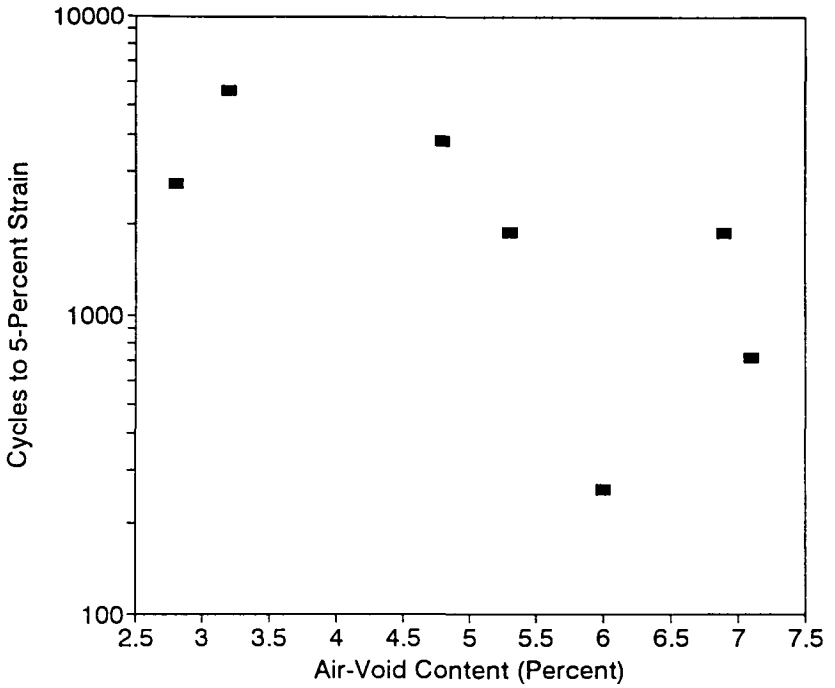

Figure 10.1. Cycles to 5 percent permanent shear strain versus air void content; asphalt content — 4.5 percent

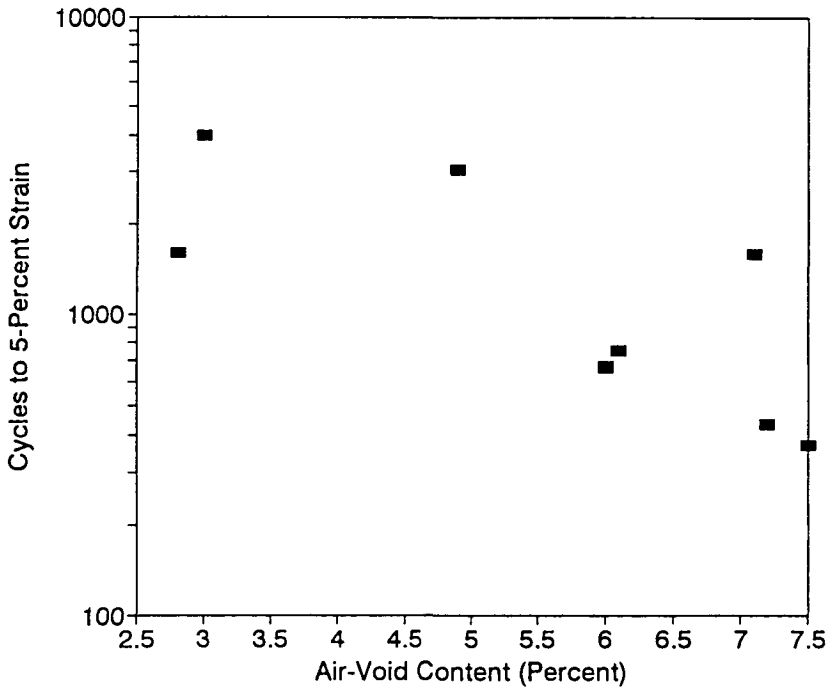

Figure 10.2. Cycles to 5 percent permanent shear strain versus air void content; asphalt content — 4.9 percent

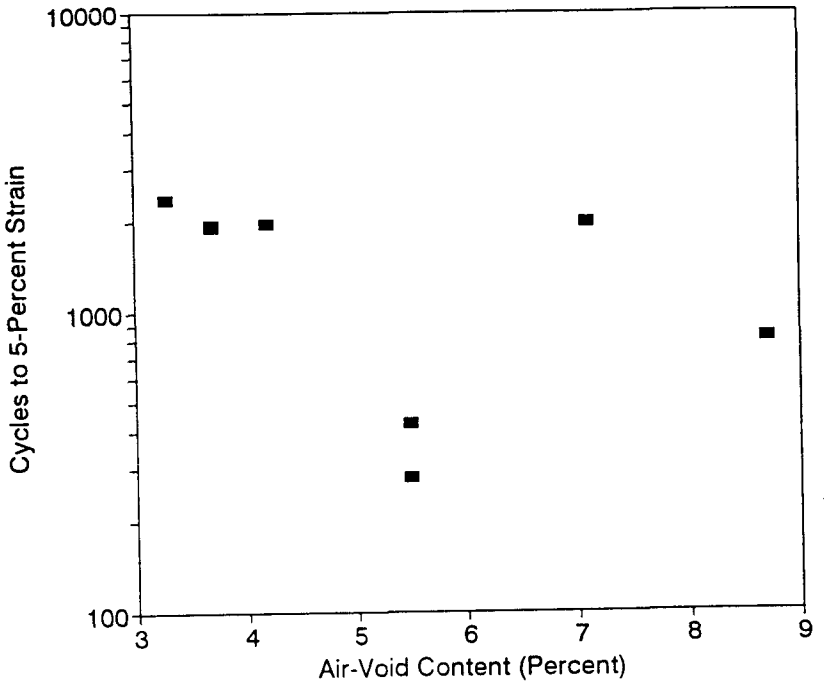

Figure 10.3. Cycles to 5 percent permanent shear strain versus air void content; asphalt content — 5.5 percent

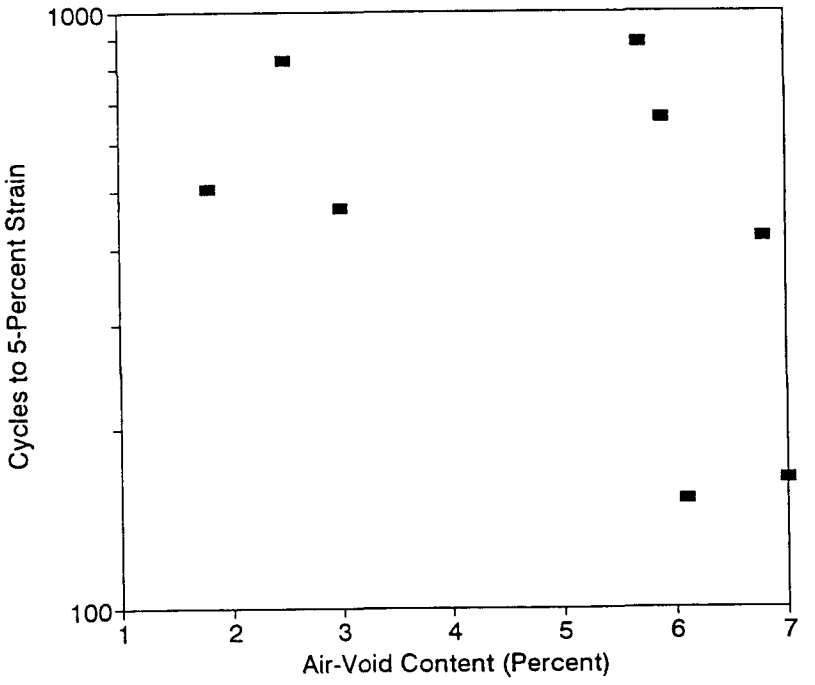

Figure 10.4. Cycles to 5 percent permanent shear strain versus air void content; asphalt content — 6.0 percent

this region and because other work suggests a rapid decrease in resistance as air voids decrease below 3 percent.

Results of the calibration are summarized in Table 10.2 and illustrated graphically in Figures 10.5 through 10.8. In general the models were not particularly successful in capturing the variance of the data set, and the relationships were not statistically significant. Increasing the order of the polynomial not only failed to improve the accuracy of the calibrations (Table 10.2) but also produced results contrary to the a priori expectation of monotonically decreasing cycles to 5 percent strain (Figures 10.5 through 10.8). Accordingly, the linear calibrations are preferred.

The linear models yielded standard errors of estimate of Ln{Cycles} ranging from 0.578 to 0.933. The estimates do not appear to be systematically influenced by asphalt content. Using dummy variables to collectively apply the four individual models to the entire data set yields a composite standard error of estimate of 0.776 and a corresponding mean square error of 0.602. The coefficient of variation may be estimated using the following equation:

$$CV = 100\ (e^{MSE} - 1)^{0.5} \qquad (10.3)$$

where:
- CV = coefficient of variation in percent;
- e = base of natural logarithms; and
- MSE = mean square error of Ln{Cycles}.

For a mean square error of 0.602, the coefficient of variation is approximately 90 percent.

The four linear models are graphically depicted in Figure 10.9. Although they do not form the kind of family of relationships that is desired, they do verify that reductions in asphalt content improve performance for the low air void contents representative of critical in situ conditions.

10.1.2 Sample Size — Variance Relationships

To make probability statements based on laboratory measurements, the mean and variance of the measurements and the nature of their distribution must be known, measured, or assumed. For the results reported herein, the number of cycles to reach 5 percent shear strain is used as a measure of (N_{supply}) and is assumed to have a log normal distribution. The sample mean is computed in the normal manner; multiple stress levels are not used in the testing, and extrapolations are not required.

The variance of interest is the sum of the variance of the sample mean (σ^2/n) and the variance of the deviations of individual measurements from the sample mean (σ^2). This is similar to the approach taken in the fatigue investigation. Because σ^2 has been determined to be approximately 0.6 as shown above, the relationship between sample size (n) and variance is known in advance. Using terminology similar to that employed in the fatigue investigation

Table 10.2. Calibration Summary

Asphalt Content Percent	Order of Polynomial	Coefficient of Determination	Standard Error of Estimate (Ln{Cycles})	Probability
4.5	First	0.45	0.933	0.15
	Second	0.49	1.038	0.36
	Third	0.74	0.903	0.36
4.9	First	0.68	0.578	0.02
	Second	0.69	0.643	0.10
	Third	0.71	0.719	0.24
5.5	First	0.16	0.816	0.33
	Second	0.43	0.735	0.24
	Third	0.60	0.686	0.25
6.0	First	0.12	0.759	0.50
	Second	0.33	0.762	0.54
	Third	0.46	0.843	0.69

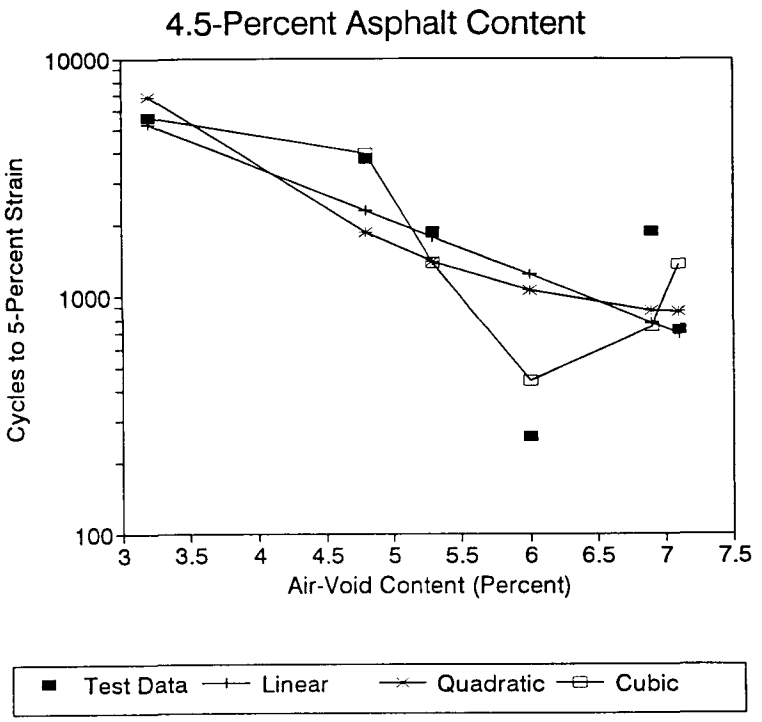

Figure 10.5. Calibration summary, asphalt content — 4.5 percent

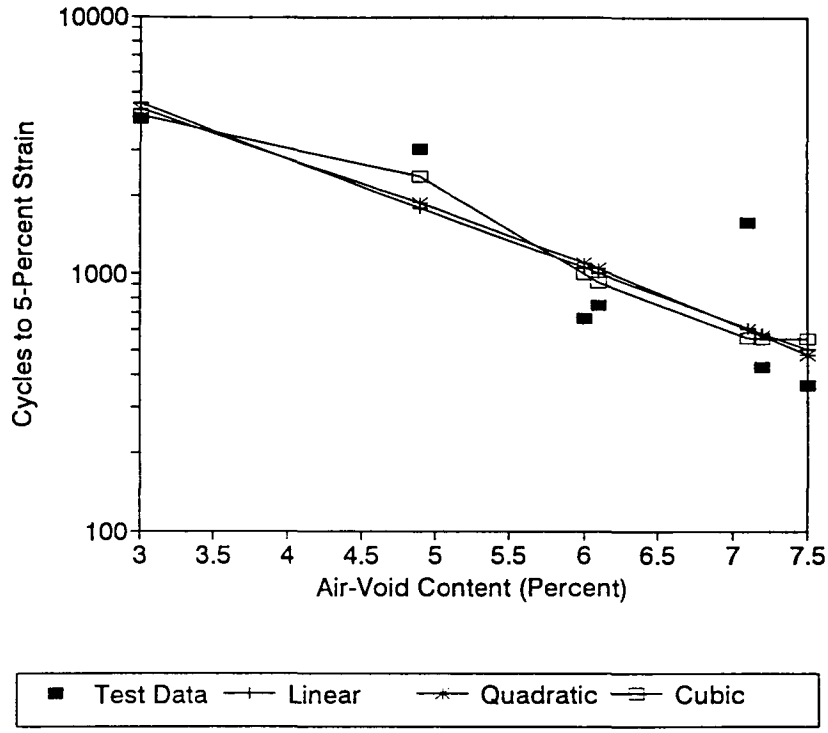

Figure 10.6. Calibration summary, asphalt content — 4.9 percent

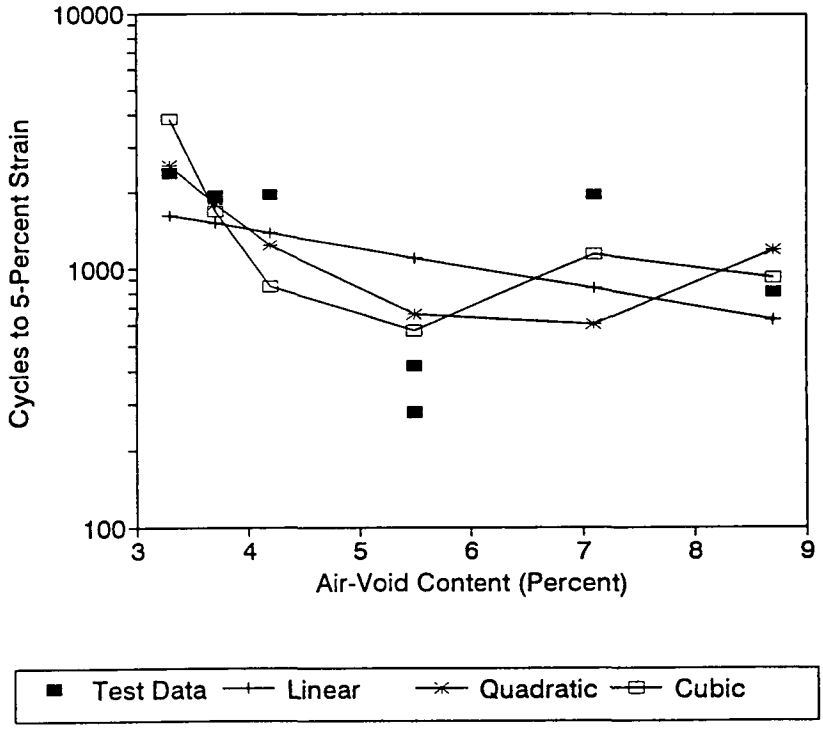

Figure 10.7. Calibration summary, asphalt content — 5.5 percent

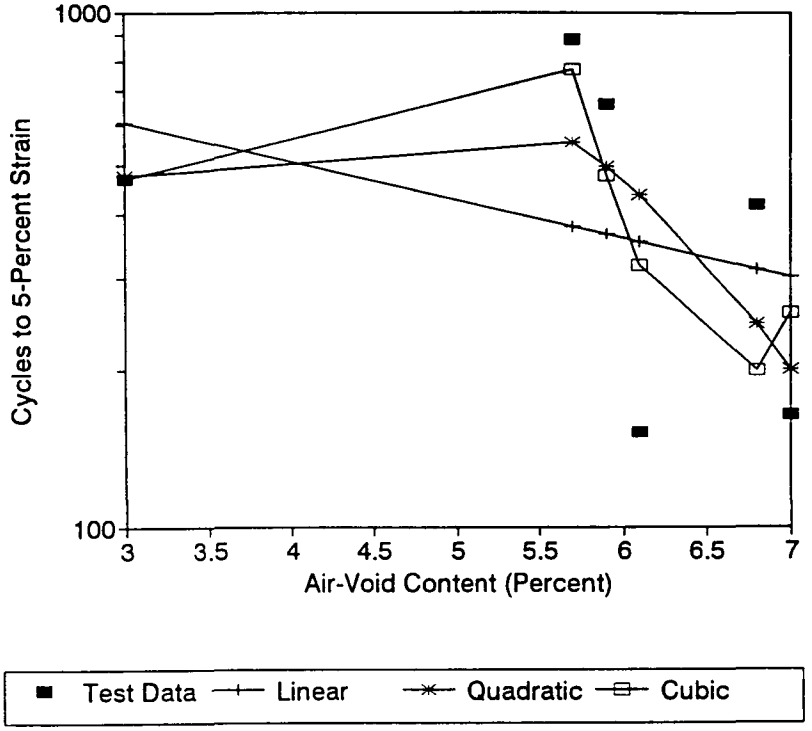

Figure 10.8. Calibration summary, asphalt content — 6.0 percent

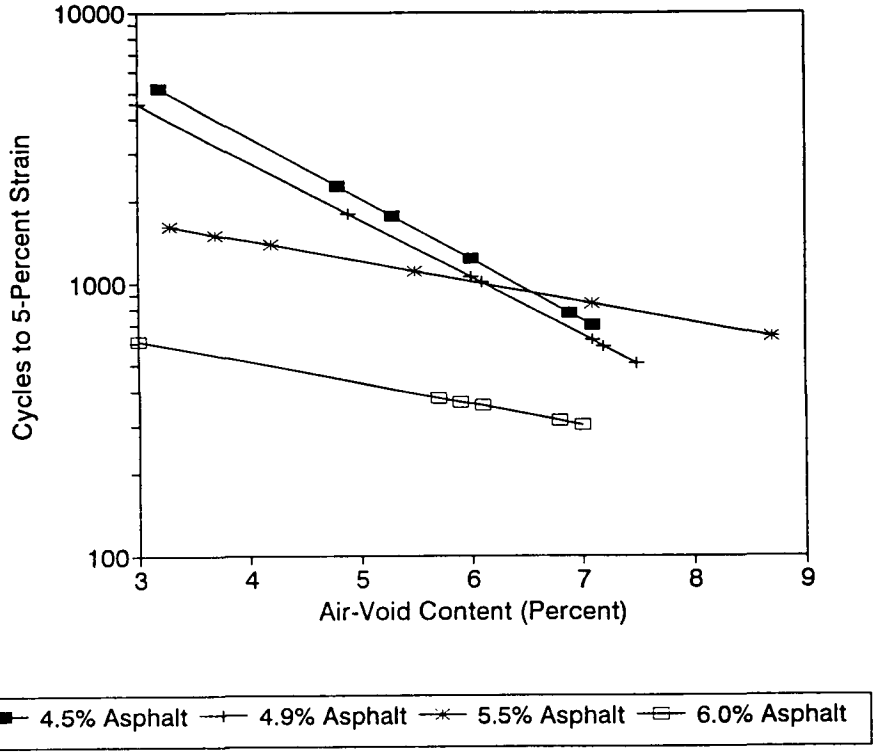

Figure 10.9. Comparison of linear models for four asphalt contents

(Tayebali et al. 1993), the standard deviation of predicted Ln (N_{supply}) can be determined from the following equation:

$$\text{Std. Dev. of Predicted Ln } (N_{supply}) = [\text{Std. Dev. Ln } (N_{5\%})^2 \cdot (1 + 1/n)]^{1/2} \quad (10.4)$$

where: $N_{5\%}$ = number of repetitions to 5 percent strain in constant height repeated load simple shear test; and

n = number of specimens tested at specific condition (e.g., one binder content and one air void content).

Results of the computations are shown in the following tabulation:

Number of Specimens Tested	Standard Deviation of Predicted Ln(N_{supply})
1	1.095
2	0.949
4	0.866
8	0.822

Variability in the results of the repeated load simple shear tests can be caused by variations in all of the following:

- batching, mixing, and compaction of the mix;
- measurement of the maximum specific gravity;
- measurement of the bulk specific gravity of the cored/cut specimen, and with the maximum specific gravity, calculation of the air voids content;
- mounting of the end caps;
- placement of the horizontal LVDT on the side of the specimen, parallel to the plane of movement of the shear (horizontal) platen of the testing machine;
- repetitive simple shear testing, with the specimen being maintained at a constant height (The precision of the constant height test depends on the gain setting of the electronics of the test machine. The gain setting that can be used depends on the stiffness of the specimen, which depends on the mix and the test temperature.); and
- extrapolation of the results obtained for 1 or 2 hours of testing (5000 to 10,000 repetitions) to the failure strain, which is required for specimens with higher

permanent shear deformation resistance and those tested at lower temperatures, as well as the inherent variability in the materials.

10.1.3 Reliability Multiplier, M

As noted earlier, for a mix to be satisfactory,

$$N_{supply} \geq M \cdot N_{demand} \tag{10.1}$$

the reliability multiplier can be determined from the following equation:

$$Ln(M) = Z_R \cdot [Var\{Ln(N_{supply})\} + Var\{Ln(N_{demand})\}]^{0.5} \tag{10.5}$$

where: Z_R = a function of the reliability level, which assumes values of 0.253, 0.841, 1.28, and 1.64 for reliability levels of 60, 80, 90, and 95 percent, respectively;
$Var\{Ln(N_{supply})\}$ = variance of the natural logarithm of N_{supply}; and
$Var\{Ln(N_{demand})\}$ = variance of the natural logarithm of N_{demand};

or taken directly from Table 10.3.

Table 10.3. Reliability multipliers

		Reliability Multiplier			
Sample Size	Variance of $Ln(N_{demand})$	60 Percent Reliability (Z_R = 0.253)	80 Percent Reliability (Z_R = 0.841)	90 Percent Reliability (Z_R = 1.28)	95 Percent Reliability (Z_R = 1.64)
1	0.2	1.349	2.704	4.545	6.957
	0.4	1.377	2.896	5.046	7.955
	0.6	1.404	3.090	5.567	9.022
	1.0	1.455	3.480	6.673	11.381
2	0.2	1.304	2.416	3.830	5.587
	0.4	1.334	2.609	4.305	6.490
	0.6	1.363	2.802	4.797	7.456
	1.0	1.417	3.188	5.839	9.592
4	0.2	1.280	2.270	3.482	4.945
	0.4	1.312	2.464	3.946	5.805
	0.6	1.342	2.657	4.425	6.723
	1.0	1.397	3.042	5.437	8.754
8	0.2	1.267	2.197	3.313	4.640
	0.4	1.300	2.392	3.772	5.479
	0.6	1.331	2.585	4.245	6.375
	1.0	1.388	2.970	5.243	8.356

10.2 Summary

Considerations of reliability for the constant height repeated load simple shear test have been briefly examined in this chapter. From a study of one mix prepared over a range in asphalt and air void contents, results of the constant height repeated load simple shear test (the only procedure evaluated in this investigation) suggest a mean square error of 0.60. This results in a coefficient of variation (CV) of about 90 percent. While this may seem large, the equipment and procedures have only recently been developed. As measuring equipment and test methodologies are improved, this variation can be significantly reduced as already has been demonstrated for the fatigue test (reduction in CV from about 90 percent to 40 percent).

With the above information, reliability multipliers have been determined which permit a mix design to be selected so that the estimated rut depth for the design traffic will not exceed some prescribed amount, e.g., 1.25 cm (0.5 in.), with a prescribed level of reliability such as 80 percent. These multipliers are applied to the estimated traffic (N_{demand}), which has been converted to its equivalent repetitions at the critical temperature. The higher the level of reliability desired for a given level of traffic variability and a specific number of specimens tested in the laboratory, the greater the value of the multiplier. For example, for a variance in Ln (N_{demand}) of 0.2 and a sample size of four specimens tested, the value of M is increased by a factor of about 2.2 to improve the reliability of the estimate from 80 percent to 95 percent. As noted at the outset of this chapter, such a change may reduce the number of acceptable mixes for a specific project.

11

Shift Factor

A shift factor must be applied to the traffic forecast to enable direct comparison to be made between field- and laboratory-traffic estimates. This shift factor will account for traffic wander, construction variability, differences between laboratory and actual (field) states of stress, and other factors.

Proposed herein is the use of such a shift factor and defined as follows:

$$N_{demand} = SF \cdot (ESAL)_{Tc} \quad (11.1)$$

where:

N_{demand}	=	design traffic demand (laboratory-equivalent repetitions of standard load);
$(ESAL)_{Tc}$	=	design ESALs adjusted to the critical temperature, T_c, for the site in which the mix is to be used; and
SF	=	empirically determined shift factor.

To this time, relatively little research has been directed to the definition of shift factors for permanent deformation estimates. The Shell researchers (van de Loo 1976), based on a analysis of the influence of traffic wander on permanent deformation, have suggested that when the effects of single and dual tires are considered together, the amount of rutting with wander is about the same as would be obtained if all vehicles traveled in one path.

In other studies where the creep test has been used within the framework of the layer-strain procedure (Monismith et al. 1987, van de Loo 1976), coefficients in the range 1 to 2 have been used to multiply the laboratory-estimated rutting values to permit them to correspond to field-measured values. For example, in a reasonably controlled study in Saudi Arabia, a factor of 1.5 was used to establish correspondence between laboratory-predicted (using the layer-strain procedure and creep test results) and field-measured values (Monismith et al. 1987).

Unfortunately, time limitations have not permitted the development of well documented shift factors in terms of load applications. Ultimately, such factors will necessarily have to

depend on the results of controlled tests (e.g., laboratory wheel-tracking, Federal Highway Administration [FHWA] Accelerated Load Facility [ALF], and Special Pavement Studies-9 [SPS-9] investigations).

Nevertheless, repeated load testing of pavement cores extracted from a limited number of General Pavement Studies (GPS) sites has provided an opportunity for developing first-generation estimates of appropriate shift factors. These first-generation estimates are a starting point from which mix designers can make adjustments to reflect local experiences with mixes known to be either good or poor performers. The sections to follow briefly describe the methodology followed; at this time only one value for the shift factor is presented.

11.1 Field Data

Selected GPS sections that had been identified by the A-005A contractor and used in the validation studies associated with that contract provided the data used in the analyses. Subsequently, additional sites for which rut depth measurements and equivalent single axle loads (ESALs) were known were made available by the Colorado Department of Transportation. Table 11.1 provides a summary of the data which includes site number and state, rut depth measurements, and the estimated ESALs associated with the rut depth measurements. Rut depths were measured using the Pasco Equipment, the Dynatest dipstick, or a difference in elevation relative to a 1.2 m (4 ft) straight edge.

Fifteen centimeter (6 in.) diameter cores were obtained from each of the sites for simple shear testing in the laboratory. To define the test temperature for the simple shear tests on specimens from a specific site, temperature data from two or three stations near the site with at least 20 years of records were obtained.

11.2 Temperature Analysis

At the time of testing, the concept of the critical temperature was just evolving. However, the Strategic Highway Research Program (SHRP) binder specification had already incorporated the use of a maximum pavement temperature. This temperature is defined as the maximum average temperature for seven consecutive days. The mean highest average 7-day maximum temperature was obtained from the average of the 20 to 30 values from the years of record.

Pavement surface temperature was computed from Equation 11.2 (Solaimanian and Kennedy 1993),

$$422\alpha\tau_a^{\frac{1}{\cos z}}\cos z + 0.7\sigma T_a^4 - 90k - h_c(T_s - T_a) - \epsilon\sigma T_s^4 = 0 \qquad (11.2)$$

where: z = zenith angle (approximately;
z = latitude -20° (for latitudes over 22°);

Table 11.1. Summary of test conditions and results

GPS Sites	GPS Core Designation	State	Max Pav Temp (°F)	Void Content (%)	Age (yrs)	ESAL	Rut Depth (in.)	Shear Strain (in./in.)	No. Cycles CHRSST	Rejection Criterion
21,001	GX21-1	AK	90	6.1	7	399,844	0.18	0.0164	87	
21,004	GX1-1	AK	90	3.9	13	1,791,505	0.33	0.0300	3419	
41,007	GX41-1	AZ	138	2.8	11	21,365,008	0.41	0.0373	576	out
41,021	GX-19	AZ	135	1.0	11	11,549,655	0.52	0.0473	26,876	void
					12	12,633,956	0.53	0.0482	28,553	void
41,025	GX22-1			0.0	13	13,651,008	0.16	0.0145	286	void
41,036	GX8-1	AZ	138	6.6	6	4,322,385	0.14	0.0127	11,523	
					7	4,769,968	0.14	0.0127	11,523	
53,071	GX64-1	AR	125	3.9	1	637,500	0.14	0.0127	6872	
					2	1,275,000	0.16	0.0145	9694	
					3	1,657,500	0.16	0.0145	10,585	
68,153	GX51-1	CA	120	3.4	12	614,903	0.16	0.0145	376	
68,156	GX26-1	CA	120	6.3	15	820,162	0.14	0.0127	30,063	
82,008	GX10-1	CO	125	1.5	17	1,225,650	0.42	0.0382	19,963	
					18	1,283,072	0.46	0.0418	28,155	
131,031	GX33-1	GA	128		9	227,047	0.28	0.0255	4763	
					10	256,209	0.28	0.0255	4763	
161,020	GX61-1	ID	120	6.0	3	142,749	0.14	0.0127	44	
					4	178,200	0.15	0.0136	52	
171,003	GX32-1	IL	125	3.5	3	139,986	0.12	0.0109	185	
					4	179,982	0.17	0.0155	395	
					5	216,645	0.15	0.0136	299	
201,009	GX29-1	KS	130	7.9	4	284,935	0.20	0.0182	451	
					5	404,268	0.23	0.0209	582	
211,014	GX14-1	KY	120	4.1	5	1,418,454	0.18	0.0164	3089	
					6	2,051,845	0.19	0.0173	3827	
231,012	GX44-1	ME	110	2.1	4	980,000	0.23	0.0209	756	
					5	1,190,000	0.25	0.0227	931	
261,012	GX3-1	MI	115	6.5	9	714,861	0.23	0.0209	803	
					10	802,748	0.26	0.0236	1031	
271,019	GX11-1	MN	115	9.0	9	435,438	0.22	0.0200	83,390	void
					10	472,975	0.23	0.0209	9324	void
341,030	GX23-1	NJ	120	0.5	18	1,115,000	0.56	0.0509	14,355	void
					19	1,160,000	0.68	0.0618	23,103	void

Table 11.1 (continued). Summary of test conditions and results

GPS Sites	GPS Core Designation	State	Max Pav Temp (°F)	Void Content (%)	Age (yrs)	ESAL	Rut Depth (in.)	Shear Strain (in./in.)	No. Cycles CHRSST	Rejection Criterion
341,031	GX31-1	NJ	120	1.0	16	5,075,000	0.37	0.0336	486	void
					17	5,325,000	0.38	0.0345	512	void
351,022	GX62-1	NM	120	5.2	6	724,306	0.15	0.0136	1304	
401,015	GX43-1	OK	130	2.1	13	955,031	0.23	0.0209	2016	
					14	1,040,193	0.24	0.0218	2692	
404,164	GX35-1	OK	130	4.0	14	633,750	0.15	0.0136	19076	
					15	686,250	0.14	0.0127	15860	
479,025	GX30-1	TN	125	8.1	9	233,159	0.14	0.0127	19804	void
					11	288,553	0.18	0.0164	37120	void
481,039	GX71-1	TX	130	3.9	7	1,637,481	0.16	0.0145	1105	
					8	1,993,484	0.23	0.0209	2170	
481,047	GX18-1	TX	130	2.5	18	5,500,000	0.20	0.0182	1625	out
481,048	GX42-1	TX	130	1.1	15	786,000	0.20	0.0182	251,336	void
					17	856,600	0.16	0.0145	131,878	void
481,069	GX81-1	TX	130	2.3	13	2,573,568	0.34	0.0309	8205	
					14	2,751,168	0.32	0.0291	7185	
481,077	GX15-1	TX	130	1.8	7	1,394,648	0.38	0.0345	3039	
811,805	GX65-1	CN	110	4.3	9	1,190,182	0.25	0.0227	133	out
851,801	GX4-1	CN	90	4.1	5	1,183,357	0.21	0.0191	2668	
891,011	GX63-1	CN	115	4.8	10	853,376	0.17	0.0155	813	
					11	933,380	0.20	0.0182	1258	
CO Sites	CO Core Designation	State	Max Pav Temp (°F)	Void Content (%)	Age (yrs)	ESAL	Rut Depth (in.)	Shear Strain (in./in.)	No. Cycles CHRSST	Rejection Criterion
14	14H	CO	124	4.6	23	3,282,000	0.80	0.0727	166839	
29	29I	CO	120	7.1	9	5,002,000	0.30	0.0273	4442	
30	30H	CO	120	6.6	9	4,622,000	0.60	0.0545	3122	
13	13A	CO	124	7.5	6	1,257,000	0.10	0.0091	1030	
13	13B	CO	124	7.1	6	1,257,000	0.10	0.0091	675	

τ_a	=	sunshine factor (0.81 for sunny conditions, 0.62 cloudy conditions);
α	=	solar absorptivity (default: 0.9);
σ	=	Stefan-Boltzman Constant (0.1714 E-8 Btu/(hr.ft^2.R^4);
h_c	=	surface coefficient of heat transfer (default = 3.5 Btu/(hr.ft^2.F);
k	=	thermal conductivity (default: 0.8 Btu/(hr.ft^2.F)/ft);
ϵ	=	surface emissivity (default: 0.9);
T_a	=	maximum air temperature in Rankine (°R) (°R=°F + 460); and
T_s	=	maximum pavement surface temperature (°R).

The maximum pavement temperature at the surface is determined using Equation 11.2. The relationship can be solved iteratively. For example, if one desired to compute the surface pavement temperature at a site with a latitude of 38° and a value for T_{air} = 31.7°C (89°F), each of the terms of Equation 11.2 would be computed as follows:

$422\alpha\ t_a^{1/\cos z} \cos z$	=	422 (0.9) (0.8) $^{1/\cos(38-20)}$ cos(38-20)	= 286
$0.7\sigma\ T_a^4$	=	0.7 (0.1714 E-8) $(89+460)^4$	= 109
$-h_c\ (T_s - T_a)$	=	-(3.5) (***32***)	= -112
-90k	=	-90 * 0.8	= -72
$e\sigma T_s^4$	=	-0.9 (0.1714E-8) (***121*** + 460)^4	= -176
		SUM	= 35

Note that the terms in bold italics are initial assumptions. Note also that the equation requires temperatures to be expressed in degrees Rankine. Iteratively the equation would finally converge to a sum of zero.

The maximum pavement temperature for any depth less than 20 cm (8 in.) is found through the following empirical formula (Solaimanian and Kennedy 1993):

$$T_d = T_s\ (1 - 0.063d + 0.007d^2 - 0.0004d^3) \qquad (11.3)$$

where d is the depth in inches, T_s is the maximum pavement temperature (°F) at the surface, and T_d is the maximum pavement temperature (°F) at depth d.

For reasons discussed earlier, the maximum pavement temperature at 5 cm (2 in.) depth was selected as the testing temperature for each of the GPS sections. Table 11.1 contains the test temperatures determined for each of the test sites according to the procedure described above.

11.3 Laboratory Tests

Constant height repeated load simple shear tests were conducted on 15 cm (6 in.) diameter by 5 cm (2 in.) high specimens obtained from cores for each of the sections shown in Table 11.1. The test temperature for each section was that determined according to

Equation 11.3. A shear stress of 70 kPa (10 psi) was used with a loading time of 0.1 s in the form of a haversine and a time interval between loading (rest period) of 0.6 s. Each specimen was subjected either to the number of repetitions required to produce a permanent shear strain of 5 percent or to 5000 repetitions[10] if the 5 percent level was not reached.

Prior to the repeated load shear testing, each specimen was heated for a period of 2 hours at the predetermined pavement temperature, Table 11.1.

Results of some of the repeated load shear tests are shown in Figure 11.1. Differences in performance among mixes are observed in this figure.

11.4 Analyses

Analysis was limited to those GPS sections shown in Table 11.2.[11] In each case, the pavement had been in service for fewer than 9 years and the asphalt layer exceeded 12.5 cm (5 in.) in thickness. Laboratory test results are summarized in Table 11.3.

To obtain the values for permanent shear strain shown in Table 11.3, Equation 6.34 was used, i.e.:

$$\text{Rut depth (in.)} = 11 \bullet (\gamma_p)_{max} \tag{6.34}$$

For example, for the GPS site GX64-1 the shear strain of 1.27 percent (0.0127) was obtained by dividing the rut depth 0.14 in. by the factor 11.

For this analysis, ESALs were adjusted to their equivalents at the 7-day average maximum pavement temperature at a 5 cm (2 in.) depth by applying a constant factor of 0.0724, Table 11.4. This average appears reasonable in light of information available for the nine FHWA regions, e.g., Table 6.5. Analysis of the data resulted in the following equation:

$$N_{demand} = 0.0562\ ESAL_{T'}^{0.924} \tag{11.4}$$

where: N_{demand} = number of repetitions required in constant height repeated load simple shear test; and

$ESAL_{T'}$ = number of design-lane ESALs after conversion to its equivalent at the average maximum pavement temperature at a 5 cm (2 in.) depth, T'.

---

[10]For the test conditions used, this required about 1 hour of repeated loading in shear.

[11]Another analysis has been performed which is not included herein. Details are described in Sousa and Solaimanian 1994.

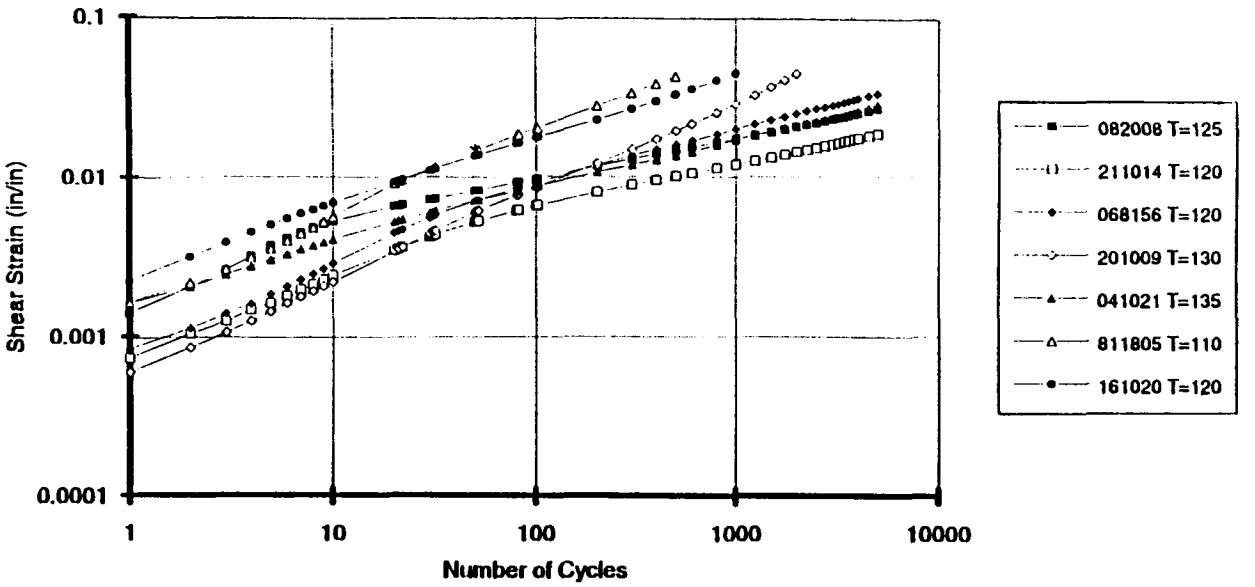

Figure 11.1. Variation of permanent shear strain in constant height repeated load simple shear test with number of stress repetition for specimens from selected GPS sites

Table 11.2. GPS sections included in calibration

UCB Identification (SHRP Site #)	Surface Thickness (in.)	Age (yrs)	Average Maximum Daily Temp. (°F)	Rut Depth (in.)	Traffic Loading (ESALs)
GX64-1 (053071)	16.7	1	52	0.14	637,550
		2	52	0.16	1,275,000
GX32-1 (171003)	12.0	3	52	0.12	139,986
		4	52	0.17	179,982
GX29-1 (201009)	10.0	4	54	0.20	284,935
		5	54	0.23	404,268
GX14-1 (211014)	13.0	5	49	0.18	1,418,454
		6	49	0.19	2,051,845
GX44-1 (231012)	9.5	4	43	0.23	980,000
		5	43	0.25	1,190,000
GX62-1 (351022)	6.6	6	49	0.15	724,306
GX71-1 (481029)	7.7	7	54	0.16	1,637,481
		8	54	0.23	1,993,484

Notes: 1 in. = 2.54 cm
°C = (°F - 32) 5/9

Table 11.3. Laboratory test results

UCB Identification (SHRP Site #)	Age (yrs)	Test Temperature (°C)	Test Results	
			Permanent Shear Strain (%)	Cycles to Permanent Shear Strain
GX64-1 (053071)	1	52	1.27	6872
	2	52	1.45	9694
GX32-1 (171003)	3	52	1.09	185
	4	52	1.54	395
GX29-1 (201009)	4	54	1.82	451
	5	54	2.09	582
GX14-1 (211014)	5	49	1.64	3089
	6	49	3.36	3827
GX44-1 (231012)	4	43	2.09	756
	5	43	1.86	931
GX62-1 (351022)	6	49	1.36	1304
GX71-1 (481039)	7	54	1.45	1105
	8	54	2.09	2170

Table 11.4. Shift factor determinations

Variable	For Laboratory Testing at Maximum Temperature	For Laboratory Testing at Critical Temperature
Average Temperature Conversion Factor (Nationwide)	0.0725	0.0898
Average CH Cycles/ESAL	0.0362	0.0292
Average ESALs/CH Cycles	51.8	64.2
Equation	CH $N=0.0562\ ESAL^{0.924}$	CH $N=0.0461\ ESAL^{0.924}$
Coefficient of Determination	0.51	

The coefficient of determination for this expression is 0.51, and the variability is graphically demonstrated in Figure 11.2a.

Because of the relative weakness in the regression of this equation and in the database from which it was derived, and because the exponent of $ESAL_{T'}$ is so close to one, a simple shift factor relating N_{demand} to $ESAL_{T'}$ should *initially* suffice for mix-design purposes. It appears that a factor on the order of 0.04 might be an appropriate beginning point when testing and analysis is conducted at the critical, instead of the maximum, pavement temperature, Figure 11.2b.

Thus, to determine N_{demand} for mix-design purposes, the traffic estimate (ESAL) is first converted to its equivalent at the critical temperature through use of the appropriate temperate conversion factor (Table 6.7). Then N_{demand} is simply the product of 0.04 and the ESALs at the critical temperature.

11.5 Summary

In this section an approach has been described that permits a direct comparison to be made between field- and laboratory-traffic estimates. The study used the results of simple shear tests on cores from GPS pavement sections from throughout the United States from which traffic and associated rutting data were available. This comparison was made through a *shift factor* that converts the field traffic to laboratory-equivalent repetitions of a standard load in the constant height repeated load simple shear test.

The shift factor proposed should be considered a first generation factor from which mix designers can make adjustments to reflect local experiences with mixes known to be either good or poor performers from a rutting standpoint.

While testing of the cores was done at the average maximum pavement temperature (for a 7-day period) at a 5 cm (2 in.) depth for each site, the recommended shift factor for pavement analysis and design purposes is that associated with the critical temperature at the same depth. As noted in Chapter 9, this temperature is believed to ensure optimum results in pavement deformation assessment.

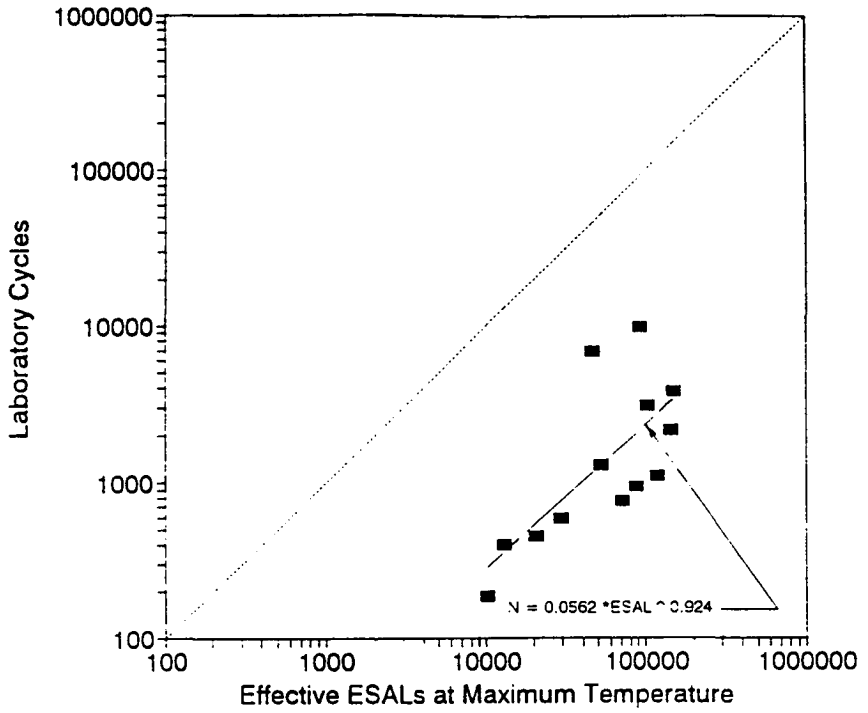

a. maximum pavement temperature

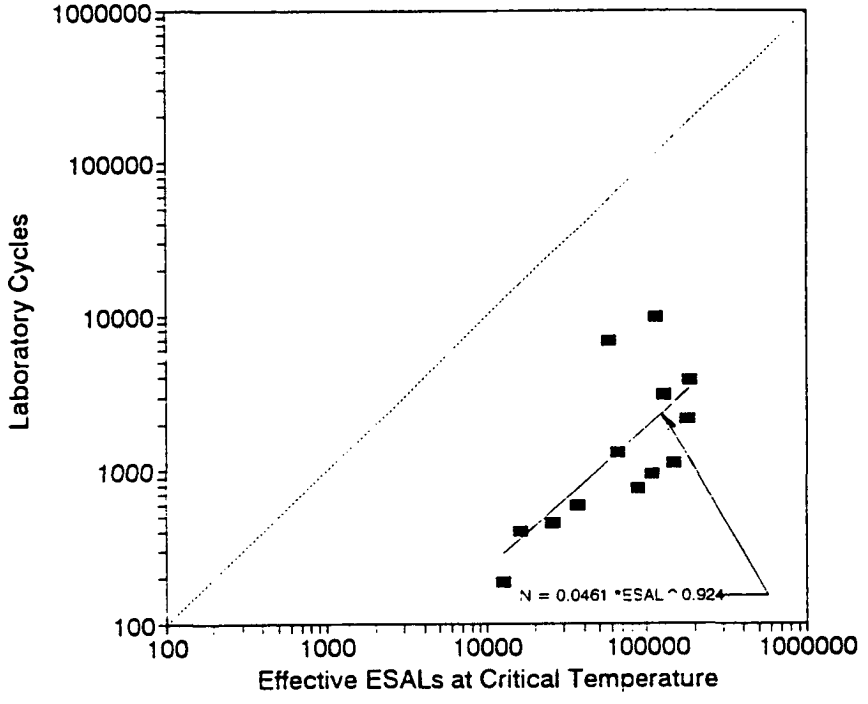

Figure 11.2. Relationship between laboratory cycles, N, and effective ESALs

12

Tests on Mixes Containing Modified Binders

The purpose of this phase of the research program was to investigate the influence of modified binders on the permanent deformation characteristics of mixes as defined by the constant height repeated load simple shear test. Results of this test program are briefly summarized.

Another part of the study, intended to be a part of the validation effort for the permanent deformation test, was conducted by SWK Pavement Engineering on prototype pavements constructed in the University of Nottingham's Pavement Test Facility. This study included mixes containing a conventional asphalt and a modified binder. Results of the SWK test program are summarized as well.

12.1 Constant Height Repeated Load Simple Shear Test Program

Specimens for this study were fabricated at the Southwestern Laboratories (SWL) in Houston, Texas, (the Strategic Highway Research Program [SHRP] A-004 Contractor), using a modified gyratory compactor (Texas type). The compacted specimens were shipped to the University of California's Richmond Field Station where they were sawed to the appropriate size and tested in the simple shear device.

12.1.1 Materials

The testing phase for the program included mixes containing two aggregates (RB and RL), three asphalts (AAD-1, AAG-1, and AAK-1), and four modifiers coded as 401, 412, 415, and 416. Mixes containing the binders in the unmodified condition were also tested (code 000).

Air void determinations on mixes containing the RL aggregate exhibited considerable variability as well as air void contents as high as 17 percent. Accordingly, specimens

containing this aggregate were not tested. In addition, specimens containing asphalt AAD-1 were not tested.

12.1.2 Procedures

The mixes were received as compacted specimens 15 cm (6 in.) in diameter by 15 cm (6 in.) high. These were sawed to produce test specimens approximately 5 cm (2 in.) high.

Before testing in the simple shear device, air void determinations were performed on specimens approximately 5 cm (2 in.) high. Two methods were used: (1) with parafilm (wp); and (2) without parafilm (np). Results of the tests are reported in the next section.

Constant height repeated load simple shear tests were performed on the 5 cm (6 in.) diameter by 5 cm (2 in.) high specimens to which caps had been bonded for shear stress application. As with tests reported earlier, an epoxy resin adhesive was used. Tests were conducted at 40°C (104°F). Each specimen was first conditioned with a shear stress of 7 kPa (1 lb/in^2) applied for 100 repetitions with a loading time of 0.1 s (haversine pulse) and a time interval of 0.6 s between loads. After conditioning, each specimen was subjected to a shear stress of 70 kPa (10 psi) using the same loading time and frequency. Tests were continued for 5000 load repetitions or until a maximum shear strain of 5 percent was attained so long as it occurred at or before 5000 repetitions.

12.1.3 Air Void Content Data and Specimen Uniformity

Table 12.1 contains a summary of air void determinations by both the A-004 contractor and the University of California, Berkeley, (UCB) staff. Note that the without-parafilm procedure used at UCB provides about the same *average* results as those reported by the A-004 contractor, although there are some individual differences. On the other hand, the air void contents as determined using parafilm indicate significantly higher levels, approximately 12 percent versus 6.8 percent.

A similar pattern is observed for the 5 cm (2 in.) high specimens sawed from the 15 cm (6 in.) high cylinders as seen in Table 12.2. Also, it will be noted in this table that differences exist across the height of the 15 cm (6 in.) specimens (e.g., FM00K L1, L2, and L3-14.5 to 17.2 percent). It is likely that variability exists across the diameter of the specimen as well. This is illustrated by the photograph of the failed surface of one of the specimens accidently loaded in tension, Figure 12.1. Around the periphery of the specimen there is about a 2.5 cm (1 in.) annulus in which the specimen has a different density than the remainder of the specimen. Such differences have been reported by Bonnot (1976) as well as more recently in studies associated with the A-003A contract (e.g., Eriksen 1992).

These data reinforce earlier recommendations contained in Chapter 5 regarding specimen preparation.

Table 12.1. Air void contents for 15 cm (6 in.) in diameter by 15 cm (6 in.) high specimens

Specimen Designation	Air Void Content (Percent)		
	Repeated by A-004 Contractor	Determined by A-003A Staff	
		np	wp
DM000DB2	6.1	6.7	11.7
DM000GL1/2	6.7	7.2	11.7
DM000GL3	6.8	6.5	10.6
D/FM000GB3	6.7	6.2	9.4
D/FM000KL1	6.8	5.7	12.1
D/FMOOOKL3	6.9	7.3	12.8
DM401GL3	7.9	7.8	15.0
DM401KB3	7.4	7.3	12.8
DM401KL1/2	6.8	6.0	10.5
DM401KL3	7.6	8.2	14.2
DM412GB2	6.9	6.7	11.0
D/FM415GB2	6.6	6.2	11.7
FM000FL2	6.0	6.1	11.8
FM000FL3	7.5	7.1	11.0
FM000KL2	7.6	6.4	13.0
FM000KL3	6.8	6.9	8.8
FM405FB1/2	6.0	6.5	11.7
FM405FB3	6.1	6.0	12.0
FM405FL1	6.4	4.5	10.9
FM405FL1	6.4	4.9	9.9
FM405FL3	6.9	8.7	15.2
FM405FL3	6.9	6.0	11.5
FM405KB1	6.8	7.0	14.0
FM405KL1	6.9	5.9	10.0
FM405KL1/2	6.9	7.2	14.8
FM405KL3	6.1	7.9	13.7
FM405KL3	6.1	8.4	14.2
Average	6.8	6.7	12.1

Table 12.2. Air void contents for 6 in. in diameter by 2 in. high specimens

Specimen Designation	Air Void Content (Percent)		
	Repeated by A-004 Contractor	Determined by A-003A Staff	
		np	wp
DM415KB3	6.3	7.1	10.2
DM416GB1	6.8	7.9	10.6
DM416GB2	6.1	7.3	8.5
DM416GB3	6.1	7.9	10.7
DM416KB1	6.2	6.1	7.3
DM416KB2	7.2	9.0	11.6
DM416KB3	7.1	8.9	10.7
FM000FB1	7.1	7.6	9.4
FM000FB1	7.1	7.0	10.8
FM000FB2	7.2	8.3	10.1
FM000FB3	7.1	8.7	10.2
FM000FL1	7.1	12.5	15.6
FM000FL2	7.1	11.8	15.8
FM000FL3	6.2	13.3	17.7
FM000GB1	6.2	6.1	10.6
FM000GB2	6.2	7.2	9.3
FM000GB3	6.7	6.8	9.4
FM000KB2	7.0	7.9	10.0
FM000KB3	6.9	6.8	10.9
FM000KL1	6.8	12.6	14.5
FM000KL2	6.1	11.9	14.9
FM000KL3	6.1	13.6	17.2
FM405FB1	6.4	6.7	9.9
FM405FB2	6.4	7.8	10.7
FM405FB3	6.4	7.9	10.8
FM405FL1	6.4	13.4	15.3
FM405FL3	6.4	12.1	15.4
FM405GB1	6.4	6.4	11.2
FM405GB2	6.3	7.5	9.3
FM405GB2	6.3	7.2	10.1
FM405GB3	6.4	7.1	10.7
FM405KB1	6.0	8.5	12.6
FM405KB1(A)	6.0	8.5	12.2
FM405KB2	6.0	8.1	10.2
FM/M405KB3	6.0	8.6	10.8
FM415KB2	6.4	6.9	11.6
FM415KB3	6.2	7.2	11.7
FM415KB3	6.2	7.4	10.2
FM415GB1	6.1	7.4	10.6
FM415GB2	6.6	6.8	10.2
FM416GB1	6.8	9.2	11.3
FM416GB2	6.1	6.9	10.6
FM416GB3	7.9	8.5	11.6
FM416KB1	6.2	7.6	8.9
FM416KB2	7.2	8.1	10.0
FM416KB3	7.1	8.1	10.3
Average	6.8	8.9	11.7

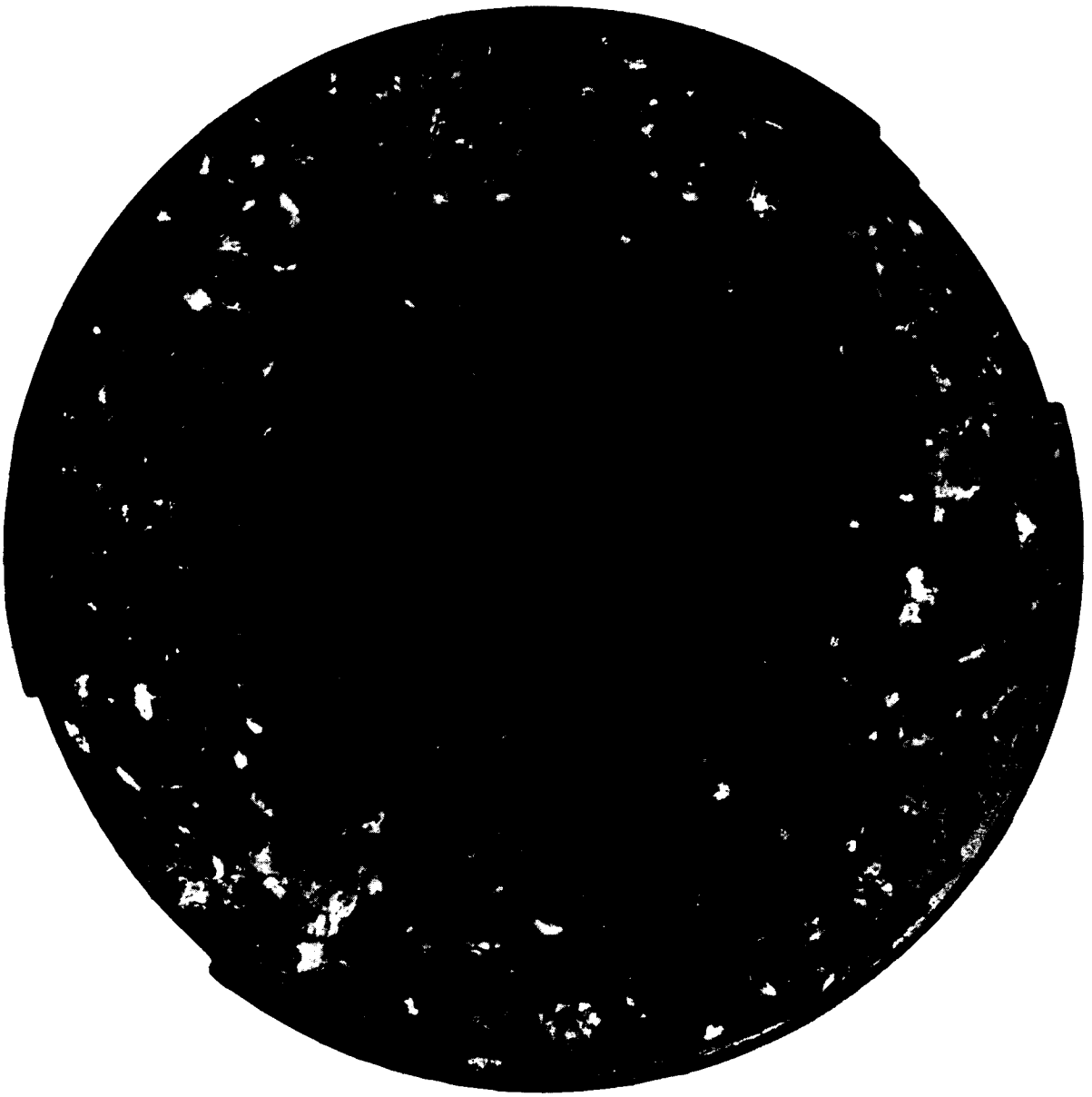

Figure 12.1. Photograph of broken specimen

12.1.4 Permanent Deformation Response

Results of the simple shear tests are summarized in Table 12.3 and presented graphically in Figures 12.2 through 12.11. As seen in Table 12.3 there are variations in the air void contents of the specimens, making comparisons among the mixes difficult, if not impossible.

One possibility for comparison is illustrated in Figure 12.12 for mixes containing asphalt AAG-1 or modified versions thereof and in Figure 12.13 for mixes containing both unmodified and modified materials utilizing AAK-1. The results presented in Figures 12.12 and 12.13 suggest the following conclusions:

Mixes containing asphalt AAG-1 appeared to be more influenced by modifiers than mixes containing asphalt AAK-1. For mixes with asphalt AAG-1, the influence of modifier on performance in rank order (high to low) is: 401, 412, 415, and 416; mixes containing the unmodified binder do not perform as well as those with modified binders.

Mixes containing modified binder utilizing asphalt AAK-1 appeared to be less sensitive to the influence of modifier, with mixes containing modifier 401 responding most favorably.

12.2 University of Nottingham Pavement Test Facility Study

Tests were performed by SWK Pavement Engineering on *four* prototype pavement structures in the University of Nottingham's Pavement Test Facility. Results of this study are contained in the report *Permanent Deformation Validation Study,* by Gibb et al. 1992. The researchers tested pavements containing mixes utilizing two aggregates, Tuff and Gravel, and two binders — a conventional 100 pen. asphalt and the same material modified with an SBR latex. The nominal pavement structures consisted of 100 mm (4 in.) of the binder/aggregate surfacing, 200 mm (8 in.) of a granular base/subbase materials resting on silty clay subgrade. Unidirectional loads were applied using the equipment shown in Figure 12.14 with a wheel load of 10 kN (2250 lb) at a pavement temperature of 30°C (86°F).

Final rut depths after 50,000 passes are illustrated for the four sections in Table 12.4. For this study the addition of an SBR latex to modify the binder significantly altered mix performance. As seen in Table 12.4, rut depths after 50,000 load applications were 3 to 5 mm (0.1 to 0.2 in.) for mixes containing the modified binder and 12 to 19 mm (0.47 to 0.75 in.) for mixes containing the conventional binder.

Tests to be completed subsequently should provide validation of the A-003A permanent deformation test. Unfortunately neither time nor funds have permitted the completion of this phase of the test program.[12]

---

[12]The materials have been placed in the Materials Reference Library (MRL) by SWK Pavement Engineering.

Table 12.3. Constant height repeated load simple shear test results

Specimen Designation	Air Void Content (percent)	Specimen Height (in.)	$N_{5\%}$
No Modifier			
DM000GB1	9.9	2.066	2971
DM000GB2	10.0	2.058	2230
DM000GB3	9.3	2.159	1794
DM000KB1	9.9	2.092	7973
DM000KB2	10.6	2.070	1091
DM000KB3	6.6	2.082	42244
Modifier 401			
DM401GB1	11.1	2.137	4380
DM401GB2	11.6	2.172	7298
DM401GB3	10.5	2.083	13039
DM401KB1	11.7	2.089	3649
DM401KB2	12.8	2.104	14846
DM401KB3	12.2	2.126	4231
Modifier 412			
DM412GB1	10.6	2.081	9110
DM412GB3	12.2	2.088	1712
DM412GB2	16.3	2.097	
DM412KB1	10.2	2.062	1735
DM412KB2	10.7	2.065	3883
DM412KB3	11.3	2.062	4342
Modifier 415			
DM415GB1	10.6	2.127	1191
DM415GB2	11.3	2.091	2418
DM415GM3	12.2	2.108	1688
DM415KB1	9.1	2.081	5673
DM415KB2	10.5	2.076	3431
DM415KB3	10.2	2.118	2432
Modifier 416			
DM416GB1	10.6	2.060	
DM416GB2	8.5	2.086	4156
DM416GB3	10.7	2.059	2264
DM416KB1	7.3	2.075	
DM416KB2	11.6	2.061	686
DM416KB3	10.7	2.068	2313

Note: 1 in. = 2.54 cm

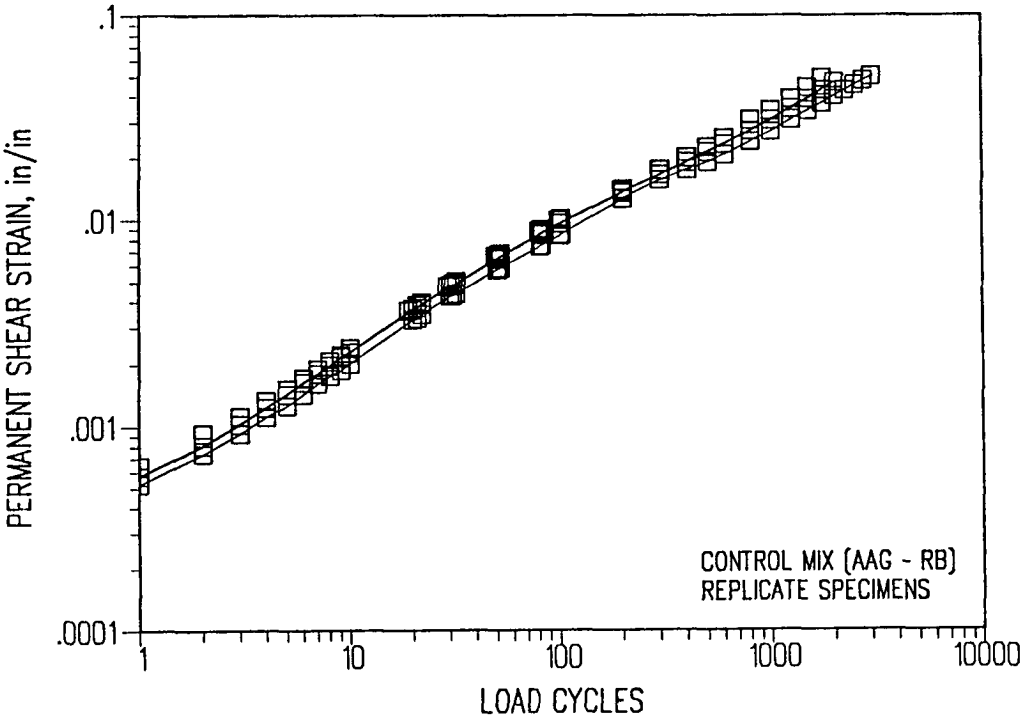

Figure 12.2. Permanent shear strain versus number of cycles for specimens with control mix (binder AAG)

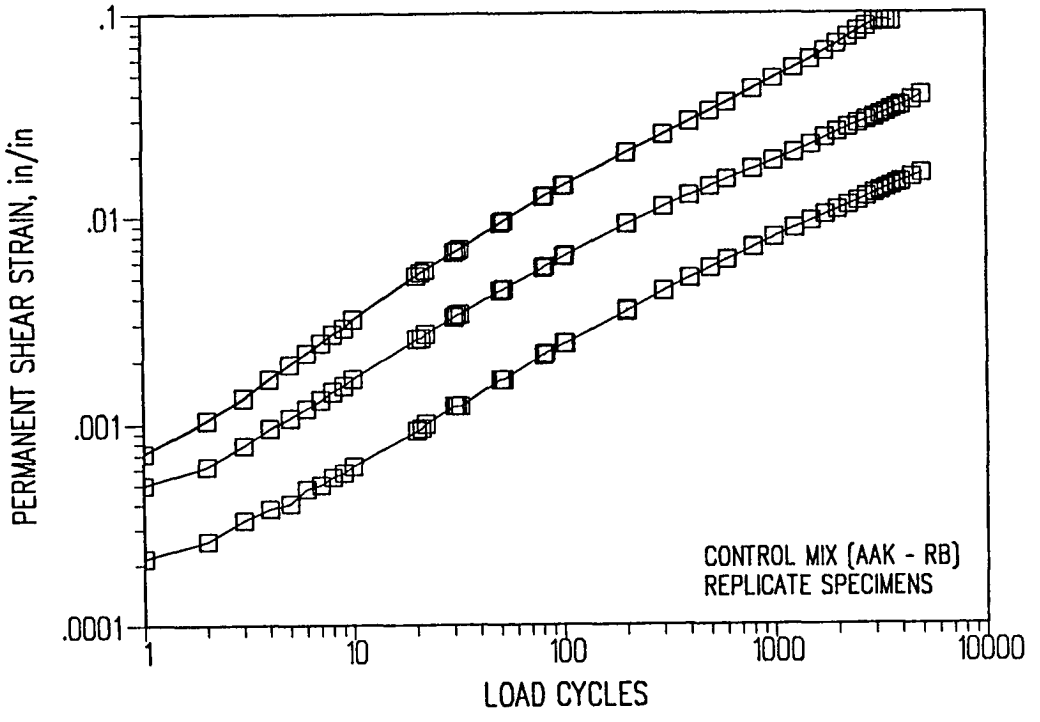

Figure 12.3. Permanent shear strain versus number of cycles for specimens with control mix (binder AAK)

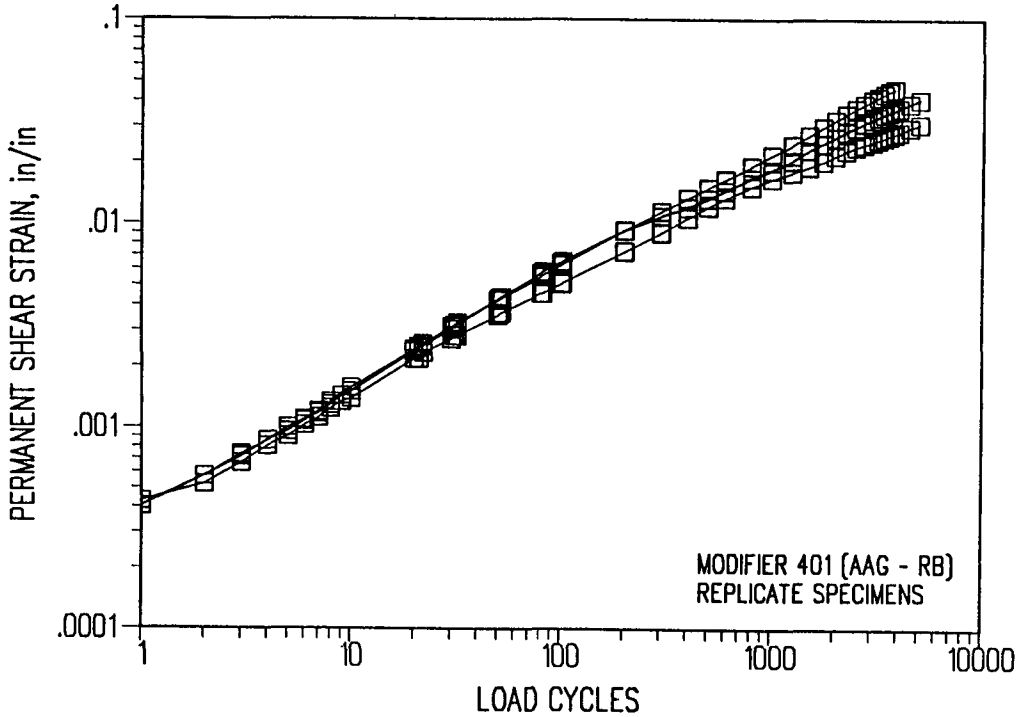

Figure 12.4. Permanent shear strain versus number of cycles for specimens with control mix containing modifier 401, binder AAG and aggregate RB

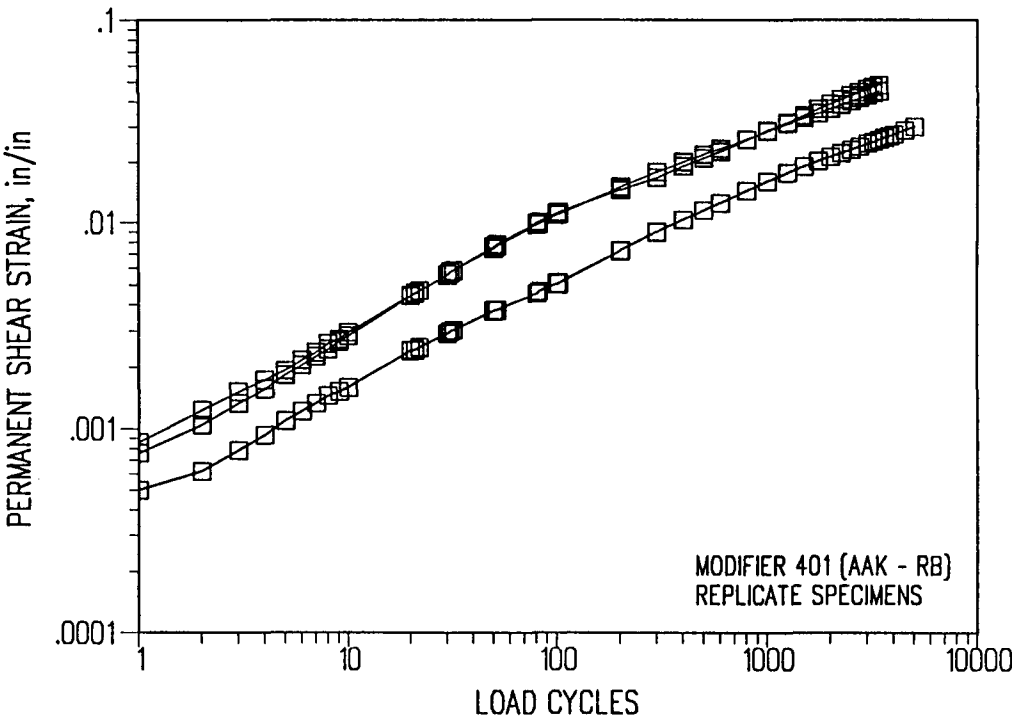

Figure 12.5. Permanent shear strain versus number of cycles for specimens with mix containing modifier 401, binder AAK and aggregate RB

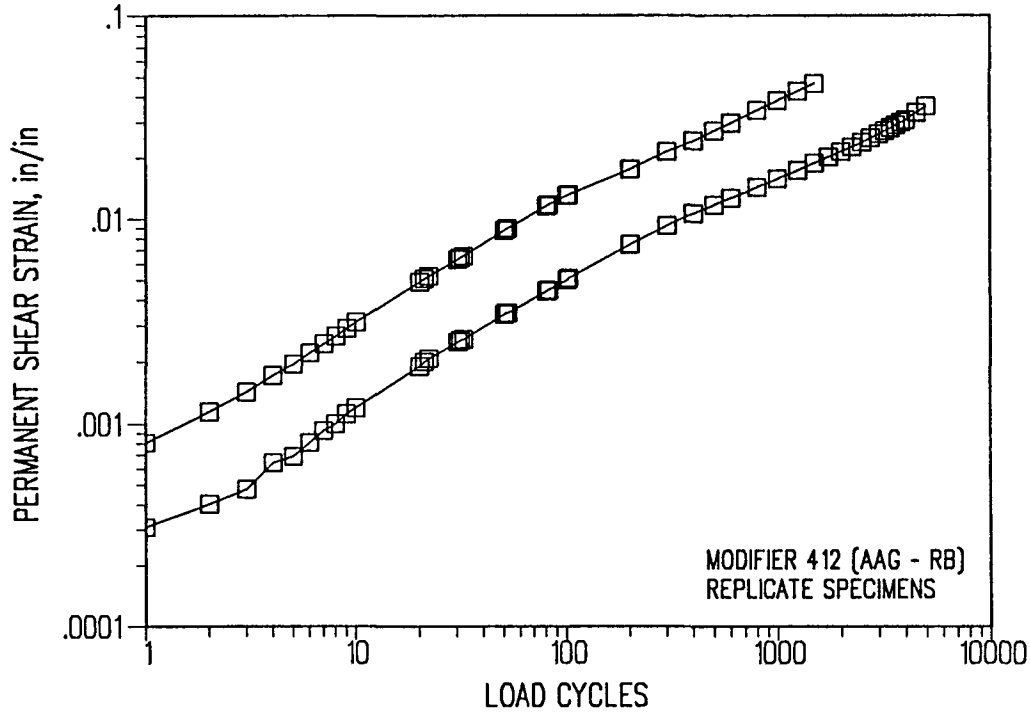

Figure 12.6. Permanent shear strain versus number of cycles for specimens with mix containing modifier 412, binder AAG and aggregate RB

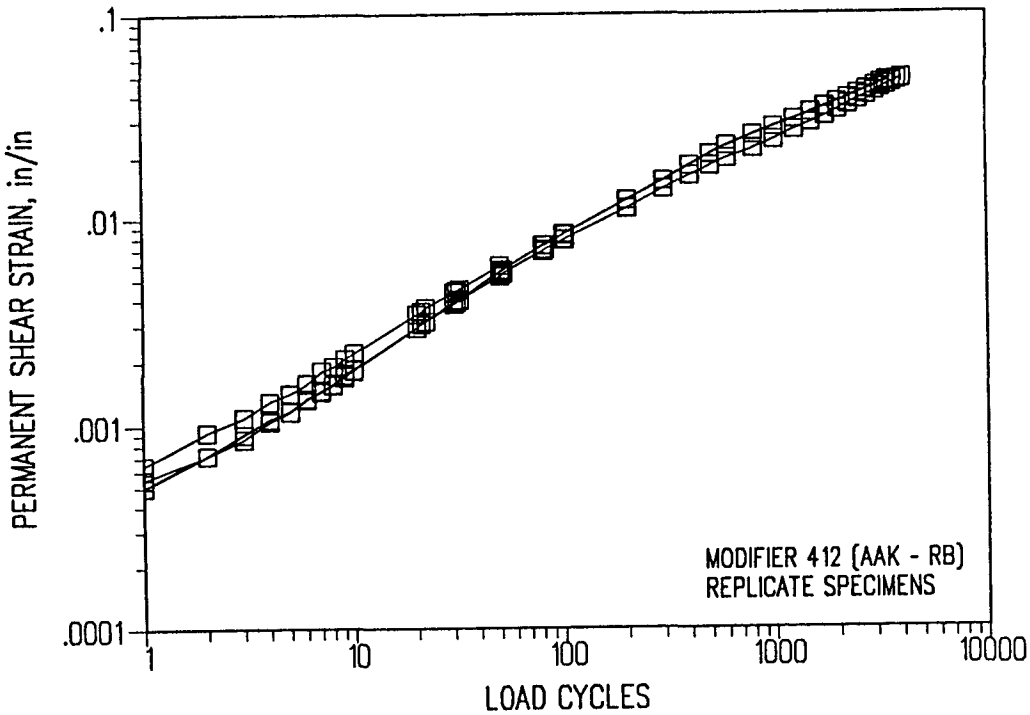

Figure 12.7. Permanent shear strain versus number of cycles for specimens with mix containing modifier 412, binder AAK and aggregate RB

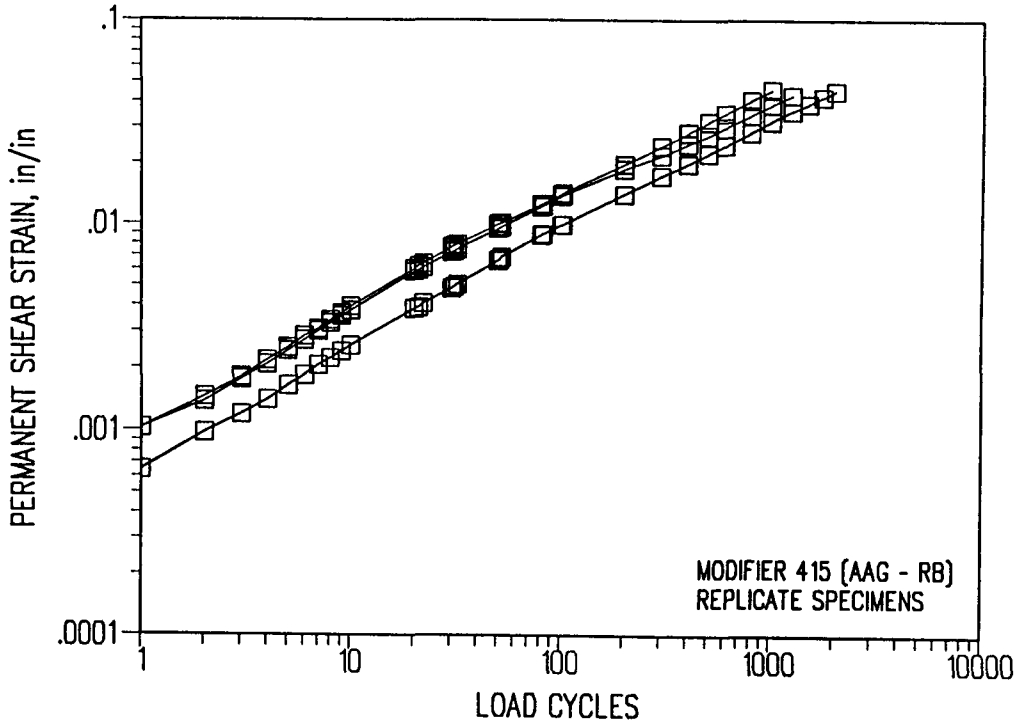

Figure 12.8. Permanent shear strain versus number of cycles for specimens with mix containing modifier 415, binder AAG and aggregate RB

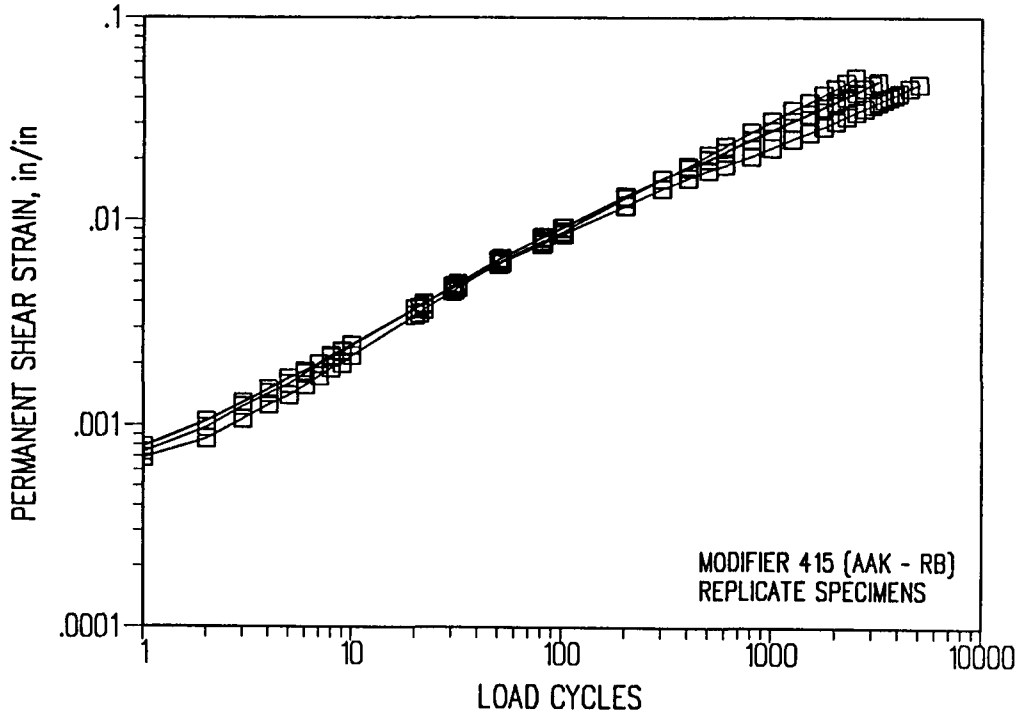

Figure 12.9. Permanent shear strain versus number of cycles for specimens with mix containing modifier 415, binder AAK and aggregate RB

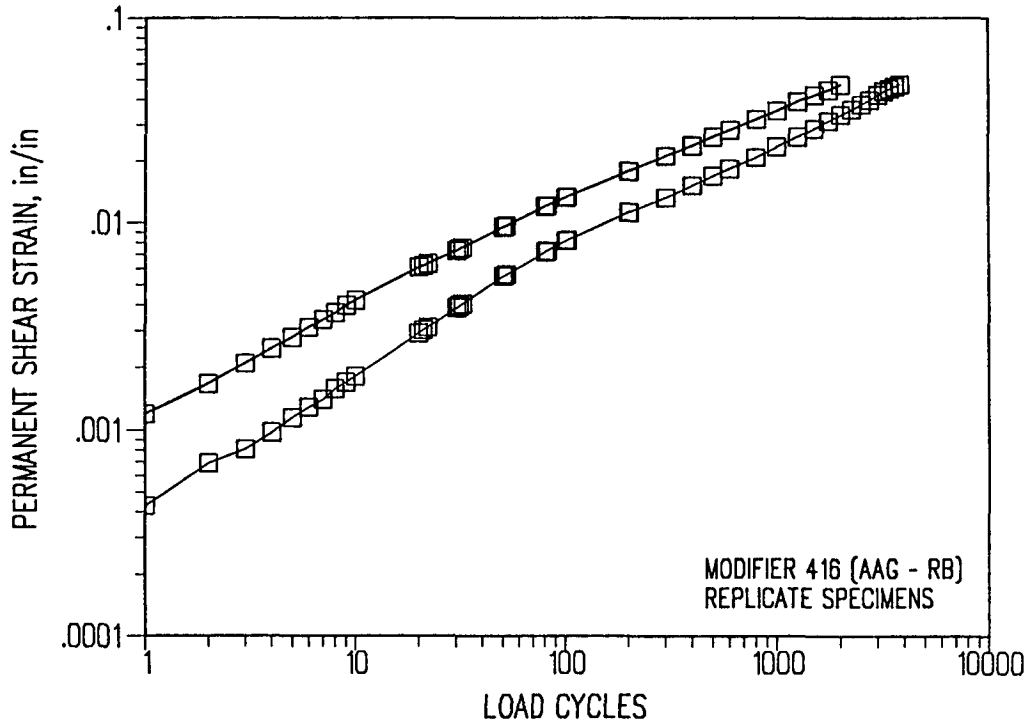

Figure 12.10. Permanent shear strain versus number of cycles for specimens with mix containing modifier 416, binder AAG and aggregate RB

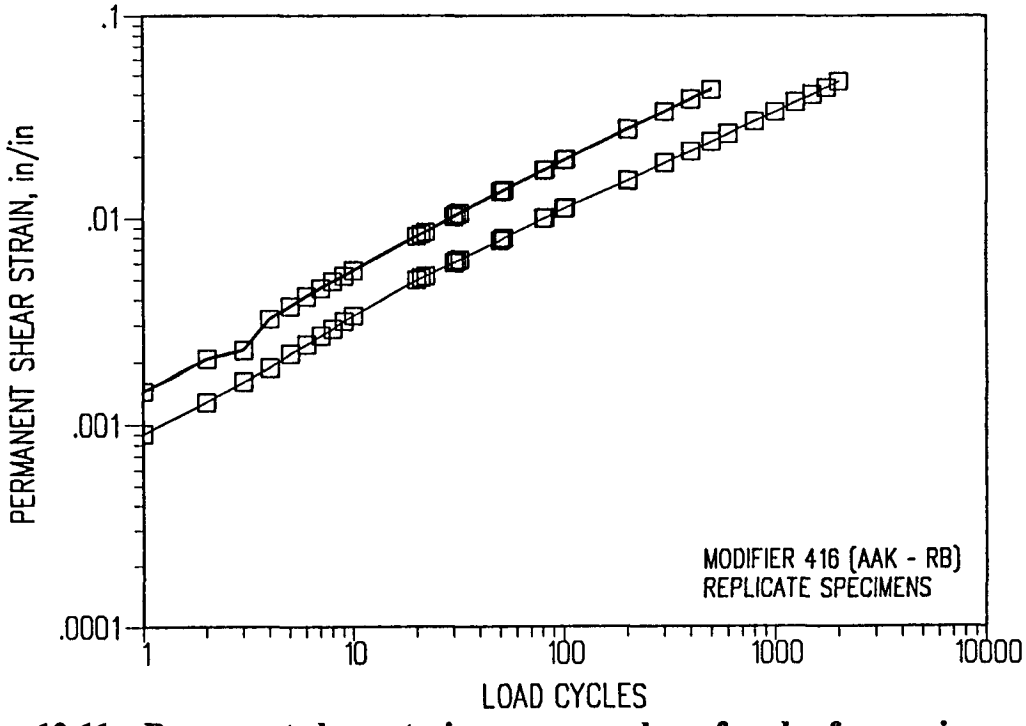

Figure 12.11. Permanent shear strain versus number of cycles for specimens with mix containing modifier 416, binder AAK and aggregate RB

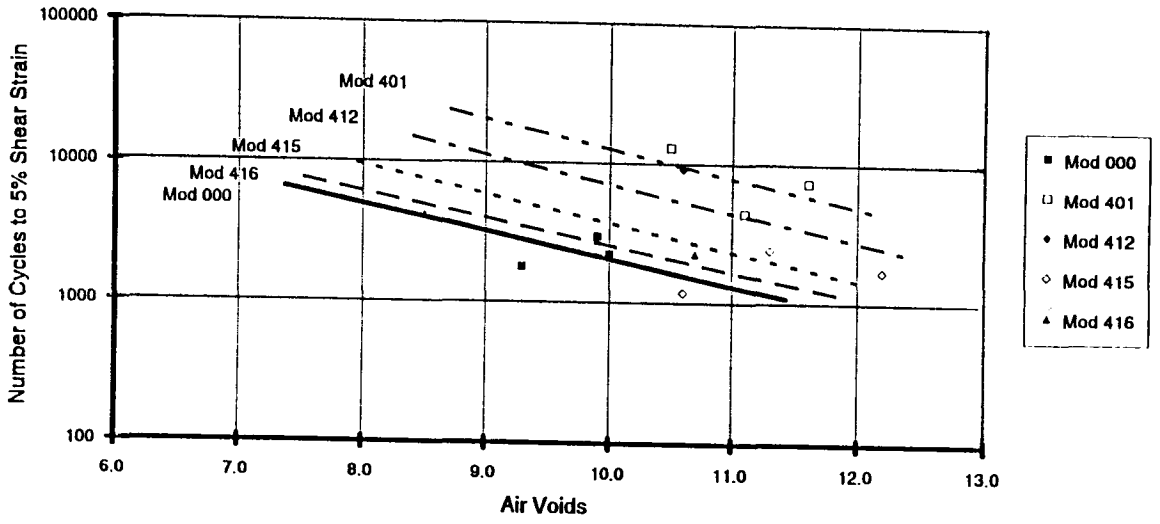

Figure 12.12. Estimated effect of binder on the number of cycles to reach 5 percent permanent shear strain (CHRSST @ 70 kPa [10 psi]) on mixes with asphalt AAG at 40°C (104°F)

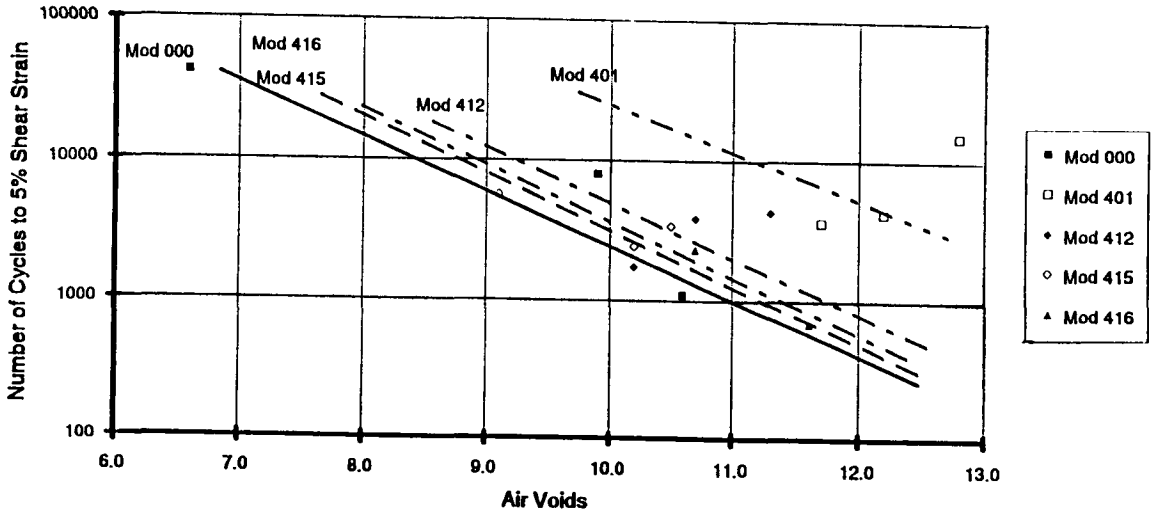

Figure 12.13. Estimated effect of binder on the number of cycles to reach 5 percent permanent shear strain (CHRSST @ 70 kPa [10 psi]) on mixes with asphalt AAK at 40°C (104°F)

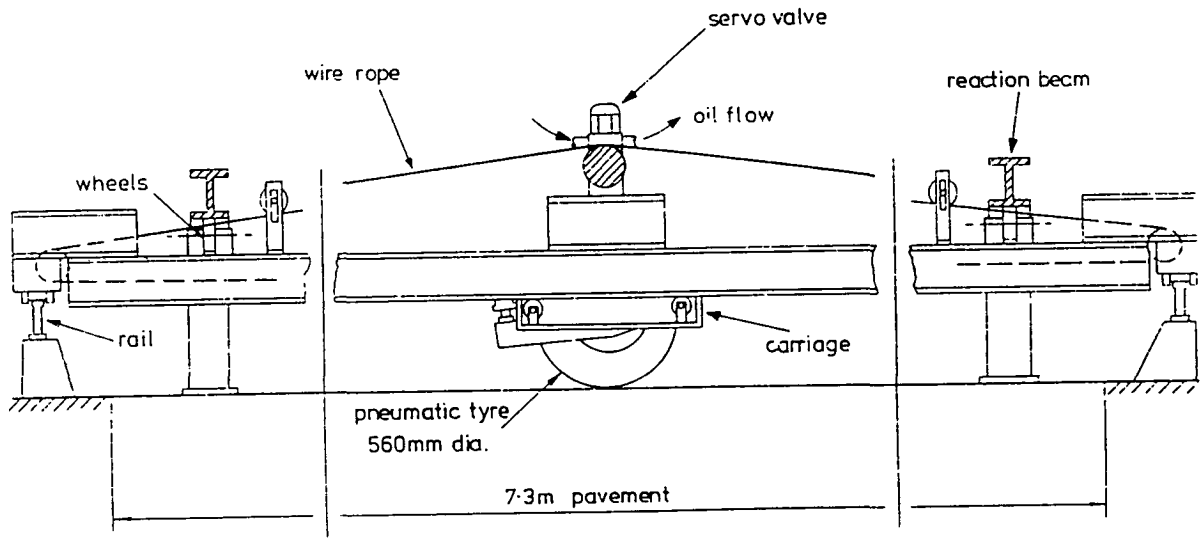

Figure 12.14. Side view of pavement testing facility

Table 12.4. Final rut depths — pavement test facility test sections

Section	Rut Depth at 50,000 Passes (mm)		
	Profile 1	Profile 2	Profile 3
Tuff/100 pen.	15	19	16
Tuff/100 pen. + SBR	5	3	4
Gravel/100 pen.	12	14	18
Gravel/100 pen. + SBR	4	5	5

12.3 Summary

The results indicated that modification of asphalt with various additives has the potential to improve the permanent deformation resistance of asphalt aggregate mixes. This is illustrated by the results of both simple shear tests and the wheel-tracking tests performed at the University of Nottingham in its pavement test facility. However, the results of the simple shear tests reveal that, for a given asphalt, not all modifiers are equally effective in improving permanent deformation resistance and that the influence of a specific modifier is asphalt dependent. Thus, it is important to evaluate a particular asphalt/modifier combination with the specific aggregate to ascertain whether the modified binder will improve the permanent deformation resistance of a mix.

It is likely that the environment, as measured by *critical temperature*, will also have an influence since some modified binders may perform well in one temperature range but no better than the unmodified asphalt in another. While this latter point was not investigated herein, since all permanent deformation testing was performed at a specific temperature — 40°C (104°F) for the simple shear tests and 30°C (86°F) for the pavement test facility program — other investigations (e.g., Harvey et al. 1994) have suggested that temperature must be considered as well. Fortunately, the simple shear test provides a useful tool to examine the effects of temperature on mix performance for a specific asphalt/modifier aggregate mix.

13

Mix Design Considerations

The constant height repeated load simple shear test provides a methodology for mix design whereby mix proportions can be selected so that the resulting rut depth will not exceed some prescribed maximum value (e.g., 1.25 cm [0.5 in.]) for a specific level of traffic.

The basis for the procedure has been described in preceding chapters. The general approach will be described, illustrated by a test program on one mix containing a conventional asphalt and aggregate. Also discussed are procedures to allow evaluation of the effects of aging and water on permanent deformation response.

13.1 Materials

Mixes containing aggregate RB and asphalt AAG-1 were prepared at binder contents of 4.5, 4.9, 5.5, and 6.0 percent (by weight of aggregate). Rolling wheel compaction (Harvey 1991) was used to prepare slabs from which specimens 10 cm (4 in.) in diameter[13] and 5 cm (2 in.) high were obtained by coring and sawing. Prior to compaction the mixes were subjected to short-term aging (loose mix, 4 hours at 135°C [275°F]).

Target air void contents for the slabs for the mixes were set at 2 to 4.5 percent, 5 to 7 percent, and 8 to 10 percent (based on measurements using parafilm). The results described in Chapter 10 for reliability considerations are the same as used herein.

13.2 Test Procedure

Resistance to permanent deformation at 50°C (122°F) was measured by means of the constant height repeated load simple shear test. A shear stress of 50 kPa (7 psi) was used;

[13]At the time this study was conducted the simple shear device permitting testing of 15 cm (6 in.) diameter specimens had not been completed.

load was applied for 0.1 s with a time interval between load applications of 0.5 s. The number of repetitions corresponding to a permanent shear strain of 5 percent was obtained for each of the specimens. Examples of the variation of permanent shear strain with load repetitions are shown in Figure 13.1.

13.3 Test Results

Test results are summarized in Table 13.1 and plotted in Figure 13.2. It will be noted that the number of cycles to 5 percent strain increases as the air void content decreases for each mix at a specific asphalt content. However, in this instance, when the air void content in reduced below about 3 percent, the number of cycles decreases, indicating a reduced resistance to permanent deformation development. This pattern of behavior is the same as observed in the results of Hveem stabilometer tests and various forms of axial loading tests in which stress versus strain properties are measured (e.g., Sousa et al. 1991).

13.4 Recommended Mix Design Procedures

Results like those presented in Table 13.1 and Figure 13.1, and information presented in Chapters 6, 9, 10, and 11, suggest the framework for a mix design procedure. However, rather than preparing specimens at a range in air void contents for simple shear testing, as was done herein, it is recommended that mixes covering a range in asphalt contents be prepared at an air void content of 3 percent ($\pm$0.3 percent). This recommendation is based on the argument that if the mix can sustain the traffic without deforming excessively at this air void content then the potential for being densified to lower air void contents is minimal.

From Figure 13.1 the number of cycles to 5 percent strain at an air void content of 3 percent can be interpolated and plotted as shown in Figure 13.2. The form of this curve is the same as that obtained from Hveem stabilometer tests. However, this curve is plotted at constant air void content, whereas the Hveem data reflect a change in both air void content and asphalt content. This difference is illustrated in Table 13.2 in which data taken from the initial mix design tests for aggregate RB and asphalt AAG-1 (Hicks 1988) are compared with the average values of air void contents for the data shown in Table 13.1 (and shown as shaded areas in the table).

The analyses presented in Chapter 6 illustrate a relationship between rut depth and maximum permanent shear strain and stated in a general form in Equation 6.35, i.e.,

$$\text{Rut depth} = k(\gamma_p)_{max} \tag{6.35}$$

For a value of k=10, $(\gamma_p)_{max}$ for a rut depth of 1.25 cm (0.5 in.) would be 0.05 or 5 percent. This then defines the level of shear strain in the simple shear test at which the number of cycles that a particular mix exhibits when tested at a fixed shear stress and at the critical temperature, T_c, would be selected, and is termed N_{supply}.

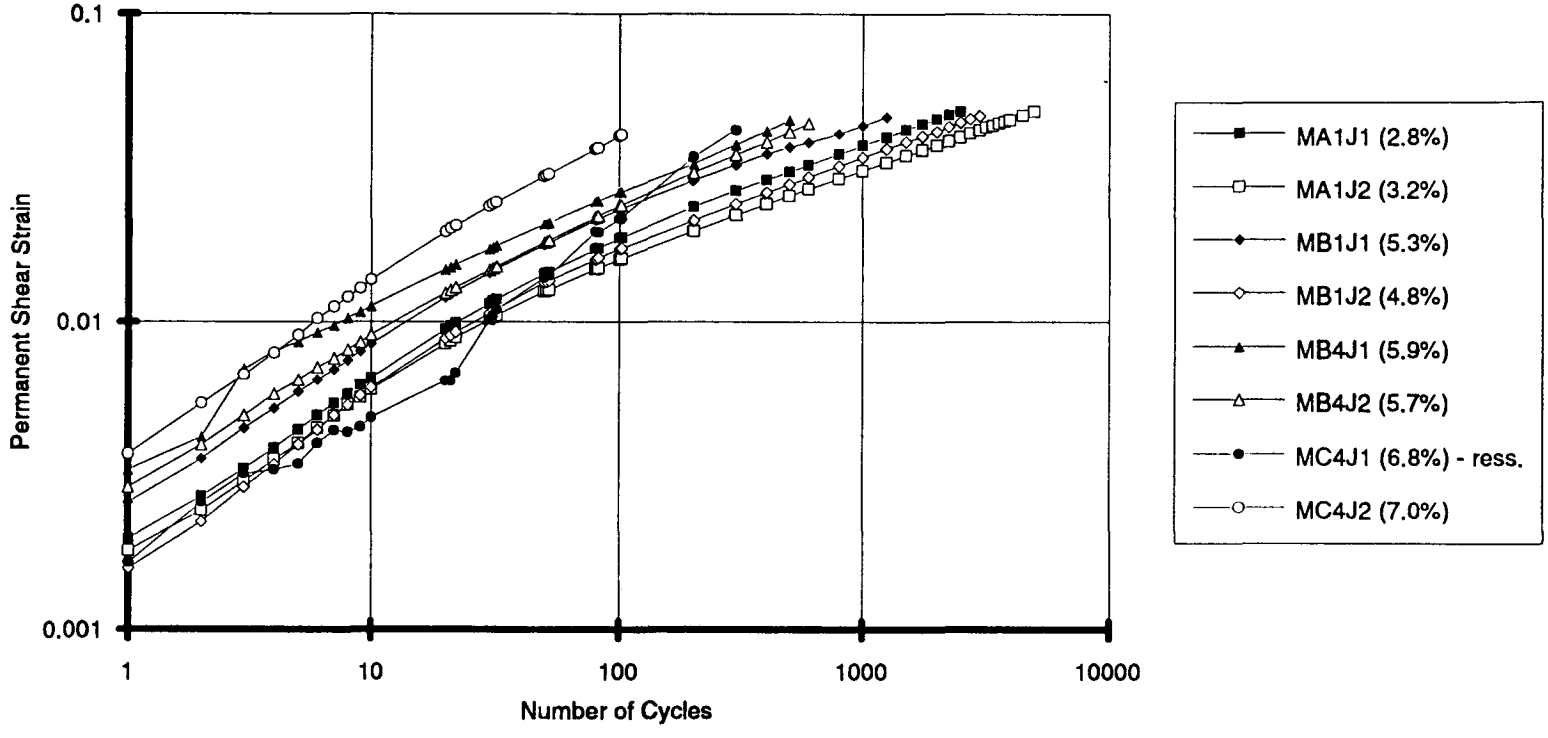

Figure 13.1. Permanent shear strain versus stress repetitions for mixes containing aggregate RB and asphalt AAG-1; tests performed at 50°C (122°F)

Table 13.1. Experimental test data

Asphalt Content (Percent)	Air-Void Content (Percent)	Cycles to 5 Percent Strain
4.5	2.8	2722
	3.2	3598
	4.8	3798
	5.3	1872
	6.0	258
	6.9	1868
	7.1	723
4.9	2.8	1595
	3.0	3979
	4.9	3067
	6.0	671
	6.1	754
	7.1	1580
	7.2	432
	7.5	369
5.5	3.3	2366
	3.7	1900
	3.7	1936
	4.2	1960
	5.5	279
	5.5	422
	7.1	1967
	8.7	812
6.0	1.8	505
	2.5	829
	3.0	468
	5.7	884
	5.9	661
	6.1	152
	6.8	419
	7.0	164

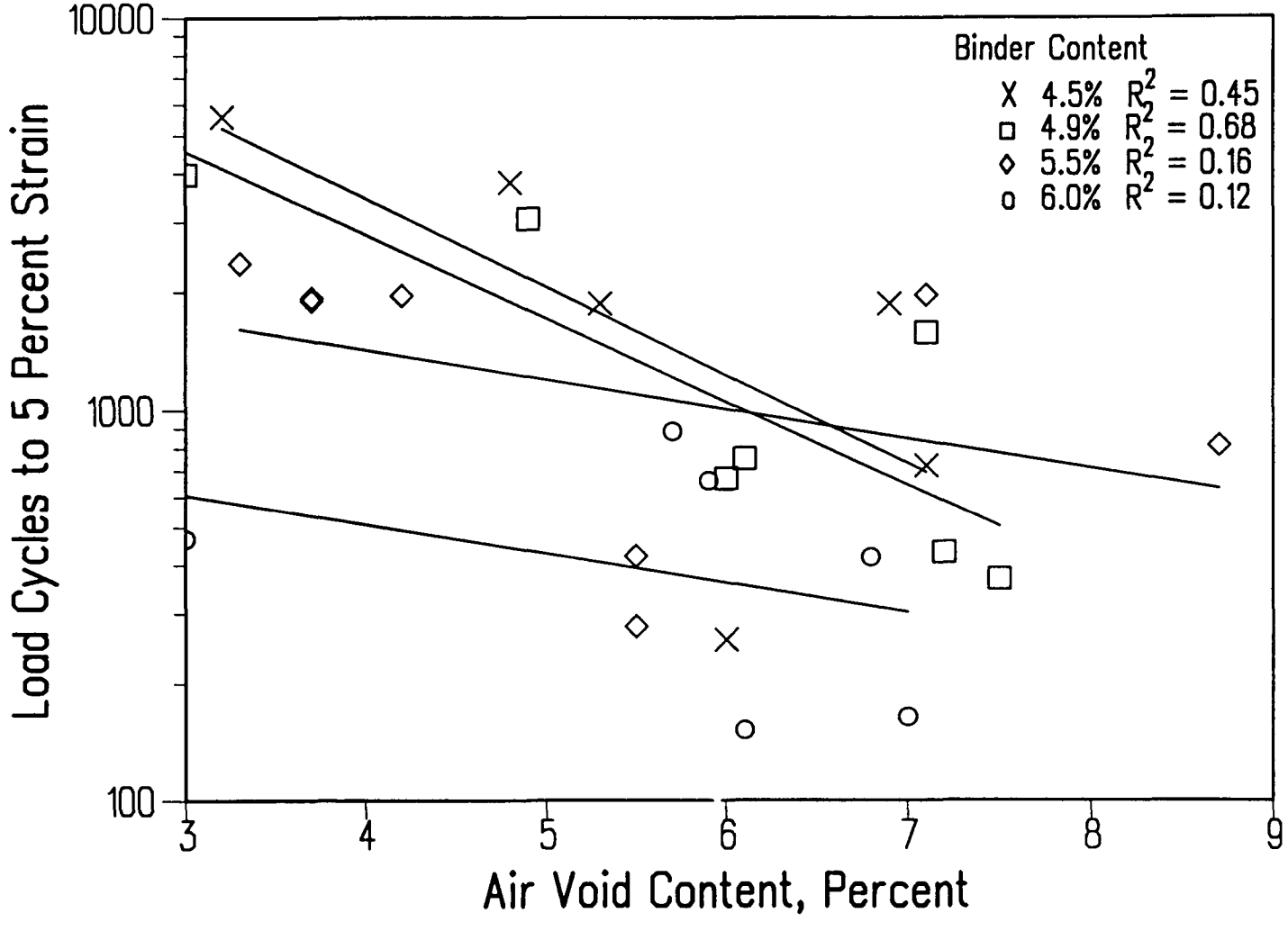

Figure 13.2. Relationships between asphalt content, air void content, and cycles to 5 percent permanent shear in constant height repeated load simple shear test

Table 13.2. Range of asphalt and air void contents examined for mix design purposes

Target Air Void Content (Table 13.1)	Asphalt Content	Void Content								
		4.25	4.50	4.75	4.90	5.25.	5.50	5.75	6.00	6.25
0 — 2.5										2.4
2.5 — 4.0			b					3.3		
4.0 — 5.0						4.7				
5.0 — 6.0				5.0						
6.0 — 7.0										
7.0 — 9.0		7.4[a]								

[a]Numbers are measured values for Hveem stabilometer specimens prepared by kneading compaction (Hicks 1988).
[b]Boxed areas indicate average values for specimens prepared by rolling wheel compaction and tested in the simple shear test.

To define which mix is suitable for the traffic, it is necessary to convert the estimated traffic, e.g., expressed in equivalent single axle loads (ESALs), to its equivalent at the critical temperature (Chapter 9) and to use a shift factor to relate the traffic to equivalent laboratory repetitions in the simple shear test, termed N_{demand}.

Referring to Table 9.7, a mean temperature conversion factor of 0.1158 (which permits the design ESALs to be converted to those at the critical temperature) has been determined for the nine Federal Highway Administration (FHWA) regions. In the example presented herein, mixes had been tested at a temperature of 50°C (122°F), a temperature above the values for the critical temperatures shown in Table 6.7. Accordingly, a temperature conversion factor of 0.04, (based on analysis performed like that shown in Chapter 9) has been used. In addition, an average shift factor of 0.04 has been selected (this based on an analysis of pavements tested at temperatures corresponding to the average maximum high 7-day temperature at a 5 cm [2 in.] depth for each of the sites investigated [Chapter 11]).

For a mix to sustain 1×10^6 ESALs the corresponding N for the simple shear test at 5 percent shear strain (N_{demand}) should be:

$$1 \times 10^6 \times 0.04 \times 0.04 = 1{,}600 \text{ repetitions}$$

For this example, it might be assumed that this corresponds to a reliability level of 50 percent. To determine the requirements for the laboratory mix, N_{supply}, (Chapter 10),

$$N_{supply} \geq M \cdot N_{demand} \qquad (10.1)$$

where, as noted earlier, M is reliability multiplier (greater than 1). From Table 10.3 for a variance in $Ln(N_{demand})$ of 0.2 and for tests on four specimens, the value of M equals 2.270 for a reliability of 80 percent that the rut depth should not exceed 0.5 in. Thus, the asphalt content should be selected at a value of $N_{5\%} \approx 3600$ repetitions from Figure 13.3; this corresponds to a value of 5.2 percent. Allowing 0.3 percent for variation in production suggests that an asphalt content of 4.9 $\pm$ 0.3 percent would be reasonable for this mix. Referring to the report by Hicks et al. (1989), this value corresponds to that used for this mix in the initial studies for evaluating mix performance in the A-003A program.

It is likely that this mix would sustain a larger number of load repetitions to a rut depth of 1.25 cm (0.5 in.) because the analysis is based on mixes that have been subjected only to short-term aging. Figure 13.4 illustrates the comparative performance of short-term and long-term aging on mix performance. There is almost one order of magnitude difference in the number of load repetitions to reach 5 percent strain for the long-term versus the short-term aged specimen. Thus, by performing constant height repeated load simple shear tests on specimens subjected to long-term aging as well as on specimens subjected to short-term aging, improved estimates of the amount of rutting which might develop will be obtained. The development of permanent shear strain corresponding to an in-service mix is hypothesized in Figure 13.5. From the information presented in this figure it is apparent that one could bound the actual amount of permanent deformation that might be anticipated in situ.

13.4.1 Effects of Water

Water may increase the propensity of a mix for permanent deformation. The effects of water may be considered in the initial mix design phase or as a part of the mix evaluation process as described herein.

It is possible to subject specimens to a water conditioning process like that developed at Oregon State University as a part of the water sensitivity studies associated with the A-003A project (Terrel et al. 1993). Results of simple shear tests performed on mixes prior to and after water conditioning are shown in Figure 13.6. The propensity for rutting in both mixes increases significantly if the mixes are subjected to sustained water saturation. With these data the increase in rutting that might occur in situ can be estimated using the procedure described earlier.

13.5 Summary

The constant height repeated load simple shear test, when used as discussed in this chapter, provides a basis for mix design that is site specific (both in terms of pavement temperature and traffic) and that permits a mix to be selected so that the amount of rutting will not exceed a prescribed amount — to a predetermined level of reliability (e.g., 80 percent).

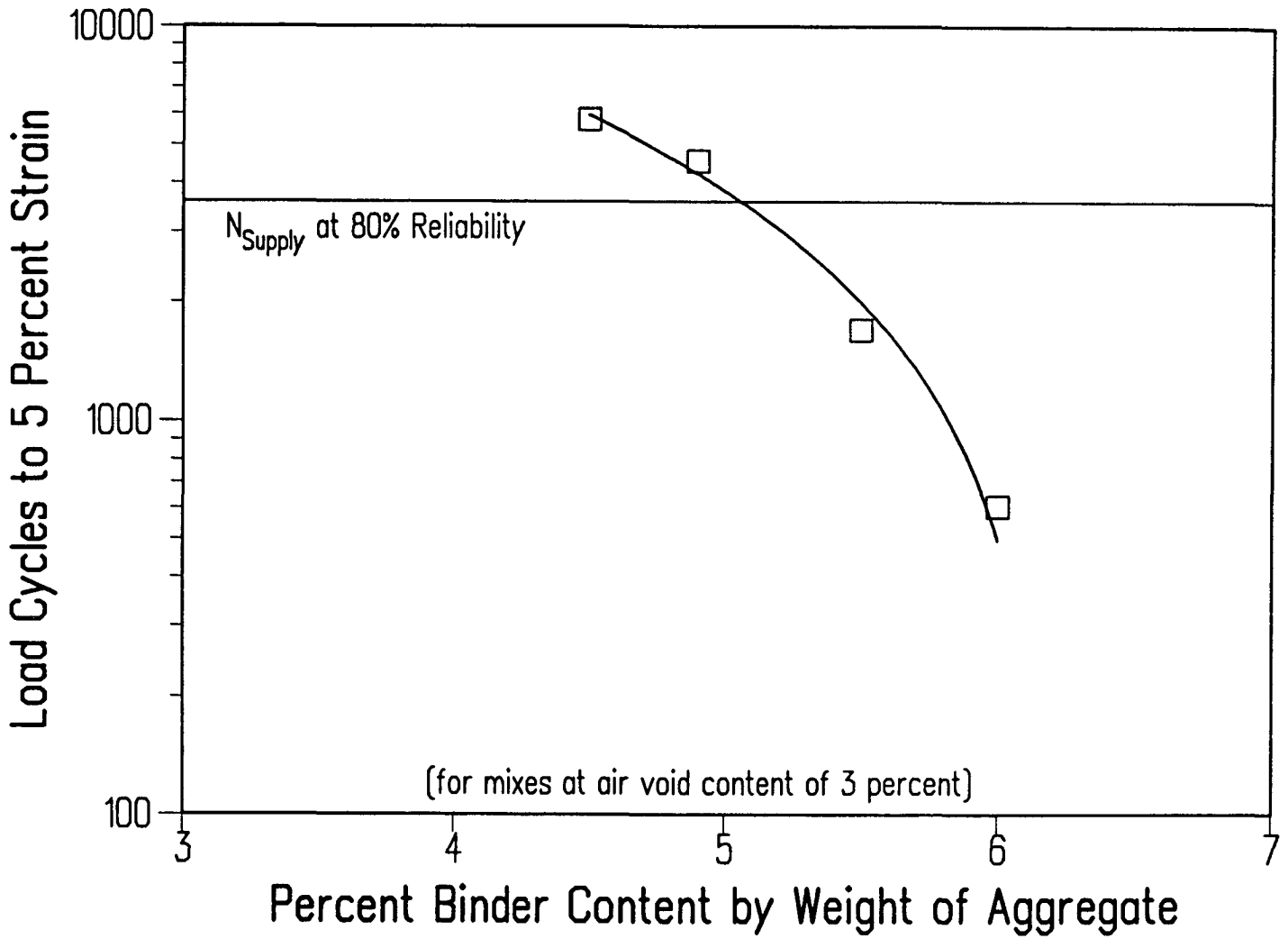

Figure 13.3. Asphalt content versus cycles to 5 percent permanent shear strain for mixes containing an air void content of 3 percent

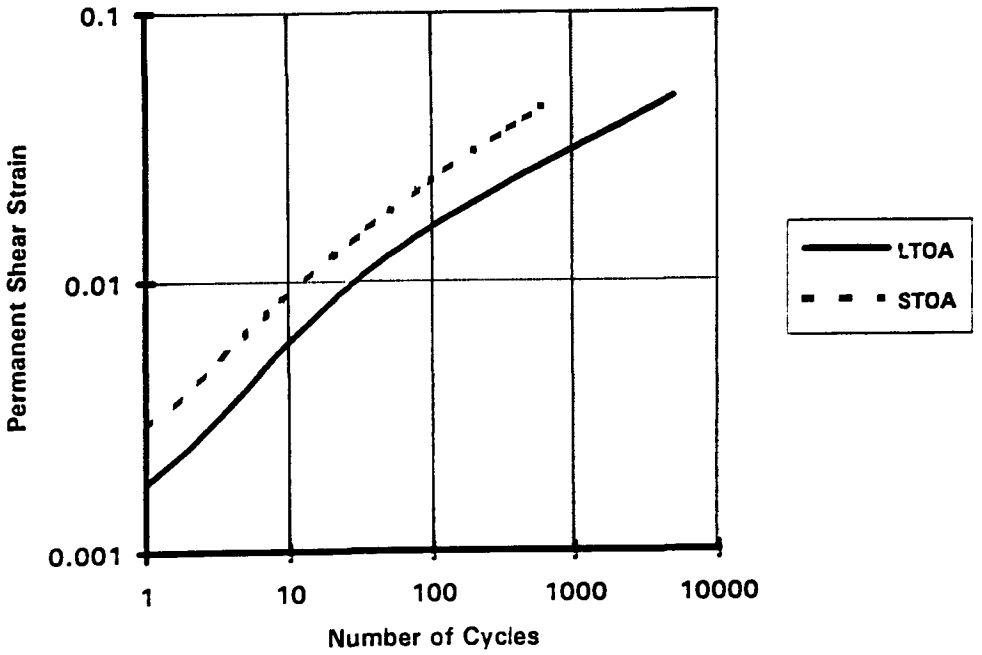

Figure 13.4. Estimated variation of permanent shear strain in constant height, repeated load, simple shear tests on specimens of the same mix subjected to short-term and long-term aging

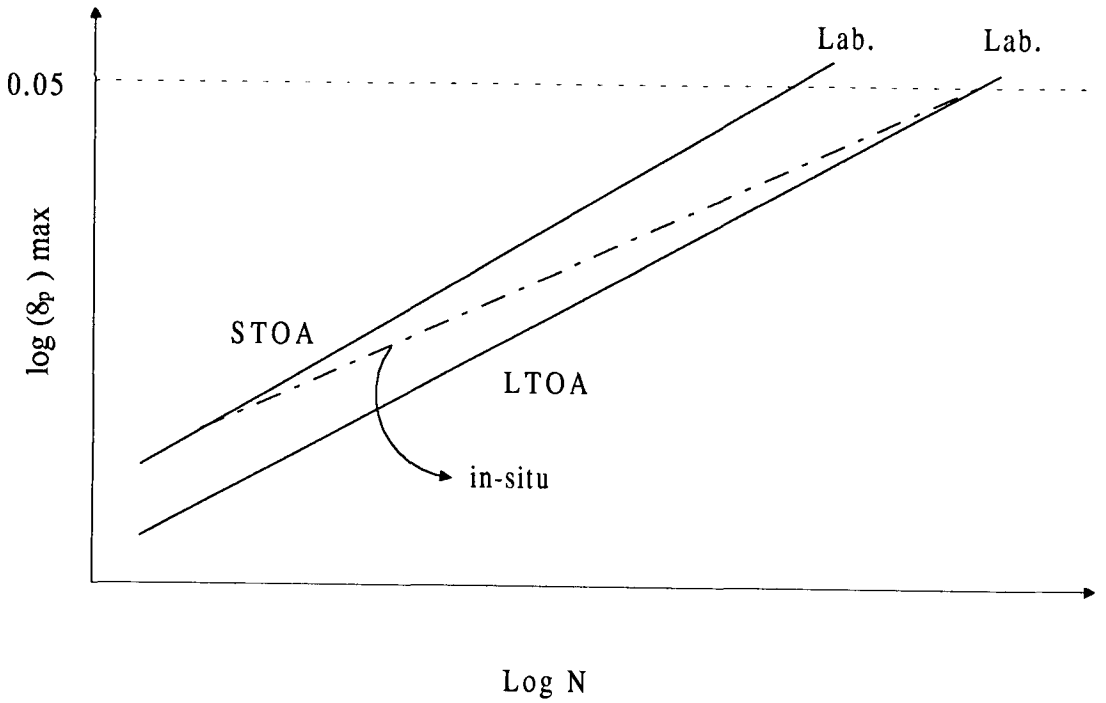

Figure 13.5. Hypothetical permanent deformation performance in situ considering the effects of aging

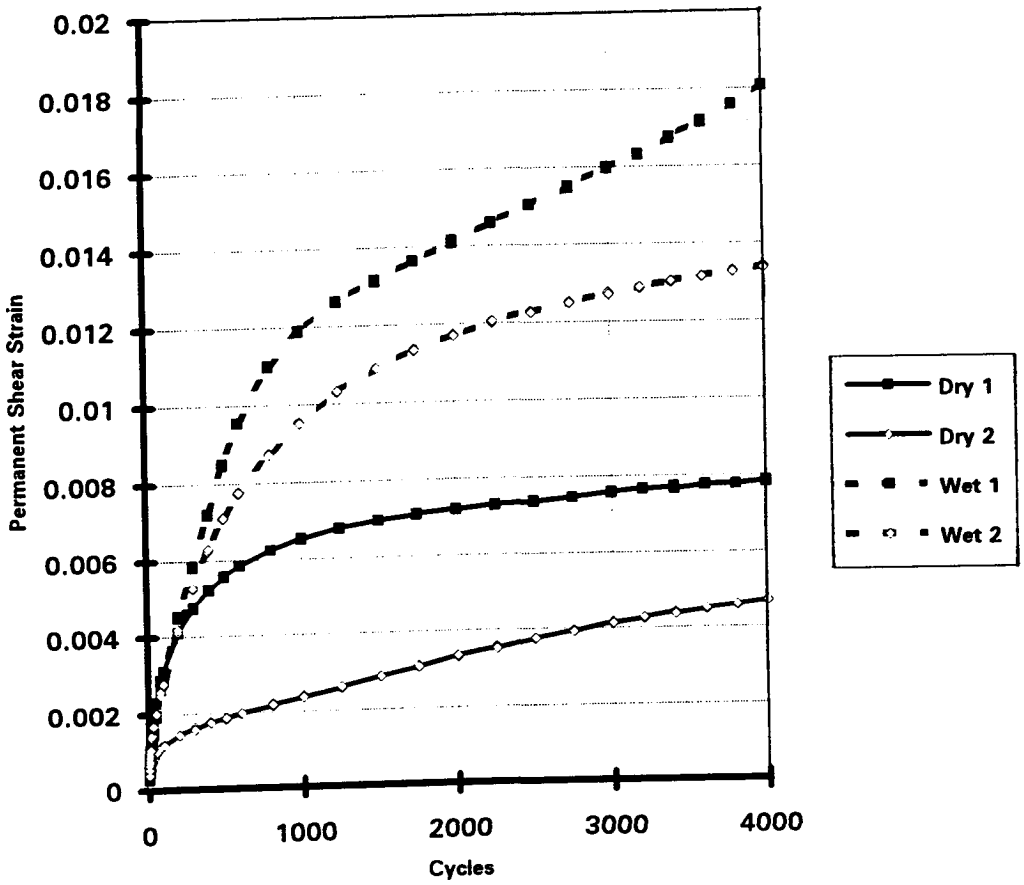

Figure 13.6. Comparison of the variation of permanent shear strain on specimens of the same mix subjected to the ECS water conditioning protocol (wet and not dry)

The process consists of compacting mixes of a specific asphalt/binder and aggregate to an air void content of about 3 percent (i.e., within prescribed limits of this value) over a range in binder contents by rolling wheel compaction and performing the constant height, repeated load, simple shear test at the critical temperature for the site in question. Selection of the design asphalt content is then accomplished by selecting the highest asphalt/binder content which permits the design traffic estimate to be carried. This procedure will be detailed in Part III of this report.

14

Summary and Recommendations

This report has described the development of the simple shear test and its potential application in mix analysis and design. In addition, the use of the test to validate a permanent deformation requirement in the Strategic Highway Research Program (SHRP) binder specification has been presented.

The simple shear test described herein permits simultaneous application of shear and axial loads to cylindrical specimens 15 or 20 cm (6 or 8 in.) in diameter and 5 or 7.5 cm (2 or 3 in.) high respectively. (Square specimens could also be tested.) Confining pressures of up to 690 kPa (100 psi) can be applied over a temperature range of -10 to +70°C (14 to 158°F). Both shear and axial loads can be applied sinusoidally, repetitively, or sustained (creep loading). For sinusoidal loading, frequencies in the range 0.01 to 20 Hz (approximately three decades) are feasible. Repeated loads using a haversine pattern can be applied with a range in times of loading and time intervals between loadings (rest periods). Shear stresses are transmitted to the specimen through end caps that have been bonded to it using an epoxy resin.

A simpler version of the equipment has also been developed. This equipment permits testing only in the upper temperature range. It has the advantage, however, that it could be used in the field as a construction control test since cores from as-constructed pavements could be tested under prescribed conditions at paving sites. Both sets of equipment permit testing of conventional dense-graded mixes, open-graded mixes, gap-graded (SMA) mixes, and large-stone (up to 3.8 cm [1.5 in.] maximum size) mixes.

With the simple shear equipment, test methodologies have been developed that permit definition of important mix characteristics necessary to define the propensity of a specific mix for permanent deformation, including (1) dilation under shear load; (2) increase in stiffness with increase in hydrostatic pressure at higher temperatures; (3) temperature and rate of loading dependence; (4) residual permanent deformation development with unloading; and (5) difference in response in creep and repeated loading.

To ensure that the test reflects mix response representative of in situ conditions, proper compaction of laboratory specimens is required. While the evidence is not exhaustive, the A-003A team recommends, based on available information, that specimens for permanent deformation testing be cored (or sawed) from slabs prepared by rolling wheel compaction.

Two levels of testing have been recommended. For mix design purposes the constant height repeated load simple shear test would appear suitable. With this test, mixes can be selected that will ensure that the design traffic will not cause ruts exceeding a preselected level (e.g., 1.25 cm [0.5 in.]) with a prescribed level of reliability.

An alternative is the simple shear test in which a fixed ratio of normal-to-shear stress is maintained. Difficulties were experienced with deformation measurements in this test and time constraints precluded studies of improved deformation measuring techniques. Accordingly, this test was not studied to the same extent as the constant height test.

The second procedure, which permits the estimation of rut depth for some design traffic volume, requires the performance of a suite of tests at 40°C (104°F) including the following:

- Uniaxial strain test. A test in which the axial load is rapidly applied and the confining pressure necessary to maintain a constant diameter of the specimen is measured.

- Volumetric test. A test in which the specimen is subjected to a hydrostatic stress state and the associated volume change is determined.

- Simple shear constant height test. A test in which a shear stress is rapidly applied while maintaining the specimen at constant height and the corresponding shear strain is measured.

In addition, frequency sweeps in shear over a range in frequencies from 0.01 to 10 Hz are performed at 4°C, 20°C, and 40°C (39°F, 68°F, and 104°F) and possibly 60°C (140°F). The shear stress is adjusted to provide a shear strain of about 0.01 percent and an axial stress is applied to maintain constant height.

The data obtained from these tests are used to define the nonlinear elastic, viscous, and plastic parameters for the constitutive relationship to define mix response.

The three-dimensional constitutive relationship developed from the suite of tests includes (1) nonlinear elastic response to capture the effects of the aggregate structure at higher temperatures including dilation and stress stiffening; (2) plastic behavior; and (3) temperature and rate of loading dependency as expressed by linear viscoelasticity.

Results from solutions of representative pavement structures have provided a useful design relationship that relates maximum permanent shear strain in the asphalt aggregate mix $(\gamma_p)_{max}$ to the rut depth at the pavement surface, i.e.,

$$\text{Rut depth} = k\,(\gamma_p)_{max} \qquad (14.1)$$

As illustrated herein it is possible to use this relationship to select a limiting value of permanent shear strain in the constant height repeated load simple shear tests for mix design purposes.

While significant progress has been made in defining the permanent deformation response of asphalt aggregate mixes using the three-dimensional constitutive relationship noted above, a number of improvements are required. One is to represent better what happens during unloading. In Chapter 6 was been demonstrated that while the loading portion of the measured data is reasonably represented by the model, improvement in the unloading estimates is required.

Other changes include the following:

- modification of the elastoplastic component of the constitutive model to be based on multiplicative decomposition of the deformation gradient;
- replacement of the Kirchhoff elasticity by a compressible Neo-Hook model in the viscoelastic component of the model;
- incorporation of plastic deformation in the volume change component to reflect reduction in air void content (compaction) by traffic; and
- incorporation of the modified constitutive model in finite deformation elements (two- and three-dimensional).

Work is also required to define material response in tension as well as in compression. Moreover, to ensure that the development of damage with load repetition is defined, a failure envelope is required. One such hypothesis is illustrated in Figure 14.1. In this instance the failure envelope is defined in the I_1 - J_2 plane, where I_1 is the first invariant of the strain tensor (indicates the change in volume) and J_2 is the second invariant of the strain deviator (indicates amount of distortion). The expected shape such a failure envelope would take is presented in Figure 14.1.

The shape presented in Figure 14.1 is motivated by the following:

- Asphalt concrete mixes perform better in compression (volume loss); hence, the area to the left of the J_2 axis is substantially larger that the area to the right of the J_2 axis.
- The resistance of asphalt concrete mixes to deviatoric stresses is known to rapidly deteriorate when the voids in the aggregate structure are essentially filled with asphalt; hence, the almost vertical boundary on the left side.
- The inter-particle friction is increased by deviatoric stresses; hence, greater volume increase is allowed on the right side when deviatoric stresses are present.

One form that the testing program to define this envelope might take is illustrated in Figure 14.2.

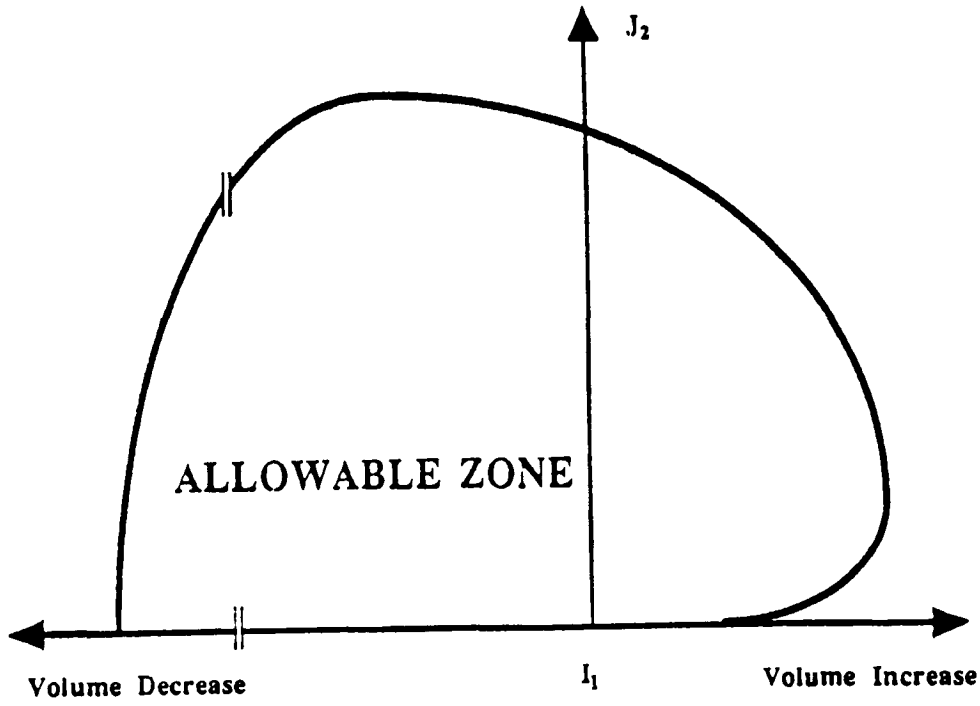

Figure 14.1. Estimated failure envelope shape

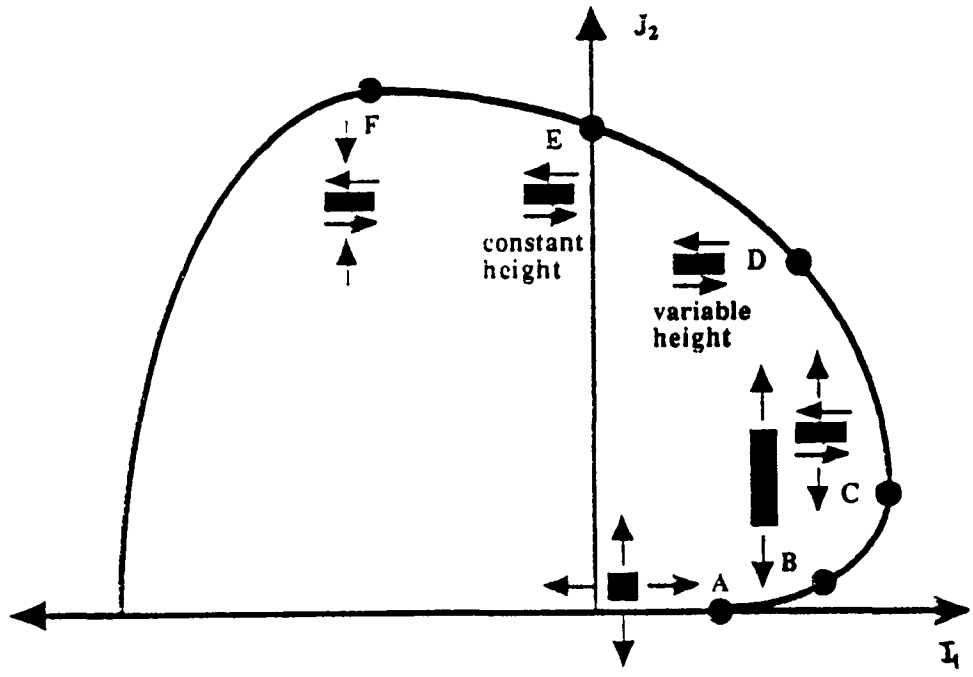

Figure 14.2. Recommended testing program

The validation testing for the SHRP binder specification indicated that binder properties can affect the permanent deformation response of asphalt aggregate mixes. However, aggregate characteristics can be equally or more significant. The results suggest that the influence of asphalt on permanent deformation response is dependent on the loading and environmental conditions to which the mix is subjected. The effect of the asphalt is comparatively small when the mix is subjected to states of stress which amplify the effects of the aggregate, e.g., the field states of stress (FS) shear test. However, in cases where mix characteristics are such that interparticle friction is low and the mix is subjected to harsh environmental and loading conditions (e.g., 60°C [140°F] and constant height [CH] shear test), the influence of the binder becomes more readily pronounced. When aggregate characteristics or compaction conditions are expected to result in a mix that is susceptible to permanent deformation, selection of a binder which can overcome these deficiencies will be important. Under these circumstances the value of $G^*/\sin\delta$ can be used to screen binders that will provide inferior performance.

From the favorable comparisons of data from the wheel-tracking and simple shear test program, it would appear that the constant height simple shear test is a suitable candidate for improved mix evaluation for design purposes.

The suitability of compound-loading simple shear tests for mix design and analysis was evaluated. Because of the variability in test measurements and relative insensitivity of the measured response to asphalt content, the tests are not considered suitable at the time for routine mix design purposes. However, because mixes are evaluated under different stress states, the compound-loading test does hold promise for mix design/analysis. *Accordingly, it is recommended that such an approach be further evaluated.*

The temperature equivalency concept has been introduced whereby a single temperature for a particular location can be defined for mix analysis and design purposes. It provides an effective way to account for both traffic and environmental effects. For conventional mixes, testing at a single temperature, the critical temperature, ensures optimum results. Temperature conversion factors, examples of which have been determined in this investigation, provide a simple, convenient way to convert traffic loading to its equivalent at a fixed temperature level permitting, in turn, direct comparisons between traffic loading in situ and single-temperature, repeated-load testing in the laboratory.

The temperature conversion factors presented are considered to be first-order approximations since they are based on a layer-strain approach. However, *when applied with care they provide an effective way to account for traffic and climatic effects in mix analysis and design.* It is recommended that the layer-strain analysis be replaced with a more accurate model of permanent deformation coupled with a range of appropriate laboratory test data to support its application, e.g., test data and analyses like those presented in Chapter 6.

Consideration has been given to reliability relative to the permanent deformation test. Initial reliability multipliers have been developed for measurements of variability in the constant height, repeated load, simple shear test. The coefficient of variation (CV) obtained from a limited test program is 90 percent (based on a mean square error of about 0.60). As experience is gained with the equivalent and improvements mode in the deformation

measuring systems, it is expected that this value of CV will be reduced. An example of this has already been demonstrated for the beam fatigue test program wherein CV was reduced from 90 percent for the earlier equipment to about 40 percent with the SHRP-developed beam fatigue unit.

Consideration has been given to relating anticipated traffic on the actual pavement to laboratory traffic estimates using a limited study of cores from selected General Pavement Studies (GPS) sections for which both rut depths and associated traffic were available. Results of this analysis suggest that a shift of about 0.04 is to be applied to the traffic expressed as repetitions at the critical temperature. Comparison with the repetitions corresponding to a preselected level of permanent shear strain (determined from the constant height, repeated load, simple shear test performed at the critical temperature) provide an indication of the suitability of the mix, i.e.,

$$N_{supply} \geq M \cdot N_{demand} \qquad (14.2)$$

where:

	M	=	reliability multiplier;
	N_{demand}	=	$SF(ESALs)_{Tc}$;
	SF	=	shift factor; and
	$(ESALs)_{Tc}$	=	estimated design traffic repetitions converted to repetitions at critical temperature.

While the results for shift factor developed from this study appear reasonable, it is recommended that additional analyses be made and the resulting factor (or factors) be validated through wheel-tracking and other forms of accelerated pavement testing. The effects of tire pressure should be included in this study.

A very limited study has been conducted of mixes containing modified binders. From the study presented herein it appears that the constant height, repeated load, simple shear test can be used to evaluate the permanent deformation response of mixes containing modified binders as well as mixes containing conventional asphalts. However, validation of this approach should be accomplished through wheel-tracking or other accelerated pavement testing.

Finally, the framework for a mix evaluation procedure has been suggested. A more detailed discussion will be presented in Part III of this report along with a specific example of the use of the methodology for a major project.

Part III — Mix Design and Analysis

J. A. Deacon
J. B. Sousa
S. L. Weissman
J. Coplantz
C. L. Monismith

15

Introduction

The primary objectives of Strategic Highway Research Program (SHRP) Project A-003A include development of a series of accelerated performance-related tests for asphalt aggregate mixes and methods for analyzing asphalt aggregate interactions that significantly affect pavement performance. Included within the scope of A-003A is consideration of permanent deformation (rutting), one of the major distress mechanisms affecting the performance of asphalt pavements. For permanent deformation evaluation, test methods use the simple shear test developed as a part of the A-003A program and described in Part II of this report.

Testing can be done at two different levels with the simple shear test equipment. At one level, the test program uses a suite of tests to permit an estimate of rutting to be made in a specific environment for an estimated level of traffic. At the other level, an estimate is made of the ability of the mix to carry the estimated traffic without exceeding a prescribed level of rutting. The latter level, termed Level 1 herein, includes considerations of reliability that reflect variabilities in both test results and traffic estimates.

The Level 1 procedure can also be used for mix design. When carried out for this purpose, the asphalt and aggregate that have been selected would be prepared with at least three asphalt contents and the resulting mixes compacted by rolling wheel compaction to an air void content of about 3 percent. This air void content provides, for a specific mix, a reasonable boundary between conditions above which the mix can carry the expected traffic with little permanent deformation and below which the potential for excessive rutting exists.

The method is dependent on a relationship between maximum permanent shear strain occurring in the asphalt concrete layer and rut depth developed from finite element analyses of a representative asphalt pavement structure. The mixes used to develop the relationship were those evaluated using the suite of tests, the results for which have been reported in Part II of this report.

In addition, two important new concepts are introduced in the Level 1 procedure, one pertaining to the test temperature and the other to the treatment of traffic. It is recommended that the tests be conducted at one temperature, termed the critical temperature. This

temperature is defined as the temperature at a 5 cm (2 in.) depth at which more rutting occurs than at other temperatures. Conversion of the design traffic level to its equivalent at the critical temperature through a temperature conversion factor then permits a comparison to be made between the results of the shear test and the applied traffic.

The purpose of this report is to describe in detail the permanent deformation analysis system that has been developed by the A-003A researchers. A discussion of general concepts, including an overview of the analysis system, immediately follows.

15.1 General Concepts

The analysis system proposed herein follows the same format as the mix design/analysis system for fatigue (Tayabali et al. 1994). That is, it is based on the premise that a trial mix has been identified, traffic and environmental conditions have been determined, and the pavement structural (cross) section has been designed. The analysis system permits determination of whether the trial mix will perform satisfactorily in service. Two alternatives are offered: (1) an estimate is made of the number of repetitions that the mix can sustain to a fixed level of rutting[14] or (2) a rut depth in the asphalt-bound layer is estimated for the prescribed conditions and compared to the tolerable level established for the site.

If the mix does not meet the requirements a number of alternatives are available. For the Level 1 procedure, the analysis can be repeated using more refined measurements (e.g., more tests to improve the reliability estimate). In both the Level 1 and Level 2 procedures, redesign of the mix can be considered. Mix redesign could include increasing the amount of crushed (rough textured) aggregate in the mix, using a more viscous grade of asphalt, using a modified binder rather than a conventional asphalt cement. The recommended approach can be summarized as follows:

(1) Determine design requirements for reliability and performance (permissible rut depth).

(2) Determine the expected distribution of in situ pavement temperatures.

(3) Estimate design traffic demand (equivalent single axle loads [ESALs]).

(4) Select trial pavement structural section.

(5) Select trial mix.

(6) Prepare test specimens and condition them as required.

---

[14]As noted earlier, this procedure can be extended to include mix design (binder content selection) as well. For this application, the binder content would be the maximum amount that could be used in the mix so that the expected rut depth will not exceed the design level for the anticipated traffic.

(7) Determine the resistance of the trial mix to permanent deformation using the cyclic shear test or the suite of tests required for rutting prediction.

(8) Apply factors to the traffic demand to account for differences between laboratory and in situ conditions and, as appropriate, to convert traffic loading to its equivalent at the laboratory test temperature.

(9) As appropriate, determine the amount of rutting associated with N_{demand}.

(10) If N_{demand} exceeds N_{supply} or the rut depth corresponding to N_{demand} exceeds the permissible rut depth, redesign the mix. It may be possible to improve the reliability of the traffic estimate to a specific level of rutting by testing more specimens or to determine a more reliable estimate of the amount of rutting for the specific traffic conditions by using the suite of tests.

Key features of this design and analysis system are described in the following sections.

15.1.1 Levels of Analysis

The proposed system recognizes that a range in testing requirements is desirable. For routine applications the testing need not be extensive. However, when unconventional mixes are used or more complex design applications are encountered, the extent of testing and analysis is increased.

Two levels have been stipulated.[15] The first level requires simple shear constant height repeated load testing at a single stress condition and a single temperature and uses the results of previously developed finite element analyses to ensure that the level of rutting will not exceed some prescribed value. The second level requires a suite of tests using the simple shear test equipment with shear stiffness measurements obtained at multiple temperatures.

15.1.2 Traffic Loading and Temperature Considerations

If the traffic is expressed in terms of ESALs per lane for structural pavement design purposes, this same measure can be used for mix design purposes as well. Development of permanent deformation in mixes is significantly affected by the magnitude of the tire contact pressure. Accordingly, an estimate of the range in tire pressures associated with the traffic must be known so that a representative tire (contact) pressure can be utilized to establish the conditions for mix evaluation.

For routine mix design, shear testing at a single temperature, termed the critical temperature, T_c, is recommended. Conversion of the design traffic level (expressed in terms of ESALs)

---

[15]In the systems for fatigue and thermal cracking three levels have been recommended. For permanent deformation, two levels of mix design and analysis are defined.

to its equivalent at the critical temperature is required. Predetermined temperature conversion factors (by climatic region) will likely suffice for this situation. For mixes of atypical temperature sensitivity, testing over a range in temperatures is desirable (until more experience is obtained), i.e., the use of the Level 2 procedure, since the temperature conversion factors have been developed for mixes containing conventional asphalts.

The critical temperature used is the temperature at highly stressed locations within the pavement structure; it has been defined as the temperature for a prescribed temporal distribution of traffic[16] at which more rutting occurs than at other temperatures. For rutting, the highly stressed locations occur in the upper portion of the asphalt (binder)-bound layer, i.e., in the upper 7.5 to 10 cm (3 to 4 in.) of the surface. More rutting occurs at the critical temperature because of both the frequency of its occurrence relative to traffic and the sensitivity of the mix to rutting at this temperature.

15.1.3 Reliability

The analysis system for Level 1 requires that the mix resistance to permanent deformation, termed N_{supply} (associated with a prescribed limiting rut depth), equal or exceed the traffic demand, N_{demand} (adjusted traffic estimate), which has been increased by an amount determined by the designer on the basis of a pre-selected level of reliability. The value of N_{demand} is increased by a reliability multiplier (M), the value of which increases with increasing design reliability and increasing variability of mix response and traffic demand estimates. Although reliability remains an important design consideration for the Level 2 analysis, specific recommendations for its treatment in such analyses have not yet been developed.

15.1.4 Mechanistic Analysis

In the procedure used for the Level 1 analysis the amount of rutting has been related to the maximum shear strain occurring in the upper part of the pavement layer; both parameters have been determined by a finite element analysis of a representative pavement structure using conventional asphalt aggregate mixes and selected values of tire contact pressure. The second level makes direct use of the finite element analyses methodology and measured mix characteristics, using the suite of tests to predict the amount of rutting for the site specific traffic and environmental conditions.

---

[16]A uniform traffic distribution has been assumed throughout the day and the year for the information presented herein.

15.1.5 Overview of Analysis Systems

Distinguishing characteristics of the permanent deformation analysis system are shown in Table 15.1. Simplified testing with the cyclic shear test distinguishes Level 1 from Level 2 which requires the complete characterization of mix response using the suite of tests described in Part II of this report. Figures 15.1 and 15.2 provide schematic frameworks for both systems.

Level 1 is expected to suffice for mixes of typical temperature sensitivity. Level 2 provides an optional procedure for other mixes, for investigative analyses, and for calibrating models such as used in the Level 1 analysis. Table 15.2 summarizes the recommended levels of permanent deformation testing and analysis for different types of mixes.

For most permanent deformation analyses (Level 1), the design traffic is expressed in terms of the number of ESALs in the critical lane during the pavement's design life, adjusted to its equivalent at the critical temperature, T_c. A shift factor, different from that used in fatigue analyses, must be applied to the traffic estimate to enable direct comparison between the traffic estimate and laboratory measurements. The shift factor attempts to account for differences in stress states, loading conditions, traffic wander, etc. The end result of the traffic analysis is an estimate of traffic demand (N_{demand}) that is commensurate with laboratory permanent deformation measurements.

Mix resistance to permanent deformation distress (N_{supply}) is determined from measurements with the simple shear equipment using the cyclic shear test for Level 1. For Level 2 the amount of rutting associated with N_{demand} is calculated based on the results of the suite of tests and compared with the tolerable level selected for the rut depth for the specific pavement site.

15.2 Temperature Equivalency Factors

To simplify testing, ensure productivity, and reduce costs, permanent deformation testing for the Level 1 analysis is limited to a single temperature and the destructive effects of anticipated traffic in the field are expressed as equivalent ESALs at the single temperature.

The temperature equivalency factors presented build upon the AASHTO load-equivalency concept. The temperature-equivalency factor, TEF_i, is defined as the number of ESALs at the common temperature, T_c, that is equivalent in destructive effect to one ESAL applied at some other temperature, T_i. If $ESAL_i$ represents the number of ESALs anticipated when the temperature is T_i, then the product, $ESAL_i$ represents the number of ESALs anticipated when the temperature is T_i, then the product, $ESAL_i \times TEF_i$, would represent the equivalent effect of the loading at the common temperature, T_c. Therefore:

$$TEF_i \times ESAL_i = \text{Equivalent } ESAL_c \, . \qquad (15.1)$$

Table 15.1. Distinguishing characteristics of permanent deformation analysis system

Variables		Level 1	Level 2
		Abbreviated analysis with limited cyclic shear testing	Comprehensive analysis with full testing
Testing	Type	Cyclic shear	Constant height simple, shear, uniaxial strain, and volumetric tests at 40°C (104°F) with frequency sweeps at 4°, 20°, 40°, and 60°C (39°, 68°, 104°, 140°F)
	Temperature	Critical temperature, T_c	
In situ Conditions	Traffic	Equivalent ESALs at T_c, 85th percentile tire pressure	ESALs by temperature class, 85th percentile tire pressure
	Structure	Critical shear stress under "standard" load at T_c	Complete stress/strain pattern from finite element analysis
	Temperature	Frequency distribution at 5 cm (2 in.) depth	Frequency distribution throughout surface layer
Analysis	Mechanistic	Finite element analysis with nonlinear viscoelastic surface properties[a]	Finite element analysis with nonlinear viscoelastic surface properties
	Damage	Preanalysis (temperature equivalency factors for design ESALs)	Integral part of finite element analysis

[a]It is possible that sufficiently accurate results for shear stress may be determined using multi-layer elastic analysis as experience is developed.

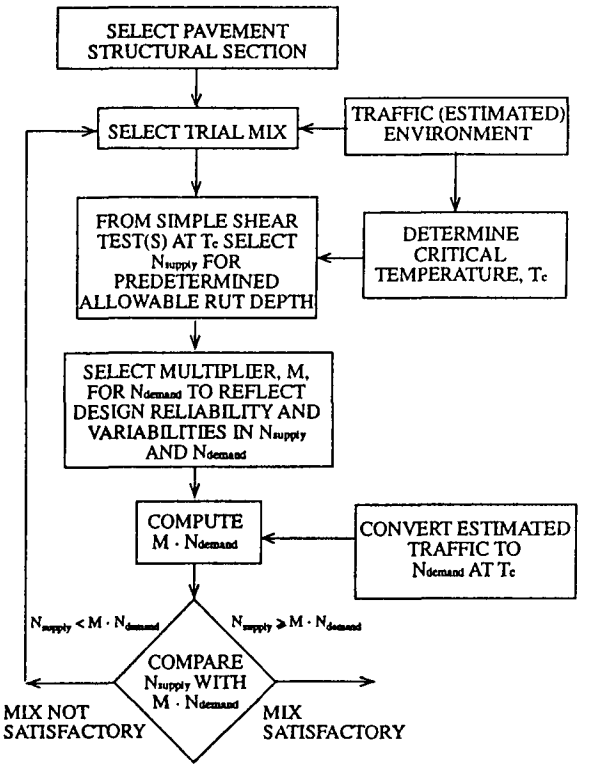

Figure 15.1. Routine mix analysis/design system

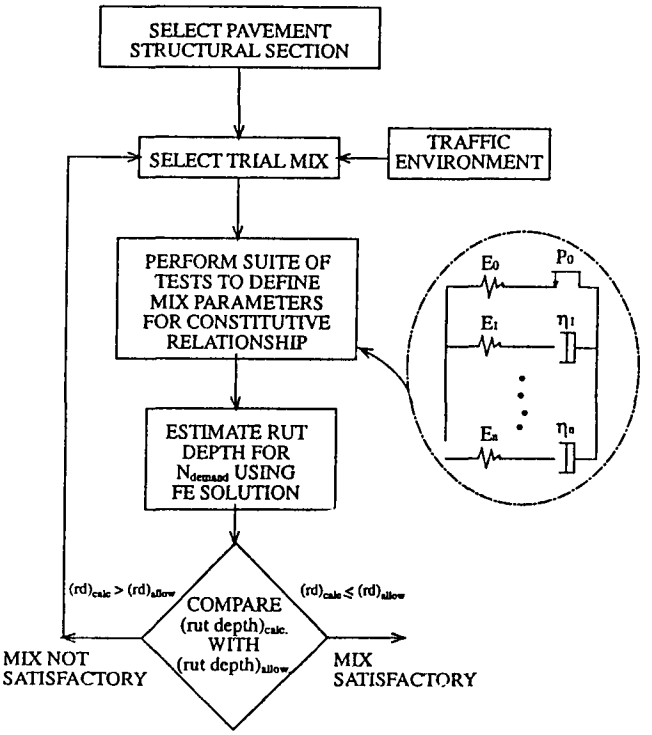

Figure 15.2. Comprehensive mix analysis/design system

Table 15.2. Recommended level of permanent deformation testing and analysis

Mix Characteristics	Level 1	Level 2
	Abbreviated analysis with limited cyclic shear testing	Comprehensive analysis with full testing
Dense graded mixes with conventional binders of typical temperature sensitivity	Recommended	Optional for investigative analyses and model calibrations
Unconventional mixes with binders of typical temperature sensitivity[1]	Recommended	Optional for investigative analyses and model calibrations
Mixes with binders of atypical temperature sensitivity[2]	Not applicable	Optional for investigative analyses and model calibrations

[1]Stone-mastic, open grade
[2]Mixes containing modified binders

alternatively,

$$TEF_i = [\text{Damage of ESAL}_c \text{ at } T_c]/[\text{Damage of ESAL}_i \text{ at } T_i]. \quad (15.2)$$

These factors have been developed for the nine climatic regions throughout the United States incorporated in the Federal Highway Administration (FHWA) program (Lytton et al. 1990) to determine environmental parameters for use in pavement analyses. Chapter 12, Part II, contains the details for the development of these factors.

Temperature-conversion factors (TCF), which convert repetitions of traffic (ESALs) to the equivalent number at the critical temperature, are shown in Table 15.3 for an 20 cm (8 in.) thick asphalt-bound layer. Their use is recommended in lieu of computations of combined frequency/temperature-equivalency factors because they yield identical results and are easier to apply since only a single multiplication is required:

$$\text{Equivalent ESALs}_{Tc} = \text{TCF} \times \text{Design ESALs} \quad (15.3)$$

in which Equivalent ESALs_{Tc} is the equivalent number of ESALs at the critical temperature, T_c, and Design ESALs represents the design traffic loading.

Also, as noted in Chapter 12, Part II, testing and analysis at multiple temperatures becomes necessary when evaluating mixes of atypical temperature sensitivity — that is, those for which standard temperature equivalency and conversion factors are not applicable — and is desirable for important paving projects demanding the utmost in accuracy. The objective of the testing would be to recalibrate the equations used to determine the factors. Following these recalibrations, temperature-equivalency and conversion factors would be determined by procedures such as those employed herein.

Table 15.3. Temperature conversion factors for permanent deformation (20 cm [8 in.] pavement)

Region	Temperature Conversion Factor	Percent Damage Within 5°C Range
IA	0.1262	70.2
IB	0.0993	69.8
IC	0.1517	74.2
IIA	0.1006	76.6
IIB	0.0707	67.8
IIC	0.1224	64.2
IIIA	0.1218	76.2
IIIB	0.1337	68.5
IIIC	0.1162	67.3
Mean	0.1158	70.5
Coefficient of Variation (%)	18.9	5.7

Testing temperatures should be carefully chosen so that they are compatible with the capabilities of laboratory test equipment and span the range within which much of the damage occurs in situ. Calculations reported in Chapter 12, Part II, and shown in Table 15.4 suggest that most of the damage occurs within a temperature range as small as 15°C (27°F). An even smaller range may eventually prove to be sufficient for permanent deformation. At the present, however, it appears that testing in the range of 30°C to 45°C (86°F to 113°F) is likely to be sufficient for the vast majority of locations within the continental United States.

Table 15.4. Extent of damage accumulation in suggested temperature ranges

Region	Percent Damage Within Indicated Temperature Range (30°C to 45°C [86°F to 113°F])
IA	89.6
IB	95.4
IC	89.3
IIA	91.3
IIB	97.4
IIC	92.3
IIIA	94.4
IIIB	78.7
IIIC	96.3
Mean	91.6

15.3 Reliability

Consideration of reliability offers the potential for assuming an acceptable level of risk in mix analysis/design without expensive overdesign. As used herein reliability refers to the probability that the mix will provide satisfactory performance during the design period; i.e., the amount of rutting will not exceed some prescribed value such as 1.25 cm [0.5 in.]. Reliability levels can be specified in the range of 60 to 95 percent, corresponding to risk levels of 40 to 5 percent respectively. Generally a lower level of risk means a higher mix cost or a reduction in the number of acceptable mixes available (including both binders and aggregates).

This analysis system requires that the mix resistance (N_{supply}) exceed the traffic demand (N_{demand}) by some factor that is based on reliability requirements. This condition can be expressed in the following form:

$$N_{supply} \geq M \bullet N_{demand} \tag{15.4}$$

where: M = reliability multiplier (greater than 1) whose magnitude is dependent upon the variability of (1) the estimated number of repetitions in the laboratory associated with a certain level of rutting in the pavement, and (2) the estimated traffic, and is also dependent upon the desired reliability of the design.

Equation 15.4 can also be written in logarithmic form:

$$\text{Ln}\,(N_{supply}) \geq \text{Ln}\,(N_{demand}) + \delta \tag{15.5}$$

where: δ = an increment (greater than 0) whose value is equal to Ln(M).

Limited data for the repeated load simple shear tests reported in Chapter 13, Part II, yield a mean square error of 0.602 for a range in binder contents. This permitted a determination of the standard deviation of $\text{Ln}(N_{supply})$ as shown in Table 15.5. Using these determinations, it was then possible to determine the reliability multiplier, M, as shown in Chapter 13, Part II.

These results are, for convenience, reproduced herein as Table 15.6.

15.4 Shift Factor

A shift factor must be applied to the traffic forecast to enable direct comparison between field and laboratory traffic estimates. This shift factor will account for traffic wander, construction variability, differences between laboratory and actual (field) states of stress and other factors.

Table 15.5. Standard deviation of prediction $Ln(N_{supply})$

Number of Specimens Tested	Standard Deviation of Predicted Ln (N_{supply})
1	1.095
2	0.949
4	0.866
8	0.822

Table 15.6. Reliability multipliers

Sample Size	Variance of $Ln(N_{demand})$	Reliability Multiplier			
		60 Percent Reliability (Z_R = 0.253)	80 Percent Reliability (Z_R = 0.841)	90 Percent Reliability (Z_R = 1.28)	95 Percent Reliability (Z_R = 1.64)
1	0.2	1.349	2.704	4.545	6.957
	0.4	1.377	2.896	5.046	7.955
	0.6	1.404	3.090	5.567	9.022
	1.0	1.455	3.480	6.673	11.381
2	0.2	1.304	2.416	3.830	5.587
	0.4	1.334	2.609	4.305	6.490
	0.6	1.363	2.802	4.797	7.456
	1.0	1.417	3.188	5.839	9.592
4	0.2	1.280	2.270	3.482	4.945
	0.4	1.312	2.464	2.946	5.805
	0.6	1.342	2.657	4.425	6.723
	1.0	1.397	3.042	5.437	8.754
8	0.2	1.267	2.197	3.313	4.640
	0.4	1.300	2.392	3.772	5.479
	0.6	1.331	2.585	4.245	6.375
	1.0	1.388	2.970	5.243	8.356

An initial development for a requisite shift factor was described in Chapter 14, Part II, of this report. It was indicated that when testing at the critical temperature the relationship between the number of repetitions in the constant height, repeated load, simple shear test (N_{demand}) and the number of ESALs at the critical temperature was as follows:

$$N_{demand} = 0.0461 \ ESALs_{Tc}^{0.924}. \quad (15.6)$$

The coefficient of determination for this expression is 0.51 and the variability is graphically demonstrated in Figure 15.3.

Because of the relative weakness in the regression equation and in the database from which is was derived, and because the exponent of $ESAL_{Tc}$ is so close to 1, a simple shift factor relating N_{demand} to $ESAL_{Tc}$ should *initially* suffice for mix-design purposes. It appears that a factor on the order of 0.04 might be an appropriate beginning point. Thus, to determine N_{demand} for mix design purposes, the traffic estimate (ESAL) is first converted to its equivalent at the critical temperature ($ESAL_{Tc}$) through use of the appropriate temperature conversion factor (Table 15.3). Then N_{demand} is simply the product of 0.04 and $ESAL_{Tc}$.

15.5 Abridged Analysis System

This abridged analysis system is that referred to as the Level 1 methodology briefly summarized in Table 15.1 and shown schematically in Figure 15.1. It is anticipated that this procedure would be used for the majority of situations in which mixes containing conventional binders would be used. It can be used to check the adequacy of a specific mix relative to rutting or to select an asphalt content for a mix so that some prescribed level of rutting is not exceeded.

This system has been developed using information determined by means of the Level 2 procedure, which treats the mix as a nonlinear viscoelastic, plastic material. Relationships between rut depth and permanent shear strain have been determined using a three-dimensional constitutive relationship for the asphalt mix and a finite element analysis. Steps in the analysis include the following:

(1) Determine design requirements for reliability and performance. The analysis system outlined permits the designer to select a specific level of reliability commensurate with the pavement site for which the mix will be utilized.

Performance requirements for permanent deformation generally call for the amount of rutting not to exceed some level, e.g., 1.02 to 1.25 cm (0.4 to 0.5 in.) in order to minimize the potential for hydroplaning.

(2) Determine expected distribution of in situ temperature. Pavement analysis in the abridged procedure requires that the mix be evaluated at the critical temperature, T_c.

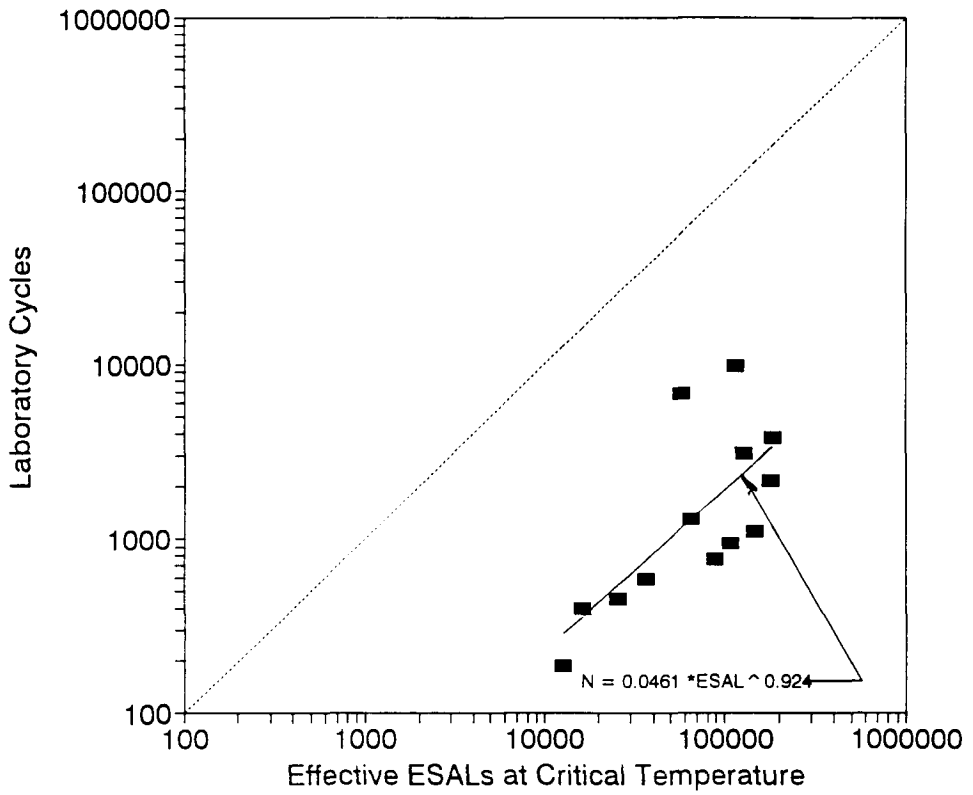

Figure 15.3. Relationship between laboratory cycles, N, and effective ESALs at critical temperature

For this mode of distress it is important to emphasize that temperatures in the upper range have a significant influence on the development of permanent deformation. Thus, if temperature data are available for a specific site in a region for which the critical temperature has been calculated using the FHWA model and if these data differ from the average for the region, then the site-specific critical temperature can be calculated following the procedure suggested herein so that the mix can be evaluated at this temperature rather than at the average for the region.

It is also important to emphasize that these computations need only be performed once for a specific region or subregion thereof.

(3) Estimate design traffic demand (ESALs). For this procedure it is necessary to estimate the number of ESALs at the critical temperature. Accordingly, temperature equivalency factors, or more simple temperature conversion factors, must be available to convert the actual number of ESALs to the equivalent number at T_c. These conversion factors need only be computed once for specific regions. Table 15.3 contains one set of such factors for the 9 FHWA regions of the U.S.

(4) Select trial mix. A trial mix with a binder and aggregate is selected. This might be done according to the SUPERPAVE™ methodology or by any procedure the responsible agency considers appropriate. Changes and redesigns are evaluated at the discretion of the design (materials) engineer.

(5) Prepare test specimens and condition as required. Cylindrical specimens 15 cm in diameter by 5 cm high (6 by 2 in.)[17] are obtained from slabs prepared by rolling wheel compaction in accordance with Harvey 1991. These specimens are cored and then sawed so that the end surfaces are smooth and parallel. The cut surfaces ensure that the specimens are comparatively uniform throughout as compared to specimens prepared in molds, which may have substantial density gradients both across their diameters and throughout their heights (e.g., Eriksen 1992).

Generally the specimens will have been subjected to the short-term oven aging procedure (Bell et al. 1994) to simulate the mix as it exists early in its constructed life. If desired, to define long-term effects, the mix could also be subjected to long-term aging (Bell et al. 1994). Moreover, if the effects of water on permanent deformation response are considered to be important, water conditioning can be accomplished using equipment and a procedure also developed as part of the A-003A contract (Terrel et al. 1993).

---

[17]For large stone mixes, 37.5 mm (1.5 in.) maximum aggregate size, 200 mm (8 in.) by 75 mm (3 in.) specimens are recommended for testing.

(6) Perform repeated load constant height simple shear tests. In the Level 1 procedure, repeated load constant height simple shear tests are performed at the critical temperature, T_c, for the specific site. At this time the recommended procedure is to use a shear stress of 70 kPa (10 psi) (associated with tire pressures of about 690 kPa [100 psi]) that is repeatedly applied for a duration of 0.1 s and a time interval between loadings of 0.6 s. The repeated loading is continued for 1 hour, permitting the specimen to be subjected to a total of about 5000 stress repetitions.

(7) Determine the resistance of the trial mix to permanent deformation. From finite element analyses it has been determined that there exists a reasonably constant ratio between the maximum shear strain obtained in representative asphalt-bound layers and the permanent shear strain obtained in the constant height simple shear test for the 690 kPa (100 psi) tire loading condition (Chapter 9, Part II). The ratio is of the order of 10 to 11. That is, a rut depth of 1.25 cm (0.5 in.) would correspond to a shear strain of about 5 percent (0.05).

Thus to develop N_{supply} for the given mix, the maximum shear strain is selected from the relation:

$$\text{Rut depth} = 10 \text{ (or } 11) \cdot (\gamma_p)_{max} \tag{15.7}$$

It is likely that this relationship between maximum shear strain and rut depth will be somewhat dependent on the structural pavement section; that is, there may be a different conversion factor for a 10 cm (4 in.) asphalt concrete overlay on a portland cement concrete pavement as compared to a comparatively thick asphalt concrete layer for which the factor shown above had been determined.

(8) Apply a shift factor to the traffic demand (ESALs). The design traffic volume, i.e., the laboratory-equivalent repetitions of the standard load, N_{demand}, is determined from:

$$N_{demand} = ESALs_{Tc} \cdot SF \tag{15.8}$$

where: $ESALs_{Tc}$ = design ESALs adjusted to the critical temperature, T_c; and
SF = empirically determined shift factor.

At this time, it is recommended that a shift factor of 0.04 be used. This shift factor, as noted earlier, was determined from analyses of a limited number of General Pavement Studies (GPS) test sites.

(9) Compare traffic demand (N_{demand}) with mix resistance (N_{supply}). Satisfactory performance requires that the mix resistance (N_{supply}) equal or exceed the traffic demand (N_{demand}). As with fatigue, a multiplier, M, should be applied

to N_{demand} since neither N_{supply} nor N_{demand} is known with certainty. This factor permits the incorporation of some level of design reliability, as well. For a mix to be satisfactory:

$$N_{supply} \geq M \bullet N_{demand} \tag{15.4}$$

where: M = multiplier whose value depends on the design reliability and on the variabilities of the estimates of N_{supply} and N_{demand}.

Determinations have been made for the variance of $Ln(N_{supply})$ as a function of the number of specimens tested and traffic level. In addition, values for M, depending on both the variance in the sample size and $Ln(N_{demand})$, for reliabilities varying from 60 to 95 percent have also been computed as shown earlier, Table 15.6.

(10) If inadequate, alter trial mix and iterate. If the particular mix is determined to be inadequate a number of alternatives are available to the designer; adjust the asphalt content, adjust the aggregate gradation, use a modified binder, select another aggregate source, or use combinations of the above.

15.6 Mix Design Using Level 1 Methodology

The Level 1 methodology can be used as a mix-design procedure to select the initial binder content. Mixes can be prepared over a range in binder contents by rolling wheel compaction to an air void content of about 3 percent. For each mix the procedure described in the previous section would be followed to select N_{supply}. The mix with the highest binder content which satisfies $M \bullet N_{demand}$ (adjusted traffic) would be selected for further evaluation. The following provides an example of the application of the procedure.

Assume that a mix is to be designed for an interstate highway and that it must accommodate 10×10^6 ESALs during its design life. A dense aggregate grading, Table 15.7, has been selected and an asphalt cement graded according to the proposed 1993 Pacific Coast Conference Specifications as a PBA-6 material (Pacific Coast Conference on Asphalt Specifications, 1993).

The critical temperature, T_c, was determined from weather records adjacent to the site to be 45°C (113°F). As noted earlier this is the temperature at which the constant height repeated load simple shear tests were performed. Based on previous experience with this material, a reasonable asphalt content was in the range 5.0 to 5.5 percent (by weight of aggregate). Accordingly, mixes were prepared at 4.5, 5.0, 5.5, and 6.0 percent (by weight of aggregate).

Table 15.7. Aggregate gradation

Sieve Size	Percent Passing[a]	Target Percent Passing
1 in.	100	100
3/4 in.	97	95
1/2 in.	81	80
3/8 in.	69	68
#4	50	48
#8	41	35
#16	29	24
#30	19	17
#50	13	12
#100	10	8
#200	8	4

[a]Wet sieve analysis — one sample

Slabs were then compacted by a form of rolling wheel compaction (Harvey 1991) to a target air void content of about 3 percent. From the slabs, cylindrical specimens 15 cm (6 in.) in diameter by 5 cm (2 in.) were obtained by coring and sawing. (The specimens were subjected only to short-term aging prior to compaction.)

Constant height repeated load simple shear tests were performed on the specimens using a shear stress of 70 kPa (10 psi), a time of loading of 0.1 sec, a time interval between loadings of 0.6 sec, and at a temperature of 45°C (113°F) (the critical temperature estimated from weather data for two sites near the project). Each specimen was subjected to about 5000 repetitions of stress and the accumulation of permanent shear strain with load repetitions was obtained. Representative results are shown in Figure 15.4. From these data the number of repetitions to a shear strain of 0.045 was estimated for each specimen, the value for strain having been determined from Equation 15.7 and a rut depth of 1.25 cm (0.5 in.) having been assumed. This number of repetitions is termed N_{supply}; Table 15.8 contains a summary of the test data for the range in asphalt contents considered. Note that considerable extrapolation is necessary to determine N_{supply} and was not accounted for in the discussion on reliability.

Equation 15.8 was used to determine N_{demand}. To adjust the estimated design ESALs to ESALs at the critical temperature a factor of 0.1158 (the mean value from Table 15.3) was used. Thus N_{demand} is as follows:

$$N_{demand} = 10 \times 10^6 \times 0.1158 \times 0.04 = 46,320 \text{ repetitions.}$$

Using Equation 15.4 the necessary value(s) for N_{supply} can be determined for various levels of reliability, assuming that $\sigma^2 = 0.602$ for the laboratory test data (the basis for the M values in Table 15.6). These levels are shown in Figure 15.5 with the test data to permit the selection of a recommended asphalt content. The variance in Ln (N_{demand}) has been assumed to be 0.2 and a sample size of four has been used.

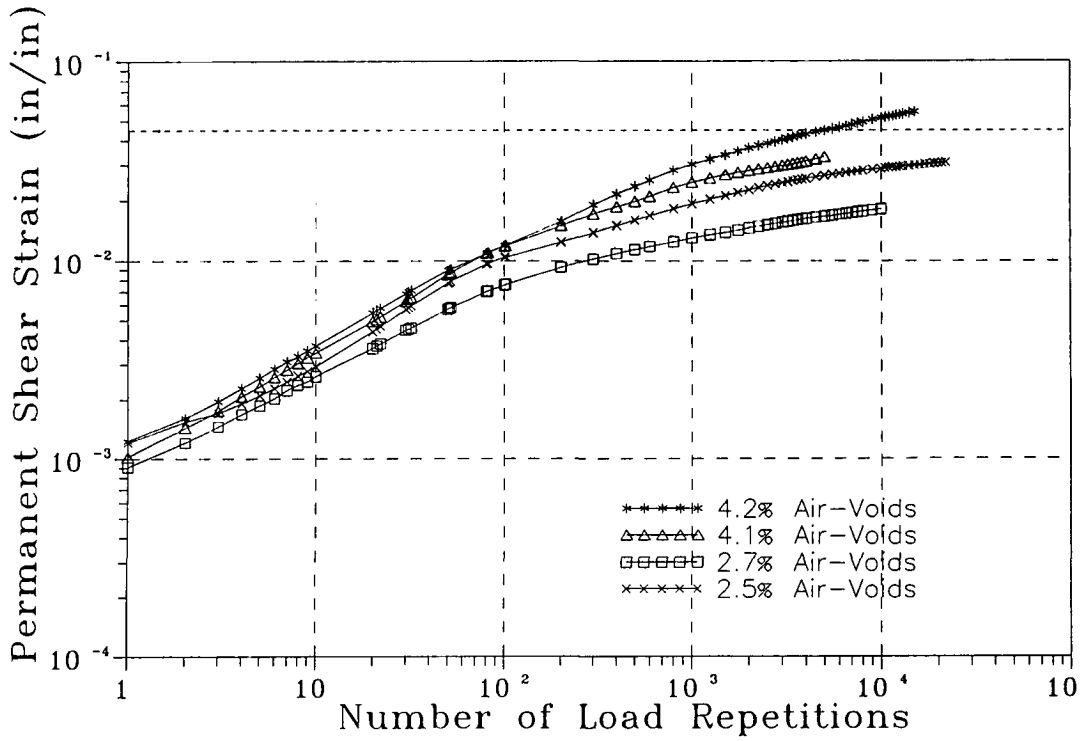

Figure 15.4. Mix design example: permanent shear strain versus stress repetitions in constant height, repeated load simple shear test; asphalt content — 5.0 percent (by weight of aggregate)

Table 15.8. Constant height simple shear repeated load tests; shear stress — 70 kPa (10 psi), test temperature 45°C (113°F)

Asphalt content by weight of aggregate — percent	Air void content — percent	N_{supply} (at $\gamma = 0.045$) $\times 10^3$	N_{supply} average $\times 10^3$
4.5	3.9	120.4	1015
4.5	3.8	22.9	
4.5	3.1	2900	
4.5	2.6	3041	
5.0	4.2	5.1	4973
5.0	4.1	30.0	
5.0	2.7	14884	
5.0	2.5	1270	
5.5	3.3	8.8	153.5
5.5	3.1	20.5	
5.5	3.0	70.7	
5.5	1.4	196.9	
5.5	1.2	470.9	
6.0	4.2	10.4	75.1
6.0	3.3	96.5	
6.0	2.9	118.5	

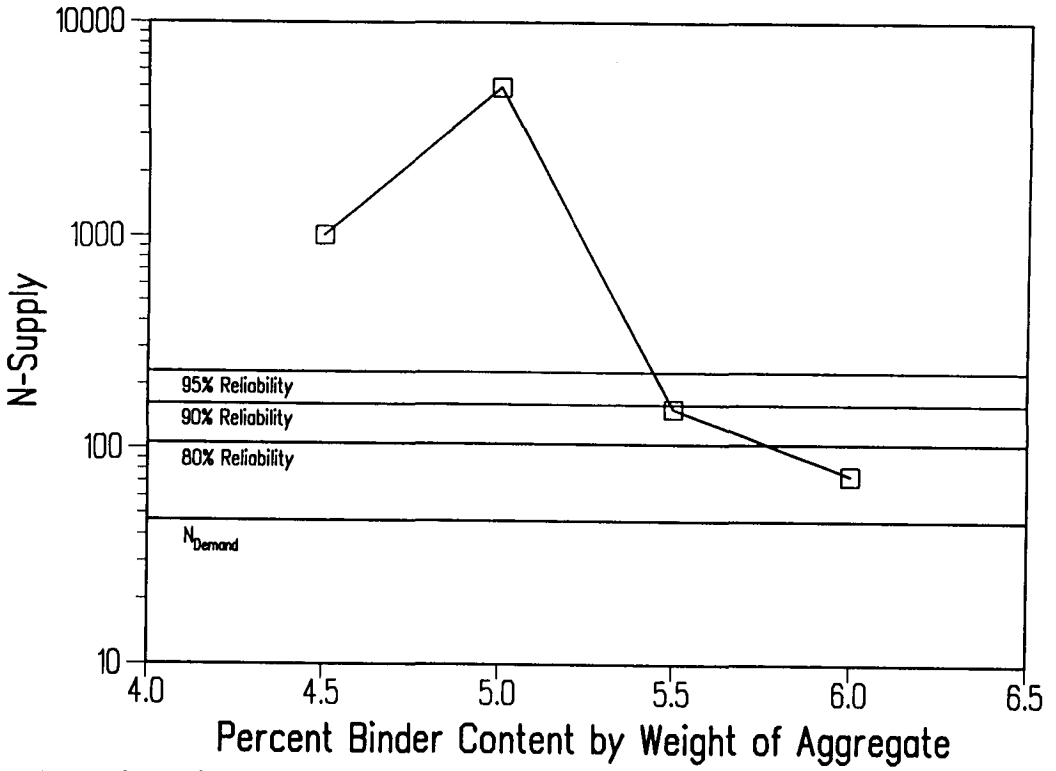

Figure 15.5. Relationship between N_{supply} (repetitions to γ_p = 0.045) and asphalt content

According to the information presented in Figure 15.5, an asphalt content of 5.4 percent could be used to achieve a high degree of reliability. However, it is necessary to recognize plant variations; accordingly, a value of 5.2 percent would be recommended as the design value in this instance.

15.7 Mix Design Using Level 2 Methodology

The comprehensive analysis system, termed Level 2, is anticipated to be used only for mix evaluations for major projects, for investigative analyses, and for model calibrations. The general framework has already been shown in Figure 15.2.

The complete procedure requires the preparation of *four* and preferably *five* specimens at a particular binder content with replication for all but the frequency sweep tests. (It should be noted that time did not permit an evaluation in the variability of the test procedures used in this analysis.)

The test program includes the following:

(1) At a temperature of 40°C (104°F) three tests are performed on three different specimens: uniaxial strain test, volumetric test, and simple shear constant height test.

2. On one specimen, *frequency sweeps* in shear over a range in frequencies from 0.01 to 10 Hz are performed at 4°, 20°, 40°, and possibly 60°C (39, 68, 104, and possibly 140°F). The shear stress is adjusted to provide a shear strain of about 0.0001 in./in. and an axial stress is applied to maintain constant height.

The data obtained from these tests are used to define the nonlinear elastic, viscous, and plastic parameters for the constitutive relationship for the mix (depicted schematically in the model illustrated in Figure 15.2).

At a temperature of 40°C (104°F) it is recommended (at least in the initial phases of the use of this procedure) that a fifth specimen be tested in the simple shear test at constant height in repeated loading at a fixed stress level, e.g., 70 kPa (10 psi).

The results of this test can be compared with those predicted from the constitutive relationship developed from the test data obtained in steps 1 and 2. Modifications in the constitutive relationship can thus be developed to ensure reasonable compatibility among all of the tests.

With a reasonable constitutive relationship it is then possible to estimate the rutting occurring in this mix in the specific pavement structure in which it will be placed by using a finite element idealization of the pavement structure (Part II of this report). If the estimated rut depth exceeds some prescribed level, a different mix must be evaluated in the same manner.

15.8 Summary

The report describes an innovative design and analysis system to evaluate the resistance of asphalt aggregate mixes to permanent deformation. The system provides an effective methodology to define the effect of asphalt aggregate interactions on pavement rutting. It combines mix testing with traffic loading (repetitions, wheel loads, and tire pressures), environmental conditions (temperature), and the pavement cross-section to ensure that permanent deformation in the form of ruts will not exceed acceptable limits.

As with the fatigue system, this analysis system assumes that a trial mix has been identified, that traffic and environmental conditions have been determined, and the pavement cross-section has been designed. It then seeks to judge, with predetermined reliability in the case of the Level 1 methodology, whether the trial mix will perform satisfactorily in service. Performance in this instance is defined in terms of a limiting rut depth which should not be exceeded when the anticipated traffic is applied. If the particular mix is not satisfactory the designer has two options available; either the mix can be redesigned, or a more comprehensive testing and analysis program (Level 2) can be performed.

For routine mix design, the testing and analysis system has been simplified to permit the test program to be completed in one day after the test specimens have been prepared. Laboratory testing is limited to constant height repeated load simple shear testing with each specimen

requiring 1 hour of testing at a single temperature. For large projects or unconventional mixes, more extensive testing and analysis are recommended.

Key features of the Level 1 method include the use of temperature conversion factors and reliability considerations. The temperature conversion factors used to convert design ESALs to their equivalent at a specific high temperature appear to be an effective way to treat temperature effects without resorting to multiple-temperature testing. Time limitations have precluded the development of temperature equivalency factors based on the Level 2 methodology and is an area that should be pursued further. The authors believe that the use of the approach will not change significantly the results reported herein. Nevertheless, this development should be pursued.

Conceptual development of the mix design/analysis has been completed as a part of the SHRP A-003A effort. Considerable progress has been made toward establishing an implementable package at Level 1. Validation of this approach, however, has been limited. Accordingly, a key task is to demonstrate its ability to discriminate among suitable and unsuitable mixes.

In terms of the test methodology, a limited study has been completed to define the reliability of the constant height repeated load simple shear test. Moreover, reliability of the test procedures associated with the Level 2 methodology has not been investigated. Thus, while an initial indication of test variability has been provided for the simple shear constant height repeated load test the authors believe that this can be improved significantly as the test is used in practice.

The Level 2 procedure provides a sound analytical basis for improved rutting prediction. The permanent deformation relationship that has been developed has some limitations, particularly in the representation of plastic behavior, and refinement of this aspect of the model is required. Computations associated with the accumulation of rutting with traffic repetitions using the finite element idealization of the pavement structure are time consuming with today's micro-computer technology; however, the speed of computers increases each year. One cannot judge the efficacy of the approach incorporated in the Level 2 methodology by today's standards. Rather, one must look a few years down the road when this approach will be implemented on a larger scale in practice.

16

References

Ahlborn, G. (1972). ELSYM 5, computer program for determining stresses and deformation in five layer systems. University of California, Berkeley.

Akhter, G. F., and M. W. Witczak (1985). Sensitivity of flexible pavement performance to bituminous mix properties. Research Record 1034, Transportation Research Board, Washington, DC.

Barksdale, R. D. (1971). Compressive stress pulse times in flexible pavements for use in dynamic testing. Highway Research Record, 345, Highway Research Board, 32-34.

Barksdale, R. D. (1972). Laboratory evaluation of rutting in base course materials. Proceedings, Third International Conference on the Structural Design of Asphalt Pavements, Vol. I, London, 161-174.

Barksdale, R. D. and J. H. Miller II (1977). Development of equipment and techniques for evaluating fatigue and rutting characteristics of asphalt concrete mixes. School of Civil Engineering, Georgia Institute of Technology, SCEGIT-77-149.

Battiato, G., F. Ronco, and C. Verga (1977). Moving loads on a viscoelastic double layer: predictions of recoverable and permanent deformations. Proceedings, Fourth International Conference on the Structural Design of Asphalt Pavements, Vol. I, Ann Arbor, 459-466.

Bell C. A., Y. AbWahab, M. E. Cristi, and D. Sosnovske. *Selection of Laboratory Aging Procedures for Asphalt-Aggregate Mixtures.* Report No. SHRP-A-383. Strategic Highway Research Program, National Research Council, Washington, DC. 1994.

Bonnot, J. (1986). Asphalt aggregate mixtures. Transportation Research Record 1096, Transportation Research Board, 42-51.

Brown, S. F. and C. A. Bell (1977). The validity of design procedures for the permanent deformation of asphalt pavements. Proceedings, Fourth International Conference on the Structural Design of Asphalt Pavements, Vol. I, Ann Arbor, 467-482.

Brown, S. F. and C. A. Bell (1979). The prediction of permanent deformation in asphalt pavements. Proceedings, The Association of Asphalt Paving Technologists, Vol. 48, 438-476.

Brown, S. F. and K. E. Cooper (1980). A fundamental study of the stress-strain characteristics of a bituminous material. Proceedings, The Association of Asphalt Paving Technologists, Vol. 49, 476-498.

Célard, B. (1977). ESSO road design technology. Proceedings, Fourth International Conference on the Structural Design of Asphalt Pavements, Vol. I, Ann Arbor, 249-268.

Eisenmann, J. and A. Hilmer (1987). Influence of wheel load and inflation pressure on the rutting effect at asphalt-pavements - experiments and theoretical investigations. Proceedings, Sixth International Conference on the Structural Design of Asphalt Pavements, Vol. I, Ann Arbor, 392-403.

Eriksen, K. (1992). Homogeneity of air voids in asphalt-aggregate mixtures compacted by different methods at different temperatures. Prepared by the Danish National Road Laboratory for SHRP-88-AIIR-13, Phase 3b. Strategic Highway Research Program, National Research Council, Washington, DC.

Francken, L. (1977). Permanent deformation law of bituminous road mixes in repeated triaxial compression. Proceedings, Fourth International Conference on the Structural Design of Asphalt Pavements, Vol. I, Ann Arbor, 483-496.

Gibb, J., Letter report transmitting wheel-tracking test data for 200 mm diameter cores, SWK Pavement Engineering, Nottingham, UK. 19 December 1991.

Harvey, J. (1991). University of California at Berkeley SHRP A-003A asphalt concrete specimen preparation protocol, Version 3.0. UCB Technical Memorandum No. TM-UCB-A-003A-91-2. Prepared for the Strategic Highway Research Program, National Research Council.

Harvey J.T., T. Lee, J. Sousa, J. Pak, and C.L. Monismith, "Evaluation of Fatigue and Permanent Deformation Properties of Several Asphalt-Aggregate Mixes Using SHRP A-003A Equipment," Paper presented at Annual Meeting of Transportation Research Board, Washington D.C. January 1994.

Hicks, R.G., (1988). State-of-the-Art on Rutting in Asphalt Concrete, *Proceedings*, Third IRF Middle East Regional Meeting, Vol. 6, 6.119-6.144.

Hills, J. F. (1973). The creep of asphalt concrete mixes. Journal of The Institute of Petroleum, November.

Huschek, S. (1977). Evaluation of rutting due to viscous flow in asphalt pavements. Proceedings, Fourth International Conference on the Structural Design of Asphalt Pavements, Vol. I, Ann Arbor, 497-508.

Kenis, W. J., J. A. Sherwood, and T. F. McMahon (1982). Verification and application of the VESYS structural subsystem. Proceedings, Fifth International Conference on the Structural Design of Asphalt Pavements, Vol. I, Delft, The Netherlands, 333-346.

Khedr, S. A. (1986). Deformation mechanism in asphaltic concrete. Journal of Transportation Engineering, American Society of Civil Engineers, Vol. 112, No. 1, 29-45.

Khosla, N. P. and M. S. Omer (1985). Characterization of asphaltic mixtures for prediction of pavement performance. Transportation Research Record 1034, Transportation Research Board, 47-55.

Kirwan, R. W., M. S. Snaith, and T. E. Glynn (1977). A computer based subsystem for the prediction of permanent deformation. Proceedings, Fourth International Conference on the Structural Design of Asphalt Pavements, Vol. II, Ann Arbor, 509-518.

Lai, J. S. and D. Anderson (1973). Irrecoverable and recoverable nonlinear viscoelastic properties of asphalt concrete. Transportation Research Record 468, Transportation Research Board, 73-88.

Leahy, R. B. (1989). Permanent deformation characteristics of asphalt concrete. Doctoral dissertation, University of Maryland, College Park, 399 pp.

Lucks, A. S., J. T. Christian, G. E. Brandow, and K. K. Høeg (1972). Stress conditions in NGI simple shear test. Proceedings, American Society of Civil Engineers, Vol. 98, No. SM1, 155-160.

Lytton, R. L., D. E. Pufahl, C. H. Michalak, H. S. Liang, and B. J. Dempsey (1990). An integrated model of the climatic effects on pavements. FHWA-RD-90-033, Texas Transportation Institute, College Station, Texas.

Mahboub, K. and D. N. Little (1988). Improved asphalt concrete design procedure. Research Report 474-1F, Texas Transportation Institute.

McLean, D. B. and C. L. Monismith (1974). Estimation of permanent deformation in asphalt concrete layers due to repeated traffic loading. Transportation Research Record 510, Transportation Research Board, 14-30.

Meyer, F. R. P. and R. C. G. Haas (1977). A working design subsystem for permanent deformation in asphalt pavements. Proceedings, Fourth International Conference on the Structural Design of Asphalt Pavements, Vol. I, Ann Arbor, 519-528.

Monismith, C. L., K. Inkabi, C. R. Freeme, and D. B. McLean (1977). A subsystem to predict rutting in asphalt concrete pavement structures. Proceedings, Fourth International Conference on the Structural Design of Asphalt Pavements, Vol. I, Ann Arbor, 529-539.

Monismith, C. L. and A. A. Tayebali (1988). Permanent deformation (rutting) considerations in asphalt concrete pavement sections. Proceedings, The Association of Asphalt Paving Technologists, Williamsburg, VA, Vol. 57, 414-463.

Nunn, M. E. (1978). Deformation testing of dense coated macadam: effect of method of specimen compaction. TRRL Laboratory Report 870, Transport and Road Research Laboratory, Crowthorne, Berkshire.

Pacific Coast Conference on Asphalt Specifications, Meeting Minutes, Twenty-fifth Meeting, May 1993, Berkeley, CA.

Romain, J. E. (1972). Rut depth prediction in asphalt pavements. Proceedings, Third International Conference on the Structural Design of Asphalt Pavements, Vol. I, London, 205-210.

Schmidt, R. J. (1972). A practical method for measuring the resilient modulus of asphalt treated mixes. Highway Research Record 404, Highway Research Board, 22-32.

SHRP, *Stage 1 Validation of Relationship Between Asphalt Properties and Asphalt Aggregate Mix Performance* Report No. SHRP-A-398. Strategic Highway Research Program, National Research Council, Washington, D.C. 1994.

Sousa, J. B. (1986). Dynamic properties of materials for pavement design. Ph.D. Thesis, University of California, Berkeley, 400 pp.

Sousa, J. B., J. Harvey, L. Painter, J. A. Deacon, and C. L. Monismith (1991). Evaluation of laboratory procedures for compacting asphalt-aggregate mixtures. TM-UCB-A-003A-90-5, Institute of Transportation Studies, University of California, Berkeley.

Sousa, J., and M. Solaimaniam, Abridged procedure to determine permanent deformation of asphalt concrete pavement. Transportation Research Board, 1994.

Tayebal, A., J. Deacon, J. Coplantz, F. Finn, J. Harvey, and C. Monismith. *Fatigue Response of Asphalt-Aggregate Mixes*. Report No. SHRP-A-404. Strategic Highway Research Program, National Research Council, Washington DC. 1994.

Terrel, R. L. and S. Al-Swailmi. *Water Sensitivity of Asphalt-Aggregate Mixtures Test Development*. Report No. SHRP-A-403. Strategic Highway Research Program, National Research Council, Washington, DC. 1994.

Thrower, E. N. (1977). Methods of predicting deformation in road pavements. Proceedings, Fourth International Conference on the Structural Design of Asphalt Pavements, Vol. I, Ann Arbor, 540-554.

Thrower, E. N. (1978). Stress invariants and mechanical testing of pavement materials. Report 810, Transport and Road Research Laboratory, Great Britain.
Uge, P. and P. J. van de Loo (1974). Permanent deformation of asphalt mixes. Koninklijke/Shell-Laboratorium, Amsterdam, November.

Uzan, J. (1982). Permanent deformation in pavement design and evaluation. Technion, Israel Institute of Technology.

van de Loo, P. J. (1974). Creep testing, a simple tool to judge asphalt mix stability. Proceedings, The Association of Asphalt Paving Technologists, Vol. 43, 253-284.

van de Loo, P. J. (1976). Practical approach to the prediction of rutting in asphalt pavements: the Shell method. Transportation Research Record 616, Transportation Research Board, 15-21.

Van Dijk, W. (1975). Practical fatigue characterization of bituminous mixes. Proceedings, The Association of Asphalt Paving Technologists, Vol. 44, pp. 38-74.

Verstraeten, J., J. E. Romain, and V. Veverka (1977). The Belgian Road Research Center's overall approach to asphalt pavement structural design. Proceedings, Fourth International Conference on the Structural Design of Asphalt Pavements, Vol. I, Ann Arbor, 298-324.

Von Quintus, J. L., J. A. Scherocman, C. S. Hughes, and T. W. Kennedy (1991). Asphalt-aggregate mixture analysis system — AAMAS. National Cooperative Highway Research Report 338, Transportation Research Board, Washington, D.C.

Appendix A

Finite Element Analysis of Simple Shear Test

The development of the constitutive relationship to define the permanent deformation response of asphalt aggregate mixes was defined in Chapter 6. This relationship includes nonlinear elastic response, which is defined by nine coefficients (material constants), C_1 through C_9 (see Equation 6.1). To determine the material constants C_2, C_4, and C_9, the simple shear test has been interpreted as a pure shear test. It is expected that some error would be present in the results obtained from such an assumption. It is furthermore expected that the magnitude of the error decreases with improved height-to-diameter ratios. The disturbances caused by the absence of complementary shear components tends to be limited to the ends. As the relative volume of the specimen under uniform states of stress increases, it is expected that the error would decrease. It is therefore important to determine the error function of the height-to-diameter ratio to identify the ratio where the error can be considered acceptable or negligible.

A finite element mesh composed of 4 × 8 × 16 elements representing half of a shear specimen (to take advantage of symmetry) was created in a finite element analysis program (FEAP). The height of the specimen (subdivided in eight rows of elements) was fixed at 5 cm (2 in.). The dimension of the side was varied between 10 and 20 cm (4 and 8 in.). The constants used for the solution were:

$C_1 = 35{,}000\ \text{lb/in}^2$
$C_2 = -300{,}000\ \text{lb/in}^2$
$C_3 = -3.9 \times 10^6\ \text{lb/in}^3$
$C_4 = 2.8 \times 10^6\ \text{lb/in}^3$
$C_5 = -5 \times 10^6\ \text{lb/in}^3$
$C_6 = 3 \times 10^9\ \text{lb/in4}$
$C_7 = 1 \times 10^9\ \text{lb/in}^4$
$C_8 = 6 \times 10^9\ \text{lb/in}^4$
$C_9 = -5 \times 10^8\ \text{lb/in}^4$

To investigate the effect of specimen geometry on the determination of material properties, the material properties used as input for the finite element were compared with those that

would have been obtained if the response were analyzed just as if it were a simple shear test. Therefore, a measure of the error can be obtained. The two important parameters that can be obtained from the shear test are G (or C_2) and C_4. For these two cases a measure of the error is presented in Figures A.1 and A.2. It will be noted that the measure of G is not sensitive to the various parameters (i.e., C_4 and others). It is also important to note that in a 15 × 15 × 5 cm (6 × 6 × 2 in.) specimen the error in measuring G is about 10 percent and that value is independent of all other values, implying that if extra accuracy is needed the value obtained can simply be multiplied by 1.1 (pending further analysis).

The error observed for C_4 is almost negligible in the realistic case when true mix behavior is simulated by using all parameters (all Cs).

The uniformity of stress distribution was investigated for the 15 × 15 × 5 cm (6 × 6 × 2 in.) specimen. Figures A.3 and A.4 diagram the variation of the shear stress and axial stress throughout the specimen. It can be concluded that the variation of the shear stresses is for the most part uniform. The axial stresses, however, present stress concentrations near the edge of the specimen. This factor could be of importance in failure analysis, as it may cause crack initiation near the edge; moreover, it may or may not be detrimental. In some cases notches are created to force crack initiation. If this singularity causes a crack to start, then it could be beneficial, since one would know exactly where the crack would start and its growth could be monitored. However, prior to failure, the results obtained from the test can be considered reliable and accurate.

Deformation patterns were also examined in the analysis, the results of which are shown in Figure A.5. It will be noted that, with exception of the end columns of elements, the shear deformations are parallel to the direction of shear stress, indicating that the assumption of simple shear response is reasonable.

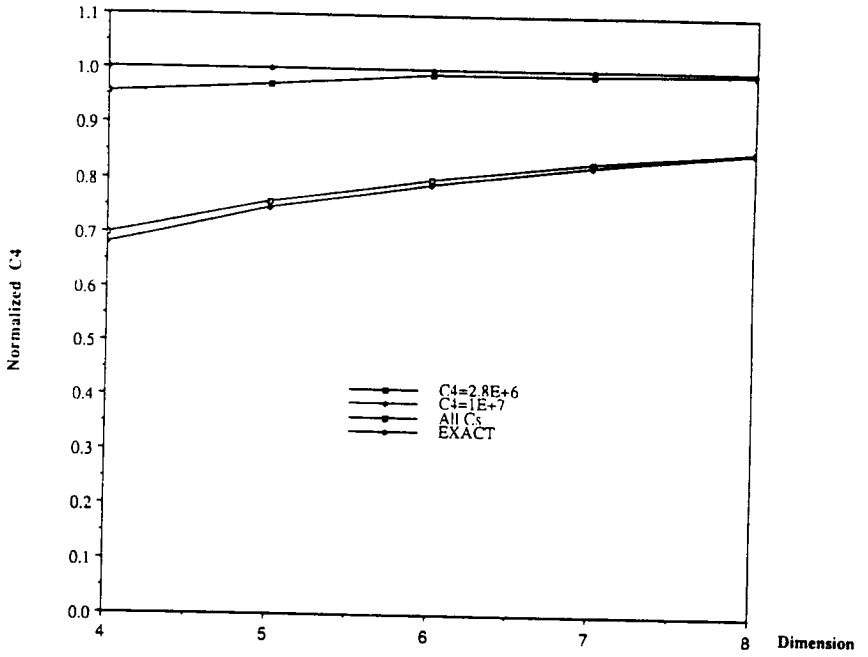

Figure A.1. Effect of changing base dimension on measured C_4, normalized

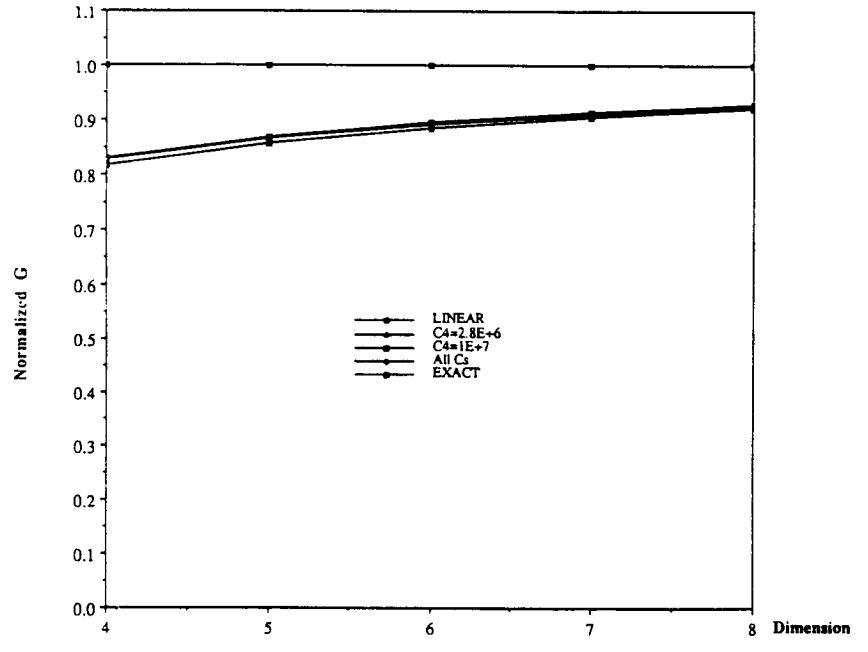

Figure A.2. Effect of changing base dimension on measured G, normalized

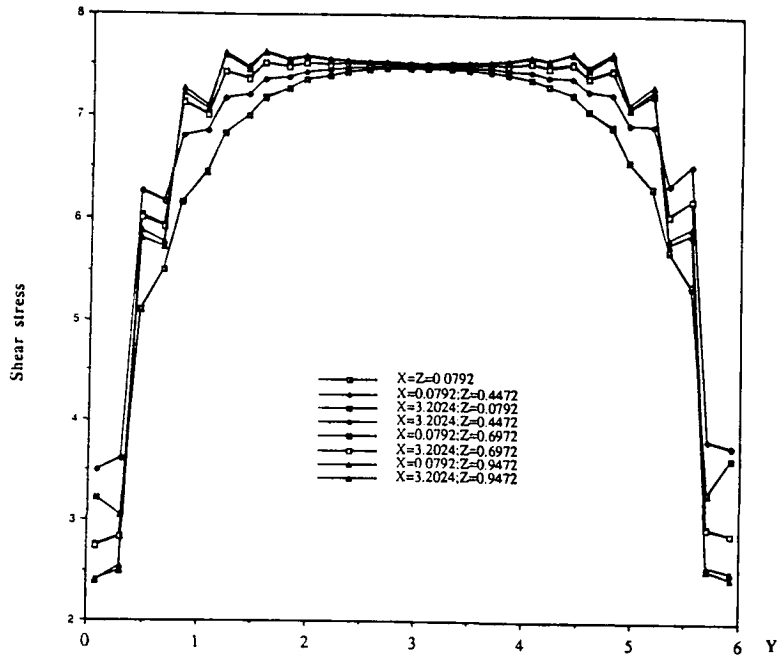

Figure A.3. Variation of the shear stress in the Y direction

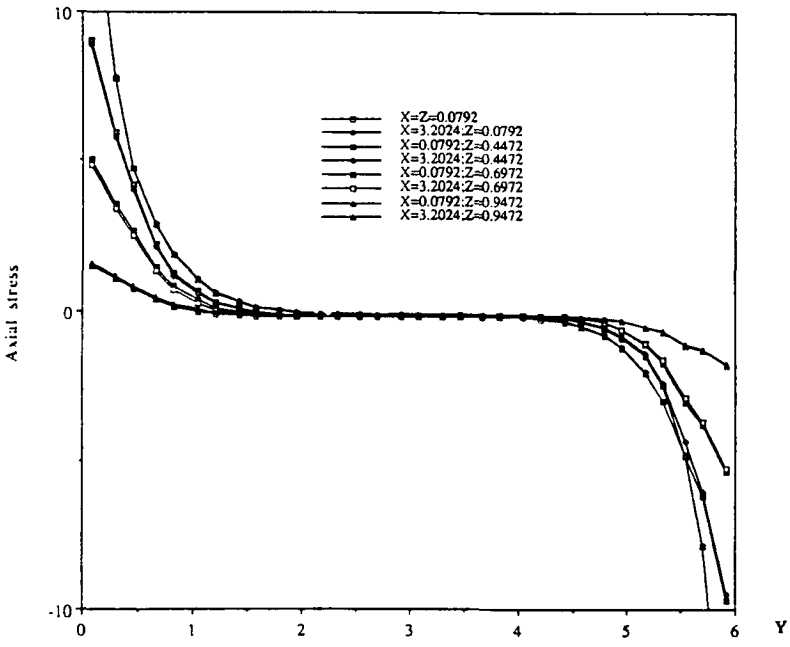

Figure A.4. Variation of the axial stress along the Y axis

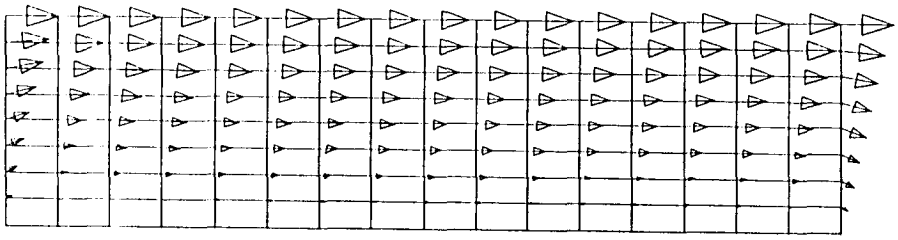

Figure A.5. Deformation pattern, simple shear, finite element idealization

Appendix B

Nonlinear Viscoelastic Characterization

In the initial phase of the development of the constitutive relationship for the permanent deformation response of asphalt aggregate mixes, four mixes were selected, containing aggregates RB and RL and asphalt AAK-1 and AAG-1. These mixes were:

(1) V0W0 — Aggregate RB, asphalt AAG-1, low asphalt content, low void content;

(2) B0W0 — Aggregate RB, asphalt AAK-1, low asphalt content, low void content;

(3) B1T1 — Aggregate RL, asphalt AAK-1, high asphalt content, high void content; and

(4) V0T1 — Aggregate RL, asphalt AAG-1, low asphalt content, high void content.

Wheel-tracking tests had been performed by SWK Pavement Engineering at the University of Nottingham (SWK/UN) on these mixes and the ranking in order of increasing normalized rutting rate was as follows: V0W0 < B0W0 < B1T1 < V0T1.

To permit the comparisons to be made the following steps were followed:

(1) Determination of nonlinear elastic parameters at 4°C (39°F) (to minimize viscous effect). (40°C [104°F] is now recommended.)

(2) Determination of the viscous parameters over a range of temperatures (4°, 20° and 40°C [39°, 68°, and 104°F]) and frequencies (0.01, 0.02, 0.05, 0.1, 0.2, 0.5, 1.0, 2.0, 5,0 and 10 Hz).

(3) Determination of damage parameters.

(4) Simulation, using FEAP, of the response of the mix in a repetitive simple shear test (constant height) at 40°C (104°F), using 0.1 s loading time and a time interval between load applications of 0.6 s.

(5) Perform repetitive simple shear test at 40°C (104°F) for same conditions as (4).

(6) Compare observed and predicted behavior and evaluate possible cause of discrepancies and corrections to be made either in the model or in the determination of the material parameters.

It should be noted that in this procedure, evaluation of the model behavior is made through a test from which no material parameters were obtained and which is of a totally different nature than those used to determine the material properties (i.e., the validation test was a repetitive test while the tests used to obtain material properties were either constant rate of loading or sinusoidal in nature). It is important to be able to match performance not only at different stress levels but also at varying rates of loading and unloading.

Specimens for testing were fabricated using the University of California at Berkeley (UCB) rolling wheel compaction procedure. All specimens of one mix were obtained from the same slab by coring, and cores (6 in. diameter by 2 in. high) were stored at 20°C (68°F) prior to testing.

To determine the nonlinear elastic parameters, the requisite tests were performed at 4°C (39°F). This temperature was selected because, at the time, it was thought to be a temperature at which the viscous response of mixes would be minimized during the testing sequence even though the loads/deformations/pressures could not be applied instantaneously. (N.B. While tests were conducted on the four mixes listed, a complete series was not done for the V1T0 mix due to some test difficulties, hence comparisons between measured and computed results are not presented for this mix.)

Simple shear constant height tests permit the direct determination of three of the nine parameters defining nonlinear response (i.e., C_2, C_4, and C_9).[18] Data presented in Figures B.1 through B.3 illustrate the variation of shear strain with the shear stress obtained during the test with that predicted from the model (assuming that the data contained no viscous response).

Figures B.4 through B.6 illustrate the axial stress developed during the tests as a function of the shear strain for each of the mixes tested. One of the most significant aspects of these results is the fact that dilation occurred at 4°C (39°F). This suggests that dilation is strain-related and is associated with the granular structure of dense mixes. Its influence can normally be neglected at low temperatures because the asphalt concrete mix is so stiff that conventional traffic loads are not sufficient to generate strains large enough to mobilize the dilational component. At higher temperatures, however, where the mix is less stiff, traffic-induced stresses can generate strains sufficient to allow dilation to become an important aspect in determining the stability of a mix.

[18]Chapter 6 contains a discussion of the methodology used to obtain all of the constants, C_1 through C_9.

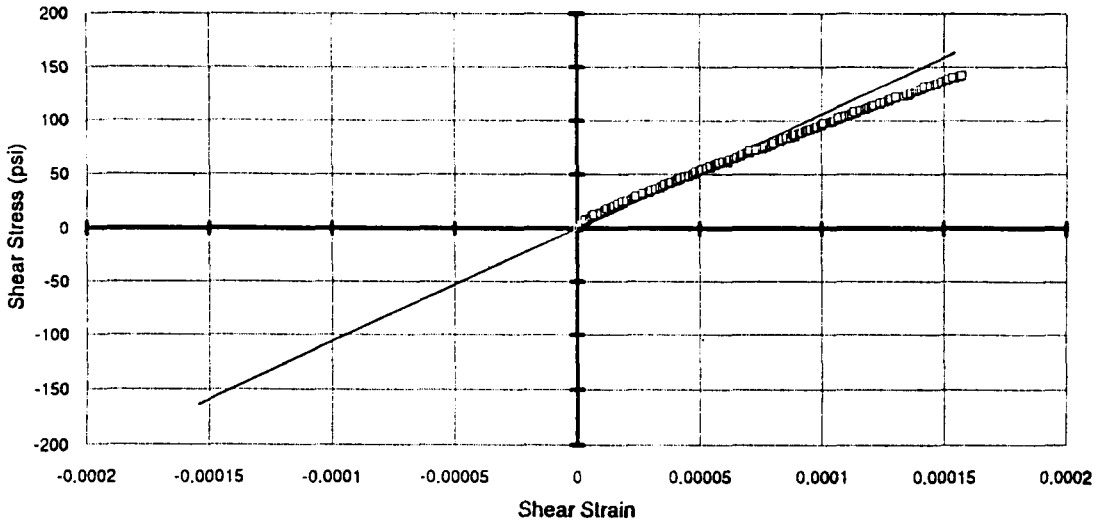

Figure B.1. Variation of shear stress with shear strain for simple shear tests at 4°C (39°F) and 70 kPa/s (10 psi/s) ramping shear stress (model and actual data) — aggregate RB, asphalt AAG-1 (V0W0)

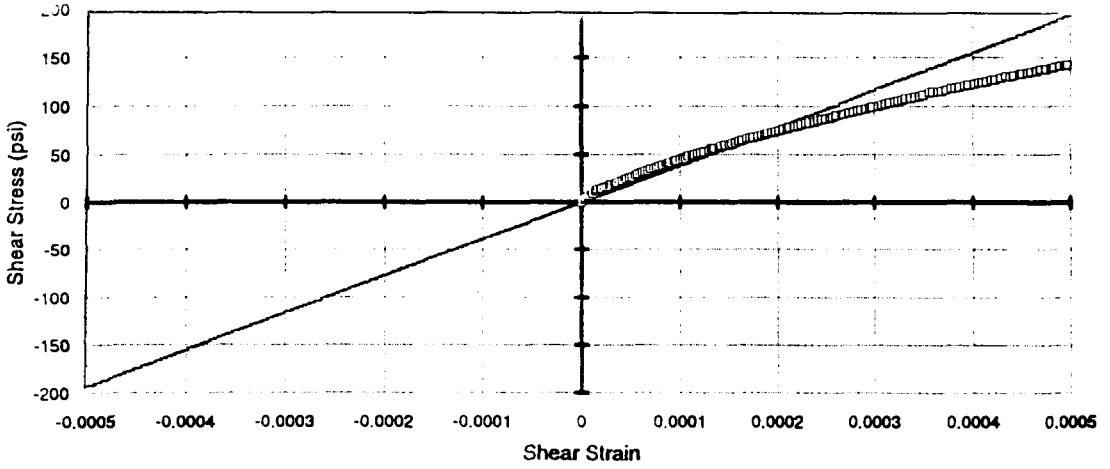

Figure B.2. Variation of shear stress with shear strain for simple shear tests at 4°C (39°F) and 70 kPa/s (10 psi/s) ramping shear stress (model and actual data) — aggregate RB, asphalt AAK-1 (B0W0)

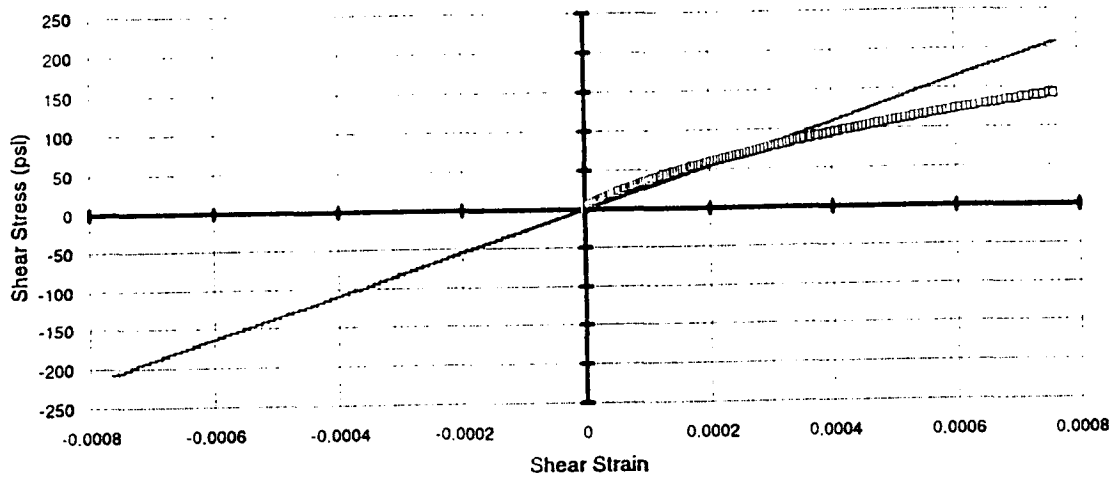

Figure B.3. Variation of shear stress with shear strain for simple shear tests at 4°C (39°F) and 70 kPa/s (10 psi/s) ramping shear stress (model and actual data) — (aggregate RL, asphalt AAK-1) (B1T1)

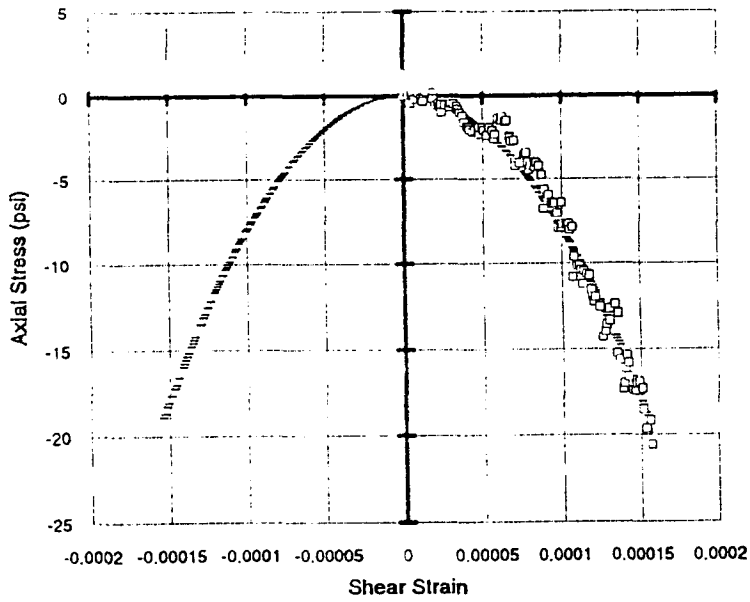

Figure B.4. Variation of Axial stress with shear strain for simple shear tests at 4°C (39°F) and 70 kPa/s (10 psi/s) ramping shear stress (model and actual data) — aggregate RB, asphalt AAG-1 (V0W0)

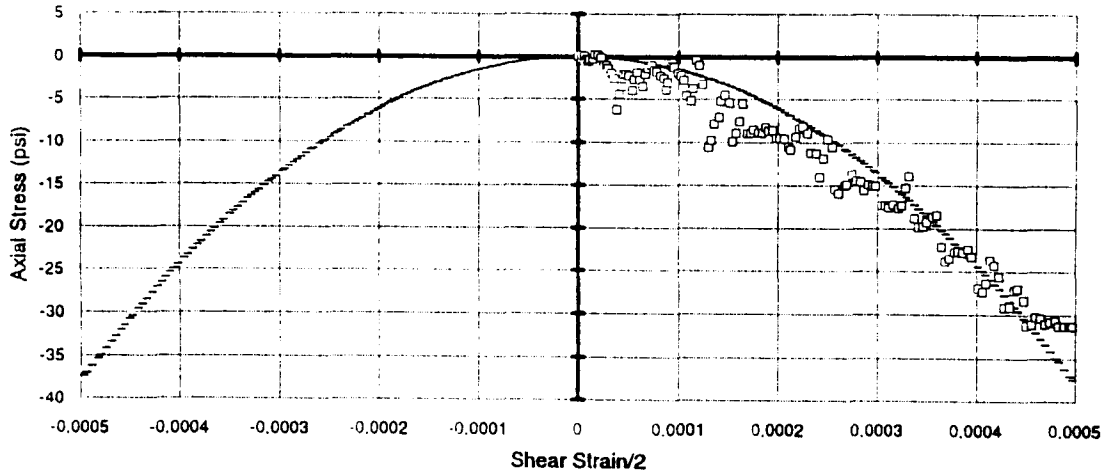

Figure B.5. Variation of axial stress with shear strain for simple shear tests at 4°C (39°F) and 70 kPa/s (10 psi/s) ramping shear stress (model and actual data) — aggregate RB, asphalt AAK-1 (B0W0)

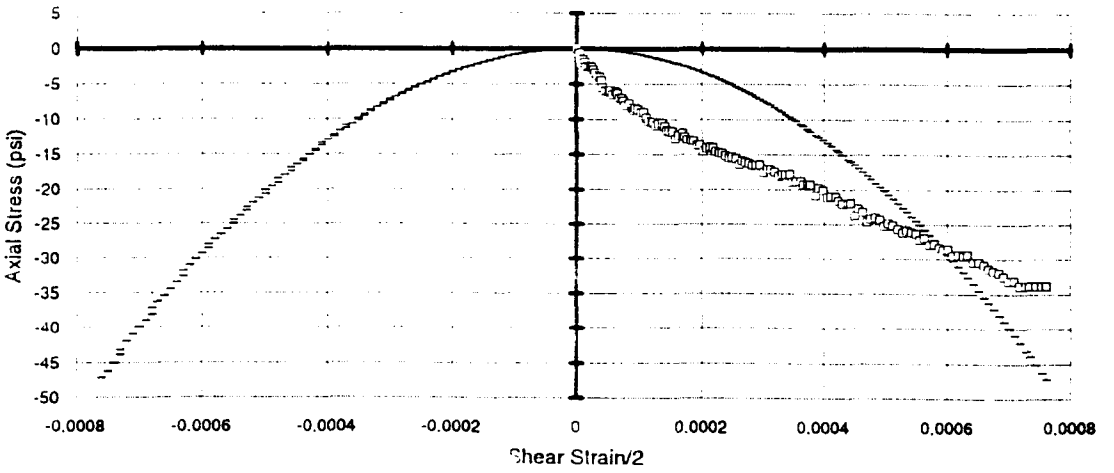

Figure B.6. Variation of axial stress with shear strain for simple shear tests at 4°C (39°F) and 70 kPa/s (10 psi/s) ramping shear stress (model and actual data) — aggregate RL, asphalt AAK-1 (B1T1)

Comparison of the model with the actual data in Figures B.4 through B.6 suggests that the model "captures" the dilation observed in the mixes.

Uniaxial strain tests permit the direct determination of the coefficients C_1, C_3, C_6, and C_7 and also provide a check for C_2 and C_4 (obtained from the simple shear test at constant height). This assumes that there is no viscous deformation contributing to the response (or if there is, that both tests are executed at the same rate). Figures B.7 through B.12 illustrate the response of three of the mixes and the best fit obtained with the model parameters.

Figure B.13 compares the variation of the axial stress with the axial strain for the three mixes while Figure B.14 compares the variation of the confining stress with the axial strain. In Figure B.14 it is interesting to compare the relative performance of the mixes. While the V0W0 mix (aggregate RB, asphalt AAG-1) required a confining stress of only 117 kPa (17 psi) to ensure a state of uniaxial strain, the B1T1 (aggregate RL, asphalt AAK-1) mix required about 324 kPa (47 psi) even though both were subjected to the same axial stress — approximately 827 kPa (120 psi), Figure B.13. This indicates that mix B1T1 is less stable than mix V0W0. These results are quite significant; they demonstrate that the uniaxial strain test is capable of differentiating among mixes of different stabilities. It is interesting to note that the Hveem stabilometer would rank the mixes in the same order,[19] since that test is similar to the uniaxial strain test.

Volumetric test results, with the constants obtained from the simple shear and uniaxial strain tests, permit the two remaining constants, C_5 and C_8, to be estimated. Also, a check on the sum of the constants $C_1 + C_2$ can be made from the results from the volumetric test. Figures B.15 through B.18 compare the results obtained from the data with those fitted with the model parameters. Figure B.19 compares the response for the four mixes tested.

Results for the C coefficients obtained from the tests are summarized in Table B.1. Note that all tests were performed with a load rate of about 70 kPa/s (10 psi/s) at 4°C (39°F). While 4°C (39°F) and the 70 kPa/s (10 psi/s) rate were selected to minimize viscous deformation in the determination of the nonlinear elastic constants, some creep was still present. Accordingly, the C coefficients shown in Table B.1 include some viscous deformation.

Results shown in Table B.1 allow some encouraging comparisons. For example it can be observed that the values of C_2 and C_4 obtained from the simple shear test for the B0W0 mix compare reasonably well to those obtained from the uniaxial strain test. Also, the values predicted for the constant, A ($A=3*C_1 + 2*C_2$), of the volumetric test (i.e., the coefficient for the linear strain term) using those obtained from the uniaxial strain test compare reasonably well to those measured in the volumetric test for all of the mixes.

---

[19]Mix design data reported earlier indicate that the B1T1 mixture is less stable than the V0W0 mixture as measured by the stabilometer "S" value.

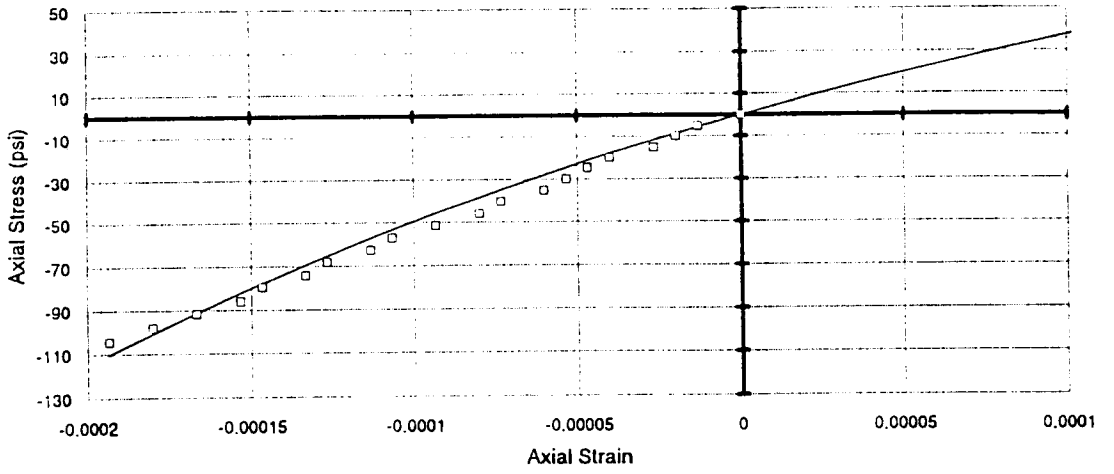

Figure B.7. Variation of axial stress with axial strain for uniaxial strain tests at 4°C (39°F) and 70 kPa/s (10 psi/s) ramping for axial stress (model and actual data) — aggregate RB, asphalt AAG-1 (V0W0)

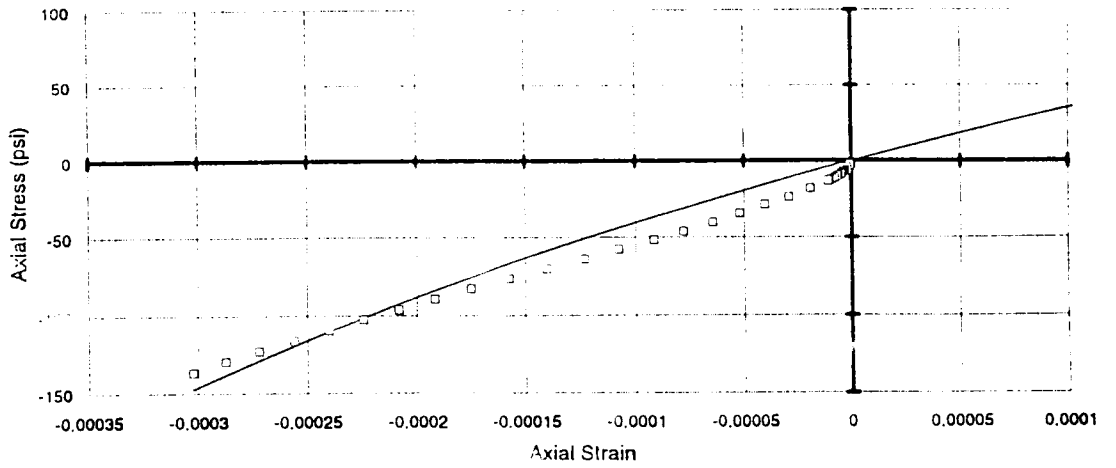

Figure B.8. Variation of axial stress with axial strain for uniaxial strain tests at 4°C (39°F) and 70 kPa/s (10 psi/s) ramping for axial stress (model and actual data) — aggregate RB, asphalt AAK-1 (B0W0)

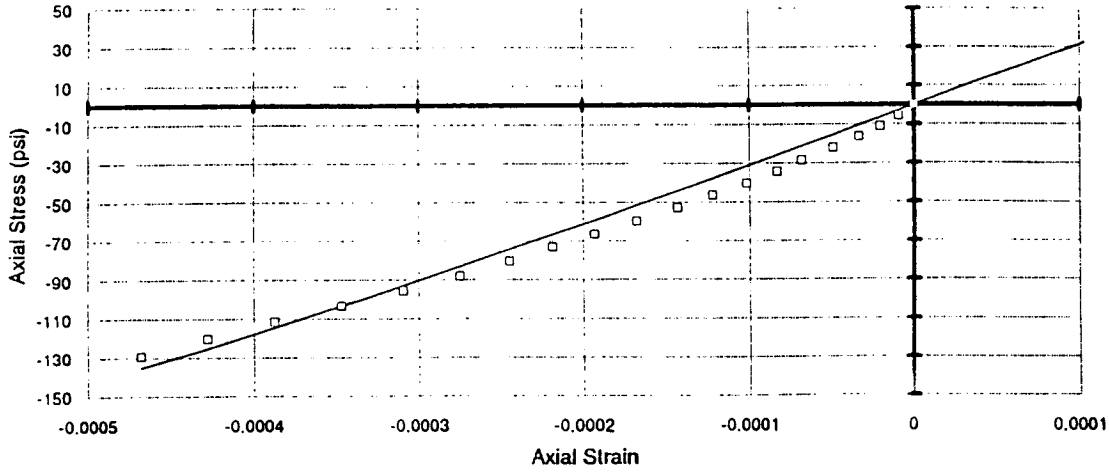

Figure B.9. Variation of axial stress with axial strain for uniaxial strain tests at 4°C (39°F) and 70 kPa/s (10 psi/s) ramping for axial stress (model and actual data) — aggregate RL, asphalt AAK-1 (B1T1)

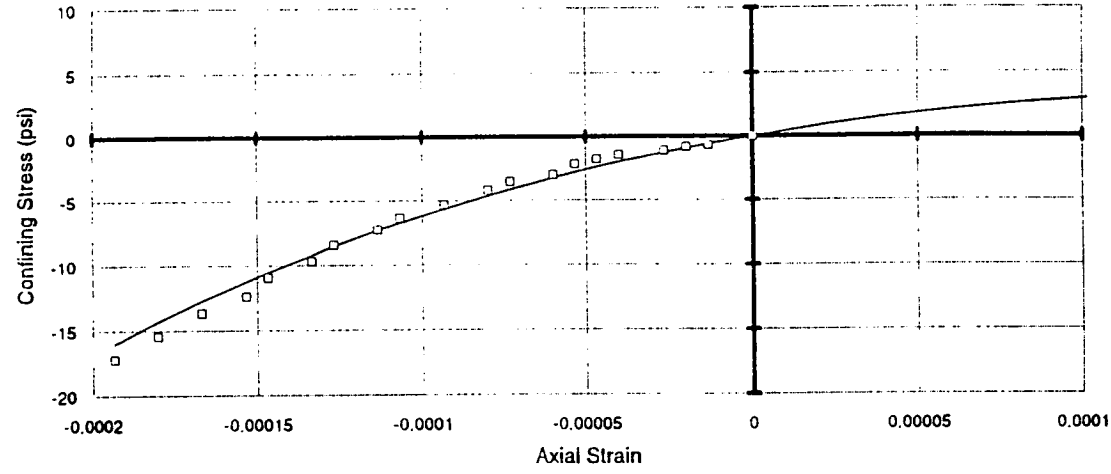

Figure B.10. Variation of confining stress with axial strain for uniaxial strain tests at 4°C (39°F) and 70 kPa/s (10 psi/s) ramping for axial stress (model and actual data) — aggregate RB, asphalt AAG-1 (V0W0)

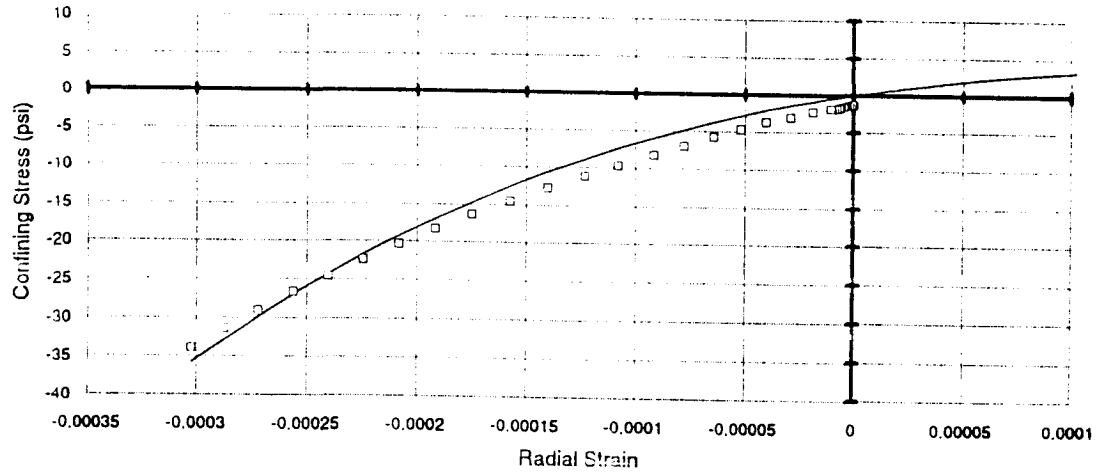

Figure B.11. Variation of confining stress with axial strain for uniaxial strain tests at 4°C (39°F) and 70 kPa/s (10 psi/s) ramping for axial stress (model and actual data) — aggregate RB, asphalt AAK-1 (B0W0)

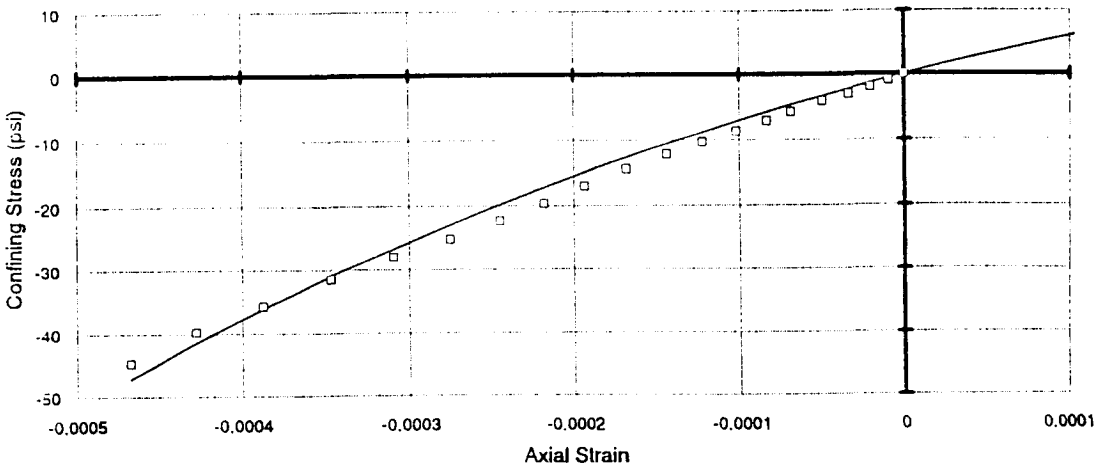

Figure B.12. Variation of confining stress with axial strain for uniaxial strain tests at 4°C (39°F) and 70 kPa/s (10 psi/s) ramping for axial stress (model and actual data) — aggregate RL, asphalt AAK-1 (B1T1)

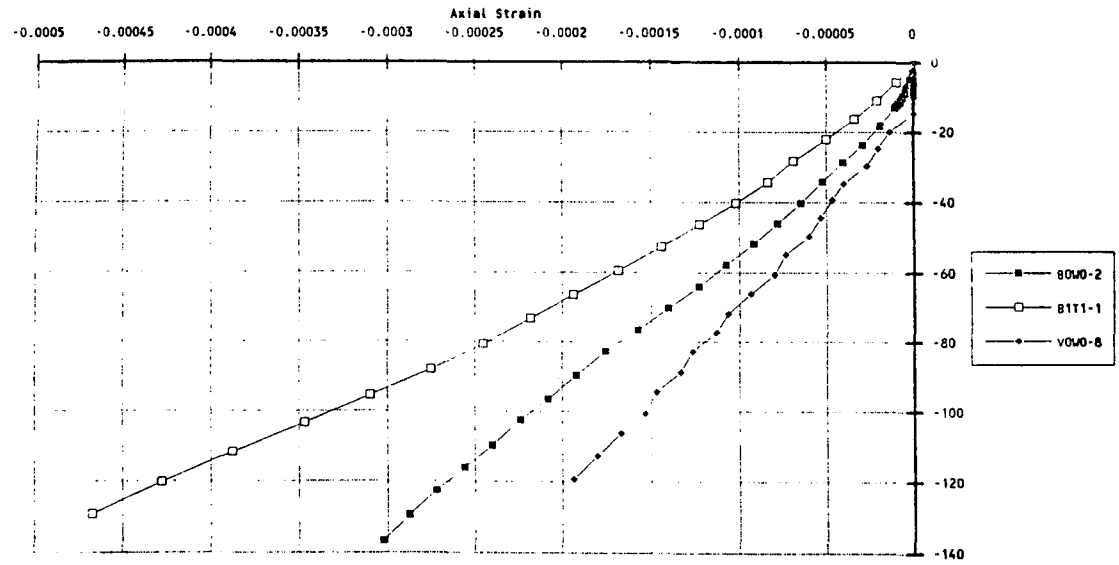

Figure B.13. Axial stress versus axial strain; uniaxial strain test

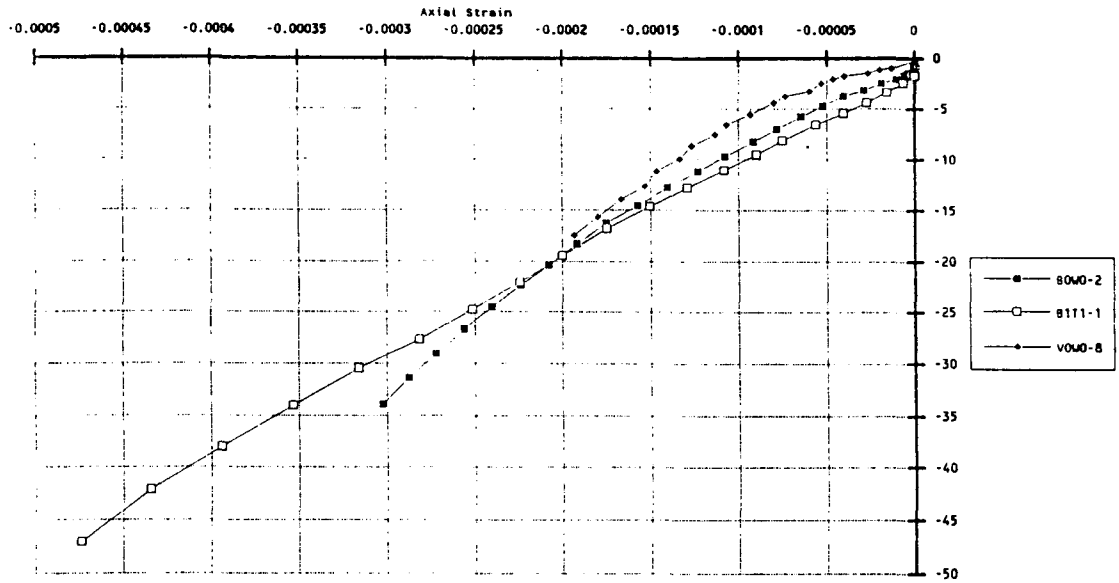

Figure B.14. Confining stress versus axial strain; uniaxial strain test

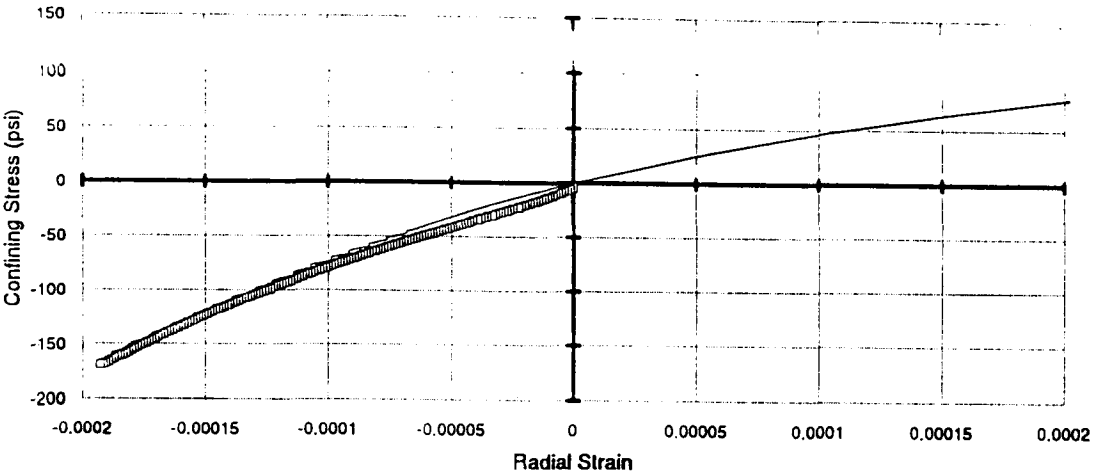

Figure B.15. Variation of confining stress with radial strain for volumetric tests at 4°C (39°F) and 105 kPa/s (15 psi/s) ramping for stress (model and actual data) — aggregate RB, asphalt AAG-1 (V0W0)

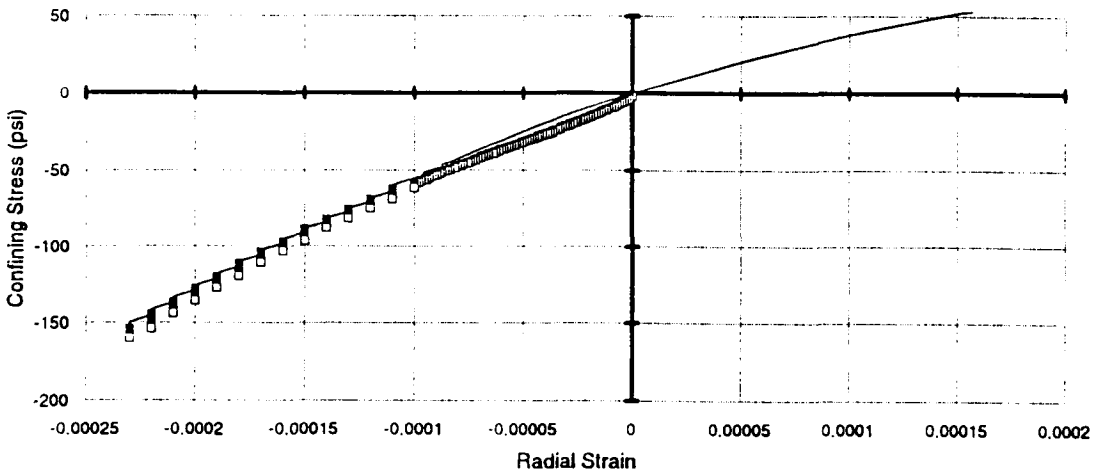

Figure B.16. Variation of confining stress with radial strain for volumetric tests at 4°C (39°F) and 105 kPa/s (15 psi/s) ramping for stress (model and actual data) — aggregate RB, asphalt AAK-1 (BOWO)

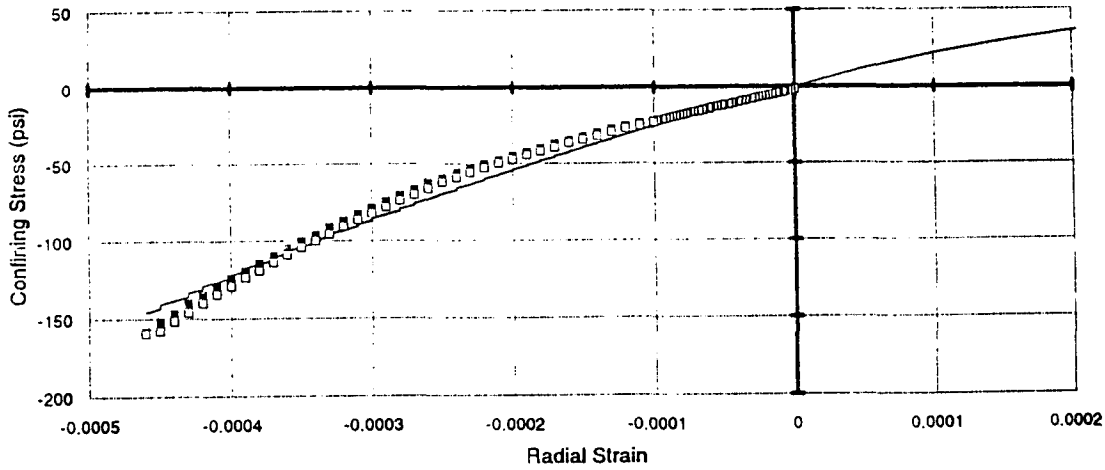

Figure B.17. Variation of confining stress with radial strain for volumetric tests at 4°C (39°F) and 105 kPa/s (15 psi/s) ramping for stress (model and actual data) — aggregate RL, asphalt AAK-1 (B1T1)

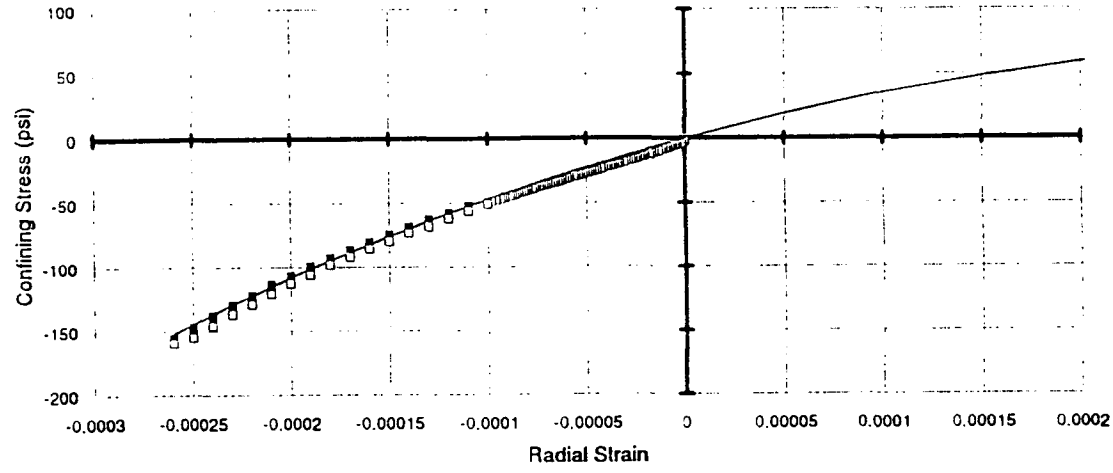

Figure B.18. Variation of confining stress with radial strain for volumetric tests at 4°C (39°F) and 105 kPa/s (15 psi/s) ramping for stress (model and actual data) — aggregate RL, asphalt AAG-1 (V1T0)

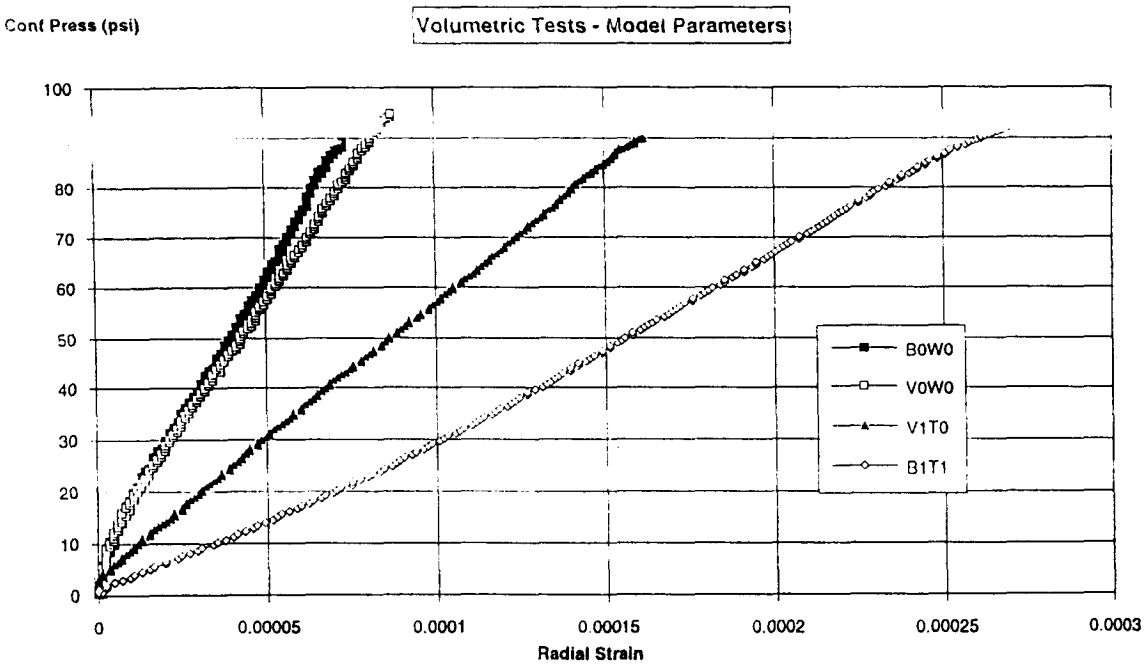

Figure B.19. Variation of radial strain with confining pressure — volumetric tests

Table B.1. Summary of C coefficients determined from the simple shear, uniaxial strain, and volumetric tests

	Simple Shear Tests		
	B0W0	V0W0	B1T1
C_2=	-3.88E+05	-1.06E+06	-2.74E+05
C_4=	1.52E+08	7.94E+08	8.14E+07
C_9=	-2.50E+11	-1.00E+10	-2.50E+09
	Uniaxial Strain Tests		
	B0W0	V0W0	B1T1
C_1=	3.71E+05	4.27E+05	3.11E+05
C_2=	-3.24E+05	-3.83E+05	-2.46E+05
C_3=	-2.94E+08	-6.15E+08	1.39E+07
C_4=	1.17E+08	4.48E+08	-6.84E+07
C_6=	2.91E+11	6.91E+11	-6.73E+10
C_7=	-9.67E+10	-6.01E+11	1.16E+11
Verif. Av=	4.66E+05	5.14E+05	4.40E+05
	Volumetric Tests		
	B0W0	V0W0	B1T1
A	4.66E+05	5.39E+05	2.52E+05
B	-6.89E+08	-8.22E+08	-4.03E+08
C	2.72E+11	3.17E+11	1.65E+11
C_5=	8.97E+08	6.77E+08	8.78E+07
C_8=	-6.50E+11	-6.20E+10	-5.40E+11

Note: All units are in psi.

In most instances the comparisons of the C's determined from the tests are reasonable. In the case of C_4 for the mix B1T1, however, a positive value was obtained in the simple shear test but a negative value was obtained in the uniaxial strain test. Some of the difference might be attributed to the use of different specimens in the two tests and their varying void contents.

It must be recognized, as stated earlier, that some viscous deformations are incorporated in these tests. Accordingly, the C values are probably smaller than they should be. This has led to the necessity of developing an algorithm that will permit determination of the true values for the nonlinear elastic coefficients, recognizing that load applications require finite times rather than being instantaneous (i.e., values which do not include viscous deformation).

The viscous components for the materials were determined from frequency sweep tests at 4°, 20°, and 40°C (39°, 68°, and 104°F). Strain control tests in shear were performed at frequencies of 0.01, 0.02, 0.05, 0.1, 0.2, 0.5, 1, 2, 5, 10 Hz at an amplitude of 0.0001 in./in. Tests were performed from the high frequency to low frequency at a particular temperature and from low temperature to high temperature. Master curves for each of the mixes were determined using the computer program IRIS. (N.B. These

computations are based on the assumption that the mixes exhibit thermorheologically simple behavior.) The assumption of thermorheologically simple response appears reasonable for the deformations used in the test as seen in Figure B.20.

The IRIS program was also used to determine the number and values for constants of the Maxwell elements in parallel required to match the master curves. Table B.2 contains the output of IRIS and includes the constants for the Williams Landel Ferry (WLF) equation. The constants permit the determination of the viscous parameters at any temperature, thus permitting performance predictions at any pavement temperature.

The fitted master curves and the values of G′ and G″ obtained from the tests are presented in Figures B.21 through B.24. The results suggest that the assumption of Maxwell elements in parallel represent the dynamic response to a reasonable degree.

It should be noted that the strain control, shear frequency sweep test is proving to be comparatively easy to perform and provides a reliable measure of the viscous response for a range in temperatures and frequencies. This test may also prove useful to investigate the influence of strain on the magnitude of the parameters.

To illustrate the influence of asphalt and aggregate type on mix stiffness, variation of G* and phase angle with frequency for the four mixes are shown in Figures B.25 and B.26. Note that the mixes containing asphalt AAG-1 exhibit different response than mixes containing asphalt AAK-1 relative to phase angle variation, Figure B.26. At lower frequencies (higher temperatures) the mixes with aggregate RB exhibit higher stiffnesses than the mixes with RL material. At higher frequencies the influence of the asphalt (stiffness) predominates.

Damage parameters were estimated from tests performed at 20°C (68°F) and 1 Hz frequency. Strain control shear tests were performed with strain amplitudes of 0.0001, 0.0002, 0.0005, 0.001, and 0.002 in./in. to investigate the influence of strain level on damage. In this analysis it was assumed that only one dashpot out of the 10 or 12 usually obtained for a mix from the IRIS program would be significantly influenced for the frequency and temperature used.

Figure B.27 illustrates the variation of stiffness ratio (stiffness at any strain amplitude divided by stiffness at small strain amplitude) with strain magnitude. It appears that the strain amplitude has comparatively small influence in reducing the spring stiffness, although slight strain softening is observed.

Figure B.28 suggests that the dashpot viscosity is strongly influenced by strain amplitude. In this figure the ratio of the viscosity at any strain amplitude to that of a strain level of 0.0001 in./in. is plotted as a function of strain amplitude. Moreover, when the ordinate, termed damage, has a value of 1, the dashpot is considered undamaged. As the value of the ordinate decreases, i.e., approaches 0, the damage to the dashpot increases.

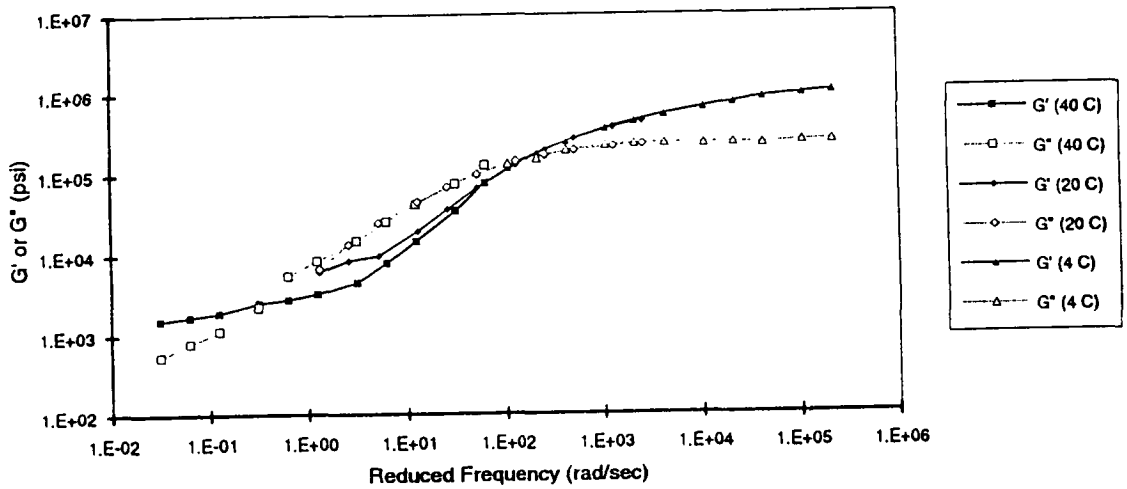

Figure B.20. Variation of G′ and G″ for an asphalt concrete mix with temperature and frequency (tests performed with strain control at a shear strain amplitude of 0.0001 in./in.)

Table B.2. Discrete relaxation spectra from computer program IRIS[20]

i	B0W0		V0W0		B1T1		V1T0	
	g_i	λ_i	g_i	λ_i	g_i	λ_i	g_i	λ_i
1	.2489E+07	.1493E-06	.4561E+06	.4763E-05	.2310E+07	.2652E-06	.2676E+06	.2757E-05
2	.2932E+06	.8310E-05	.2565E+06	.4029E-04	.2196E+06	.1240E-04	.2080E+06	.2102E-04
3	.2296E+06	.6178E-04	.2396E+06	.2042E-03	.1949E+06	.7684E-04	.1936E+06	.1144E-03
4	.1314E+06	.3468E-03	.2482E+06	.1155E-02	.1101E+06	.4544E-03	.1818E+06	.6875E-03
5	.8485E+05	.1915E-02	.1439E+06	.5862E-02	.5393E+05	.2643E-02	.1212E+06	.3886E-02
6	.2889E+05	.1064E-01	.7844E+05	.2986E-01	.1694E+05	.1677E-01	.5058E+05	.2087E-01
7	.1929E+05	.4147E-01	.4295E+04	.1758E+00	.2819E+04	.2982E-01	.7978E+04	.1037E+00
8	.8068E+04	.3931E+00	.1789E+04	.1199E+01	.4719E+04	.1409E+00	.2923E+04	.8906E+00
9	.2423E+04	.6496E+01	.6061E+03	.1051E+02	.2758E+04	.8117E+00	.5123E+03	.5411E+01
10	.3085E+04	.1859E+03	.1435E+04	.2688E+03	.2085E+04	.5739E+01	.9074E+03	.1698E+04
11					.1240E+04	.1404E+04		

[20]Spectra determination procedure by M. Baumgaertel and H. Winter.

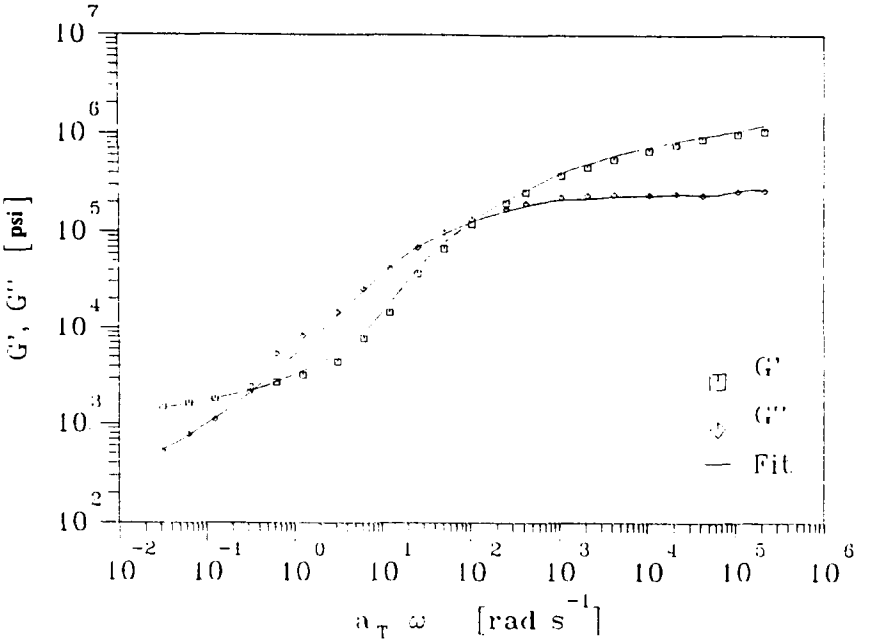

Figure B.21. Variation of G′ and G″ with frequency for mix V0W0 (aggregate RB, asphalt AAG-1) at a reference temperature of 40°C (104°F)

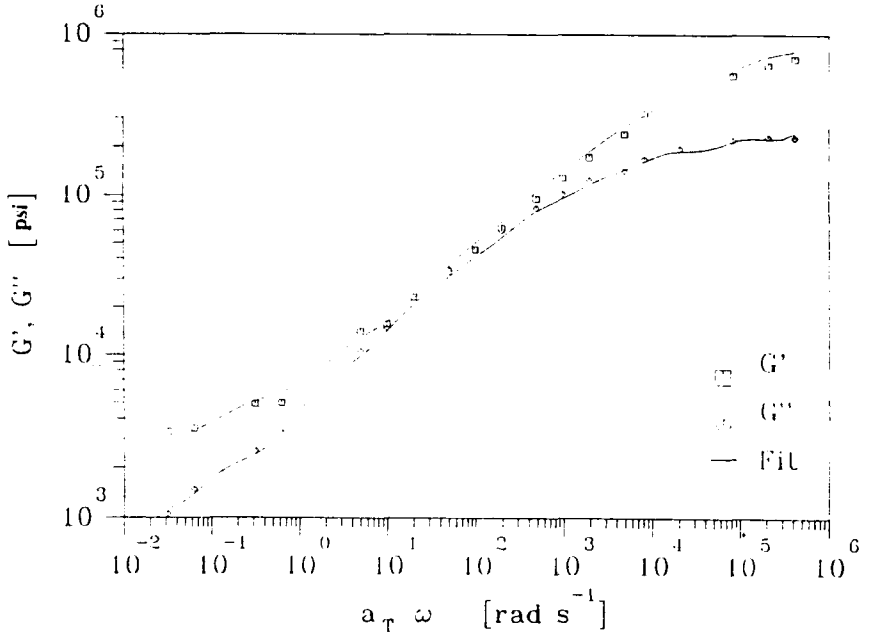

Figure B.22. Variation of G′ and G″ with frequency for mix B0W0 (aggregate RB, asphalt AAK-1) at a reference temperature of 40°C (104°F)

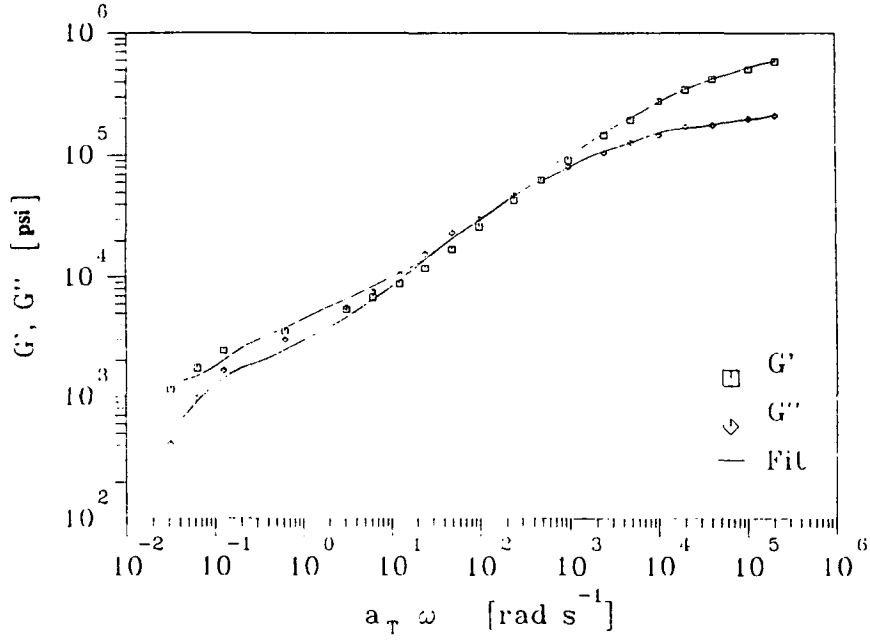

Figure B.23. Variation of G′ and G″ with frequency for mix B1T1 (aggregate RL, asphalt AAK-1) at a reference temperature of 40°C (104°F)

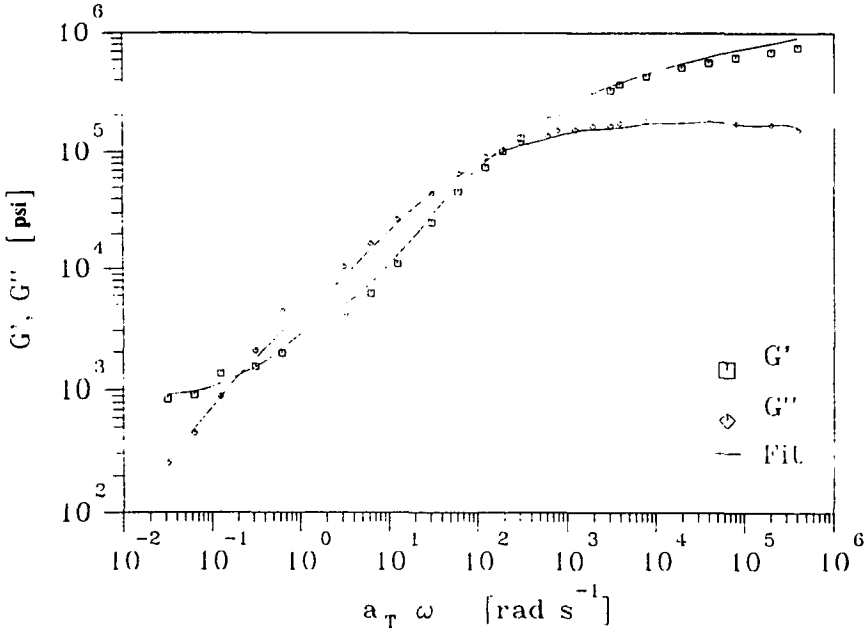

Figure B.24. Variation of G′ and G″ with frequency for mix V1T0 (aggregate RL, asphalt AAG-1) at a reference temperature of 40°C (104°F)

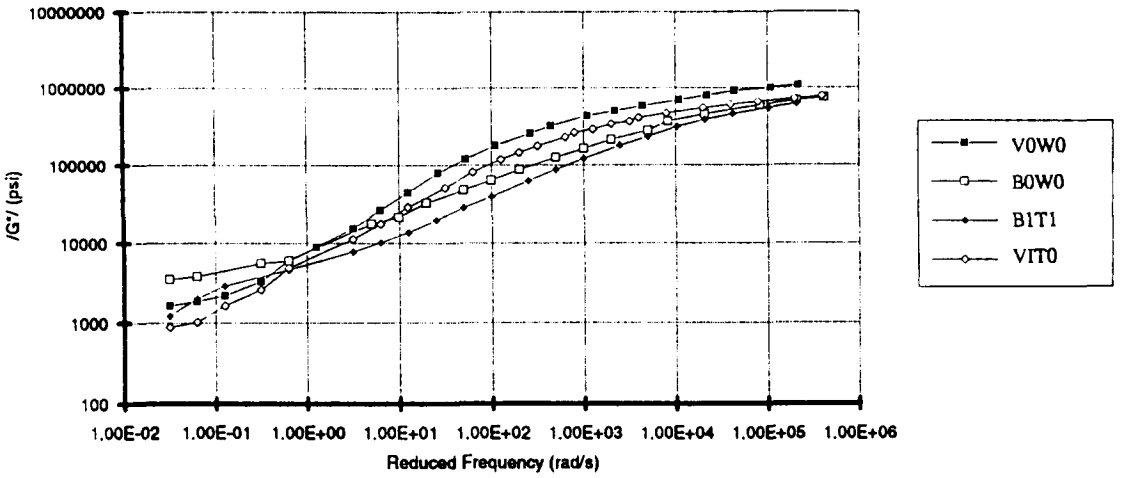

Figure B.25. Complex shear modulus versus reduced frequency (40°C [104°F] reference) from shear frequency sweeps

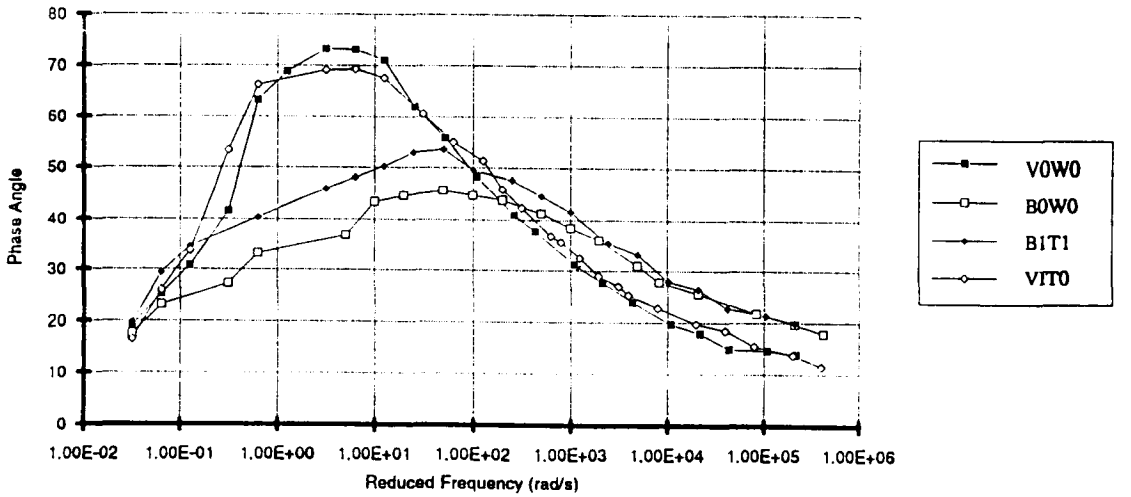

Figure B.26. Phase angle versus reduced frequency (40°C [104°F] reference) from shear frequency sweeps

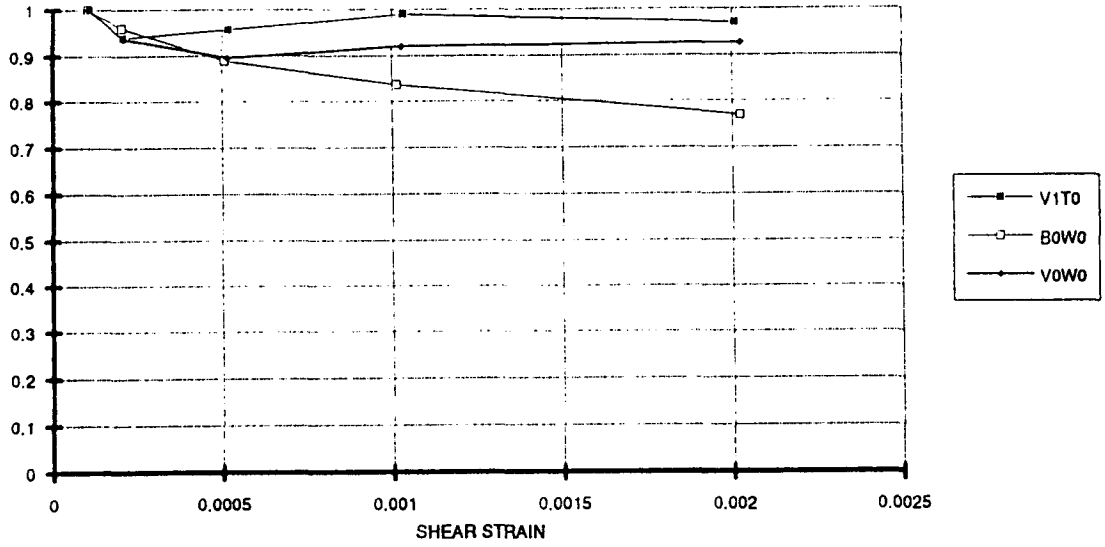

Figure B.27. Variation of stiffness ratio (E/E_0) in strain sweep tests at 20°C (68°F) and 1 Hz

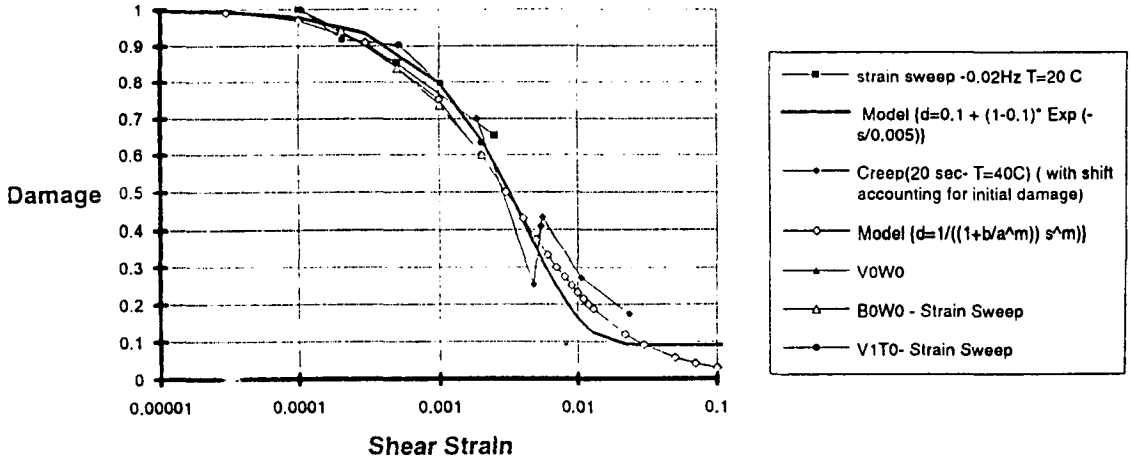

Figure B.28. Comparison of the shape of the damage function obtained from shear strain sweeps and from shear creep tests with proposed damage model

In Figure B.28, development of damage with strain level obtained from creep tests is presented. The variation of the damage parameter with strain magnitude appears to follow a similar path for both strain sweep and creep tests. These results suggest a highly nonlinear behavior in the dashpots; however, the nonlinearity appears to be independent of the mix composition.

Table B.3 contains a summary of the material properties obtained for the four mixes that have been subjected to the battery of permanent deformation tests. Note that the values of C_2 obtained from the frequency sweep tests are higher than those obtained from the simple shear, uniaxial strain, and volumetric tests. This is not surprising. Tests performed in the frequency sweep tests at 4°C (39°F) and 10 Hz yield higher values for G* than those obtained at 0.1 Hz frequency at the same temperatures. It can be argued that the finite times of loading in the simple shear, uniaxial strain, and volumetric tests are analogous to those associated with tests performed at 0.1 Hz and therefore provide lower values for the C's than if they had been determined at a rate corresponding to 10 Hz.

To match the viscous parameters and C constants, the C_1 and C_2 values were corrected proportionally. Unfortunately, time has not permitted the other C values to be corrected. *A program to determine all the nonlinear elastic, viscous, and damage parameters, taking each of these factors into consideration by using an iterative procedure with a quadratic convergency, is under development and should yield consistent and accurate parameters rapidly.*

The data in Table B.2 (using the higher values for C_1 and C_2) provide the basis for predicting the performance of the mixes in some other form of loading and thus serve to provide validation of the permanent deformation model.

A repetitive simple shear test at constant height was selected for the validation process. This test was conducted at 40°C (104°F) using a time of loading of 0.1 s and a time interval between load applications of 0.6 s. The magnitude of the repeated shear stress was 52 kPa (7.5 psi). The height of each specimen was maintained within ± 0.00005 in. Results from the tests on the four mixes are presented in Figure B.29 as permanent shear strain versus the number of load applications.

Generally, results appear reasonable, although the B0W0 mix (aggregate RB, asphalt AAK-1) should have performed better than the V0W0 mix (aggregate RB, asphalt AAG-1). Other than that, the ranking of the mixes is as expected. Specimens with RB aggregate perform much better than those containing RL aggregate.

For validation purposes, a two-element finite element mesh representing half of the shear specimens was used to take advantage of the antisymmetry of the load. The model assumes that the state of stress in the true specimen is perfect (i.e., that a state of pure shear stress exists within the cylindrical specimen).

Table B.3. Mix parameters for permanent deformation model; 4 mixes

	B0W0	V0W0	B1T1	V1T0
Asphalt Type	AAK-1	AAG-1	AAK-1	AAG-1
Asphalt Content		4.5		
Aggregate Type	RB	RB	RL	RL
Void Level (%)	3.7	3.6	7.9	3.1
Compaction Type	rolling	rolling	rolling	rolling
Nonlinear Elastic Constants (psi)				
C_1	3.71E+05	4.27E+05	3.11E+05	
C_1 corrected	7.54E+06	3.19E+06	7.37E+06	
C_2	-3.24E+05	-3.83E+05	-2.46E+05	
C_2 corrected	-6.58E+06	-2.86E+06	-5.84E+06	
C_3	-2.94E+08	-6.15E+08	1.39E+07	
C_4	1.17E+08	4.48E+08	-6.84E+07	
C_5	8.97E+08	6.77E+08	8.78E+07	
C_6	2.91E+11	6.91E+11	-6.73E+10	
C_7	-9.67E+10	-5.01E+11	1.16E+11	
C_8	8.97E+08	6.77E+08	8.78E+07	
C_9	-1.00E+12	-6.20E+10	-5.40E+11	
Viscous Parameters				
Ref. Temp (°C)	40	40	40	40
C_1 (WLF)	48.02	7.35	53.5	30.4
C_2 (WLF)(K)	-416.57	110.77	583.2	324
Viscous Poisson's	0.489	0.489	0.489	0.489
Ratio	5.94E+05	3.99E+05	1.76E+06	7.74E+05
η_o (psi)	3.29E+06	1.43E+06	2.92E+06	1.04E+06
α_i	7.57E-01	3.19E-01	7.91E-01	2.59E-01
	8.91E-02	1.79E-01	7.52E-02	2.01E-01
	6.98E-02	1.67E-01	6.68E-02	1.87E-01
	3.99E-02	1.73E-01	3.77E-02	1.76E-01
	2.58E-02	1.01E-01	1.85E-02	1.17E-01
	8.78E-03	5.48E-02	5.80E-03	4.89E-02
	5.86E-03	3.00E-03	9.66E-04	7.71E-03
	2.45E-03	1.25E-03	1.62E-03	2.82E-03
	7.37E-04	4.24E-04	9.45E-04	4.95E-04
	9.38E-04	1.00E-03	7.14E-04	8.77E-04
			4.25E-04	

Table B.3 (continued). Mix parameters for permanent deformation model; 4 mixes

	B0W0	V0W0	B1T1	V1T0
β_i	6.26E-07	5.45E-06	3.49E-07	4.76E-07
	4.10E-06	2.59E-05	1.55E-06	2.82E-06
	2.39E-05	1.23E-04	8.53E-06	1.43E-05
	7.67E-05	7.19E-04	2.85E-05	8.07E-05
	2.74E-04	2.12E-03	8.12E-05	3.04E-04
	5.18E-04	5.88E-03	1.62E-04	6.82E-04
	1.35E-03	1.89E-03	4.79E-05	5.34E-04
	5.34E-03	5.38E-03	3.79E-04	1.68E-03
	2.65E-02	1.60E-02	1.27E-03	1.79E-03
	9.66E-01	9.68E-01	6.81E-03	9.95E-01
			9.91E-01	
Damage Parameters (Simo Max Strain Model)				
alpha 1	0.004	0.004	0.004	0.004
beta 1	0.09	0.09	0.09	0.09
m	n/a	n/a	n/a	n/a
Damage Parameters (Shmuel Max Strain Model)				
alpha 1	0.0003	0.0003	0.0003	0.0003
beta 1	0.1	0.1	0.1	0.1
m	1	1	1	1

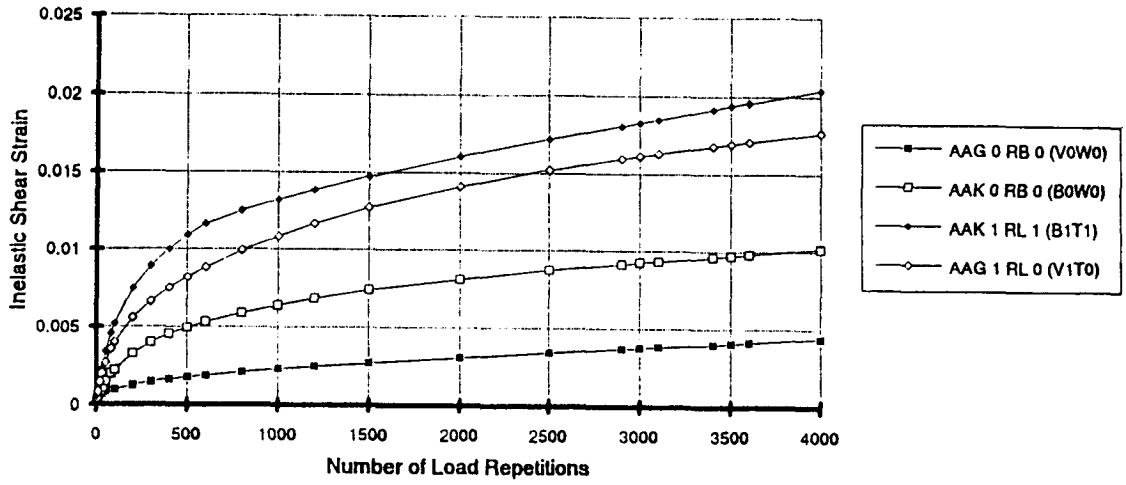

Figure B.29. Accumulation of permanent shear strain with number of load repetitions (52 kPa [7.5 psi]) in simple shear constant height tests at 40°C [104°F], 0.1 s loading, 0.6 s rest period)

Using this model and material properties presented in Table B.3, 100 cycles of 0.1 s loading and 0.6 s unloading were simulated (Figure B.30). The simulations ranked the mixes according to their known permanent deformation resistance. This was an important demonstration considering that mix properties used in the simulations were based on measurements not only made at different frequencies and times of loading, but measured in totally different types of tests.

Figure B.31 compares results obtained from the test of B1T1 mix with predictions obtained from the model assuming several levels of damage. Adding a damage component to the mix model significantly improves the ability to simulate test measurements. Figure B.32 shows a similar comparison for the V0W0 mix.

Results indicate that the mix model has the potential to capture some of the important aspects of the asphalt aggregate mix response. Also, based on this investigation, testing at 4°C (39°F) in an effort to minimize the viscous component of the mix response was no longer necessary. Rather, it was decided to perform the suite of tests at 40°C (104°F). It was decided to include a fourth temperature, 60°C (140°F), to the frequency sweep tests to extend the number of loading cycles that can be reasonably simulated.

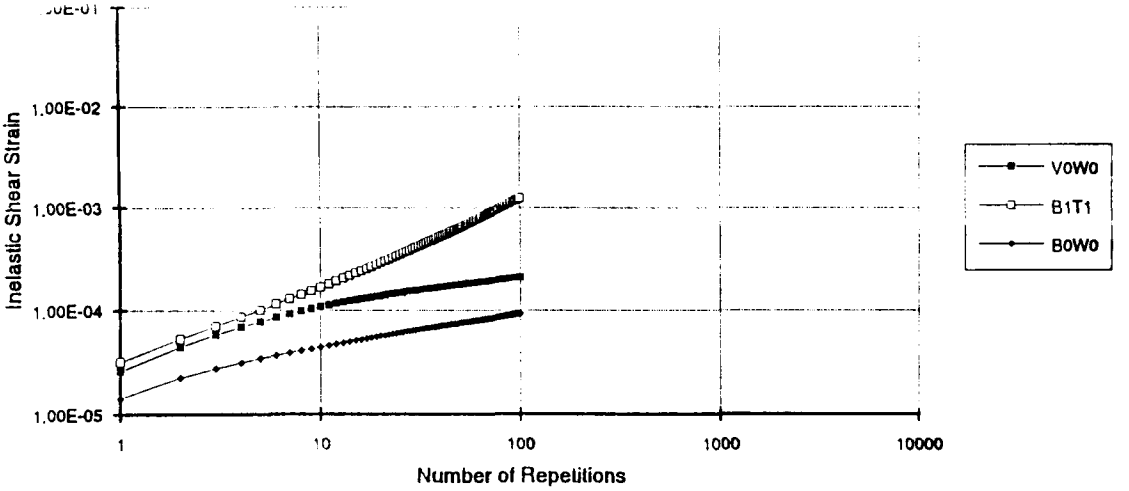

Figure B.30. Model prediction of accumulation of permanent deformation in the repetitive simple shear test

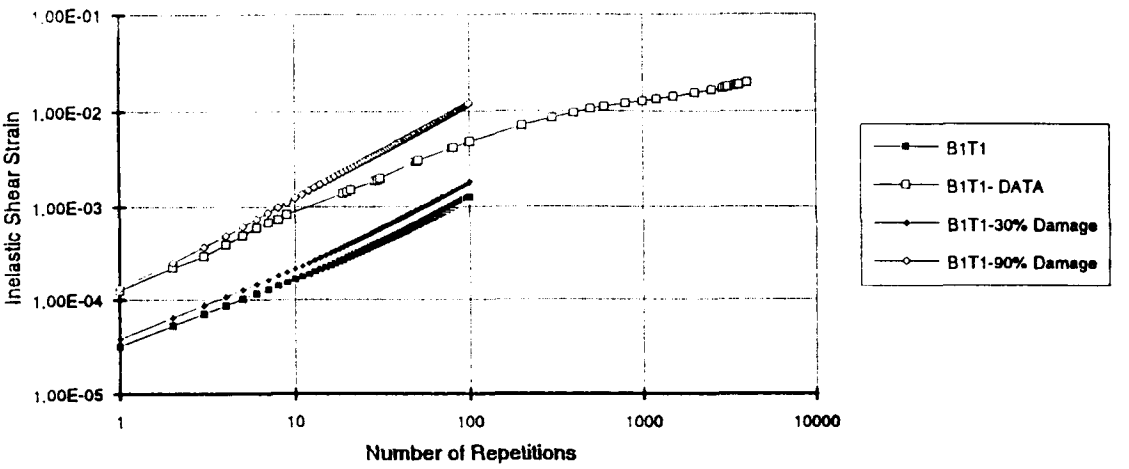

Figure B.31. Comparison between data and model prediction of accumulation of permanent deformation in the repetitive simple shear test for B1T1

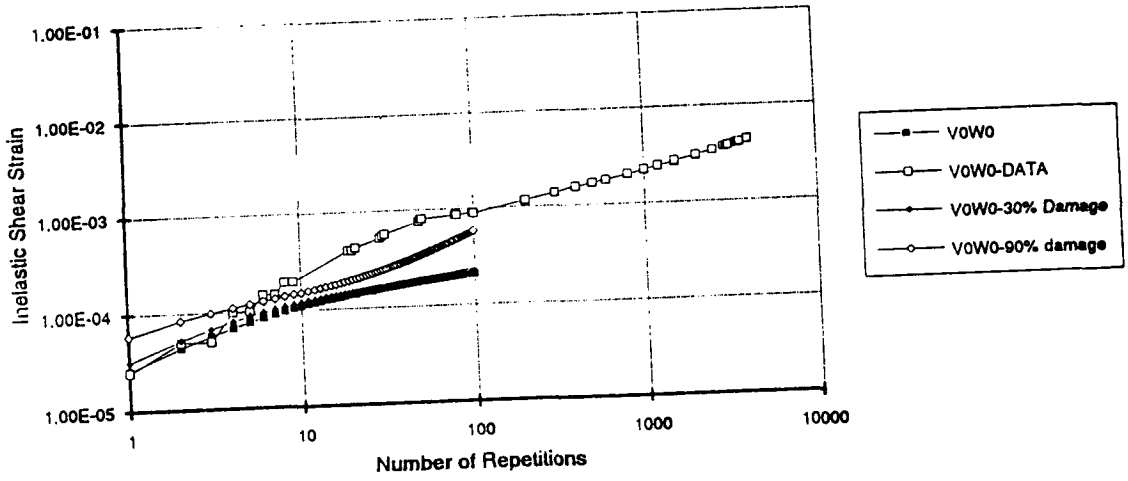

Figure B.32. Comparison between data and model prediction of accumulation of permanent deformation in the repetitive simple shear test for V0W0

Appendix C

Effects of Tire Pressure, Pavement Thickness, and Underlying Support Stiffness on Relationship Between Maximum Permanent Shear Strain and Rut Depth

Analyses of the permanent deformation response of the pavement section shown in Figure C.1 have been conducted to ascertain the influence of tire pressure on the relationship between maximum permanent shear strain and rut depth. For these analyses only the nonlinear elastic and viscous properties were incorporated in the constitutive relationship used in the finite element analysis to investigate relationships between tire pressure, rut depth, and permanent shear and axial strains (Chapter 6).

The relationship between rut depth and permanent shear strain presented as Equation 6.34 in Chapter 6 was based on a tire pressure of 690 kPa (100 psi). For the analyses, two additional stress levels for the tire loading, 1380 and 3450 kPa (200 and 500 psi), were used and were applied as a pulse loading with a duration of 0.3 s and an interval of 0.4 s between pulses. The conditions of high tire pressure and comparatively long time of loading were selected so that large ruts and the associated large permanent strains could be obtained with relatively few load cycles.

The magnified deformed finite element mesh is shown in Figure C.2 at the end of the second load cycle for the 3450 kPa (500 psi) tire loading condition. Figures C.3 and C.4 show the changes in pavement profile with load applications for the 1380 and 3450 kPa (200 and 500 psi) conditions. For the 3450 kPa (500 psi) loading, note that considerable upheaval of the pavement surface occurs between the tires. For the 1380 kPa (200 psi) condition this upheaval is less pronounced. The difference may be due in part to the fact that the magnitude of the elastic strain is smaller for the 1380 kPa (200 psi) loading. Our research indicates that dilation exhibits a nonlinear dependence on the magnitude of the shear strain, essentially a nonlinear increase with increase in shear strain.

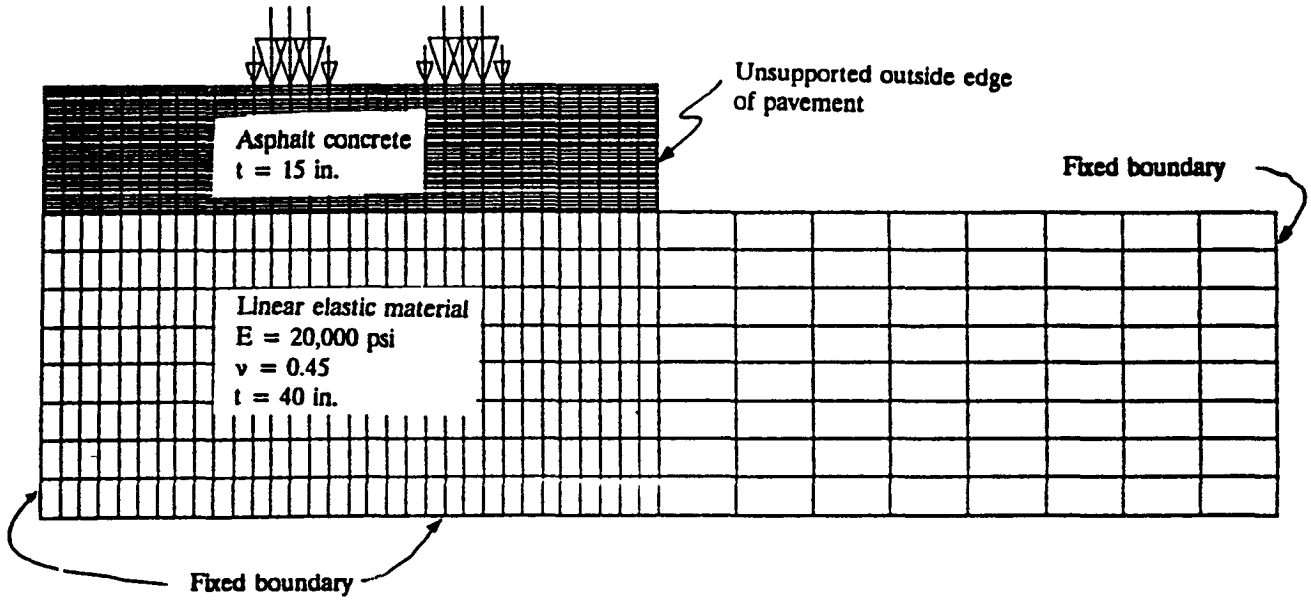

Figure C.1. Pavement cross-section represented by two-dimensional finite-element mesh

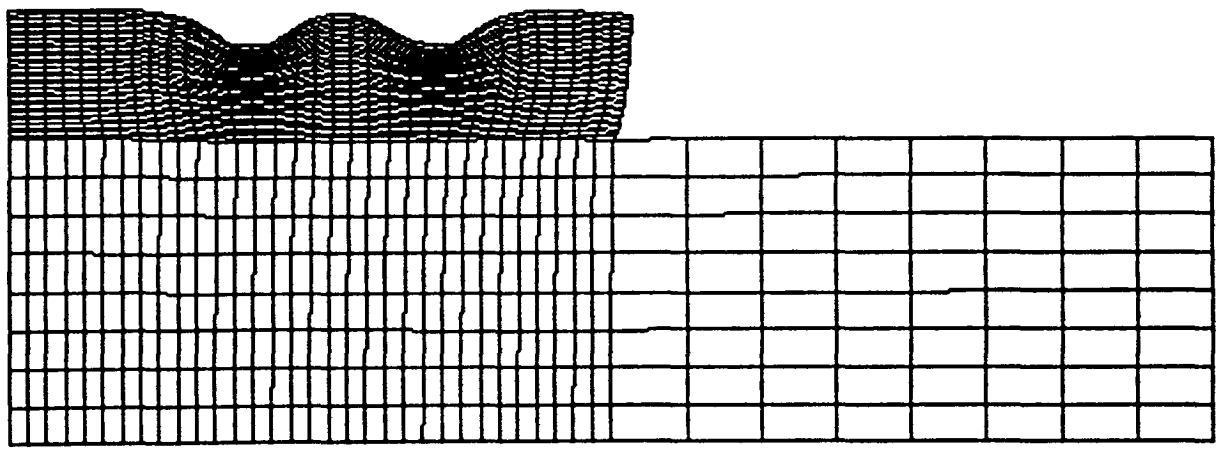

Figure C.2. Deformed finite-element mesh, second loading cycle

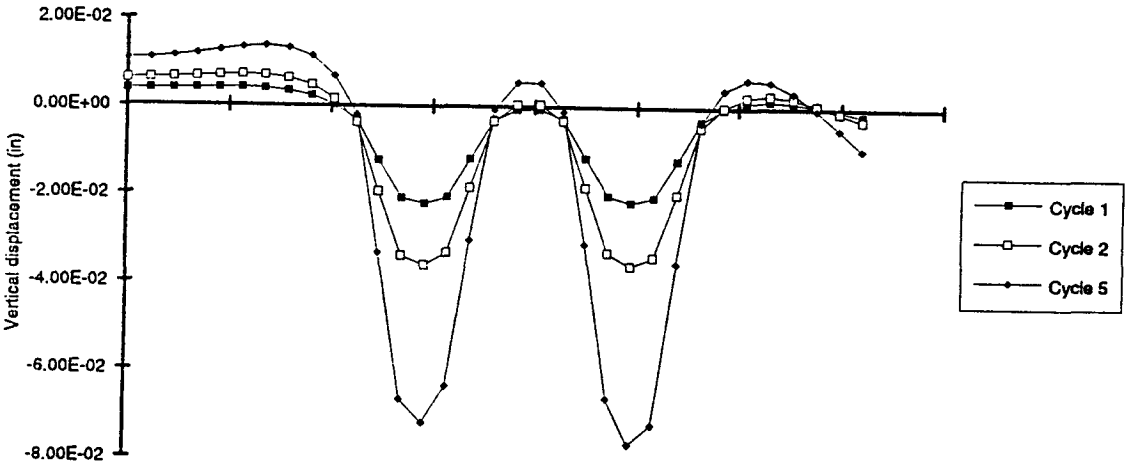

Figure C.3. Variation of pavement profile with the number of load applications, stress level 3450 kPa (500 psi), loading time 0.3 s, rest period 0.4 s

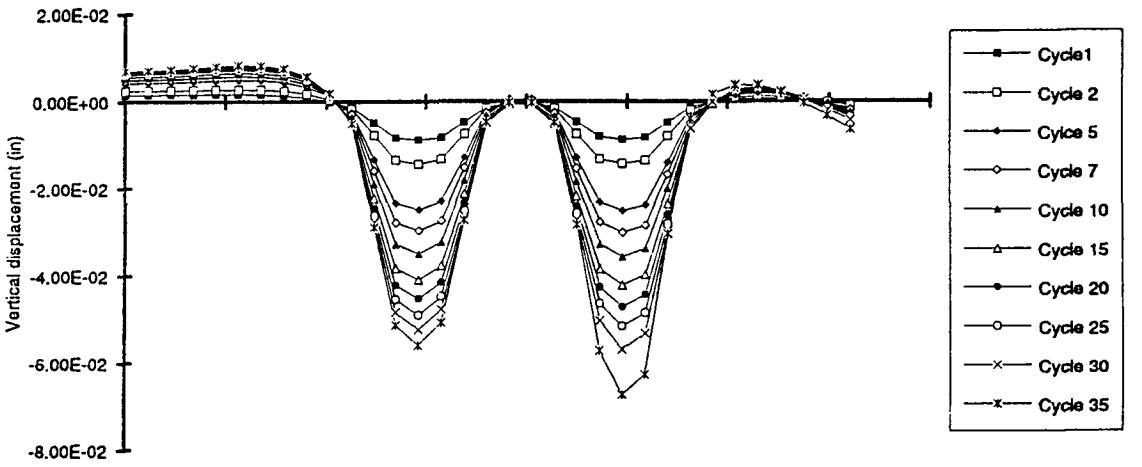

Figure C.4. Variation of pavement profile with the number of load applications, stress level 1380 kPa (200 psi), loading time 0.3 s, rest period 0.4 s

Figure C.5 suggests that there may be a linear relationship between rut depth and maximum permanent shear strain. (N.B. Some of the nonlinearity at the larger rut depths may be due to instability in the computational procedure.) In Figure C.5, note that the shear strains are larger than the axial strains.

Using the same values for C_1 and C_2 and the viscous components as in the previous runs, but eliminating the nonlinear elastic part of the material response, i.e., setting the coefficients C_3 through C_9 equal to 0, the change of the pavement profile with the number of cycles was determined. Figure C.6 shows the results. It is clear the upheaval at the edge of each tire has been significantly reduced and that there is almost no upheaval between tires. This observation confirms the need to model the nonlinear behavior of the material if realistic permanent deformation profiles are to be predicted.

Also as noted in Chapter 6, Symplectic Engineering to incorporate plasticity, improved the constitutive relationship over that described earlier in this section.

With initial material characteristics according to the model mathematically described in Chapter 6 for a mix containing asphalt AAM-1 and aggregate RH with an air void content of approximately 4 percent, a series of analyses were performed for the pavement structure analysis and loading conditions shown in Figure C.7. For this analysis (690 kPa [100 psi] tire pressure) a load duration of 0.1 s and a time interval between load application of 0.6 s were used.

Variation of rut depth with shear strain is illustrated in Figure C.8. It was from this relationship that the linear relationship between permanent shear strain and rut depth was further evaluated; as noted in Chapter 13, this is important to the development of a simplified procedure for mix evaluation.

Figure C.9 presents the variation of the rut depth and maximum shear strain with the number of cycles. In this figure the accumulation of permanent deformation computed in constant height repetitive simple shear tests at different stress levels is also presented. These are values predicted by modeling the shear test using only two finite elements. It is important to note that the variation with the number of cycles of the maximum permanent shear strain in the pavement and the permanent shear strain in the test at 140 kPa (20 psi) is almost identical. This would indicate that if tests were performed under these conditions, predictions of rut depth could be made, provided that the adequate material properties are obtained.

Figure C.10 compares the maximum shear strain obtained in the pavement with the results obtained from constant height simple shear tests on several mixes. It is likely that the material properties used for the mix with asphalt AAM-1 and aggregate RH requires adjustment to the parameters of the plastic component.

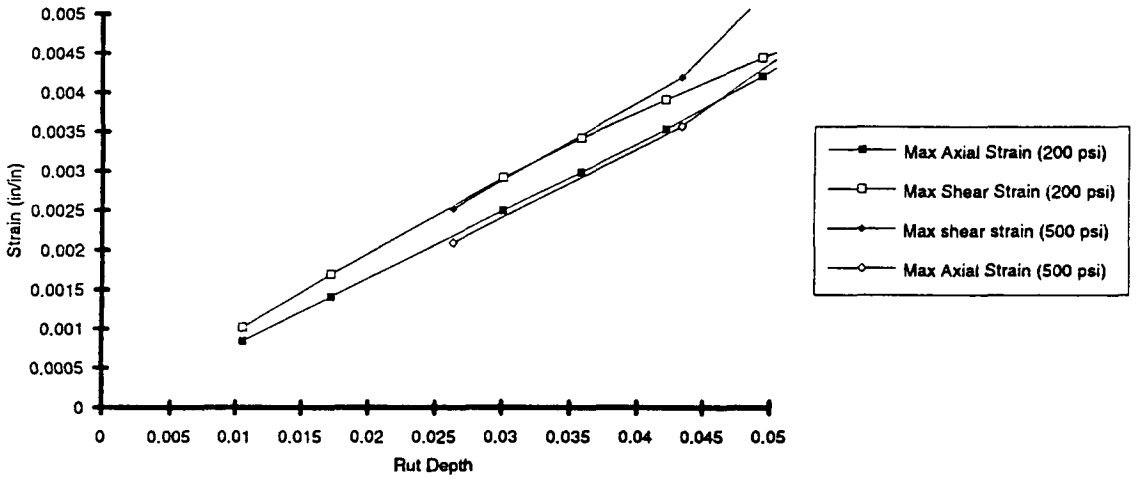

Figure C.5. Comparison of relationships between rut depth and strain for 1380 and 3450 kPa (200 and 500 psi) load levels

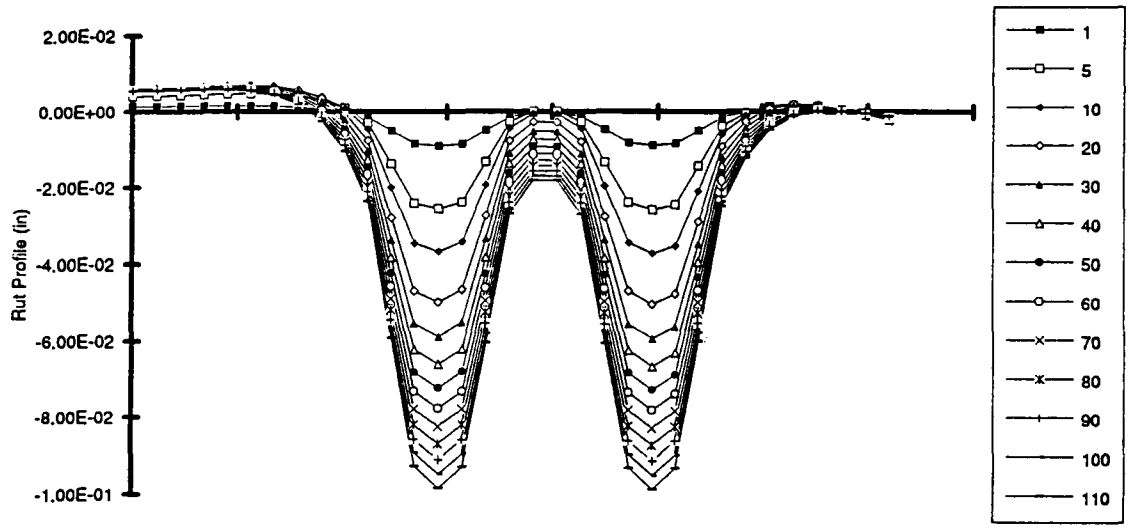

Figure C.6. Variation of pavement profile with number of cycles (1380 kPa [200 psi] tire pressure)

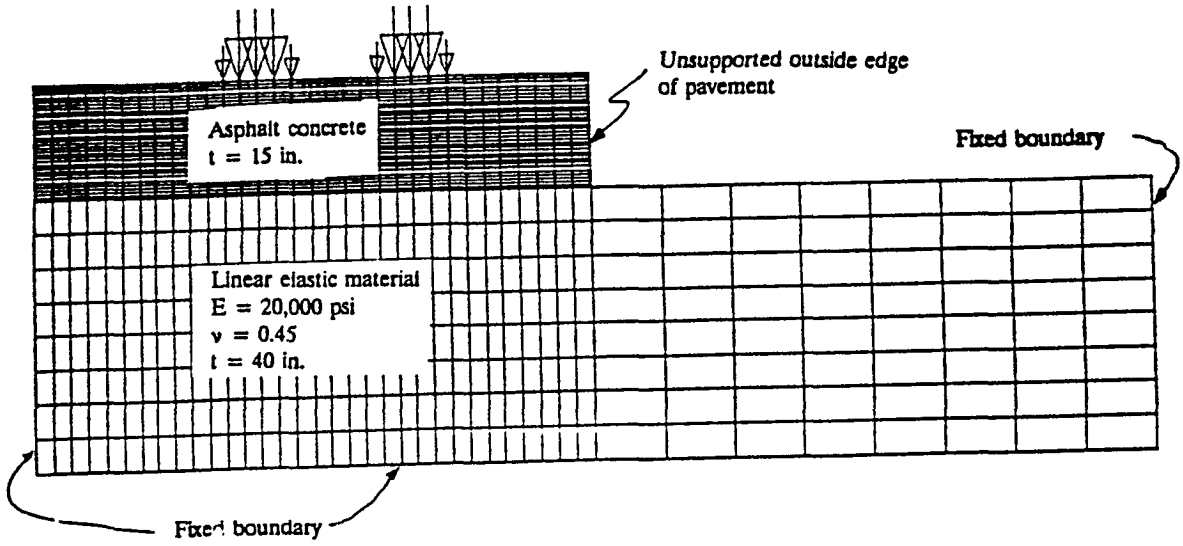

Figure C.7. Sample two-dimensional mesh

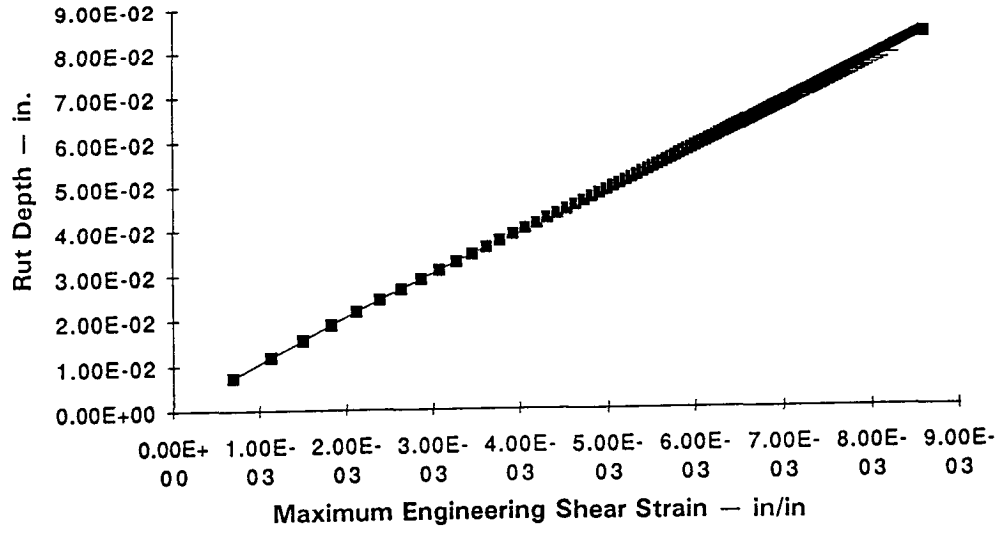

Figure C.8. Rut depth as a function of the maximum engineering shear strain

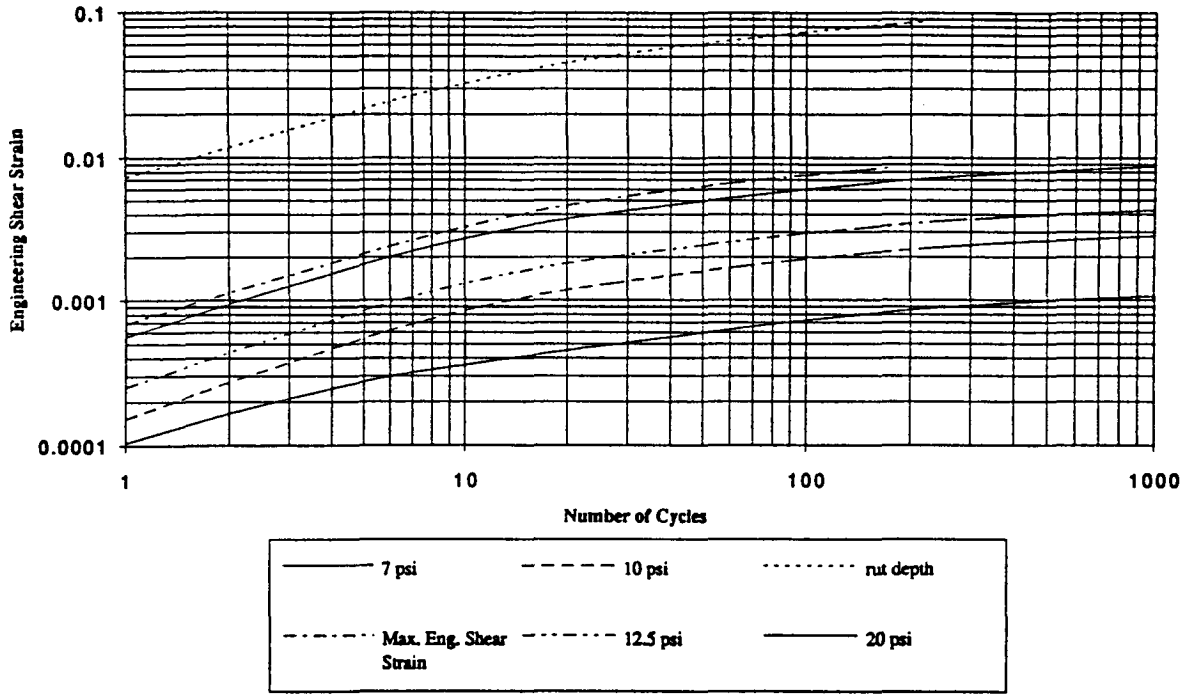

Figure C.9. Simple shear constant height test, engineering strain as a function of the number of cycles

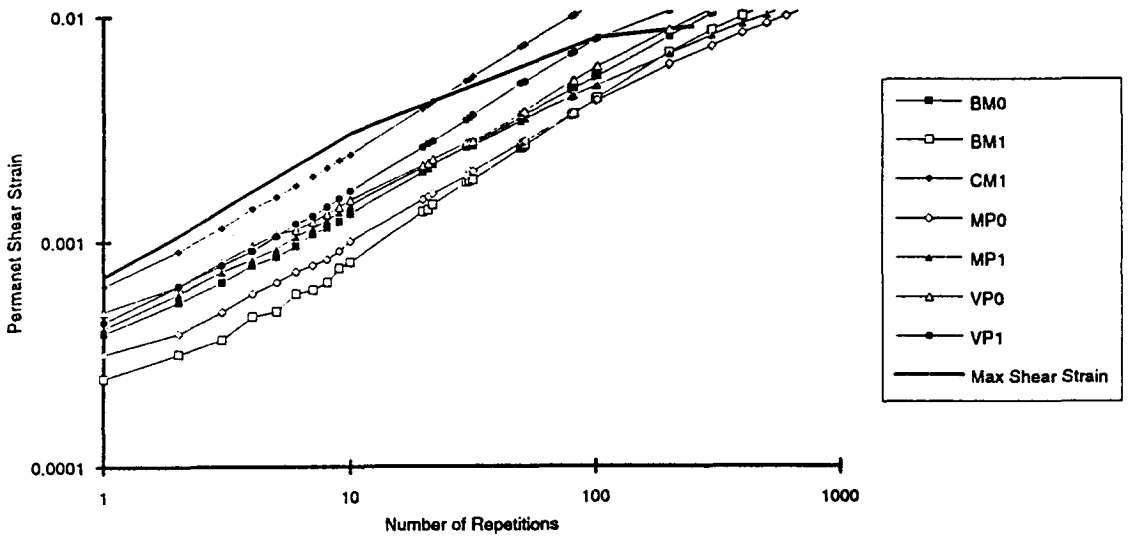

Figure C.10. Permanent deformation versus number of repetitions in constant height simple shear tests at 40°C (104°F) (0.1 s, .6 s) (47 kPa [6.8 psi] shear stress)

Influence of Pavement Thickness and Underlying Support Stiffness in the Relationship Between Maximum Permanent Shear Strain and Rut Depth[21]

To determine the effects of asphalt concrete thickness on the relationship between rut depth and shear strain, the pavement structure shown in Figure C.11 (similar to the structure shown in Figure C.7) was analyzed using the following asphalt concrete layer thicknesses and other material characteristics:

AC Thickness (in.)	Basic Layer Modulus, E (ksi)	Poisson's Ratio
4	30	0.35
6	25	0.35
9	20	0.35
12	15	0.35

Three of the mixes whose characteristics have been described in Chapter 6 — low and high void content mixes containing binders AAK, AAM, and AAG— were utilized for the analyses. These three mixes were considered to represent stiff, medium, and soft mixes, respectively.

Plane-strain finite-element simulations of the pavement sections subjected to 300 cycles of loading (0.1 s haversine pulse of 690 kPa [100 psi] followed by 0.6 s rest period) were conducted. The results obtained for these pavement sections are shown in Figures C.12 through C.51.

To determine the effects of underlying layer stiffness on permanent deformation response, three thicknesses of asphalt concrete — 10 cm, 15 cm, and 20 cm (4 in., 6 in., and 8 in.) — resting on a 15 in. thick layer of portland cement concrete (whose modulus was assumed to be 5.0×10^6 psi) were analyzed for the same loading conditions. These results are shown in Figures C.34-C.51.

To determine the parameter K in Equation 6.35, i.e.,

$$\text{Rut depth} = K \cdot (\gamma_p)\ \text{max}, \tag{6.35}$$

relationships between the ratio of rut depth to engineering shear strain were obtained from information contained in Figures C.23 to C.25 and Figures C.30 to C.32. The results are shown in Figure C.33. Similar types of information could be obtained from Figures D.34

[21]This study was completed by Symplectic Engineering after the Strategic Highway Research Project (SHRP) contract had been terminated (May 1993). Funds from another source were used. It was considered important enough to the overall goals of this permanent deformation project to be included.

through C.36. Average values for these ratios are shown in Figure C.52 for both cases examined herein.

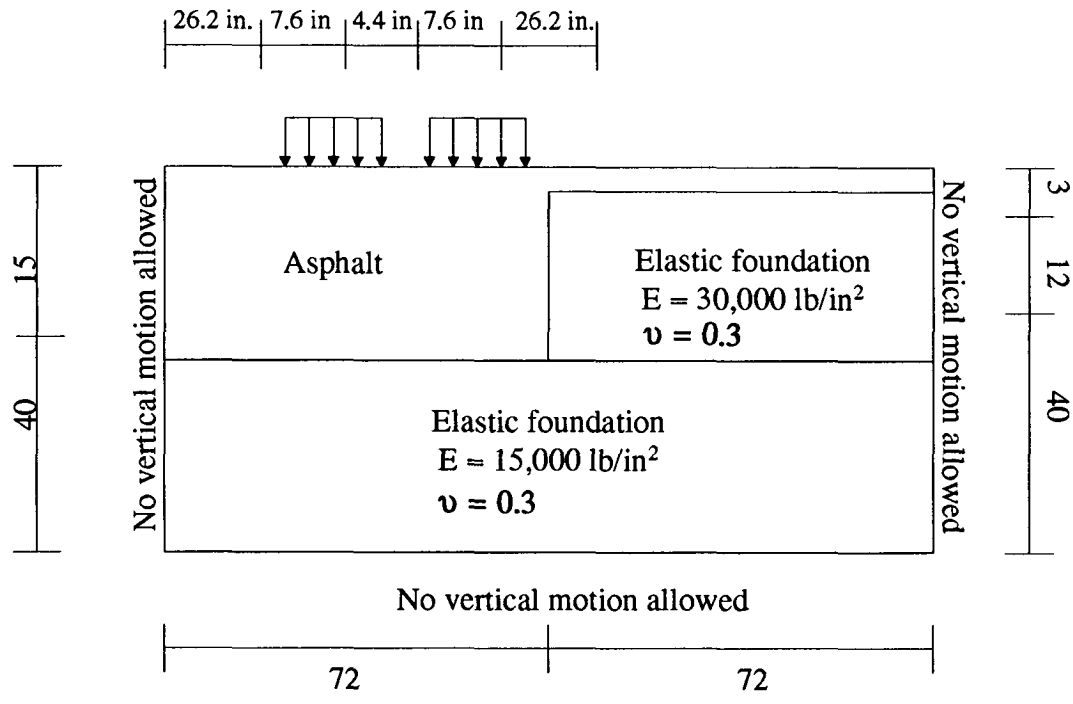

Note: All dimension in inches

Figure C.11. Pavement and load geometry for effect of layer thickness

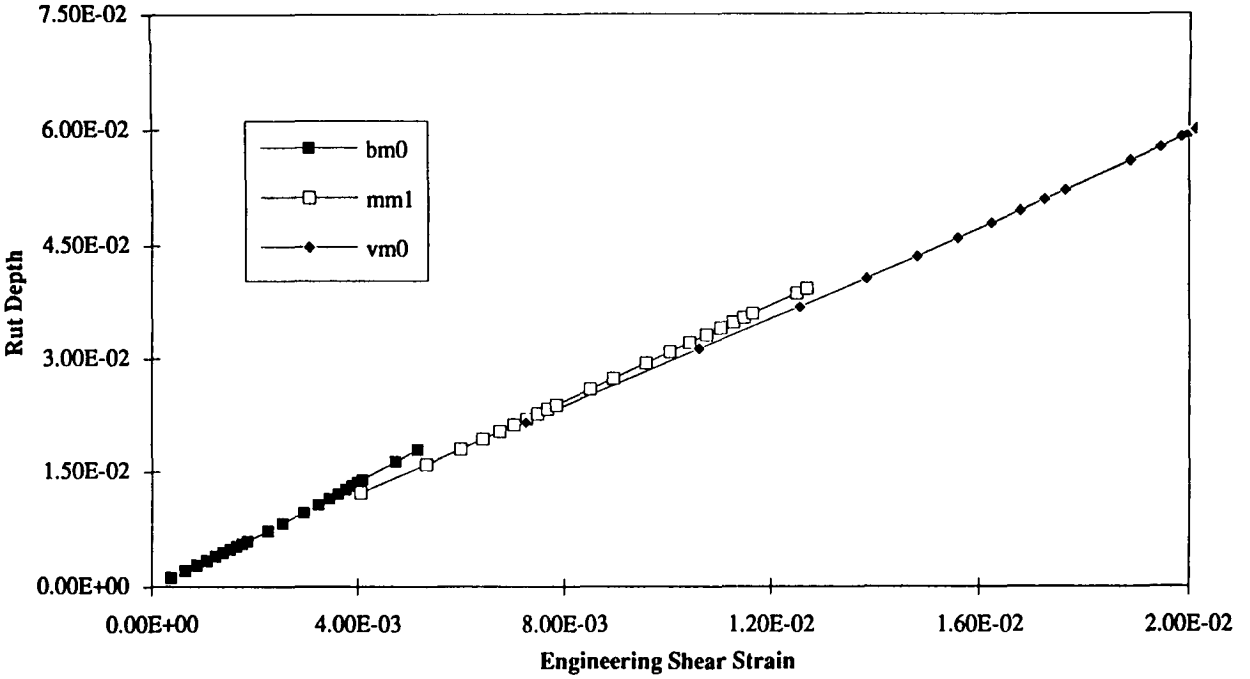

Figure C.12. Rut depth to maximum engineering shear strain ratio; 10 cm (4 in.) AC on 100 cm (40 in.) of elastic foundation

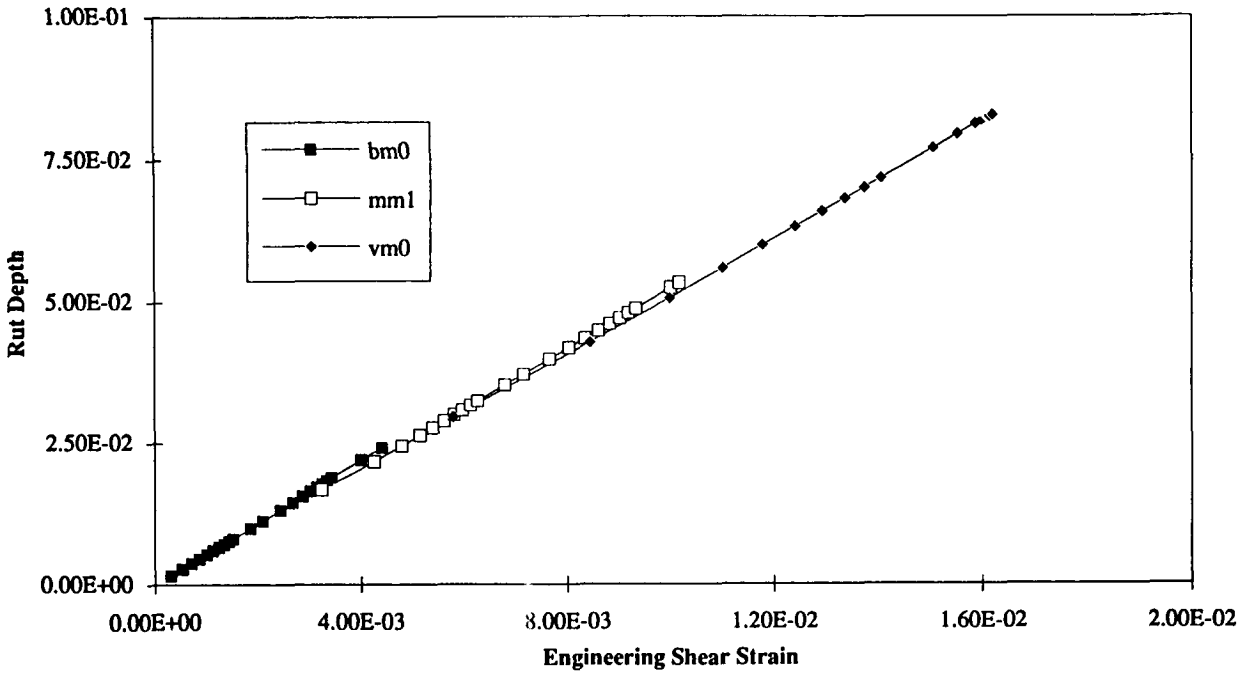

Figure C.13. Rut depth to maximum engineering shear strain ratio; 15 cm (6 in.) AC on 100 cm (40 in.) of elastic foundation

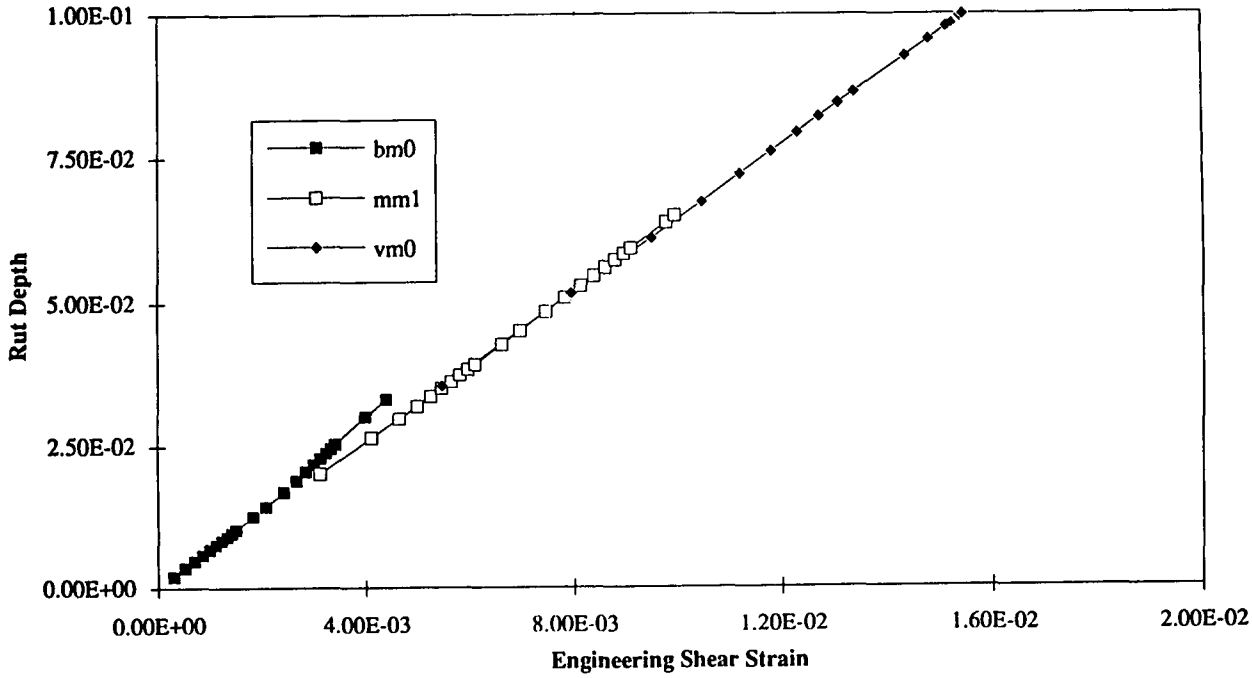

Figure C.14. Rut depth to maximum engineering shear strain ratio; 22.5 cm (9 in.) AC on 100 cm (40 in.) of elastic foundation

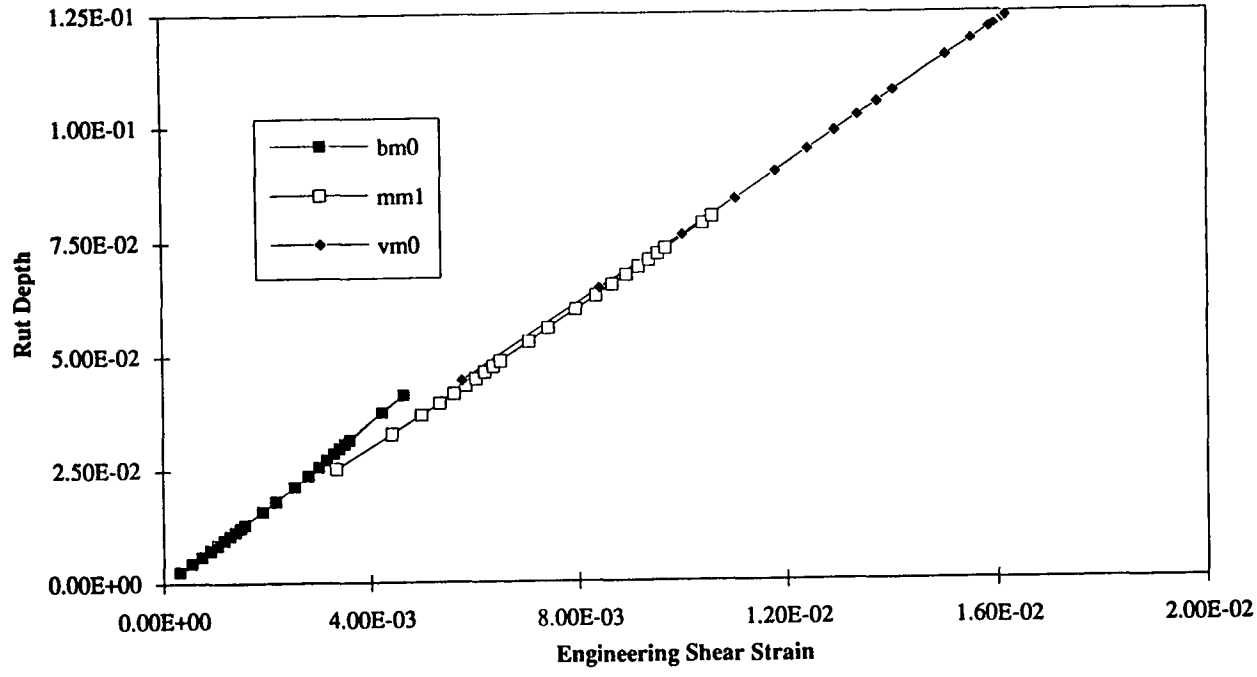

Figure C.15. Rut depth to maximum engineering shear strain ratio; 30 cm (12 in.) AC on 100 cm (40 in.) of elastic foundation

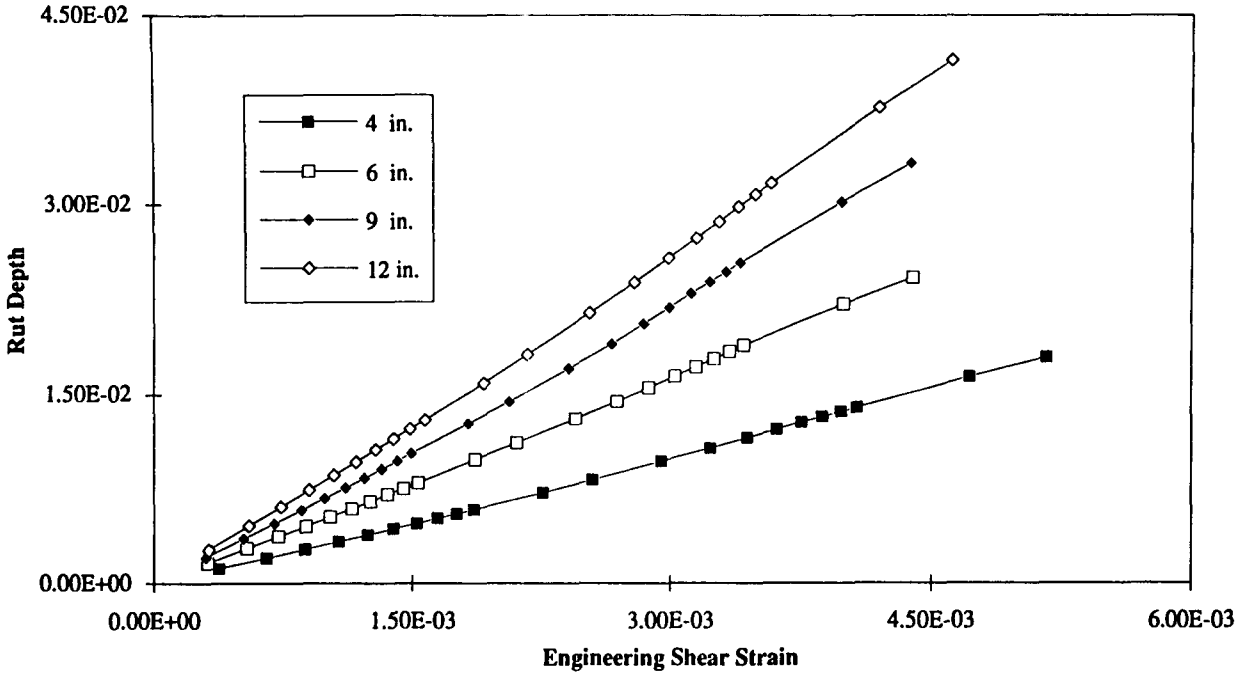

Figure C.16. Rut depth to maximum engineering shear strain ratio; bm0 mix on 100 cm (40 in.) of elastic foundation

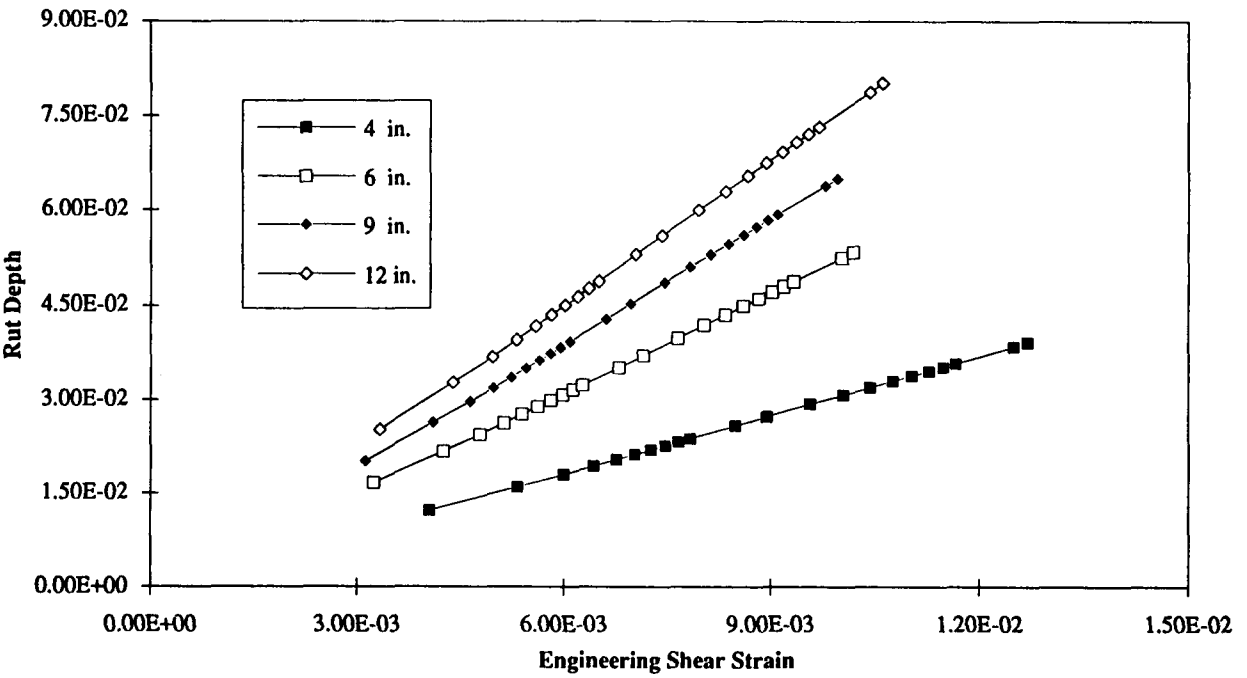

Figure C.17. Rut depth to maximum engineering shear strain ratio; mm1 mix on 100 cm (40 in.) of elastic foundation

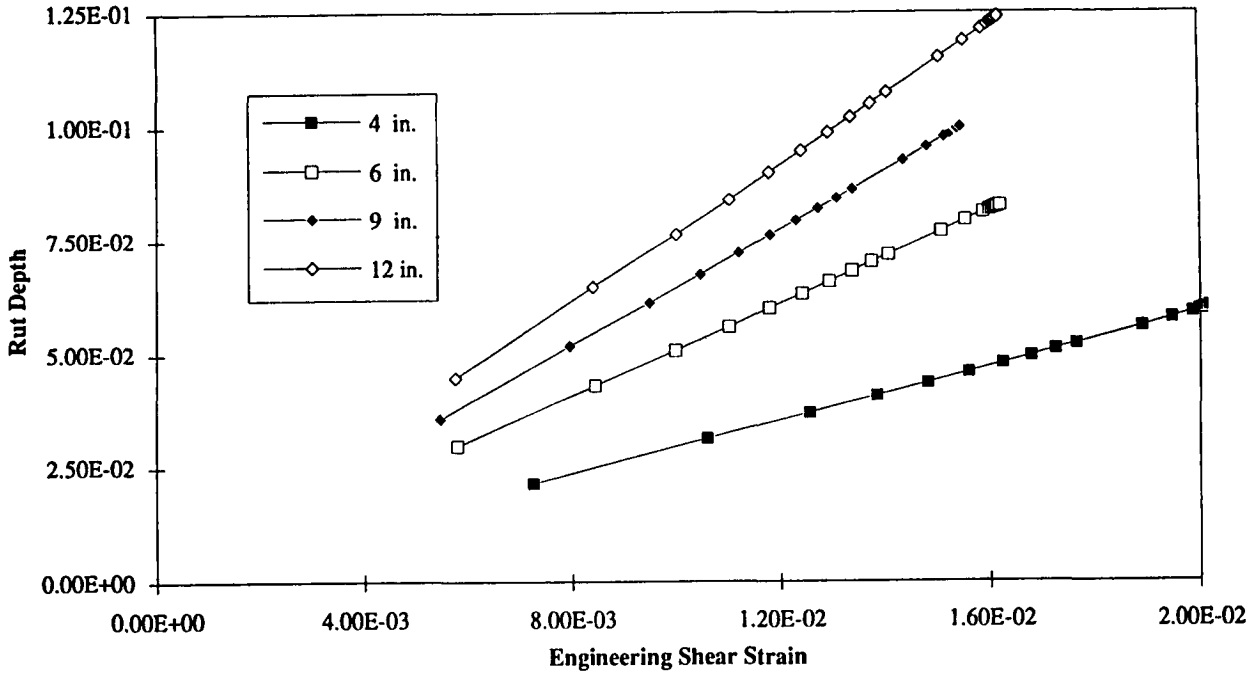

Figure C.18. Rut depth to maximum engineering shear strain ratio; vm0 mix on 100 cm (40 in.) of elastic foundation.

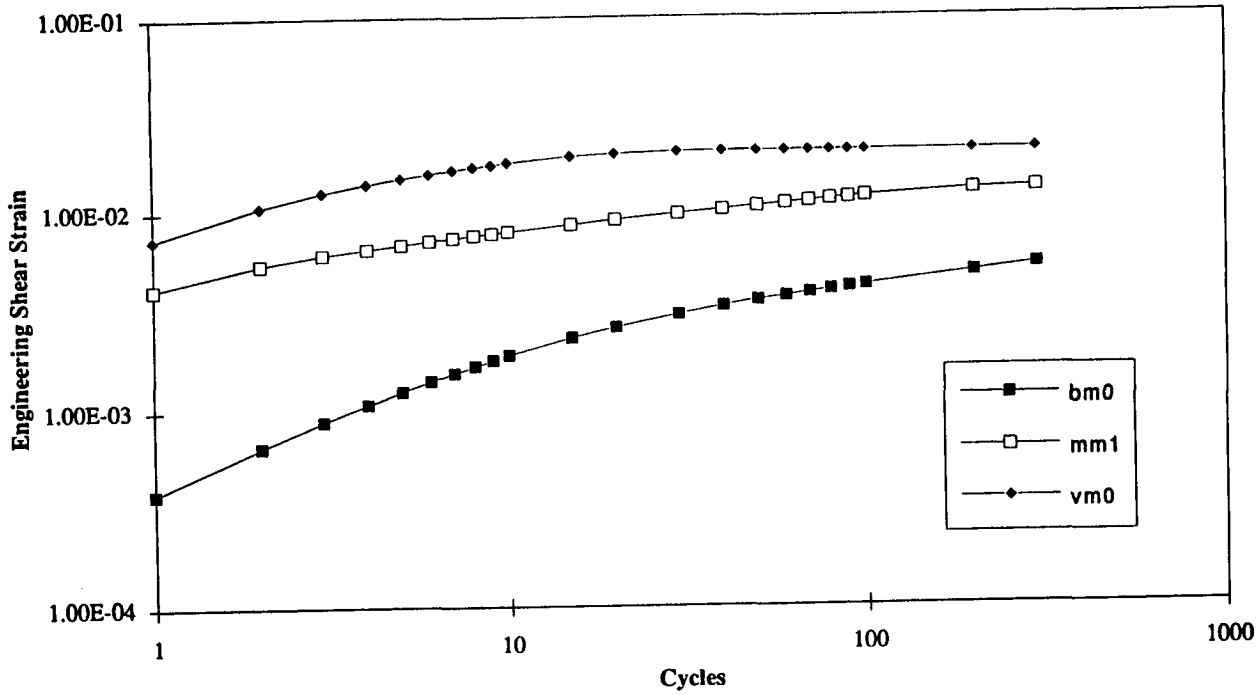

Figure C.19. Engineering shear strain versus number of cycles; 10 cm (4 in.) AC on 100 cm (40 in.) of elastic foundation

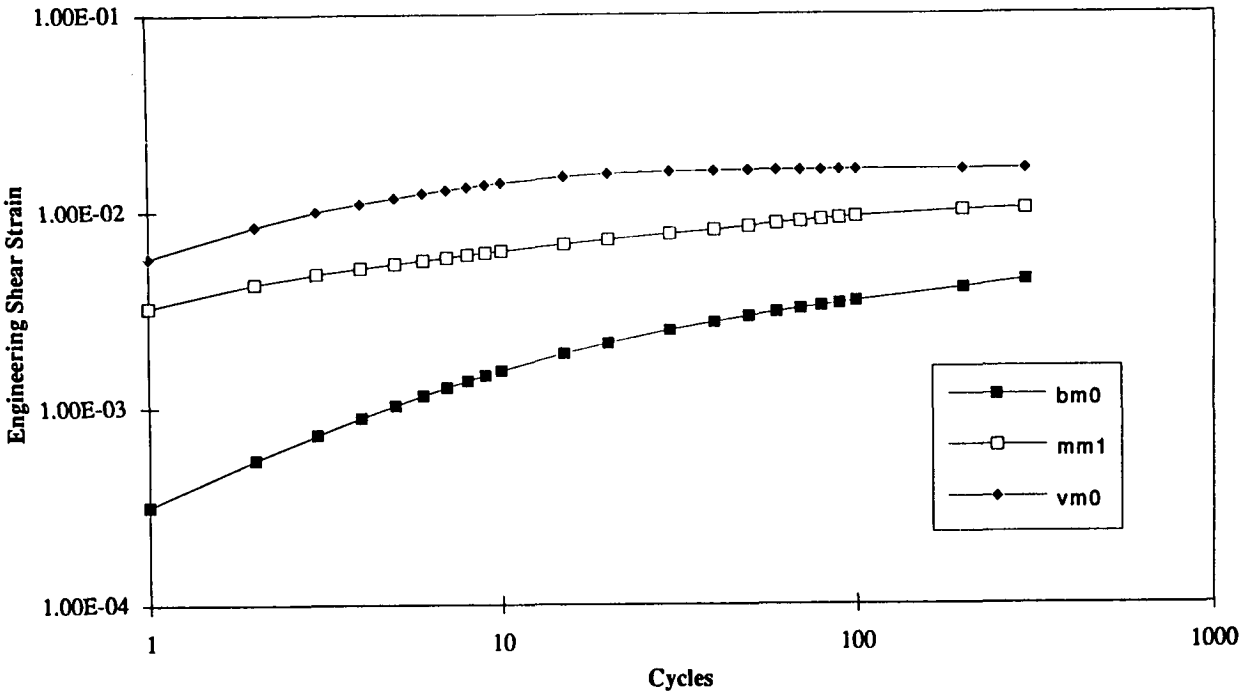

Figure C.20. Engineering shear strain versus number of cycles; 15 cm (6 in.) AC on 100 cm (40 in.) of elastic foundation

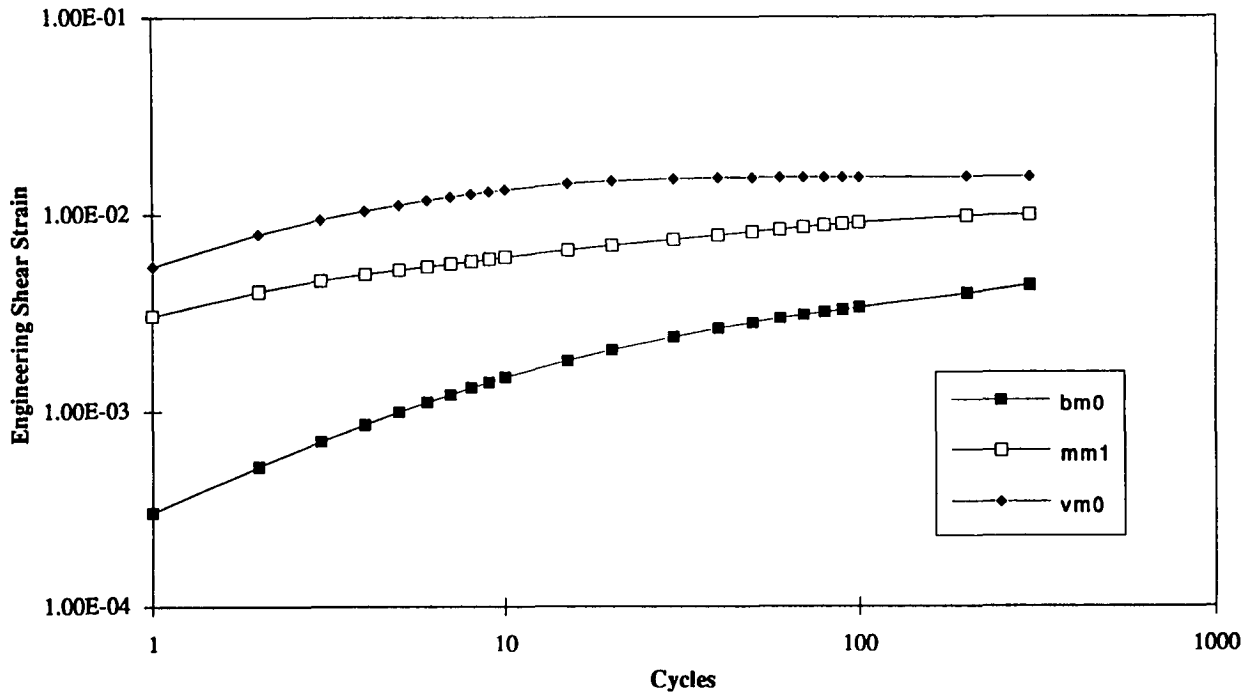

Figure C.21. Engineering shear strain versus number of cycles; 22.5 cm (9 in.) AC on 100 cm (40 in.) of elastic foundation

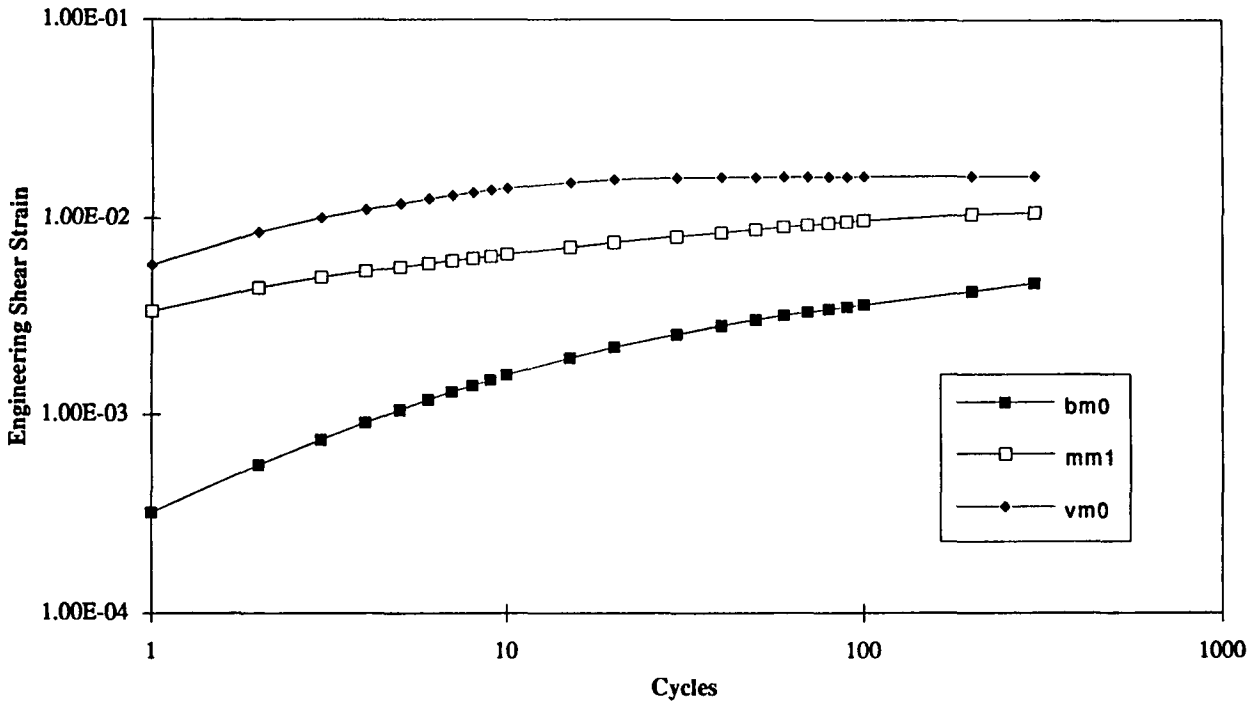

Figure C.22. Engineering shear strain versus number of cycles; 30 cm (12 in.) AC on 100 cm (40 in.) of elastic foundation

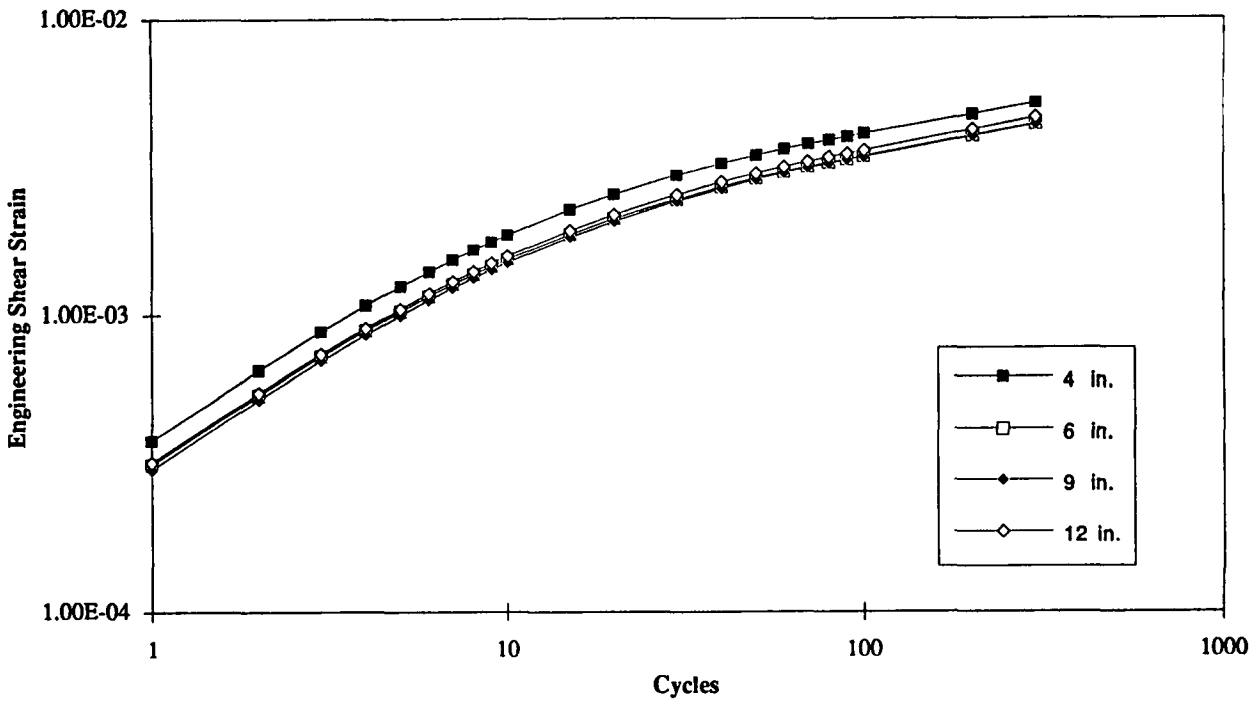

Figure C.23. Engineering shear strain versus number of cycles; bm0 mix on 100 cm (40 in.) of elastic foundation

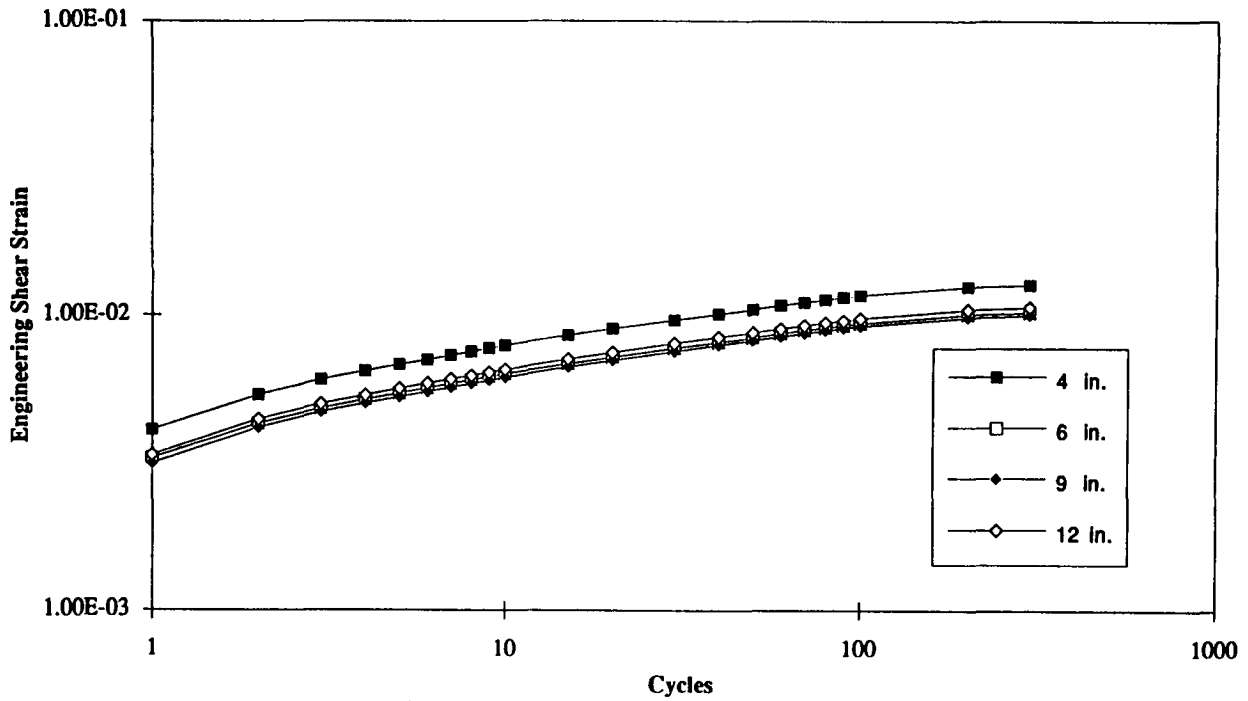

Figure C.24. Engineering shear strain versus number of cycles; mm1 mix on 100 cm (40 in.) of elastic foundation

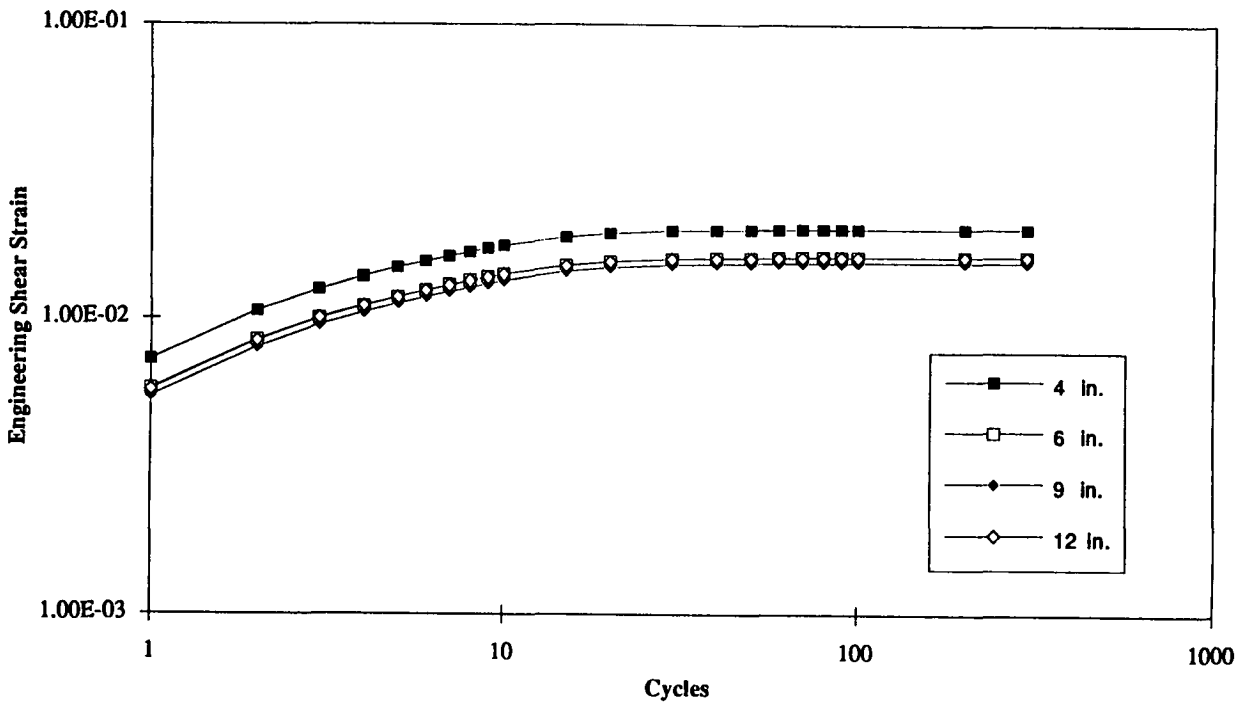

Figure C.25. Engineering shear strain versus number of cycles; vm0 mix on 100 cm (40 in.) of elastic foundation

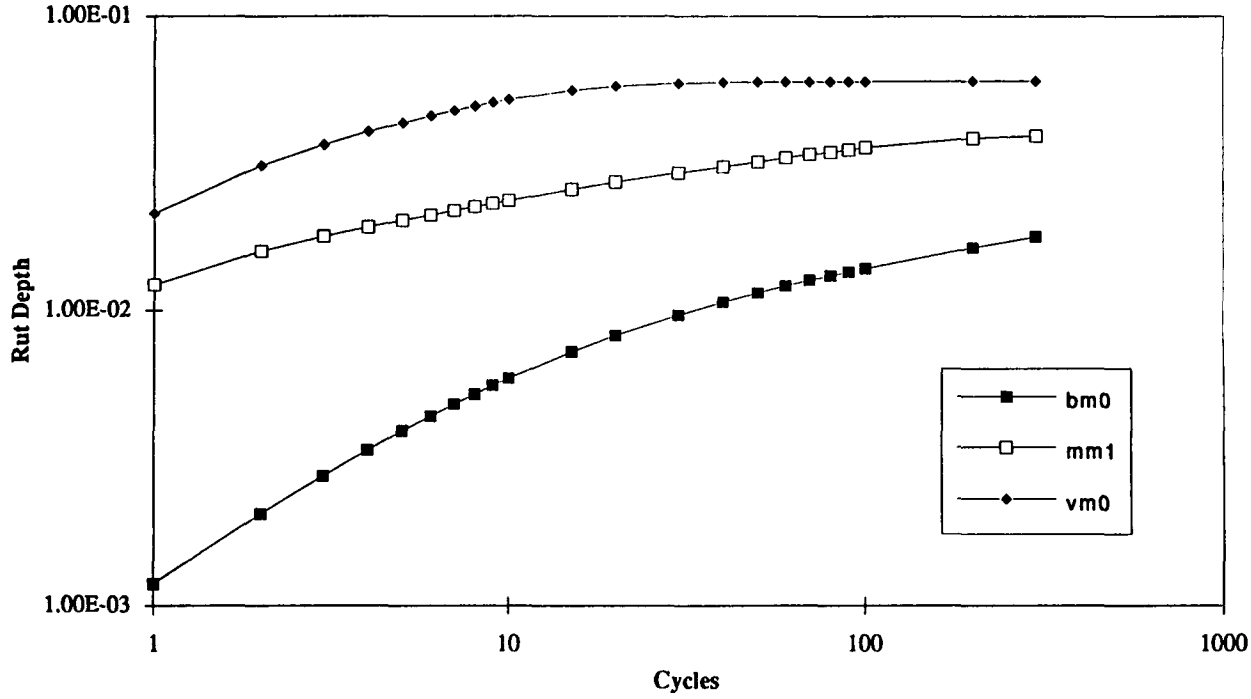

Figure C.26. Rut depth versus number of cycles; 10 cm (4 in.) AC on 100 cm (40 in.) of elastic foundation

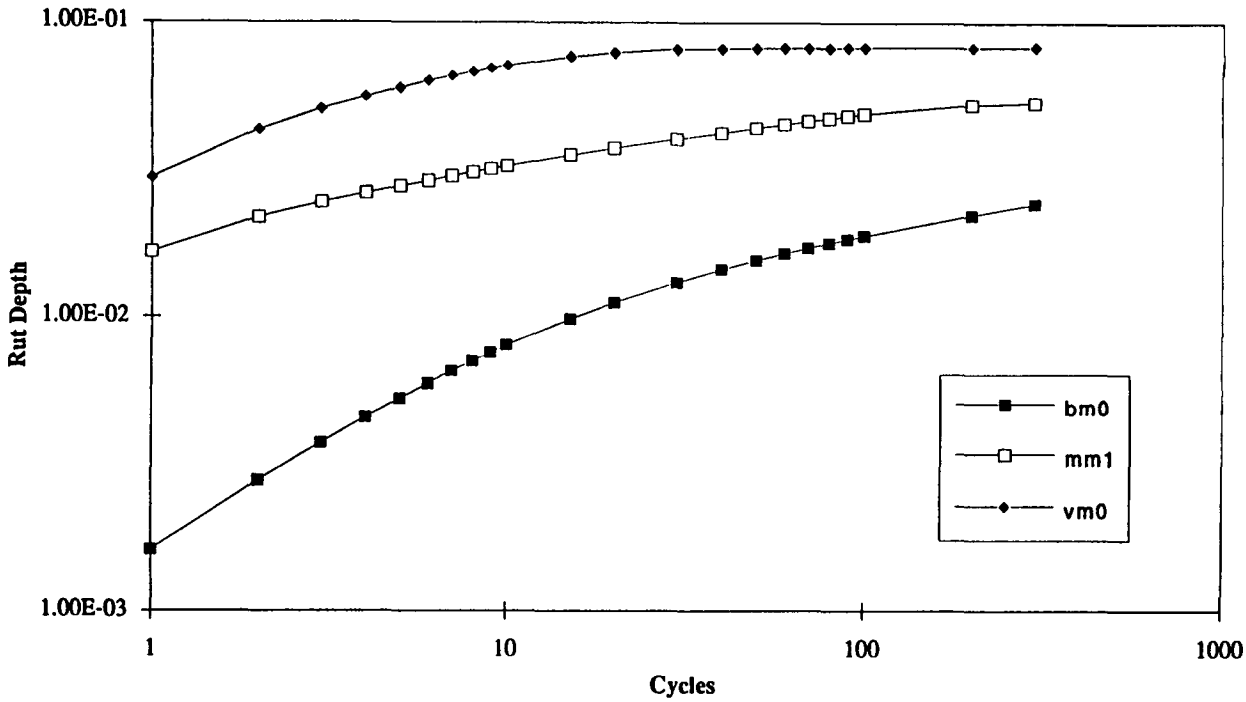

Figure C.27. Rut depth versus number of cycles; 15 cm (6 in.) AC on 100 cm (40 in.) of elastic foundation

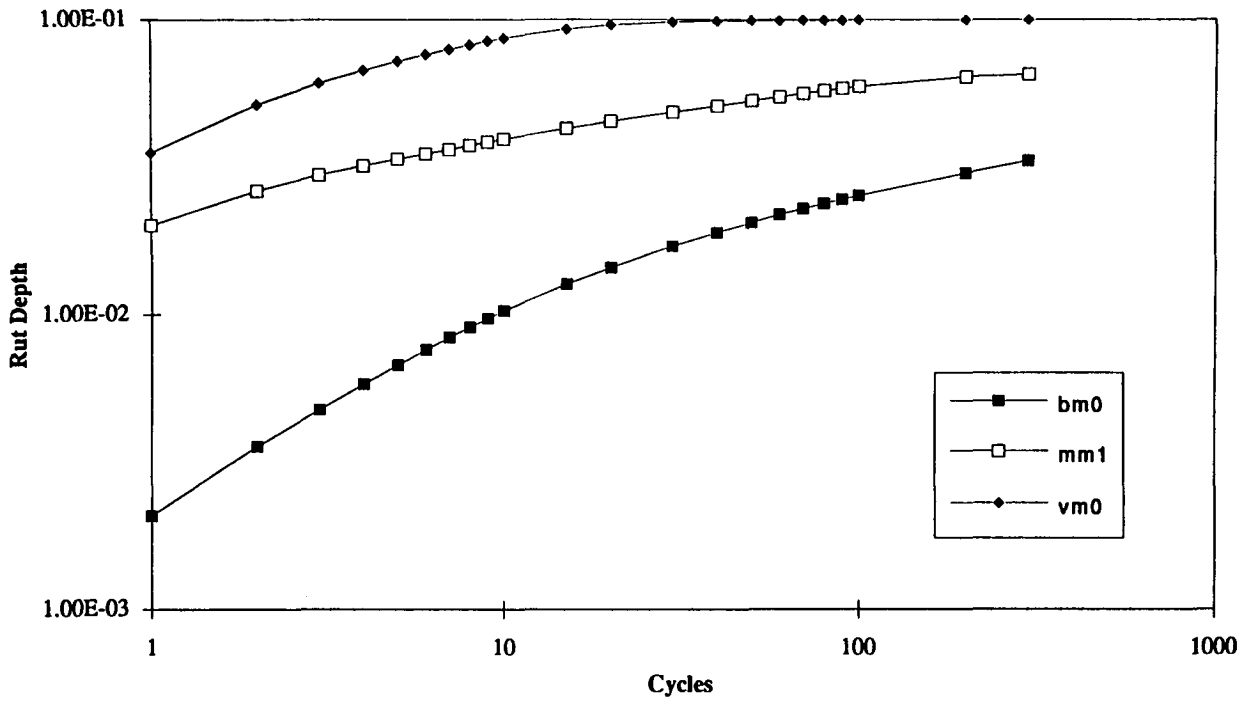

Figure C.28. Rut depth versus number of cycles; 22.5 cm (9 in.) AC on 100 cm (40 in.) of elastic foundation

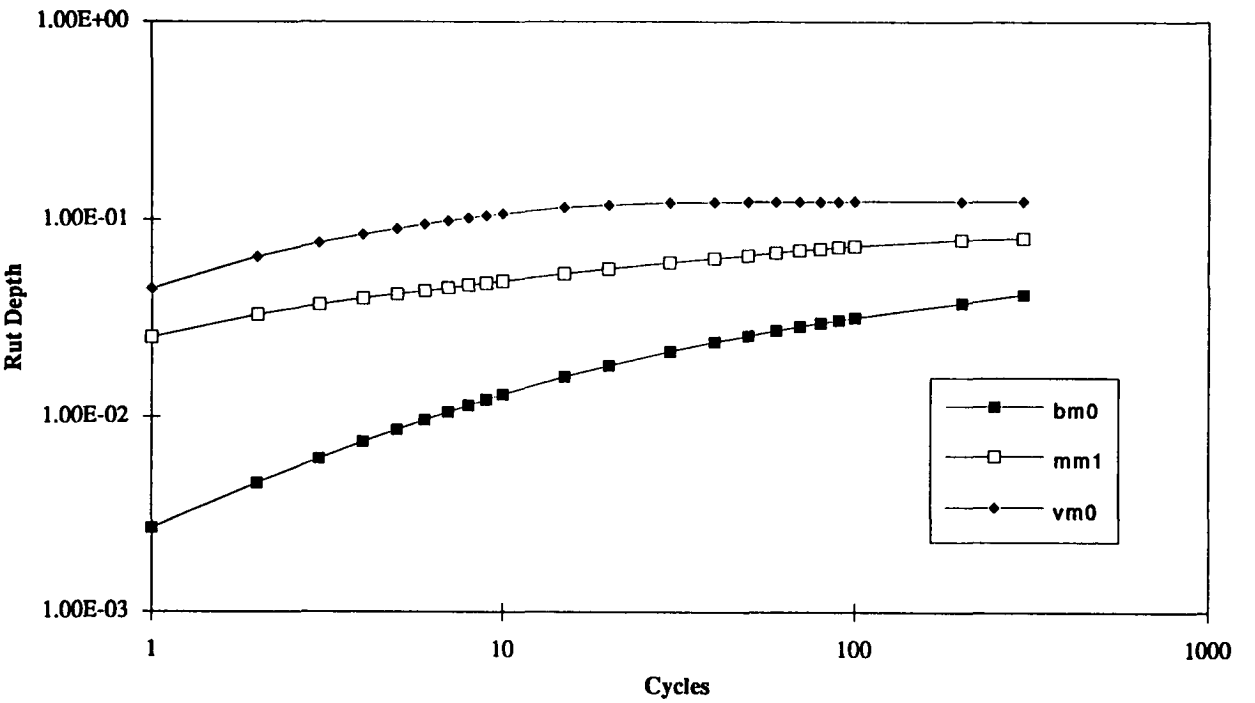

Figure C.29. Rut depth versus number of cycles; 30 cm (12 in.) AC on 100 cm (40 in.) of elastic foundation

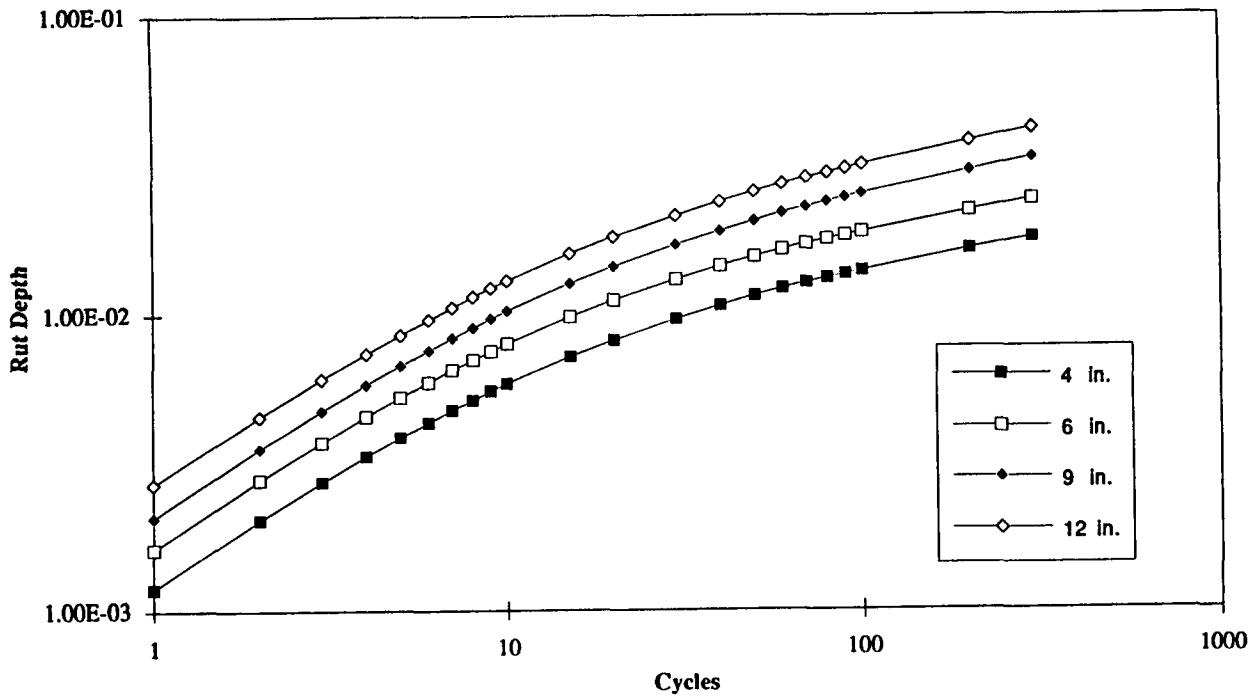

Figure C.30. Rut depth versus number of cycles; bm0 mix on 100 cm (40 in.) of elastic foundation

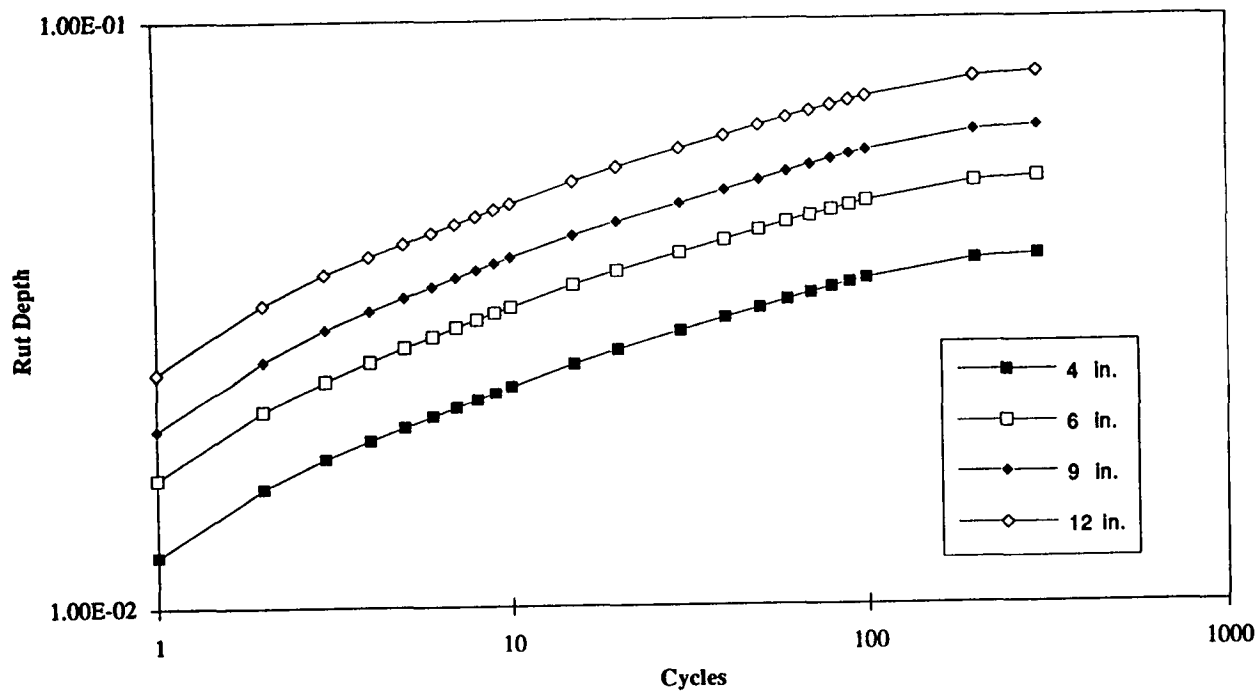

Figure C.31. Rut depth versus number cycles; mm1 on 100 cm (40 in.) of elastic foundation

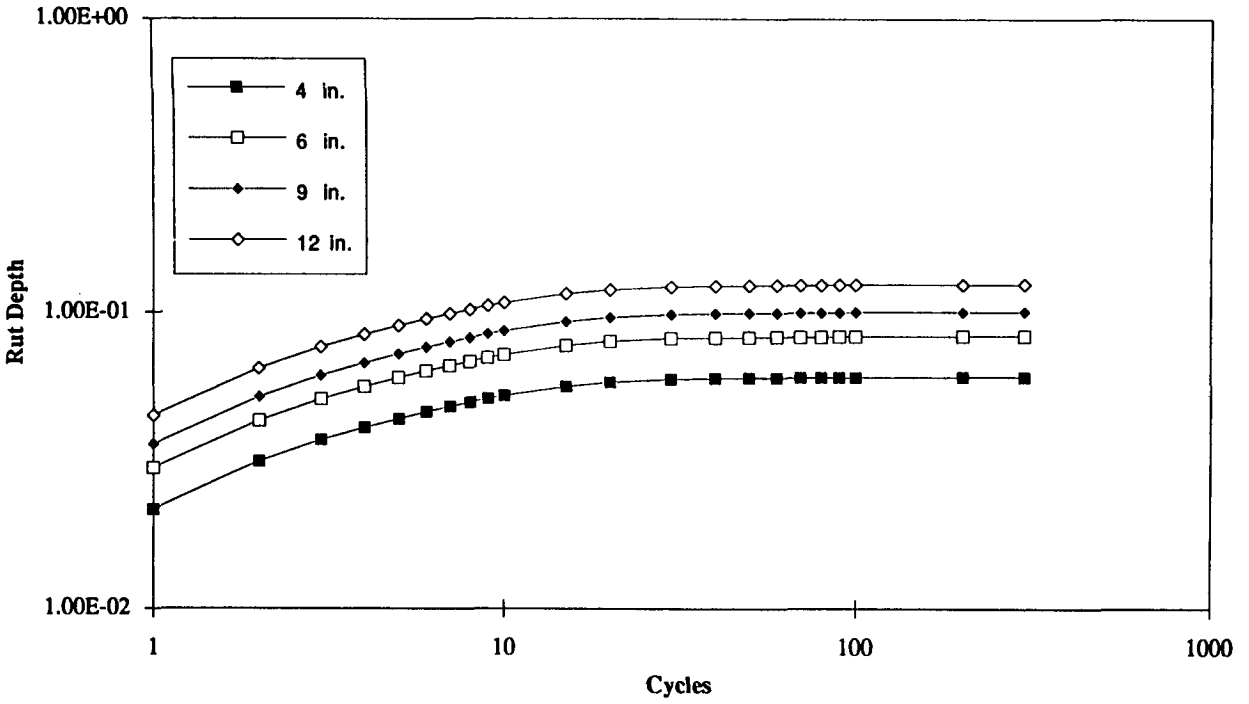

Figure C.32. Rut depth versus number of cycles; vm0 mix on 100 cm (40 in.) of elastic foundation

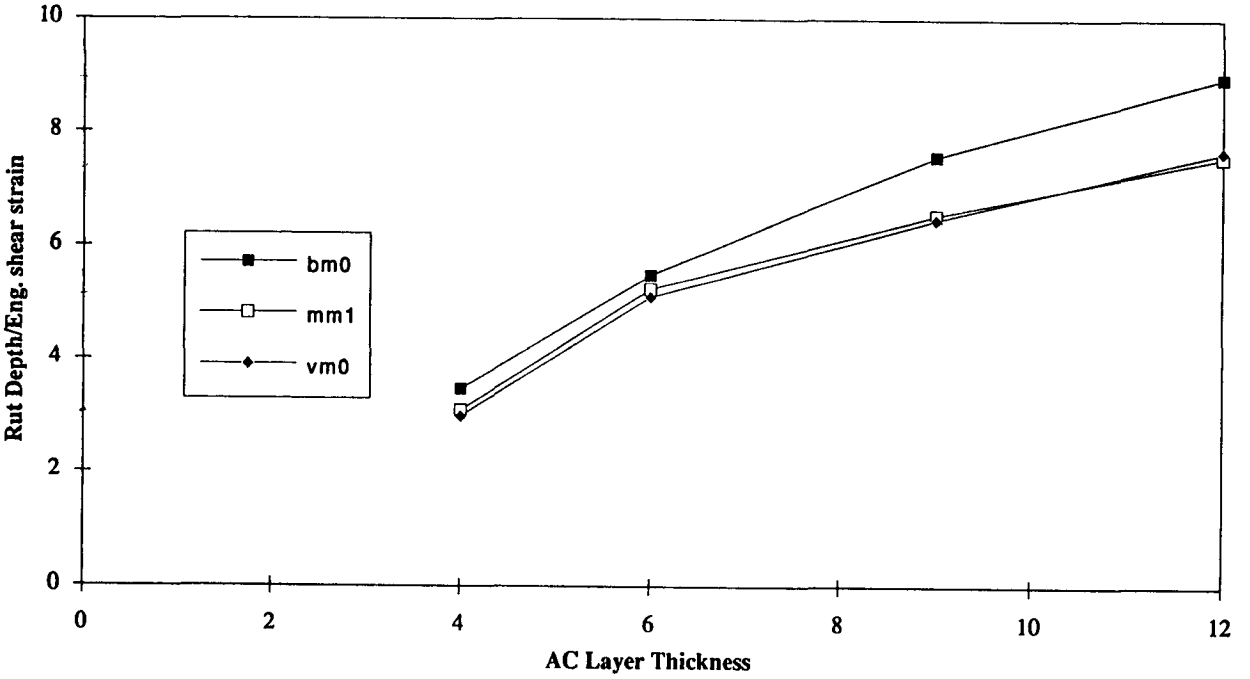

Figure C.33. Rut depth versus maximum engineering shear strain as a function of the AC layer's thickness (after 300 cycles)

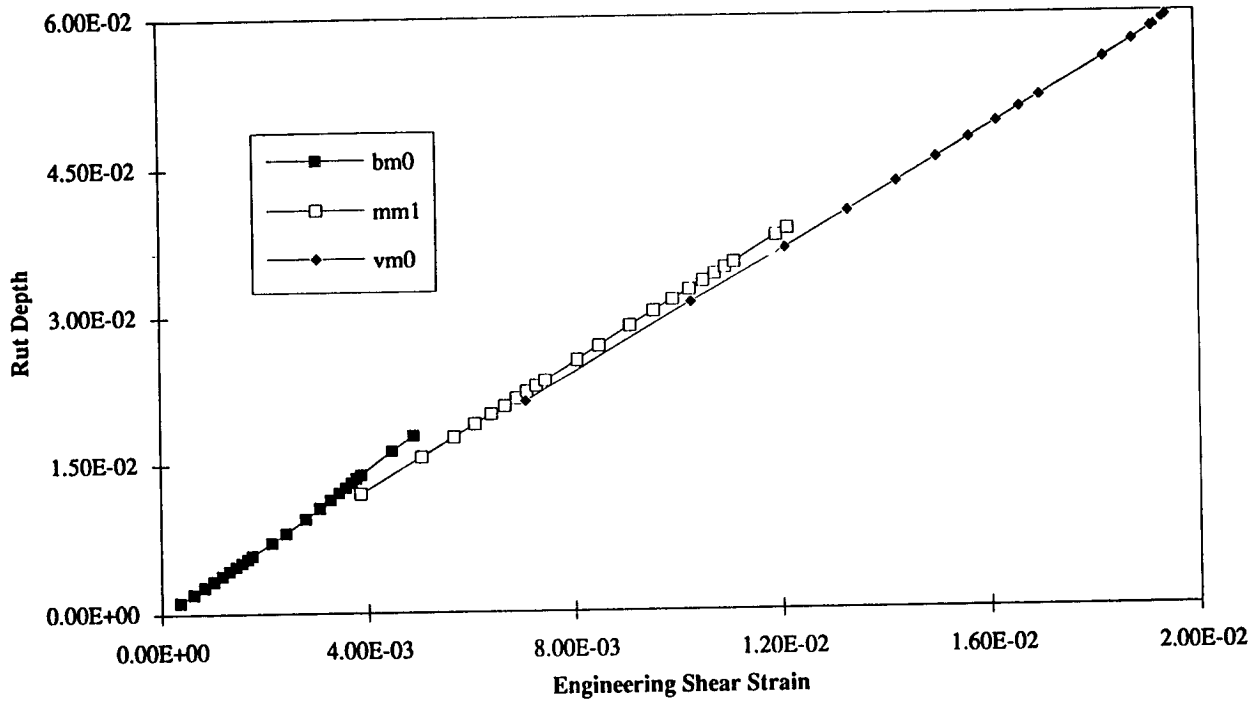

Figure C.34. Rut depth to maximum engineering shear strain ratio; 10 cm (4 in.) AC on 37.5 cm (15 in.) concrete

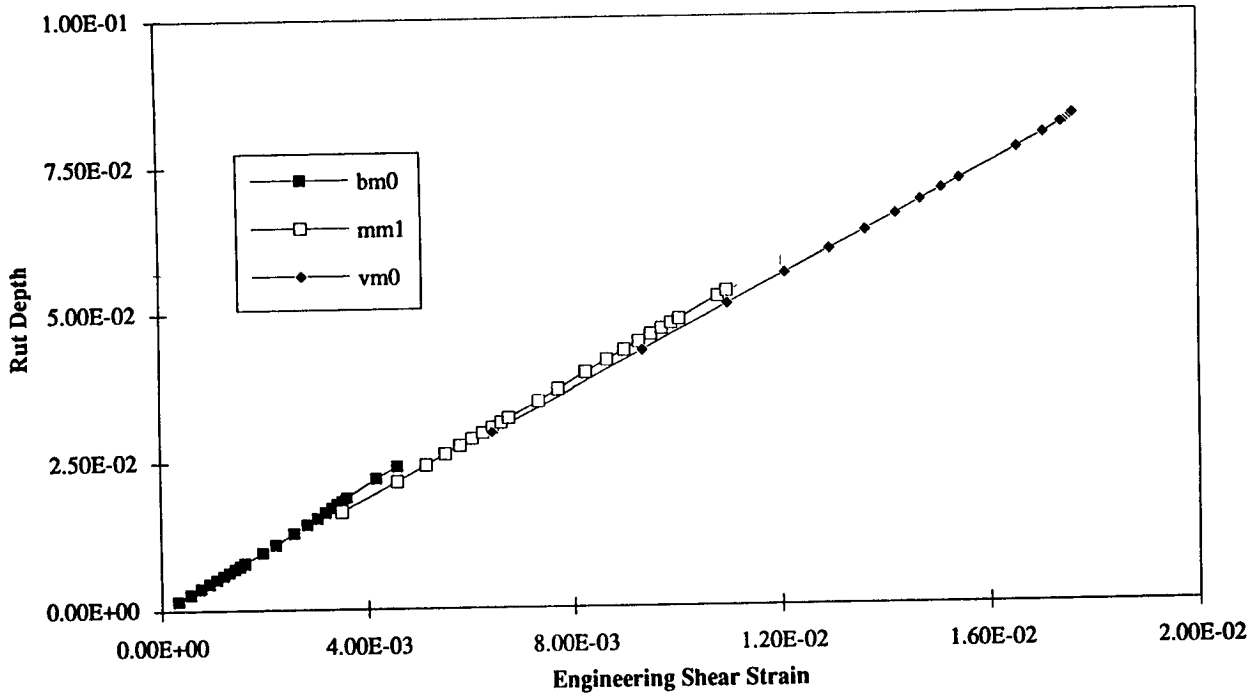

Figure C.35. Rut depth to maximum engineering shear strain ratio; 15 cm (6 in.) AC on 37.5 (15 in.) concrete

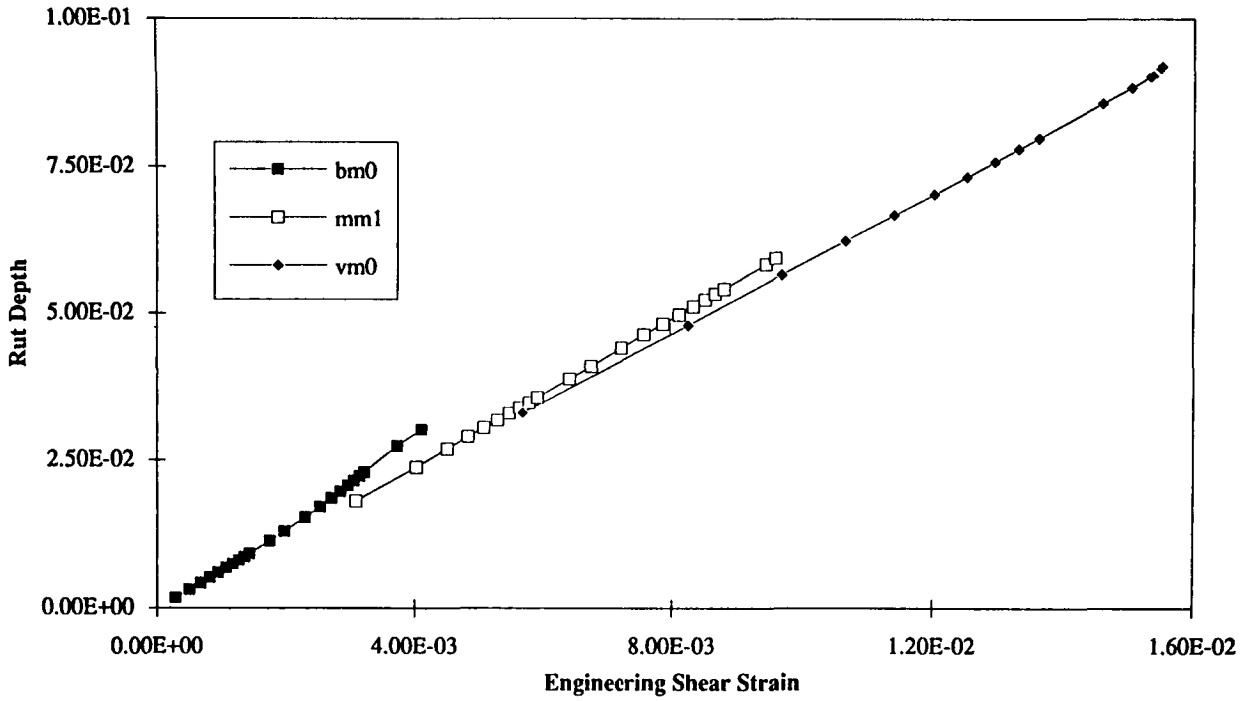

Figure C.36. Rut depth to maximum engineering shear strain ratio; 20 cm (8 in.) AC on 37.5 cm (15 in.) concrete

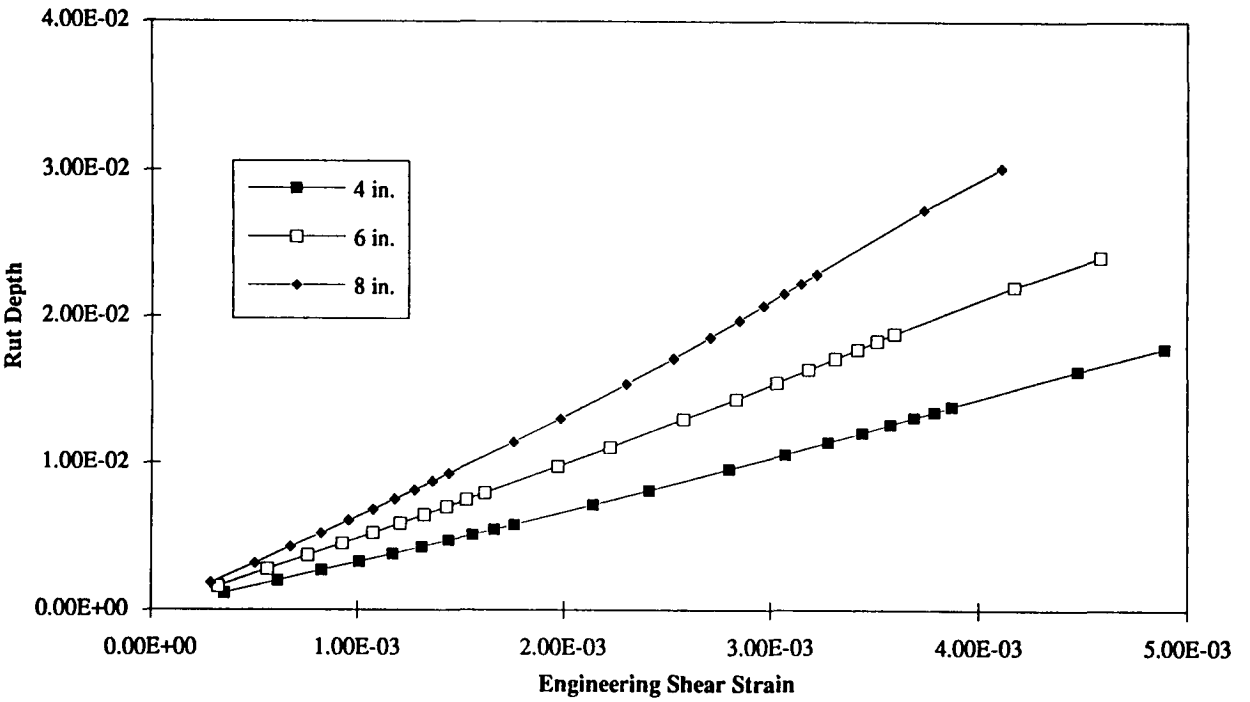

Figure C.37. Rut depth to maximum engineering shear strain ratio; bm0 mix on 37.5 cm (15 in.) concrete

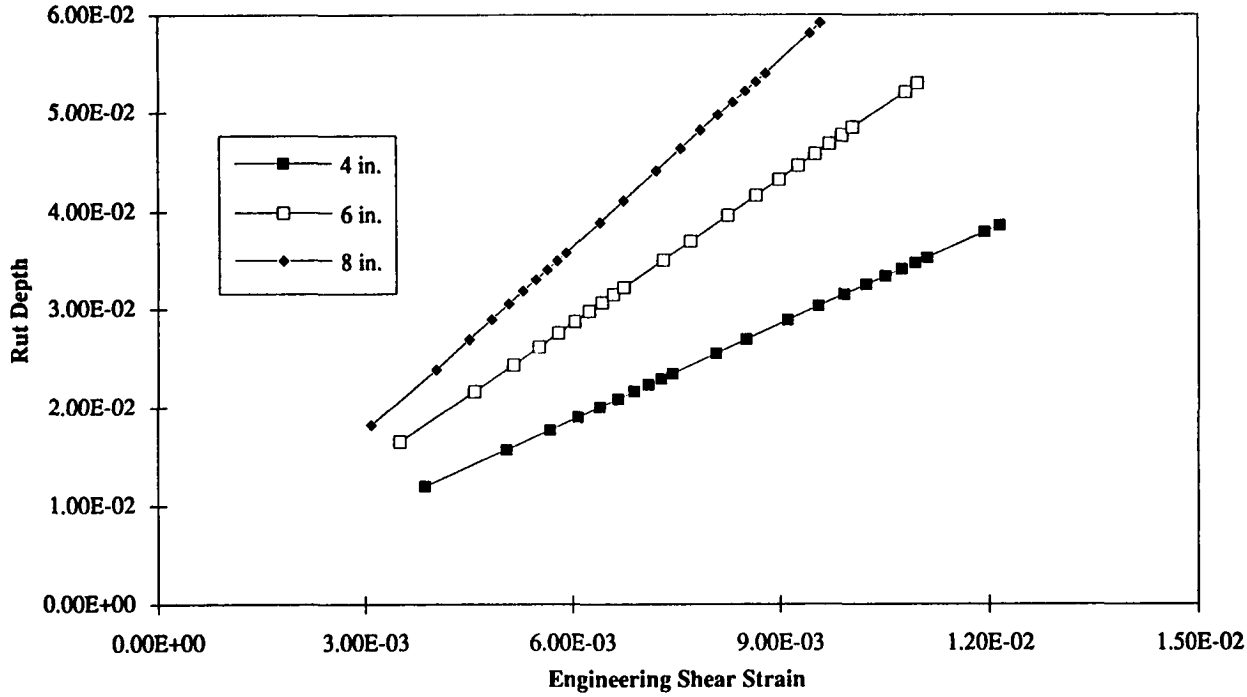

Figure C.38. Rut depth to maximum engineering shear strain ratio; mm1 mix on 37.5 cm (15 in.) concrete

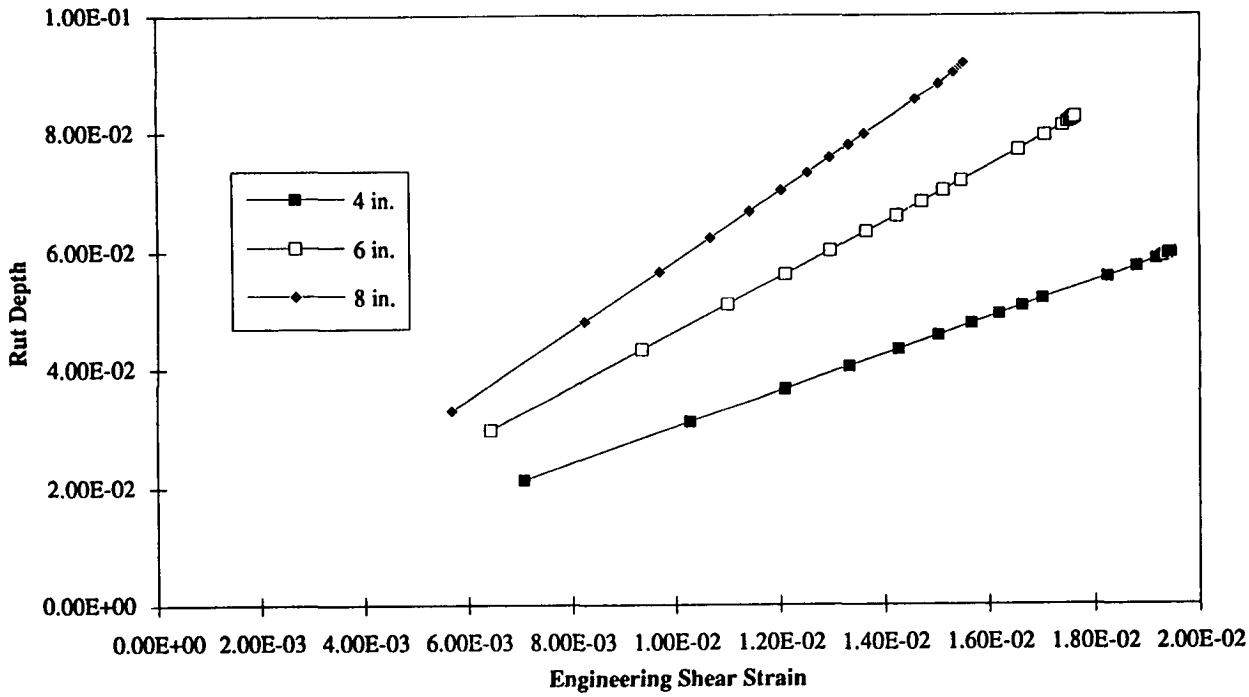

Figure C.39. Rut depth to maximum engineering shear strain ratio; vm0 mix on 37.5 cm (15 in.) concrete

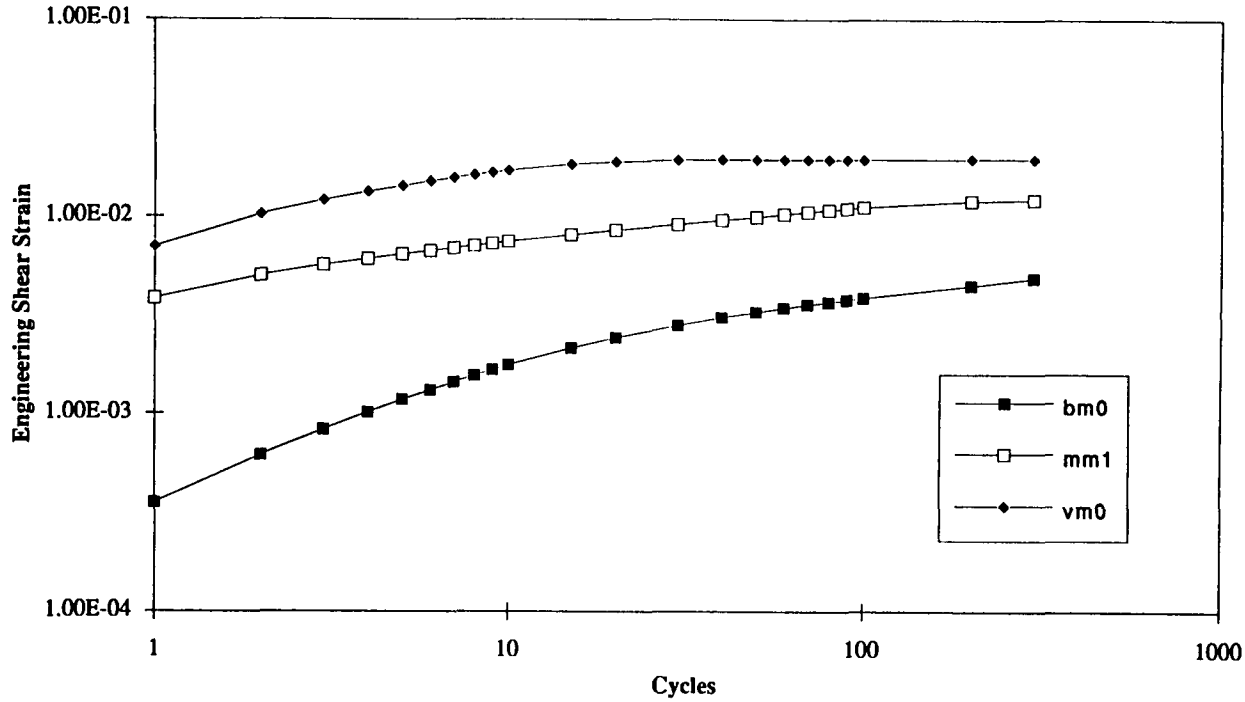

Figure C.40. Engineering shear strain versus number of cycles; 10 cm (4 in.) AC on 37.5 cm (15 in.) concrete

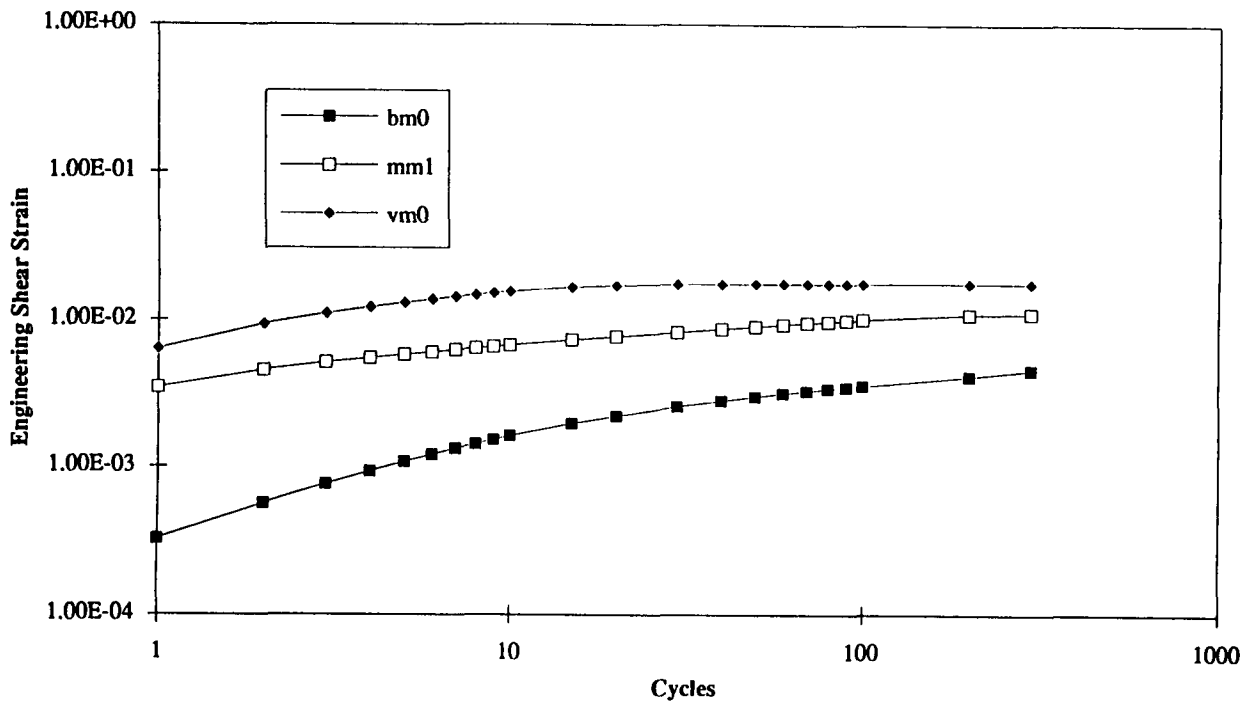

Figure C.41. Engineering shear strain versus cycles; 15 cm (6 in.) AC on 37.5 cm (15 in.) concrete

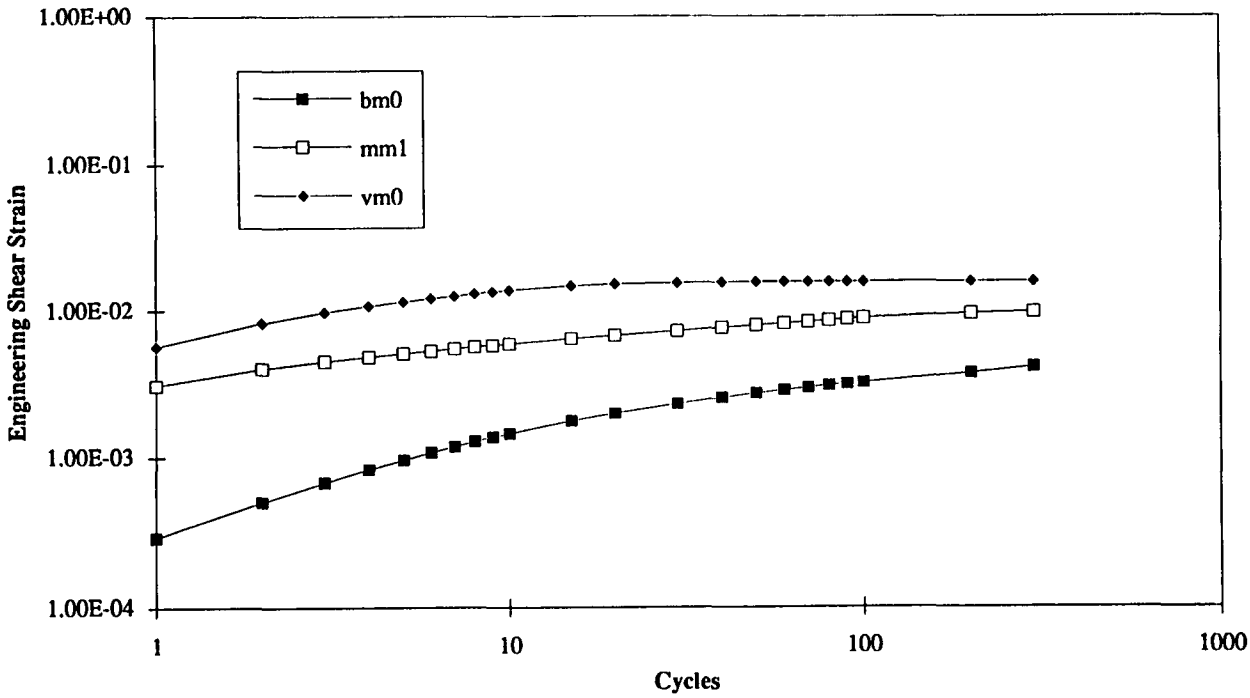

Figure C.42. Engineering shear strain versus cycles; 20 cm (8 in.) AC on 37.5 cm (15 in.) concrete

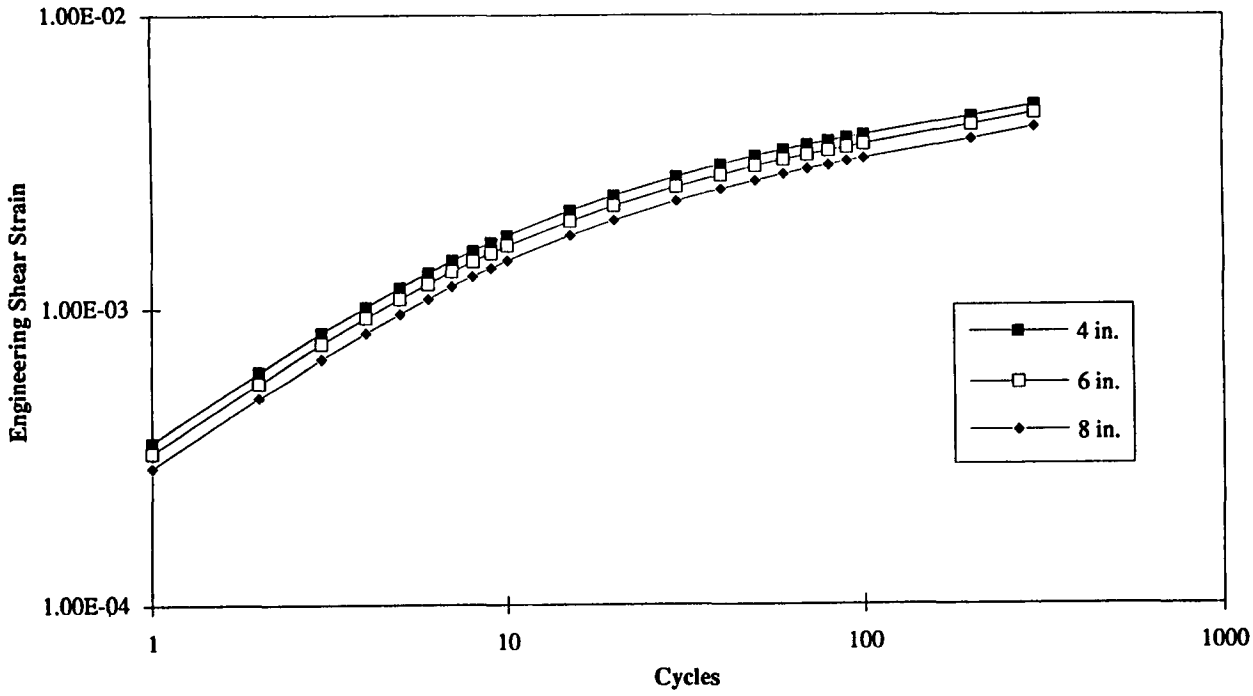

Figure C.43. Engineering shear strain versus cycles; bm0 mix on 37.5 cm (15 in.) concrete

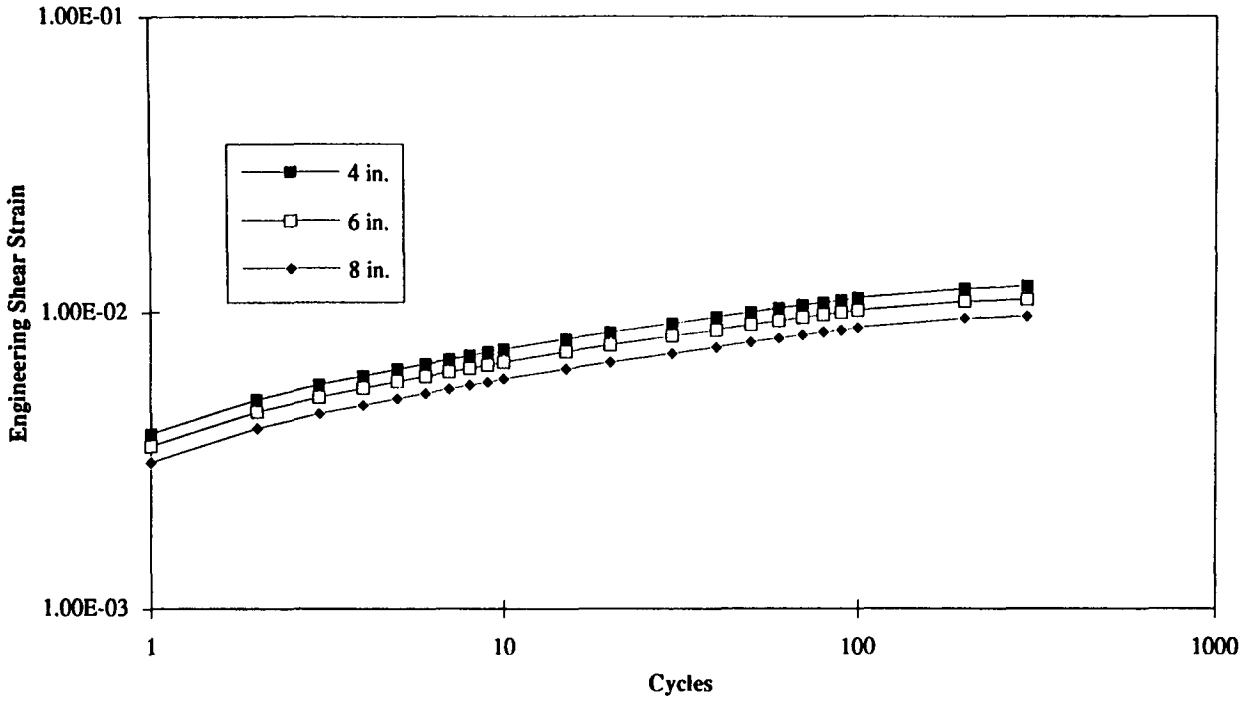

Figure C.44. Engineering shear strain versus cycles; mm1 mix on 37.5 cm (15 in.) concrete

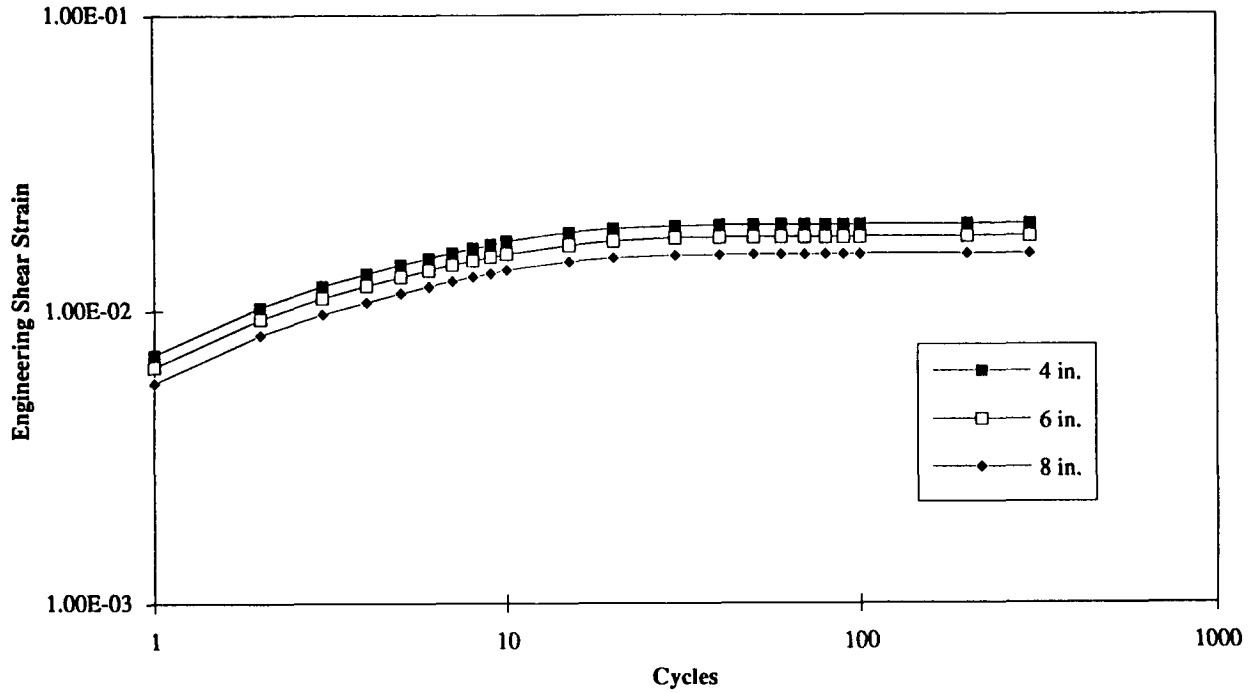

Figure C.45. Engineering shear strain versus cycles; vm0 mix on 37.5 cm (15 in.) concrete

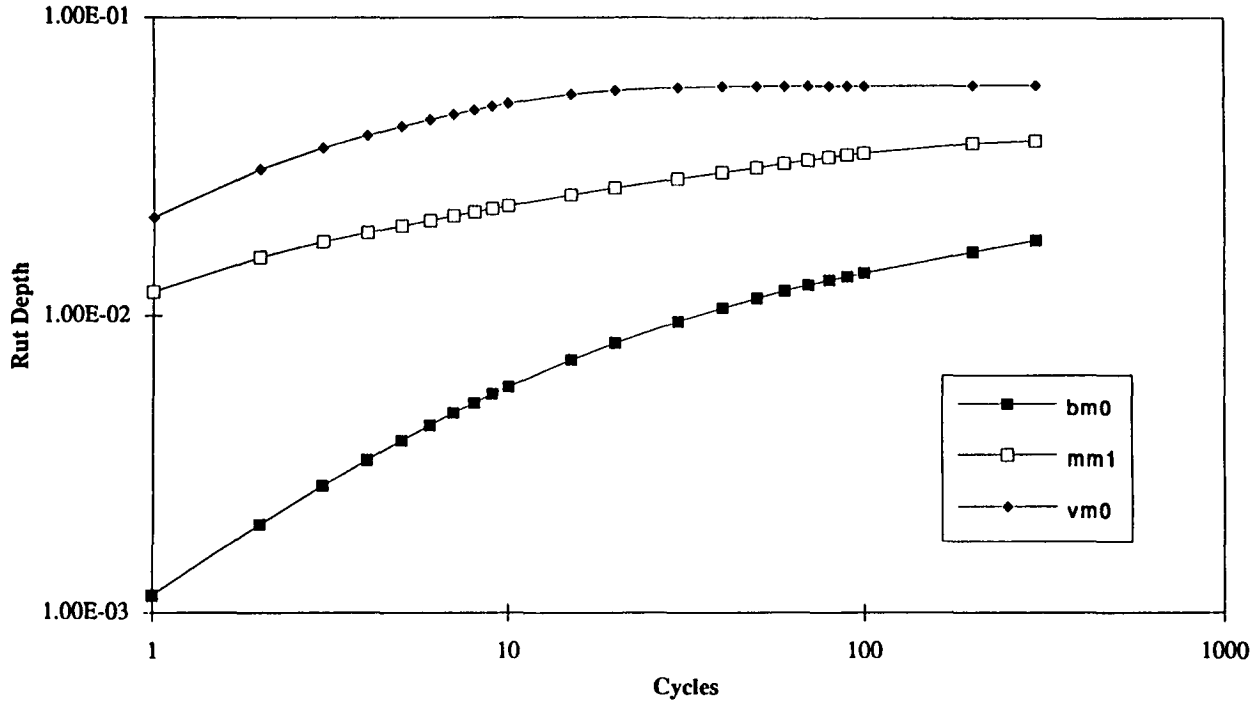

Figure C.46. Rut depth versus number of cycles; 10 cm (4 in.) AC on 37.5 cm (15 in.) concrete

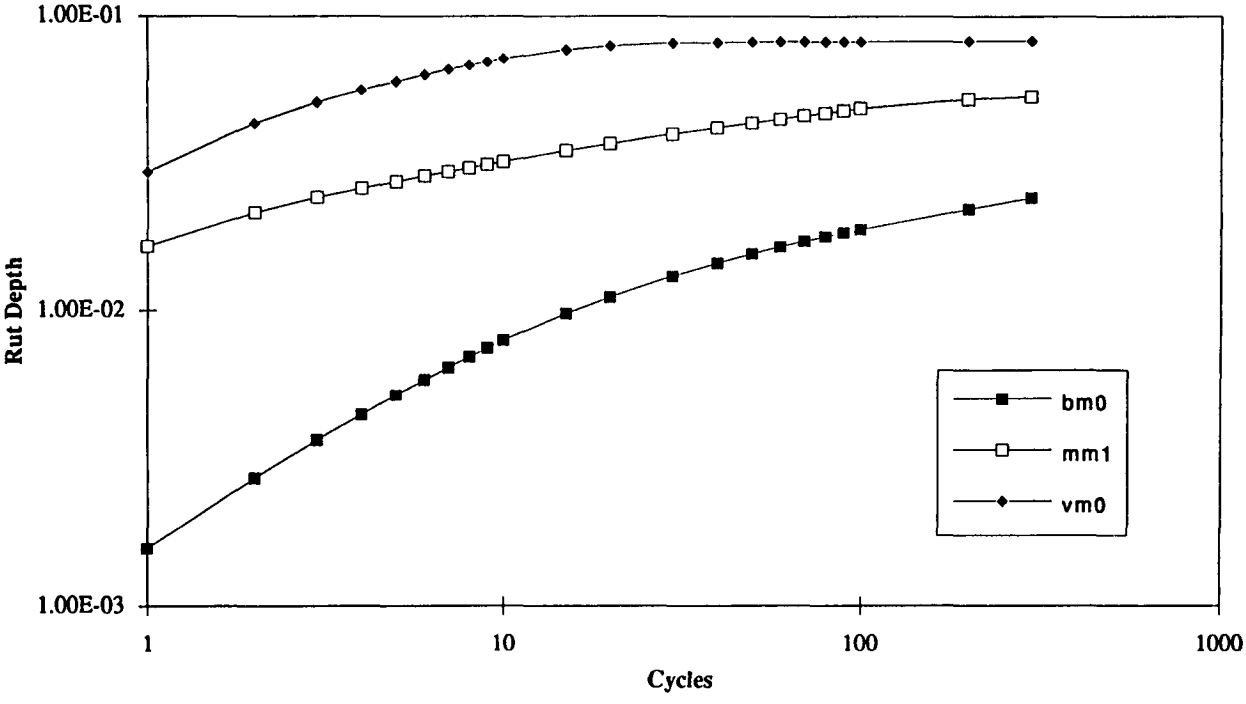

Figure C.47. Rut depth versus number of cycles; 15 cm (6 in.) AC on 37.5 (15 in.) concrete

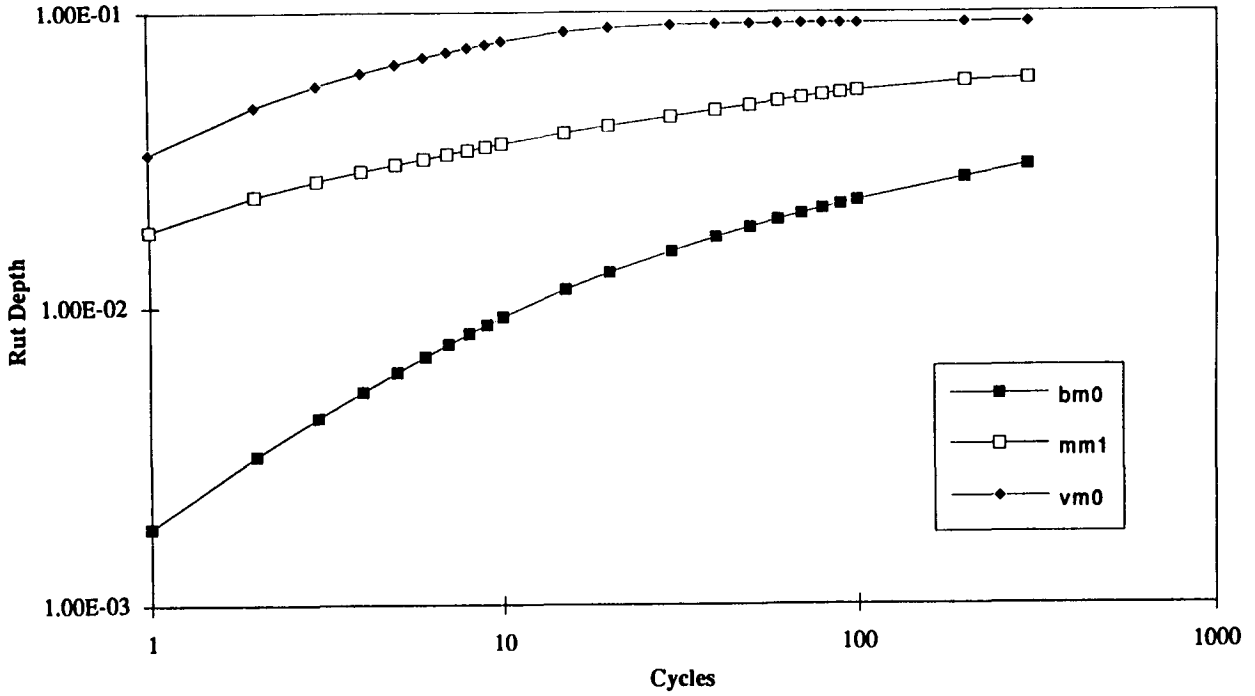

Figure C.48. Rut depth versus number of cycles; 20 cm (8 in.) AC on 37.5 cm (15 in.) concrete

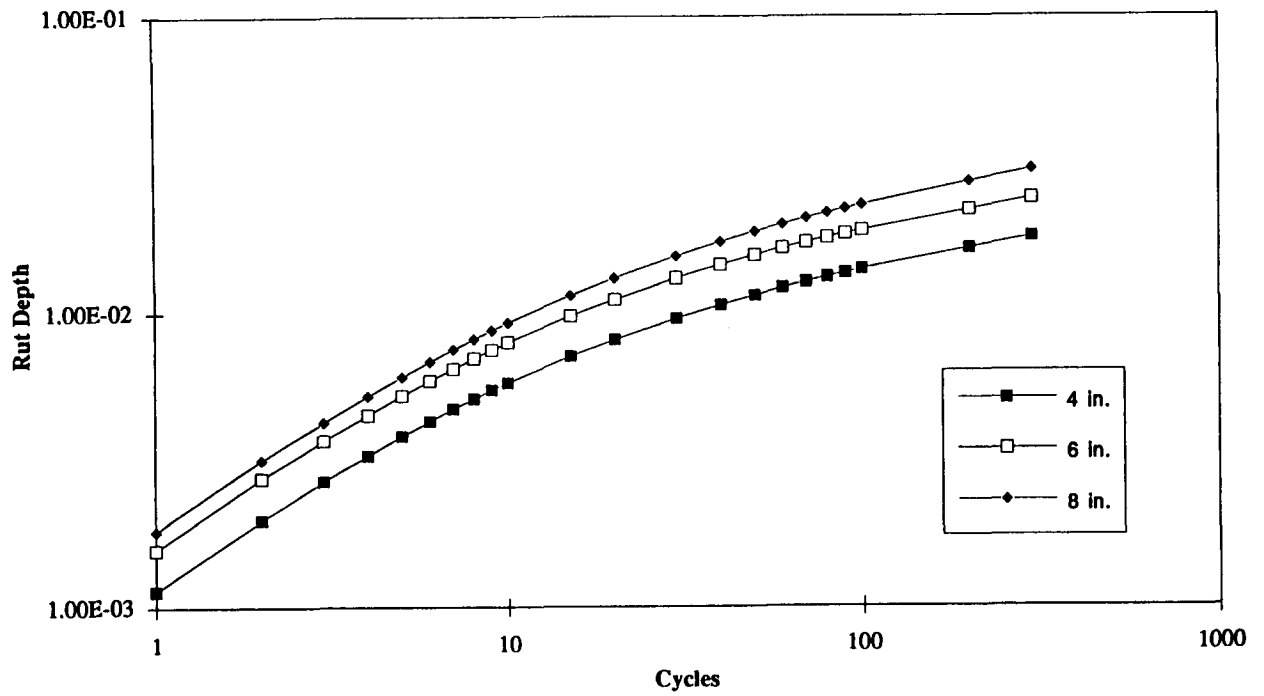

Figure C.49. Rut depth versus number of cycles; bm0 mix on 37.5 cm (15 in.) concrete

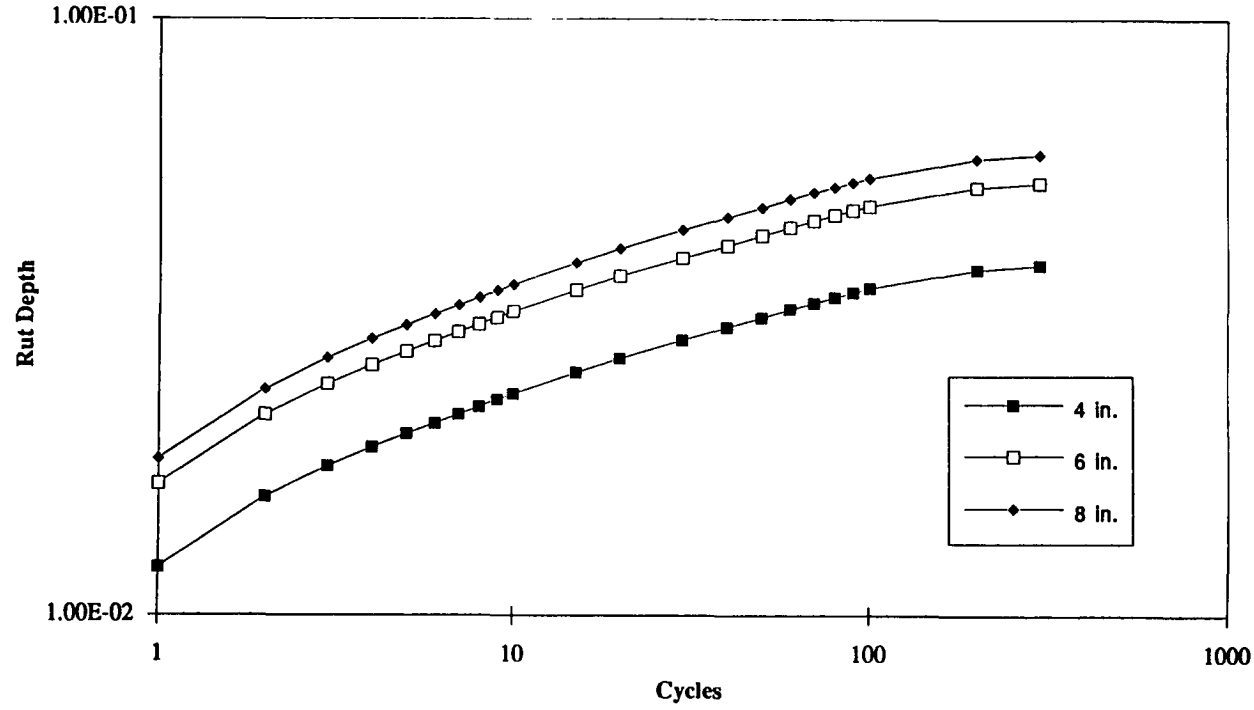

Figure C.50. Rut depth versus number of cycles; mm1 mix on 37.5 cm (15 in.) concrete

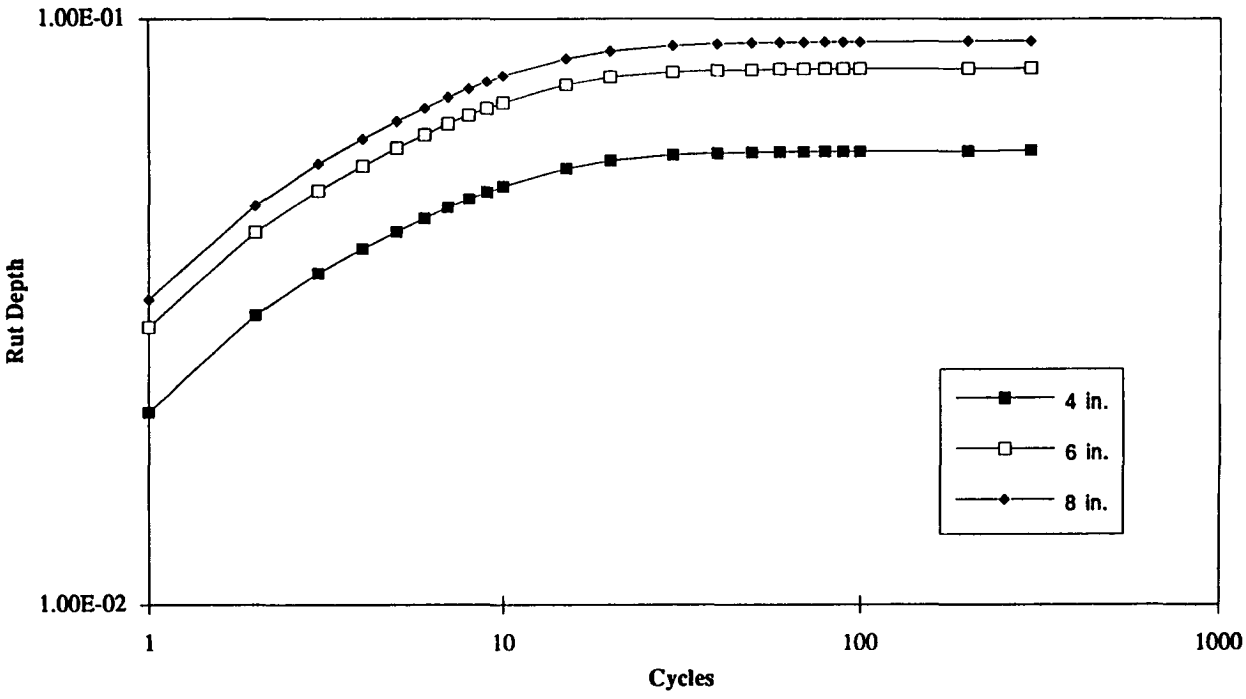

Figure C.51. Rut depth versus number of cycles; vm0 mix on 37.5 cm (15 in.) concrete

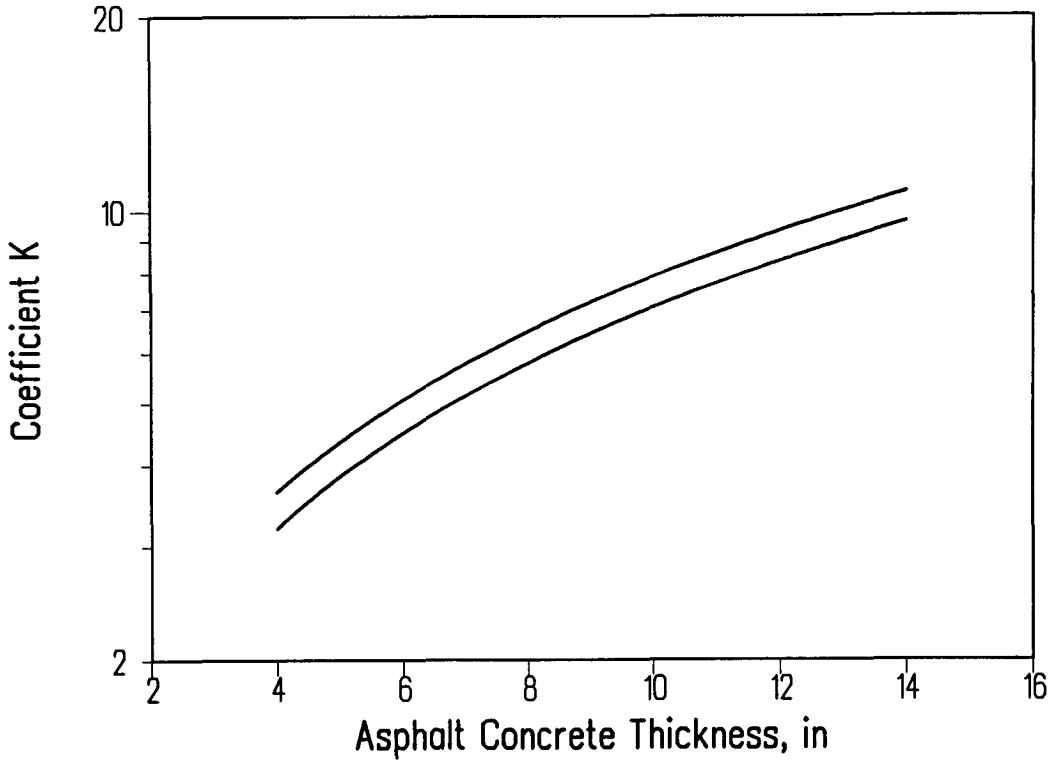

Figure C.52. Variation of parameter K in Equation 6.35 with pavement thickness

Appendix D

SWK/UN Wheel-Tracking Test Results for 64 Mixes

Table D.1. Wheel-track rutting results, adjusted for air voids (after STOA, @ 40°C [104°F]and 20/rads)

Asphalt Source	Aggregate Source	Air Voids (%)	Total Rut Depth at 5000 passes (mm)	Normalized Rut Rate between 2000 and 4000 passes (mm/MPa/hr)
AAA	RD	4.0	2.07	0.37
AAA	RD	7.0	1.90	0.47
AAA	RH	4.0	2.75	0.71
AAA	RH	7.0	3.07	0.84
AAB	RD	4.0	1.38	0.34
AAB	RD	7.0	2.45	0.37
AAB	RH	4.0	1.50	0.36
AAB	RH	7.0	2.80	0.57
AAC	RD	4.0	1.23	0.23
AAC	RD	7.0	1.01	0.21
AAC	RH	4.0	4.64	1.49
AAC	RH	7.0	5.57	1.52
AAD	RD	4.0	0.96	0.26
AAD	RD	7.0	2.43	0.47
AAD	RH	4.0	3.06	1.02
AAD	RH	7.0	3.70	1.18
AAF	RD	4.0	1.21	0.36
AAF	RD	7.0	0.89	0.22
AAF	RH	4.0	1.01	0.31
AAF	RH	7.0	2.04	0.66
AAG	RD	4.0	1.03	0.21
AAG	RD	7.0	2.53	0.84
AAG	RH	4.0	1.57	0.40
AAG	RH	7.0	3.72	0.95
AAK	RD	4.0	1.51	0.31
AAK	RD	7.0	1.92	0.64
AAK	RH	4.0	2.05	0.46
AAK	RH	7.0	1.31	0.34

Table D.1 (continued). Wheel-track rutting results, adjusted for air voids (after STOA, @ 40°C [104°F] and 20 rads)

Asphalt Source	Aggregate Source	Air Voids (%)	Total Rut Depth at 5000 passes (mm)	Normalized Rut Rate between 2000 and 4000 passes (mm/MPa/hr)
AAL	RD	4.0	1.70	0.34
AAL	RD	7.0	2.36	0.43
AAL	RH	4.0	3.27	0.79
AAL	RH	7.0	3.11	0.95
AAM	RD	4.0	1.31	0.17
AAM	RD	7.0	1.04	0.27
AAM	RH	4.0	1.08	0.22
AAM	RH	7.0	1.85	0.43
AAV	RD	4.0	1.46	0.36
AAV	RD	7.0	2.04	0.44
AAV	RH	4.0	2.20	0.66
AAV	RH	7.0	2.56	0.78
AAW	RD	4.0	1.36	0.21
AAW	RD	7.0	1.52	0.27
AAW	RH	4.0	0.83	0.23
AAW	RH	7.0	3.13	1.04
AAX	RD	4.0	1.35	0.15
AAX	RD	7.0	1.80	0.35
AAX	RH	4.0	1.05	0.31
AAX	RH	7.0	1.93	0.62
AAZ	RD	4.0	1.13	0.22
AAZ	RD	7.0	1.96	0.59
AAZ	RH	4.0	2.18	0.49
AAZ	RH	7.0	2.69	0.77
ABA	RD	4.0	1.04	0.28
ABA	RD	7.0	1.77	0.31
ABA	RH	4.0	1.48	0.41
ABA	RH	7.0	2.82	0.54
ABC	RD	4.0	0.81	0.16
ABC	RD	7.0	1.19	0.29
ABC	RH	4.0	1.13	0.38
ABC	RH	7.0	1.63	0.63
ABD	RD	4.0	1.68	0.31
ABD	RD	7.0	1.67	0.58
ABD	RH	4.0	1.83	0.70
ABD	RH	7.0	1.89	0.74

Appendix E

Load Conditions for Laboratory Tests Based on Estimates of Stresses in Upper Part of Asphalt-Bound Layer

The primary candidate for the accelerated performance test for the abridged permanent deformation analysis system is the compound axial-cyclic shear test. Current plans are to subject each mix to both a constant height cyclic shear test and a compound cyclic axial-shear test. Thus, if the compound test eventually proves unsuitable, a default test will be available.

Cyclic Shear

(1) The cyclic shear test is attractive because the prevailing belief is that permanent deformation is primarily a shear phenomenon; cyclic tests demonstrate greater sensitivity than creep tests to asphalt properties (including modifiers); and specimen size and shape are convenient (much more so than axial, for example). (Tanco 1992, pp 136 and 139, suggests that cyclic shear is inferior to cyclic axial.)

(2) We are unlikely to be able to *directly* relate laboratory stress levels to in situ stress levels. Laboratory stresses must be set at smaller levels because there is no "healing" effect similar to that resulting from traffic wander and because the absence of confinement not only increases deformation during the loading phase but also possibly reduces or retards recovery during the rest phase. Regarding recovery, fatigue testing provides an interesting analogy.

(3) Performance measures generally include slope of ln $\dot{\epsilon}^i$ - ln N relationship; N at fixed (terminal) level of $\dot{\epsilon}^i$; and $\dot{\epsilon}^i$ at fixed level of N, etc. Any performance measure requiring extrapolation is inferior because of inaccuracy, either real or perceived.

(4) Mixes cannot be reliably compared at very small numbers of loading cycles.

(5) Test results are more variable than desired. With less sophisticated equipment, as many as four to seven replicates per test condition may be necessary for reliable measurements.

(6) Permanent deformation can be assumed to be a state variable, and the time-hardening concept is valid for compound loading.

(7) Although ranking of the permanent deformation resistance of various mixes may be affected by stress level, testing under a range of stresses has been too limited to yield conclusive results.

Constant Height Cyclic Shear

(1) Because the axial stress is uncontrolled, this test is more likely to be perceived as an index test rather than a test of fundamental mix properties.

(2) The confining pressure due to axial loading is likely to be too small generally and almost certainly is too small for weak mixes.

(3) The inability to set the axial stress reduces the ability to duplicate in situ stress states.

(4) Testing abnormalities (if they exist) will result in rejection by potential users or dissatisfaction by experienced users. Such abnormalities may include peculiar ln ϵ^i - ln N curves (reverse curvature, discontinuities, etc.); specimen fracturing without discernable effect on performance measurements; and excessive percentage of questionable tests.

(5) Experience: proven ability to discriminate among asphalts must be considered.

Field-Stress Cyclic Shear

(1) Attractiveness stems primarily from its ability to reproduce in situ stress states better than any other reasonable alternative.

(2) Primary disadvantage is the complexity associated with the confining pressure, including, primarily, the necessity for a membrane but including hardware requirements as well.

(3) Experience: N at 2 percent strain is not well correlated with ϵ^i at 602 cycles (A-002A hypothesis testing), and with stresses heretofore utilized, the test is very sensitive to aggregate but insensitive to asphalt.

Cyclic Axial-Shear

(1) Synchronized axial and shear load pulses with constant ratio of axial-to-shear stress.

(2) Because the axial stress is preselected, the cyclic axial-shear test is better able to duplicate the in situ stress state than is the constant height cyclic shear test. Because the axial stress is controllable during testing, the test is not as likely to be considered an index test.

(3) Lack of experience with this test is a significant complication.

Alternative Test

(1) Stress state (as identified above) includes constant height cyclic shear, cyclic axial-shear, and field-stress cyclic shear.

(2) Loading pattern

a. Simple — In testing each specimen, the amplitudes of the stress pulses are maintained at constant levels.

b. Compound — In testing each specimen, the amplitudes of the stress pulses are varied according to some predetermined pattern. As envisioned herein, stress levels would progressively increase at the end of each test block of some fixed number of cycles such as 400. Compound loading is advantageous because "premature" failure is eliminated, extrapolation is unnecessary, lengthy testing is avoided even with "strong" mixes, and stress-level effects can be characterized with limited testing.

Test Conditions and Interpretation of Test Measurements

(1) Selection of stress conditions

From elastic analysis of a two-layer structure with a 30 cm (12 in.) surface (Poisson's ratio of 0.35) over a subgrade with modulus of 138 MPa (20,000 psi) (Poisson's ratio of 0.45), surface modulus varied from 172 to 1033 MPa (25,000 to 150,000 psi). Tire pressure on a 44 kN (10,000-pound) dual tire (30 cm [12 in.] center to center) varied from 552 kPa to 828 kPa (80 psi to 120 psi). Critical condition was assumed to be outside edge of tire at depth of 5 cm (2 in.).

Because of the apparently constant ratio of normal-to-shear stress as shown in Table E.1, a more complete analysis was undertaken. Normalized shear stress is shown in Table E.2. Maximum principle shear stresses and the corresponding ratio of normal-to-shear stress were calculated at a number of locations within the pavement. The location of the critical shear stress was confirmed to be near the outside edge of the tire and at a shallow depth (Figure E.1). At the critical locations, the ratio of normal-to-shear stress was approximately 1.5 instead of approximately 1.2 as determined above (Figure E.2). Greater confinement at locations more directly beneath the tire centerline produced larger ratios, and more distant locations experienced smaller ratios. A somewhat finer grid confirmed these findings (Figures E.3 and E.4).

The critical conditions, the maximum shear stress with the least confinement (smallest axial-to-shear ratio), are readily apparent from plots of the axial-to-shear ratio versus maximum shear stress for each of the points on the grid. For the 690 kPa (100 psi) tire pressure and 345 MPa (50,000 psi) surface modulus, the critical shear stress is about 25 kPa (32.6 psi) and the critical ratio about 1.5 (Figure E.5). Figures E.6 through E.10 confirm that the critical ratio is about 1.5 for all tire pressures and for surface moduli of 345 MPa (50,000 psi) and 690 MPa (100,00 psi). The maximum shear stresses are shown in Table E.3.

(2) Selection of performance measures

a. Alternatives are slope or intercept of ln ϵ^1-ln n relationship; N at fixed (threshold) level of ϵ^1; ϵ^1 at fixed level of N; and modulus (total, resilient, or permanent), etc.

b. The abridged analysis system under consideration requires a laboratory estimate of N_{pd}, the number of loading cycles (under representative stresses) corresponding to a design strain level. Thus, test stresses and inelastic strain limits would vary, depending upon design conditions.

c. As experience develops, it may prove possible to obtain a general perception of likely mix performance by measuring (or estimating) N_{pd} at typical test stresses and strain limits.

Table E.1. State of stress for various tire pressures

Tire Pressure (psi)	Surface Modulus (psi)	Maximum Shear Stress (psi)	Corresponding Normal Compressive Stress (psi)	Ratio of Normal- to-Shear Stress
80	25,000	23.2	26.8	1.16
	50,000	23.6	27.8	1.18
	100,000	24.1	29.2	1.21
	150,000	24.5	30.3	1.24
100	25,000	28.3	32.4	1.15
	50,000	28.6	33.5	1.17
	100,000	29.1	35.0	1.20
	150,000	29.3	36.1	1.23
120	25,000	33.0	37.5	1.14
	50,000	33.3	38.6	1.16
	100,000	33.7	40.2	1.19
	150,000	33.9	41.3	1.22

Table E.2. Normalized shear stress

Surface Modulus (psi)	Normalized Shear Stress Relative to 100 psi Tire Pressure		
	80 psi Tire Pressure	100 psi Tire Pressure	120 psi Tire Pressure
25,000	0.82	1.00	1.17
50,000	0.82	1.00	1.16
100,000	0.83	1.00	1.16
150,000	0.84	1.00	1.16

Table E.3. Maximum shear stress

Surface Modulus (psi)	Maximum Shear Stress (psi)		
	80 psi Tire Pressure	100 psi Tire Pressure	120 psi Tire Pressure
50,000	26.2	32.6	38.8
100,000	24.9	32.0	38.3

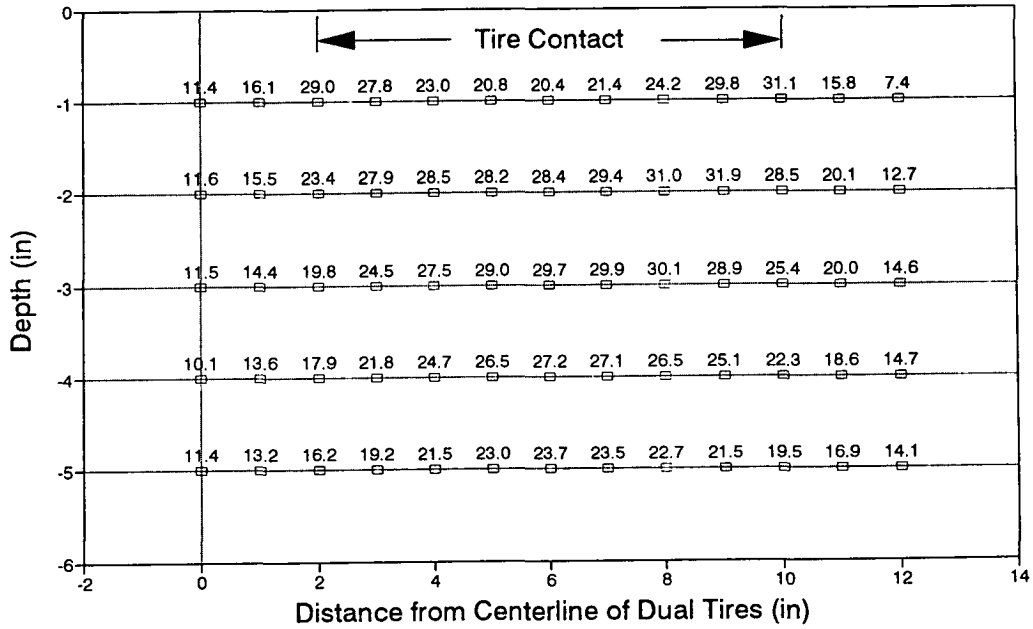

Figure E.1. Maximum shear stresses resulting from 10,000 lb load, 690 kPa (100 psi) tire pressure, asphalt concrete modulus — 345 MPa (50,000 psi)

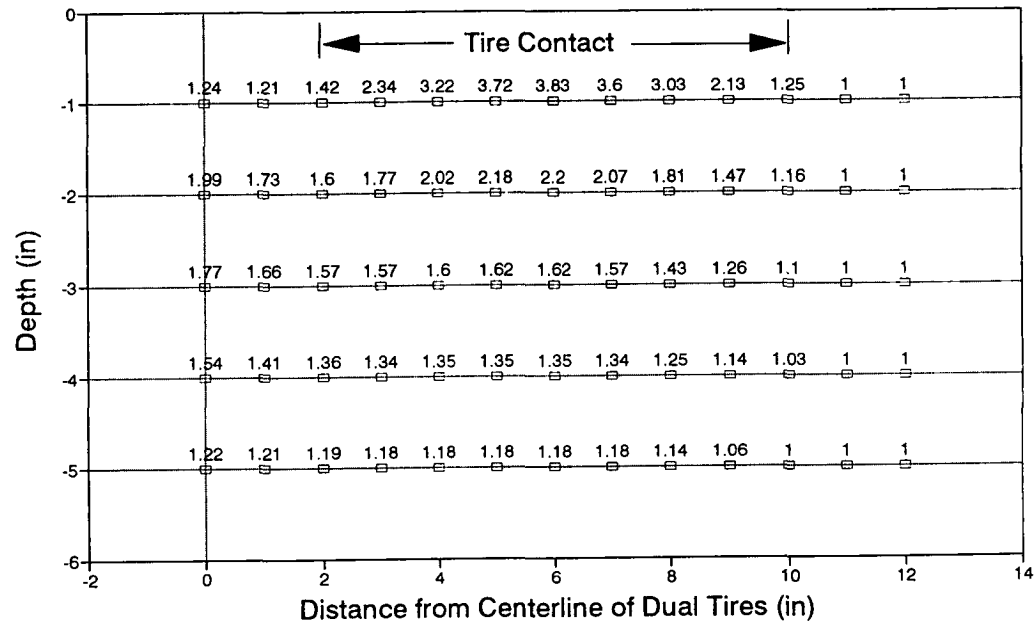

Figure E.2. Ratio of axial-to-shear stress for conditions of Figure E.1

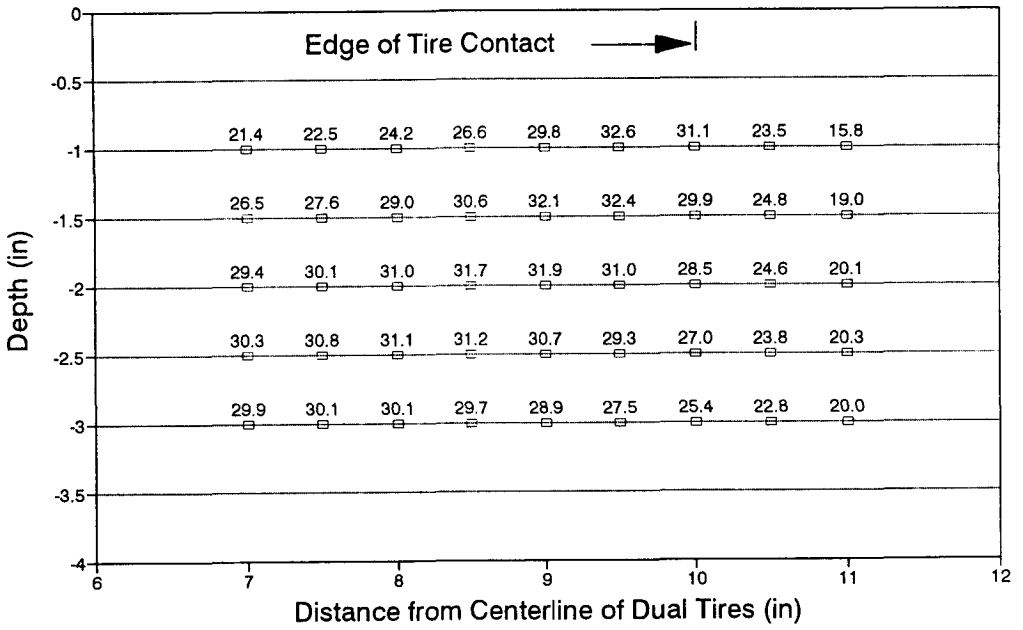

Figure E.3. Maximum shear stresses; same conditions as Figure E.1

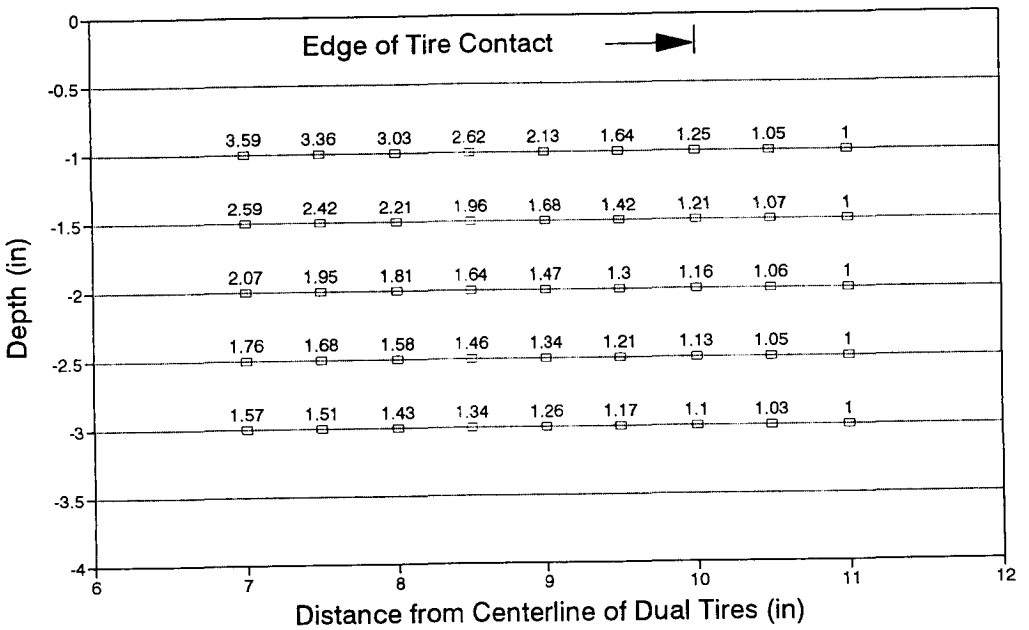

Figure E.4. Ratio of axial to shear for conditions of Figure E.3

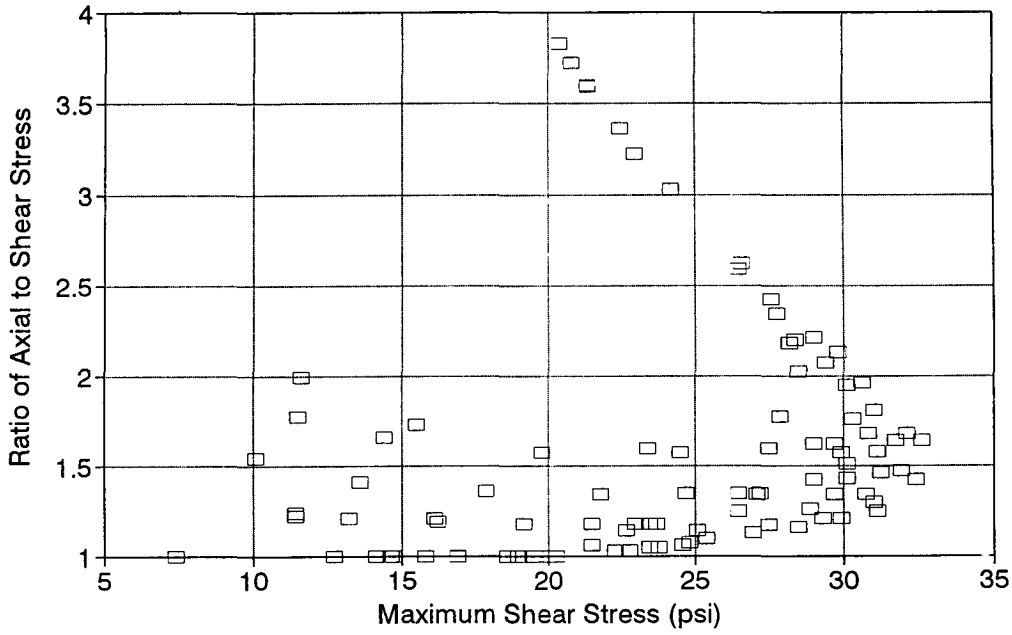

Figure E.5. Cyclic axial-shear test conditions, conditions of Figure E.1

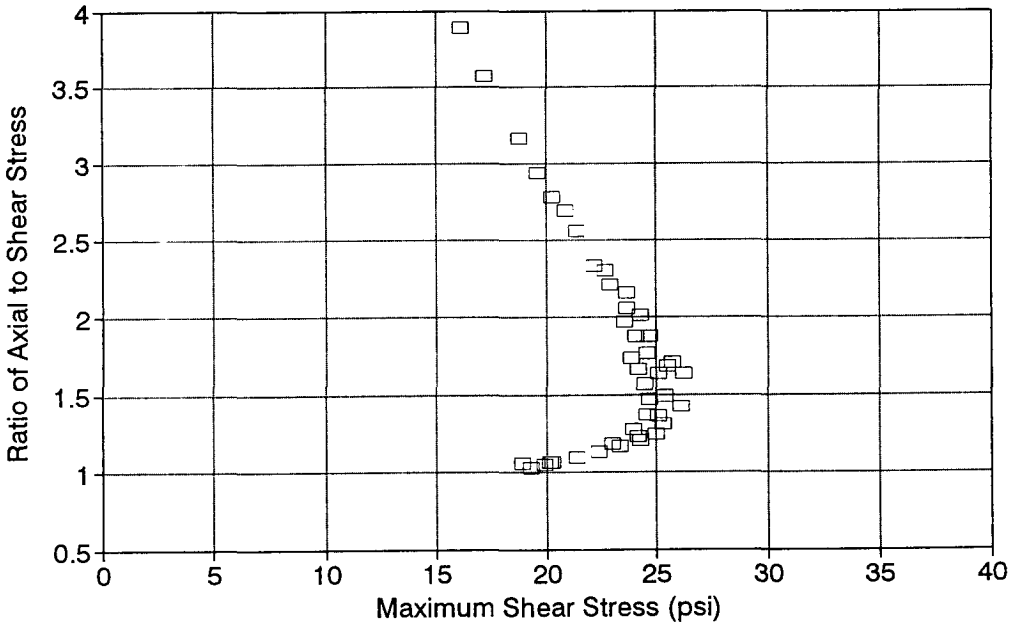

Figure E.6. Cyclic axial-shear test conditions — 552 kPa (80 psi) tire pressure; other conditions same as Figure E.1

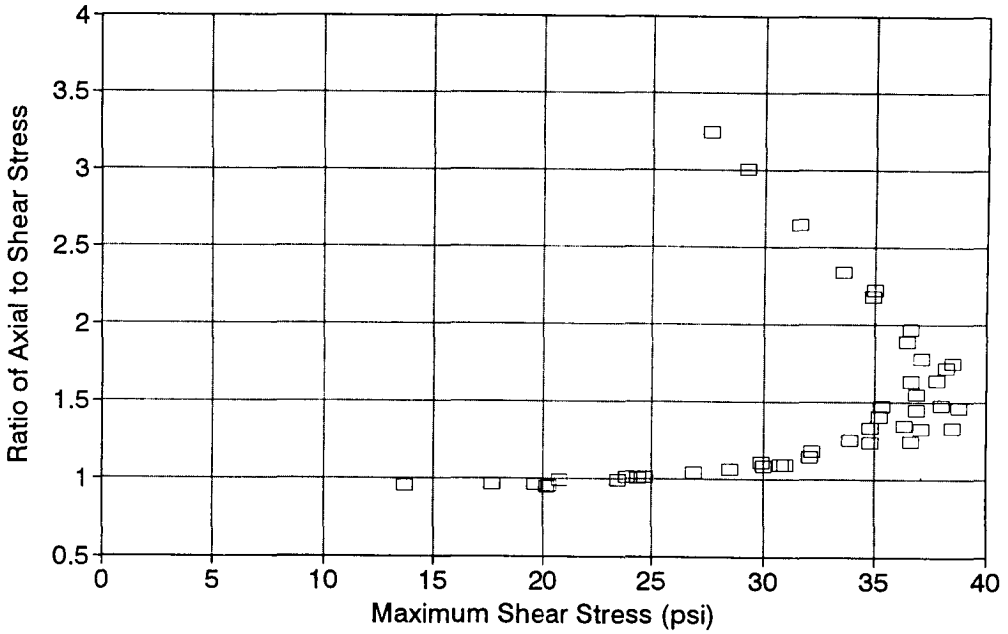

Figure E.7. Cyclic axial-shear test conditions — 828 kPa (120 psi) tire pressure; other conditions same as Figure E.1

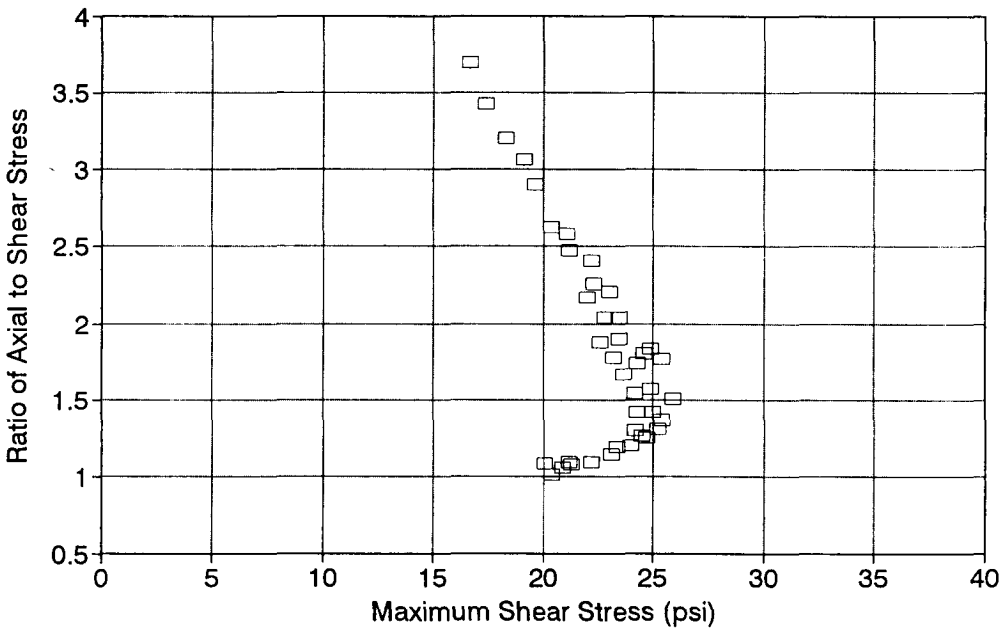

Figure E.8. Cyclic axial-shear test conditions; 10,000 lb load; tire pressure — 552 kPa (80 psi); layer modulus = 689 MPa (100,00 psi)

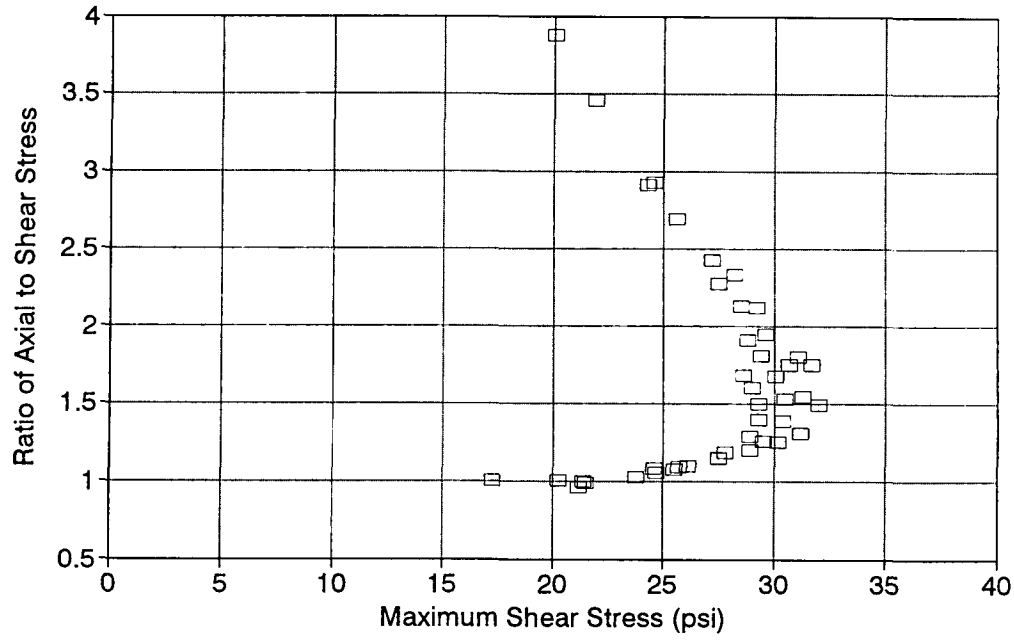

Figure E.9. Cyclic axial-shear test conditions; 10,000 lb load; tire pressure — 690 kPa (100 psi)

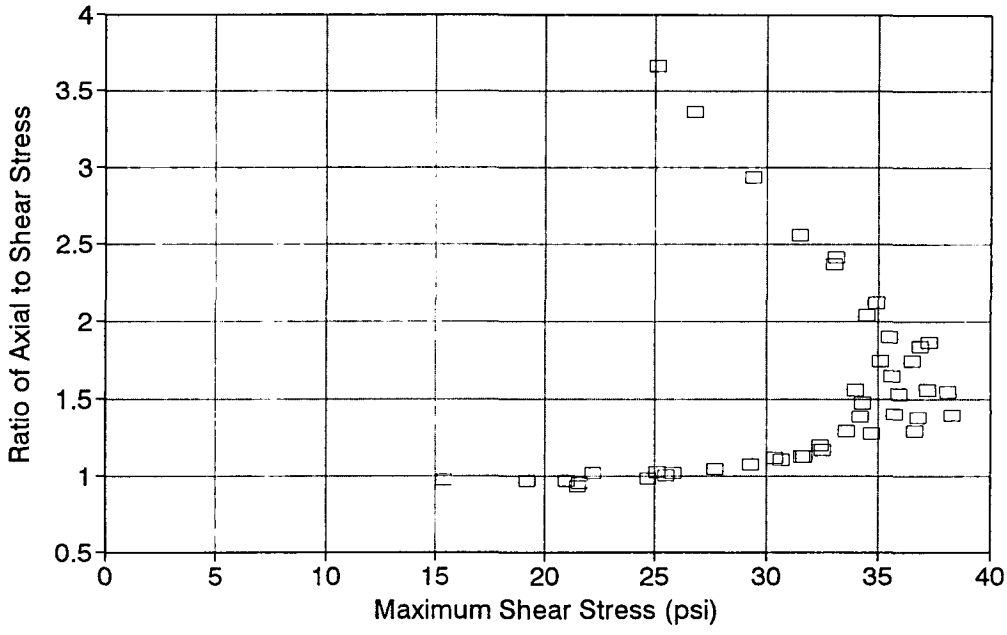

Figure E.10. Same as Figure E.9; tire pressure = 828 kPa (120 psi)

(3) Extrapolations to conditions representative of in situ pavements

The abridged analysis system compares a test measurement or estimate, N_{pd}, with a traffic estimate, N_{design}. Because these are expected to be large quantities, limitations on laboratory testing time will prevent testing at the low stress levels corresponding to N_{pd}. Accordingly, testing must be conducted at larger stress levels with estimates of N_{pd} being based on extrapolations or models.

(4) Treatment of reliability

The treatment of reliability depends on the kinds of test measurements, the methods used in their interpretation, and the nature of their use in the analysis system. The reliability portion of the abridged analysis system requires an estimate of the variance of N_{pd}. Obtaining such an estimate is complicated by the likelihood that N_{pd} will be estimated instead of measured because of long testing times at low stress levels. Estimates will likely be based either on extrapolations (as in fatigue) or in a model that captures the effects of stress on N_{pd}.

Validation Activity

What must be done to demonstrate that the accelerated test accurately measures the ability of asphalt aggregate mixes to resist permanent deformation in situ?

Compound Cyclic Axial-Shear

(1) It is assumed that a simple cyclic shear test yields a relationship between inelastic shear strains, ϵ^i, and number of loading cycles, N, as follows:

$$\epsilon^i = a\, N^b$$

where: a and b = constants for each fixed stress condition.

(2) The compound loading test is justifiable only if inelastic strain is a state variable — that is, future response depends only on the existing strain state and not the manner in which it was reached — or, alternatively, if the time-hardening concept is valid.

(3) The interpretation begins with the following basic equation relating ϵ^i with N for simple loading:

$$\epsilon^i = a\, N^b.$$

At the end of the first loading block or sequence:

$$\epsilon_1^i = a_1 \Delta N^{b1}$$

where: ϵ_1^i = inelastic strain at the end of the first loading block;
ΔN = fixed number of cycles in each loading block; and
a_1 and b_1 = constants appropriate to the first stress level.

If N_2 is the number of cycles at the second stress level which would have yielded a strain of ϵ_1^i in a simple loading test, then N_2 can be determined as follows:

$$\epsilon_1^i = a_2 N_2^{b2}$$

and

$$N_2 = (\epsilon_1^i/a_2)^{(1/b2)}.$$

If ϵ_2^i is the inelastic strain at the end of the second loading block, then

$$\epsilon_2^i = a_2 (N_2 + \Delta N)^{b2}$$

where: a_2 and b_2 = constants appropriate to the second stress level

and

$$\epsilon_2^i = a_2[(\epsilon_1^i/a_2)^{(1/b2)} + \Delta N]^{b2}.$$

Generalizing

$$\epsilon_j^i = a_j[\epsilon_{j-1}^i/a_j)^{(1/bj)} + \Delta N]^{bj}$$

where: ϵ_j^i = the inelastic shear strain at the end of the jth block of a compound loading cycle; and
a_j and b_j = constants appropriate to the jth stress level.

(4) The first "successful" compound cyclic shear test — performed on a V0W0 specimen — yielded the following ϵ^i - N relationship:

$$\epsilon^i = 0.0002\ \tau\ N^{0.30} = 0.0002\ \tau$$

where: ϵ^i = inelastic shear strain;
τ = shear stress; and
N = number of cycles.

Each test block consisted of 400 loading cycles of progressively increasing shear stress beginning at 6.9 kPa (1 psi) and proceeding in 6.9 kPa (1 psi)

increments until reaching 105 kPa (15 psi). The magnitude of the axial stress was 1.2 times that of the shear stress.

Figure E.11 illustrates the test data and a curve of best fit obtained manually by trial and error. The anomaly at the first three stress levels resulted primarily from inaccurate control of the vertical stress levels.

Figure E.12 illustrates the simulation of *simple* cyclic axial-shear tests using the above ϵ^i - N model calibration from the compound loading testing. Note especially in this case the relative insensitivity to the slopes of the lines to the level of stress.

Figure E.13 compares simulations from the compound loading test with two other sets of test data, one developed from a typical cyclic constant height shear test of V0W0 and the second from a simple cyclic axial-shear test of V0W0. Unfortunately, the axial-shear test was interrupted after only 300 loading cycles because control of the axial load was lost. Although these comparisons are not conclusive, they do support the relationship that had been expected. In comparison with the constant height test, the added "confinement" within the axial-shear test increases resistance to permanent deformation (e.g., at a given number of cycles, the inelastic strain is less in the axial-shear test). Additionally, the compound loading test yields estimates that appear to be very much in line with actual measurements from the other two tests. Because of the nature of the ϵ^i - N model being employed, however, the compound loading test will not be able to duplicate curved portions of any double logarithmic plot of actual measurements.

(5) Lack of experience with the compound cyclic axial-shear test confounds the task of selecting proper test parameters. Fortunately, the test does not require a priori determinations of the design shear stress and the design strain limit. What is required, however, is a selection of the ratio of axial-to-shear stress, the size of the test block, and the sequence of increasing shear stresses.

Ideally, the ratio of axial-to-shear stress can be maintained at a single level. Based on the above calculations, a constant ratio of approximately 1.5 seems appropriate. Further investigation is in order using structural analysis programs and finite element idelizations.

Trial testing has used test blocks of 400 loading cycles each. Thus far, there is no indication that this block length is unsuitable.

The sequence of shear stresses in prior testing has begun at 6.9 kPa (1 psi) and increased in increments of 6.9 kPa (1 psi). This may result in excessive testing time for the more resistant mixes. To develop some understanding of the range in stresses that might be practically expected, the one available equation ($\epsilon^i = 0.0002\ \tau\ N^{0.30 + 0.0002\ \tau}$) was used to produce the data shown in Table E.4.

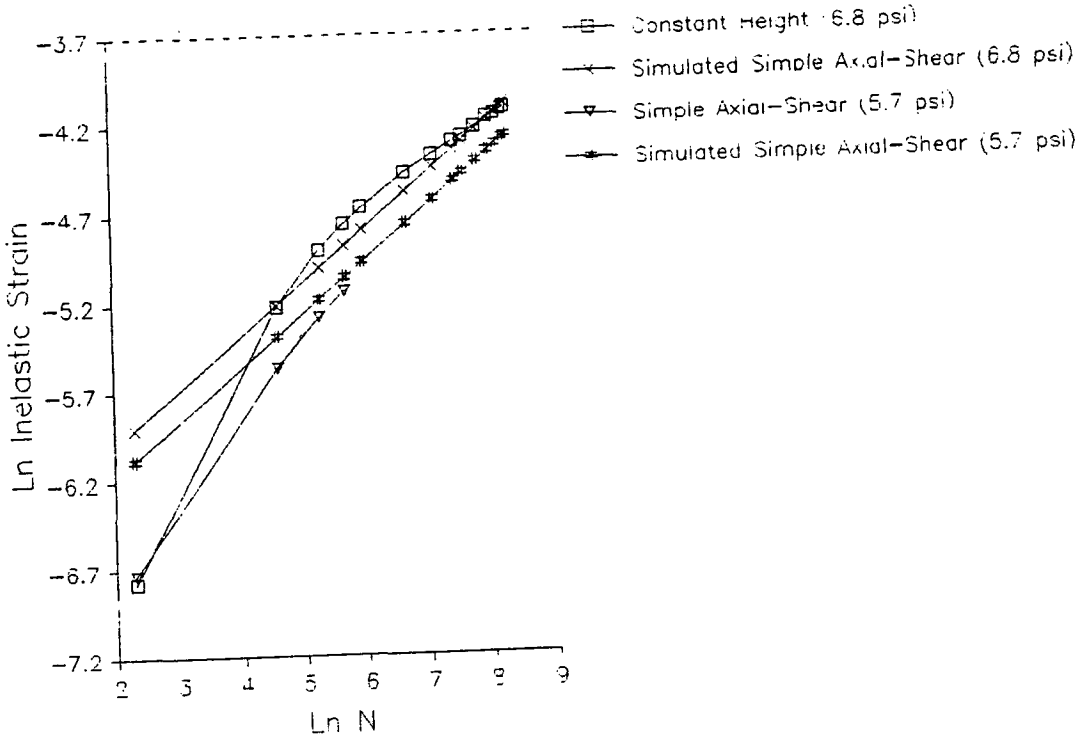

Figure E.11. Compound cyclic shear test (aggregate RB, asphalt AAG-1) 400 cycles, 6.9 to 105 kPa (1 to 15 psi) shear stress, 1.2 axial/shear ratio

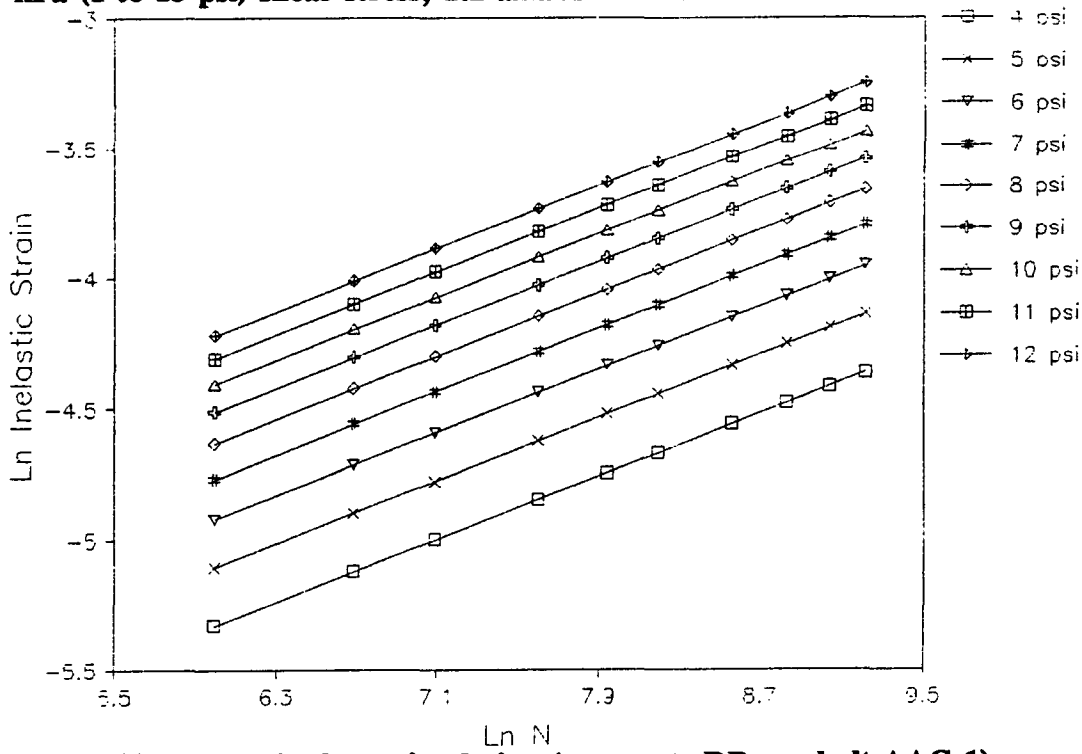

Figure E.12. Simple cyclic shear simulation (aggregate RB, asphalt AAG-1)

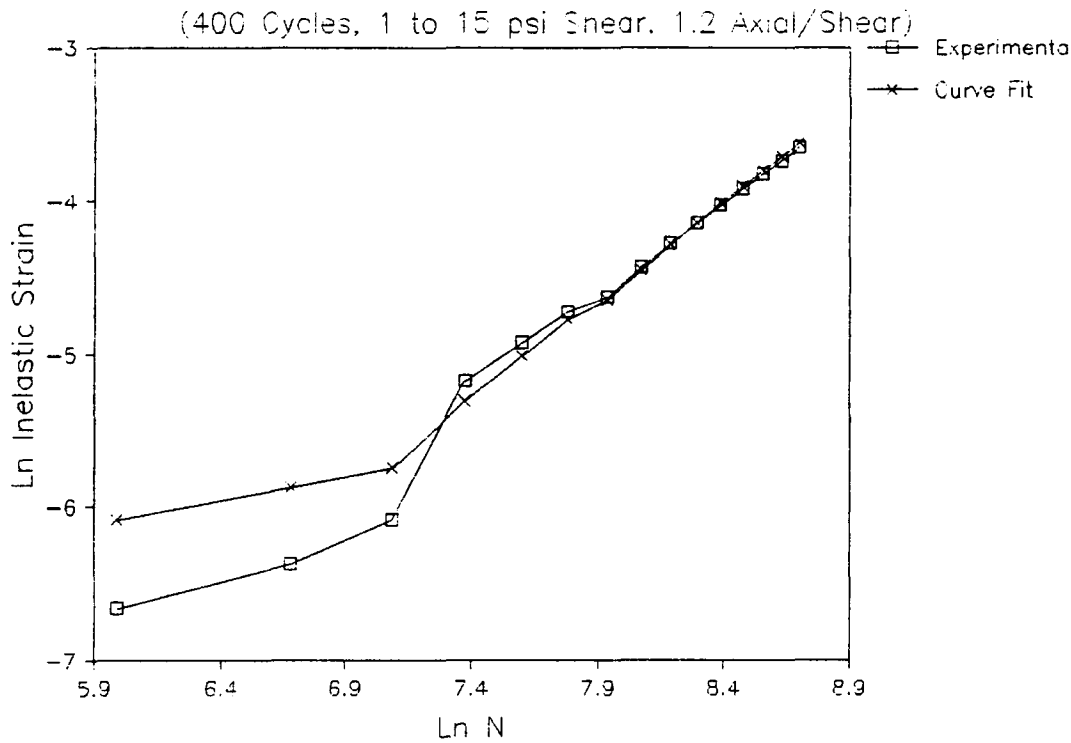

Figure E.13. Constant height versus simple shear (aggregate RB, asphalt AAG-1)

Table E.4. Design strain for various load cycles

Anticipated Number of Load Cycles	Shear Stress (psi) 1 Percent Design Strain	2 Percent Design Strain
50,000	1.94	3.86
100,000	1.58	3.14
500,000	0.98	1.95
1,000,000	0.79	1.58

To the extent that the model calibration is reasonably accurate, it thus appears that test stresses may generally be small, most likely below 34 kPa (5 psi) and perhaps extending to 6.9 kPa (1 psi) or even less. The stress sequence shown in Table E.5 is appropriate for adequately accommodating this range without requiring excessively long tests:

Table E.5. Testing sequence for various shear stresses

Shear Stress (psi)	Comments
0.5	Primarily "conditioning"
1	Stress range of greatest interest
2	Stress range of greatest interest
3	Stress range of greatest interest
4	Stress range of greatest interest
5	Stress range of greatest interest
7	Accelerated loading to "failure"
9	Accelerated loading to "failure"
11	Accelerated loading to "failure"
13	Accelerated loading to "failure"
15	Accelerated loading to "failure"
17	Accelerated loading to "failure"
etc.	Accelerated loading to "failure"

Testing would be terminated when the inelastic strain reached some reasonable maximum such as 3 percent.

Appendix F

Compound Loading Test Results

Table F.1 Identification of specimens used in normal tests

Asphalt Content (Percent)	Air Void Content (Percent)		
	2.5-3.5	4.5-5.5	6.5-7.5
4.5	MA1B1 MA1B2	MB1B1 MB1B2	MC1B1 MC1B2
4.9	MA2B1 MA2B2	MB2B1 MB2B2	MC2B1
5.5	MA3B1	MB3B1	MC3B1 MC3B2
6.0	MA4B1	MB4B1	MC4B1

Table F.2. Identification of specimens used in constant height tests

Asphalt Content (Percent)	Air Void Content (Percent)		
	2.5-3.5	4.5-5.5	6.5-7.5
4.5	MA1H1 MA1H2	MB1H1 MB1H2	MC1H1
4.9	MA2H1 MA2H2	MB2H1 MB2H2	MC2H2
5.5	MA3H1	MB3H1	MC3H1 MC3H2
6.0	MA4H1	MB4H1	MC4H1 MC4H2

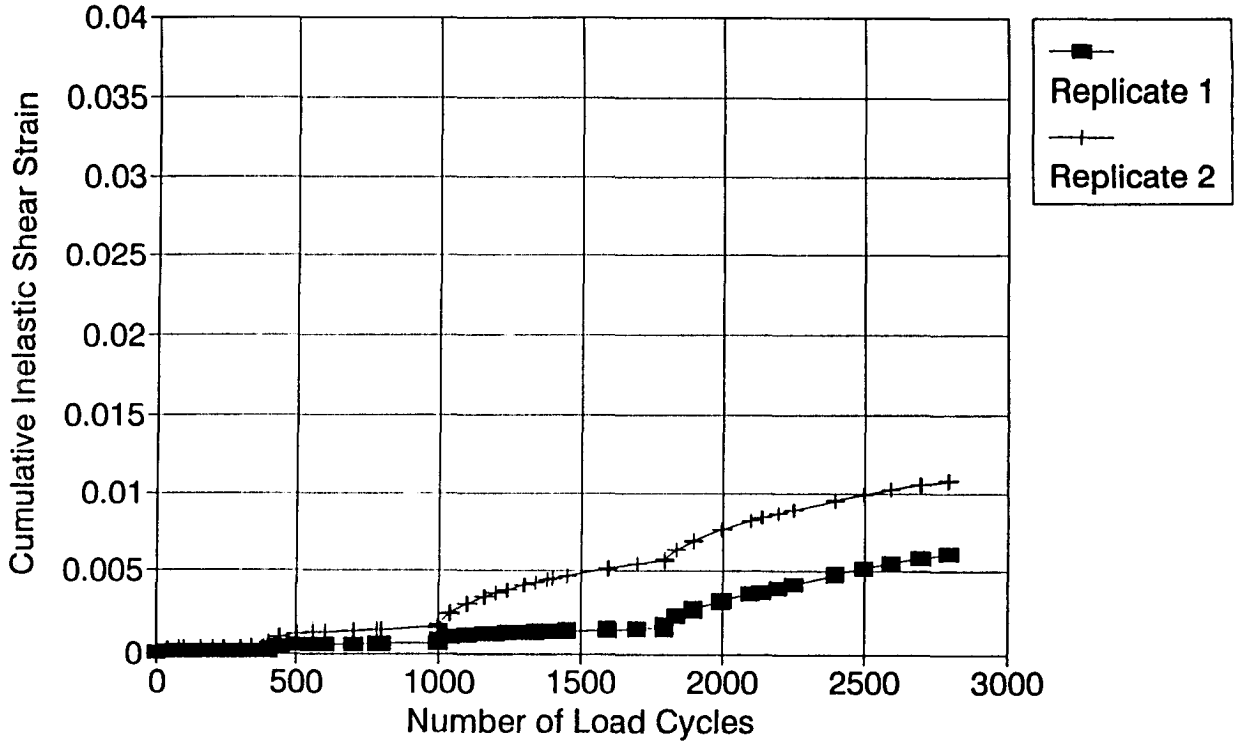

Figure F.1. Compound normal test (Mix A1)

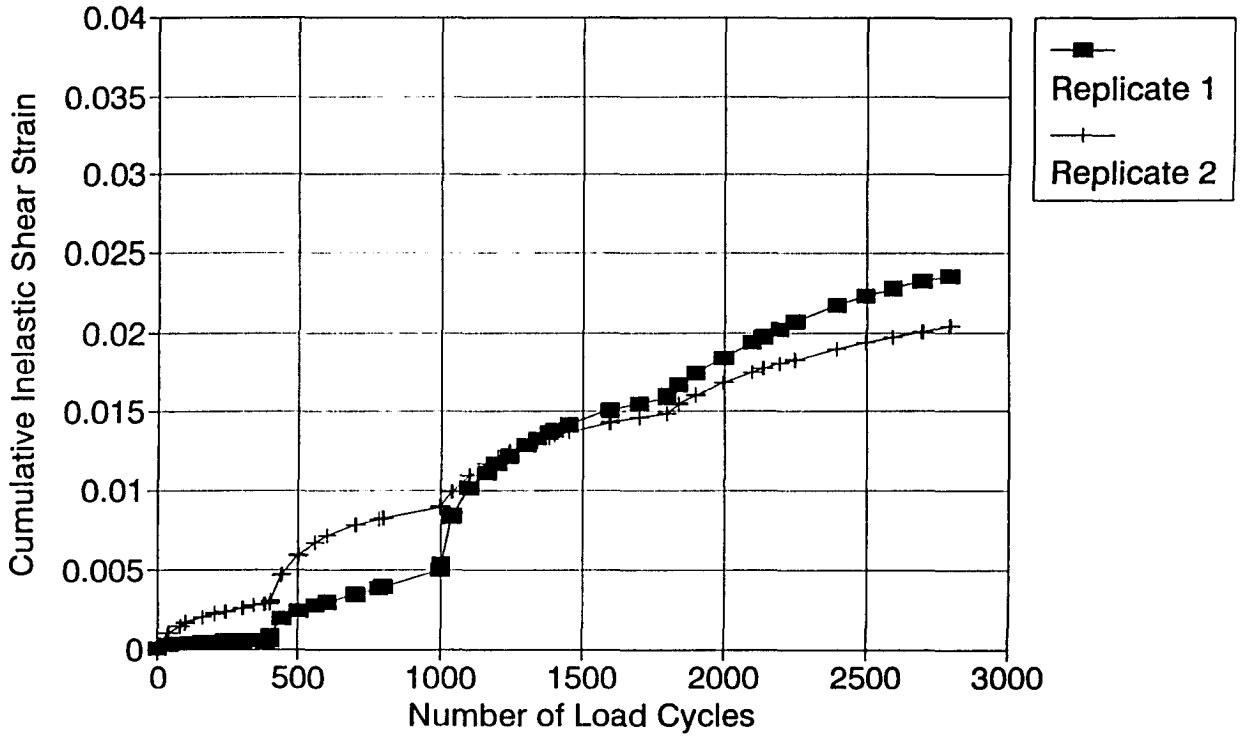

Figure F.2. Compound normal test (Mix A2)

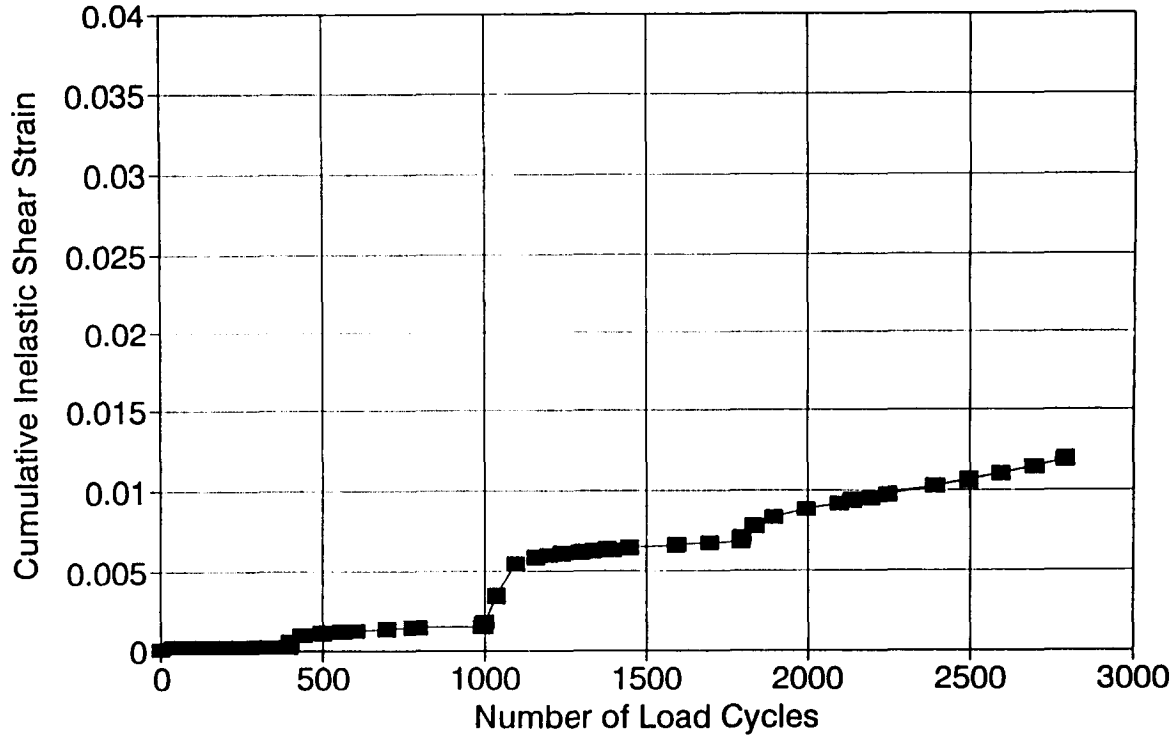

Figure F.3. Compound normal test (Mix A3)

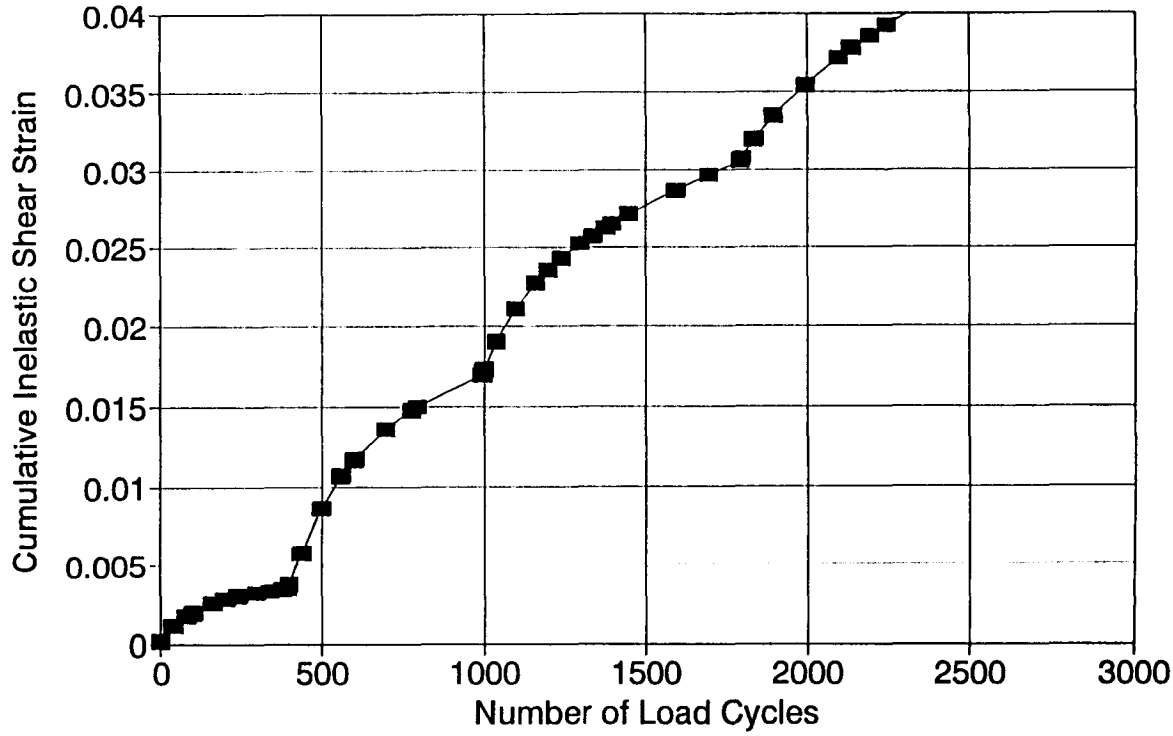

Figure F.4. Compound normal test (Mix A4)

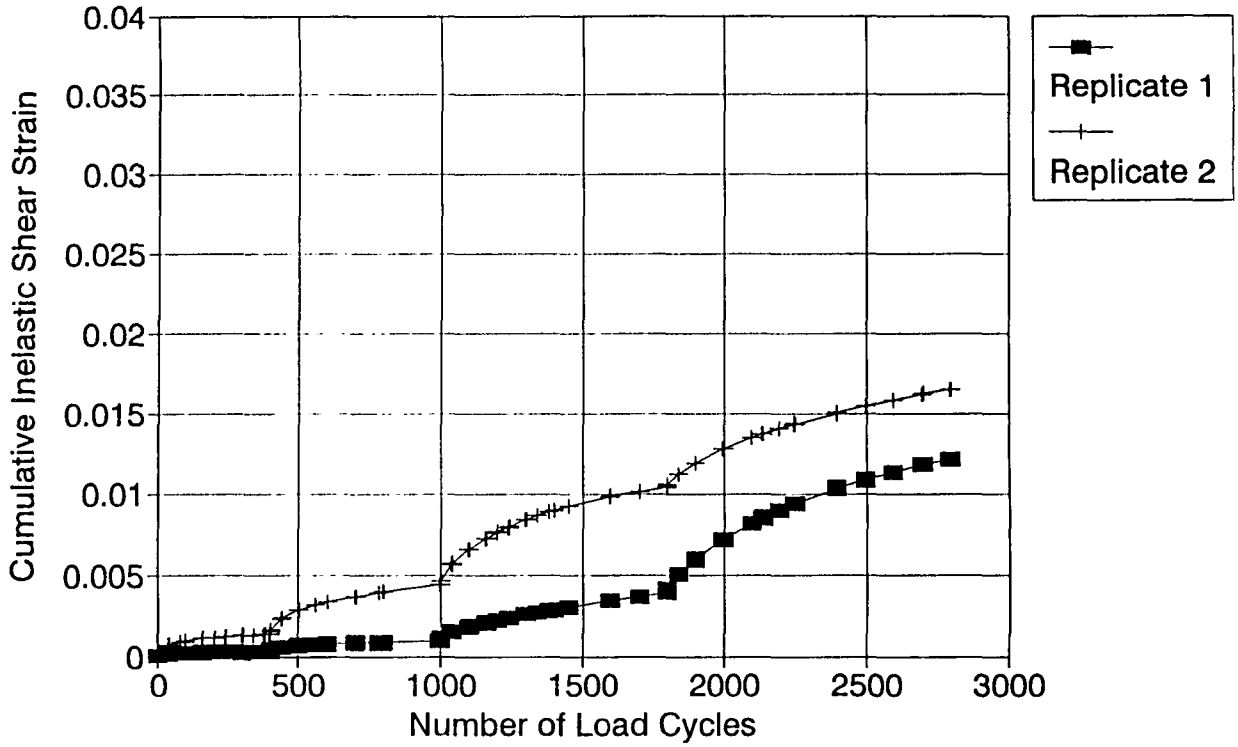

Figure F.5. Compound normal test (Mix B1)

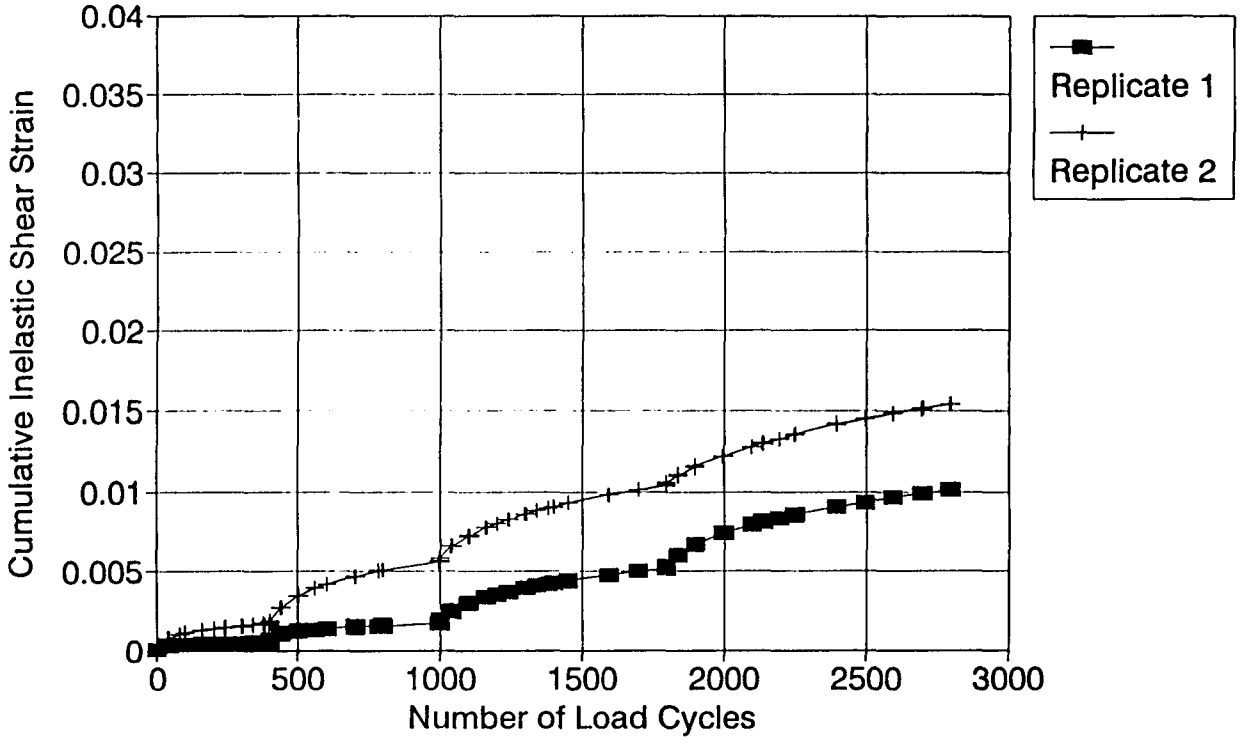

Figure F.6. Compound normal test (Mix B2)

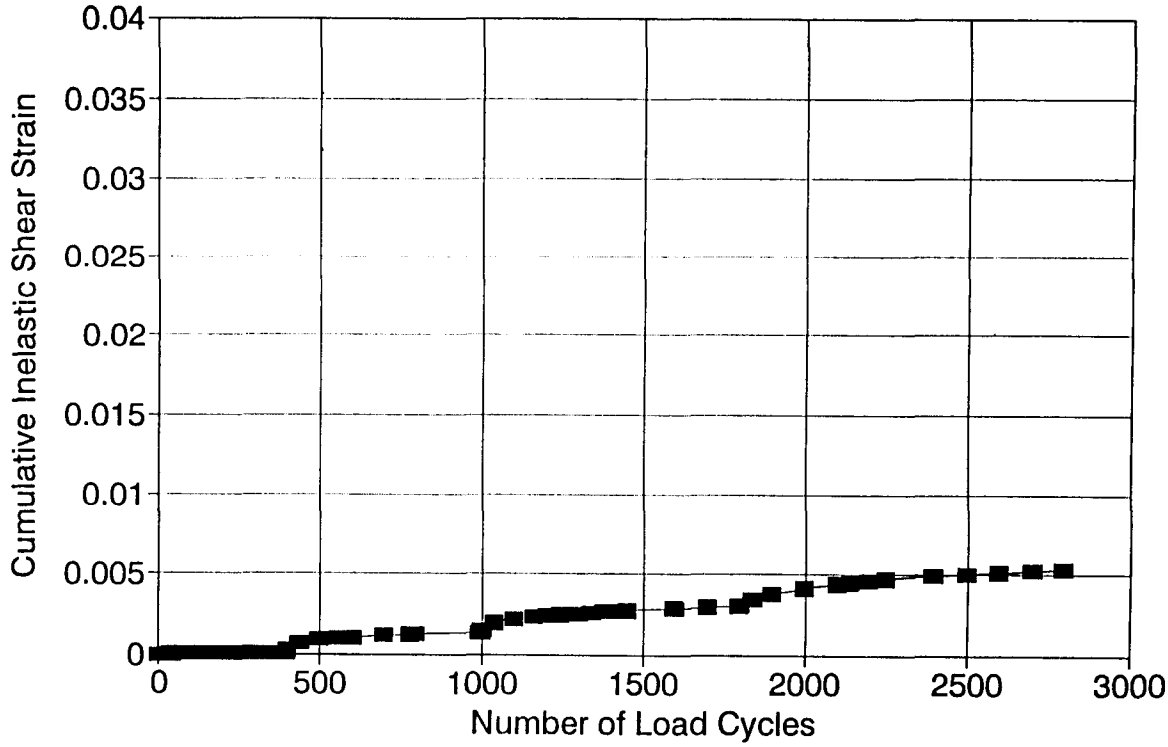

Figure F.7. Compound normal test (Mix B3)

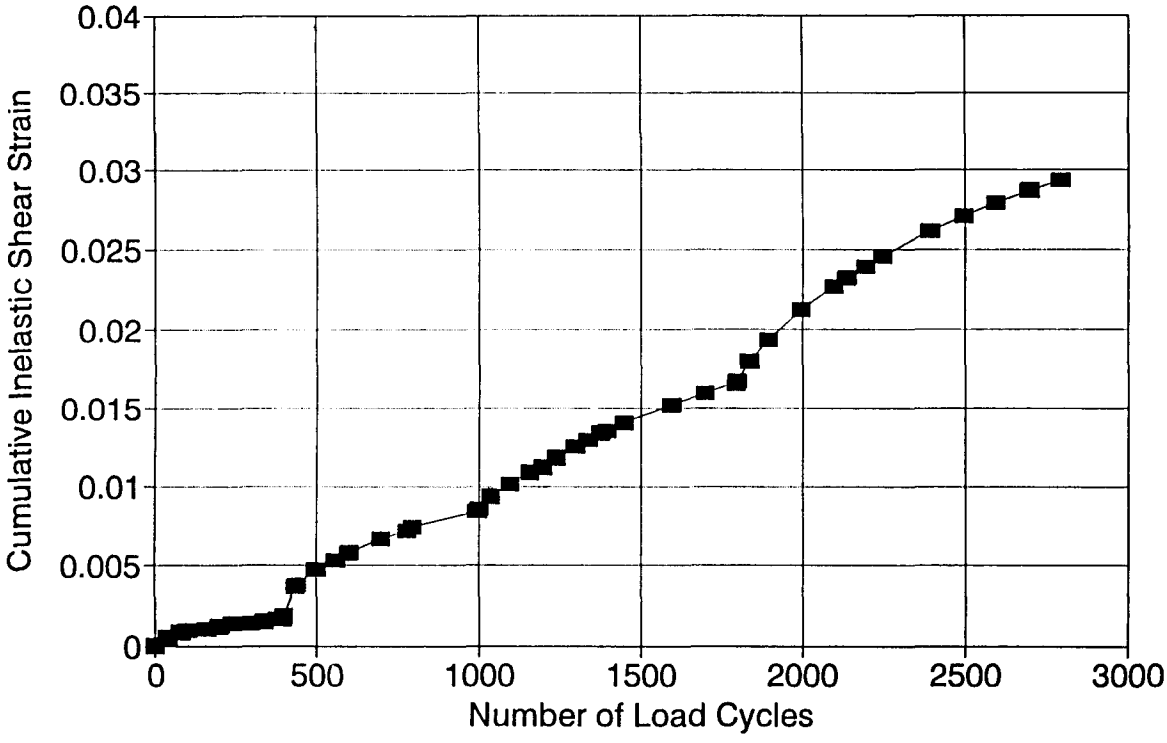

Figure F.8. Compound normal test (Mix B4)

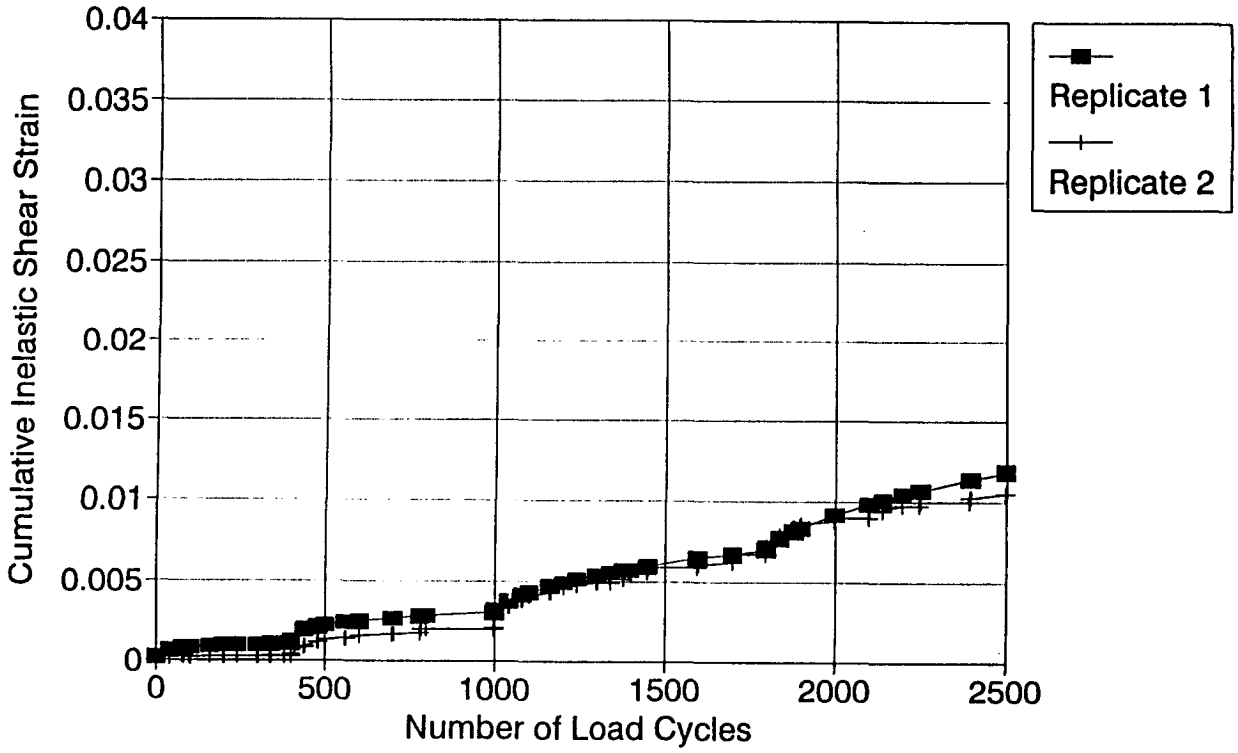

Figure F.9. Compound normal test (Mix C1)

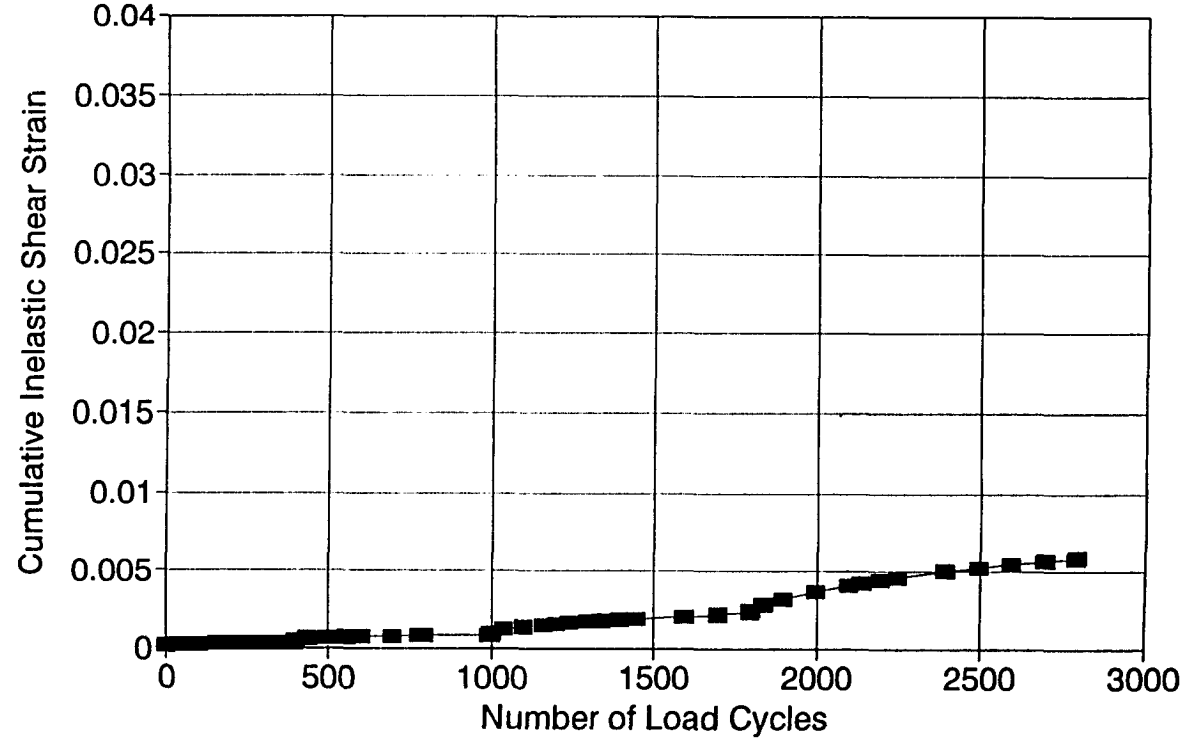

Figure F.10. Compound normal test (Mix C2)

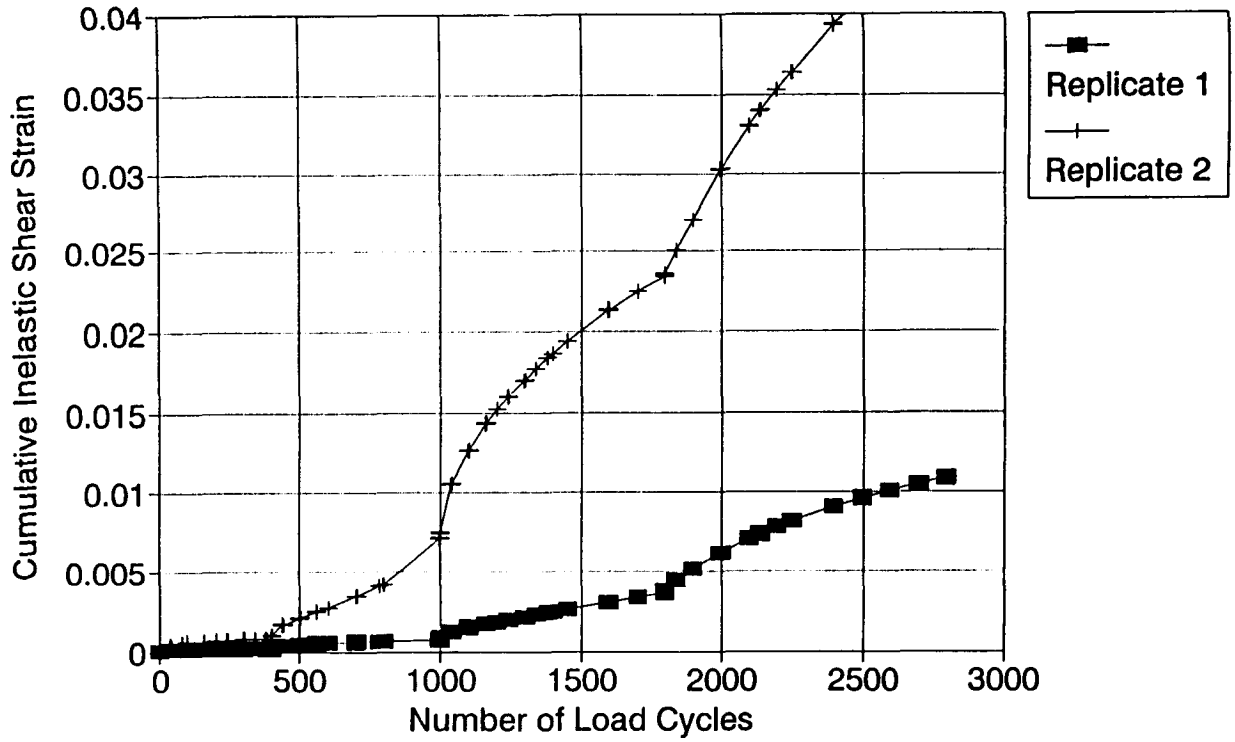

Figure F.11. Compound normal test (Mix C3)

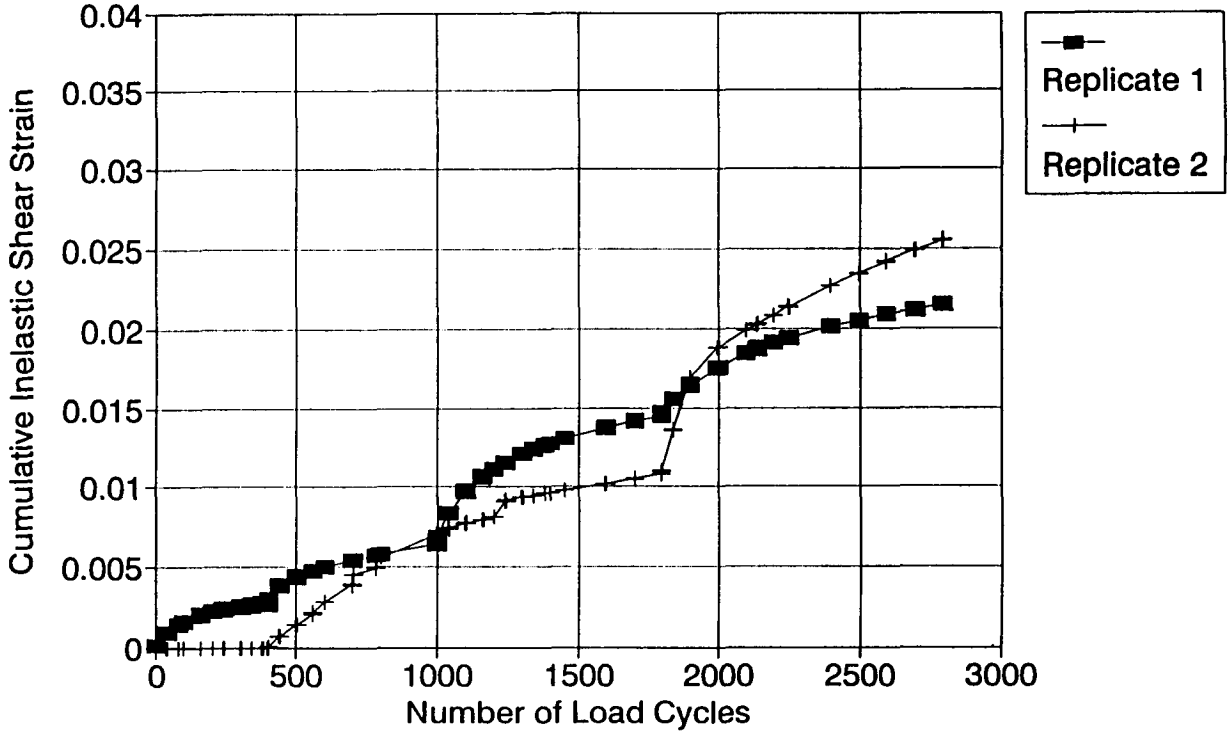

Figure F.12. Compound constant height test (Mix A1)

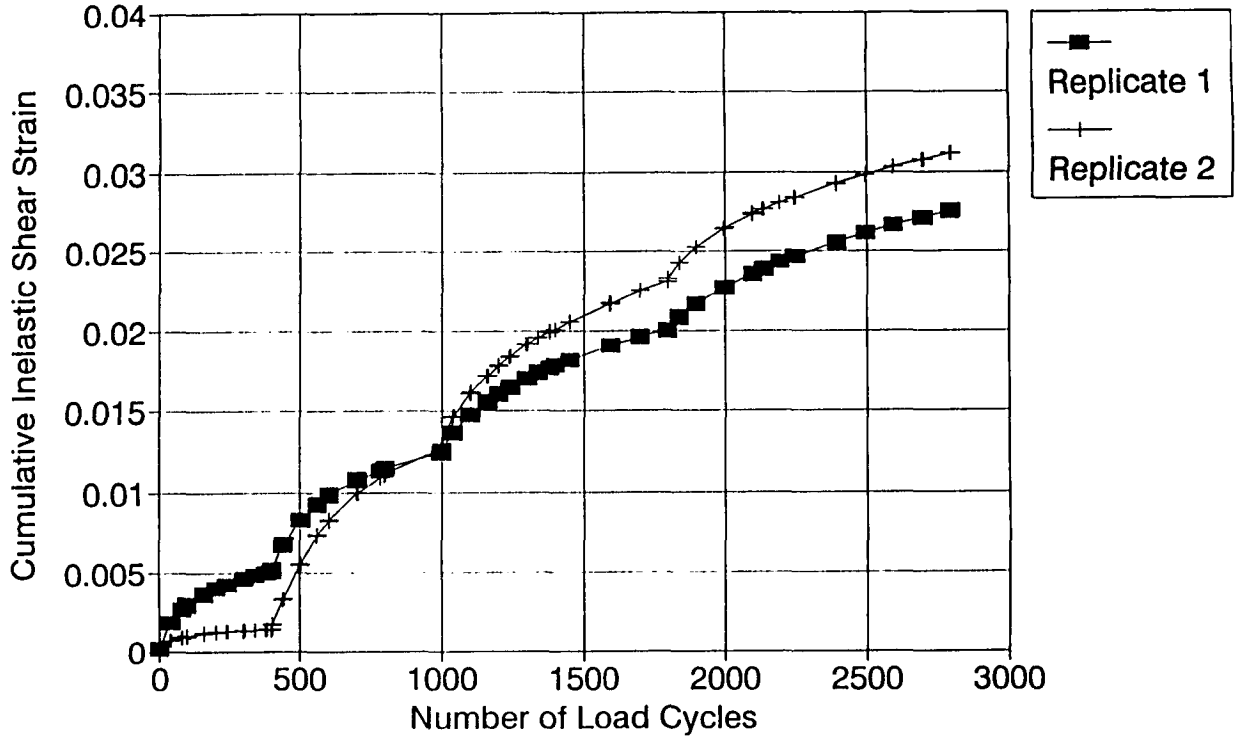

Figure F.13. Compound constant height test (Mix A2)

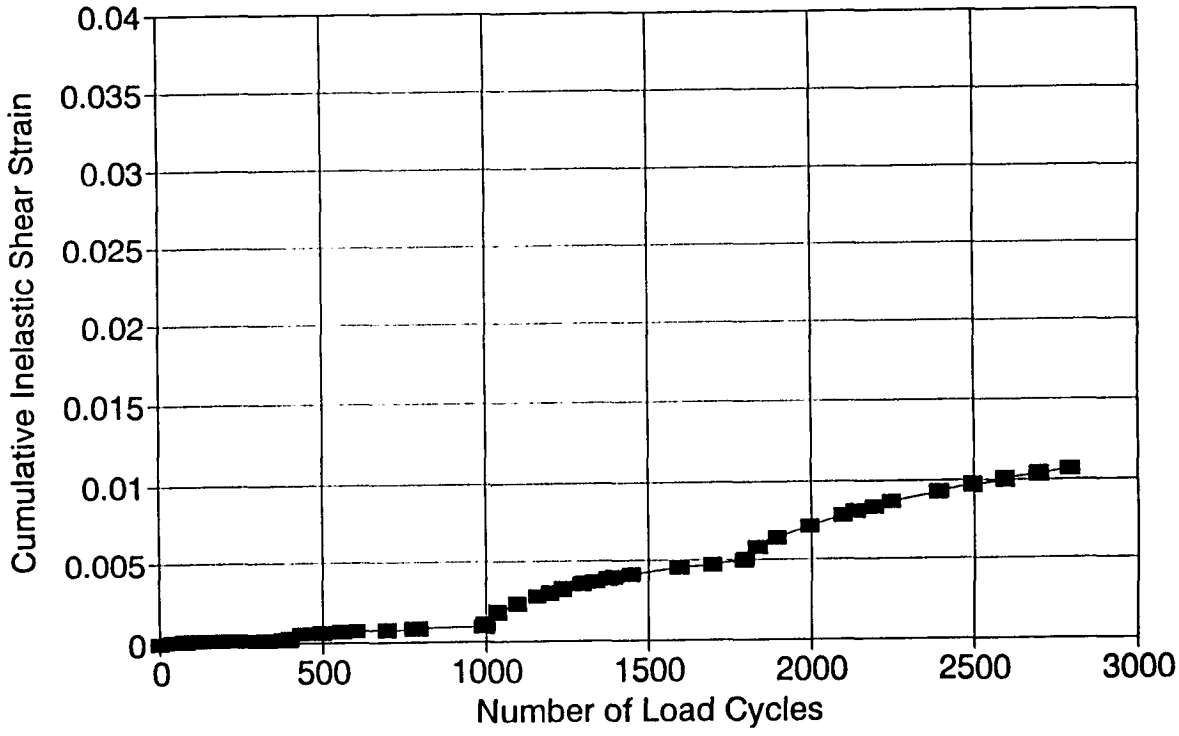

Figure F.14. Compound constant height test (Mix A3)

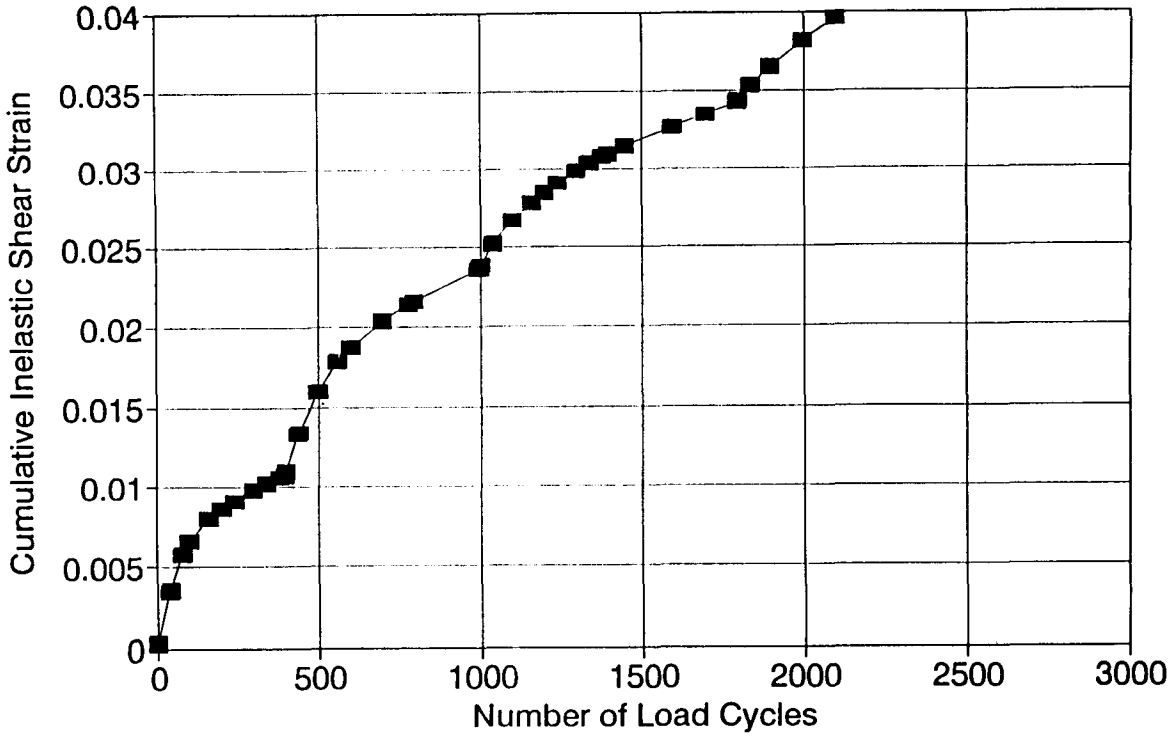

Figure F.15. Compound constant height test (Mix A4)

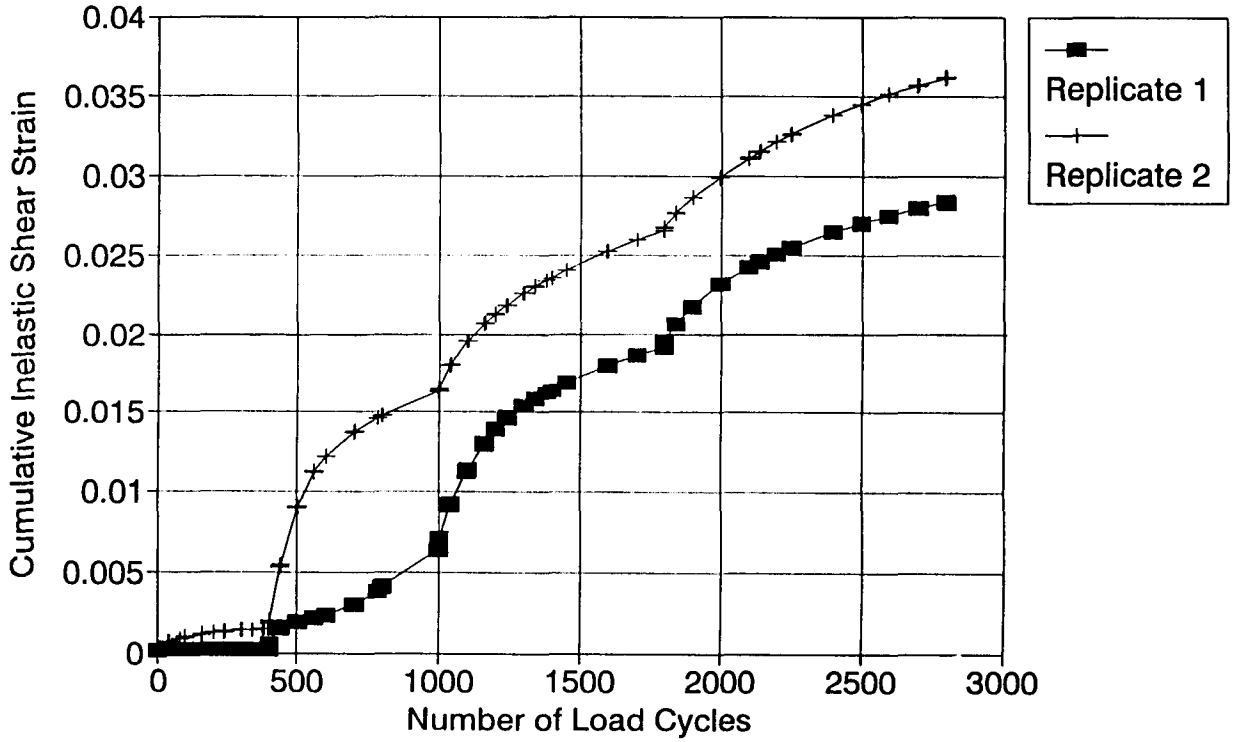

Figure F.16. Compound constant height test (Mix B1)

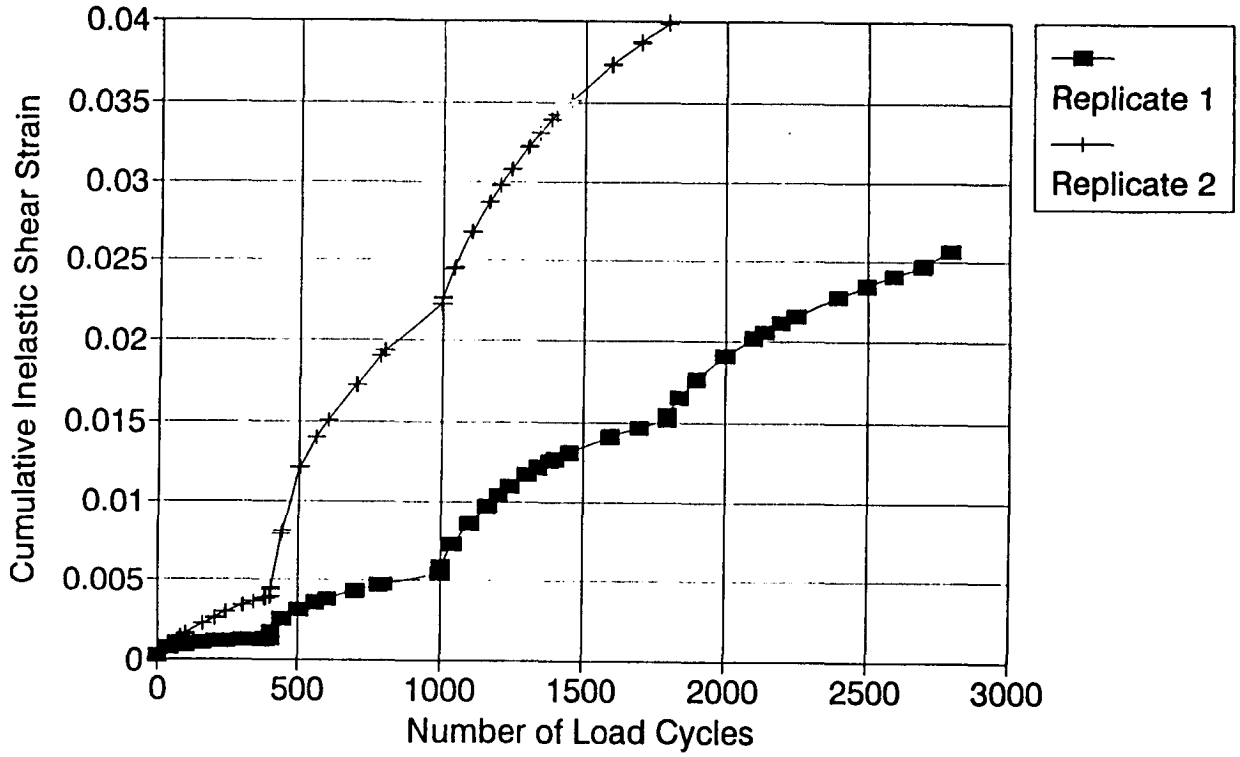

Figure F.17. Compound constant height test (Mix B2)

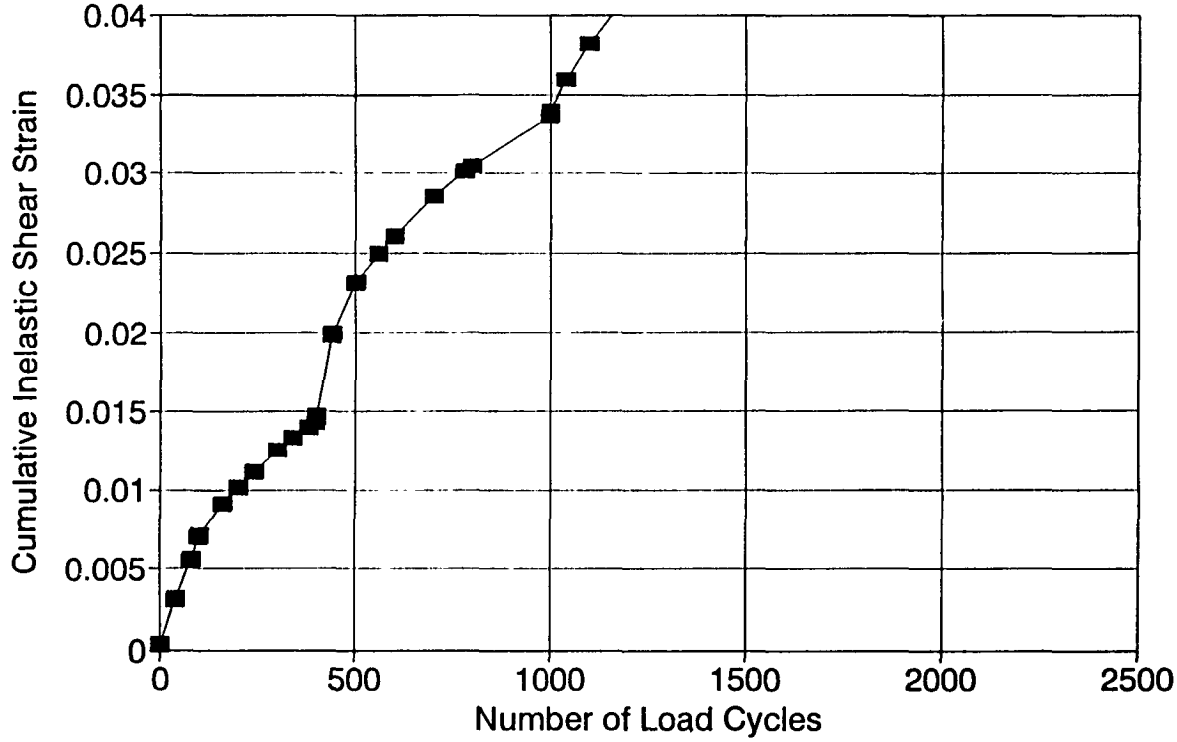

Figure F.18. Compound constant height test (Mix B3)

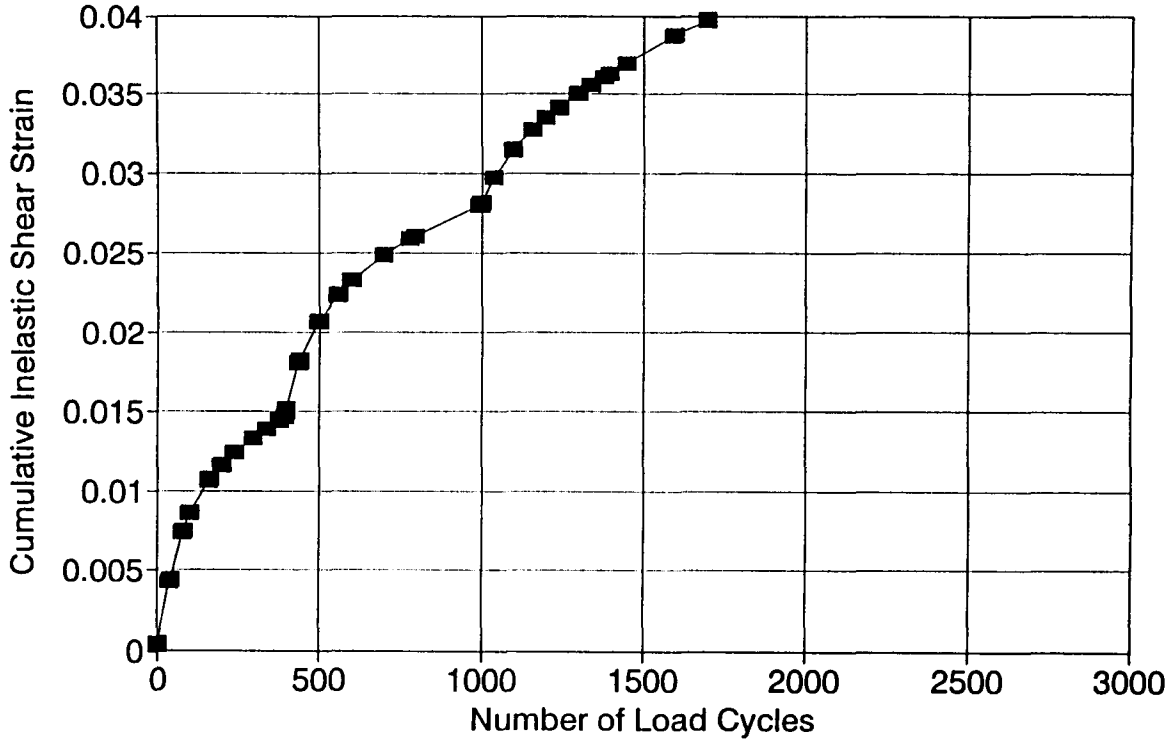

Figure F.19. Compound constant height test (Mix B4)

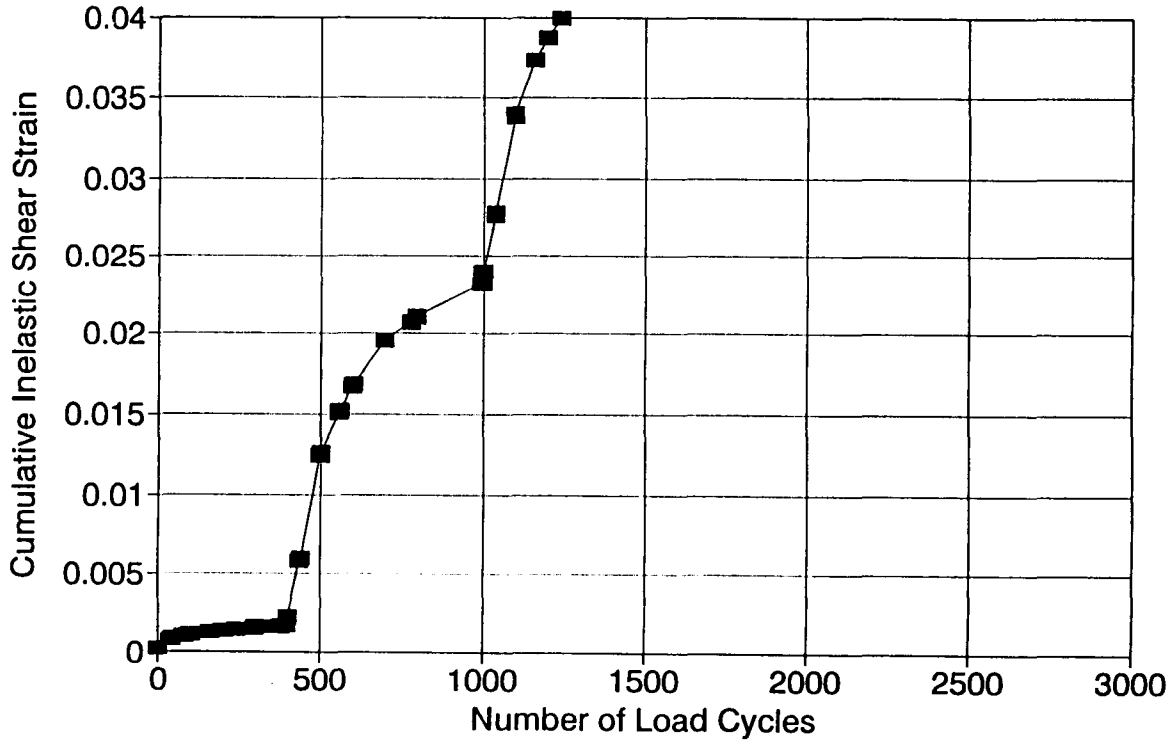

Figure F.20. Compound constant height test (Mix C1)

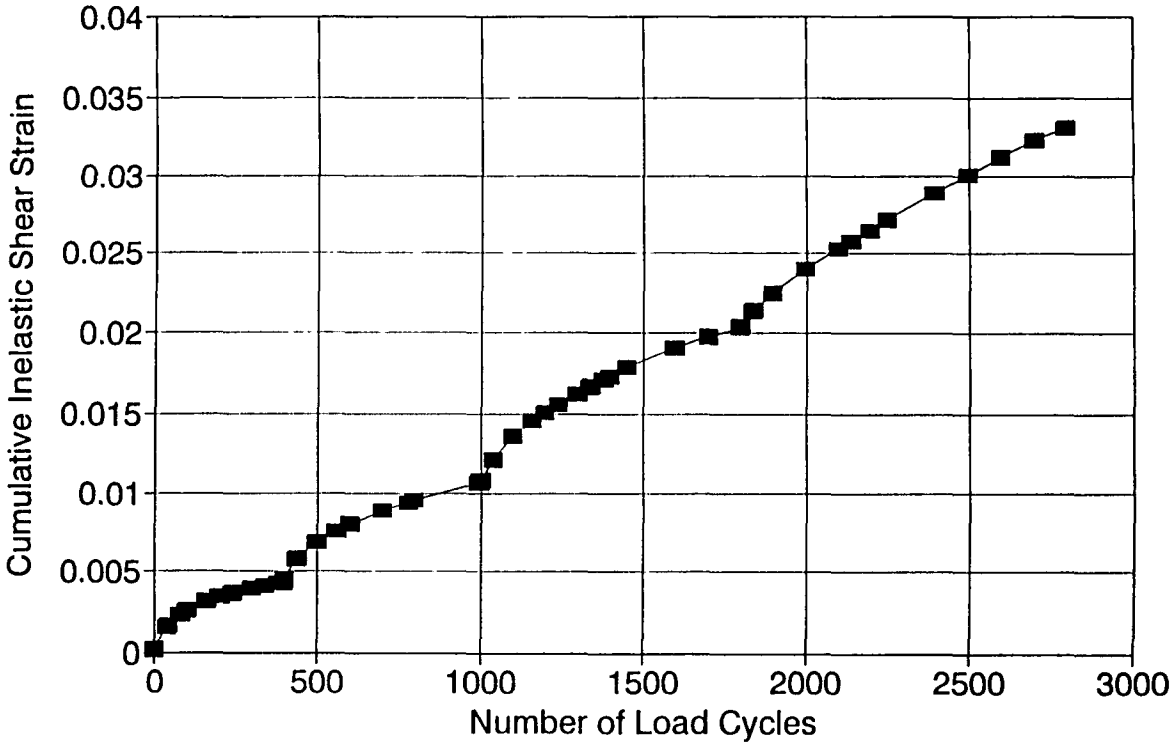

Figure F.21. Compound constant height test (Mix C2)

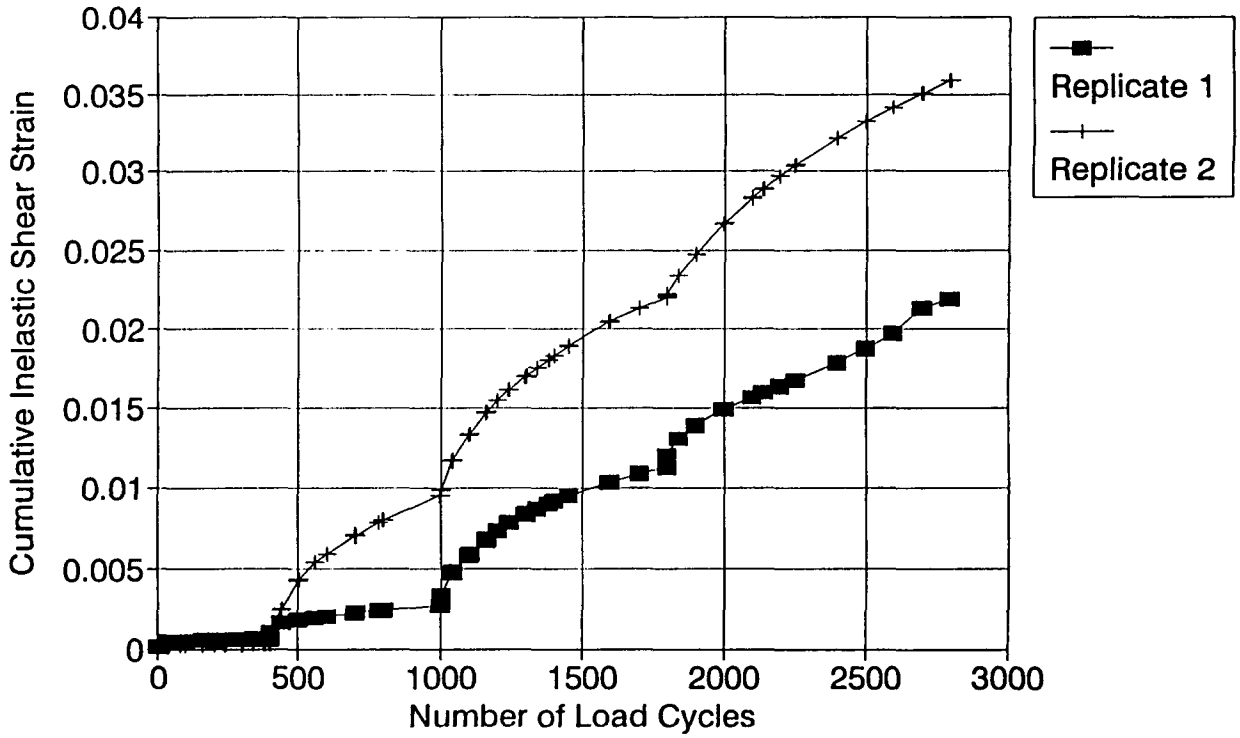

Figure F.22. Compound constant height test (Mix C3)

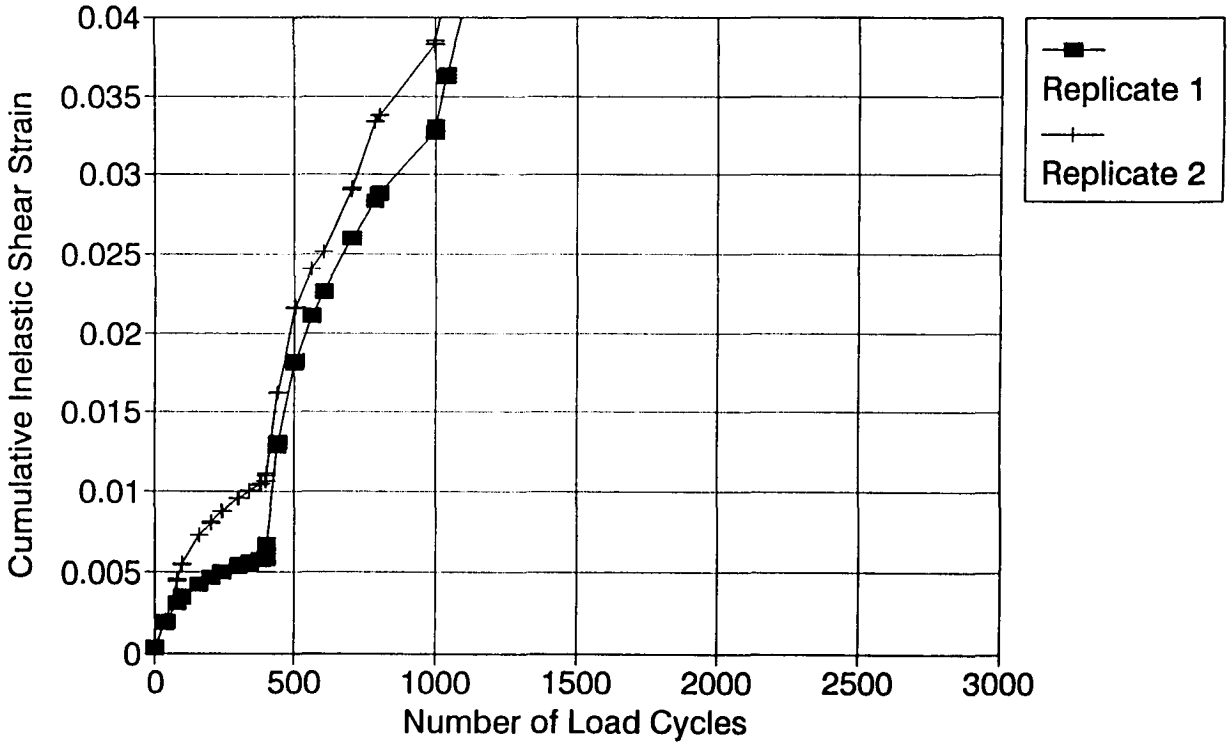

Figure F.23. Compound constant height test (Mix C4)